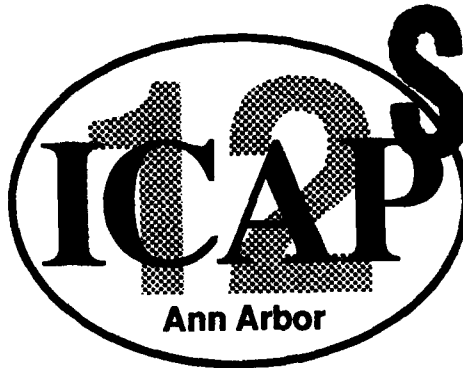


AD-A259 250



1

Twelfth International Conference
on
ATOMIC PHYSICS



DTIC
ELECTE
DEC 14 1992
A D

ABSTRACTS of
CONTRIBUTED PAPERS

This document has been approved
for public release and sale; its
distribution is unlimited.

University of Michigan
Ann Arbor

July 29 - August 3, 1990

92 12 10 025

REPORT DOCUMENTATION PAGE

1a. REPORT SECURITY CLASSIFICATION Unclassified		1b. RESTRICTIVE MARKINGS	
2a. SECURITY CLASSIFICATION AUTHORITY		3. DISTRIBUTION/AVAILABILITY OF REPORT Unlimited Distribution	
2b. DECLASSIFICATION/DOWNGRADING SCHEDULE			
4. PERFORMING ORGANIZATION REPORT NUMBER(S) N00014-90-J-1196		5. MONITORING ORGANIZATION REPORT NUMBER(S)	
6a. NAME OF PERFORMING ORGANIZATION University of Michigan	6b. OFFICE SYMBOL (if applicable)	7a. NAME OF MONITORING ORGANIZATION	
6c. ADDRESS (City, State, and ZIP Code) Department of Physics Ann Arbor, MI 48109		7b. ADDRESS (City, State, and ZIP Code)	
8a. NAME OF FUNDING/SPONSORING ORGANIZATION Office of Naval Research	8b. OFFICE SYMBOL (if applicable)	9. PROCUREMENT INSTRUMENT IDENTIFICATION NUMBER	
8c. ADDRESS (City, State, and ZIP Code) 800 North Quincy Street Arlington, Virginia 22217-5000		10. SOURCE OF FUNDING NUMBERS	
		PROGRAM ELEMENT NO	PROJECT NO
		TASK NO	WORK UNIT ACCESSION NO
11. TITLE (Include Security Classification) "12th International Conference on Atomic Physics"			
12. PERSONAL AUTHOR(S) Robert R. Lewis			
13a. TYPE OF REPORT Grant	13b. TIME COVERED FROM 11/15/89 TO 11/14/90	14. DATE OF REPORT (Year, Month, Day) 1990 Sept 26	15. PAGE COUNT
16. SUPPLEMENTARY NOTATION			
17. COSATI CODES		18. SUBJECT TERMS (Continue on reverse if necessary and identify by block number)	
FIELD	GROUP	SUB-GROUP	
19. ABSTRACT (Continue on reverse if necessary and identify by block number) The final report on this grant consists of a book of abstracts of papers submitted to the conference.			
20. DISTRIBUTION/AVAILABILITY OF ABSTRACT <input type="checkbox"/> UNCLASSIFIED/UNLIMITED <input type="checkbox"/> SAME AS RPT <input type="checkbox"/> DTIC USERS		21. ABSTRACT SECURITY CLASSIFICATION	
22a. NAME OF RESPONSIBLE INDIVIDUAL		22b. TELEPHONE (Include Area Code)	22c. OFFICE SYMBOL

Twelfth International Conference
on
ATOMIC PHYSICS



**ABSTRACTS of
CONTRIBUTED PAPERS**

University of Michigan
Ann Arbor

July 29 - August 3, 1990

Edited by W. E. Baylis, G. W. F. Drake
and J. W. McConkey

92-31270



51488

92 12 10 025

Department of Physics, University of Windsor
Windsor, Ontario, Canada N9B 3P4
July 1990

Local Organizing Committee

W. E. Baylis, Windsor
R. S. Conti, Ann Arbor
G. W. F. Drake, Windsor
G. W. Ford, Ann Arbor
D. W. Gidley, Ann Arbor
M. A. Gongora, Mexico City
R. R. Lewis, Ann Arbor
Conference Co-Chairman
W. J. McConkey, Windsor

S. Rand, Ann Arbor
A. Rich, Ann Arbor
Conference Chairman
D. Steel, Ann Arbor
S. Williams, Ann Arbor
P. W. Zitzewitz, Ann Arbor
J. C. Zorn, Ann Arbor
Conference Co-Chairman

International Program Committee

B. Bederson, New York
P. Bender, Boulder
C. Cohen-Tannoudji, Paris
T. W. Hänsch, Munich

H. J. Kimble, Pasadena
R. R. Lewis, Ann Arbor
Conference Co-Chairman
N. F. Ramsey, Cambridge, Mass.

International Organizing Committee

E. Arimondo, Pisa
G. Backenstoss, Basel
V. I. Balykin, Troitzk
M. A. Bouchiat, Paris
E. Commins, Berkeley
R. J. Damburg, Riga
T. Dohnalik, Krakow
G. W. F. Drake, Windsor
N. Fortson, Seattle
M. Gavril, Amsterdam
S. Haroche, Paris
V. W. Hughes, New Haven
I. B. Khriplovich, Novosibirsk

D. Kleppner, Cambridge, Mass.
F. Lin, Shanghai
C. Manus, Saclay
H. Narumi, Hiroshima
G. zu Putlitz, Heidelberg
A. Rich, Ann Arbor
Chairman
P. G. H. Sandars, Oxford
I. A. Sellin, Washington, D. C.
S. J. Smith, Boulder
P. E. Toschek, Hamburg
H. Walther, Munich

DTIC QUALITY IMPROVED 2

Accession For	
NTIS CRA&I	<input checked="" type="checkbox"/>
DTIC TAB	<input type="checkbox"/>
Unannounced	<input type="checkbox"/>
Justification	
By _____	
Distribution / _____	
Availability Codes	
Dist	Availability for Special
A-1	

Conference Sponsors:

International Union of Pure and Applied Physics

National Science Foundation

Office of Naval Research

Air Force Office of Scientific Research

University of Michigan
College of Engineering
College of Literature, Science and the Arts
Rackham Graduate School
Department of Physics

Ford Motor Company

IBM Corporation

Harold Early

TABLE OF CONTENTS

Poster Sessions Tuesday, 31 July (I-VI) and Thursday, 2 August (VII-XII)

I. Fundamental Laws and Constants

- I-1 *Quantum-mechanical phase-space trajectories and their application to scattering*
Hai-Woong Lee
- I-2 *Antimatter gravity and the weak equivalence principle*
M. H. Holzscheiter, R. E. Brown, J. Camp, T. Darling, P. Dyer, T. Goldman, D. B. Holtkamp, R. J. Hughes, N. Jarmie, N. S. P. King, M. M. Nieto, R. A. Kenefick, D. Oakley, R. Ristinen, F. C. Witteborn
- I-3 *Quadrupole moment of the $nS_{1/2}$ state of the hydrogen atom*
M. Yu. Kuchiev, A. V. Solov'yov, V. L. Yakhoutov
- I-4 *Classical constraints on the electron*
W. E. Baylis
- I-5 *Relativistic calculations of P- and T-violating properties in Cs and Tl*
Adam C. Hartley, Eva Lindroth and Ann-Marie Mårtensson-Pendrill
- I-6 *Parity non-conservation in atomic bismuth*
M. J. D. Macpherson, K. P. Zetie, D. N. Stacey
- I-7 *Separated-oscillatory-field phase-variation technique for measurement of the $n=2$ Lamb Shift in He^+*
M. E. Poitzsch and F. M. Pipkin
- I-8 *Particle-antiparticle frequency comparisons and the weak equivalence principle*
Richard J. Hughes
- I-9 *A measurement of the $2^2S_{1/2}$ - $2^2P_{3/2}$ fine-structure interval in muonium*
S. H. Kettell, H. E. Ahn, A. Badertscher, F. C. Chmely, M. Eckhause, P. Guss, V. W. Hughes, J. R. Kane, Y. Kuang, B. E. Matthias, H.-J. Mundinger, B. Ni, H. Orth, G. zu Putlitz, H. R. Schaefer, K. A. Woodle
- I-10 *On the possibilities of some new P and P,T violation experiments*
D. Budker, E. D. Commins, D. DeMille and M. Zolotarev

- I-11 *Systematic effects in the Berkeley electron electric-dipole experiment*
Stephen B. Ross, Kamal Abdullah, Conny Carlberg, E. D. Commins and Harvey Gould
- I-12 *A new apparatus for the study of parity nonconservation in atomic thallium*
D. DeMille, D. Budker, and E. D. Commins
- I-13 *Evidence for fractional charge and associated color charge in atoms and ions*
J. L. McKibben
- I-14 *Proposed test of the symmetrization postulate and exclusion principle*
J. D. Gillaspay, K. Deilamian, and D. E. Kelleher
- I-15 *Status report on the gamma-ray component of a determination of $N_A h/c$*
M. S. Dewey, E. G. Kessler, R. D. Deslattes, G. L. Greene and H. Börner
- I-16 *New techniques for simultaneous precision frequency spectroscopy of freely precessing ^3He , ^{21}Ne and ^{129}Xe*
E.R. Oteiza, R.J. Hoare, T.E. Chupp
- I-17 *Coherence in freely precessing ^{21}Ne and results of tests of local Lorentz invariance and linearity of quantum mechanics*
T. E. Chupp, R. J. Hoare, E. R. Oteiza, J. M. Richardson, M. E. Wagshul
- I-18 *Test of QED in helium-like and hydrogen-like uranium with a Doppler-tuned spectrometer*
J. H. Lupton, D. D. Dietrich, C. J. Hailey and K. P. Ziock
- I-19 *Precision measurements of $n=3$ to $n=3$ transition energies in very highly charged ions*
D. D. Dietrich, C. L. Bennett, T. E. Cowan, M. H. Chen, K.-T. Cheng, D. A. Knapp, R. E. Marrs, A. L. Osterheld and J. H. Scofield
- I-20 *Berry phase in a Stern-Gerlach experiment: example of mixing of the spin states*
V. A. Andreev, P. B. Lerner
- I-21 *Semi-empirical approach to the calculation of PNC E1 transitions in caesium and thallium*
A. C. Hartley and P. G. H. Sandars

- I-22 *An experiment to measure the fine structure of $n=2$ positronium*
T. D. Steiger, B. Ghaffari, A. Rich, and R. S. Conti
- I-23 *Electron-screening correction to the self energy in high-Z atoms*
Paul Indelicato and Peter J. Mohr
- I-24 *Self energy of excited states in a strong Coulomb field*
Peter J. Mohr and Yong-Ki Kim
- I-25 *Search for time-reversal symmetry violation in thallium fluoride using a jet source*
D. Cho, K. Sangster and E. A. Hinds
- I-26 *Deflection of an atomic beam by the Casimir force*
C. I. Sukenik, M. G. Boshier and E. A. Hinds
- I-27 *Cavity QED level shifts of simple atoms*
E. A. Hinds and V. Sandoghdar
- I-28 *The Runge-Lenz vector for the two-dimensional hydrogen atom*
M. Lieber, X. L. Yang, and F. T. Chan
- I-29 *First test of CP invariance in the decay of positronium*
Mark Skalsey and James Van House
- I-30 *Accurate calculation of parity nonconservation in cesium*
S. A. Blundell, W. R. Johnson, J. Sapirstein
- I-31 *Variational eigenvalues and QED effects in the $n=10$ states of helium*
G. W. F. Drake
- I-32 *Study of scalar and pseudoscalar particle production and QED vacuum birefringence (Delbruck scattering) using a polarized light beam -- status report*
F. Nezrick, R. Cameron, G. Cantatore, A. C. Melissinos, Y. Semertzidis, H. Halama, D. Lazarus, A. Prodell, J. Rogers, C. Rizzo and E. Zavattini
- I-33 *Improved anisotropy measurement of the Lamb shift in He^+*
A. van Wijngaarden, J. Kwela and G. W. F. Drake
- I-34 *A test of the linearity of quantum mechanics in spin $-3/2$ ^{201}Hg*
P. K. Majumder, B. J. Venema, S. K. Lamoreaux, B. R. Heckel, and E. N. Fortson

II. Atom and Ion Manipulation

- II-1 *First experiments with extracted ions following electron impact excitation in an electron beam ion trap*
D. Schneider, M. W. Clark, D. DeWitt, R. Schuch, C. L. Cocke, R. Schmieder, K. Reed, R. Marrs, M. Levine, R. Fortner
- II-2 *Studies on the process of slowing atoms with the Zeeman tuned technique*
V. S. Bagnato, S. C. Zilio, C. Salomon and R. Napolitano
- II-3 *Electronic g-factor of Ba⁺*
H. Knab, M. Hubrich, K. H. Knöll and G. Werth
- II-4 *⁴He - D₂ mass difference measurement in a Penning trap*
Ch. Gerz, D. Wilsdorf, D. Hagen and G. Werth
- II-5 *Laser cooling of an atomic beam utilizing the Stark effect*
R. J. Knize and J. R. Yeh
- II-6 *The effect of long-range collisions between atoms on laser cooling*
A. M. Smith and K. Burnett
- II-7 *A compensated Penning trap mass spectrometer and the ³H-³He mass difference*
R. S. Van Dyck, Jr., D. L. Farnham, F. L. Moore and P. B. Schwinberg
- II-8 *Consistency of the electron g-factor in a Penning trap*
R. S. Van Dyck, Jr., P. B. Schwinberg and H. G. Dehmelt
- II-9 *Sodium vapor drift observed upon resonance radiation pressure*
S. Gozzini, G. Paffuti, C. Gabbanini, G. Nienhuis and L. Moi
- II-10 *Preliminary experiment of laser isotope enrichment via magnetic deflection*
Xiwen Zhu, Guilong Huang, Ganghua Mei and Delin Yang
- II-11 *Demonstration of miniature Paul-Straubel trap with well defined potential well*
N. Yu, H. Dehmelt and W. Nagourney
- II-12 *Photodissociation recoil source for ultra-slow molecules*
Christopher Sweeney, Frederick Weihe, and Jens Zorn

- II-13 *Laser cooling of $^9\text{Be}^+$ at the Heidelberg test storage ring TSR*
W. Petrich, V. Balykin, M. Bock, C. Ellert, M. Grieser, R. Grieser, D. Habs, G. Huber, E. Jaeschke, R. Klein, T. Kühl, H. Miesner, M. Music, R. Neumann, S. Schröder, D. Schwalm, P. Sigray, M. Steck, B. Wanner, A. Wolf
- II-14 *Laser focusing of atoms: a particle optics approach*
J. J. McClelland and M. R. Scheinfein
- II-15 *Monte Carlo simulation studies of cavity-confined positronium*
Paul W. Zitzewitz, Lisa Lapidus, Jeffrey Nico and David Gidley
- II-16 *Progress on laser cooling of stored relativistic Li^+ ions*
R. Klein, N. Boos, R. Grieser, G. Huber, I. Hoog, P. Merz, S. Schröder, Th. Kühl, R. Neumann, V. Balykin, D. Habs, C. Ellert, W. Petrich, D. Schwalm, B. Wanner, A. Wolf and the TSR group
- II-17 *Observation of the laser cooling force due to multiphoton "Doppleron" resonances*
R. G. Hulet, J. J. Tollett, J. Chen, J. G. Story, N. W. M. Ritchie and C. C. Bradley

III. Nonlinear Physics and Chaos

- III-1 *Atoms in strong fields: chaotic dynamics, localization, and "scars"*
R. V. Jensen
- III-2 *Nonlinear optical interactions involving the real Gaussian field*
Chen Xie, G. Klimeck, Ce Chen and D. S. Elliott
- III-3 *Multiphoton transitions in non-monochromatic fields*
J. C. Camparo and P. P. Lambropoulos
- III-4 *Phase-sensitive above-threshold ionization at 8 Gigahertz*
D. A. Tate, D. G. Papaioannou and T. F. Gallagher
- III-5 *Attractor geometry of a quasiperiodically perturbed two-level atom*
J. C. Camparo and R. P. Frueholz
- III-6 *Induced chaotic amplitude variations in a hydrogen maser*
Ronald L. Walsworth, Edward M. Mattison and Robert F. C. Vessot

IV. Quantum Optics and Other Laser Techniques

- IV-1 *Saturation lineshapes in phase conjugation by non-collinear wave mixing*
O. di Lorenzo-Filho, P. C. de Oliveira and J. R. Rios Leite

- IV-2 *Inhibited spontaneous emission and thresholdless microlasers*
Y. Yamamoto, S. Machida and G. Björk
- IV-3 *New aspects of Holstein's treatment of radiation trapping*
W. Falecki and W. Hartmann
- IV-4 *Use of atomic frequency mixing effects for frequency stabilization of laser diodes in experiments with two-photon step by step excitation*
W. Falecki, W. Hartmann and R. Strobel
- IV-5 *A proposed compression method for a spin-polarized ^3He nuclear target*
L. D. Schearer and R. Vandiver
- IV-6 *Photon statistics in resonance fluorescence: results from an atomic beam deflection experiment*
M. D. Hoogerland, M. N. J. H. Wijnands, H. A. J. Senhorst, H. C. W. Beijerinck and K.A.H. van Leeuwen
- IV-7 *Calculations for the Hanle Effect in non-monochromatic laser light*
R. Ryan and T. Bergeman
- IV-8 *Resonances in 1D scattering with asymptotically linear potentials: A simplified model of atoms in a quadrupole magnetostatic trap*
H. Sporn, T. Bergeman, and N. D. Balazs
- IV-9 *Magneto-optical compression of slow atomic beams*
J. Nellesen, G. Hennig, J. H. Müller, K. Sengstock, U. Spangenberg, J. Werner and W. Ertmer
- IV-10 *Polarization gradient cooling: multipole interpretation of light forces in 3D-laserfields*
H. Wallis and W. Ertmer
- IV-11 *Effects of quantum noise on a two-level system in a single-mode cavity*
Linda Vahala
- IV-12 *Photodetachment-threshold shifts in two-color radiation fields*
L. A. Bloomfield
- IV-13 *Observation of the $^2S_{1/2} - ^2D_{5/2}$ transition in laser cooled trapped Yb^+*
A. S. Bell, H. A. Klein, G. P. Barwood, P. Gill, A. P. Levick and W. R. C. Rowley

- IV-14 *Linear trap for high-accuracy spectroscopy of stored ions*
M. G. Raizen, J. C. Bergquist, Wayne M. Itano and D. J. Wineland
- IV-15 *Subharmonic excitation of trapped electrons' cyclotron resonance*
Carl S. Weimer, F. L. Moore, and D. J. Wineland
- IV-16 *Coupled trap spectroscopy*
D. J. Heinzen, J. J. Bollinger, W. M. Itano, F. Moore and D. J. Wineland
- IV-17 *Diode laser measurements of Rb optical pumping parameters*
M. E. Wagshul and T. E. Chupp
- IV-18 *Observation of the channeling of atoms in three dimensional optical interference patterns*
N. P. Bigelow and M. Prentiss
- IV-19 *Observations of distortions in the fluorescence lineshapes of cold atoms in 3-D optical interference patterns*
N.P. Bigelow and M. Prentiss
- IV-20 *Studies of a single laser cooled, trapped strontium ion*
A. A. Madej, M. Houssin and J. D. Sankey
- IV-21 *Velocity-selective coherent population trapping for laser cooling in two and three dimensions*
F. Mauri and E. Arimondo
- IV-22 *Excitation of a single trapped electron by squeezed back-action*
Peter B. Lerner and P. Tombesi
- IV-23 *Effects of radiation trapping on optically trapped atoms*
T. Walker, D. Sesko and C. Wieman
- IV-24 *Cooperative stimulated radiation: coherence in atomic reaction induced by laser*
K.T. Lu

V. Photoionization Processes

- V-1 *PCI in the angular distribution of Auger-electrons for inner-shell atomic photoionization*
M. Yu. Kuchiev and S. A. Sheinerman

- V-2 *The radiative self-forces in semiclassical theory and the anomalously small luminescence of atomic systems*
N. N. Bezuglov, E. N. Borisov and V. P. Proshihin
- V-3 *Spin-orbit perturbation in atomic rubidium through photo-electron angular distributions*
Yi-Yian Yin, Ce Chen and D. S. Elliott
- V-4 *Phase sensitive multi-photon ionization*
Ce Chen, Yi-Yian Yin and D. S. Elliott
- V-5 *The calculation of the photoionization cross sections of the 7^2L excited states of Cs*
N. B. Avdonina and M. Ya. Amusia
- V-6 *A new method to compute atomic and molecular photoionization cross sections by use of basis sets*
L. Veseth
- V-7 *Photodetachment cross sections for Ca^+ , Sr^+ and Ba^+*
G. F. Gribakin, B. V. Gul'tsev, V. K. Ivanov, M. Yu. Kuchiev
- V-8 *Near-threshold photodetachment of H^- ions in parallel and crossed electric and magnetic fields*
I. I. Fabrikant
- V-9 *Spin and channel coupling in photoionization of Na*
Alfred Z. Msezane and Francis Nyandeh
- V-10 *Higher retardation and multipole corrections to the dipole angular distribution of inner shell photoelectrons*
A. Bechler and R. H. Pratt
- V-11 *Theoretical investigations of photon-electron polarization correlations in ns-subshell photoionization of uranium*
Y. S. Kim, I. B. Goldberg and R. H. Pratt
- V-12 *Energy and angular distribution of shake-off electrons of He near threshold*
R. Wehlitz, O. Hemmers, B. Langer, A. Menzel and U. Becker

- V-13 *Decay of the Ar 2p⁵nd core resonances: an Auger spectrum dominated by shake processes*
J. E. Hansen, M. Meyer, E. V. Raven and B. Sonntag
- V-14 *Study of dielectronic and radiative recombination of few-electron ions in the heavy-ion storage ring TSR*
A. Wolf, J. Berger, M. Bock, D. Habs, B. Hochadel, G. Kilgus, A. Müller, M. Music, G. Neureither, U. Schramm, R. Schuch, D. Schwalm and M. Wagner
- V-15 *Photodetachment in infrared and microwave fields*
D. J. Larson, P. S. Armstrong, M. C. Baruch, W. G. Sturuss, N. D. Gibson, and L. P. Ratliff
- V-16 *Photodissociation of H₂ very near threshold -- half-collisions at very low energy*
E. E. Eyler and E. McCormack
- V-17 *Theoretical evaluation of cross-sections for Compton scattering from inner shell atomic electrons*
T. Suric, P. M. Bergstrom, K. Pisk and R. H. Pratt
- V-18 *Exact calculation of multi-photon processes by a single longitudinal mode pulsed laser*
Edward S. Fry, ShiFang Li, Feng Gao and XingFu Li
- V-19 *Retardation effects in Rayleigh scattering by K-shell electrons*
A. Costescu, P. M. Bergstrom and R. H. Pratt
- V-20 *Study of Mg 3pnd and 3pns (J=1) autoionization spectra*
G. W. Schinn, C. J. Dai and T. F. Gallagher
- V-21 *Ionization of Rydberg atoms by a circularly polarized microwave field*
J. M. Hetteema, C. Y. Lee, Panming Fu, T. J. Scholz, T. F. Gallagher
- V-22 *Collective effects on ionization of Rydberg sodium atoms by blackbody radiation*
F. Fuso, M. Allegrini, R. Dygdala, F. Giammanco and E. Arimondo
- VI. Plasma Physics**
- VI-1 *Fast electron relaxation on Langmuir oscillations in collisional low-temperature plasma*
V. I. Demidov, T. V. Rudakova and V. Y. Simonov

- VI-2 *Coincidence study of heavy noble gas excitation by electron impact in the regime of large impact parameters*
K. E. Martus, S. H. Zheng and K. Becker
- VII. Atomic Spectroscopy and Structure - Theory**
- VII-1 *Spline solutions of the helium pair equation*
C. F. Fischer
- VII-2 *Current status of atomic spectroscopic data compilations at NIST*
W. L. Wiese, J. R. Fuhr, W. C. Martin, A. Musgrove and J. Sugar
- VII-3 *Analytical exactness of estimating eigenquantum defects from Lu-Fano plots*
Liu Xuewen and Yu Gengsun
- VII-4 *Multichannel quantum-defect theory of lifetimes for highly excited states of atoms*
Liu Xuewen and Z.-W. Wang
- VII-5 *Variational principle with nondifferentiable functions for equivalent electrons*
I. L. Beigman
- VII-6 *An analytical approach to the calculation of the electron energy levels for a many-electron atom*
Sebastiano Tosto
- VII-7 *Configuration interaction between Rydberg series in C I*
L. Bureyeva
- VII-8 *Investigation of the bound even-parity $J=0,2$ spectra of neutral tin*
Mingxing Jin, Dajun Ding, Hang Liu and Shoufu Pan
- VII-9 *Higher-order effects in the hyperfine structure and isotope shift in heavy elements*
G. Klemz and H.-D. Kronfeldt
- VII-10 *Spectroscopic data for highly charged ions*
S. Li, Y. Sun, G. Han, H. Yang, Y. Yang and L. Chen
- VII-11 *Calculation of $2p^4(3P)nl(l=s,d)$ Rydberg spectra of the fluorine isoelectronic sequence*
Z.-W. Wang and X.-Z. Qian
- VII-12 *Quantum electrodynamic perturbation theory for high-Z few-electron atoms*
V. M. Shabaev

- VII-13 *Determination of configuration-mixing coefficients from fine-structure data*
Edward S. Chang
- VII-14 *Stark effect in the high-L Rydberg lines of magnesium in the solar infrared spectrum*
William G. Schoenfeld and Edward S. Chang
- VII-15 *Reanalysis of the isotope shift and nuclear charge radii in radioactive potassium isotopes*
A.-M. Mårtensson-Pendrill, L. Pendrill, S. Salomonson, A. Ynnerman and H. Warston
- VII-16 *Variational method for the many-particle Dirac equation*
K. Aashamar and J. D. Talman
- VII-17 *Effective multiconfigurational potential for many-body perturbation calculations*
Z. W. Liu and H. P. Kelly
- VII-18 *Anomalous doublet splittings of binding energies in Dirac-Fock calculations*
Chien-Tsun Chen and Keh-Ning Huang
- VII-19 *A theoretical survey of the neon isoelectronic sequence*
E. Biémont
- VII-20 *A theoretical investigation of transition rates and wavelengths in the x-ray spectra of nickel-like ions (Ge V - Pb LV)*
P. Quinet and E. Biémont
- VII-21 *Comparison of the saddle-point method and the Feshbach-type projection method*
Kwong T. Chung
- VII-22 *Identification of high-resolution Auger spectrum of beryllium*
Kwong T. Chung
- VII-23 *Finite element analysis of the three-body Coulomb system*
J. Shertzer
- VII-24 *The spectrum of photoexcited Nd^{3+} ions in LaCl_3*
J. Shertzer, N. Pelletier-Allard and R. Pelletier
- VII-25 *Fine structure of the alkaline earth negative ions*
V. A. Dzuba, V. V. Flambaum, G. F. Gribakin, O. P. Sushkov

- VII-26 *Dirac-Fock basis set calculations for atoms and molecules*
Ajaya K. Mohanty and E. Clementi
- VII-27 *The exact Born-Oppenheimer oscillator strength distribution moments in the continuum for $H_2^+(1s\sigma_g)$*
J.W. Liu
- VII-28 *Brillouin's theorem and the role of single excitations in multiconfiguration Hartree-Fock calculations*
T. M. Luke and J. D. Talman
- VII-29 *Spectroscopic factors of subvalent electrons in argon and xenon*
M. Ya. Amusia and A. S. Kheifets
- VII-30 *Positiveness of free-free Coulomb dipole matrix elements*
S. D. Oh and R. H. Pratt
- VII-31 *Ab Initio Calculations Of Orthogonal Parameters For Complex Configurations Using B-Splines*
Y.-T. Shen, M. Landtman and J.E. Hansen
- VII-32 *A relativistic many-body study of the energy levels of the Hg $16p^2$ resonances*
Z. Cai, D. R. Beck and W. F. Perger
- VII-33 *Non-variational series solution to the non-relativistic helium problem using a standard angular momentum decomposition*
Douglas McColm and Glen Erickson
- VII-34 *Widths of the $n1'$ autoionisation resonances in the rare gas atoms*
M. Ya. Amusia, V. L. Tsemekhman, K. L. Tsemekhman
- VII-35 *An extended relativistic Hamiltonian for spin 1/2 particles*
S. P. Goldman
- VII-36 *Relativistic variational calculations for hydrogenic atoms in strong magnetic field*
Z. Chen and S. P. Goldman
- VII-37 *Relativistic finite basis set calculations for atoms*
H. M. Quiney and I. P. Grant
- VII-38 *Software for relativistic atomic structure theory: the grasp project at Oxford*
F. A. Parpia and I. P. Grant

- VII-39 *An efficient method for computing relativistic mixing in complex spectra*
K. Aashamar, T. M. Luke and J. D. Talman
- VII-40 *Relativistic configuration interaction method for atomic systems*
Takashi Kagawa and Shuji Kiyokawa
- VII-41 *Potential energy surface for H_3^+ via Z-dependent perturbation theory -- a third-order study*
Moh'd Abu-Jafar, Frank C. Sanders and Donald H. Galvan
- VII-42 *Second-order contribution to the width and shift of autoionizing states of two-electron atoms below the $n=2$ threshold*
Lonnie W. Manning and Frank C. Sanders
- VII-43 *Relativistic coupled-cluster calculations*
I. Lindgren, E. Lindroth, H. Persson, S. Salomonson and P. Öster
- VII-44 *Coupled-cluster calculations for atoms*
I. Lindgren, A.-M. Mårtensson-Pendrill, S. Salomonson, A. Ynnerman and P. Öster
- VII-45 *Analysis of the nonlinear dichroic Voigt effect and its relation with nonlinear Faraday effect and nonlinear Hanle effect*
X. Chen
- VII-46 *Photoionization calculations for the 3D subshell of barium*
M. Kutzner, D. Winn, W. Radojevic and H. P. Kelly
- VII-47 *Hydrogen-like atom in a strong magnetic field*
N.N. Ablyazov, M. Yu. Kuchiev
- VII-48 *A data management system for high-precision UV laser spectroscopy based on relativistic quantum-defect theory*
K. T. Lu, Dennis T. Baba and Keri Carpenter
- VIII. Atomic Spectroscopy and Structure - Experiment**
- VIII-1 *Superfluorescent transitions between high-lying atomic levels in an electric field*
T. Becker and R.-H. Rinkleff
- VIII-2 *Experimental study of heavy atomic spectroscopy using discharge sputtering*
Fucheng Lin

- VIII-3 *Hyperfine structures of stable terms in ^{14}N -ions*
H. Winter and A. Schirmacher
- VIII-4 *On-line collinear fast beam laser spectroscopy of ^{88}Kr and ^{90}Kr to study nuclear charge radii beyond the $N=50$ shell closure*
H. A. Schuessler, R. M. Evans, M. Brieger, and Y. F. Li
- VIII-5 *Perturbation of the 2D series in aluminum; an old problem solved with new measurements*
A. Dönszelmann, M. Davidson and E. P. Buurman
- VIII-6 *One-photon resonant two-photon ionization processes of atomic lead*
Dajun Ding, Mingxing Jin and Hang Liu
- VIII-7 *Beam-foil study of two-electron transitions in Cu-like ions of soft-x-ray laser interest*
E. Träbert, J. Sugar, G. Möller, P. H. Heckmann
- VIII-8 *Lifetime of the 2^3S_1 state of helium-like $^{79}\text{Br}^{33-}$*
R. W. Dunford, C. J. Liu, H. G. Berry, M. L. A. Raphaelian, R. C. Vondrasek, and B. J. Zabransky
- VIII-9 *Magnetic-field decoupling of alkali excited-state hyperfine structure*
W. A. van Wijngaarden and J. Sagie
- VIII-10 *Hyperfine structure studies of ^{93}Nb using laser optical galvanic spectroscopy*
Ranjit Singh and G. N. Rao
- VIII-11 *Cascade-corrected lifetime measurements for the $3s3p^2\ ^2S$, 2P and 2D levels of Ti X, Fe XIV and Ni XVI*
E. H. Pinnington, A. Tauheed, W. Ansbacher, E. Träbert, P. H. Heckmann and G. Möller
- VIII-12 *Laser spectroscopy on copper and silver atoms*
J. Bengtsson, J. Carlsson, P. Jönsson, J. Larsson, L. Sturesson and S. Svanberg
- VIII-13 *Laser spectroscopy of atomic hydrogen*
C. D. Thompson, G. H. Woodman, C. J. Foot, P. Hannaford, D. N. Stacey, P. E. G. Baird, J. B. Swan and G. K. Woodgate
- VIII-14 *Circular-metastable di-excited states of barium*
L. Chen, G. Spiess, F. Roussel, M. Cheret, T. Bolzinger, J. Hare and M. Gross

- VIII-15 *High-precision isotope shift measurement in helium*
P. Zhao, J. R. Lawall, and F. M. Pipkin
- VIII-16 *Sternheimer-free determination of the ^{47}Ti nuclear quadrupole moment from hyperfine-structure measurements*
E. Stachowska, J. Dembczynski, W. Ertmer
- VIII-17 *The sodium D-lines in magnetic fields up to 1 Tesla*
M. Musso, L. Windholz, H. Jäger
- VIII-18 *Spectroscopy of high angular momentum Rydberg states in Si^{10+}*
A. E. Livingston, F. G. Serpa, and E. J. Galvez
- VIII-19 *Doubly-excited $6p\ 1/2, 3/2np\ J=1$ and $4f\ 5/2, 7/2nf\ J=5, 6$ autoionizing Rydberg series in barium*
R.J. de Graaff, M. Abutaleb, W. Ubachs and W. Hogervorst
- VIII-20 *High-resolution study of the $B^2\Sigma_u^- - X^2\Sigma_g^-$ system of $^{15}\text{N}_2^+$*
T. J. Scholl, A. W. Taylor, R. A. Holt and S. D. Rosner
- VIII-21 *Laser spectroscopy investigations of the Eu-I line 5765\AA*
W. Pietsch, M. Musso, L. Windholz
- VIII-22 *Lyman alpha stark beats*
J. F. Williams
- VIII-23 *Measurement of the Lamb shift in lithium-like uranium (U^{89+})*
J. Schweppe, A. Belkacem, L. Blumenfeld, Nelson Claytor, B. Feinberg, Harvey Gould, V. E. Kostroun, L. Levy, S. Misawa, R. Mowat, and M. Prior
- VIII-24 *First two-photon spectroscopy of singlet helium*
W. Lichten, D. Shiner and Zhi-Xiang Zhou
- VIII-25 *Lineshapes of ionizing Stark resonances in helium*
E. E. Eyler, A. Nussenzweig, T. Bergeman, E. Pollack
- VIII-26 *Precision wavelength measurement of the $1s2s\ ^3S - 1s2p\ ^3P^o$ transitions in helium-like boron*
T. P. Dinneen, N. B. Mansour, H. G. Berry, L. Young and R. C. Pardo

IX. Molecular Spectroscopy and Structure, Surfaces and Clusters

- IX-1 *DV-X α calculation of x-ray absorption spectra of resonances for SF₆*
H. Nakamatsu, T. Mukoyama and H. Adachi
- IX-2 *Solution of the interface problem between two chains using a Green's matrix method*
M. A. Abdel-Raouf
- IX-3 *Recombination spectroscopy of alkali and alkaline-like ions in superfluid helium*
H. Bauer, M. Beau, J. Fischer, H. J. Reyher, J. Rosenkranz and K. Venter
- IX-4 *Neutral mass-selected lead cluster beams*
M. Abshagen, J. Kowalski, M. Meyberg, G. zu Putlitz, J. Slaby and F. Träger
- IX-5 *The experimental determination of the electron charge density of diatomic molecules by electron diffraction*
Y. Zhang, A. W. Ross and M. Fink
- IX-6 *The spectroscopic investigation of excited dissociation products of cluster ions desorbed by electrons*
I. P. Bogdanova, V. A. Vladimirov and V. I. Yakovleva
- IX-7 *Zn₂ potential curves: a simple theoretical treatment of intershell effects*
M. Couty, G. Chambaud and W. E. Baylis

X. Atomic, Ionic and Molecular Collisions

- X-1 *Recent developments in collision induced intramultiplet mixing with Ne^{**}{(2p)⁵(3p)} atoms*
W. Boom, J. P. H. Sanders, H. C. W. Beijerinck and B. J. Verhaar
- X-2 *Collisional ion drift selfalignment as a tool for electric field determination in ionized gas*
S. A. Kazantsev, A. G. Petrashen, N. T. Polezhaeva, V. N. Rebane, and T. K. Rebane
- X-3 *Free-particle model for charge-changing process at relativistic velocity collision*
S. Karashima
- X-4 *Collisional multipole relaxation in the ⁷F ground term of samarium*
P. Hannaford, R. M. Lowe and R. J. McLean

- X-5 *Relativistic coupled-channel calculations with Coulomb boundary conditions*
N. Toshima and J. Eichler
- X-6 *Atomic polarization produced in Na-Ar and Na-Xe optical collisions*
D. Olsgaard and M. Havey
- X-7 *Polarized N^{++} ion beam formed by electron capture in a polarized sodium target*
C. J. Liu, R. W. Dunford, Y. Azuma, N. B. Mansour, H. G. Berry and D. A. Church
- X-8 *Determining the absolute scale for $Mg^+ + He$ differential scattering cross sections at 30-, 66.7-, and 150-keV Mg^+ energies*
E. Redd
- X-9 *State-selective KKL RTEA measurements for collisions of 0.25-2 MeV/u F^{7+} with H_2 and He targets*
D. H. Lee, P. Richard, T. J. M. Zouros, J. M. Sanders and J. L. Shipaugh
- X-10 *Molecule-like behaviour of H^- in collision dynamics*
M. Matsuzawa, N. Koyama, M. Maeda and T. Ishihara
- X-11 *Resonance scattering involving tri-atomic systems*
Sung-Ho Salk and C. K. Lutrus
- X-12 *Scaling of Rydberg charge-transfer cross sections: initial measurements with a new detector*
S. B. Hansen, K. B. MacAdam and L. G. Gray
- X-13 *Associative ionization between sodium and cesium*
M. Biagini, C. Gabbanini, S. Gozzini, A. Lucchesini and L. Moi
- X-14 *A study of $H^0 + H_2$ collisions*
E. J. Quintana, J. A. Lozano, and E. Pollack
- X-15 *Double ionization of helium by fast He^+ projectiles*
J. L. Forest, J. A. Tanis, M. W. Clark, S. M. Ferguson and K. Lifrieri and V. L. Plano
- X-16 *Impact-parameter treatment of atomic collisions including noninertial nuclear-electronic terms*
Gabriel Hose

- X-17 *On the transition time in Landau-Zener model*
S. V. Bobashev, V. A. Kharchenko
- X-18 *Absolute L-mixing cross sections for slow K^+ + Na Rydberg atom collisions*
W. W. Smith., T. F. Gallagher, P. Pillet, R. Kachru and N. H. Tran

XI. Electron and Positron Collisions

- XI-1 *The final-state interaction in K-shell ionization during the β -decay*
E. G. Drukarev
- XI-2 *Theory of positron-atom and positron-ion collisions*
M. A. Abdel-Raouf
- XI-3 *Electron impact ionization of the 3^1P state in magnesium*
Rajesh Srivastava
- XI-4 *Electron scattering by atomic hydrogen*
S. N. Tiwary
- XI-5 *Measurements of electron-impact excitation cross sections and oscillator strengths in rare gas atoms*
Y. Sakai, T. Suzuki, G. P. Li, T. Takayanagi, K. Wakiya, H. Suzuki, T. Inaba, S. S. Kano and H. Takuma
- XI-6 *Cross sections and spin polarizations for e^- scattering from cadmium*
Sultana N. Nahar
- XI-7 *Wannier's threshold law and adiabatic representation*
S. Watanabe
- XI-8 *Positron collision with rubidium*
T. T. Gien
- XI-9 *Wallace approximation for e^- scattering*
T. T. Gien and Z. C. Yan
- XI-10 *Cross sections and electron collision excitation functions of some $5p^56p$ Xe levels*
I. P. Bogdanova and S. V. Yurgenson
- XI-11 *Coherent excitation of the heavy rare gases by electron impact*
J. J. Corr, P. J. M. van der Burgt and J. W. McConkey

- XI-12 *Collision data for electric quadrupole transitions in Ca^+*
A. Burgess, M. C. Chidichimo and J. A. Tully
- XI-13 *Elastic scattering of low-energy electrons by Ca, Sr, and Ba atoms*
G. F. Gribakin, B. V. Gul'tsev, V. K. Ivanov, M. Yu. Kuchiev
- XI-14 *Low energy electron impact excitation in H and He^+ : $n \leq 5$ state calculations*
K. M. Aggarwal, K. A. Berrington, P. G. Burke, A. E. Kingston and A. Pathak
- XI-15 *Electron impact excitation with Ca XV and Fe XXI*
K. M. Aggarwal, K. A. Berrington, W. B. Eissner and P. H. Norrington
- XI-16 *Theoretical differential cross sections and spin polarizations for elastic electron scattering from Xe atoms*
Q. Hou, J. M. Li and R. H. Pratt
- XI-17 *Electron impact ionization of highly charged Na-like ions*
K. J. Reed, M. H. Chen and D. L. Moores
- XI-18 *Absolute electron scattering cross sections for the $2S \rightarrow 2P$ transition in Zn^+ using energy-loss and merged-beams methods*
Steven J. Smith, K.-F. Man, R. J. Mawhorter, I. D. Williams and A. Chutjian
- XI-19 *Electron scattering by neon-like selenium using the Dirac R-matrix theory*
W. P. Wijesundera, I. P. Grant, F. A. Parpia
- XI-20 *Electron scattering by oxygen-like krypton using the Dirac R-matrix theory*
W. P. Wijesundera, F. A. Parpia, I. P. Grant
- XI-21 *Eikonal evaluation of cross section asymmetry in atomic break-up process by polarized electrons*
T. Onaga and H. Narumi
- XI-22 *Complete electron impact excitation parameters for the 3^3D state of helium*
H. J. Beyer and H. Kleinpoppen
- XI-23 *Photon Stokes parameters of alkali resonance lines in electron impact excitation of spin-polarized alkali atoms*
M. A. H. Bukhari, H. J. Beyer and H. Kleinpoppen

- XI-24 *Superelastic $3P \rightarrow 3S$ cross sections for 3 eV electrons scattered by sodium*
T. Y. Jiang, M. Zuo, L. Vuskovic, and B. Bederson
- XI-25 *Dielectronic recombination in helium-like heavy ions*
R. Ali, C. P. Bhalla, C. L. Cocke, P. Richard and M. P. Stockli
- XI-26 *Elastic scattering of positrons on mercury: a negative-energy Dirac-Fock treatment*
J. E. Sienkiewicz and W. E. Baylis

XII. Exotic Atoms and Special Topics

- XII-1 *Radiation of atomic electrons in the processes of nuclear transformations*
A. V. Solov'yov
- XII-2 *Evidence of fast excited positronium formation from $n=2$ fine-structure transition*
R. Ley, K. D. Niebling and G. Werth
- XII-3 *Free muonium from silica aerogels*
V. Ebert, K. Jungmann, V. W. Hughes, S. Kirches, S. Koppe, F. Maas, H.-J. Munding, G. zu Putlitz, J. Rosenkranz, W. Schäfer, W. Schwarz, Z. Zhang
- XII-4 *Angular distribution measurement of beam-foil muonium*
H. E. Ahn, F. Chmely, V. W. Hughes, S. H. Kettell, Y. Kuang, B. E. Matthias, H.-J. Munding, B. Ni, G. zu Putlitz, H. R. Schaefer, K. A. Woodle
- XII-5 *Atomic physics searches for bound state beta decay*
D. E. Murnick and Namik Kwon
- XII-6 *Physics with laser polarized nuclei*
T. E. Chupp

I. FUNDAMENTAL LAWS AND CONSTANTS
(QED, Symmetries, Basic Physics ...)

**QUANTUM-MECHANICAL PHASE-SPACE TRAJECTORIES AND THEIR
APPLICATION TO SCATTERING**

Hai-Woong Lee
Department of Physics
Korea Institute of Technology, KAIST
Taejon, 305-701, KOREA

The concept of quantum-mechanical phase-space trajectories is introduced, which offer a visual interpretation of quantum scattering dynamics.

Theory

Wigner distribution function

$$W(q, p, t) = \frac{1}{\pi\hbar} \int_{-\infty}^{\infty} dx \exp(-2ipx/\hbar) \psi^*(q-x, t) \psi(q+x, t)$$

time development

$$\frac{\partial W(q, p, t)}{\partial t} = -\frac{p}{m} \frac{\partial W(q, p, t)}{\partial q} + \int_{-\infty}^{\infty} dj W(q, p+j, t) J(q, j)$$

where

$$J(q, j) = \frac{i}{\pi\hbar^2} \int_{-\infty}^{\infty} dy [V(q+y) - V(q-y)] \exp(-2iyj/\hbar)$$

Define $\tilde{V}(q, p, t)$ such that

$$\frac{\partial \tilde{V}(q, p, t)}{\partial q} \frac{\partial W(q, p, t)}{\partial p} = \int_{-\infty}^{\infty} dj W(q, p+j, t) J(q, j)$$

Then

$$\frac{\partial W(q, p, t)}{\partial t} = -\frac{p}{m} \frac{\partial W(q, p, t)}{\partial q} + \frac{\partial \tilde{V}(q, p, t)}{\partial q} \frac{\partial W(q, p, t)}{\partial p}$$

which immediately yields

$$\frac{dq}{dt} = \frac{p}{m}, \quad \frac{dp}{dt} = -\frac{\partial \tilde{V}(q, p, t)}{\partial q}$$

Thus, each phase-space point (q, p) of the Wigner distribution function moves along a classical trajectory under the influence of the "quantum potential" $\tilde{V}(q, p, t)$. Such a trajectory, called "Wigner trajectory", can be considered as a visual manifestation of quantum-mechanical motion of the phase-space point.

Example : Scattering of a Gaussian wave packet by a potential step

potential

$$V(q) = \begin{cases} V_0, & q \geq 0, \\ 0, & q < 0. \end{cases}$$

initial wave packet

$$W(q, p, t = 0) = \frac{1}{\pi \hbar} \exp[-(q - q_0)^2 / 2(\Delta q)^2] \exp[-(p - p_0)^2 / 2(\Delta p)^2]$$

where

$$(\Delta p) = \frac{\hbar}{2(\Delta q)}$$

Assume weak scattering ($\frac{\hbar^2}{2m} \gg V_0$) and neglect spreading. Then

$$W(q, p, t) \cong \frac{1}{\pi \hbar} \exp[-(q - q_0 - \frac{p_0 t}{m})^2 / 2(\Delta q)^2] \exp[-(p - p_0)^2 / 2(\Delta p)^2]$$

Straightforward algebra yields (see the first equation in the box in the previous page)

$$\frac{\partial \tilde{V}(q, p)}{\partial q} \cong \frac{V_0}{\hbar} \sqrt{\frac{2}{\pi}} (\Delta p) \exp[-2(\Delta p)^2 q^2 / \hbar^2] \sum_{n=0}^{\infty} \frac{(-1)^n}{(2n+1)!} \left(\frac{p-p_0}{\sqrt{2}\Delta p}\right)^{2n} H_{2n}\left(\frac{\sqrt{2}(\Delta p)q}{\hbar}\right)$$

and

$$\begin{aligned} \tilde{V}(q, p) = \tilde{V}(q) = & \frac{V_0}{\sqrt{\pi}} \left\{ \frac{\sqrt{\pi}}{2} \left[1 + \operatorname{erf}\left(\frac{\sqrt{2}(\Delta p)q}{\hbar}\right) \right] \right. \\ & \left. + \exp[-2(\Delta p)^2 q^2 / \hbar^2] \sum_{n=1}^{\infty} \frac{(-1)^{n+1}}{(2n+1)!} \left(\frac{\delta p}{\sqrt{2}\Delta p}\right)^{2n} H_{2n-1}\left(\frac{\sqrt{2}(\Delta p)q}{\hbar}\right) \right\} \end{aligned}$$

where H_n denotes the Hermite polynomial, erf is the error function, and $\delta p = p - p_0$. Graphs for the quantum potential \tilde{V} and the corresponding Wigner trajectories will be shown at the conference.

ANTIMATTER GRAVITY AND THE WEAK EQUIVALENCE PRINCIPLE

M. H. Holzscheiter, R. E. Brown, J. Camp, T. Darling, P. Dyer, T. Goldman,
 D. B. Holtkamp, R. J. Hughes, N. Jarmie, N. S. P. King, M. M. Nieto,
 Los Alamos National Laboratory, Los Alamos, NM 87545;
 R. A. Kenefick, Texas A&M University, College Station, Texas 77843;
 D. Oakley, R. Ristinen, University of Colorado, Boulder, Colorado 80309;
 F. C. Witteborn, NASA Ames Research Center, Moffett Field, California 94305

We are developing an experiment to compare the acceleration, g , of antiprotons in the earth's gravitational field with that of particles of normal matter, such as protons or negative hydrogen ions [1]. This experiment will test for the first time whether antiprotons respect the weak equivalence principle. The weak equivalence principle is itself based upon the experimental result that different types of matter fall with the same accelerations with extraordinary accuracy (parts in 10^{11}). It was the profound implication of such results which led Einstein to his general theory of relativity, in which the gravitational force couples to all types of energy with equal strength. Despite the well-known successes of general relativity it is vitally important to continue to test experimentally the principle of equivalence on which it is founded, particularly with particles such as the antiproton, which are not readily encountered in a gravitational context.

Several arguments have been made which suggest that antiprotons must respect the weak equivalence principle. The suggestion that CPT symmetry between matter and antimatter requires the antiproton to fall with the same acceleration as the proton involves a misuse of CPT. One must remember that a falling antiproton is not an isolated particle and so the CPT operation must also be applied to the source of the gravitational field. CPT symmetry therefore relates the gravitational acceleration of a proton to the acceleration of an antiproton towards an "antiearth," and so has no bearing on the result of our experiment. Morrison identified some apparent difficulties with energy conservation and the gravitational red-shift if antiprotons do not respect the equivalence principle [2]. It can be shown that energy is conserved, but at the price of an anomalous red-shift in "clocks" composed of antimatter [3]. Indeed, since Morrison wrote his paper it has become well-known that the red-shift is only a test of weak equivalence for the energy content of "clocks," rather than a property of photons [4]. M. L. Good showed [5] that a violation of equivalence in the neutral kaon system would show up as an apparent CP-violating effect which can be experimentally constrained. These constraints could have some bearing on the question of equivalence for the antiproton if gravity couples with an anomalous strength to the energy of antiquarks, although Good's calculation needs to be reassessed in such a model. Conversely, there are other models in which Good's considerations have no implications for antiprotons [6]. L. I. Schiff argued [7] that equivalence principle tests on ordinary matter already imply some limits on equivalence for antimatter since virtual positrons contribute to the binding energy of atoms. However, as Schiff himself realized, his calculation was plagued with unknown divergent contributions, and so his argument can only be regarded as qualitative. None of these arguments can therefore be regarded as removing the necessity for an experimental measurement of the gravitational acceleration of the antiproton.

Our method of measuring g has been adopted from the experiment to measure g for free electrons [8]. Low energy particles are launched upwards and the time for them to traverse a height difference of 1 m under the influence of gravity is recorded. The distribution of flight times (due to the distribution of initial velocities of the particles) will exhibit a cutoff time. This time is directly related to g for the launched particles and is independent of the particle's inertial mass and distribution of initial velocities. The cutoff would occur at about 1/2 sec for a 1 m flight path, and we propose to measure this cutoff time to an accuracy of better than 1%.

The cutoff time of 1/2 sec corresponds to particles having an initial velocity of

approximately 4 m/sec, which is equivalent to a kinetic energy of 10^{-7} eV for an antiproton. This is 13 orders of magnitude below the lowest energy antiprotons that are currently available (2 MeV at LEAR). To achieve the first and largest step in energy reduction we will pass a 200 nsec long bunch of these high energy antiprotons through a thin foil. If the thickness is chosen correctly a significant number of antiprotons will emerge with energies below 50 keV and can be captured into a Penning trap. By using a combination of electron cooling [9] and resistive cooling [10], the average energy can be reduced to 4 K. Once the particles are cooled to 4 K they are ready to be launched into a region of space which is sufficiently free of electric fields and magnetic-field gradients that the force of gravity is dominant.

The technical problems of this experiment can be separated into two areas: (1) A large number of antiprotons must be captured into a trap and cooled to 4 K; (2) A region of space free of electric fields larger than 10^7 V/m and magnetic gradients larger than 1 part in 10^5 must be provided. With respect to item (1), we have successfully tested the foil degrading of 5-MeV antiprotons at LEAR [11] and have experimentally verified the expected efficiency. Independently, we have used a small accelerator to inject 5-20 keV H^+ and H^- ions into an elongated, multi-electrode trap. This trap allows the capture of a longer length beam bunch than does a standard Penning trap, but still maintains a certain degree of harmonicity. Subsequently, we constructed a beam line that combines the degrading and trapping. Here we pass 5-MeV protons from a Van de Graaff accelerator through a foil located at the entrance of an 18" long trap and capture particles below 50 keV. With respect to item (2), we plan to provide a drift region inside a metal cylinder. This "drift tube" will be situated in a uniform magnetic field to constrain the ions to move along its axis. The major problem in fabricating such a tube is to control the fluctuating electric field produced by the patch effect (variations in the work function along the tube's inside surface). Therefore, we have built a vibrating probe apparatus (Kelvin probe) to study surface potentials on small samples of different materials. We have succeeded in identifying candidates for the drift-tube surface, but the sensitivity of these measurements is limited to a field 100 times stronger than ultimately needed. To improve on these results we will have to use gravity itself as a probe. Therefore, we have assembled a test experiment where different mass ions from an ion source will be launched into a drift tube. A micro channel plate detector will be used at the exit of the tube to detect the ions and to study the time-of-flight distribution. Detecting ions moving under the influence of gravity will constitute the ultimate test of having achieved sufficient shielding of stray electric fields. As for the magnetic gradient fields, we have commissioned a superconducting magnet which provides a 2-tesla field with a homogeneity of better than 1 part in 10^5 over a cylinder of 50 cm length and 1 cm diameter. Once the drift-tube has been tested, we will replace the ion source with a Penning trap and use the drift-tube as a tool to analyze the launching of ultra-low energy particles from the trap.

After measuring g for protons and negative hydrogen ions at Los Alamos the experiment will be moved to LEAR in order to measure the gravitational acceleration of antiprotons and thereby perform the first test ever of the weak equivalent principle for antimatter.

1. N. Beverini, et. al.; CERN/PSCC/86-2/P-94 (1986)
2. P. Morrison, Am. J. Phys. 26, 358 (1958).
3. R. J. Hughes, Proc. Moriond Workshop on "New and Exotic Phenomena", 1990.
4. K. Nortvedt, Phys. Rev. D11, 245 (1975);
J. S. Bell in "Fundamental Symmetries," Ph. Bloch et al.eds., Plenum NY (1986).
5. M. L. Good, Phys. Rev. 121, 311 (1961).
6. K. Macrae and R. J. Riegert, Nucl. Phys. B244, 513 (1984).
7. L. I. Schiff, Phys. Rev. Lett. 1, 254 (1958).
8. F. C. Witteborn, W. M. Fairbank, Phys. Rev. Lett. 19, 1049 (1967)
9. G. Gabrielse, et.al; Phys. Rev. Lett. 63, 1360 (1989)
10. H. G. Dehmelt, Adv. At. Mol. Phys. 3, 53 (1967) and 5, 109 (1969)
11. N. Hill, D. B. Holtkamp, N. S. P. King, to be published

QUADRUPOLE MOMENT OF THE $nS_{1/2}$ -STATE OF THE HYDROGEN ATOM.M.Yu.Kuchiev⁺, A.V.Solov'yov⁺, V.L.Yakhoutov⁺⁺+ A.F.Ioffe Physical-Technical Institute of the Academy of Sciences
of the USSR, Leningrad, 194021

++ Polytechnical Institute, Leningrad, USSR, 195251

Recently, in the papers [1-2] it was pointed out that an account for the hyperfine interaction (HFI) of the atomic electrons with the nucleus with spin $I \neq 0$ gives rise to the non-zero quadrupole moment (QM) value of the atom with the ground-state term $S_{1/2}$. Previously it was supposed that the QM of the atom with the $S_{1/2}$ -term should strictly be equal to zero. The origin of the QM of $S_{1/2}$ term is the HFI. It provides the admixture of the states with $D_{3/2}$ term to the initial state. These states possess the QM, hence the initial $S_{1/2}$ state also obtains the non-zero QM. The calculations were performed previously for $1S_{1/2}$ and $2S_{1/2}$ states of H. The ground-state QM is $Q_{1S}^{(H)} = -7.65 \cdot 10^{-25} e \text{ cm}^2$ [1-2]. This result was generalised to the case of hydrogen-like ions with the arbitrary nuclear charge values, nuclear magnetic moment values and nuclear spin values [3]. In the papers [4-5] the computation of the hydrogenic $2p_{1/2}$ state QM value $Q_{2p_{1/2}}^{(H)}$ was carried out.

In $2p_{1/2}$ the present work the calculation of QM value of the $nS_{1/2}$ state with the total moment $F=1$ of the hydrogen atom is carried out for arbitrary n .

There is the feature, which makes the problem rather peculiar for $n \geq 3$. Namely, in the non-relativistic approximation the two important magnitudes: firstly, the matrix element, causing ns - nd mixing, and, secondly, the energy denominator of the mixing coefficient, are both equal to zero. Thus, computation of the coefficient of the $ns_{1/2}$ - $nd_{3/2}$ state admixture can not be carried out in the non-relativistic limit. The relativistic corrections to both the matrix element and the energetic denominator are of the order of α^2 . As a result we come across the interesting situation: one has to carry out the computation with an accuracy, being of order α^2 , whereas the resultant mixing coefficient is independent of α .

The functional dependence of Q_{ns} on n turns out to be rather peculiar. If one takes into account the admixture of only the $n'd_{3/2}$

($n' \neq n$) and $d_{3/2}$ state to the $nS_{1/2}$ one, it results in the following expression :

$$Q_{ns} = -\frac{4}{3} \mu_e \mu_p n = Q_{1s} \cdot n \quad (1)$$

which coincides with that, obtained in the paper of Amusia et al. (1986). Here $\mu_e = |e| \hbar / 2m_e c$; $\mu_p = |e| \hbar / 2m_p c$ - are the electron and the photon magnetic moments.

In the present work we have shown that an account for the admixture of all $d_{3/2}$ -states, including $nd_{3/2}$ gives

$$Q_{ns} = -\frac{4}{3} \mu_e \mu_p (n^2 + 2) = Q_{1s} \cdot \frac{n^2 + 2}{3} \quad (2)$$

Thus an account for the $nS_{1/2}$ - $nd_{3/2}$ mixing causes the more rapid increase of Q_{ns} with n . An interesting fact is the absence of the terms $\sim \alpha n^4 + \beta n^3$ in (2). One may expect them to be present in the final result, since the radius of the $nS_{1/2}$ state increases with the increase of n as n^2 . And in fact, the terms of such type arise in the intermediate stage of calculations, whereas finally they vanish.

1. V.G.Baryshevsky and S.A.Kuten, Phys.Lett.A., 64 (77) 238; 67(78) 355.
2. I.B.Khriplovich, J.Phys.B 17 (1984) L803.
3. R.E.Moss and I.A.Sadler, J.Phys. B 19 (1986) L503.
4. M.Ya.Amusia, V.L.Yakhontov, J.Phys. B.: At.Mol.Phys. 1984, V.17, L203.
5. M.Ya.Amusia, M.Yu.Kuchiev, V.L.Yakhontov, Izv. AN SSSR, ser. fiz., v. 50, n7, 1285 (1986) (in Russian)

CLASSICAL CONSTRAINTS ON THE ELECTRON

W. E. Baylis, Dept. of Physics, University of Windsor, Windsor, Ontario N9B 3P4, Canada

Some properties of the electron which are usually associated with its quantum nature are shown to be required by a consistent classical picture. The 4-velocity and orientation of an "elementary particle" is given classically by the instantaneous Lorentz transformation from its rest frame to the observer's frame. This transformation behaves as a *spinor*; it is the classical *eigenspinor* Λ of the particle. The particle is said to be "elementary" if a single eigenspinor is sufficient to describe its motion. The eigenspinor trivially satisfies a 4-momentum relation which is the exact classical analog of the Dirac equation of relativistic quantum theory, and the bilinear covariants formed with the eigenspinor are closely associated with those from quantum theory, including current density and spin. If the particle is charged, the evolution of Λ is also constrained by the Lorentz-force equation. It can be shown that the time-development equation for an elementary charge should be linear in Λ and that linearity implies a precession like that for a spin with a g-factor of 2.

The arguments are developed here in the covariant extension of the Pauli algebra \mathcal{P} . [1,2] In \mathcal{P} , any element p is the sum of scalar (p_0), pseudoscalar (iq_0), vector (\mathbf{p}), and pseudovector ($i\mathbf{q}$), parts $p = p_0 + iq_0 + \mathbf{p} + i\mathbf{q}$. The restricted Lorentz transformation $L \in \text{SL}(2, \mathbb{C})$ of a 4-vector like the 4-velocity u is given by

$$u \rightarrow u' = LuL^* \quad (1)$$

where $L = \exp(-i\bar{\theta}/2 + w/2)$ is a unimodular element of \mathcal{P} : $L\bar{L} = 1$. The bar indicates the *spatial reversal*, obtained by changing the sign of the vector and pseudovector parts, whereas the *hermitean conjugate*, denoted by a dagger, has the signs on the pseudoscalar and pseudovector parts reversed. If $\bar{\theta} = 0$, L is hermitean and describes a pure boost with boost parameter w . On the other hand, if $w = 0$, then L is unitary and describes a pure rotation by the angle θ about the axis $\bar{\theta}$. The eigenspinor Λ is the particular L which transforms the particle from its rest frame S_0 to the observer's frame S . The scalar $\Lambda\bar{\Lambda} = 1$ is the bilinear covariant corresponding to the normalization condition of the Dirac tetrad.

The 4-velocity of the particle is found by applying Λ to the rest 4-velocity, which for a positive-energy particle (in units with $c = 1$) is $u_{rest} = 1$: $u = \Lambda u_{rest} \Lambda^* = \Lambda \Lambda^*$. This is another bilinear covariant; it corresponds exactly to the quantum current density. More generally, however, Λ gives not only the 4-velocity but also the orientation of the particle as seen in the observer's frame S . If the particle is observed in a different frame S' , Λ must be replaced by the transformed

$$\Lambda \rightarrow \Lambda' = L\Lambda, \quad (2)$$

where L transforms quantities from S to S' .

The motion of an elementary particle is determined if the evolution of its eigenspinor is known. An equation of motion for $\Lambda(\tau)$ takes the form given by the trivial identity

$$\dot{\Lambda} = G\Lambda, \quad G = \Lambda\bar{\Lambda}. \quad (3)$$

Since $\Lambda \bar{\Lambda} = 1$, $\dot{\Lambda} \bar{\Lambda} = -\Lambda \dot{\bar{\Lambda}} = -\dot{\bar{\Lambda}} \Lambda$ where the dot indicates a derivative with respect to the proper time τ , and we noted that the order of the derivative and the spatial reversal may be interchanged. As a result, G is the negative of its spatial reversal and is therefore a vector plus a pseudovector. By (2), G transforms as a "6-vector": $G \rightarrow LG\bar{L}$.

The 4-acceleration \dot{u} is related to $\dot{\Lambda}$ by

$$\dot{u} = \dot{\Lambda} \Lambda^* + \Lambda \dot{\Lambda}^* = Gu + uG^* \quad (4)$$

This is exactly the form of the Lorentz-force equation in \mathcal{P} . [2] For the motion of a charge e of mass m in an external electromagnetic field $F = E + iB$,

$$G = \frac{e}{8m} [(2+g)F + (2-g)\Lambda \Lambda^* F^* \bar{\Lambda}^* \bar{\Lambda}] \quad (5)$$

where g is a scalar constant and F is the field on the world line of the particle. An analysis of the rotation predicted by (3) and (5) shows that even though the charge was not assumed to be spinning, it precesses like a particle with spin and a g -factor g . If a single Λ is to describe the motion of a possibly rotating charge of any nonzero extension, then the equation of motion (3) must be linear in Λ , and hence by (5), $g = 2$. The classical bilinear covariants corresponding to the spin are the 6-vector $S = i\Lambda \dot{\Lambda}$ and its pseudovector dual $\uparrow = i\Lambda \dot{\Lambda}^*$.

Radiation reaction can be derived for the classical motion by expanding the retarded self-field F_{ret} along the worldline $r(\tau)$ of the charge and adding this to the external field with which the charge interacts at x . The self-field is the usual Liénard-Wiechert solution to Maxwell's equations $\partial F_{ret}(x) = 4\pi k \bar{j}$ with $j = eu(\tau)\delta[x - r(\tau)]$ except that the light-cone condition on the separation $R = x - r(\tau)$ is satisfied only in the limit $R \rightarrow 0$. A mass renormalization is then all that is required to obtain the Lorentz-Dirac equation. Radiation reaction is incorporated into the time-development of Λ by adding the effective internal field $\frac{2kq}{3} d(\dot{u}\bar{u})/d\tau$ to F .

The "classical Dirac equation" is simply the spinor form of the equation relating the 4-momentum and the 4-velocity: $p = mu$ and its spatial reverse. From the bilinear covariants for unimodularity and 4-velocity, these relations can be written in the linear form

$$p\bar{\Lambda}^* = m\Lambda, \quad \bar{p}\Lambda = m\bar{\Lambda}^* \quad (6)$$

Classically $p = p^*$ and the two equations (6) are equivalent. They are also equivalent quantum mechanically if $\bar{p}\Lambda = -i\hbar\partial\Lambda\dot{\Lambda} - e\bar{A}\Lambda = -(\hbar\partial S + e\bar{A})\Lambda$ where S is the 6-vector spin (see above). The four components of a minimal 2×2 matrix representation of Λ correspond directly to the four components of the usual Dirac tetrad and expressions in terms of gamma matrices and have exactly their usual quantum forms.

This research is supported by the Natural Sciences and Engineering Council of Canada.

1. W. E. Baylis and G. Jones, *J. Math. Phys.* **29**, 57-62 (1988).
2. W. E. Baylis and G. Jones, *J. Phys. A* **22** 1-16; 17-29 (1989).

RELATIVISTIC CALCULATIONS OF P- AND T-VIOLATING PROPERTIES IN Cs AND Tl

Adam C Hartley¹, Eva Lindroth² and Ann-Marie Mårtensson-Pendrill²,

1) Clarendon Laboratory, Oxford, OX1 3PU, England

2) Dept. of Physics, Chalmers University of Technology, S-412 96 Göteborg, Sweden

The demands for accurate calculations for the interpretation of atomic experiments studying parity non-conserving (PNC) phenomena has stimulated the development of techniques for relativistic many-body techniques. The exchange of a Z_0 boson leads to a parity non-conserving electron-nucleon interaction

$$h^{PNC} = \frac{G_F}{2\sqrt{2}} Q_W \rho_N(r) \gamma_5$$

where $Q_W/(-N) = 0.9793 - (Z/N) [0.9793 - 3.8968 \sin^2 \theta_w]$ and $\sin^2 \theta_w = 0.230 \pm 0.005$. The value of Q_W can be extracted from the ratio between experimental and theoretical results, thereby giving information about the weak interaction parameters at low energies – provided both theory and experiment are sufficiently accurate. The atomic calculations are particularly challenging due to the need to treat two perturbations simultaneously – the applied electric field and the weak interaction – in addition to the Coulomb interaction between the electrons. This makes the calculations relatively complicated already at the one-particle level. However, it is known from calculations of other properties that inclusion of correlation effects, which require the simultaneous excitation of two orbitals, are required in order to get reliable results.

In this work we performed correlation calculations using a numerical basis set, obtained from a diagonalization of the discretized representation of the Dirac hamiltonian, as described in /1/, to perform explicitly the summations over intermediate states. For the atoms Cs and Tl we have calculated the lowest-order correlation contributions to energies, hyperfine structures and transition matrix elements /2/, as well as to parity non-conserving electric dipole (PNC-E1) transition matrix elements and to atomic electric dipole moments (EDM) /3/ in terms of a possible electron EDM, which, if found, is a manifestation of simultaneous P- and T-violation. Table 1 shows some of the results obtained. The hyperfine structure and PNC results for Cs are in agreement with earlier calculations /4,5/, when results at the same level of approximation are compared. Our Cs EDM calculation is the first to include correlation effects. When our result, $R=114(3)$ is combined with the experimental limit from ref. /6/, $d(\text{Cs})=(2.3 \pm 7.8 \pm 1.4) \cdot 10^{-24}$ e·cm, this gives the current lowest limit for the electron EDM: $d_e=(1.9 \pm 6.5 \pm 1.2) \cdot 10^{-26}$ e·cm. The Tl results show larger correlation contributions than earlier, formally equivalent, calculations, /7,8,9/, in particular for the hyperfine structure /7/ and the EDM /9/ contributions. The discrepancy is

probably caused by the larger basis set and higher intermediate angular momenta used in the present work. The TI results make it clear that a more complete treatment, especially of the interaction between the $6p_{1/2}$ and the two $6s$ core electrons, is needed before the TI results can be relied on.

Table 1: Results for the ground state hyperfine structure (in GHz) from Ref /2/, for the PNC-E1 transition matrix element, $6s \rightarrow 7s$ and $6p_{1/2} \rightarrow 7p_{1/2}$, respectively (in units of $10^{-11} e a_0 Q_W / (-N)$) and for the enhancement factors for a possible electron EDM /3/.

	Cs			TI		
	hfs	PNC-E1	EDM	hfs	PNC-E1	EDM
HF	1.427	0.736	126	17.57	-6.63	-1906
+RPA	1.720	0.890	115	21.88	-9.65	-1041
+BO	2.365	0.946	117	24.21	-7.40	-293
+BO-RPA	2.405	0.936	114	24.06	-7.83	-179
Exp:	2.298 ^a	(0.899 $\pm 0.09 \pm 0.06$) ^b		21.31 ^c	(-7.2 \pm 1.7) ^d	

a) E Arimondo *et al* Rev. Mod. Phys. **49** 31 (1977)

b) M C Noecker *et al* Phys. Rev. Lett. **61** 310 (1988)

c) A Lurio and A G Prodell, Phys. Rev. **101** 79 (1956)

d) P S Drell and E D Commins, Phys. Rev. **A32** 2196 (1985)

References:

1. S Salomonson and P Öster, Phys. Rev. **A40** 5548, 5559 (1989)
2. A C Hartley and A-M Mårtensson-Pendrill, Z. Phys. A, in print
3. A C Hartley, E Lindroth and A-M Mårtensson-Pendrill, J Phys. B, submitted
4. W R Johnson *et al*. Phys. Rev. **A35** 3220 (1987),
V A Dzuba *et al*. J. Phys. **B17** 1953 (1984)
5. W R Johnson *et al*. Phys. Rev. **A37** 307, 1395 (1988)
V A Dzuba *et al*. Phys. Lett. **A141** 147 (1989)
6. S A Murthy *et al*. Phys. Rev. Lett. **61** 310 (1989)
7. V A Dzuba *et al*, J. Phys. **B20** 1399 (1987)
8. V A Dzuba *et al*, J. Phys. **B20** 3297 (1987), Physica Scripta **35** 69 (1987)
9. A Ya Kraftmakher, J. Phys. **B21** 2803 (1988)

PARITY NON-CONSERVATION IN ATOMIC BISMUTH

M.J.D. Macpherson, K.P. Zetie, D.N. Stacey.
Clarendon Laboratory, Oxford University,
Parks Road, Oxford, OX1 3PU, England.

The exchange of Z^0 bosons between the electrons and the nucleus in an atom causes parity non-conserving optical rotations near M1 (E1 parity forbidden) transitions [1]. This rotation depends on the ratio of the M1 and PNC-induced E1 transition matrix elements and is enhanced by a factor of Z^3 in heavy atoms [2]. The experimentally determined quantity

$$R = \text{Im} \left(\frac{E1_{PNC}}{M1} \right)$$

can be compared to a calculated value which depends on the nuclear weak charge, Q_w , and hence used to test electroweak theory [3]. Such measurements in atoms are important because they provide a test of electro-weak theory at low energy, and are sensitive to an orthogonal combination of the quark-lepton coupling constants C_{1u} and C_{1d} to that measured in high energy experiments such as those at CERN and SLAC. The work has also stimulated progress in the theory of the structure of heavy atoms [4].

Our experiment measures the effect near the allowed M1 transition at 876 nm in bismuth ($Z = 83$, $I = \frac{9}{2}$). Our published result of $R_{876} = (-10 \pm 1) \times 10^{-8}$ [5], when combined with the most recent theoretical value [6] of $(11.0 \pm 1.3) \times 10^{-8} Q_w/N$ (using $Q_w = -[N - (1 - 4 \sin^2 \theta_w)Z]$), gives $\sin^2 \theta_w = 0.215(33)$. This is consistent with the value of 0.221(3) from high energy experiments [7].

The aims of the present phase of the experiment are firstly to improve the precision and secondly to make an unambiguous observation of the nuclear anapole moment (caused by parity mixing of nuclear wavefunctions), described by Ze'ldovich [8]. This gives a nuclear spin-dependent term in the electron-nucleus Hamiltonian leading to a PNC rotation which is estimated to be of order 1% of that from the familiar nuclear spin-independent term [9] and is distinguishable from it by its spectrum (see figure 1).

The experimental technique is essentially as described in [5] but changes have been made which have improved both the statistical accuracy (now 1%) and, more importantly, discrimination against systematic effects. The changes include:

1. Standing wave laser upgraded to a Coherent CR-699 ring dye laser. This has higher power output and allows us to scan 30 GHz, covering the whole hyperfine structure of the 876 nm line. This gives optimum discrimination between nuclear spin-dependent and spin-independent effects.

2. Improvements in the oven heating system so that operation is at a constant temperature. We can also reach a higher bismuth vapour density than before.

3. Real-time calibration of the frequency scale.

We will present the first data obtained with the new system.

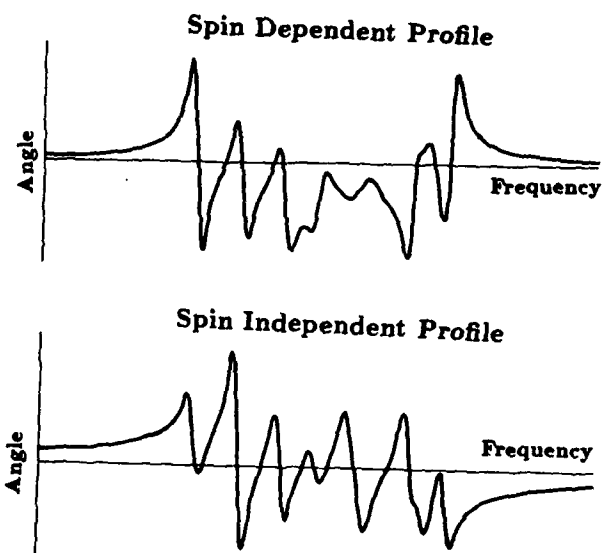


Figure 1: Comparison of nuclear spin-dependent and spin-independent rotations

REFERENCES:

1. eg Lynn (1984) *Atomic Physics* 9 World Scientific
2. M.A. Bouchiat & C. Bouchiat (1974) *Journal de Physique* 35 899
3. eg Sandars (1984) *Atomic Physics* 9 World Scientific
4. eg Dzuba et al (1988) *Europhys Lett* 7 413
5. Macpherson et al (1987) *Europhys Lett* 4 811
6. Flambaum et al (1990) *Novosibirsk Preprint* 89-111
7. Quoted by Blundell et al (1990) *University of Notre Dame Preprint*
8. Ze'ldovich (1957) *Sov Phys JETP* 6 1184
9. Flambaum & Khriplovich (1980) *Sov Phys JETP* 52 835

SEPARATED-OSCILLATORY-FIELD PHASE-VARIATION TECHNIQUE
FOR MEASUREMENT OF THE N=2 LAMB SHIFT IN He⁺ •

M. E. Poitzsch and F. M. Pipkin
Lyman Laboratory of Physics, Harvard University
Cambridge, MA 02138

The 14 GHz $2^2S_{1/2} - 2^2P_{1/2}$ Lamb shift in He⁺ provides an important test of QED atomic structure calculations, since this simple atomic system is both precisely calculable and amenable to powerful spectroscopic methods. At present, experimental precision can attain roughly the level of the uncertainty in the theoretical value [1,2].

To measure the Lamb shift, we use the separated-oscillatory-fields (SOF) technique of atomic-beam spectroscopy, which is due to Ramsey [3]. This technique has been used for precise rf spectroscopy of various fine-structure levels in hydrogen and He⁺ [4]. In this method, the atoms or ions, excited into the metastable $2^2S_{1/2}$ state, pass through two separated rf interaction regions whose electric fields are alternately in phase and 180° out of phase. An "interference signal" is detected as the difference between the rf quenching signals for these two relative phases. This interference signal can be narrowed substantially below the natural linewidth of the interval -- a major advantage, since the natural linewidth for the He⁺ (n=2) Lamb shift is 1.6 GHz.

In the experimental set-up, a small linear accelerator produces a beam of He⁺ ions at an energy of 127 keV. Ions in the metastable $2^2S_{1/2}$ state are produced when the beam passes through a nitrogen gas target. The SOF interaction regions consist of a pair of tunable microwave cavities fed by a 20-watt traveling-wave tube amplifier through a large-solid-angle, tantalum-cathode detector that monitors the population of ions surviving in the metastable $2^2S_{1/2}$ state by detecting the 30.4 nm photons emitted when those ions are quenched by an applied static electric field. Finally, a Faraday cup measures the beam current for use in normalizing the signals.

Despite the narrowing achieved by the SOF technique, this system still requires a very rigorous understanding of the behavior of the cavities and precise control of the microwave electric field strength over a broad frequency band. We have, however, demonstrated a phase-variation technique [5] that gives a precise determination of the transition frequency using fewer different frequency points that need not be as far from resonance. In this method, we introduce an additional, variable phase shift between the two microwave electric field regions by varying the path length of one of the waveguide feed arms. At a fixed frequency, varying this phase causes the interference signal to behave exactly as a cosine of calculable period. The Lamb-shift transition frequency can be determined by varying this phase for several neighboring frequencies and, at each frequency, finding the phase value

at which the interference signal is a maximum. The graph of these maximal phases versus frequency crosses the abscissa at the transition frequency.

An extensive series of numerical simulations has been carried out to provide a better understanding of the dependence of the signal on the microwave electric field in and between the cavity interaction regions. A numerical solution of Maxwell's equations is used to determine the spatial dependence of the microwave electric field. Improved cavities with greater tuning range, finer tunability, and well-defined electric field geometries are currently being constructed and will soon be implemented.

-
- Research supported by NSF Grant PHY87-04527
 - 1. G. W. F. Drake, J. Patel, and A. van Wijngaarden, Phys. Rev. Lett. 60, 1002 (1988).
 - 2. M. S. Dewey and R. W. Dunford, Phys. Rev. Lett. 60, 2014 (1988).
 - 3. N. F. Ramsey, Molecular Beams (Oxford U.P., London, 1956), pp. 124-134.
 - 4. See, e.g., S. R. Lundeen and F. M. Pipkin, Metrologia 22, 9 (1986); P. K. Majumder and F. M. Pipkin, Phys. Rev. Lett. 63, 372 (1989).
 - 5. H. A. Klein, E. W. Hagley, P. K. Majumder, F. M. Pipkin, and M. E. Poitzsch, Phys. Rev. A36, 3494 (1987).

PARTICLE-ANTIPARTICLE FREQUENCY COMPARISONS AND
THE WEAK EQUIVALENCE PRINCIPLE

Richard J. Hughes
University of California,
Los Alamos National Laboratory,
Physics Division P-15,
Los Alamos, NM 87545.

Improvements in the precision spectroscopy of single particles or antiparticles in an ion trap[1] will allow a comparison of the influence of gravity on the trapped particles to be made. In particular, the comparison of electron and positron, or proton and antiproton cyclotron frequencies, which are used as tests of CPT symmetry for their inertial masses[2,3], will become sensitive to a violation of the weak equivalence principle by the antiparticle in the earth's gravitational field[4]. An experiment to test this fundamental principle of physics for antimatter has yet to be performed[5], although a measurement of the gravitational acceleration of the antiproton is under development[6].

The cyclotron frequency of a charged particle in a magnetic field constitutes a local clock. It is well known that the gravitational redshift of the rates of two clocks which are separated by some height in a gravitational field results from the coupling of gravity to the energy content of the clocks[7], and that a measurement of the redshift provides a test of weak equivalence for the clock energy[8]. Therefore, although the cyclotron frequencies of an electron or proton in a magnetic field will exhibit the usual redshift of general relativity in a gravitational field, the positron or antiproton cyclotron frequencies would not if these antiparticles do not obey the weak equivalence principle.

This observation leads to the possibility of testing the equivalence principle for positrons and antiprotons by comparing their cyclotron frequencies with those of the electron and antiproton, respectively, in the same magnetic fields and at the same height in the earth's gravitational field. This is because although the cyclotron frequencies of these particle-antiparticle pairs would be identical in the absence of gravity (at "infinity"), under the assumption of exact CPT symmetry, they would have different redshifts between "infinity" and the surface of the earth if the antiparticle violated the weak equivalence principle, and this would produce a non-zero frequency

difference. The conventional redshift between "infinity" and the surface of the earth is $GM_{\oplus}/R_{\oplus}c^2 \sim 6 \times 10^{-10}$. Therefore, if it is found that the cyclotron frequencies of the proton and antiproton are equal to 1 part in 10^9 in the same magnetic field[2], this result would rule out the possibility that the antiproton experiences a gravitational acceleration which is double (or opposite) that of the proton in the earth's gravitational field. Moreover, if the precision of this frequency comparison can be improved to the 10^{-12} level[1], such an experiment would provide a test of weak equivalence for the antiproton in the earth's gravitational field at the 10^{-3} level, and likewise for the electron and positron.

References.

1. D. J. Heinzen and D. J. Wineland, "Laser-Cooled Refrigerator and Detector," NIST Report (1989), to be published in Phys. Rev. A.
2. G. Gabrielse et al., "Progress Report by the Trap Collaboration (PS-196)," CERN/PSCC/89-7/PSCC/M297;
G. Gabrielse et al., Phys. Rev. Lett. 63, 1360 (1989).
3. P. B. Schwinberg, R. S. VanDyck, Jr., and H. G. Dehmelt, Phys. Lett. A81, 119 (1981).
4. R. J. Hughes, "Do Positrons and Antiprotons respect the Weak Equivalence Principle?" LA-UR-90-1026, to appear in the proceedings of the Moriond workshop on "New and Exotic Phenomena", Les Arcs, France, January 1990; M. H. Holzschneider and R. J. Hughes (in preparation).
5. T. Goldman and M. M. Nieto, Phys. Lett. 112B, 217 (1988);
T. Goldman, R. J. Hughes, and M. M. Nieto, Phys. Lett. 171B, 217 (1988).
6. N. Beverini et al., "A Measurement of the Gravitational Acceleration of the Antiproton," CERN/PSCC/85-21/P-83 (1985).
7. A. Einstein, Ann. Phys. 35, 898 (1911);
R. H. Dicke in "Relativity, Groups and Topology," C. DeWitt and B. DeWitt, eds. (Gordan and Breach, New York, 1964).
8. K. Nordvedt, Phys. Rev. D11, 245 (1975).

A MEASUREMENT OF THE $2^2S_{1/2} - 2^2P_{3/2}$ FINE STRUCTURE INTERVAL IN MUONIUM

S.H. Kettell¹, H.E. Ahn¹, A. Badertscher³, F.C. Chmely¹, M. Eckhause⁴,
 P. Guss⁴, V.W. Hughes¹, J.R. Kane⁴, Y. Kuang¹, B.E. Matthias¹, H.-J. Munding²,
 B. Nil¹, H. Orth², G. zu Putlitz², H.R. Schaefer¹, K.A. Woodle¹

Yale University¹, Universität Heidelberg², Paul Scherrer Institute³,
 College of William and Mary⁴

The ($2^2S_{1/2} - 2^2P_{3/2}$) fine structure transition in muonium has been observed for the first time at LAMPF. The energy level diagram is shown in Fig. 1 and the experimental setup in Fig. 2. Muonium atoms (μ^+e^-) in the metastable 2S state are produced by the beam-foil technique¹ with a low momentum, 8 MeV/c, subsurface muon beam. The incident μ^+ are detected in a low pressure multiwire proportional chamber, and M(2S) is formed by electron capture in the production foil immediately downstream. Transitions from hfs sublevels of the $2^2S_{1/2}$ state to hfs sublevels of the $2^2P_{3/2}$ state are induced in the microwave cavity, and the spontaneously emitted $2P \rightarrow 1S$ photons are detected by four UV phototubes. The resulting ground state M atoms are detected upon striking the microchannel plate. A delayed triple coincidence between a MWPC count, a phototube count and a microchannel plate count is designated an event. The signal is the difference between the number of events with microwaves on and off. Fig. 3 shows the signal as a function of microwave frequency.

The value for the $2^2S_{1/2} - 2^2P_{3/2}$ interval, which is determined from the data using theoretical values for the hyperfine structure intervals, is 9895^{+35}_{-30} MHz. Adding the theoretical value² for the Lamb shift ($2^2S_{1/2} - 2^2P_{1/2}$), $S_M = 1047.5(3)$ MHz, to the measured $2^2S_{1/2} - 2^2P_{3/2}$ interval gives a value for the fine structure splitting $2^2P_{3/2} - 2^2P_{1/2}$ of $10\,943^{+35}_{-30}$ MHz, which is in agreement with the theoretical value³ of $10\,921.832(2)$ MHz. The experimental sensitivity is such that we begin to test the reduced mass corrections to the fine structure splitting. Alternatively, by combining the theoretical value for the fine structure interval with our measurement we can derive a value for the Lamb shift of 1027^{+30}_{-35} MHz. This value is in agreement with the QED prediction and is independent of previous direct measurements. Previous experimental values^{4,5} for the Lamb shift in muonium are 1070^{+12}_{-15} MHz and 1042^{+21}_{-23} MHz. Combining our new result for the Lamb shift with the previous measurements gives a new experimental value of 1058^{+10}_{-12} MHz for the Lamb shift in muonium.

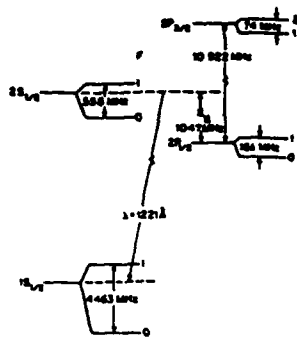


Fig. 1. Energy level diagram for muonium in its $n=1$ and $n=2$ states, including fine structure, Lamb shift, and hfs terms.

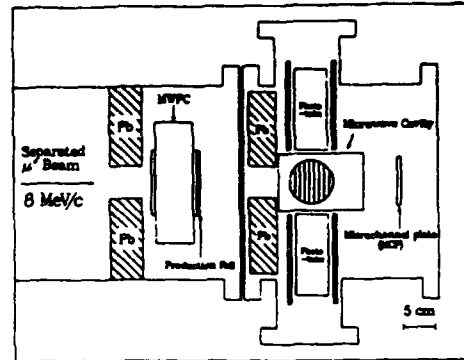


Fig. 2. Apparatus used in the microwave spectroscopy experiment to measure the fine structure in the $n=2$ state of muonium.

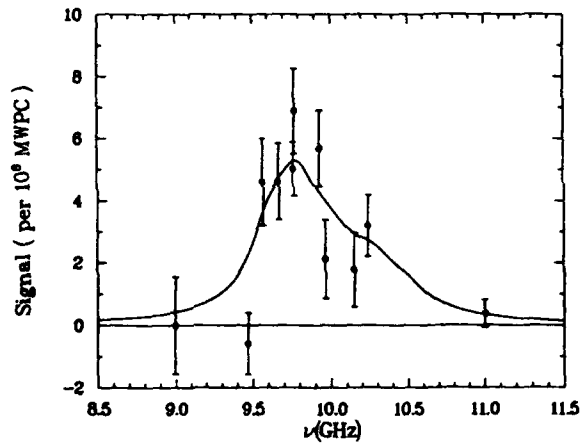


Fig. 3. Microwave resonance data and the best fit line shape to the transitions $2^2S_{1/2} + 2^2P_{3/2}$, $\Delta F=0, \pm 1$.

This work was supported by DOE, NSF, and BMFT.

¹Bolton, P.R. et al., Phys. Rev. Lett. 44B, 199 (1973).

²Sapirstein, J.R. and Yennie, D.R., in *Quantum Electrodynamics*, ed. by T. Kinoshita, (World Scientific, to be published, 1990).

³G.P. Lepage and D.R. Yennie, *Precision Measurement and Fundamental Constants II*, Natl Bur. Stand. (U.S.) Spec. Publ. No. 617, ed. by B.N. Taylor and W.D. Phillips (U.S. GPO, Washington, D.C., 1984) p. 185.

⁴C.J. Oram, *Atomic Physics 9*, ed. R.S. van Dyck and E.N. Fortson (World Scientific, Singapore, 1984) p. 75.

⁵K.A. Woodle et al., Phys. Rev. A41, 93 (1990); A. Badertscher et al., *Atomic Physics 9*, ed. R.S. van Dyck and E.N. Fortson (World Scientific, Singapore, 1984) p. 83.

ON THE POSSIBILITIES OF SOME NEW P AND P,T VIOLATION EXPERIMENTS

D.Budker, E.D.Commins, D.DeMille and M.Zolotarev[#]

Department of Physics, University of California
Berkeley, California 94720, USA

[#] Lawrence Berkeley Laboratory, University of California
Berkeley, California 94720, USA

In this paper we will discuss possibilities of P and P,T violation experiments in the situation where the mixing states of opposite parity are quasi-degenerate. A specific example of such a system is atomic dysprosium (Z=66) where there is a pair of opposite-parity levels with the same total angular momentum and energy separation $\lesssim 10^{-2} \text{ cm}^{-1}$ (E=19797.96 cm^{-1} , J=10). Further advantages may arise from the fact that both of these levels are likely to be metastable ($\tau \sim 10^{-3} - 10^{-4}$ sec). A preliminary experiment to measure the lifetimes and electric polarizabilities of these levels is underway.

SYSTEMATIC EFFECTS IN THE BERKELEY ELECTRON ELECTRIC DIPOLE EXPERIMENT*

Stephen B. Ross^{1,2}, Kamal Abdullah^{1,2}, Conny Carlberg², E. D. Commins^{1,2},
and Harvey Gould²

¹Physics Department, University of California

²Materials and Chemical Sciences Division,

Lawrence Berkeley Laboratory

Berkeley, California 94720

We present a discussion of the primary systematic effects associated with our electric dipole moment (EDM) search. Fundamental to our measurement is a set of auxiliary experiments used to isolate and eliminate systematic effects that could mimic a true electron EDM.

Our main experiment employs two counter-propagating beams of thallium atoms in the ground state, which pass through a 100 kV/cm electric field E , and a weak uniform magnetic field B parallel to E . The atoms of interest are in a coherent superposition of $F=1$, $m_F=\pm 1$ states. A non-zero electron EDM would cause a phase shift between these two components. However, such a phase shift can also arise from the following false effects:

- Interaction of the atomic magnetic moment with the motional magnetic field $E \times v/c$: A false edm arises if B is not exactly parallel to E , if B is inhomogeneous, and if the two counter-propagating beams experience different average values of B . Stringent limits on the $E \times v$ effect are achieved by imposing magnetic field gradients several hundred times larger than those occurring in the main experiment, and by measuring, first, the resonant frequency differences between the two beams, and second, the false EDM effect itself. These two auxiliary measurements provide the same limit on the false effect. Our measurements are also sensitive to a term proportional to $(vE/c)^2$ if the electric field does not reverse exactly.
- A geometric phase effect: A false EDM can arise if B has a component parallel to the beam axis with different magnitudes at the two ends of the electric field region. We have detected this effect in circumstances where such a magnetic field is deliberately imposed, and our observations are in agreement with theoretical expectations. The contribution of the geometric phase to a false EDM arising from residual field gradients can be isolated and eliminated by carrying out the real experiment at several resonant frequencies, and comparing the results.

*This work supported by the Director: Office of Energy Research, Office of Basic Energy Science, Chemical Sciences Division; of the U.S. Department of Energy under contract DE AC03 76SF00098.

A NEW APPARATUS FOR THE STUDY OF PARITY NONCONSERVATION IN
ATOMIC THALLIUM

D. DeMille, D. Budker, and E. D. Commins
Physics Department, University of California, Berkeley
Berkeley, California 94720

We have constructed and are now testing a new apparatus designed with the goal of making improved measurements of parity nonconservation (PNC) in the $6p_{1/2} \rightarrow 7p_{1/2}$ transition in atomic thallium. Thallium atoms in an intense hypersonic beam are excited by linearly polarized pulsed laser light (polarization ϵ) in the presence of crossed \mathbf{E} and \mathbf{B} fields. Interference between Stark and electroweak amplitudes leads to a term proportional to $(\mathbf{e} \cdot \mathbf{B})(\mathbf{e} \cdot \mathbf{E} \times \mathbf{B})$ in the $6p_{1/2} \rightarrow 7p_{1/2}$ transition probability. $7p_{1/2}$ atoms are detected by pulsed-laser induced ionization and subsequent collection of the ions. In comparison with previous measurements of PNC in the same transition—which employed thallium in a vapor cell and detection of $7p_{1/2}$ atoms by observation of decay fluorescence¹—the present apparatus offers the possibility of a significant gain in statistics. Our efforts to this point have been directed primarily towards two goals: the characterization and optimization of the performance of the hypersonic beam, and the elimination of background signals in the ionization detector. Details of the results of these efforts and of the proposed PNC experiment will be presented.

¹P. S. Drell and E. D. Commins, Phys. Rev. A 32, 2196 (1985).

EVIDENCE FOR FRACTIONAL CHARGE AND
ASSOCIATED COLOR CHARGE IN ATOMS AND IONS

Joseph L. McKibben
Retired from LANL
113 Aztec Ave., Los Alamos, NM 87544 USA

The Search for Fractionally-Charged Particles. Since the proposed existence of quarks in 1964, there has been much effort to find fractionally-charged particles among atoms and molecules with negative results, see Smith [1]. High-energy accelerators experiments have also given negative results [2]. The contention is made herein that a considerable number of fractionally-charged particles, having associated color charge, exist on the nuclei of ^4He , ^8Be , ^{12}C , etc. and color-neutral triads of these nuclei exist. Fully assembled, they pass for atoms and so the usual methods of searching are ineffective. While the numbers of these "atoms" may be large, they are still too scarce to be detected by the most sensitive type of mass spectrograph—sensitivity one part in $\sim 10^{15}$. Isotope concentration using evaporative techniques may bring them into the detectable range. Other methods lying in the realm of experimental atomic physics may also detect these particles.

Experimental Observation of Fractionally Charged Particles: There are several experiments that have been done that give support to the above interpretation but the one that had the most impact on the development of this concept was done in 1967 by Stevens, Schiffer, and Chupka. Information was not published on it until nine years later [3].

This experiment consisted of trying to evaporate fractionally-charged particles from manganese nodules, sending the ions through a fractional-charge filter and collecting them on a platinum filament. This ion-loaded filament was then taken to a 15 kV accelerator and negative ions emitted by it were sent through a crossed-field analyzer. The secondary electrons produced by the ions striking an aluminum plate were detected by an electron multiplier. The count rate was plotted against the current through the iron-core magnet. Many peaks observed were not identified. This was the first experiment with a new crossed-field analyzer. At the same time a new fused quartz sample holder was used.

Important unpublished information was made available to the author by Stevens in 1982. Analysis of these data forms the basis of this paper. An important aspect of this analysis is the existence of high diffusivity of ions within fused quartz.

The Particles. The data consisted of m/Z values. To determine the masses it was necessary to assume a charge for each ion. Some ions were obvious— H^- , $^{19}\text{F}^-$, $^{35}\text{Cl}^-$, $^{37}\text{Cl}^-$, CN^- , etc. Others appeared to have fractional charges. Only the correct assumptions on these give a self-consistent set of particles and "atoms". That the up quark has charge $+2e/3 = +e/6 + e/2$ and the down quark has charge $-e/3 = +e/6 - e/2$ made this analysis possible.

Present was a free particle I call A [4] with charge $+e/6$ and mass of ~ 1.14 amu and bound to a nucleus its mass is noticeably lower. Also present was a free particle I call B with charge $+e/2$ and mass ~ 0.13 amu. Particle C with charge $-e/2$ and particle A seem to be together and so form a down quark attached a nucleus. C appeared more massive than B.

Recently the author became aware of the 1981 haplon model of Fritzsche and Mandelbaum [5] who proposed the existence of four basic particles. Three of their particles have the same

fractional charge and possibly the same color charge. No mass values were given. The two particles corresponding to B and C have spin $\hbar/2$ while the one resembling A has no spin.

"Atoms" Formed Primordially: The attachment of particle A to the nucleus of helium must have taken place in the Big Bang when these particles might be available. The binding energy of A to ${}^4\text{He}$ is ≈ 0.10 amu. A triad of helium nuclei, with their attached particles A of different color along with a triad of particles B, can form a molecule resembling an atom of oxygen. This may be written as $({}^4\text{He-A})_3\text{B}_3$. Also particle A can firmly bind two helium nuclei together and a triad of the ${}^8\text{Be-A}$ ions with a triad of particles B can form a molecule resembling an atom of silicon. The $-e/2$ ions of both the "oxygen atom" and "silicon atom" showed up in the data [3]. The $-e/2$ ions lack a particle B but have an extra electron.

Very prominent in the negative ions emitted by the filament [3] were particles with charge of $-2e/3$ and with an apparent mass of ≈ 26.9 amu/Z. These likely were formed in the quartz sand (used to make fused quartz) by cosmic rays separating out dual ${}^8\text{Be-A}$ ions from normal ${}^8\text{Be-A}$ triads. This component resembles oxygen, except for its extra charge of $+e/3$, and so often replace oxygen atoms and stay within the crystal. The single silicon component of ${}^8\text{Be-A}$ and both the single and dual components of ${}^4\text{He-A}$ have over the years diffused out along the crystal axes. With only the dual ${}^8\text{Be-A}$ ions present in them, grains of quartz sand may often have both fractional charge and color charge.

Experiments to Verify these Concepts: There are several interesting experiments needed to confirm the above concepts that are in the expertise area of atomic and molecular physicists. The most basic experiment required is reproduction and extension of the experiment described above [3]. The source of the ions should be fused quartz tubing or quartz sand. After the ions have passed through the crossed-field analyzer, occasional tests should be made to determine the charge on the ions. This can be done by stripping off an electron by a gas cell and observing the shift in magnetic deflection.

An interesting possibility would be the observation of particles A and B in apparatus similar to that described at this conference by Dehmelt. This would allow their spins to be determined. Another important experiment that might be done with this apparatus would be the observation of the variation of the long-range color force between a pair of dual ${}^8\text{Be-A}$ ions as a function of their separation.

It may be possible to take quartz sand and separate a significant quantity of its fractionally-charged grains from ordinary grains by allowing the grains to fall through a transverse electric field. With some ingenuity and persistence—perhaps using Dehmelt's apparatus for detection—it may be possible to separate the grains according to their color charge. Placing the separated grains on the vertices of a triangle would produce a large-size color-static field. A small-size color field exists between the triad nuclei with particles A on them.

[1] P. F. Smith, *Annu. Rev. Nucl. Part. Sci.* **39**, 73-111 (1989).

[2] L. Lyons, *Phys. Rep.* **129**, 225-84 (1985) and L. Lyons *et al.*, *Z. Phys.* **C36**, 363 (1987).

[3] C. M. Stevens, J. P. Schiffer, and W. Chupka, *Phys. Rev.* **D14**, 716 (1976). See page 717.

[4] While in this abstract I am using A, B, and C to designate the particles, I have frequently called A the subquark, B the positive hemitron, and C the negative hemitron.

[5] H. Fritzsch and G. Mandelbaum, *Phys. Lett.* **102B**, 319 (1981) and **109B**, 224 (1982).

PROPOSED TEST OF THE SYMMETRIZATION POSTULATE AND EXCLUSION PRINCIPLE

J. D. Gillaspay, K. Deilamian, and D. E. Kelleher
Center for Atomic, Molecular, and Optical Physics
National Institute of Standards and Technology
Gaithersburg, MD. 20899

The Pauli exclusion principle (PEP) dictates the stability of matter and the shell structure of atoms and nuclei. Yet, despite this pervasive influence, PEP stems from the symmetrization postulate (SP) which cannot be derived from more fundamental principles without unproven assumptions. In his 1945 Nobel address, Pauli stated: "*Already in my original paper I stressed the circumstances that I was unable to give a logical reason for the exclusion principle or to deduce it from more general assumptions.*" In his book *General Principles of Quantum Mechanics*, Pauli noted that "*The fact that quantum mechanics yields more states than actually occur in nature (and all of them equally possible) is still a puzzle.*" These statements were made years after the spin-statistics theorem was established.

The symmetrization postulate states that the wavefunction of a system of identical fermions is antisymmetric under exchange of any two of the particles (and symmetric for bosons). The two-electron helium atom provides the simplest atomic example of an antisymmetric system. Its wavefunction can be written:

$$\Psi = \frac{1}{\sqrt{2}} (\Psi(r_1, r_2) - \Psi(r_2, r_1)) .$$

PEP is a special case of SP; when two identical fermions are in the same state, the terms in the above expression are identical and Ψ vanishes.

The two permutation symmetries allowed by SP, antisymmetric and symmetric, are built into field theories via the bilinear commutation relations of the field operators. In 1953 Green¹ showed that different symmetries result if trilinear commutation relations are used. However, these other symmetries, if they existed at all, would be as likely as the usual ones, and thus readily observable. Recent theoretical work in this area has tried to find a model which allows *small* violations of SP. In 1987, several theoretical groups claimed to have produced such models. However, it was subsequently shown that the most promising model also predicted small negative norms for certain states of four particles or more. Recently, a new model² has been developed which does not suffer this drawback.

If one takes the indistinguishability of identical particles to be axiomatic, the types of violations considered for SP are different than in other symmetry breaking. The "superselection rule" expresses the fact that there cannot be a symmetry-breaking term in the Hamiltonian for a system of identical particles. The Hamiltonian must be symmetric under permutation of the particles because any term which couples different symmetries would provide a basis for distinguishing them. Thus the only possible violations of SP are the occurrence of symmetries which, though inconsistent with SP, are consistent with the indistinguishability of identical particles. The simplest example of this is a symmetric state of two identical fermions. Other examples, such as those described by Green¹, would include more complex symmetries for greater than two particles.

Until recently there have been few precision experimental tests of SP and PEP. The experiment which claimed by far the greatest sensitivity was subsequently shown to be invalid because it looked for observables which violated the superselection rule. Recently, two new experimental results have been reported. These experiments involved looking for signatures of particular atoms with three electrons in the K shell, i.e. $1s^3$. One such experiment involved looking for X rays emitted from a current-carrying copper strip³; the other experiment involved using a mass spectrometer to search for atoms which behave chemically like a halogen but have the mass of a noble gas⁴. These experiments found null results with sensitivities in the range of one part in 10^{16} - 10^{26} .

We propose an experiment to look for excited states of helium that are symmetric upon permutation of the two electrons. These SP-violating states are nearly degenerate with normal helium states which

STATUS REPORT ON THE GAMMA-RAY COMPONENT OF A DETERMINATION OF $N_A h/c$

M. S. Dewey, E. G. Kessler, R. D. Deslattes, and G. L. Greene
*National Institute of Standards and Technology
Gaithersburg, Maryland 20899*

H. Börner
Institut Laue-Langevin, Grenoble, France

Absolute wavelength determinations in the several-MeV region can be combined with mass spectroscopic measurements to yield the combination of fundamental constants $N_A h/c$ where N_A , h , and c are the Avogadro constant, Planck constant, and the speed of light respectively. [1] This combination of constants follows from the relation

$$(\Delta M \times 10^{-3}) \lambda = N_A h/c \quad (1)$$

where ΔM is the mass change in a.m.u. of a system undergoing radiative decay (the factor of 10^{-3} arises from the definition of the Avogadro constant which relates to gram atomic weight) and λ is the photon's wavelength. In turn, $N_A h/c$ may be used to derive a value for α , the fine structure constant, through the relation

$$\alpha^{-2} = \left[\frac{M_p \times 10^{-3}}{2R_\infty (m_p/m_e) (N_A h/c)} \right] \quad (2)$$

where M_p is the proton mass in atomic mass units, R_∞ is the Rydberg Constant, and m_p/m_e is the ratio of the proton to electron mass. M_p , m_p/m_e , and R_∞ are all known to about 0.02 ppm or better so a 0.1 ppm determination of $N_A h/c$ yields a value for α with an uncertainty of 0.05 ppm. [2] This is comparable with the present stated uncertainty on α . [3] A particularly promising system appears to be the spectroscopic mass doublet $^{15}\text{NH}_3$ - $^{14}\text{NDH}_2$ which has a mass change corresponding to approximately 8 MeV. The goal of this work has been to measure the wavelength of the 'photon' involved in this 8 MeV transition in units of meters with an accuracy of 0.1 ppm or better. It should be noted that the considerable progress which has been made recently in the technology of atomic mass spectroscopy using trapped ions [4] suggest that sufficiently accurate determinations of ΔM may be possible.

The method employed relies on crystal diffraction from highly perfect flat crystals of silicon or germanium. A wavelength measurement follows from the Bragg-Laue relation $\lambda = 2d \sin \theta$. The three steps involved in the measurement chain linking gamma-ray wavelengths to visible wavelengths and their present status are as follows:

1. In the first step, the lattice spacing of a Si crystal is measured in terms of the wavelength of an iodine-stabilized He-Ne laser operating in the visible near 633 nm. This step employs simultaneous x-ray and optical interferometry and yields a calibrated Si crystal sample. Currently lattice parameter values obtained in an individual measurement have a statistical

imprecision near 0.01 ppm. However there are unexplained systematic residual patterns and nonreproducibility of lattice parameter values of approximately 0.2 ppm [5,6]. It is likely that the NIST lattice spacing measurement will produce results which are consistent with and have an uncertainty comparable to or less than that reported in reference 7 (0.06 ppm).

2. In the second step, the lattice spacings of various other crystals are compared to the calibrated Si crystal to yield a family of crystals whose lattice spacings are known relative to the optical wavelength. This method employs an x-ray crystal comparator. Currently lattice spacing differences obtained with our comparator show a statistical uncertainty near 0.01 ppm[6]. This level of precision needs to be regarded as preliminary pending evaluation of possible systematic errors especially associated with the angle measuring interferometer. However, a final uncertainty near 0.01 ppm appears likely from this lattice comparison step.
3. In the final step (GAMS4) gamma-rays are diffracted by the crystals calibrated in step two and the diffraction angles are accurately measured. By combining the measured lattice spacing and diffraction angles, gamma-ray wavelengths are determined. Currently the measurements are limited by our ability to measure small diffraction angles and excessively broad profiles resulting from crystal imperfection and environmental disturbances. Low order diffraction angles for 2-5 MeV gamma-rays are a few tenths of a degree. These angles are measured by Michelson angle interferometers which have a sensitivity of $\sim 1 \times 10^{-4}$ arcsec, but possible nonlinearities of $\sim 1 \times 10^{-3}$ arcsec. The broad profiles limit the precision with which the diffraction angles can be determined. Assuming counting statistics which permit profile division of FWHM/100, the angular pointing precision is $\geq 1 \times 10^{-4}$ arcsec. If nonlinearities are eliminated, angle measurement uncertainties of a few tenths ppm should result.

In summary, if the optimistic scenarios described above are assumed, the uncertainty of high energy gamma-ray wavelength measurements which would contribute to a determination of $N_A h/c$ is likely to be a few tenths ppm.

-
1. R.D. Deslattes and E.G. Kessler, Jr., Atomic Masses and Fundamental Constants-6, J.A. Nolan, Jr. and W. Beneson, eds., New York, NY: Plenum Press, 1979, p. 203.
 2. M.S. Dewey et al., Nucl. Instrum. Methods A 284, 151 (1989).
 3. B.N. Taylor and E.R. Cohen, The 1986 Adjustment of the Fundamental Physical Constants, CODATA Bulletin 63, CODATA, 1986.
 4. E.A. Cornell et al., Phys. Rev. Lett 63, 1675 (1989).
 5. R.D. Deslattes et al., IEEE Trans. Instrum. Meas., IM-36, 166 (1987).
 6. R.D. Deslattes and E.G. Kessler, IEEE Trans. Instrum. Meas. (to be published).
 7. P. Becker et al., Phys. Rev. Lett. 46, 1540 (1981).

**NEW TECHNIQUES FOR SIMULTANEOUS PRECISION FREQUENCY
SPECTROSCOPY OF FREELY PRECESSING ^3He , ^{21}Ne AND ^{129}Xe ***

E.R. Oteiza, R.J. Hoare, T.E. Chupp
Lyman Laboratory of Physics, Harvard University
Cambridge, Massachusetts 02138

Techniques for frequency spectroscopy of freely precessing noble gas atoms have been developed to search for the Permanent Electric Dipole Moment of ^{129}Xe , to detect geometric phases (e.g. Berry's phase) and to test Lorentz Invariance and the Linearity of Quantum Mechanics. These techniques have achieved sensitivity on the order of 10^{-6} Hz for measurement intervals of one hour which is possible with narrow line-widths ($<10^{-3}$ Hz) and large signal to noise ratios ($>10^4$). In order to monitor systematic effects we make simultaneous measurements on two or more of the noble-gas species, ^3He , ^{21}Ne and ^{129}Xe . Two techniques have been used in simultaneous detection schemes. They are magnetic induction detection of the rotating magnetization of each species and a form of Rb magnetometry of the noble gas nuclear polarization.

In the magnetic induction technique the precessing magnetization is detected by a near-by pick-up-coil. Signal size, therefore, is proportional to the precession frequency (1 -10 kHz at 3 Gauss) and the total magnetization of each species. Noise is limited by the Johnson noise of the pick-up network. A signal-to-noise ratio of 10^4 for a bandwidth of 1/(1 hr) has been achieved.

In the Rb magnetometry technique, the signal is produced by the transmission of circularly polarized resonance light through Rb vapor in a magnetic field of 1 mGauss. The spin-polarized noble-gas atoms, during binary collisions with the Rb, induce a torque on the Rb spins. Signal size is determined by the polarization and density of each noble-gas species and by the strength of the hyperfine coupling between each of the noble-gas species and rubidium. Both techniques have been used in simultaneous detection schemes with comparable signal-to-noise ratios.

*Supported by the National Science Foundation.

**COHERENCE IN FREELY PRECESSING ^{21}Ne AND
RESULTS OF TESTS OF LOCAL LORENTZ INVARIANCE AND
LINEARITY OF QUANTUM MECHANICS ***

T.E. Chupp, R.J. Hoare, E.R. Oteiza, J.M. Richardson, M.E. Wagshul
Lyman Laboratory of Physics, Harvard University
Cambridge, Massachusetts 02138

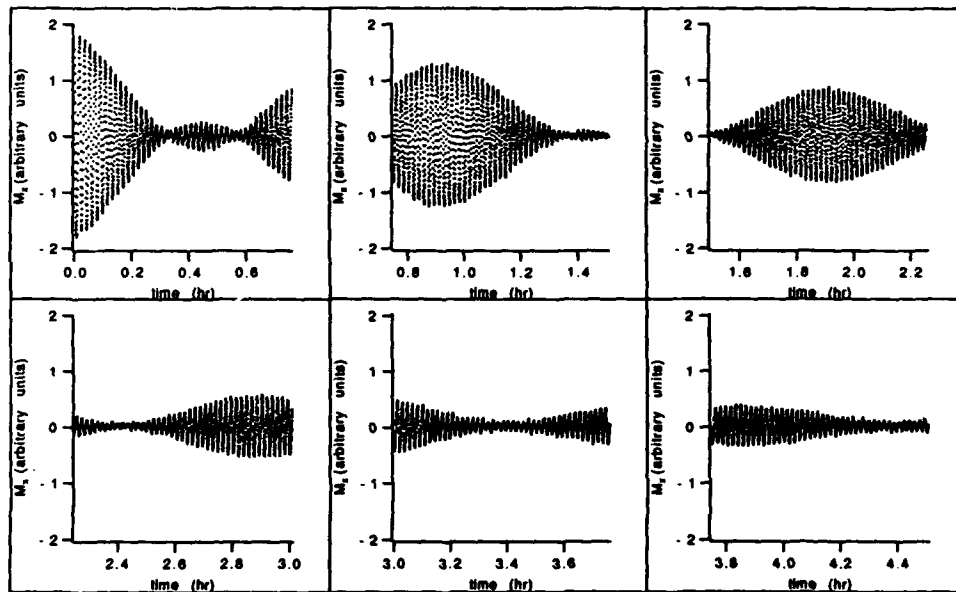
We have observed coherence among the four magnetic sublevels of freely precessing ^{21}Ne ($I=3/2$) for times of 4.5 hours. The coherence is demonstrated by measuring the component of magnetization transverse to a static magnetic field. Since the magnetization is due to the ensemble average, a coherent superposition of amplitudes, the time dependence of the transverse magnetization shows that the relative phases of the amplitudes evolve at different rates. In the presence of a net average electric quadrupole interaction in addition to the magnetic dipole interaction, three frequencies result producing the beat pattern in the time-domain behavior illustrated in the figure below. Data of this nature can be used to extract components of the frequency spectrum with precision better than 10^{-6} Hz for one hour measurement intervals. This has allowed the first direct detection of the quadrupole component of coherence relaxation as well as searches for Local Lorentz Violating Mass Anisotropy and nonlinear corrections to Quantum Mechanics.

Mass Anisotropy would be evident in a time dependence of the quadrupole splitting of the Zeeman levels in ^{21}Ne for an apparatus that is stationary in the lab. A component at twice the Earth's sidereal frequency would suggest a preferred direction relative to the fixed stars which affects the local physics of the ^{21}Ne nucleus. Systematic variations of the quadrupole component at multiples of the earth's solar frequency do arise, mostly due to temperature variations, but can be suppressed by combining data taken at different times of year such that the solar and sidereal day change relative phase. Our data produce an upper limit of 2×10^{-21} eV (0.45×10^{-6} Hz) on the Lorentz-Invariance-violating contribution to the binding energy, a limit that is comparable to that of the most sensitive previous experiment.

Nonlinear corrections to quantum mechanics would be revealed by the

dependence of the coherence frequencies on the amplitudes of the four magnetic sublevels of ^{21}Ne . The lowest order corrections to the coherence frequencies would be linear combinations of $|\psi_i|^2$ where the subscript labels the magnetic sublevel. Invoking rotational invariance, the quadrupole component of the frequency spectrum would be proportional to the tensor polarization T_2 with the constant of proportionality as a measure of the size of the nonlinear correction. We have found this correction to be less than 1.3×10^{-19} eV (30×10^{-6} Hz) at the $1-\sigma$ confidence level.

*Supported by the National Science Foundation.



**TESTS OF QED IN HELIUM-LIKE AND HYDROGEN-LIKE URANIUM
WITH A DOPPLER TUNED SPECTROMETER**

James H. Lupton
University of Michigan
Physics Department, Ann Arbor, MI 48109

Daniel D. Dietrich, Charles J. Hailey, Klaus P. Ziock
Lawrence Livermore National Laboratory
Livermore, CA 94550

Uranium ions with one or two electrons are the simplest atomic systems available for tests of quantum electrodynamics in the high field limit. We report ongoing results of our analysis of an experiment to measure the absolute $2p_{3/2}-1s_{1/2}$ transition energy in H-like uranium. The Lawrence Berkeley Laboratory's BEVALAC supplied highly charged uranium ions at 422 MeV/nucleon. Standard beam foil techniques were used to strip the ions to ~40% U^{+91} , 40% U^{+90} in a Cu stripper foil. The remaining 20% of the beam is predominantly U^{+92} . A 15 μm Au target foil is used to excite the transitions of interest. Because of limited count rate and secondary electron bremsstrahlung background in the highly stripped uranium ion/beam-foil environment, a Doppler tuned spectrometer was used to observe x-rays from the transition.¹

The Doppler spectrometer exploits the angular dependant Doppler shift of x-rays emitted by the in-flight ion interacting in the target foil. A k-edge absorption filter is placed at the angle where its k-edge energy is in resonance with the Doppler shifted x-rays emitted by the ion. Since a k-edge filter preferentially transmits x-rays with energies below the k-edge, behind the filter, one observes a step in the number of x-rays as a function of angle. By measuring the angle, θ , with respect to the beam direction at which the step occurs and with knowledge of the beam velocity, β , and k-edge energy, E_{lab} , one obtains the rest frame x-ray energy with the familiar expression:

$$E_0 = \gamma E_{lab} (1 - \beta \cos \theta)$$

where E_0 is the line energy and β and γ are the usual relativistic velocity parameters. For this experiment, $\beta = .72$ was selected to optimize the H-like and He-like charge state fraction in the target.² To take advantage of relativistic forward beaming and to optimize systematic uncertainties, a uranium absorber foil was chosen. Uranium has its K-edge at 115.62 KeV which requires a 57.5° angle of observation to match the 102.18 KeV, $2p_{3/2}-1s_{1/2}$ transition in H-like uranium.³ To record the Doppler angle of each event, x-ray detectors with ~1mm spatial resolution⁴ were placed behind absorber foils, at an angle of 57.5° with respect to the beam. Similar detectors were placed behind Hf absorber foils (65.31 KeV) at 96.0°. Two k-edge energies and two angles, allow the elimination of the poorly known beam velocity from the Doppler expression. To reduce systematic alignment errors the double Doppler angle setup was duplicated on opposite sides of the beam.

Uncertainties in the BEVALAC beam due to the 30 mm-mr beam emittance at the target area present difficulties for any measurement of H-like and He-like $n=2$ to $n=1$ transitions in uranium. We used scintillation hodoscopes to determine ion locations on an event-by-event basis. A hodoscope of minimal scintillator thickness (0.5 mm) with a position resolution of 1.4 mm, was used 14 m upstream of the target. Downstream another hodoscope with a position resolution of 0.9 mm gave the ion location just after the target. The inner product of the beam trajectory vector with the x-ray vector gives the Doppler angle. This procedure reduces the beam emittance to an effective value of 0.1mm-mr. Current precision alignment of the target foil, x-ray detectors and beam hodoscopes, limit the systematic errors due to alignment to 2.8 eV.

The H-like $2p_{3/2}-1s_{1/2}$ transition as well as the He-like $2^3P_1 - 1^1S_0$ transition are observed simultaneously in the Doppler spectrometer.⁵ We anticipate the total statistics accumulated during our most recent run will permit an energy determination to 45 eV of the 300 eV wide step observed for each of these transitions. We estimate that better statistics from future runs planned at GSI will improve the precision to ~3 eV. At this precision the systematics of determining the step location become important and changes to limit the step width will be implemented.

High precision measurements on H-like uranium provide a test of QED calculations of the 352 eV self energy contribution to the $2p_{3/2}-1s_{1/2}$ transition energy.³ The He-like $2^3P_1 - 1^1S_0$ energy measured relative to the H-like system will probe two electron correlation effects in the high field regime. Other high field experiments, such as 5g-4f transitions in muonic lead,⁶ complement the uranium measurements providing independent probes of the vacuum polarization and nuclear size corrections.⁷

This work was performed under the auspices of the U. S. Dept. of Energy by Lawrence Livermore National Laboratory under Contract No. W-7405-ENG-48.

¹R.W. Schmieder and R. Marrus, Nucl. Instr. Meth. **110**, 459 (1973).

²H. Gould, D. Greiner, P. Lindstrom, T.J.M. Symons, and H. Crawford, Phys. Rev. Lett. **52**, 180 (1984).

³W.R. Johnson and G. Soff, Atomic Data and Nuclear Data Tables **33**, 406 (1985).

⁴C.J. Hailey, F. Harrison, J.H. Lupton, and K.P. Ziock, Nucl. Instr. Meth. **A272**, 340 (1989).

⁵J.H. Lupton, D.D. Dietrich, C.J. Hailey, K.P. Ziock, SPIE proc. **1152**, 223 (1989).

⁶G. Backenstoss, S. Charalambus, H. Daniel, Ch. von der Malsburg, G. Poelz, H. P. Povel, H. Schmitt, and L. Tauscher, Phys. Rev. Lett. **B 31**, 233 (1970); P.J.S. Watson and M.K. Sundaresan, Can. J. Phys. **52**, 2037 (1974).

⁷E. Borie and G.A. Rinker, Rev. Mod. Phys., **54**, 67 (1982).

PRECISION MEASUREMENTS OF $n=3$ TO $n=3$ TRANSITION ENERGIES IN VERY HIGHLY CHARGED IONS

D.D. Dietrich, C.L. Bennett, T.E. Cowan, M.H. Chen, K-T. Cheng, D.A. Knapp,
R.E. Marrs, A.L. Osterheld and J.H. Scofield
Lawrence Livermore National Laboratory
Livermore, California 94550

The study of highly ionized atoms can address several unsolved fundamental problems in atomic physics. Despite the excellent agreement between theory and experiment at low Z , precision tests of theory at high Z remain relatively scarce. We have embarked on an experimental program¹ to provide critical tests of many body relativistic theory and benchmarks for the underlying theory of atomic structure, quantum electrodynamics. We have performed a series of x-ray spectroscopic measurements of high Z ions trapped in the LLNL electron beam ion trap, with a vacuum coupled Johann crystal spectrometer. A sample spectra of highly ionized platinum spanning the energy range from 645 to 660 eV is shown in Fig 1. Clearly evident are lines from sodiumlike and magnesiumlike platinum.

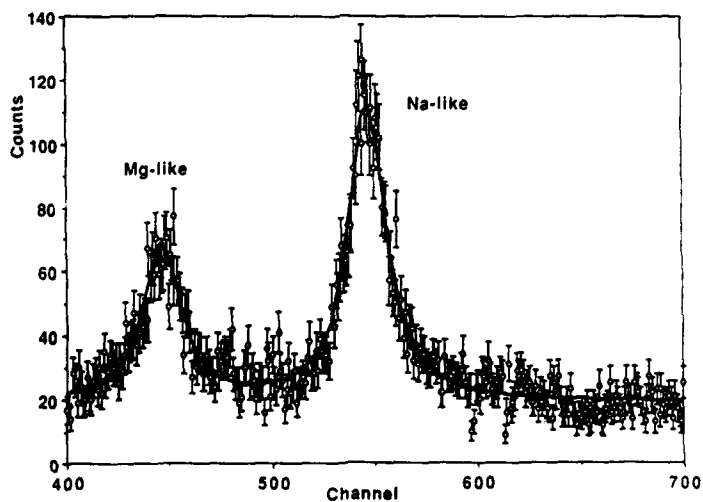


Figure 1. Summed spectrum of Pt 3s-3p transitions taken with 18.5 Kev electron beam energy.

Table 1

Platinum n=3 to n=3 transition energies (in eV)

Transition	Experiment	Theory	Th-Exp
$3S_{1/2}-3P_{3/2}$ (Na)	653.44(5)	654.07	0.63
$3s^2(1S_0)-3s3p(1P_1)$ (Mg)	665.53(6)	666.75	1.22
$3s^23p(2P^{\circ}_{1/2})-3s3p^2(2P_{3/2})$ (Al)	658.95(8)	659.80	0.85
$3s^23p(2P^{\circ}_{1/2})-3s3p^2(2P_{1/2})$ (Al)	669.77(6)	671.48	1.71
$3s^23p^2(3P_0)-3s3p^3(3S^{\circ}_1)$ (Si)	663.32(8)	662.87	-0.45
$3P_{1/2}-3D_{3/2}$ (Na)	679.07(18)	679.98	0.91

In Table 1 the measured transition energies are compared with a multi-configuration relativistic Hartree-Fock calculation² run in the optimized level mode using radiative corrections obtained in the extended average level mode. We will discuss the implications of this work for isoelectronic extrapolations³ and the reliability of various *ab initio* calculations.

Work performed under the auspices of the U.S. Department of Energy by the Lawrence Livermore National Laboratory under contract number W-7405-ENG-48.

1. T.E. Cowan, C.L. Bennett, D.D. Dietrich, J. Bixler, C.J. Hailey, J.R. Henderson, D.A. Knapp, M.A. Levine, R.E. Marrs and M.B. Schneider, Phys. Rev. Lett. (submitted).
2. I.P. Grant, B.J. McKenzie, P.H. Norrington, D.F. Mayers and N.C. Pyper, Comput. Phys. Commun. **21**, 207 (1980); B.J. McKenzie, I.P. Grant, P.H. Norrington, Comput. Phys. Commun. **21**, 233 (1980).
3. J.F. Seely and R.A. Wagner, Phys. Rev. **A41**, 5246 (1990).

**Berry Phase in a Stern-Gerlach Experiment:
Example of Mixing of the Spin States**

V. A. Andreev

Lebedev Institute for Physical Sciences, Ac. Sci. USSR
Moscow 117924, U. S. S. R.

P. B. Lerner

Department of Electrical Engineering, University of Michigan
Ann Arbor, MI 48109

The 2π -pulse in a Rabi's experiment configuration provides the recurrence of the initial spin state. However, the adiabatic cyclic evolution of parameters of the Rabi device results in nontrivial Berry phase. The Berry phase in the case of Rabi experiment provides a possibility of distinction between different superpositions of the pure spin states of the input beam with equal probabilities of the projections. This distinguishability of the spin states with different constant phase shift between the spin components is a consequence of a valid quantum measurement. The impact of the measurement procedure on the fluctuations is described as a rotation of the quantum fluctuations in the plane of the angular momentum components J_1 - J_2 .

The Berry phase of the fermions was extensively studied in the recent experimental papers /1,2,9/. Also the experimental test of Aharonov-Casher effect should be mentioned in this context /3/. Rabi device /4/ used for the determination of the magnetic moments of the heavy particles, usually works in the regime of maximum separation of the different spin components due to the spin-flip in the auxiliary radio-frequency field what corresponds to the $\pi/2$ dynamical phase shift, induced by external fields in the spin state of a particle. However, 2π dynamical phase shift results in a total recurrence of a spin state of a given particle.

The quantity measured in the Rabi experiment is the flux of particles coming to the detector or essentially the probability of the spin-flip in the case of pure state. One supposes the slow cyclic evolution of the parameters of the problem which are constant magnetic field $H_0(t)$, rf-field amplitude $H_1(t)$ and phase modulation $\psi(t)$. We admit that the particle in the initial state /5/ has the probability of $\sin^2(\theta/2)$ to have say 'spin up' and the probability $\cos^2(\theta/2)$ to have 'spin down' or vice versa. The phase difference between those amplitudes is α . The global phase shift of the particle beam is unessential and cannot be measured. The phase α is vice versa a physically meaningful quantity and it is precisely the measure of the quantum nature of the spin projection. The particles with different α has the same probability to be observed in the 'spin up' or 'spin down' states, however they are not identical and could be distinguished macroscopically. The expression for Berry phase has the form

$$(1) \quad \delta_B = \int_0^{2\pi} \frac{\Delta d\psi}{2\Omega} \quad \Omega^2 = \Delta^2 + R_1^2 \quad \Delta = \frac{1}{2}(\omega - 2R_0) \quad R_{0,1} = \mu \frac{H_{0,1}}{h}$$

It has properties, similar to the Berry phase in the Jaynes-Cummings model /6/. The simultaneous change of all three parameters of the model Δ , H_1 and ψ is necessary to obtain non-trivial phase shift. The readout of the particle detector of the Rabi device is proportional to $|S_2(T)|^2$. The formula for the detector readout gives the expression with the interference term proportional to the Berry phase. For the pure state of spin at the output beam, the modulation of the detected signal due to Berry phase is absent (compare it with /7/).

In the experiment, the Berry phase could be changed providing the information about the polarization of the particle beam. This method is, in some sense, unique, because it can distinguish mixtures with the only difference in the phase between amplitudes of the spin components.

This procedure of measurement through adiabatic evolution of the parameters of the Rabi experiment admits interpretation in the terms of quantum fluctuations. The magnetic moment of a quantum particle is observable vector which components are represented by SU(2) group operators $\hat{J}_1, \hat{J}_2, \hat{J}_3$. For the state (1) the dispersions of the angular momentum operators takes the form /8/ :

$$(2) \quad \begin{aligned} \Delta J_1^2 &= \frac{1}{2}(1 - \sin^2 \phi \sin^2 \alpha) \\ \Delta J_2^2 &= \frac{1}{2}(1 - \cos^2 \phi \sin^2 \alpha) \\ \Delta J_3^2 &= \frac{1}{2}(1 - \cos^2 \phi) \end{aligned}$$

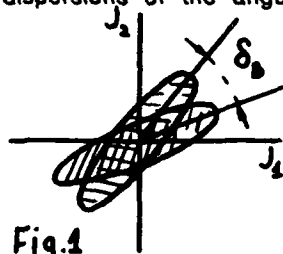


Fig.1

After the cyclic evolution the dispersion of the operator ΔJ_3^2 remains unchanged, while the quantum fluctuations of the operators J_1, J_2 change in such a way, that if the initial quantum fluctuations represented on a J_1 - J_2 plane as a dotted ellipsis (Fig. 1), the evolution of the quantum fluctuations during the measurement procedure results in a turn of this ellipsis in an angle, equal to the Berry phase.

References.

1. D. Dubbers *Physica B&C* **151** (1988) 93
2. H. Weinfurter, G. Badurek. *Phys. Rev. Lett.* **64** (1990) 1319
3. A. Cimmino et al. *Phys. Rev. Lett.* **63** (1989) 380
4. I.I. Rabi. *Phys. Rev.* **51** (1937) 652, see also J. Schwinger, *ibid.* P. 648
5. C. Cohen-Tannoudji, B. Diu, F. Laloe. *Quantum Mechanics*, Wiley 1977
6. V. A. Andreev, A. B. Klimov, P. B. Lerner. *JETP Lett.* **50** (1989) 74
7. Y. Aharonov, J. Anandan. *Phys. Rev. Lett.* **57** (1987) 1574
8. K. Wodkewich, J. H. Eberly. *JOSA B* **2** (1985) 458
9. H. Rauch. *Helv. Phys. Acta* **61** (1988) 589

SEMI-EMPIRICAL APPROACH TO THE CALCULATION OF
PNC E1 TRANSITIONS IN CAESIUM AND THALLIUM

A. C. Hartley and P. G. H. Sandars

The Clarendon Laboratory, Oxford

Atomic parity non-conservation (PNC) is now well established experimentally in agreement with the predictions of the unified theory of electro-weak interactions. Experiments in caesium have now reached a precision of 2% and an accuracy of 1% is expected in the near future. If the corresponding atomic theory can be carried out to the same accuracy, electro-weak radiative effects and other new phenomena beyond the tree-level standard model may become observable.

To go beyond lowest order PNC correlation calculations using MBPT is not easy. One alternative approach is to use a combination of many-body perturbation theory and semi-empirical techniques. Our approach is based on the observation that in an atom like caesium with a single active electron outside a relatively tightly bound core, the corrections to the simplest one-particle calculation of the PNC E1 transition amplitude can be divided into four classes:

- (i) Corrections to the effective central potential seen by the valence electron. These corrections will include a number of high order correlation effects which may not be easy to calculate.
- (ii) PNC core polarization in which the short range electron-nucleus PNC interaction polarises the core and this is propagated to the valence electron via the normal Coulomb interaction.
- (iii) Dipolar shielding in which the valence electron transition dipole moment induces a moment in the core which adds a correction to the total atomic transition moment.
- (iv) Complex many-body effects which are not included in (i) to (iii) above.

Complex effects of type (iv) contribute very little to the PNC matrix element for caesium. The core polarisation (ii) and the dipolar shielding (iii) are one-particle effects which can be treated relatively easily by standard self-consistent techniques. The main thrust of our approach is to use semi-empirical methods to choose the most appropriate effective potential of type (i) above.

In addition to this a semi-empirical correction can be applied to the results based on rescaling arguments for the hyperfine constants and electric dipole transition matrix elements. When this is applied to our calculations we achieve an estimated accuracy of 2% for the caesium $6s_{1/2}$ to $7s_{1/2}$ PNC transition. We have also applied our method (without the semi-empirical rescaling) to the $6p_{1/2}$ to $7p_{1/2}$ and $6p_{1/2}$ to $6p_{3/2}$ PNC transitions in thallium with accuracies of about 7%.

AN EXPERIMENT TO MEASURE THE FINE STRUCTURE OF $n = 2$ POSITRONIUM

T.D. Steiger, B. Ghaffari, A. Rich, and R.S. Conti
 Randall Laboratory of Physics, University of Michigan
 Ann Arbor, MI 48109, U.S.A.

An experiment to make precision measurements of the $n = 2$ fine structure intervals (ν_J) between the 2^3S_1 and 2^3P_J ($J = 0, 1, 2$) states of positronium (Ps) is currently underway at the University of Michigan. This experiment will provide an excellent test of quantum electrodynamics (QED) in a bound-state, equal-mass system which is free from nuclear size effects and hadronic interactions. The planned precision (~ 15 ppm) will probe QED terms $\propto \alpha^4 \text{Ry}$. Recent measurements of the 1^3S_1 Ps lifetime^{1,2} indicate either new physics or unexpectedly large coefficients for high order QED terms. In either case the present experiment should be sensitive to similar effects. Such tests in Ps have applicability to hadronic systems due to the strong analogy between the QED of Ps and the quantum chromodynamics of quark/anti-quark systems.³ The experimental motivation for this second-generation experiment is a new detection scheme which promises to improve the detection efficiency by a factor of 500.

The intervals in question were calculated to terms $\propto \alpha^3 \text{Ry}$ in 1954⁴ and have been measured previously.^{5,6} The results are (in MHz):

ν_J	THEORY	EXP.	
ν_0	18496.1	18504.1 ± 10.1	Ref. 5
ν_1	13010.9	13001.3 ± 4.0	Ref. 5
ν_2	8625.2	8619.6 ± 2.8	Ref. 5
		8631 ± 7	Ref. 6

The marginal disagreement between the values for ν_1 and ν_2 from Ref. 5 and the $\mathcal{O}(\alpha^3 \text{Ry})$ theory can be attributed to a shift of ~ -7 MHz in the 2^3S_1 energy level. Such a shift is within the range of the expected contribution from the uncalculated $\mathcal{O}(\alpha^4 \text{Ry})$ terms. The precision of the present experiment will be sufficient to definitively establish the size of these $\mathcal{O}(\alpha^4 \text{Ry})$ contributions.

In order to perform the desired experiment it is necessary to detect either the initial state (2^3S_1) or one of the final states (2^3P_J). Both previous experiments relied on detection of the 2^3P_J states by collecting the Lyman- α UV photon emitted upon decay to the ground state. The transition frequencies were determined by scanning the microwave frequency and searching for a resonant appearance of the 2^3P_J states (a "flop in" experiment). The efficiency of that detection method was only $\sim 0.1\%$, which proved to be the limiting factor in those experiments.

The current experiment is designed to detect the 2^3S_1 state. A schematic of the proposed experimental apparatus is shown in the figure. This experiment utilizes a microwave waveguide

1 C.I. Westbrook *et al.*, Phys. Rev. A **40**, 5489 (1989).

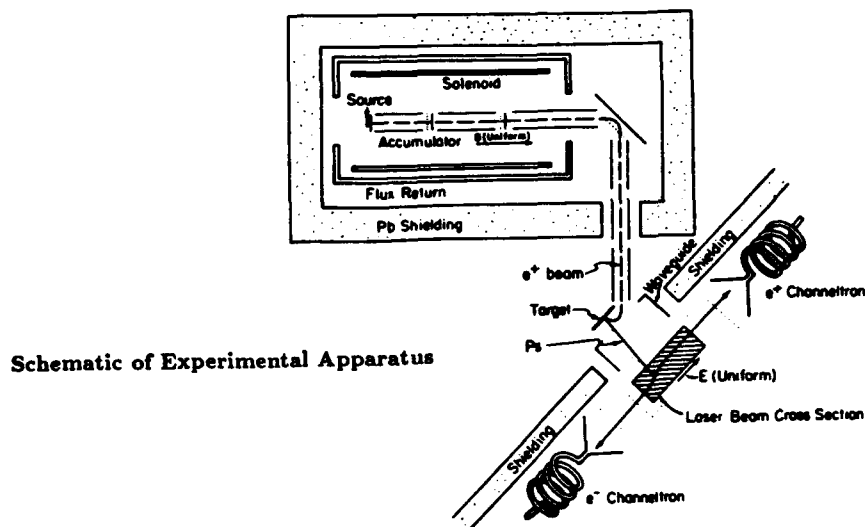
2 J.S. Nico *et al.* this conference.

3 E.D. Bloom and G.J. Feldman, Sci. Amer. **246**, 66 (May 1982).

4 T. Fulton and P.C. Martin, Phys. Rev. **95**, 811 (1954).

5 S. Hatamian *et al.*, Phys. Rev. Lett. **58**, 1833 (1987).

6 A.P. Mills, Jr. *et al.*, Phys. Rev. Lett. **34**, 1541 (1975), S. Berko and H.N. Pendleton, Ann. Rev. Nuc. Part. Sci. **30**, 543 (1980).



Schematic of Experimental Apparatus

which has a large hole in each side. These holes allow the Ps to enter, traverse, then exit the waveguide but are covered with conducting mesh to confine the microwaves. Positronium is formed by slow (~ 100 eV) positrons impinging on a metal target. In principle Ps may be formed in any excited state (Ps^*) in this manner. Once formed, the Ps^* enters the waveguide where it interacts with the microwaves. If the microwaves are tuned to a resonance then a transition ($2^3S_1 \rightarrow 2^3P_1$) is driven. The Ps^* then exits the waveguide and enters the detection region.

Of all the possible states of Ps only two - 1^3S_1 and 2^3S_1 - have lifetimes long enough to permit them to traverse the waveguide and enter the detection region. Laser ionization will distinguish the 2^3S_1 state from the 1^3S_1 state. Photons energetic enough to ionize the 2^3S_1 state (< 729 nm) but not energetic enough to ionize the 1^3S_1 state (> 182 nm) will be applied and the resultant positrons will be efficiently detected ($\sim 50\%$). The measurement is accomplished by scanning the microwave frequency and observing a resonant disappearance of the 2^3S_1 state (a "flop out" experiment).

In order to ionize efficiently it is necessary to deliver ~ 10 mJ of laser energy during the time it takes the Ps^* to cross the laser beam (~ 10 ns). This is only possible with a pulsed laser. Since the 2^3S_1 state may only be detected when a laser pulse is present it is crucial to pulse the positron beam in synchronicity with the laser beam. Positrons from a radioactive source may be accumulated in a Penning trap and then ejected suddenly in a short pulse. Such a device is currently in the testing stage.⁷ Preliminary tests have produced pulses of positrons (~ 140 ns FWHM) and have shown $\sim 100\%$ trapping efficiency. Eventually a pulsed beam with ~ 1000 positrons per pulse is expected. This should be sufficient to measure ν_0 , ν_1 , and ν_2 to 300, 150, and 100 kHz respectively which will constitute the most sensitive test to date of Ps energy levels.

⁷ R.S. Conti *et al.*, Proc. of the 7th Symp. on Rad. Meas. and Appl. to be published in Nuc. Instr. and Meth.

ELECTRON SCREENING CORRECTION TO THE SELF ENERGY IN HIGH-Z ATOMS

Paul Indelicato[†] and Peter J. Mohr
National Institute of Standards and Technology
Gaithersburg, MD 20899, USA

In high-Z atoms, quantum electrodynamic (QED) corrections are an important component in the theoretical prediction of atomic energy levels. The main QED effect in electronic atoms is the Coulomb self energy correction which is known for a large number of states. At the next level of precision, an estimate of the effects of electron interactions on the self energy is necessary. A proper way to account for these corrections in high-Z few-electron atoms or inner shells of many-electron atoms is to evaluate the vertex diagram corresponding to the combined effect of self energy and photon exchange between two electrons.[1-3] A first approximation to this correction, and a first step toward the complete evaluation of the vertex diagram, is to evaluate the effect of the static potential of each electron on the self energy of the other electrons.

This paper reports on the status of a calculation of the electron screening effect on the self energy in an external Coulomb field. The calculation is done to first order in the perturbing potential and to all orders in the strong nuclear Coulomb field. The particular case studied here is the effect of screening potentials that arise from hydrogenic electrons. To first order, these corrections add linearly in atoms with more than two electrons. We expect to generalize this calculation to an arbitrary screening potential subsequently.

This calculation is particularly applicable to QED corrections in lithiumlike uranium where a measurement of the Lamb shift has been made,[4] as well as to numerous other cases where this correction is expected to be the dominant difference between theory and experiment.

The method of evaluation will be discussed and preliminary results will be presented.

[†] Permanent address: LPAN, University Pierre et Marie Curie, 4 Place Jussieu, 75252 Paris Cedex 05, France.

1. S. J. Brodsky and P. J. Mohr, in *Structure and Collisions of Ions and Atoms*, ed. by I. A. Sellin (Springer, Berlin, 1978), p. 3.
2. P. J. Mohr, *Phys. Rev. A* **32**, 1949 (1985).
3. P. J. Mohr, *Nucl. Inst. Meth.* **B9**, 459 (1985).
4. J. Schweppe, et al., *Bull. Am. Phys. Soc.* **35**, 1178 (1990).

SELF ENERGY OF EXCITED STATES IN A STRONG COULOMB FIELD

Peter J. Mohr and Yong-Ki Kim
National Institute of Standards and Technology
Gaithersburg, MD 20899, USA

Quantum electrodynamic (QED) corrections are an important component in the prediction of atomic energy levels in many cases. Experiments have been done on high- Z isoelectronic sequences that are sufficiently precise that QED corrections for levels with $n > 2$ are needed for a theoretical prediction with a comparable accuracy.[1,2] Also, in singly-ionized helium, a precision experiment has recently been done on $n = 4$ states.[3]

This paper focuses on the self energy, which is the largest radiative correction in most atoms. Preliminary results of a calculation of the self energy in a strong Coulomb field for excited states will be given. Results of this study are applicable to the above-mentioned experiments.

A remarkable degree of regularity in the behavior of the results for a given angular momentum symmetry as a function of n appears in the results. Some of the details of the calculation will be presented. Comparisons with experiment will be made.

1. J. Reader et al., J. Opt. Soc. Am. B 4, 1821 (1987).
2. Y.-K. Kim et al. J. Opt. Soc. Am. B 5, 2225 (1988).
3. P. K. Majumder and F. M. Pipkin, Phys. Rev. Lett. 63, 372 (1989).

SEARCH FOR TIME REVERSAL SYMMETRY VIOLATION IN THALLIUM FLUORIDE USING A JET SOURCE

D. Cho, K. Sangster and E. A. Hinds
*Department of Physics, Yale University
New Haven, Connecticut 06511.*

Since the discovery of CP-violation in 1964 [1] the permanent electric dipole moments (EDM) of various systems have been measured carefully in the search for direct evidence of T-violation. One of the most interesting and extensively studied systems in this regard is the molecule thallium fluoride (TlF) [2]. A heavy polar molecule is in general a sensitive system in which to search for evidence of T-violation [3]. In this particular one, the Tl nucleus is massive (atomic number = 81) and has one unpaired proton, making it uniquely suited for a measurement of the proton EDM (d_p). The large nuclear charge causes the motion of the electrons to be relativistic in the vicinity of the nucleus which makes the molecule sensitive also to the electron EDM d_e [4]. In addition, the molecule is very sensitive to the possible T-violating neutral weak interactions between the electrons (ψ_e) and nucleons (ψ_n). One can imagine both scalar and tensor types of weak interaction:

$$H_{\text{scalar}} = iC_S(G_F/\sqrt{2})(\bar{\psi}_e\psi_n)(\bar{\psi}_e\gamma_5\psi_e)$$

$$H_{\text{tensor}} = iC_T(G_F/\sqrt{2})(\bar{\psi}_e\sigma^{\mu\nu}\psi_n)(\bar{\psi}_e\gamma_5\sigma_{\mu\nu}\psi_e).$$

In our experiment [5], the molecule is polarized by an external electric field (\vec{E}_C) so the interaction of the Tl nuclear spin ($\vec{\sigma}$) with the rest of the molecule can be effectively described by

$$H = -\mu_n\vec{\sigma} \cdot \vec{B}_0 - d\hbar\vec{\sigma} \cdot \vec{\lambda}.$$

The first term is the usual (T-conserving) hyperfine interaction of the nuclear magnetic dipole moment $\mu_n\vec{\sigma}$ with the internal magnetic field \vec{B}_0 of the molecule. On the other hand, the second term describes the T-violating electric dipole interaction that we are interested in. Here $\vec{\lambda}$ is a unit vector pointing from the Tl nucleus to the F nucleus, d is a measure of T-violation in TlF and \hbar is Planck's constant. At the operating field of $E_C = 29.5$ kV/cm, the projection $\vec{\sigma} \cdot \vec{\lambda}$ was 0.542. We measured d using a molecular beam technique to determine the change in the Tl nuclear magnetic resonance frequency (near 120 kHz) as either the electric (\vec{E}_C) or magnetic field (\vec{B}_0) was reversed.

The measurement was performed on one of the hyperfine sublevels within the first rotational state ($J=1$) and in the electronic and vibrational ground states ($^1\Sigma, v=0$). To select a particular hyperfine level with the Tl nuclear spin pointing in one direction, we used an electrostatic quadrupole lens together with a so-called state selector. First, the lens focussed those molecules in the $|J=1, M_1=0\rangle$ states. Next, the nuclear spin states were resolved in the state selector by a 27 G magnetic field, and an oscillating electric field drove a transition from one of the focussed states to a single hyperfine sublevel of the manifold $|J=1, M_1=\pm 1\rangle$. The Tl

nuclear spin transition was then induced in that state using separated oscillating magnetic fields to produce a narrow resonance line. Finally, a second combination of state selector and electric quadrupole rendered the nmr transition observable; it focussed the beam onto a hot wire detector when σ was unchanged but defocussed it when σ had been flipped.

In the work reported here we successfully developed and implemented a pure TIF supersonic jet source, in contrast with previous experiments on TIF which used more conventional effusive sources. Our supersonic source produced an intense, rotationally-cold beam with greatly enhanced population in the J=1 manifold. The nmr strength was larger by a factor of 100 than in our previous work and under optimal operating conditions the signal-to-noise ratio was increased by 20.

The experiment consisted of looking for a frequency difference in the nmr transition with the electric field (\vec{E}_c) either parallel or antiparallel to the magnetic fields of the state selectors which served as spin quantization axes. After 45 hours of data-taking we determined that the frequency difference was $(1.4 \pm 2.4) \times 10^{-4}$ Hz [5], which constitutes a tenfold improvement over the previous measurement [6].

The measured shift is a null result which can be used to set the following upper limits on T-violating parameters:

$d_p = (-3.7 \pm 6.3) \times 10^{-23} e\text{cm}$	$C_T = (1.7 \pm 3.0) \times 10^{-7}$
$d_s = (-1.4 \pm 2.4) \times 10^{-25} e\text{cm}$	$C_S = (5.4 \pm 9.2) \times 10^{-6}$

In the uncertainty quoted above, the contributions of experimental systematic errors are negligible. However, this was achieved only after making some compromises in the operating parameters in order to minimize a background signal from higher rotational states. As a result, we were unable to take full advantage of the new source. We are now working on other ways of eliminating this undesirable background and will report on our progress toward the next factor of ten improvement.

-
- [1] J. H. Christenson, J. W. Cronin, and V. L. Fitch, R. Turlay, *Phys. Rev. Lett.* **13**, 138 (1964).
- [2] E. A. Hinds, in *Atomic Physics 11* (S. Haroche, J. C. Gay, and G. Grynberg, eds.) p.151 (1989), World Scientific, Singapore.
- [3] P. G. H. Sandars, *Phys. Rev. Lett.* **19**, 1396 (1967).
- [4] V. V. Flambaum and I. B. Khriplovich, *Zh. Eksp. Teor. Fiz.* **89**, 1505 (1985) [*Sov. Phys. JETP* **62**, 872 (1985)].
- [5] D. Cho, K. Sangster, and E. A. Hinds, *Phys. Rev. Lett.* **63**, 2559 (1989).
- [6] D. Schropp Jr., D. Cho, T. Vold, and E. A. Hinds, *Phys. Rev. Lett.* **59**, 991 (1987).

DEFLECTION OF AN ATOMIC BEAM BY THE CASIMIR FORCE

C. I. Sukenik, M. G. Boshier, and E. A. Hinds,
Department of Physics, Yale University
New Haven, Connecticut 06511.

The force experienced by an atom inside a parallel-plate waveguide is one of the basic phenomena of cavity QED [1]. The full QED expression for this force is a complicated function, which depends upon the atomic oscillator strengths, the position of the atom, and the width of the cavity [2]. For ground-state atoms one can distinguish two simple limits. (i) When the gap is sufficiently small, the force takes on the form of a van der Waals interaction between the instantaneous electric dipole of the atom and its multiple images in the walls of the waveguide. (ii) When the gap is large enough and the atom is far from the walls, the force is quite different and can be understood as a Casimir force produced by a gradient of the vacuum fluctuation energy density. Whereas the van der Waals force between atoms and conductors has previously been studied experimentally [3,4], the Casimir force has not. Here we report the first observation of atom deflection by the Casimir force.

The heart of our apparatus was a parallel-plate waveguide consisting of two gold-coated mirrors facing each other across a gap that could be varied between 450 nm and 1575 nm. The cavity mirrors formed a channel 8 mm long through which passed a beam of ground-state sodium atoms. Any atoms that landed on the mirrors stuck to the surface and were lost from the beam. At the exit of the channel, two cw laser beams (589 nm and 420 nm) were used to excite the emerging atoms to the 14S state so that they could be ionized in a static electric field and counted using a channeltron. The number of atoms per second transmitted by the channel was measured as a function of the width of the channel with the results shown in Fig. 1.

When the width of the gap was larger than 1300 nm, the intensity of the transmitted beam followed the curve expected for simple ballistic trajectories, indicating that atoms in the gap experienced no significant cavity forces. On the other hand, when the spacing was reduced below 1300 nm, the transmitted beam intensity fell much more rapidly than the ballistic value, becoming an order of magnitude less by the time the width reached 800 nm. This attenuation of the beam is due to the deflection of atoms onto the mirrors by the Casimir force.

Previous deflection experiments carried out using the ground states of Cs, Rb and K [3] and Rydberg states of cesium and sodium [4] demonstrated cavity QED forces only in the short-range, van der Waals regime where the atom-cavity interaction is indistinguishable from that of a fluctuating classical dipole. In our case, however, the waveguide is "large" - the atoms are sufficiently far from the cavity walls that the atom-cavity interaction is in the Casimir regime. Here the actual atom-cavity force is expected to be much weaker than the force corresponding to a van der Waals potential, as we illustrate in Fig. 2 for the central portion of a 1000 nm-wide cavity [5]. Since the channel is so long, the transmitted atoms must travel close to the potential maximum and therefore it is precisely this central region that determines the transmission of the gap.

We are now engaged in calculations to show that our measured transmission curve confirms the theoretical cavity QED potential.

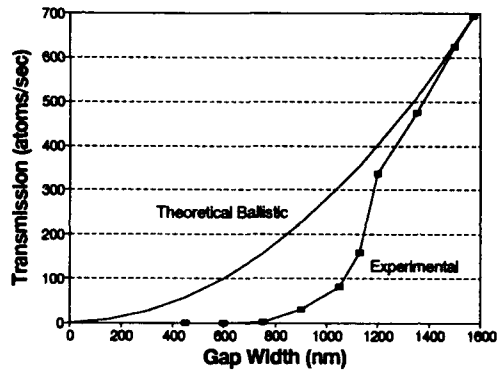


Fig. 1.

Transmission of an atomic beam through an 8 mm-long gold channel of variable width. Transmission drops sharply below a width of 1300 nm as a result of deflection by the Casimir force on the atoms.

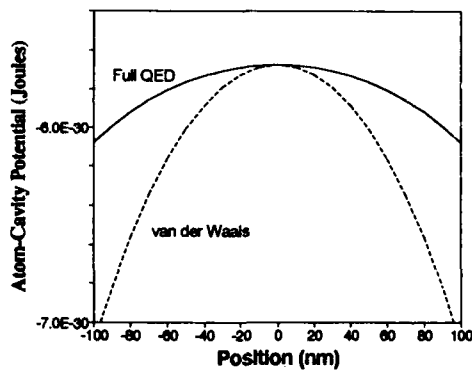


Fig. 2.

Comparison of the full QED potential near the center of a 1000 nm cavity with the potential assuming a simple van der Waals interaction [5]. The slope of the physical potential gives the Casimir force which deflects the atoms.

- [1] See, for example, E. A. Hinds in *Advances in Atomic, Molecular and Optical Physics*, (Bates and Bederson eds.) 87, 235 (1990), Academic Press, New York.
- [2] G. Barton, *Proc. Roy. Soc. Lond.* A410, 141 (1987).
- [3] A. Shih and V. A. Parsigian, *Phys. Rev.* A12, 835 (1975), and references therein.
- [4] A. Anderson, S. Haroche, E. A. Hinds, W. Jhe, and D. Meschede, *Phys. Rev.* A37, 3594 (1988).
- [5] A constant has been subtracted from the physical potential to bring the curves into coincidence at the center of the gap.

CAVITY QED LEVEL SHIFTS OF SIMPLE ATOMS

E. A. Hinds and V. Sandoghdar

Department of Physics, Yale University, New Haven, Connecticut 06511

We have made a quantitative theoretical study of quantum electrodynamic corrections to the energy of simple atoms near a metallic surface. The atoms considered are (i) the fictitious two-level system, (ii) hydrogen, and (iii) alkalis. The main purpose is different in each case. The two-level atom provides a simple framework within which we discuss the van der Waals and Casimir level shifts and explore the long-range shifts of excited states. Our calculations on hydrogen concern the possible cavity QED corrections to the $n=1$ and $n=2$ Lamb shift measurements. The shifts of alkali resonance lines are of interest because they might be studied in the laboratory as a test of cavity QED.

We have set about quantifying the magnitude of the cavity level shifts and the range over which they may be observed. In order to be specific, we consider the simplest "cavity" boundary: an infinite plane conducting mirror surface. The level shifts are computed here using perturbation theory to order e^2 in the atom-field coupling. Although the perturbative approach is unsuitable for cavities of very high quality factor, it does provide a good approximation in this non-resonant problem. A full account will be presented, although there is space here only for the bare results.

(I) THE TWO LEVEL ATOM

It is well known [1] that the ground-state energy of an atom close to a plane conductor tends at small distance z to the instantaneous van der Waals potential $-(2 \langle g | d_z^2 | g \rangle + \langle g | d_p^2 | g \rangle) / 64\pi\epsilon_0 z^3$, while at the other extreme, when the atom is far away from the mirror, the ground state level shift tends to the Casimir potential $-3\hbar c \alpha_{stat} / (32\pi^2 \epsilon_0 z^4)$, where α_{stat} is the static electric polarizability.

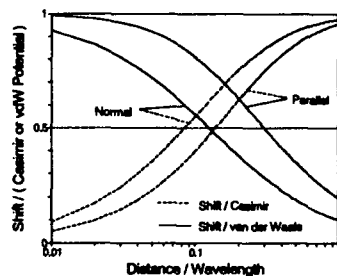


Figure 1. Ratio of exact ground state energy shifts in a two level atom to the van der Waals and Casimir potentials. The cases of normal and parallel dipole are shown separately.

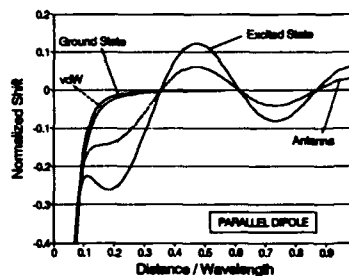


Figure 2. QED level shifts in a two level atom near a plane mirror due to a parallel dipole. The van der Waals potential and the interaction energy of a classical antenna are also shown.

We have calculated the full QED ground state level shift for all distances. Figure 1 displays the ratio of this shift to the limiting van der Waals and Casimir potentials. As well as depicting the asymptotic behaviour, this figure provides quantitative information about the behaviour of the potential at intermediate distances. It reveals the remarkably simple result that, within a factor of two, the van der Waals potential is correct when $z < 0.12\lambda$ while the Casimir potential is correct at larger distances.

We have also calculated the shift of the upper level and show the results in Fig. 2 for the case when the two levels are coupled by a dipole parallel to the conducting surface. For comparison we show the interaction energy of a classical antenna whose mean square dipole is equal to that of the excited atom. The two agree at small distance but not at long range. Further discussion of this interesting point will be given.

(II) CORRECTIONS TO THE HYDROGEN LAMB SHIFT

Our view of the $2S_{1/2}$ and $2P_{1/2}$ level shifts is in striking disagreement with that of Cheon [2] who considered the shifts of these same levels when the hydrogen atom is placed between two plane parallel mirrors separated by $1 \mu\text{m}$. Of course, the one- and two- mirror shifts should differ but only by relatively minor numerical factors [3]. The main discrepancy is that Cheon finds no shift of $2P_{1/2}$ and a -894 kHz shift of $2S_{1/2}$ whereas we find a large ($\sim 500 \text{ kHz}$) oscillating shift of $2P_{1/2}$ and a very small ($\sim 2 \text{ kHz}$) $2S_{1/2}$ shift.

Of course, Lamb shift experiments are not conducted at a distance of $1 \mu\text{m}$ from a mirror. We presume that in any such measurement, the hydrogen is at least 1 mm away from reflecting surfaces. Then the $2S_{1/2}$ shift is negligible (μHz) while the oscillating $2P_{1/2}$ shift is no greater than 500 Hz - less than 10% of current experimental accuracy [4]. We conclude therefore that the existing Lamb shift measurements require no cavity QED correction.

Future experiments are more likely to focus on the narrow $1S - 2S$ two-photon uv laser transition which may eventually be used to determine the ground state Lamb shift at the 1 Hz level of accuracy. Our conclusion is again in disagreement with that implied by the work of Cheon: we show that in this case the cavity QED shifts should be much less than 1 Hz and would introduce no significant correction.

(III) THE ALKALI RESONANCE LINES NEAR A SURFACE

We have obtained a general, analytical expression for the shifts of the lowest S and P levels of alkalis. As an example, Fig. 3 shows a result for sodium. There is some experimental evidence for shifts of this type in Rb [5].

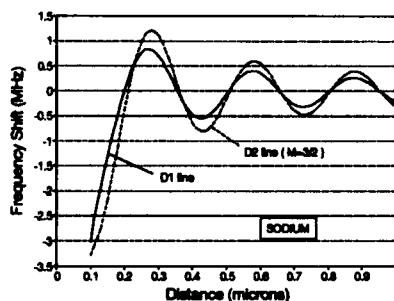


Figure 3. Frequency shifts of the sodium D-lines versus distance of the atom from a plane perfect mirror.

1. G. Barton, Proc. R. Soc. Lond. **410**, 141 (1987).
2. Il-Tong Cheon, Phys. Rev. A **37** 2785 (1988).
3. E. A. Hinds, in *Advances in Atomic and Molecular Physics* (D. Bates and B. Bederson eds.) **87**, 235 (1990). Academic Press, New York.
4. S. R. Lunde and F. M. Pipkin, *Metrologia* **22**, 9 (1986); V. G. Pal'chikov, Yu. L. Sokolov and V. P. Yakovlev *Metrologia* **21**, 99 (1985).
5. M. Oria, D. Bloch, and M. Ducloy, in *Laser Spectroscopy IX* (M. S. Feld, J. E. Thomas and A. Mooradian, eds.), p.51 (1990). Academic Press, New York.

THE RUNGE-LENZ VECTOR FOR THE TWO-DIMENSIONAL HYDROGEN ATOM

M. Lieber, X.L. Yang, and F.T. Chan
University of Arkansas
Fayetteville, AR 72701

Much interest has been developing in the properties of two dimensional systems. The existence of Chern-Simon terms¹ and the existence of anyons² which violate the theorem on spin and statistics are but two examples. There are also examples where two-dimensional behavior has been exhibited experimentally, such as the propagation of electrons in high- T_c superconductors, where the two-dimensionality is apparently imposed by the planes of copper atoms³. For the latter systems in particular the analysis of the two-dimensional hydrogen atom may be particularly relevant.

It is by now well-known that the hydrogen atom in three dimensions exhibits an "accidental degeneracy" due to a "hidden" four dimensional rotational group ($O(4)$) symmetry and the presence of an additional conserved vector, most commonly called the Runge-Lenz vector (although actually much older than these two authors⁴). Indeed, in 1935 Fock⁵ showed how to cast the momentum-space form of the Schrödinger integral equation into the equation for $O(4)$ hyperspherical harmonics. The connection of this approach with the older Runge-Lenz vector approach utilized by Pauli⁶ in his solution of the hydrogen atom problem was exhibited by Bargmann⁷, who showed that linear combinations of the components of the Runge-Lenz vector and the angular momentum vector obeyed the commutation relations of the Lie algebra of $O(4)$ (or more precisely, of $O(3) \times O(3)$ which is isomorphic to $O(4)$).

The approach of Fock was generalized to d dimensions by Alliluev⁸. In particular, he showed that the hydrogen atom in d dimensions exhibits the symmetry of the $d+1$ dimensional rotation group when expressed in momentum space, and the wave functions are nothing more than hyperspherical harmonics. His solution also pertains for the case $d=2$.

However, the analogous $d=2$ generalization of the Runge-Lenz vector does not appear to have been previously discussed, so that is the gap which we feel it is now opportune to fill.

REFERENCES

1. J. Schoenfeld, Nucl. Phys. **B185**, 157 (1981); R. Jackiw and S. Templeton, Phys. Rev. **D24**, 2291 (1981); S. Deser, R. Jackiw, and S. Templeton, Phys. Rev. Lett. **48**, 975 (1982) and Ann. Phys. (N.Y.) **140**, 372 (1982)
2. F. Wilczek, Phys. Rev. Lett. **48**, 1144 (1982), *ibid.* **49**, 957 (1982)
3. R.B. Laughlin, Science **242**, 525 (1988)
4. H. Goldstein, *Classical Mechanics*, 2nd Ed., (Addison-Wesley, Reading, Mass. 1980), page 103
5. V.A. Fock, Z. Phys. **98**, 145 (1935)
6. W. Pauli, Jr., Z. Phys. **36**, 336 (1926)
7. V. Bargmann, Z. Phys. **92**, 576 (1936)
8. S.P. Alliluev, Sov. Phys. JETP **6**, 156 (1958)

FIRST TEST OF CP INVARIANCE IN THE DECAY OF POSITRONIUM

Mark Skalsey and James Van House

Randall Laboratory of Physics

The University of Michigan

Ann Arbor, MI 48109 USA

Since the discovery of CP violation [1], many experiments have attempted to detect CP non-conservation in systems other than neutral kaons, all with negative results. The positronium (Ps) atom is an interesting candidate for testing CP invariance since it is a purely leptonic particle-antiparticle system and it is also an eigenstate of C. Discovery of CP violation in the Ps system would thus provide new insights into the mechanisms responsible for CP violation.

We have recently completed the first experiment to search for CP violation in the Ps system. The experiment uses an angular correlation in the 3- γ decay of spin aligned Ps, as first discussed by Arbib et al. [2]. This angular correlation is:

$$C_{cp}(\hat{S} \cdot \hat{k}_1)(\hat{S} \cdot \hat{k}_1 \times \hat{k}_2) \quad (1)$$

where C_{cp} is the coefficient of the angular correlation, \hat{S} is the Ps spin and \hat{k}_1 , \hat{k}_2 and \hat{k}_3 are the momenta of the three γ -rays, with:

$$|\hat{k}_1| > |\hat{k}_2| > |\hat{k}_3| \quad (2)$$

We note in eqn. 1 that the vector product $\hat{k}_1 \times \hat{k}_2$ forms the normal, \hat{n} , to the decay

plane of the three γ -rays. Since eqn. 1 contains 2 \hat{S} 's, it requires spin aligned (tensor polarization), as opposed to spin polarized (vector polarization) Ps. The degree of this alignment is given by:

$$A_1 = \sum_{m=0,\pm 1} N_m \frac{(3m^2 - 1)}{2} / \sum_{m=0,\pm 1} N_m \quad (3),$$

where N_m is the number of atoms in the substate with magnetic quantum number m . A high degree of alignment is achieved if the normally degenerate $m=0$ and $m=\pm 1$ states of triplet Ps can be resolved from each other. We achieve such separation in our experiment by forming the Ps in a 3.7 kG magnetic field to quench the $m=0$ triplet state and thereby shorten its lifetime, allowing the easy resolution of the $m=0$ state from the unperturbed long lived $m=\pm 1$ states by means of the induced difference in lifetimes.

The γ -ray energies and directions in eqns. 1 and 2 are determined experimentally by the use of three NaI detectors placed at angles relative to each other which, as determined from the Dalitz plot of the decay phase space, maximize the desired effect. Experimentally, we determine or set limits on the degree of CP violation in the angular correlation (1) by using two pairs of the NaI detectors to determine when the normal, \hat{n} , to the decay plane is up or down. We then form the asymmetry, A , between the number of events with \hat{n} up and \hat{n} down. This asymmetry was measured in a large number of systematically different runs to be $A = (-0.4 \pm 1.1) \times 10^{-3}$. The analyzing power which relates A to C_{cp} in eqn. 1, given by:

$$S_{an} \equiv A/C_{cp} \quad (4)$$

is determined to be $S_{an} = 0.072 \pm 0.015$. Using this value of S_{an} gives our limit on the angular correlation coefficient $C_{cp} = (-0.6 \pm 1.5) \times 10^{-2}$, consistent with CP invariance.

1. J. H. Christenson, J. W. Cronin, V. L. Fitch and R. Turlay, Phys. Rev. Lett. **13**, 138 (1964).
2. B. K. Arbic et al. Phys Rev. **A37**, 3189 (1988).

ACCURATE CALCULATION OF PARITY NONCONSERVATION IN CESIUM

S.A. Blundell[†], W.R. Johnson, J. Sapirstein

Department of Physics, University of Notre Dame, Notre Dame, Indiana 46556, U.S.A.

We present a new calculation of the parity nonconserving (PNC) electric dipole amplitude $E1^{\text{PNC}}$ for the 6s-7s transition in atomic cesium, with a theoretical error less than 1%. We have obtained agreement between two different approaches to the correlation problem. In the first approach, we saturate the sum over intermediate many-body states in the expression for $E1^{\text{PNC}}$ using wavefunctions obtained from a relativistic, linearized coupled-cluster code that we have recently developed. This technique includes single and double excitations and a subset of triple excitations in the wavefunctions. In our second approach, the single-particle states acquire opposite-parity admixtures, and we consider the effect of RPA and Brueckner orbital corrections to the Dirac-Hartree-Fock approximation, together with various smaller, higher-order terms. These two very different calculational schemes agree with one another to within our estimated theoretical error, and our final result for the dominant, nuclear-spin-independent, electron-nucleus term is

$$E1^{\text{PNC}} = -0.900[6] 10^{-11} i e |a_0 (Q_W - N),$$

where Q_W is the weak charge of the ^{133}Cs nucleus, and $N=78$ the neutron number. We have investigated the source of uncertainty associated with the neutron distribution, finding it to be negligible in comparison with the above uncertainty in the many-body calculation. In a similar manner, we also obtain $\beta = 27.06[20] a_0^3$, where β is the vector transition polarizability for 6s-7s.

We also consider three smaller PNC terms: the neutral-current electron-electron interaction, the nuclear anapole term, and the nuclear-spin-dependent electron-nucleus interaction. We find the first term to be negligible at the 0.1% level, and obtain factors that allow the sum of the last two terms to be isolated from measurements on different hyperfine transitions.

When combined with the measurement of Noecker *et al.*,¹ our results lead to a value of $\sin^2\theta_W$ in agreement with the value which follows from the recent highly accurate measurement of the Z mass. Using the $\overline{\text{MS}}$ scheme, we find:

$$\sin^2\theta_W(m_W) = \begin{cases} 0.2328 (m_t = 100 \text{ GeV}) \\ 0.2301 (m_t = 200 \text{ GeV}) \end{cases} \quad \begin{matrix} \text{Z mass} \\ \text{PNC in Cs} \end{matrix} \quad \sin^2\theta_W(m_W) = \begin{cases} 0.2268(66)[29] (m_t = 100 \text{ GeV}) \\ 0.2241(66)[29] (m_t = 200 \text{ GeV}) \end{cases}$$

(parentheses indicate experimental error, and brackets theoretical error). It should be noted that the inferred value of $\sin^2\theta_W$ in each case depends on the value assumed for the top quark mass, m_t .

We point out that, when the implicit dependence of $\sin^2\theta_W$ on m_t is taken into account, the standard model prediction for Q_W is relatively insensitive to the mass of the top quark, so that future improvements in theory and experiment can be expected to offer a test of the standard electroweak theory free of uncertainty from this source.

¹ M.C. Noecker, B.P. Masterson, and C.E. Wieman, *Phys. Rev. Lett.* **61**, 310 (1988)

[†] *Present address:* Lawrence Livermore National Laboratory, Livermore, California, 94550

Variational Eigenvalues and QED Effects in the $n = 10$ States of Helium

G. W. F. Drake
 Department of Physics, University of Windsor
 Windsor, Ontario N9B 3P4, Canada.

The calculation of high precision eigenvalues for the Rydberg states of helium which go significantly beyond simple screening approximations or polarization models has been a long-standing problem in atomic physics. We have recently developed new variational techniques [1] which are extensions of traditional methods involving Hylleraas co-ordinates. The new techniques involve the use of basis sets which include explicitly the screened hydrogenic wave function, together with multiple non-linear exponential parameters for the remaining Hylleraas-like terms. A complete optimization is performed with respect to the non-linear parameters. An important advantage is that the new techniques do not suffer from the usual rapid loss in accuracy as one goes to more highly excited states of a given symmetry. Results as accurate as $\pm 10^{-17}$ a.u. (± 0.1 Hz) for the nonrelativistic energies are now available for all two-electron states up to $1s10k$ ($L = 7$).

The $n = 10$ manifold of states is of particular interest because of high precision measurements of the transition frequencies by Lundeen and co-workers [2], and the possibility of detecting long range Casimir-Polder retardation effects as residual energy shifts after relativistic and quantum electrodynamic corrections have been subtracted. The calculation of these corrections will be discussed and detailed comparisons with experiment made. Table 1 below compares the theoretical predictions with the currently available experimental values. Relativistic and QED

Table 1. Comparison of theory and experiment for the 10 F - 10 G, 10 G - 10 H, 10 H - 10 I and 10 I - 10 K transition frequencies of ^4He (in MHz).

Transition	Experiment [†]	Theory	Difference
$^1\text{F}_3 - ^1\text{G}_4$	2017.325(3)	2017.326	-0.001(3)
$^3\text{F}_2 - ^3\text{G}_3$	2037.910(5)	2037.911	-0.001(3)
$^3\text{F}_3 - ^3\text{G}_4$	2043.452(5)	2043.451	0.001(5)
$^3\text{F}_4 - ^3\text{G}_5$	2044.984(4)	2044.989	-0.005(4)
$^1\text{G}_4 - ^1\text{H}_5$	486.866(2)	486.8612	0.005(2)
$^3\text{G}_3 - ^3\text{H}_4$	488.672(2)	488.6662	0.006(2)
$^3\text{G}_4 - ^3\text{H}_5$	495.561(2)	495.5578	0.003(2)
$^3\text{G}_5 - ^3\text{H}_6$	491.971(2)	491.9662	0.005(2)
$^1\text{H}_5 - ^1\text{I}_6$		154.66857	
$^3\text{H}_4 - ^3\text{I}_5$		155.81501	
$^3\text{H}_5 - ^3\text{I}_6$		159.64956	
$^3\text{H}_6 - ^3\text{I}_7$		157.63054	
H - I (mean)	157.0518(26)	157.05367	-0.0019(26)
$^1\text{I}_6 - ^1\text{K}_7$		59.31404	
$^3\text{I}_5 - ^3\text{K}_6$		60.08753	
$^3\text{I}_6 - ^3\text{K}_7$		62.43227	
$\text{I}_7 - ^3\text{K}_8$		61.19670	
I - K (mean)	60.8156(18)	60.81677	-0.0012(18)

[†]Hessels *et al* [2]. Numbers in brackets denote the experimental uncertainty in the final figure quoted.

corrections are included, but not the Casimir Polder effect proper.

In addition, the predictions of core polarization models [3] based on an asymptotic potential for the outer Rydberg electron provide valuable insight into the physical meaning of the variational calculations. A number of interesting comparisons between the two will be made, and the regions of validity of the core polarization model clearly defined. Table 2 below compares the singlet-triplet average of the $n = 10$ nonrelativistic eigenvalues with the predictions of the core polarization model. The extraordinarily good agreement for $L = 4$ and 5 is a somewhat fortuitous co-incidence that cannot be expected to apply in general.

Table 2. Comparison of the spin-averaged variational eigenvalues $\Delta \bar{E}_{\text{var}}$ for the $n = 10$ states of helium with the corresponding $\Delta \bar{E}_{\text{pol}}$ obtained from Drachman's [3] asymptotic expansion (in MHz).

	$L = 3$	$L = 4$	$L = 5$	$L = 6$	$L = 7$
V_4	-2819.48	-747.5889	-258.7808	-105.9769	-48.6392
V_6	90.08	6.4204	0.8280	0.1489	0.0328
V_7	--	1.4622	0.1067	0.0123	0.0018
V_8	--	-2.5035	-0.1260	-0.0116	-0.0015
Δ_2	-4.27	-0.2064	-0.0192	-0.0026	-0.0005
Total	-2778.71	-741.8955	-257.9817	-105.8303	-48.6067
Uncertainty	45.04	-0.5207	-0.0097	0.0003	0.0002
Variational	-2760.626	-741.8936	-257.9830	-105.82968	-48.606514
Difference	18.08	0.0019	-0.0013	0.0006	0.0002

$E_{\text{tot}} = E_{3H} + \Delta E$ with $E_{3H} = (-2 - \frac{1}{2n^2}) 2R_H$, and $\Delta E_{\text{pol}} = V_4 + V_6 + \frac{1}{2}(V_7 + V_8) + \Delta_2 + \frac{1}{2}(V_7 + V_8)$ with $V_4 = -\frac{1}{2}\alpha_1(1/r^4)$, $V_6 = -\frac{1}{2}(\alpha_2 - 6\beta_1)(1/r^6)$, $V_7 = \frac{1}{2}(\delta + 16\gamma/5)(1/r^8)$, $V_8 = -\frac{1}{2}\{\alpha_3 - 15\beta_2 + \epsilon - \alpha_1\beta_1 + 72\gamma[1 + L(L+1)/10]\}(1/r^8)$ and Δ_2 is the second-order dipole polarization correction.

1. G. W. F. Drake, J. Phys. B 22, L651 (1989).
2. E. A. Hessels, F. J. Deck, P. W. Arcuni and S. R. Lundeen, Phys. Rev. A 41, 3663 (1990).
3. R. J. Drachman, Phys. Rev. A 26, 1228 (1982); 31, 1253 (1985); 37, 979 (1988).

STUDY OF SCALAR AND PSEUDOSCALAR PARTICLE PRODUCTION AND QED VACUUM
 BIREFRINGENCE (DELBRUCK SCATTERING) USING A POLARIZED LIGHT BEAM
 - STATUS REPORT

F. Nesrick

Fermi National Accelerator Laboratory, Batavia, IL 60510

R. Cameron, G. Cantatore, A.C. Melissinos, and Y. Semertzidis

University of Rochester, Rochester, New York 14627

H. Halama, D. Lazarus, A. Prodell, and J. Rogers

Brookhaven National Laboratory, Upton, NY 11973

C. Rizzo

Istituto Nazionale di Fisica Nucleare, 34127 Trieste, Italy

E. Zavattini

Dipartimento di Fisica, Università di Trieste, 34127 Trieste, Italy

Strong theoretical indications are that light scalar or pseudoscalar particles may exist which, so far, have remained undetected. The difficulty in their detection is due to their very weak coupling to ordinary matter. Such particles do, however, couple to two photons because of the triangle anomaly. Typical examples are the axion and certain supersymmetric scalars. We have exploited the coupling to two photons to search for the coherent production of light bosons by a polarised laser beam propagating through a transverse magnetic field as first proposed by Maiani, et al. We have constructed a sensitive ellipsometer based on a 12-m long optical cavity placed in a 5-T magnetic field. The calibration of the ellipsometer is confirmed by measuring the Cotton-Mouton constant for nitrogen gas. The projected sensitivity of the instrument should allow a measurement of the QED vacuum birefringence. The first phase of the experiment is operational. We present early results from this instrument and give limits on the relevant coupling strengths.

The coupling to two photons for a pseudoscalar and scalar is described respectively by the Lagrangians $L_p = g_{p\gamma\gamma} \mathbf{E} \cdot \mathbf{B} \phi_p$ and $L_s = g_{s\gamma\gamma} (\mathbf{E}^2 - \mathbf{B}^2) \phi_s$, where \mathbf{E} is the electric field of the incident laser beam, \mathbf{B} is the external magnetic field, ϕ_p , (ϕ_s) is the pseudoscalar (scalar) field, and $g_{p\gamma\gamma}$ ($g_{s\gamma\gamma}$) is the coupling constant of the pseudoscalar (scalar) field to two photons.

The principle of the experiment can be understood from the graphs in Fig. 1. If the mass of the pseudoscalar (scalar) m_a is less than the photon energy ω , pseudoscalars (scalars) can be produced according to the graph in Fig. 1(a) and propagate freely. For pseudoscalars, only the component of \mathbf{E} parallel to \mathbf{B} will be attenuated; thus light polarised at 45° to the direction of the magnetic field will exhibit dichroism, which manifests itself as a small rotation of the polarisation vector. The pseudoscalar can convert back to a photon as shown in Fig. 1(b), in which case the component of polarisation parallel to \mathbf{B} is retarded but not attenuated. In that case, if the incident light is linearly polarised at 45° to the field direction, it will emerge with a small elliptical polarisation; this effect can take place even if $m_a > \omega$. Both graphs give rise to observable effects of order $g_{p\gamma\gamma}^2 B^2$, and are equally applicable to massless particles that couple to two photons. For the scalars the induced rotation of the polarisation vector is in the opposite sense to that induced by pseudoscalars. Therefore, by measuring both the polarisation rotation and ellipticity the mass and coupling of the pseudoscalar (scalar) can be determined.

The experimental setup is shown schematically in Fig. 2. The light source was an argon-ion laser operating at 514.5 nm vertically polarised at a power level of $\sim 2\text{W}$. The polarisation was rotated to an angle of 45° relative to the external magnetic

field by a half wave plate and precision polarized by a Glan-Thompson polariser. The beam entered the optical cavity with physical length 1256 cm and magnetic field length 880 cm. High reflectivity ($>99.8\%$) interferometric mirrors were used to achieve a large number of reflection (790 ± 35). One of the cavity mirrors was slightly deformed so the light pattern better filled the mirror aperture. The light exiting the cavity passed through a glass Faraday cell driven at 260 Hz, and was then incident on a second Glan-Thompson polarizer which was set for best extinction. The transmitted light was detected by a photodiode, amplified, and then Fourier analyzed by a Hewlett-Packard fast-Fourier-transform signal analyzer. The magnetic field was provided by two superconducting CBA dipoles, which for these data runs were modulated from 1.71 T to 2.47 T with a period of 25.6 s.

To calibrate the apparatus we measured the ellipticity induced by the transverse magnetic field (Cotton-Mouton effect) on nitrogen gas at low pressure. Our measurement was within 5% of the known Cotton-Mouton constant for nitrogen. After the calibration, the cavity was evacuated to a pressure of 3.5×10^{-6} Torr to search for an induced rotation and/or ellipticity. A signal was seen which we attribute to motion of the cavity mirrors in phase with the magnetic-field modulation. This motion (which was measured at the level of 5×10^{-9} m) modulates the amplitude and static ellipticity of the light beam exiting the cavity.

The residual signal corresponds to a rotation angle of 4.3×10^{-8} rad. Treating the residual signal as an upper limit, we exclude the production of pseudoscalars with $M_p < 7 \times 10^{-4}$ eV with coupling strengths $g_{\gamma\gamma} > 2.5 \times 10^{-6}$ GeV $^{-1}$. The ellipticity limit for the QED vacuum polarisation was determined from the residual signal, when the optical cavity had 38 reflection, to be 2.9×10^{-8} while the theoretical value is 1.8×10^{-13} .

The mirror support system has been rebuilt to minimize coupling to the magnetic field modulation. It is expected that substantial improvements (several orders of magnitude) will be realized. This experiment was performed at Brookhaven National Laboratory and was supported in part by the U.S. Department of Energy.

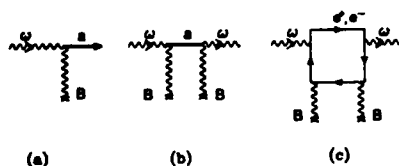


Figure 1 Possible coherent interactions of a photon in a static magnetic field. (a) Primakoff production; (b) virtual production; (c) QED vacuum-polarisation loop.

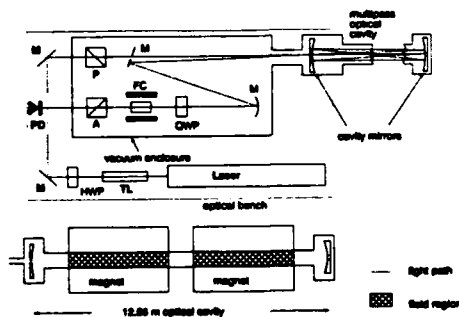


Figure 2 Schematic diagram of the apparatus and optical path with analyser A, Faraday cell FC, half-wave plate HWP, mirrors M, polariser P, photodiode PD, quarter-wave plate QWP and telescope TL.

Improved Anisotropy Measurement of the Lamb Shift in He⁺

A. van Wijngaarden, J. Kwela and G. W. F. Drake
 Department of Physics, University of Windsor
 Windsor, Ontario N9B 3P4, Canada.

Measurements of the Lamb shift in one-electron atoms and ions remain one of the important tests of quantum electrodynamics in the presence of strong Coulomb fields. Of particular importance is the high precision (9 ppm) microwave resonance measurement in neutral hydrogen by Lundeen and Pipkin [1]. However, the interpretation of this experiment is clouded by uncertainties in the proton radius, and the agreement with theory for the higher order QED corrections is not good.

In previous work [2,3] we have developed an alternative quenching anisotropy method of measuring the $2s_{1/2} - 2p_{1/2}$ Lamb shift in one-electron ions. The method is based on the observation that when the metastable $2s_{1/2}$ state is quenched in a static electric field to the ground state, the emitted Ly- α radiation is not isotropic, but has an anisotropy relative to the electric field direction which is proportional to the Lamb shift. The anisotropy is caused by an interference between the alternative decay routes through the $2p_{1/2}$ and $2p_{3/2}$ intermediate states, which become mixed with the $2s_{1/2}$ initial state by the electric field. An important advantage of the method is that the accuracy is not limited by the large width of the $2p$ state relative to the Lamb shift. A schematic diagram of the apparatus is shown in Fig. 1 below.

Measurements in He⁺ are of particular interest because the nuclear radius correction to the Lamb shift is known to exceptionally high precision from independent measurements of the fine structure in muonic helium. In addition, because the higher order QED corrections become larger than the lowest order term in proportion to Z^2 , a measurement in He⁺ is four times as sensitive to the higher order corrections.

The accuracy of our previously reported [3] Lamb shift in He⁺ has now been improved by a factor of two to 13 ppm. The improvement in accuracy was made possible by modifications to the detection system which brought about a significant improvement in the signal to noise ratio. Our new value for the Lamb shift is 14042.58 ± 0.19 MHz. This agrees with, but is larger than our previous value of 14042.22 ± 0.35 MHz. It also agrees with, but is now substantially more accurate than the theoretical value of 14042.26 ± 0.50 MHz, corresponding to an assumed nuclear radius of 1.673 ± 0.001 fm. The theoretical uncertainty of ± 0.50 MHz comes primarily from the higher order electron self-energy corrections of order $\alpha^3 Z^6$ a.u. (compared with the lowest order $\alpha^3 Z^4$ a.u. term) and beyond. There is now clearly a need for an improvement in the accuracy of these higher order terms.

1. S. R. Lundeen and F. M. Pipkin, *Metrologia* **22**, 9 (1986).
2. J. Patel, A. van Wijngaarden and G. W. F. Drake, *Phys. Rev. A* **36**, 5130 (1987).
3. G. W. F. Drake, J. Patel and A. van Wijngaarden, *Phys. Rev. Lett.* **60**, 1002 (1988).

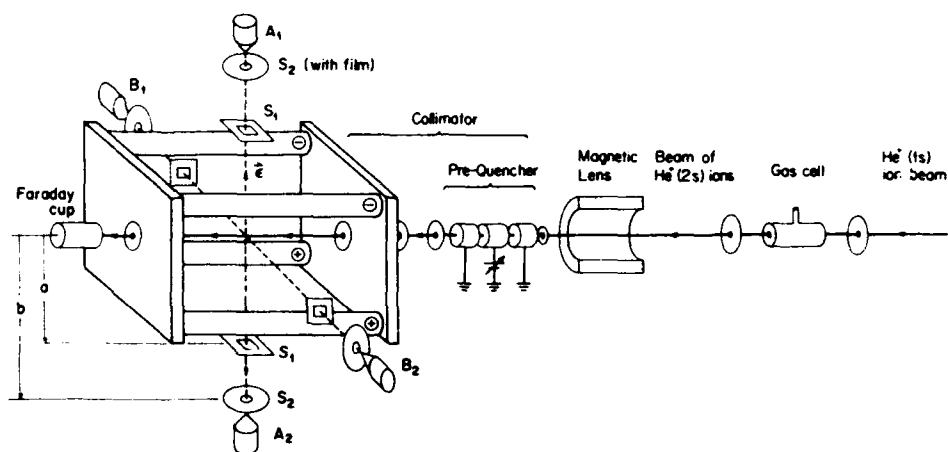


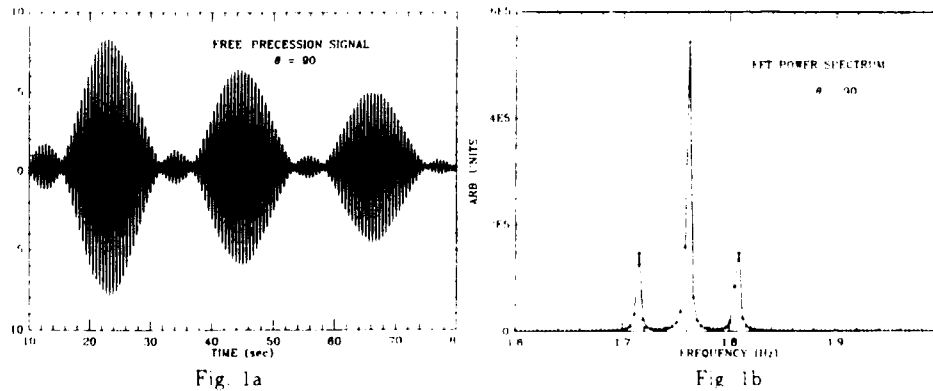
Fig. 1. Diagram of the apparatus, showing a He^+ ion beam entering from the right, and the observation cell on the left. The electric quenching field at the center of the cell is produced by applying potentials to the four quadrupole rods as shown, and the quenching radiation is observed simultaneously in four directions by the detection systems A_1 , A_2 and B_1 , B_2 .

A TEST OF THE LINEARITY OF QUANTUM MECHANICS IN SPIN-3/2 ^{201}Hg

P.K. Majumder, B.J. Venema, S.K. Lamoreaux, B.R. Heckel, and E.N. Fortson
Physics Dept., FM-15, University of Washington, Seattle, WA 98195

Recently, Weinberg has formulated a generalized version of quantum mechanics by introducing non-linear terms into the Schrodinger equation [1]. This has led to several experimental efforts to search for observable consequences of such a theory [2,3,4]. Here we discuss the results of a measurement of the spin-precession frequencies of optically pumped ^{201}Hg . We find that the possible contribution of non-linear quantum mechanical (NLQM) effects is less than 1.3×10^{-27} of the binding energy per nucleon of ^{201}Hg , representing an improvement over all previous limits.

In addition to the 'ordinary' quantum mechanical Hamiltonian, Weinberg's generalized theory contains terms proportional to powers of $(\psi^* \psi)$ making the overall energy proportional to the square of the wave function amplitude. Consider the discrete four-level system described by the ground state Zeeman levels of ^{201}Hg ($I = F = 3/2$) in a magnetic field. Because of rotational invariance in Weinberg's theory, the NLQM shifts of each level depend in a uniquely specified way on the population distribution of the ensemble of atoms. In our experiment, ground state atoms are optically pumped by circularly polarized resonance light. After pumping, the atoms are made to precess around a final quantization axis located at an angle θ with respect to the initial pump direction. The walls of the quartz cell containing the atoms provide a small ensemble-averaged electric field gradient. The resulting 100 MHz quadrupole shift easily allows us to resolve the three coherences associated with the four ground state sublevels. Figures 1a and 1b show a typical free-precession signal (90 second coherence lifetime) and its fast fourier transform. The signal represents the modulation in transmission of (weak) circularly polarized light induced by the precessing atoms.



Weinberg's theory predicts that the three observed coherence frequencies will manifest a shift which is a function of the optically pumped spin polarization and the cone-angle of precession, θ . The spin polarization has dipole, quadrupole and octupole components. These decay to zero at distinct

rates by isotropic relaxation at the walls, thus causing any NLQM shifts to vary with time. In an effort to distinguish a possible NLQM effect from systematics which can cause the Larmor frequency or quadrupole splitting to drift, we search for a time-dependent shift of the center with respect to the average of the outer two frequencies. Such a residual 'octupole' frequency shift due to ordinary quantum mechanics is very small, and is independent of polarization and cone-angle. The predicted NLQM octupole frequency shift is non-zero and has the form,

$$\Omega_{NL} = \left(\frac{\epsilon \mathcal{P}}{\hbar}\right) \times \frac{6}{\sqrt{5}} \cos \theta \left(e^{-\gamma_1 t} - \frac{9}{4} \left(\frac{\mathcal{O}}{\mathcal{P}}\right) (5 \cos^2 \theta - 3) e^{-\gamma_3 t} \right),$$

where \mathcal{P} and \mathcal{O} are the dipole and octupole polarization of the optically pumped ensemble, γ_1 and γ_3 are their respective relaxation rates, and ϵ is a small parameter characterizing the strength of any NLQM effect. After independently measuring \mathcal{P} , \mathcal{O} , γ_1 , and γ_3 , analyzing the precession frequencies of atoms for a known value of θ can provide a direct measure of ϵ . Time-domain data taken at a variety of cone-angles are fitted using a function which parametrizes the precession signal in terms of a central Larmor frequency (to which we add the term Ω_{NL}), as well as two quadrupole splittings. Typical frequency uncertainties for a single 250 second free-precession signal ranged from 5 to 40 μHz depending on the value of θ . Reversing the sense of circular polarization of the pumping light has the effect of reversing the overall sign of any resolved Ω_{NL} . We can use the fit results to compute experimentally predicted values for Ω_{NL} at $t=0$. In Fig. 2 we have averaged the results for right and left circularly polarized pumping light for various values of θ . Also plotted are the theoretical predictions for the case of $\epsilon = \pm 5 \mu\text{Hz}$. A preliminary comparison of data and theory implies that $\epsilon = 0.4(2.0) \mu\text{Hz}$. The corresponding upper limit of 1.3×10^{-27} on the binding energy per nucleon which could be due to NLQM effects represents a factor of 3 and 12 improvement over results of refs. [2] and [3] respectively. Experimental details and improved results will be presented.

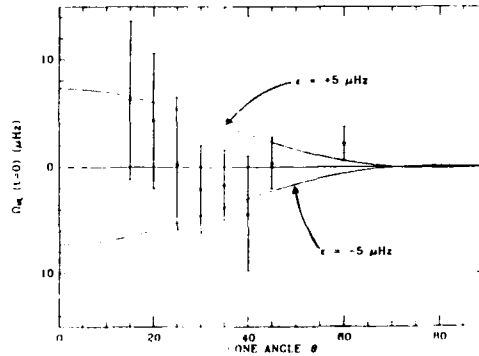


Fig. 2

- 1 S. Weinberg, Phys. Rev. Lett. **62**, 485 (1989); Ann. Phys. (N.Y.) **194**, 336 (1989)
- 2] J.J. Bollinger, *et al.*, Phys. Rev. Lett. **63**, 1031 (1989)
- 3] T.E. Chupp, and R.J. Hoare, Phys. Rev. Lett. **64**, 2261 (1990)
- 4] R.L. Walsworth, *et al.* (to be published).

II. ATOM AND ION MANIPULATION
(Cooling, Trapping ...)

FIRST EXPERIMENTS WITH EXTRACTED IONS FOLLOWING
ELECTRON IMPACT EXCITATION IN AN ELECTRON BEAM ION TRAP

D. Schneider, M. W. Clark, D. DeWitt, R. Schuch,+ C.L. Cocke,++
R. Schmieder,+++ K. Reed, R. Marrs, M. Levine, R. Fortner
Lawrence Livermore National Laboratory
P. O. Box 808
Livermore, CA 94550

Highly charged Ar (up to 18^+), Xe (up to 48^+) and U (up to 69^+) ions produced through electron impact ionization and excitation in an electron beam ion trap (EBIT) have efficiently been extracted from the trap and mass and charge analyzed. Yields for the production of Ar^{16+} , Xe^{34+} , and Xe^{44+} ions relative to "background" oxygen and carbon ions, have been deduced as a function of electron beam energies. The charge state distribution data are compared to theoretical predictions and to data recently obtained from x-ray spectroscopy measurements following the electron excitation of the trapped ions.

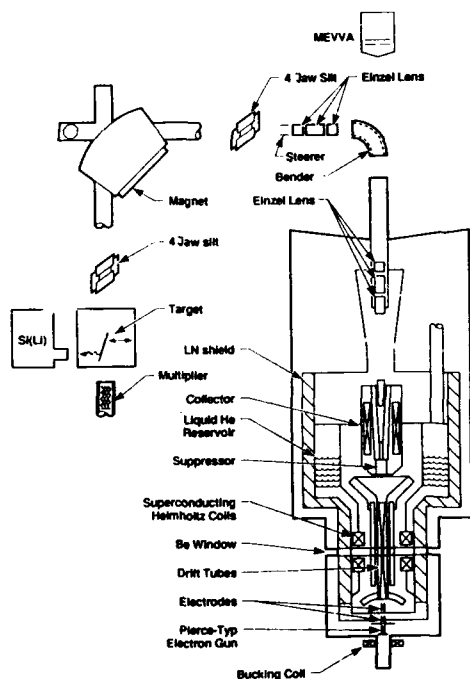


Fig. 1 shows EBIT and the extraction system. The ions are produced in the ion trap volume which consists of a copper cylinder of 20 mm length and 10 mm diameter. The electron beam is produced by a Pierce gun and injected into a magnetic field produced by superconducting coils around the trap. For details regarding the trap see Ref. 1 and references quoted therein. The Ar and Xe ions were produced by inducing Ar and Xe gas through the side ports at the trap.

Fig. 1. Schematic of EBIT including the ion extraction system and a MEVVA ion source for injection.

The uranium ions were produced by pulsing ions axially into the trap from the MEVVA ion source. The einzel lens before the "bender" focuses ions during injection and extraction. The ion extraction was performed in a continuous and pulsed mode. The pulsed mode gives an increase in the average yield by about an order of magnitude. Ion rates up to about $10^6/s$ have been obtained.

Ar K and Xe L x-ray emission following Ar^{17+} , Ar^{18+} and Xe^{44+} , Xe^{45+} and Xe^{48+} ion impact on a Cu surface has been observed, demonstrating electron capture into high n states of the highly ionized atoms in the radiative recombination process.

This work demonstrates the extension of capabilities of an electron beam ion trap (EBIT) by applying an ion extraction system to study the physics of highly charged high Z ions. The scope of new experimental possibilities may include a re-trapping of ions for the purpose of ion crystallization or studies of ion/photon interaction involving synchrotron and laser radiation.

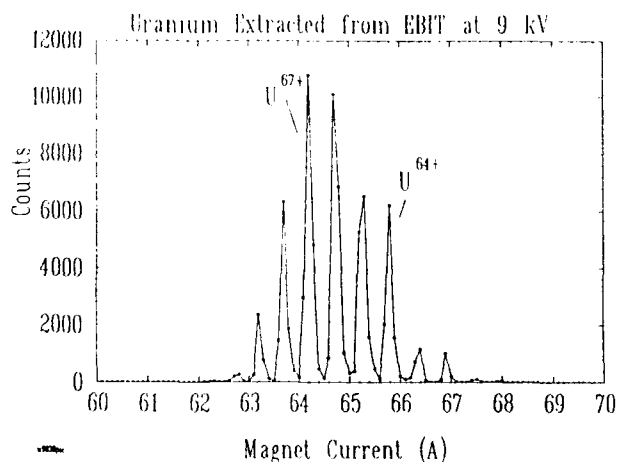


Fig. 2 Section of a typical charge state distribution of U-ions extracted from EBIT. The extraction potential (electron beam energy) was 9 kV.

Ref. 1. M.A. Levine, R.E. Marrs, J.R. Henderson, D.A. Knapp, and M.B. Schneider, *Phys. Scr.* **T22** 157 (1988), R.E. Marrs, M.A. Levine, D.A. Knapp, and J.R. Henderson, *Phys. Rev. Lett.* **60**, 1715 (1988).

Work performed under the auspices of the U.S. Department of Energy by the Lawrence Livermore National Laboratory under contract number W-7405-ENG-48.

*Manne Siegbahn Institute, **Kansas State University, ***Sandia National Laboratories

STUDIES ON THE PROCESS OF SLOWING ATOMS WITH THE ZEEMAN TUNED TECHNIQUE

V. S. Bagnato, S. C. Zilio, C. Salomon and R. Napolitano
Departamento de Física e Ciência dos Materiais,
Instituto de Física e Química de São Carlos, Universidade de São Paulo
13560, São Carlos, São Paulo, Brasil.

In using radiation forces to decelerate an atomic beam we face two problems: the undesired optical pumping and the changing Doppler effect as the atoms slow down. Both can interrupt the slowing process after just a few photons absorption. One of the alternatives to avoid them is to use a spatially varying magnetic field to compensate the Doppler shift, which also helps avoiding optical pumping when circularly polarized light is used. This technique, conveniently called Zeeman tuned has been proposed a few years ago⁽¹⁾ and successfully used^(2,3,4) to demonstrated deceleration of atoms.

We present a work where we study the influence of optical pumping and adiabatic following effects on the deceleration process in the Zeeman tuned technique.

Observing the atomic fluorescence along the deceleration path we observe that depending on the slowing laser detuning the atoms ceases to fluoresce much before expected. Figure 1 shows the results of this observation for deceleration of Na atoms. For blue detuning the dramatic drop on the fluorescence profile is associated with the fact that the atoms are actually stopping inside the solenoid. For red detuning the drop of fluorescence occurs because atoms can not follow the field adiabatically ($k v(z) \sim -\Delta + \mu B(z)$) due to the fact that for those laser frequencies the local deceleration required for the atoms to follow the magnetic field is above the maximum possible value ($a_{max} = \frac{\hbar k \Gamma}{2 S \hbar^2}$) with $k = 2\pi/\lambda$, Γ the natural line width of the transition and S the saturation parameter). This fact shows the impossibility of producing slow atoms outside the solenoid. One way of avoiding this is to work with a convenient magnetic field profile such that the atoms can follow all way along the field profile.

By controlling the field gradient is possible to decelerate the atoms using the $S_{1/2}(F=2) \rightarrow P_{3/2}(F=3)$ transition till they get close to the end of the solenoid where they are pumped out of the $S_{1/2}(F=2)$ state to $S_{1/2}(F=1)$ which do not interact with the slowing laser, allowing the atoms to move freely out of the magnet.

In Fig. 2 we observe the atomic distribution of sodium atoms along the two hyperfine states emerging from the slowing solenoid. It is clear that atoms in $S_{1/2}(F=2)$ do not follow the magnetic field down to very low values. However atoms that emerges in $S_{1/2}(F=1)$ are consistent with been decelerated of following $B(z)$ down to very low values and after that been optically pumped to this state. In this paper we explore those facts in a systematic way.

Supported by FAPESP (Fundação de Amparo à Pesquisa do estado de São Paulo), Fundação Banco do Brasil and projeto BID-USP.

References:

- [1] W. D. Phillips and H. Metalf. Phys. Rev. Lett. **48**, 596 (1982).
- [2] J. V. Prodan, W. D. Phillips and H. Metalf. Phys. Rev. Lett. **49**, 1149 (1982).
- [3] V. S. Bagnato, G. P. Lafyatis, A. Martin, E. Raab, R. Bitar and D. Pritchard Phys. Rev. Lett. **58**, 2194 (1987).
- [4] V. S. Bagnato, A. Aspect and S. C. Zilio Opt. Comm. **72**, 76 (1989).

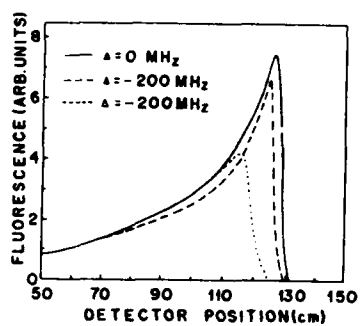


Fig.1. Fluorescence profile along the slowing magnet for different laser detunings

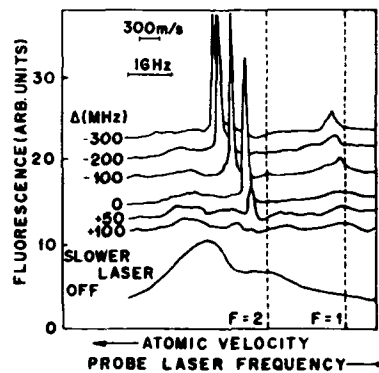


Fig. 2. Atomic velocity distribution emerging from the slowing magnet.

II-3
ELECTRONIC g-FACTOR OF Ba⁺

H. Knab, M. Hubrich, K.H. Knöll and G. Werth
Institut für Physik, Universität Mainz
D-6300 Mainz, Fed.Rep.Germany

Ba⁺ ions have been stored in a Penning ion trap with a superimposed 6T magnetic field

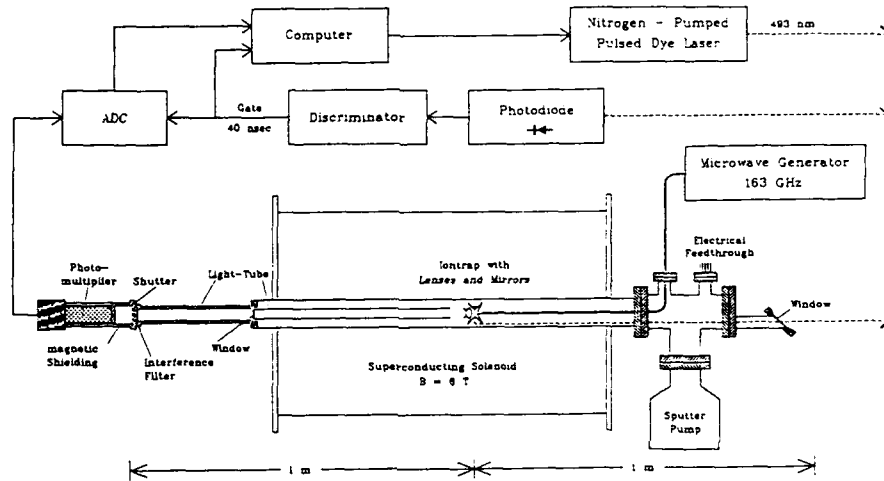


Fig.1: Experimental setup

(Fig.1). Pulsed Dye-Laser excitation of the $6S_{1/2} - 6P_{1/2}$ resonance transition shows the Zeeman splitting of the ground and excited state (Fig.2). Fixing the laser to one of the transitions we polarize the ground state by optical pumping. It is depolarized by an induced $\Delta m, = 1$ transition at 163 GHz, which is detected by an increase in fluorescence intensity (Fig.3) From the resonance frequency and the value of the magnetic field strength at the position of the ions the groundstate g -factor can be deduced.

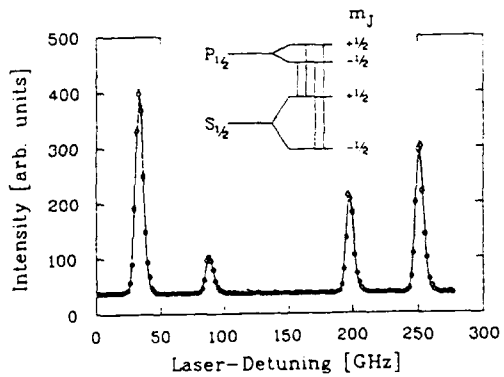


Fig.2: Laserscan at 493.1nm

The magnetic field strength is measured by the cyclotron resonance of electrons stored in the same field (Fig.4). At present the Zeeman-transition linewidth is limited by the phase

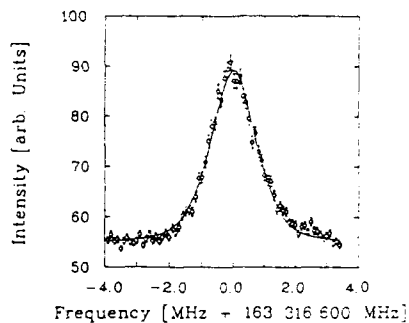


Fig.3. $\Delta m = 1$ Groundstate resonance of stored Ba-ions

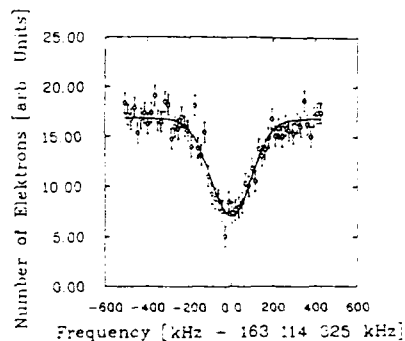


Fig.4. Cyclotron resonance of stored electrons

noise of the available microwave source. To account for the fact, that the stored ions and electrons might not cover the same volume in space we take half of the electrons' linewidth as uncertainty. The preliminary value for the $6^1S_{1/2}$ g-value in Ba^+ is 2.0024899(60). Apart from first order calculations [1], no theoretical value exists to our knowledge. For comparison the $6^1S_{1/2}$ g-factor of the isoelectronic Cs atom is 2.002 51032(20) [2].

From the Zeeman-splitting of Fig.2 the g-factor of the $6P_{1/2}$ state can be derived. We obtain $g(6^1S_{1/2}) = 0.66605(22)$ as compared to 0.66586 from first order calculation [1].

The work is supported by the Deutsche Forschungsgemeinschaft.

Reference

- [1] W.R. Johnson, private communication
- [2] E. Arimondo et al., Rev.Mod.Phys. **49**, 31 (1977)

$^4\text{He} - \text{D}_2$ MASS DIFFERENCE MEASUREMENT IN A PENNING TRAP

Ch. Gerz, D. Wilsdorf, D. Hagen and G. Werth
 Institut für Physik, Universität Mainz
 D-6500 Mainz, Fed.Rep.Germany

Eigenfrequencies of a stored ion in an ideal Penning quadrupole trap with hyperbolic electrodes are

$$\begin{aligned} \nu_z &= (2eU/mR^2)^{1/2} \\ \nu_c' &= \nu_c/2 + (\nu_c^2/4 - \nu_z^2/2)^{1/2} \\ \nu_m &= \nu_c/2 - (\nu_c^2/4 - \nu_z^2/2)^{1/2} \end{aligned}$$

where $2\pi\nu_c = e/m \cdot B$ is the ion cyclotron frequency, R the trap radius, U the applied voltage, z the trap axis and $B = B_z$. The ratio of cyclotron frequencies $\nu_c = \nu_c' + \nu_m$ for two different ions gives directly the mass ratio, from which the mass difference is obtained.

We have excited ν_c' and ν_m for single stored $^4\text{He}^+$ and D_2^+ ions and detected the resonance by a change in time of flight, when the ions are excited, kicked out of the trap and travel a distance of 45 cm in the inhomogeneous part of the magnetic field, which is produced by a superconducting solenoid. Figure 1 shows the apparatus, Fig. 2 and 3 typical ν_c' and ν_m resonances, respectively. Systematic uncertainties are reduced by correction electrodes to compensate for deviations from the quadratic trap potential, by shim coils to cancel a z^2 -component in the magnetic field and by adiabatic change of the trapping voltage to drive the ion into the trap center and to minimize the effect of the trap materials diamagnetism [1]. Typical statistical uncertainty of the center frequency of ν_c' is $1-2 \cdot 10^{-9}$. After correction of a linear drift in the magnetic field strength and taking into account the difference in ionization energy for both ions we obtain

$$\Delta m (\text{D}_2 - ^4\text{He}) = 25\,600\,331 (5) \cdot 10^{-9} \text{ amu.}$$

The Work is supported by the Deutsche Forschungsgemeinschaft.

Reference

- [1] Ch. Gerz, D. Wilsdorf, and G. Werth, Nucl. Instr. Meth. (accepted)

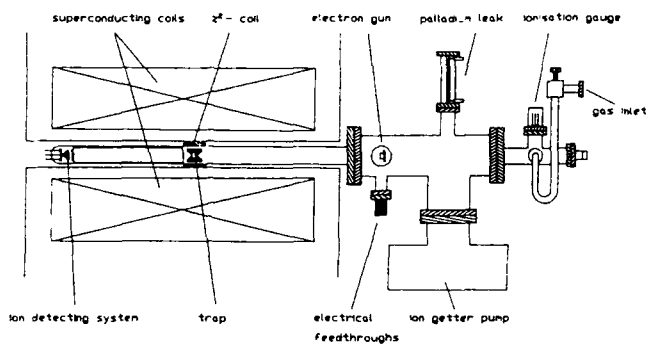


Fig. 1 : apparatus (schematic)

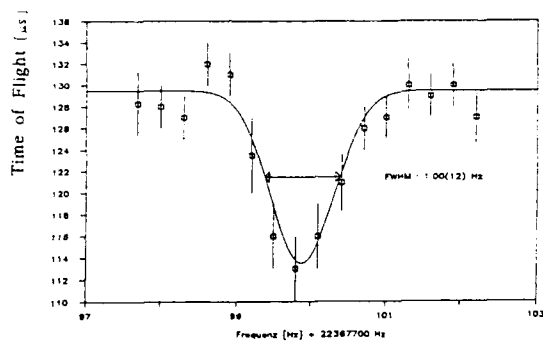


Fig 2 : ν_c - Resonance of D_2^+ (22367799.95(3) Hz)

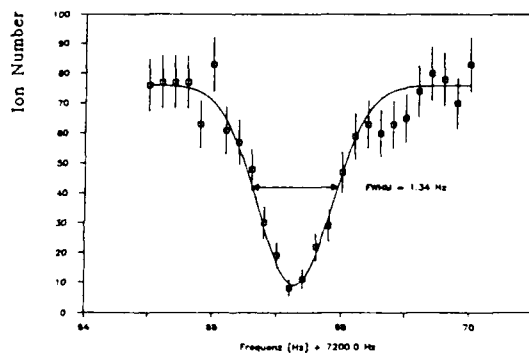


Fig 3 : ν_m - Resonance of D_2^+ (7267.25(3) Hz)

Laser Cooling Of An Atomic Beam Utilizing The Stark Effect

R. J. Knize and J. R. Yeh
Physics Department
University of Southern California
Los Angeles, CA 90089-0484, USA

We show the possibility of laser cooling of a neutral atomic beam by using the Stark Effect. The resonance frequency of an atom is shifted with a spatially varying electric field to match the Doppler shift as the atom cools. The most common methods for laser cooling of neutral atomic beams involve either laser chirping or the Zeeman Effect method. The laser chirping method cannot provide a continuous beam of cooled atoms and the Zeeman Effect method can only cool atoms in a particular sublevel and transverse heating occurs. Using the Stark Effect, it is possible to cool all the atoms in the atomic beam. This Stark Effect method also has another important feature, it allows us to simultaneously perform transverse cooling. Since all the atoms can be cooled longitudinally and transversely, it should be possible to produce an intense continuous slow neutral atomic beam. This intense slow beam would be useful in experiments involving frequency standards, searches for electric dipole moments in atoms and the observation of quantum collective behavior in atomic vapors. We will present our initial result for laser cooling of a Cs atomic beam using the Stark Effect.

THE EFFECT OF LONG-RANGE COLLISIONS BETWEEN ATOMS ON LASER COOLING

A.M. Smith and K. Burnett

Clarendon Laboratory, University of Oxford

Parks Road, Oxford, OX1 3PU

UNITED KINGDOM

There has been a considerable amount of investigation, both on theoretical and experimental levels, into the phenomenon of laser cooling of atoms. One of the critical issues this research addresses is the minimum temperature to which a beam of neutral atoms may be cooled. It was thought that this would be the doppler limit, or even the recoil limit, but various authors have suggested that heating from short-range collisions might have to be included in some situations. However we would now like to show that very long-range collisions can also give rise to heating/cooling effects that are significant compared to the laser cooling process. It may be that this will be important in determining minimum temperatures for beams of moderate or high density.

To demonstrate this we present a theory to describe collisions between pairs of atoms being cooled by a laser field. The derivation is made in the Heisenberg Picture by extending the method of Knight and Milloni [1] to a two atom system. The result is a set of coupled Optical Bloch equations where the spontaneous emission from each atom is represented by coupling to a single reservoir. Although in principle the procedure is completely quantum-mechanical, it proves necessary to make a classical path approximation in order to obtain solutions. This corresponds to defining an explicit trajectory for each atom. The solution is facilitated by defining correlation variables relating the internal behaviour of atom 1 to that of atom 2. The Bloch equations are then converted into a system of linear equations, which may be easily numerically integrated. By adopting the same techniques, based on the Heisenberg equations, equations are obtained for the motion of each atom, which are then integrated in conjunction with the equations for the internal degrees of freedom.

In the limit of no interaction between the atoms our results display all the known characteristics of laser cooling. The equations are sufficiently robust to examine both the low and high intensity regimes of laser cooling and the now well known dependency on detuning is observed.

If the interaction is turned on there is a clear effect from the collision on the atomic velocity, which depends on how close the atoms approach each other. The collision may result in heating

to oppose the laser cooling, or extra cooling, decided by the relative orientations of the atomic dipoles and the geometry of the approach. It should however be emphasised that the range of these collisions is on the order of the optical wavelength of the transition. This is much greater than the range where the quasi-molecule theory of Gallagher and Pritchard [2] applies. One consequence of this is that it is necessary to treat all orders of magnitude in the interaction (both real and imaginary) and not just the resonant dipole-dipole interaction of order $1/R^3$.

From the results it appears as if there are two mechanisms giving rise to the long-range collisions. The first is because of the change in the atomic energy levels as the atoms approach each other, leading to a jump in velocity which may be either heating or cooling. The second effect arises from the two atom damping terms in the equations (i.e, there is an extra spontaneous emission path where one atom emits a photon, the other atom absorbs it, but then immediately spontaneously emits) and causes a dip in velocity as the atoms approach and an increase in velocity as they go past each other. However during this time the laser cooling process is interrupted.

Both of these processes have an interpretation in terms of the dressed state picture, which provides the most physical explanation of the cooling mechanism in laser cooling [3]. The energy shift term (which derives from the inter-atomic potential) causes a sudden change in the amplitude of the oscillation of the dressed states. This leads to spontaneous emission occurring when the atom has much greater (or less) energy than usual and hence extra heating or cooling. Further the cooling process relies on the dressed state levels connected by the damping being exactly in phase. However in the two atom-spontaneous emission the atoms are continuously moving in and out of phase, so that the average effect is a breakdown of the cooling cycle whilst the interaction is important.

For long-range collisions it is found that the first mechanism cancels to zero when an average is taken over impact parameters. It is therefore the interruption of the laser cooling which is more likely to limit temperatures obtainable by this process. A preliminary calculation suggests that it is important to include the effect of long-range collisions for moderate to high densities. Certainly it does appear as if they will dominate over short-range collisions at these densities.

[1] P.L. Knight and P.W. Milloni, *Phys. Reports* **66** 22-105 (1980).

[2] A. Gallagher and D.E. Pritchard, *Phys. Rev. Lett.* **63** 957 (1989).

[3] J. Dalibard and C. Cohen-Tannoudji, *J. Opt. Soc. Am.* **2B** 1707 (1985).

**A COMPENSATED PENNING TRAP MASS SPECTROMETER
AND THE ^3H - ^3He MASS DIFFERENCE***

R.S. Van Dyck, Jr., D.L. Farnham, F.L. Moore, and P.B. Schwinberg
Department of Physics, University of Washington
Seattle, Washington 98195, USA

The compensated Penning trap is ideally suited for ultra-precise mass measurements relative to some calibration ion [1]. Sample economy is at its highest since only single ions are required for this spectrometer. Cryogenic operation at 4 K enhances signal-to-noise and yields very long (essentially infinite) containment times when combined with the use of non-destructive rf detection techniques. Such cryogenic use also provides for negligible interactions with background gas (whose pressure is less than 10^{-16} Torr). The use of multiply-charged ions enhances the observed signal, increases the coupling to the ion (in terms of its linewidth) and allows easy systematic checks by comparing different charge states of the same ion. In addition, the electric and magnetic trapping fields can be reasonably controlled and a simple analysis can recover the trap-independent cyclotron frequency, ω_c , which is inversely proportional to the ion's charge-to-mass ratio, q/m . This analysis involves the use of the quadrature invariance equation [2] in which ω_c^2 is the quadrature sum of the three observable normal-mode frequencies of a single ion located at the center of the trap (i.e. the ideal axial, magnetron, and shifted-cyclotron frequencies).

This instrument has already been used to obtain a 20-ppb measurement [3] of m_p/m_e and a 3-ppb determination [4] of the proton's atomic mass. These two results can be combined to yield a more precise value for the electron's atomic mass:

$$m_e = 0.000,548,579,901(11) \text{ amu.}$$

Another quantity, which is interesting because of its relevancy to the neutrino's possible non-zero rest mass, is the mass difference between tritium and helium-3. In order to determine this quantity, both single tritium and single helium-3 ions are separately loaded into the Penning trap spectrometer. However, since at present, we are limited to self-contained sources inside the cryogenically-cooled vacuum envelope, a few watts of power are required to liberate the desired gas. This heating causes significant magnetic field shifts, thus preventing a sequential measurement of the two ions. Instead, each is calibrated relative to some easily obtained multiply-charged ion such as C^{4+} or O^{6+} .

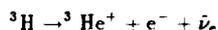
So far, several helium-3 cloud-runs have been made, calibrated against C^{4+} and one single helium-3 run, calibrated against O^{6+} . The fitted residuals for the latter are shown in Fig. 1 and yield

$$M(^3\text{He}) = 3.016,029,304,0(6,6) \text{ amu.}$$

At present, only one single tritium run has been made, calibrated relative to C^{4+} . This run yielded

$$M(^3\text{H}) = 3.016,049,262,0(9,4) \text{ amu.}$$

Combining all runs to date for both tritium and helium-3, we can obtain a *preliminary* endpoint energy, E_0 , for the reaction,



which, when determined relative to the neutral ground state, is

$$E_0 = 18,594(10) \text{ eV.}$$

This result is consistent with the most accurately measured value [5] obtained by Lippmaa [18,599(2) eV] and the more recent value [6] determined by Robertson [18,589.2(3.2) eV]. The major limitation up to now has been magnetic field uniformity and stability, but a new magnet promises to remedy both of these problems.

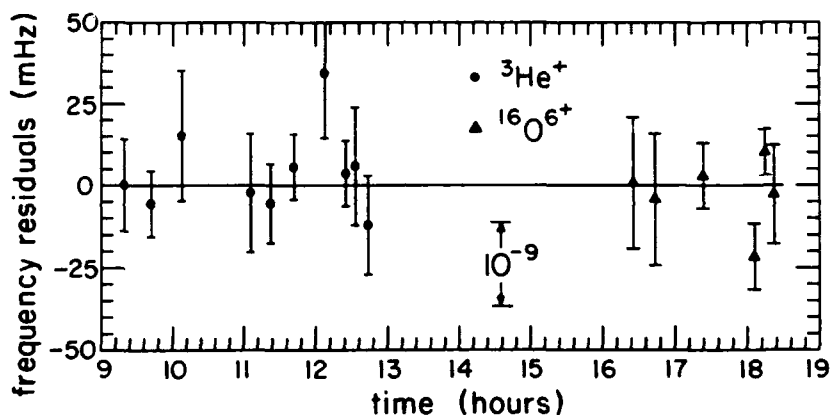


Fig. 1 Fitted Residuals for the single ${}^3\text{He} - {}^{16}\text{O}^{6+}$ comparison relative to the ${}^3\text{He}$ cyclotron frequency = 25,852,475,965 mHz, after removing a quadratic field drift. The ${}^{16}\text{O}^{6+}$ resonances (triangles) are plotted on the same graph after being scaled by the fitted mass ratio. The solid line represents the weighted average for all data.

*This work is supported by the National Science Foundation under the "Mono-Ion Research II" grant.

1. R.S. Van Dyck, Jr., *et al.*, *Physica Scripta* **T22**, 228 (1988) and F.L. Moore, *et al.*, *Nuc. Instrum. Meth. Phys. Res.* **B43**, 425 (1989)
2. L. Brown and G. Gabrielse, *Phys. Rev. A* **25**, 2423 (1982).
3. R.S. Van Dyck, Jr., *et al.*, *Int. J. Mass Spectrom. Ion Phys.* **66**, 327 (1985); *Bull. Am. Phys. Soc.* **31**, 244 (1986).
4. R.S. Van Dyck, Jr., *et al.*, in *Frequency Standards and Metrology*, edited by A. De Marchi (Springer-Verlag, Berlin, Heidelberg, 1989), p. 349.
5. E. Lippmaa, *et al.*, *Phys. Rev. Lett.* **54**, 285 (1985).
6. S.T. Staggs, *et al.*, *Phys. Rev. C* **39**, 1503 (1989).

CONSISTENCY OF THE ELECTRON G-FACTOR IN A PENNING TRAP*

R.S. Van Dyck, Jr., P.B. Schwinberg, and H.G. Dehmelt
Department of Physics, University of Washington
Seattle, Washington 98195, USA

It had been proposed [1] and experimentally verified [2] that the trapping volume of the compensated Penning trap is a microwave resonant cavity as illustrated by the observed inhibition of radiation from the cyclotron motion. This inhibition was quite fortuitous in the recently reported measurements of g -factors for both single electrons and single positrons, since the ten times inhibited damping of the cyclotron motion made it easier to excite and observe than the corresponding motion subject to free-space damping. However, the major drawback of such cavity interactions is that frequency pulling will occur for the resonant frequencies of the oscillators involved.

In order to address this possibility, the electron-geonium experiment has been repeated using an entirely new compensated Penning trap. To reduce the Q -factor of the cavity, which determines the magnitude of the possible shifts, the trap was constructed with copper endcaps and a phosphor bronze ring electrode as well as a more open structure compared to the all-molybdenum trap used in previous g -2 experiments [3]. Earlier, we reported [4] that this new trap did indeed have a cavity Q much lower than those previous traps, exhibiting a cyclotron decay time consistent with the theoretical free space value. In addition, this new trap was built with a variable magnetic bottle [5] which can be tuned over ± 250 G/cm². Such a bottle is required for the axial frequency shift detection method known as the continuous Stern Gerlach effect [6].

Several systematic effects were characterized in this trap such as the dependences on cyclotron and axial drive powers. The corrected data for about 14 runs, taken at the two extremes of the variable bottle, yielded the non-statistical distribution shown below. The resulting g -factor anomalies fall almost uniformly between the two limits, about 12 ppb apart. This distribution is now believed to be due to a slow (≈ 6 h) oscillation of the magnetic field with about the same peak-to-peak amplitude, induced into the superconducting solenoid by the movement of a nearby hydraulic elevator. The simple average of these runs yields $a_e = 1,159,652,185.5(4.0) \times 10^{-12}$ which is consistent with our previous result [3]: $a_e = 1,159,652,188.4(4.3) \times 10^{-12}$.

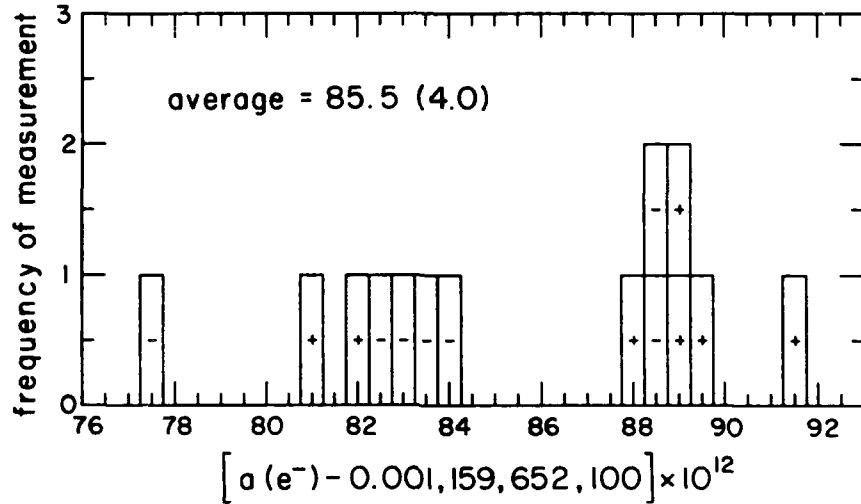


Fig. 1 The distribution of $g-2$ runs taken at the extremes of the variable magnetic bottle in the new compensated Penning trap. The "+" represents the positive extreme of $+245$ G/cm² and the "-" represents the negative extreme of -262 G/cm².

*This work is supported by the National Science Foundation under the "Single Elementary Particles at Rest in Space" grant.

1. H. Dehmelt, in *Atomic Physics 7*, edited by D. Kleppner and F.M. Pipkin, (Plenum Publishing Corp. New York, 1981) p. 337; also L.S. Brown, *et al.*, *Phys. Rev. Lett.* **55**, 44 (1985).
2. G. Gabrielse and H. Dehmelt, *Phys. Rev. Lett.* **55**, 67 (1985).
3. R.S. Van Dyck, Jr., P.B. Schwinberg, and H. Dehmelt *Phys. Rev. Lett.* **59**, 26 (1987).
4. R.S. Van Dyck, Jr., P.B. Schwinberg, and H. Dehmelt, *Bull. Am. Phys. Soc.* **30**, 2349 (1988).
5. R.S. Van Dyck, Jr., F.L. Moore, D.L. Farnham, P.B. Schwinberg, *Rev. Sci. Instrum.* **57**, 593 (1986).
6. H. Dehmelt, *Proc. Natl. Acad. Sci. USA* **83**, 2291 (1986).

SODIUM VAPOR DRIFT OBSERVED UPON RESONANCE RADIATION PRESSURE

S. Gozzini, G. Paffuti, C. Gabbanini, G. Nienhuis* and L. Moi
Istituto di Fisica Atomica e Molecolare del CNR
via del Giardino 7 - 56127 Pisa - Italy

Resonance Radiation Pressure (RRP), that is due to the photon-atom momentum transfer in the absorption-emission processes, is currently used to decelerate and cool down atoms in beams and traps. RRP was put in evidence on a sodium beam for the first time many years ago [1] but only recently it has been observed also on sodium vapor [2].

In case of a gas confined in a capillary cell, the collisions between the atoms and with the cell walls cannot be avoided and the collision rate is, in general, high. After each collision the atom changes its velocity and, eventually, shifts out of resonance. The RRP effect is, then, continuously interrupted and the atomic velocity thermalized. This imposes, in order to describe the RRP effect, to take into consideration the whole gas diffusion instead of the ballistic motion of the isolated atoms. The diffusion of the gas is modified by the presence of the resonant laser which exerts a force proportional to the instantaneous fraction of excited atoms. As the absorption line is Doppler broadened, this force depends on the vapor-laser coupling and, when a single mode laser is used, it is in general very weak.

To optimize the laser-vapor coupling a broad band laser with special configuration ("lamp-laser" [3]) has been adopted. The laser cavity has been extended up to a length $L=15$ m, which corresponds to a mode spacing of 10 MHz. The effectiveness of this kind of excitation has been already demonstrated in experiments dealing with light induced drift where high drift velocities have been observed [4].

Another limitation in RRP experiments is represented by the collisions with the cell walls which can be highly inelastic so that the resulting friction may be strong enough to make negligible any laser-induced diffusion. To minimize the surface friction effects a coating made by an ether solution of dimethylpolysiloxane, which reduces the adsorption energy of the sodium atoms at the cell walls, has been applied to the cell [5].

Our experiment is carried out in a capillary cell 50 cm long with a sodium reservoir at one end. The effect is detected by switching on/off the laser and monitoring the fluorescence evolution of the vapor via a fast transient digitizer. The compression of the vapor in the capillary cell has been observed [6]. The evolution in the optically thin regime can be reasonably described by a diffusion equation with a drift term, assuming that the diffusion coefficient D and the drift velocity v are independent on z . Moreover the laser intensity is assumed to be constant and the fluorescence is proportional to the density.

The equation has been solved for a finite cell with the metal reservoir to one end. The reservoir imposes the boundary condition of constant density for $z=L$, while at the

* Permanent address: Fysisch Laboratorium, Rijksuniversiteit Utrecht, Postbus 80 000 - 3508 TA Utrecht - The Netherlands

other end the flux vanishes.

The diffusion equation is justified when the thermalization by wall collisions drives the atomic velocity distribution to equilibrium on a time scale that is slow compared to the time scale at which density variations occur. The diffusion coefficient D is determined by the thermalization rate of the particles due to wall collisions, and the drift velocity v results from the balance of the radiation force and the wall friction.

In figure 1) we report the fit of the experimental data with the theoretical curves. In fig. 1a) the laser enters from the reservoir side, it pushes the atoms inside the capillary, so that we observe a density increase; in fig. 1b) the laser comes from the opposite direction, it pushes the atoms away so that we obtain a density decrease.

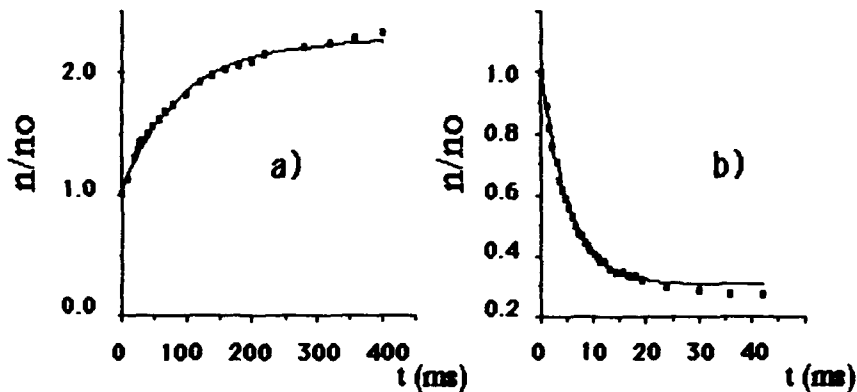


Fig.1- Fluorescence intensity versus time. The solid curves represent the theoretical solution, the points represent the experimental data. $I_L = 120$ mW, $L=15$ m; a) $z_0 = 35$ cm, $D= 4.3 \pm 1.4$ m²/s, $v = 22 \pm 7$ m/s; b) $z_0 = 24$ cm, $D= 8.4 \pm 1.6$ m²/s, $v = 39 \pm 6$ m/s

As one can see, the theoretical curves fit very well the experimental results, while the values of D and v seem to indicate that the thermalization is not complete. Experiments to evaluate surface effects are in progress.

1. O.R.Frisch, Z.Phys. **86**, 42 (1933)
2. J.H.Xu and L.Moi, Optics Commun. **67**, 282 (1988)
3. M.Allegri, P.Bicchi, S.Gozzini and J.H.Xu, SPIE vol. **701**, 176 (1987)
4. S.Gozzini, J.H.Xu, C.Gabbanini, G.Paffuti and L.Moi, Phys.Rev.A **40**, 6349 (1989)
5. J.H.Xu, M.Allegri, S.Gozzini, E.Mariotti and L.Moi, Optics Commun. **63**, 43 (1987)
6. S.Gozzini, G.Paffuti, D.Zuppini, L.Moi and G.Nienhuis, Phys.Rev.A, submitted

PRELIMINARY EXPERIMENT OF LASER ISOTOPE ENRICHMENT
VIA MAGNETIC DEFLECTION*

ZHU Xiwen, HUANG Guilong, MEI Ganghua and YANG Delin
Laboratory of Magnetic Resonance and Atomic and Molecular Physics,
Wuhan Institute of Physics, Academia Sinica, Wuhan 430071, P. R. China

Among various methods of laser isotope separation a few has been developed to the phase approaching industrial applications and the most remains in laboratory studies. Recently we proposed a method of laser isotope enrichment (LIE) via magnetic deflection of a polarized atomic beam [1]. It is based on the selective polarization of different isotopes in different senses by laser pumping and the selective deflection of a polarized atomic beam through an inhomogeneous magnet. For this method, much lower intensity than the others is needed, the knowledge of the level structures of the ground state and a few lowly-excited states of isotopes is sufficient and the technical feasibility is not difficult. However, it can be applied so far only for isotopes polarized directly by optical pumping.

At least two lasers are usually needed to polarize several isotopes in different senses simultaneously. In our case of a single mode ring dye laser available, we realized the enrichment of Li-6 by pumping the midway of the occasionally close lines of Li-6 and Li-7.

The experimental setup and procedures of LIE are similar to those of previous experiment on atomic beam polarization [2]. A Li beam with natural abundance, effused and collimated from the source chamber, is polarized in the interaction chamber by a normally incident laser beam from a SP 380D dye laser, and then detected by a quadrupole mass spectrometer in the detection chamber after passing through a hexapole magnet. The laser is in σ polarization and its intensity and interaction time with atoms in the beam are met the requirement that atoms be highly polarized in the strong magnetic field by resonant pumping. As the residual Doppler width of atomic spectra and the laser bandwidth without frequency stabilization are about 40 MHz, Li-7 in the beam is highly negatively polarized and Li-6 partially positively polarized in certain frequency range when the laser frequency is tuned, automatically

*The project supported by National Natural Science Foundation of China.

or manually, from the transition line $S_{1/2} (F=2) \leftrightarrow P_{1/2} (F=1)$ for Li-7 through that $S_{1/2} (F=1/2) \leftrightarrow P_{3/2} (F=1/2, 3/2)$ for Li-6 (separated from the former about 30 MHz) to that $S_{1/2} (F=2) \leftrightarrow P_{1/2} (F=2)$ for Li-7. Similar enrichment effects of Li-6 are measured by two detection schemes, i. e., by scanning the laser frequency and keeping the mass number of the mass spectrometer fixed at 6 and 7 and by scanning the mass number and setting the laser frequency somewhere in the range mentioned above. The highest abundance of Li-6 is enhanced to near 1/3 from the natural value 1/12. The results are consistent with the evaluated values of atomic polarizations and compared with the case when Li-7 polarized alone.

In conclusion, we succeeded in demonstration of LIE via magnetic deflection with a single laser. An improvement of its enrichment efficiency is restricted by the facts that a single laser could not resonantly pump Li-6 and Li-7 simultaneously and that Li-6 could not get highly positive polarization by F-multiplet pumping.

1. ZHU Xiwen, Acta. Phys. Sin. **33**, 1605 (1984) (in Chinese); English translation in: Chinese Physics **5**, 375 (1985).

2. G. Baum, C. D. Caldwell and W. Schroder, Appl. Phys. **21**, 121 (1980).

**DEMONSTRATION OF MINIATURE PAUL-STRAUBEL TRAP
WITH WELL DEFINED POTENTIAL WELL**

N. Yu. H. Dehmelt, and W. Nagourney
Department of Physics, University of Washington
Seattle, Washington 98195

Conventional Paul traps used in ion-trapping experiments are made of a ring and two endcaps. The shapes of the electrodes approximate ideal quadrupole potential surfaces. Typical size traps are of 1 mm ring diameter. The small size makes controlling orientation in space of the principal axes of the confining potential difficult and no previous design has succeeded in doing so. To increase the trapping strength, an even smaller size has to be used. A more serious problem with all the traps used has been the stray offset dc fields. They result largely from non-uniform potentials on the surfaces of the electrodes due to adsorbed layers. Such offset potentials introduce a large unwanted micromotion of the trapped ions.

In this abstract, We report a recently developed simple miniature trap as shown in figure 1. In this trap, a Paul-Straubel trap, the usual two endcap electrodes are replaced by two parallel metal plates perpendicular to the z-axis, placed a large distance away from the ring electrode. Two pairs of auxiliary plates are placed on the four sides of the ring perpendicular to the x- and y-axes respectively. Any stray dc potentials on the plates would have a much smaller effect at the center of the ring. The simplest version of the ring is made of a piece of long tungsten strip with a small round hole ($2R_0=250\mu\text{m}$) bored at the center. By running a large current through the strip, it can be heated up to a very high temperature at which any surface layer would be cleaned up to the atomic level. This operation, suggested by our experiment, greatly reduces, if not completely removes, the contact potential on the ring surface and accordingly the stray electric fields present at the center of the pseudopotential well. Any residual stray dc fields at the center of the trap can be made null by applying small dc fields between plates. Preliminary experimental tests showed that the least micromotion was obtained with no applied plate voltages.

The axial symmetry of the trapping potential is broken by the presence of the ring leads, which removes the radial secular frequency degeneracy. The principal oscillation axes of the effective trapping potential are therefore well defined as x, y, and z the directions and fall parallel and perpendicular to the leads. By directly exciting the ion secular motions in the above mentioned trap, we found $\omega_x=2\pi\times 1.16\text{MHz}$, $\omega_y=2\pi\times 0.90\text{MHz}$, and $\omega_z=2\pi\times 2.40\text{MHz}$, with $\Omega=2\pi\times 36\text{MHz}$, and $V_{rf}=700\text{V}$.

Compared with a conventional Paul trap using endcaps and of the same ring size, the Paul-Straubel trap requires a more than five times as large rf voltage for the same trapping strength, depending on the geometry of the actual ring. This loss can be compensated by making the ring small, since the secular frequency increases inversely proportional to the square of the ring size $\omega_z \sim V_{rf}/R_0^2\Omega$. In fact, the very simple design allows the new trap to be extremely small in size. An $R_0 = 50\mu\text{m}$ trap has been built and trapped single ions.

The overall anharmonicity of the new trap is severe, but is not a problem for an experiment with a single cooled ion. The ring geometry is mainly chosen to optimize the field strength and input and output optics. The absence of the endcaps makes the alignment of input laser beams and detection optics easy. The smallness of the trap offers the opportunity for a trap with high secular frequency, which is needed for a proposed experiment. It should be noted that a strong trapping fields will help in suppressing the micromotion at the same time.

The research is supported by the National Science Foundation under the SINGLE ATOMIC PARTICLE AT REST IN FREE SPACE project.

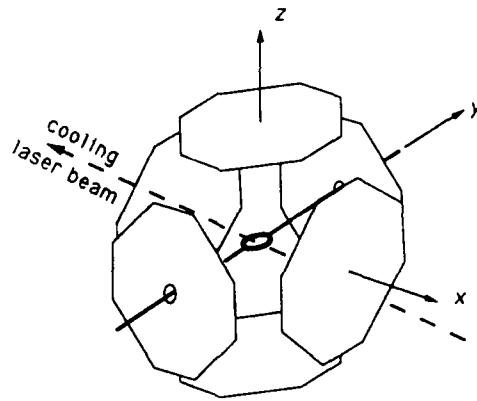


Figure 1. The configuration of the Paul-Straubel trap.

PHOTODISSOCIATION RECOIL SOURCE FOR ULTRA-SLOW MOLECULES*

Christopher Sweeney, Frederick Weihe, and Jens Zorn

Physics Dept., University of Michigan, Ann Arbor, MI 48109

Photodissociation in a hypersonic molecular beam can yield photofragments that are moving slowly in the laboratory frame of reference if the dissociating molecule happens to be aligned nearly antiparallel to the direction of the primary molecular beam [1]. In the dissociation process, some of the energy that remains after the photon breaks the molecular bond goes into kinetic energy of the fragments. If the molecule, the beam conditions, and the photon energy are chosen appropriately, a significant number of the photofragments will have a very low velocity in the laboratory frame of reference. This way of generating ultra-slow samples does not rely on the many-fold repetition of a given optical transition; it is done with a single photon and thus is suitable even if the ground state of the species to be slowed has multiple levels from rotational, vibrational, or spin degrees of freedom. Thus one may extend the interesting measurements done on ultra-slow, simple atoms to more complicated atoms and to molecules. Our method differs from the approach suggested by Basov *et al.*[2] in that we actively use the recoil of dissociation to produce fragments that move less rapidly than molecules of the primary beam.

In our first experiments with this method[3], a pulsed excimer laser dissociated large target molecules in a pulsed jet beam. A dye laser, tuned for resonant 2-photon ionization of the neutral, molecular photofragment, was pulsed at a time t after the excimer

pulse. The resultant ions went to a time-of-flight mass analyzer, the output of which, plotted as a function of t , showed only hints of ultra-slow neutral photofragments. The evidence suggests that the ultraslow fragments are particularly vulnerable to collisions with residual gas molecules in this arrangement.

To overcome this problem, we now arrange for the ultra-slow sample to be removed from the heavy flux of the primary molecular beam: The photodissociation takes place at the entrance to a multipole field that acts as a collector and focuser to guide a significant, state-selected fraction of the neutral, ultra-slow photofragments to a remote experimental region. A magnetic multipole focuser is appropriate for atoms and molecules that have magnetic dipole moments, but in the interest of simplicity, we are first exploring the use of an electric multipole focuser for polar molecules.

Our current emphasis is on the production of ultra-slow diatomic molecules, as well as production of ultra-slow NH_3 , by dissociating larger molecules. The substantial effective dipole moments permit focusing with electric fields of modest strength. The approach seems promising for a realization of Wing's proposed[4] neutral molecule storage ring and for exploration of maser operation under unusual conditions.

*Sponsored in part by the Michigan Memorial Phoenix Project

1. J.C. Zorn, **ICAP-9 Abstracts B-22** (Seattle, 1984)
2. Basov, Belenov, Gubin Kurdoglyan, Nikitin, Oraevskii and Cichov, **Sov. J. Quantum Electron.** 17, 919-992 (1987)
3. Pang, Sin, Lubman, and Zorn, **Analytical Chemistry** 58, 1581-84 (1986)
4. W. Wing, **NBS Special Publication 653**, 74-93 (1983)

LASER COOLING OF ${}^9\text{Be}^+$ AT THE HEIDELBERG TEST STORAGE RING TSR

W. Petrich¹, V. Balykin⁴, M. Bock¹, C. Ellert¹, M. Griesser¹, R. Griesser², D. Habs¹,
 G. Huber², E. Jaeschke¹, R. Klein², T. Kühl³, H. Miesner¹, M. Music¹, R. Neumann³,
 S. Schröder², D. Schwalm¹, P. Sigray⁵, M. Steck¹, B. Wanner¹, A. Wolf¹

¹Physikalisches Institut der Universität Heidelberg and Max-Planck-Institut für Kernphysik,
 D-6900 Heidelberg, Federal Republic of Germany

²Institut für Physik der Universität Mainz, D-6500 Mainz, Federal Republic of Germany

³Gesellschaft für Schwerionenforschung, D-6100 Darmstadt, Federal Republic of Germany

⁴ on leave from Academy of Sciences, Toizk, Moskow Region, USSR

⁵ on leave from Manne - Siegbahn - Institut, Stockholm, Sweden

At the Heidelberg Test Storage Ring TSR, laser cooling of relativistic ${}^7\text{Li}^+$ ions has successfully been performed for the first time [1]. Beside the experiments with ${}^7\text{Li}^+$ ions, a 7.3 MeV ${}^9\text{Be}^+$ beam has been laser cooled [2]. In contrast to the ${}^7\text{Li}^+$ beam [3], all ${}^9\text{Be}^+$ ions are in the groundstate and can interact with the laser field. At very low temperatures, the behaviour of such a cold beam differs considerably from the hot beam: plasma waves may be excited like in electron cooling experiments [4]; crystallisation of the beam seems feasible (see e.g. ref. [5]).

In the ${}^9\text{Be}^+$ laser-cooling experiment, the energy of the beam is chosen in such a way, that the strong 300 nm line of an Ar^+ ion laser can excite the ${}^2\text{S}_{1/2} \rightarrow {}^2\text{P}_{3/2}$ transition ($\lambda_0=313\text{nm}$) via the Doppler shift. Due to the relatively small laser - line width only ions in a very narrow part of the broad velocity distribution fulfill this resonance condition. However, the hyperfine splitting of the ${}^2\text{S}_{1/2}(F=1,2)$ and the ${}^2\text{P}_{3/2}(F=0,1,2,3)$ levels causes optical pumping, which would prevent the ions from further interaction and thus disable the cooling [2]. On the other hand, methods have been found to circumvent the effect of optical pumping in these experiments [2].

Fig. 1a shows a scheme of the laser-cooling setup in one of the four TSR straight sections. For probing the ion velocity profile, a high-voltage tube is locally scanning the velocity distribution across the above mentioned resonance condition. The fluorescent light is monitored perpendicular to the ion beam axes and is measured as a function of applied voltage. From the fluorescent light spectrum shown in fig. 1b, the relative momentum spread of $(\Delta p/p)_{\parallel}=3 \cdot 10^{-4}$ of the uncooled distribution is determined, which corresponds to a longitudinal temperature of $T_{\parallel}=3700\text{K}$. Out of the various laser cooling methods, which have been performed in a storage ring for the first time [2], the combination of the accelerating laser - cooling force and an induction decelerator was most successful. In this procedure, the Ar^+ ion laser power is increased from below 1 mW to 100 mW. The laser frequency can be fine tuned and is set to excite the low - energy end of the broad ${}^9\text{Be}^+$ velocity distribution. Hence, the slower ions experience an accelerating laser cooling force. An induction decelerator [6] then shifts the complete velocity distribution across the Doppler resonance condition. This procedure piles up the ions in a narrow velocity range. After compressing the velocity distribution, the above described probing scan yields an upper limit for the longitudinal temperature after cooling of $T_{\parallel}^f < 6\text{K}$, corresponding to $(\Delta p/p)_{\parallel} < 1 \cdot 10^{-5}$ (fig. 1c). An independent way of ion beam diagnostics is given by measuring the so-called Schottky noise of the coasting beam (see e.g. ref. [4]). The Schottky spectra which are obtained after laser cooling show clear evidence for collective phenomena such as the creation of plasma waves.

However, the transverse temperature of $T_{\perp} \approx 10^6\text{K}$ is hardly affected by the longitudinal laser

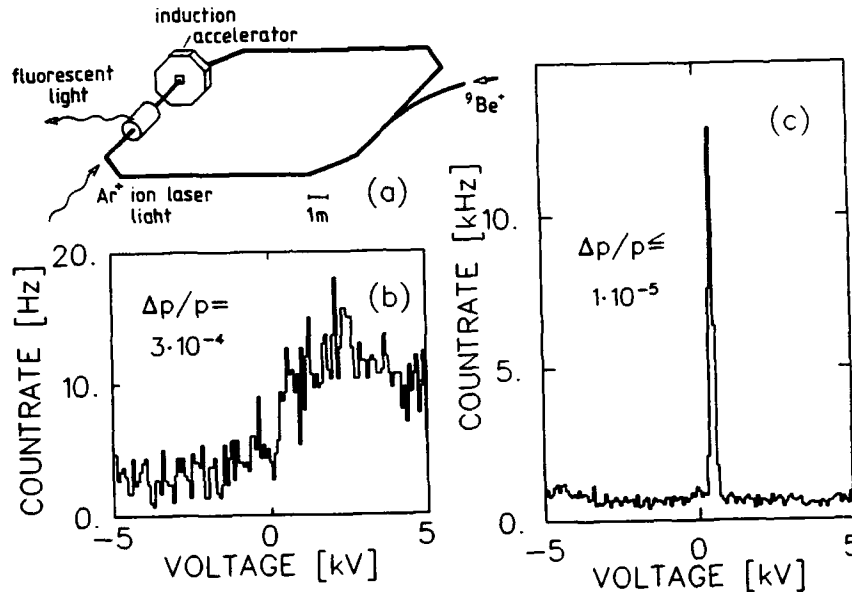


Figure 1: Fluorescent light spectra of (b) an uncooled and (c) a cooled ${}^9\text{Be}^+$ velocity distribution. The spectra were obtained by rapidly scanning the high voltage applied to the tube shown in (a).

cooling procedure. The coupling between the longitudinal and the transverse degree of freedom by intrabeam scattering is very likely to hamper a further reduction of the longitudinal temperature. Hence, transverse cooling by means of the TSR electron cooler is investigated. By electron cooling, the longitudinal temperature is reduced from 3700 K to 250 K with a cooling time of 600 ms. Further measurements show, that also the transverse temperature is substantially decreased.

In future experiments, electron pre-cooling will be of great importance when aiming for longitudinal temperatures in the millikelvin region. Even more, for a transversely cold beam intrabeam scattering and thus the above mentioned coupling will be strongly enhanced. Therefore it seems feasible, that the longitudinal laser cooling can also further reduce the transverse temperature. Then the ion movement will be dominated by their repulsive Coulomb potentials which may lead to crystallisation of the ion beam.

This work has been funded by the German Federal Minister for Research and Technology (Bundesministerium für Forschung und Technologie) under contract No. 06HD133I.

- [1] S.Schröder *et al.*, Phys. Rev. Lett. **64** (1990) 2901
- [2] W.Petrich *et al.* in: Proceedings of the ECOOL'90, Legnaro, Italy (1990), to be published
- [3] R.Klein *et al.*, this conference
- [4] V.Parkhomchuk *et al.*, Sov. Phys. Tech. Phys. **25** (1980) 7
- [5] D. Habs in: 'Frontiers in Particle Beams', Lecture Notes in Physics **296** (1986) 310
- [6] C.Ellert *et al.*, in preparation for Nucl. Instr. Meth.

LASER FOCUSING OF ATOMS: A PARTICLE OPTICS APPROACH

J.J. McClelland and M.R. Scheinfein
 Electron Physics Group
 National Institute of Standards and Technology
 Gaithersburg, MD 20899

The use of a TEM_{01}^* ("donut") mode laser beam has been proposed as a means of focusing an atomic beam to extremely small spot sizes.¹ In the initial analysis, Balykin and Letokhov showed that when a donut mode laser beam is focused to a small spot of order $1 \mu\text{m}$, and an atom beam is passed concentrically through the focus, the dipole force on the atoms has the correct radial dependence to produce first order focusing. They then estimated the effects of atomic diffraction (due to the deBroglie wavelength of the atom), spherical and chromatic aberration, and diffusion arising from spontaneous emission. It was found that spot sizes of order a few Angstroms could be obtained with reasonable values for atomic beam collimation and monochromaticity, and laser power and detuning.

Subsequently, Gould and Gallatin² showed that the assumption of thin lens conditions made by Balykin and Letokhov is not generally valid, and also that the cancellation of spherical aberration at a certain combination of laser power and detuning is incorrect. Using path integral formalism, they solved Schrödinger's equation for the motion of the atom through the lens, and also obtained estimates of the spherical and other aberrations in the thin lens limit. They predicted spot sizes of a few tens of Angstroms for conditions similar to those discussed by Balykin and Letokhov.

We have analyzed the classical trajectories of atoms through a donut mode laser beam using methods developed for particle optics. The potential generated by the dipole force is expanded in r (radius), and the equation of motion is solved. The first order paraxial equation is of exactly the same form as the equation first solved by Glaser in 1941³ for magnetic electron microscope lenses. A simple analytic solution exists, which gives focal lengths and principal plane locations valid for the thick lens in either the asymptotic or immersion limit. This solution shows that the lens has a minimum focal length, equal to the Rayleigh length of the laser beam. For higher laser powers (or changes in any other parameter which make the lens stronger), the lens forms multiple crossovers.

We have also analyzed the third order aberrations of the laser lens (which are different from those in the magnetic field case solved by Glaser) and have obtained thick-lens analytic expressions for the spherical, chromatic and diffusion aberrations. Diffraction of the atom beam is treated in the Fraunhofer limit, where the diffraction spot diameter (FWHM) is given by $\delta = 0.61\lambda_{dB}\alpha^{-1}$ (λ_{dB} is the deBroglie wavelength of the atom, and α is the angle made by the trajectory at the focus).

The results obtained in this work allow the investigation of the properties of a donut mode atomic lens over a broad range of laser and atom beam parameters. Comparisons with previous work and overall optimization of the lens will be discussed.

References

- ¹V.I. Balykin and V.S. Letokhov, *Optics Comm.* **64**, 151 (1987).
- ²P.L. Gould and G. Gallatin, *Bull. Am. Phys. Soc.* **35**, 1143 (1990).
- ³W. Glaser, *Z. Physik* **117**, 285 (1941). See also, e.g., P. Grivet, *Electron Optics*, 2nd ed. (Pergamon Press, Oxford, 1972), p. 260.

MONTE CARLO SIMULATION STUDIES OF CAVITY-CONFINED POSITRONIUM

Paul W. Zitzewitz
 Department of Natural Sciences
 The University of Michigan-Dearborn
 Dearborn, MI 48128

Lisa Lapidus, Jeffrey Nico, and David Gidley
 Department of Physics
 The University of Michigan
 Ann Arbor, MI 48109

1. Motivation

Orthopositronium (*o*-Ps) vacuum decay rate experiments¹⁻³ typically use 3x3 cm cylindrical cavities to confine the *o*-Ps to a region of uniformly high gamma detection efficiency. The *o*-Ps not only decay via three gamma annihilation, but also disappear from the detection region by escaping through the cavity aperture through which the positron beam enters. This disappearance rate was measured¹ in 1978 and found to scale with cavity aperture area, in agreement with the predictions of kinetic theory.

Orthopositronium is also expected to have a small probability of annihilation during collisions with the cavity surface. This effect was too small to be measured in 1978, but has been measured in our recent experiment³. We found a probability of annihilation per collision of 5×10^{-5} , assuming the kinetic energy of confined *o*-Ps to be 3 eV. A similar effect can occur in other cavity experiments. In particular the neutron lifetime experiment⁴ sees an analogous loss mechanism when neutrons are absorbed into the cavity walls.

In addition, in both *o*-Ps experiments we have found excess decays during the first two or three *o*-Ps lifetimes. These decays are not purely exponential, and their source has not been identified. Their effect on the experimentally measured decay rate can be eliminated by not fitting data acquired during the first 300-400 ns after *o*-Ps formation, but this discards 80-94% of all decay events. In order to investigate these decays and to improve our intuition for confined *o*-Ps, we developed a Monte Carlo simulation of confined decaying particles. The logical structure of this simulation is shown on the next page.

2. Simulations Completed

After initial tests of the simulation in MgO-coated cavities with an ideal gas, i.e. non-decaying, non-escaping particles, we investigated the escape of particles through an aperture. We confirmed the calculations of Clausing of the escape through thick apertures⁵. We also found that when aperture sizes were comparable to cavity mean-free-path, the escape rate deviated significantly from the predictions of kinetic theory. As a result, we modeled two cavities used in the experiment that were designed to have a short mean-free-path to increase the collision rate. The results obtained from these simulations were used to correct the predictions of kinetic theory. Simulations with decaying particles included a model where escaped particles entered a region where the decay rate is higher than in the cavity. This simulates the real experiment where particles escape into the uncoated positron lens system. Effects of collisional energy loss through momentum transfer to MgO grains were simulated, including models where *o*-Ps made 2-80 grain collisions for each wall encounter. Results will be discussed.

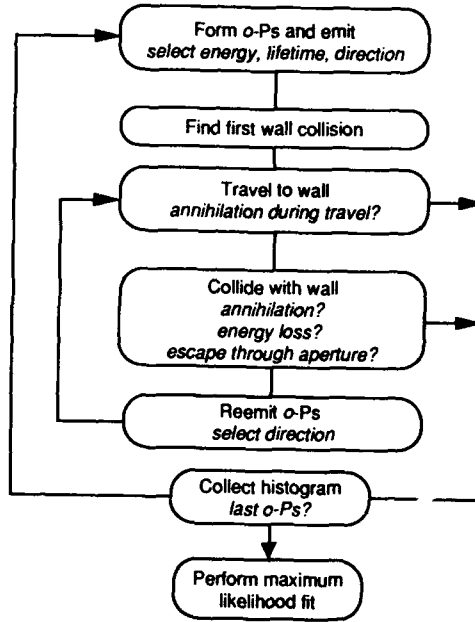
3. Future Work

Simulations to be done this year will include combinations of escape through an aperture along with inelastic cavity collisions in which particles can either lose energy or annihilate for a distribution of initial *o*-Ps energies. We expect such a combination to produce a decay spectrum that has the excessive early annihilations seen in the experiment.

4. References

1. D.W. Gidley and P.W. Zitzewitz, Phys Letts 69A, 97 (1978).
2. P. Hasbach, G. Hilbert, E. Klumpt, and G. Werth, Nuovo Cimento, 97A, 419 (1987)
3. J. Nico, D.W. Gidley, A. Rich, and P.W. Zitzewitz, submitted to Physical Review Letters, 1990.
4. W. Mampe *et al.*, Phys. Rev. Lett. 63, 593 (1989).
5. P. Clausing, Ann. Physik 12, 961 (1932).

Simulation of o-Ps in a confining cavity



PROGRESS ON LASER COOLING OF STORED RELATIVISTIC ${}^7\text{Li}^+$ IONS

R.Klein, N.Boos, R.Grieser, G.Huber, I.Hoog, P.Merz, S.Schröder
 Institut für Physik der Universität Mainz, 6500 Mainz FRG

Th.Kühl, R.Neumann
 Gesellschaft für Schwerionenforschung, 6100 Darmstadt, FRG

V.Balykin, D.Habs, C.Ellert, W.Petrich, D.Schwalm, B.Wanner, A.Wolf and the TSR group
 Physikalisches Institut der Universität Heidelberg und Max-Planck-Institut für Kernphysik,
 6900 Heidelberg, FRG

Laser cooling of a 13.3 MeV ${}^7\text{Li}^+$ beam stored at the Test Storage Ring (TSR) [1] in Heidelberg was successfully performed by two colinear laser fields operating on the ${}^3S_1(F=5/2) \rightarrow {}^3P_2(F=7/2)$ line of the metastable ions resulting in a cooling from 260 K to a final longitudinal temperature of $T \approx 3\text{K}$ [2].

The ${}^7\text{Li}^+$ ions produced by stripping of LiH^- in a gas target are accelerated by a tandem accelerator and injected into the storage ring by multiturn injection. The circumference of the TSR is 55.4 m and allows a magnetic rigidity of up to 1.7 Tm. Typically 10^7 ${}^7\text{Li}^+$ ions are stored at a velocity of $\beta = v/c = 0.064$ about 10 % being in the metastable 3S_1 state.

Recently some new schemes for laser cooling and diagnostics have been applied using an induction accelerator [3]. The actual laser force as seen by the metastable ions could be determined by means of the induction accelerator allowing a precise energy shift/turn of the stored beam. By this the initial ion distribution was shifted into and eventually across resonance with a co propagating Ar^+ laser beam acting on the closed two level transition. The force induced by the induction accelerator is compensated by the laser cooling force seen by the interacting ions. The time dependance of the resulting fluorescence signal was recorded for different strength of the induction accelerator. The life time of the ions kept at the point with zero net force was close to the storage time (5-15 sec) for induced energy shifts below 7 meV/turn and dropped sharply beyond this value. This limit is about 2 % of the calculated cooling force. This reduction is maybe due to a modulation of the Doppler shifted resonance frequency by transverse betatron motion [4] and angular mismatch between ion and laser beam. Moreover intrabeam scattering and uncontrolled induction by variation of the total magnetic flux in the ring have to be considered.

The resulting width of the momentum distribution obtained by laser cooling combined with the induction accelerator was probed independently with a tunable dye laser. Temperatures as low as 180 mK have been observed at an energy of 13.3 MeV which corresponds to a momentum precision of $\Delta p/p = 1.1 \times 10^{-8}$. This value still contains contributions from magnet instabilities and eventual collective motion.

This temperature limit could not be decreased by the combination of transverse e^- cooling and longitudinal laser cooling even so transverse beam compression by at least a factor of 10 was seen in the increase of the laser fluorescence signal. This and other observations lead to the conclusion that

the angular overlap between ion, e^- and both laser beams is not yet perfect.

We have reached by laser cooling an optical line width just about 14 times the natural width, allowing for precision experiments in atomic physics. Moreover the actual laser light pressure is already strong enough to separate in momentum the metastable 3S_1 state ions from the 1S_0 ground state $^7Li^+$ ions which corresponds to a mass resolution of about 10^{-6} .

This work has been funded by the German Federal Minister of Research and Technology (BMFT) under contract no. 06 HZ 188I and GSI Darmstadt under contract MZH1C.

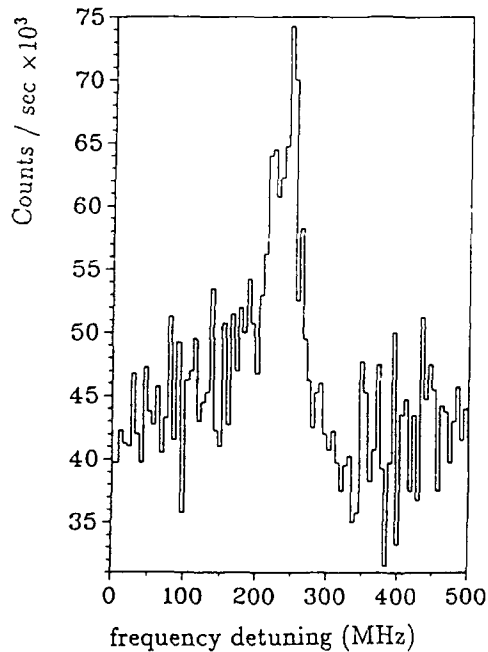


Fig. 1: Velocity distribution cooled by the combined force of a stabilized single mode Ar^+ laser and an induction accelerator. The spectrum was recorded by a single fast (500 msec) scan of an independent tunable dye laser.

1. P. Baumann et al., Nucl. Instr. Meth. **A268** 531 (1988)
2. S. Schröder et al., Phys. Rev. Lett. **64** 2901 (1990)
3. C. Ellert et al., in preparation for Nucl. Instr. Meth.
4. G. Huber et al., Laser Spectroscopy IX, ed. by M. S. Feld et al., p.295, Academic Press, Inc., 1989

**OBSERVATION OF THE LASER COOLING FORCE DUE TO
MULTIPHOTON "DOPPLERON" RESONANCES**

R.G. Hulet, J.J. Tollett, J. Chen, J.G. Story, N.W.M. Ritchie, and C.C. Bradley
Department of Physics and Rice Quantum Institute
Rice University
Houston, TX 77251

The force on an atom moving in an intense standing wave light field can be much stronger than the "usual" Doppler or "molasses" force. In addition to a large force, a plot of the force vs. velocity v exhibits a complex structure, indicative of the richness of the physical phenomena which can be observed in this system. Fig. 1 shows the results of a calculation of the mean force (averaged over a wavelength of travel) based on a numerical solution of the exact density matrix equations [1] for a particular value of the Rabi frequency Ω and the detuning from resonance Δ . Three velocity regions may be identified and, in each, the force may be ascribed to a different physical mechanism. For very low velocity, the so-called dipole force dominates. Unlike the Doppler force, this force is cooling for blue detuning [2] and does not saturate with increasing field intensity. At higher velocities, the atom may be Doppler tuned into resonance with the travelling waves which make up the standing wave. In the frame of the moving atom, the atom sees the two travelling waves at different frequency, one blue shifted by an amount kv and the other red shifted the same amount. If $\Delta = kv$, the atom will be Doppler shifted into a one-photon resonance. This is the Doppler force ("1" in Fig. 1), for which the force is due to only one of the travelling waves. For intermediate velocities, resonances may appear at high intensity. These resonances are due to multiphoton Raman transitions involving both travelling waves and occur at velocities satisfying the condition $\Delta = nk v$, where n is an odd integer. These velocity-tuned multiphoton resonances have been designated "Doppleron" resonances [3] and the quanta of energy $\hbar k v$ as a Doppleron. The first few Doppleron resonances are labelled in Fig. 1. The existence of this type of resonance was predicted in the context of saturated absorption spectroscopy [4]. More recently, Dopplerons have been employed in the cooling of the longitudinal velocity of atoms in a beam [5]. However, the force due to individual Doppleron resonances has not previously been observed.

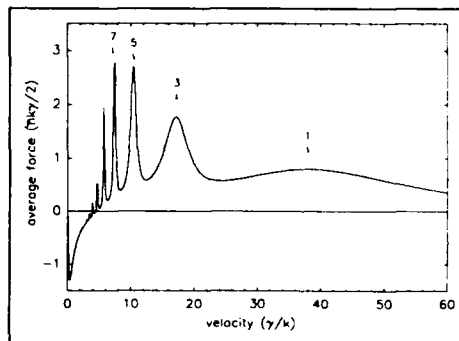


Figure 1 Exact numerical calculation for $\Omega = 60 \gamma$ and $\Delta = 30 \gamma$. The force is in units of the maximum Doppler force.

We have observed the force due to Doppleron resonances on the transverse velocity of atoms in a ^7Li atomic beam. The beam is intersected at right angles by a standing wave formed using a cw dye laser. The beam is expanded along the atomic beam axis producing a Gaussian beam waist of ~ 9.3 mm by ~ 1.1 mm. The laser frequency is tuned near the $2S_{1/2}, F=2 \leftrightarrow 2P_{3/2}, F=3$ resonance frequency of the

^7Li atom (671 nm wavelength) and is offset frequency locked by up to 300 MHz from the resonance line in a Li vapor cell. The light is circularly polarized so that atoms not initially in the $F=2$, $m_f=2$ ground state will be optically pumped into it, from where they can participate in the cooling process, or, they decay into the $F=1$ ground state hyperfine level (803 MHz hyperfine splitting) and are effectively removed from the cooling and detection processes. The laser power was 760 mW, giving a peak intensity in the standing wave of 19 W/cm^2 ($\Omega \approx 60 \gamma$, where γ is the spontaneous decay rate). The laser beam was apertured along the atomic beam axis to a 6 mm width so that the variation in Ω was ideally no more than 10% as the atoms traversed the standing wave. The transverse velocity distribution of the atoms is determined by a weak probe laser parallel to the standing wave. The probe laser frequency is tuned across the transition while a portion of the emitted fluorescence is detected. The Doppler width of the laser-induced fluorescence spectrum of the unperturbed atoms (i.e. standing wave blocked) is determined by the acceptance angle of the photodetector and is $\sim 270 \text{ MHz}$.

Fig. 2 is data for $\Omega = 60 \gamma$ and $\Delta = +30 \gamma$ (as in Fig. 1). The horizontal axis corresponds to the probe frequency detuning ν , which is related to the transverse velocity v , by $\nu = kv/2\pi$. We identify the structure in the velocity distribution as due to Doppleron resonances. The dips are due to the depletion of the heated atoms at the velocities corresponding to Doppleron resonances. The heated atoms accumulate at larger velocity where the force is relatively weak and form the peaks adjacent to the dips. The arrows indicate the positions of the 1, 3, 5, and 7 photon Doppleron resonances. The resolution of the probe laser is natural width limited to a velocity of 390 cm/s. The dipole force, which is cooling for $\Delta > 0$, creates the narrow central line peak. The dotted line in Fig. 2 is a fit resulting from numerical integration of the atoms' motion through the standing wave using the exact calculation of Fig. 1 as input. Overall, the calculation reproduces the positions and magnitude of the Doppleron features very precisely. We obtained data for other values of Ω and Δ which also agree with the calculation.

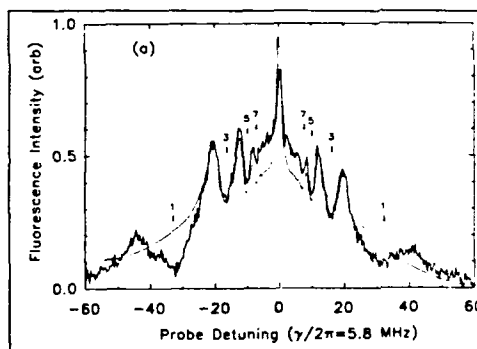


Figure 2 Solid line is data; dotted is the fit.

Our experiment is reported in a forthcoming manuscript [6] as is another experiment which has also observed the force due to Dopplerons [7]. This work was supported by the Texas Advanced Technology Program, N.I.S.T., the Welch Foundation, and the N.S.F. R.G.H. is an Alfred P. Sloan Research Fellow.

1. V.G. Minogin and O.T. Serimaa, *Opt. Commun.* **30**, 373 (1979).
2. J. Dalibard and C. Cohen-Tannoudji, *J. Opt. Soc. Am. B* **2**, 1707 (1985).
3. E. Kyrölä and S. Stenholm, *Opt. Commun.* **22**, 123 (1977).
4. S. Haroche and F. Hartmann, *Phys. Rev. A* **6**, 1280 (1972).
5. M. Prentiss and A. Cable, *Phys. Rev. Lett.* **62**, 1354 (1989).
6. J.J. Tollett, J. Chen, J.G. Story, N.W.M. Ritchie, C.C. Bradley and R.G. Hulet, submitted for publ.
7. N.P. Bigelow and M.G. Prentiss, submitted for publ.

III. NONLINEAR PHYSICS AND CHAOS

ATOMS IN STRONG FIELDS:
CHAOTIC DYNAMICS, LOCALIZATION, AND "SCARS"

R.V. Jensen

Applied Physics, Yale University

New Haven, CT 06520

Recent experimental studies of atoms in intense laser fields, strong static magnetic fields, and strong microwave fields have opened up an exciting new frontier of atomic physics. These experiments have uncovered a variety of new physical phenomena in strongly perturbed or strongly coupled quantum systems that have challenged atomic theory. In particular new theoretical ideas and methods from classical nonlinear dynamics, nuclear physics, solid-state physics, and chemical physics have been introduced to improve upon the conventional (perturbative) methods of atomic physics.

This Poster will provide an introduction to some of these new ideas that have had important applications in explaining the extensive experimental studies of the microwave ionization of Rydberg atoms^{1,2} and of the photo-absorption spectrum of Rydberg atoms in strong static magnetic fields^{3,4}. Particular emphasis will be placed on the quantum mechanisms that mimic classical *chaos*⁵, the quantum interference effects that suppress the chaotic dynamics in analogy with Anderson *localization* in solid-state physics^{6,6}, and the quantum coherence that leads to highly structured wavefunctions that appear to *scar* the paths of unstable classical orbits.^{7,8}

In addition I will present new results of applying these ideas and methods to the description of models of ground-state atoms in intense laser fields and to "chaotic" scattering problems in atomic, molecular, and solid-state physics. Finally, I will indicate how the many lessons learned from these experimental and theoretical studies in atomic physics promise to lead in turn to new results in classical, chemical, solid-state, nuclear, and perhaps even elementary particle physics.

1. E.J. Galvez, B.E. Sauer, L. Moorman, P.M. Koch, and D. Richards, Phys. Rev. Lett. **61**, 2011 (1988).
2. J.E. Bayfield, G. Casati, I. Guarneri, and D.W. Sokol, Phys. Rev. Lett. **63**, 364 (1989).
3. J. Main, G. Wienbush, A. Holle, and K.H. Welge, Physical Review Letters **57**, 2789 (1986).
4. G.R. Welch, M.M. Kash, C. Iu, L. Hsu, and D. Kleppner, Phys. Rev. Lett. **62**, 1975 (1989).
5. G. Casati, B.V. Chirikov, and D.L. Shepelyansky, Phys. Rev. Lett. **53**, 2525 (1984);
6. R.V. Jensen, S.M. Susskind, and M.M. Sanders, Phys. Rev. Lett. **62**, 1476 (1989).
7. R.V. Jensen, M.M. Sanders, M. Saraceno, B. Sundaram, Phys. Rev. Lett. **63**, 2771 (1989).
8. D. Wintgen and A. Hönig, Phys. Rev. Lett. **63**, 1467 (1989).

NONLINEAR OPTICAL INTERACTIONS
INVOLVING THE REAL GAUSSIAN FIELD

Chen Xie, G. Klimeck, Ce Chen and D. S. Elliott
School of Electrical Engineering, Purdue University
West Lafayette, IN 47907 USA

We have developed a method of generating a field whose amplitude is a randomly fluctuating variable, known as the real Gaussian field, as a means of testing the effect of the laser bandwidth on nonlinear optical interactions. The frequency of this field is constant, and its amplitude, restricted to real values, varies about a mean value of zero. (The amplitude is positive as often as it is negative.) This field differs from thermal light in that the amplitude of the latter is complex. The amplitude fluctuations of the real Gaussian field can be shown to be larger than those corresponding to thermal light. To generate the real Gaussian field, we use a stabilized c.w. tunable dye laser, whose output we modulate using an acousto-optic modulator (AOM). We drive the AOM using an r.f. signal whose amplitude is randomly modulated using an r.f. mixer. We have measured the intensity auto-correlation function of the light using a photodiode, oscilloscope and digitizing camera, and show that it has an initial value between 2.3 and 2.8 (expected value is 3) and decreases to a final value of one with a decay time inversely related to the laser bandwidth.

We are now measuring the effect of this field on nonlinear systems. The first is the 3S-5S two-photon resonance in atomic sodium. This two-photon interaction depends on the intensity auto-correlation function referred to above. (In general, two-photon absorption depends on a different fourth-order correlation function of the field.) Enhancement of the two-photon absorption rate by a factor of three is expected when compared to the absorption rate from a monochromatic field of the same average intensity.

The real Gaussian field is also being applied to studies of the transmission through a Fabry-Perot interferometer. The response of the interferometer is expected to be similar to that of an atomic system for weak fields. Although an interferometer is

a linear device, the fluctuations of the intensity transmitted it induced by fluctuations of the incident field are dependent upon higher order field properties. The intensity spectrum is expected to consist of peaks centered at zero frequency, and at the difference between the laser frequency and the peak of the interferometer transmission.

This work is supported by the Department of Energy, Office of Basic Energy Sciences.

MULTIPHOTON TRANSITIONS IN NON-MONOCROMATIC FIELDS

J. C. Camparo¹ and P. P. Lambropoulos²

¹ Chemistry and Physics Laboratory
The Aerospace Corporation
2350 East El Segundo Blvd., El Segundo, CA 90245

² Physics Department
University of Southern California
University Park, Los Angeles, CA 90089

Multiphoton interactions are fundamentally non-linear, and as such they exhibit a strong dependence on the stochastic properties of the laser radiation. This involves not only the bandwidth, but also many (often infinitely many) correlation functions of the field. The effects are particularly important for resonant multiphoton transitions under conditions of saturation. Then, a number of fundamental quantities such as AC Stark splittings and/or shifts are changed profoundly.

Most of the understanding of these phenomena is based on two extreme models: The Phase Diffusion Field and the Chaotic Field. The Phase Diffusion Field has a random phase, but stable amplitude, and is useful for the study of bandwidth effects. Furthermore, it readily lends itself to simple analytical solutions. In contrast, the Chaotic Field has severe amplitude fluctuations, exhibits photon bunching, and has application in understanding the role of higher order correlation functions in radiative interactions. We have initiated a different approach to the study of this problem based on direct Monte-Carlo simulation of the field fluctuations. As will be shown, the Monte-Carlo's Model Field is flexible, and can take on stochastic characteristics that span the range between the Phase Diffusion and Chaotic Fields. Therefore, the results from these Monte-Carlo simulations are complimentary to those obtained with the Phase Diffusion and Chaotic Fields, providing a much needed bridge between them.

In this presentation we describe the Monte-Carlo approach, the stochastic properties of our Model Field, and some of our recent results on the AC Stark shift of a 2-photon transition. Taking $\delta\omega_s$ as the AC Stark shift due to the *stochastic* field, and $\delta\omega_m$ as the AC Stark shift due to a *monochromatic* field of the same average intensity, we define a Modification Parameter M as their ratio:

$$M = \delta\omega_s / \delta\omega_m$$

For a Phase Diffusion Field $M = 1$, and for a weak Chaotic Field $M = 3$. As illustrated in Fig. 1, our Monte-Carlo results show the behavior of M as fields change from Phase Diffusion to Chaotic. In particular, we find that M is a function of the Rabi frequency, and that for strong stochastic fields M can actually be less than unity.

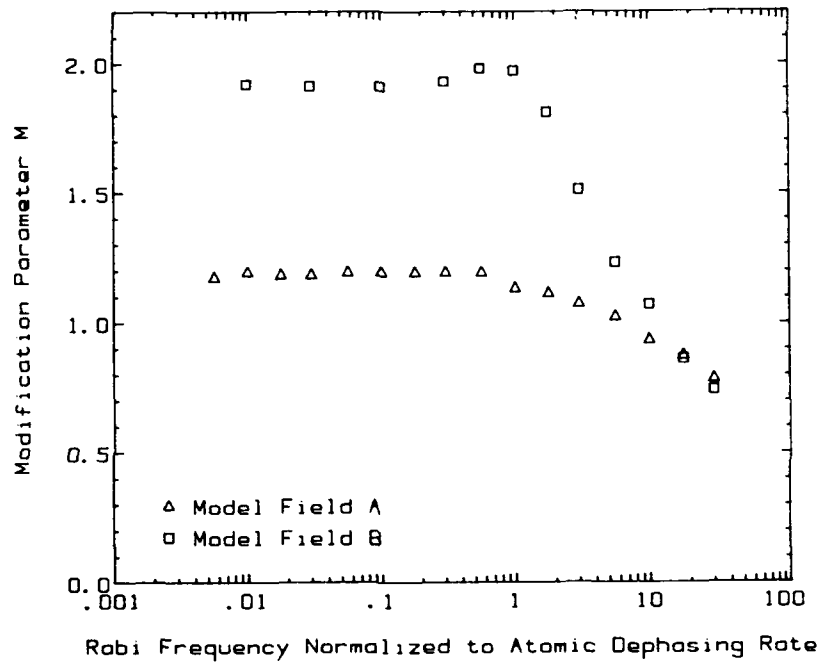


Figure 1: Modification Parameter M vs. Rabi Frequency
 Model Field B is closer to a Chaotic Field in its stochastic characteristics than A.

PHASE-SENSITIVE ABOVE-THRESHOLD IONIZATION AT 8 GIGAHERTZ.

D.A. Tate, D.G. Papaioannou and T.F. Gallagher
Department of Physics, University of Virginia,
Charlottesville, Virginia, 22901, USA.

When potassium atoms are excited to the region of the ionization limit in the presence of a strong microwave field, the ejected electrons are observed to have energies between one and three times the ponderomotive energy. We have phase locked a microwave field to the 108th harmonic of the repetition frequency of a mode locked laser, allowing excitation of Rydberg states by 5ps pulses at well defined phases of the microwave field. If the excited level is high enough in energy that it ionizes by the mechanism of field ionization, we can create free electrons effectively instantaneously with a time uncertainty which is much less than one period of the microwave field. We observe an obvious dependence of the ejected electron's energy and direction on the phase of the microwave field at which it became free of the atom. This work has been supported by AFOSR.

ATTRACTOR GEOMETRY OF A QUASIPERIODICALLY PERTURBED
TWO-LEVEL ATOM

J. C. Camparo and R. P. Frueholz

Chemistry and Physics Laboratory
The Aerospace Corporation
2350 East El Segundo Blvd., El Segundo, CA 90245

The response of matter to rapid, deterministic electromagnetic field fluctuations is an area of considerable present interest, spanning many different disciplines. Yet despite the activity in this area, it is nonetheless difficult to draw *general* conclusions concerning the dynamical behavior of quantum systems in the presence of rapidly fluctuating fields. The reason for this situation is not difficult to understand: as soon as the pattern of fluctuations becomes at all detailed, the dynamical complexity of even the simplest quantum system becomes excessive. Consequently, it becomes difficult to categorize, let alone quantify, the quantum system's temporal evolution as a function of various physical parameters like field-matter interaction strength.

In this presentation we consider what is sometimes referred to as a "kicked quantum system" from the perspective of dynamical systems theory. In the present case this kicked quantum system takes the form of a two-level atom interacting with a quasiperiodic, resonant field. The quasiperiodic nature of the field comes from the fact that the field's phase is time dependent, varying as the sum of a sinusoid and a square-wave with incommensurate frequencies. As will be shown, even though the atom's temporal evolution is exceedingly complex, the analytical tools of dynamical systems theory allow an investigation of the atomic dynamics as a function of field-atom interaction strength.

Including phenomenological relaxation rates into the Optical Bloch equations, the attractor for the atomic system is found to exist in a four dimensional phase space composed of the three Bloch vector components and the field's phase angle. To analyze the attractor, and hence the atomic dynamics, we employ two tools typically applied to the study of nonlinear, chaotic systems. Specifically, we consider Poincare sections obtained at various planes in the three dimensional Bloch space, and the Grassberger-Procaccia correlation integral. The former provides a visual representation of the atomic dynamics, while the latter yields a quantitative measure of the attractor's geometry.

We find that there are basically only two types of attractor geometry, which are differentiated by the degree of adiabaticity associated with the field's variations. Further, in the regime of adiabatic dynamics the attractor shows evidence of a non-integer scaling dimension. We attribute the attractor's fractal nature to the scaling behavior of Bloch vector trajectories in the rotating reference frame. Experiments are now in progress to validate the computational predictions.

INDUCED CHAOTIC AMPLITUDE VARIATIONS IN A HYDROGEN MASER

Ronald L. Walsworth

Lyman Laboratory of Physics, Harvard University, Cambridge, MA 02138

Edward M. Mattison and Robert F.C. Vessot

Smithsonian Astrophysical Observatory, Cambridge, MA 02138

In recent years, period doubling, quasiperiodicity, and deterministic chaos have been observed in many physical systems, and theoretical analyses have uncovered the universal nature of such seemingly random or noisy behavior. Chaos in active electromagnetic oscillators, including optical and infrared lasers and ruby masers, has been extensively studied, but has not been observed in hydrogen (H) masers. Chaos in lasers and masers is a fruitful area of research because such oscillators are accessible examples of complex systems far from thermal equilibrium and because of the implications for laser and maser performance. The quantitative modeling of the experimental results is still in its infancy, however, as few lasers or masers exhibiting chaos fully conform to the simplistic models used to analyze their dynamics.

Recently, Maan and co-workers [1] have determined the conditions under which a free-running H maser might exhibit chaotic behavior in its signal amplitude, and have found it to be feasible only at low temperatures, in a cryogenic H maser. We report here, however, an analysis that shows that chaotic behavior is possible in a room temperature H maser with a periodic modulation of a system parameter such as the maser transition linewidth. We also present preliminary experimental results of induced chaotic and other nonlinear amplitude variations in an H maser. An H maser could serve as a good test system, or paradigm, for the study of chaos in lasers and masers. Quantitative comparisons of theory and experiment are feasible with an H maser, since the system parameters can be accurately determined and controlled and since maser behavior is well described by the familiar Maxwell-Bloch equations. New ideas for the control or application of chaos might also be tested in a chaotic H maser. In addition, future work could assess the significance of nonlinear behavior on the performance of H masers as clocks, examining the likelihood that changing environmental conditions could induce unexpected variations in the maser signal.

-
1. A.C. Maan, H.T.C. Stoof, B.J. Verhaar, and Paul Mandel, *Phys. Rev. Lett.* **64**, 2630 (1990).

IV. QUANTUM OPTICS AND OTHER
LASER TECHNIQUES

SATURATION LINESHAPES IN PHASE CONJUGATION BY NON-COLLINEAR WAVE MIXING

O. di Lorenzo-Filho, P.C. de Oliveira and J.R. Rios Leite
Departamento de Física, Universidade Federal de Pernambuco
50.739 - Recife, PE, Brazil

Saturation effects in phase conjugation produced by degenerate resonant wave mixing on Doppler broadened transitions have been studied in a variety of circumstances [1]-[5]. All these works, whether experimental or theoretical consisted in quasi-collinear configuration and had the pump beams as saturating fields.

Herein we present the theoretical and experimental case where the two counterpropagating pump beams are weak and the saturation occurs by the object beam, usually called the probe beam. For small angle θ (see Figure 1) the forward pump and the object pump are interchangeable and the saturation effects known [3]. In a Doppler broadened two-level system medium with a homogeneous linewidth γ and Doppler with ku , wide angle corresponds to $\theta > \gamma/ku$. In such circumstances, the third order density matrix calculation [6] predicts lineshapes broadened from γ to ku as θ grows from zero to 90° . Such behaviour was verified for SF_6 [7] which behaves as an effective two level system while optical pumping has been properly invoked to explain different results for Na vapor [8].

Numerical solutions, with planar velocity integrations were done for the density matrix equations of a two-level system. While the object beam, incident at θ , is treated exactly within the rotating wave approximation, the two counterpropagating pump beams are taken as first order perturbations. Figure 2 shows the results for the lineshapes when all relaxation rates are taken as equal.

At the onset of saturation a single peak is obtained for $\theta \approx 0$ while a splitted line results for $\theta > \gamma/ku$. Such splitting can not be attributed to the usual dynamical Stark splitting because it is due to the different weighted contributions of third and fifth order (and higher) under double velocity integration.

Experiments to verify the predicted lineshapes were done on low pressure SF_6 with a cw CO_2 laser. The SF_6 cell was 5cm long and the laser beams had 2cm diameter. Detection was obtained with an $HgCdTe$ photodiode and a lock-in amplifier, synchronized to a mechanical chopper cutting the object beam at 800Hz.

The agreement between theory and experiment, evidenced by figures 2 and 3, is very good. The signal lineshapes were calculated using the parameters corresponding to the SF_6 experiments, including a cylindrical beams overlap correction factor. Further experimental and theoretical results, showing dynamical Stark splitting effects and their angular dependence and Doppler-free spectral lines at wide angles, will be published elsewhere.

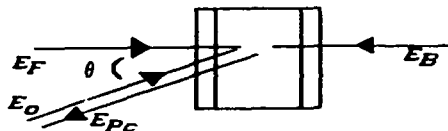


Fig 1: Scheme of phase conjugation by four wave mixing.

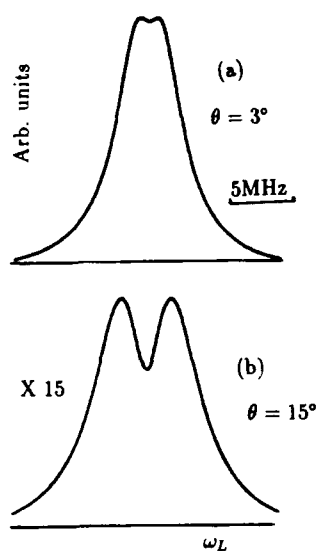


Fig 2: Numerical calculation of phase conjugation signals using $\gamma/ku = 1/10$ and $(\mu E_0/h\gamma)^2 = 0.2$

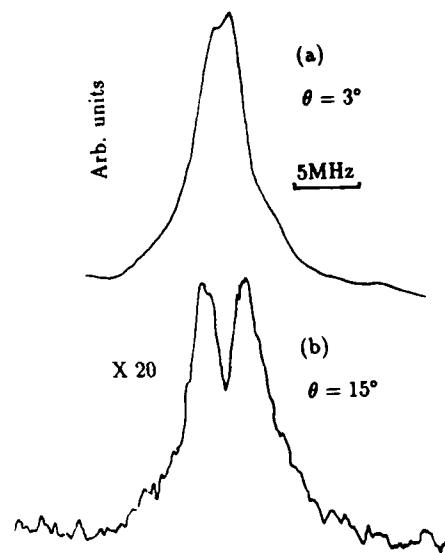


Fig 3: Experimental lineshape for the $10^2(18) CO_2$ line conjugation on SF_6 at 200 mTorr. In both figures (a) and (b), $I_F = I_B = 70mW/cm^2$ and $I_0 = 100mW/cm^2$.

References

- [1] J.P. Woerdman and M.F.H. Shuurmans; *Optics. Lett.* **6**, 239, 1981.
- [2] S. Le Boiteaux, P. Simoneux, D. Bloch, F.A.M. de Oliveira and M. Ducloy; *IEEE J. Quantum. Electronics QE-22*, 1229 (1986) (see references therein).
- [3] M. Ducloy and D. Bloch; *Optics. Commun.* **47**, 351 (1983).
- [4] G. Grynberg, M. Pinard and P. Verkerk; *Optics. Commun.* **50**, 261 (1984).
- [5] J.W.R. Tabosa, O. di Lorenzo-Filho, G. Grynberg and J.R. Rios Leite; *Europhys Lett.* **9**, 29 (1989).
- [6] M. Ducloy and D. Bloch; *J. Phys.* **42**, 711 (1981).
- [7] C.L. Cesar, J.W.R. Tabosa, P.C. de Oliveira, M. Ducloy and J.R. Rios Leite; *Optics. Lett.* **13**, 1108 (1988).
- [8] L.M. Humphrey, J.P. Gordon and P.F. Liao; *Optics. Lett.* **5**, 56 (1980).

Inhibited spontaneous emission and thresholdless microlasers

Y. Yamamoto, S. Machida and G. Björk*
 NTT Basic Research Laboratories
 Musashino-shi, Tokyo 180, Japan

A laser builds up a coherent radiation starting from spontaneously emitted photons. An atom usually emits a photon into a random direction and in a broader spectral width than the laser cavity linewidth. Thus, the coupling efficiency $\beta \equiv E_{c,v}/R_{sp}$ of spontaneous emission into a single-lasing mode is extremely small. At the oscillation threshold, the stimulated emission rate $E_{c,v}n$ must exceed the total spontaneous emission rate R_{sp} , so the number of photons n should be greater than $1/\beta$. The differential quantum efficiency jumps from β to 1 at the threshold. A typical value of β is 10^{-4} to 10^{-6} for semiconductor lasers and is 10^{-8} to 10^{-10} for other lasers. A laser is a macroscopic system in the sense that the number of photons n inside a cavity is 10^4 to 10^{10} even at pump rates just above the threshold. However, the threshold behavior disappears if the spontaneous emission into all modes except that into the single-lasing mode is inhibited by the cavity QED principle^[1]; that is, if the coupling efficiency β is increased to 1, as shown in Fig. 1. Even when the average number of photons is much smaller than 1, the differential quantum efficiency β is close to 1.

It is theoretically and experimentally demonstrated that the microcavity structure shown in Fig. 2 allows spontaneous emission to occur only into a single-cavity mode which propagates in a vertical direction. A 7.5-nm thick GaAs quantum well is embedded at the center of an $\text{Al}_{0.2}\text{Ga}_{0.8}\text{As}$ one-wavelength (260 nm) cavity layer, which is sandwiched between distributed Bragg reflectors consisting of twenty alternate quarter-wavelength layers of AlAs and $\text{Al}_{0.2}\text{Ga}_{0.8}\text{As}$. The spontaneous emission from the GaAs quantum well in the microcavity is almost all in the cavity mode, while the spontaneous emission from an ordinary GaAs quantum well embedded in thick $\text{Al}_{0.2}\text{Ga}_{0.8}\text{As}$ layers is isotropic, as shown in Fig. 3. The spontaneous emission intensity for the cavity mode is enhanced by a factor of 130 and those for other radiation continuum modes are suppressed by a factor of 1/30. Even though the present microcavity is still leaky, β can be increased to 0.95 by increasing the refractive-index difference of the DBR up to $\Delta n \equiv (n_1 - n_2)/n_1 = 0.64$.

One interesting feature of such a microcavity semiconductor laser is its quantum noise property. A constant current driven semiconductor laser produces a number-phase squeezed state at pump rates well above the oscillation threshold.^[2] At pump rates below the threshold, a small quantum efficiency destroys squeezing. At pump rates near the threshold, amplified spontaneous emission destroys squeezing. These two noise sources can be eliminated in such a microcavity laser with $\beta \simeq 1$. If a single electron is regularly injected into such a microcavity laser using the Coulomb blockade principle,^[3] a single photon state is generated.

*Permanent address: The Royal Institute of Technology, Stockholm, Sweden

References

- [1] D. Kleppner, Phys. Rev. Lett. 47, 233 (1981)
- [2] S. Machida and Y. Yamamoto, Phys. Rev. Lett. 60, 792 (1988)
- [3] M. Ueda and Y. Yamamoto, Phys. Rev. B41, 3082 (1990)

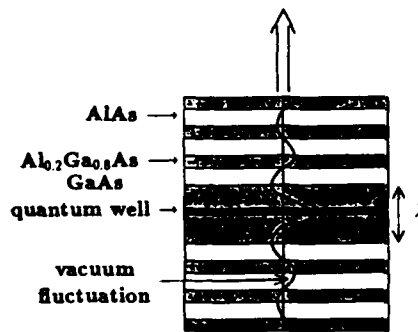
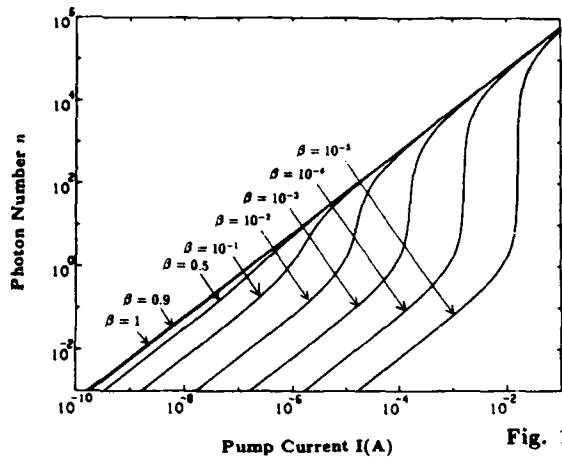


Fig.

Fig. 1 Internal photon number n vs. pump current I as a function of spontaneous emission coefficient β . $n_{sp} = 1$ and $\gamma = 10^{12} s^{-1}$.

Fig. 2 Microcavity semiconductor laser.

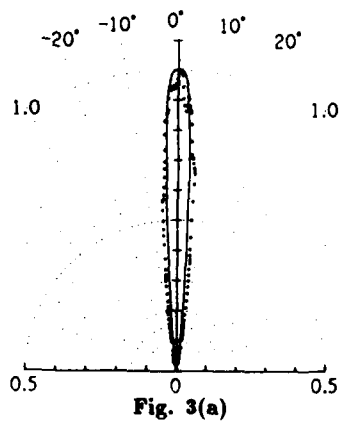


Fig. 3(a)

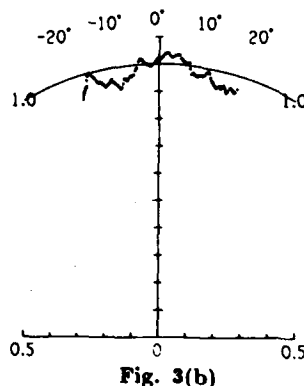


Fig. 3(b)

Fig. 3 (a) Experimental and theoretical radiation patterns from a GaAs quantum well in a one-wavelength microcavity. $\lambda_e = \lambda_0 = 800$ nm. (b) Experimental and theoretical radiation patterns from a GaAs quantum well in a thick $Al_{0.2}Ga_{0.8}As$ layer.

NEW ASPECTS OF HOLSTEIN'S TREATMENT OF RADIATION TRAPPING.

W. Falęcki¹ and W. Hartmann
 Physikalisches Institut der Universität Tübingen
 Morgenstelle 14, D-7400 Tübingen,
 Federal Republic of Germany.

The fluorescent light from atomic states that have been excited by a short pulse of light does not show a pure exponential decay if photons are reabsorbed and reemitted several times by other atoms of the sample i.e. if radiation trapping is present.

Usually, the Holstein-Bibermann [1,2] integro-differential equation is used to investigate these effects theoretically:

$$\frac{\partial n(\vec{r}, t)}{\partial t} = -(1/\tau)n(\vec{r}, t) + (1/\tau) \int_{Vol} G(\vec{r}, \vec{r}') n(\vec{r}', t) dV(\vec{r}'), \quad (1)$$

$n(\vec{r}, t)$ denotes the concentration of excited atoms, τ is the natural lifetime of the excited state and $G(\vec{r}, \vec{r}')$ is the probability that the photon emitted in \vec{r}' will be reabsorbed in \vec{r} . Solutions of (1) are frequently [1,3] given as a superposition of diffusion modes $n_i(\vec{r}) \exp(-\beta_i t)$:

$$n(\vec{r}, t) = \sum_{i=0}^{\infty} c_i n_i(\vec{r}) \exp(-\beta_i t). \quad (2)$$

From 2 the observed signal $S(t)$ can be found:

$$S(t) = const \sum_{i=0}^{\infty} \alpha_i \exp(-\beta_i t) \quad (3)$$

where $\alpha_i \propto \int n_i(\vec{r}) d\vec{r}$.

Another approach describes $S(t)$ by a sum of fractional signals S_n originating from photons that were scattered n times during their random flight to the detector [4].

$$S(t) = \sum_{n=0}^{\infty} S_n(t) = const \sum_{n=0}^{\infty} (a_n/n!) (t/\tau)^n \exp(-t/\tau) \quad (4)$$

The coefficients a_n of (4) can be interpreted as the probabilities that the photon was scattered exactly n times within the absorbing medium. In a broad variety of situations this coefficients can be calculated with Monte-Carlo procedures which are very flexible

¹Permanent address: Instytut Fizyki Uniwersytetu Jagiellońskiego, ul. Reymonta 4, PL-30-059 Kraków, Poland.

and can include various parameters as eg. line profile, geometry of the experiment, anisotropy of scattering process. The a_n 's may also be determined from Holstein's ansatz [5] by comparing (3) and (4):

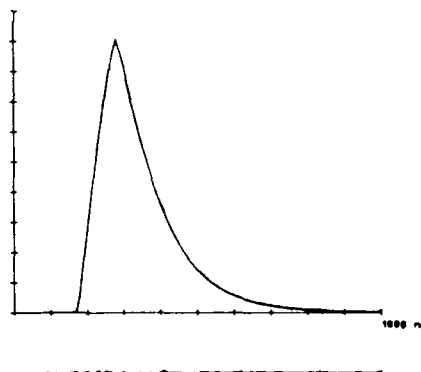
$$a_n = \frac{\tau}{\sum_{i=0}^{\infty} (\alpha_i/\beta_i)} \sum_{i=0}^{\infty} \alpha_i (1 - \tau\beta_i)^n. \quad (5)$$

As an example and as a comparison with experiments we calculate the a_n s using a simple one dimensional model, which can be solved analytically. We use a photon mean free path and a frequency independent average absorption coefficient k . In such a case the probability $G(\vec{r}, \vec{r}')$ of (1) can be expressed as $G(x, x') = 0.5k \exp(-k|x - x'|)$.

It was shown that for opacities up to about three the one dimensional model reproduces very well the a_n s calculated with the Monte-Carlo simulations of isotropic diffusion of photons with the Doppler profile of the absorption line taken into consideration [6].

To test the one dimensional model we performed experiments. The $5^2P_{3/2}$ state of rubidium was excited by pulses of light (780nm) from a laser diode. The rubidium vapour was placed in a cylindrical cell containing the natural mixture of rubidium isotopes. The time resolved fluorescence from the $5^2P_{3/2}$ level was recorded with the time resolution of 10ns. The following figure shows the comparison of a measured signals with a theoretical one.

Figure 1: Time resolved fluorescence signal from the $5^2P_{3/2}$ state of rubidium at 65°C. The natural lifetime of this state is 25.5 ns. The laser pulse duration was 100ns. The calculated mean number of scatterings of photons in the cell in presented case was about 3.6.



1. T. Holstein, Phys. Rev. **72**, 1212 (1947)
2. L. M. Biberman, Zh. Eksp. Teor. Fiz. **17**, 416, (1947)
3. C. van Trigt, Phys. Rev. **181**, 97 (1969), Phys. Rev. A **13**, 726 (1976)
4. P. Wiorkowski, W. Hartmann, Opt. Commun. **53**, 217 (1985)
5. W. Fałęcki, W. Hartmann, to be published
6. W. Fałęcki, W. Hartmann, W. Wiorkowski, Z. Phys. D **14**, 111 (1989)

USE OF ATOMIC FREQUENCY MIXING EFFECTS FOR FREQUENCY
STABILIZATION OF LASER DIODES IN EXPERIMENTS WITH TWO-PHOTON
STEP BY STEP EXCITATION.

W. Falecki¹, W. Hartmann and R. Strobel
Physikalisches Institut der Universität Tübingen
Morgenstelle 14, D-7400 Tübingen,
Federal Republic of Germany.

We performed experiments using laser two photon stepwise excitation of the $5^2D_{5/2}$ state of Rb via the transitions $5^2S_{1/2} \rightarrow 5^2P_{3/2}$ ($\lambda_1 = 780nm$) and $5^2P_{3/2} \rightarrow 5^2D_{5/2}$ ($\lambda_2 = 775.7nm$) (Fig.1). Two laser diodes were used, and it was necessary to stabilize both lasers to the respective transitions.

Usually this stabilization is effected by frequency modulating the lasers L_1 and L_2 at different reference frequencies f_1 and f_2 , and the (absorption or emission) signals associated with the transitions λ_1 and λ_2 are used to derive lock in signals which control the laser wavelength λ_{L_1} and λ_{L_2} i.e. two independent stabilizing loops at two different frequencies f_1 and f_2 are used.

This method anticipates that the $5^2S_{1/2} \rightarrow 5^2P_{3/2}$, $5^2P_{3/2} \rightarrow 5^2D_{5/2}$ two photon transition consists of two independent step transitions in the sense that the transition probability to the $5^2D_{5/2}$ state is proportional to the product of the transition probabilities of the consecutive steps.

$$P_{SD} \propto P_{SP} \cdot P_{PD} \propto \frac{1}{(\omega_{SP} - \omega_{L_1})^2 + \Gamma_1^2} \cdot \frac{1}{(\omega_{PD} - \omega_{L_2})^2 + \Gamma_2^2}$$

where ω_{SP} , ω_{PD} represent the respective transition frequencies and ω_{L_1} , ω_{L_2} are the frequencies of the laser light beams.

We used another method to stabilize both lasers to their respective transitions. The current through the first laser L_1 was modulated at a reference frequency $f_1 = 9kHz$ with an amplitude resulting in frequency modulation of a few hundred MHz. Lock-in detection of the Doppler broadened absorption signal of one of the four easily resolvable hyperfine structure components of the transition $5^2S_{1/2} \rightarrow 5^2P_{3/2}$ is used to produce the stabilizing signal. For laser L_1 this part of our set-up is similar to that described above.

The 775.7nm light from the second laser L_2 , however, is not modulated. The blue 420nm $6^2P_{3/2} \rightarrow 5^2S_{1/2}$ fluorescence from the cascade $5^2D_{5/2} \rightarrow 6^2P_{3/2} \rightarrow 5^2S_{1/2}$ is detected by use of a lock-in amplifier driven with the external reference frequency f_1 . The lock-in output as a function of the wavelength of the second laser L_2 is a dispersion curve, so that a stabilizing loop can be designed easily.

¹Permanent address: Instytut Fizyki Uniwersytetu Jagiellońskiego, ul. Reymonta 4, PL-30-059 Kraków, Poland.

This phenomenon indicates, that the $5^2S_{1/2} \rightarrow 5^2P_{3/2} \rightarrow 5^2D_{5/2}$ two photon transition occurs (partially) as a real two photon transition in the sense that second order perturbation theory must be used to calculate the $5^2S_{1/2} \rightarrow 5^2D_{5/2}$ transition probability [1,2]. Then the transition probability contains terms proportional to

$$\frac{1}{(\omega_{SP} + \omega_{PD} - \omega_{L_1} - \omega_{L_2})^2 + \Gamma^2} \quad (1)$$

If L_1 is frequency modulated ($\omega_{L_1} = \bar{\omega}_{L_1} + \delta_1 \cos f_1 t$) then the Taylor expansion of (1) results in a first order dispersion like signal synchronous with the reference frequency f_1 used to modulate the frequency of laser L_1 only.

$$\frac{2(\omega_{SP} + \omega_{PD} - \bar{\omega}_{L_1} - \omega_{L_2})}{((\omega_{SP} + \omega_{PD} - \bar{\omega}_{L_1} - \omega_{L_2})^2 + \Gamma^2)^2} \cdot \delta_1 \cos f_1 t$$

Since L_1 is locked to the $5S \rightarrow 5P$ transition ($\bar{\omega}_{L_1} = \omega_{SP}$) the dispersion curve above becomes

$$\frac{2(\omega_{PD} - \omega_{L_2})}{((\omega_{PD} - \omega_{L_2})^2 + \Gamma^2)^2} \cdot \delta_1 \cos f_1 t$$

this curve can be measured easily (Fig.2) and can be used to stabilize L_2 to the $5P \rightarrow 5D$ transition without modulating L_2 i.e. this method enables the stabilization of a laser frequency without additional distortions.

A more detailed theoretical and experimental investigation of this interesting nonlinear phenomenon will be presented at the poster session.

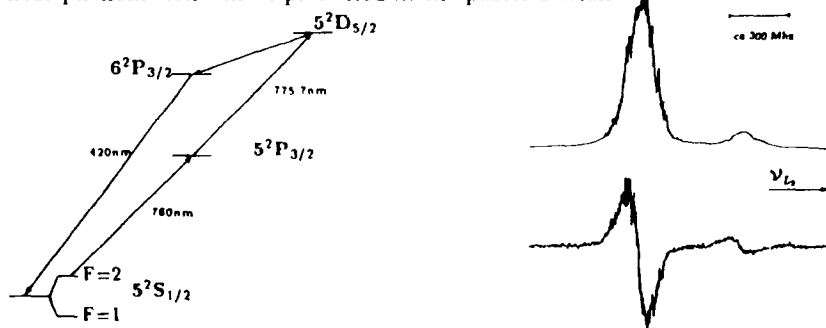


Figure 1: Scheme of involved transitions in Rb⁸⁷

Figure 2: The fluorescence 420nm light from transition $6^2P_{3/2} \rightarrow 5^2S_{1/2}$. The 780nm laser was locked to the Doppler broadened $5^2S_{1/2} \rightarrow 5^2P_{3/2}$ transition of Rb⁸⁷. Below the corresponding lock-in signals.

1. K.D. Bonin, T.J. McIlrath J. Opt. Am. B,1,52,1984.
 2. R. Loudon, The quantum theory of light, Clarendon Press, Oxford, 1973.

A PROPOSED COMPRESSION METHOD FOR A SPIN-POLARIZED
 ^3He NUCLEAR TARGET

L.D. Schearer and R. Vandiver
Physics Department, University of Missouri-Rolla
Rolla, MO 65401

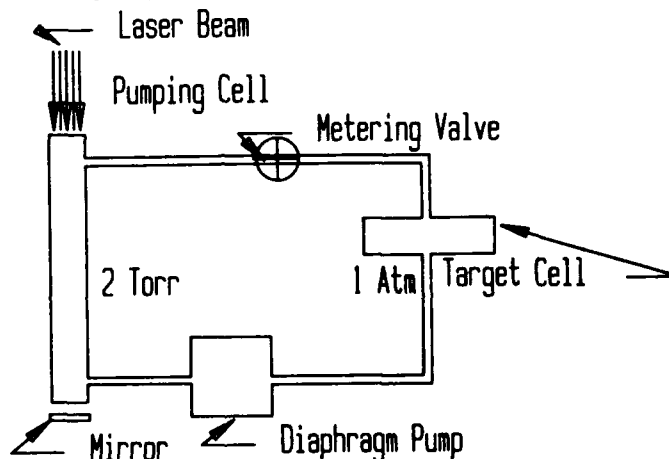
The application of optical pumping techniques to the mass-three isotope of helium results in a substantial nuclear polarization as demonstrated by Colegrove, et al. in 1963 [1]; its use as a nuclear target followed shortly [2]. Its wide application to nuclear scattering experiments was limited by the low polarization (10-20%) obtained with the helium discharge lamps used in the optical pumping process and the low densities (0.2-1 Torr) imposed by the method which first polarizes the helium metastable atoms and then depends on spin exchange collisions to transfer the angular momentum to the nuclear spin system. Both these limitations have now been removed and a number of important scattering experiments have been proposed [3].

New, tunable laser sources have been developed with 3 W or more available at the helium resonance lines to replace the discharge lamps; nuclear polarizations of 70% are now routinely available [4,5]. Higher densities can be obtained by cryogenic compression (40 Torr) [6,7] or mechanical compression [8]. Current methods of mechanical compression use a mercury Toepler pump which has some limitations, principally those associated with moving the mercury through the compression cycle. This requires the dissipation of large amounts of kinetic energy in the glass vessel. Nonetheless, a group at Mainz [9] has successfully demonstrated a Toepler pump target system obtaining compression ratios of more than 600:1 so that the method of mechanical compression is now established.

Our newly developed lasers are capable of producing polarized ^3He nuclei at a rate exceeding 10^{18} polarized nuclear spins per second. Thus, a 100 cm^3 sample at 1 atmosphere would require less than 1 hour to reach the equilibrium polarization, presumably 70% or greater. We have explored the use of other types of mechanical compression systems and mechanical/cryogenic combinations which potentially overcome the limitations mentioned above. We propose to use a multistage diaphragm pump as the first stage in the compression system. The Barodyn-100 pump, manufactured by Danielson Associates, Inc., for example, has a pumping speed of 2.5 CFM and an ultimate vacuum of 1.5 Torr. These pumps are oil-free and can be built to have leakage rates less than 10^{-6} Torr-liter sec^{-1} and consequently can be used in a closed system. Pumps are available with aluminum bodies internally coated with teflon. Pump dimensions are nominally $40 \times 32 \times 24$ cm. The target cell density can be further increased by cooling to LN2 temperatures. This has the added advantage that residual, volatile impurities may be trapped and prevented from reaching the

optical pumping region. The figure illustrates the use of such a pump in a closed system.

The pump cell is a 1 l ^3He -filled glass cell in which a weak discharge populates the metastable levels. The oil-free diaphragm pump circulates the gas and maintains a 1.5 Torr to 1 Atm. pressure differential across the metering valve. The all-glass target cell has a volume of 100 cm^3 . The cell can be cooled if additional density is desired. The pumping speed need only be large enough to ensure that all the atoms circulate through the system in a time shorter than the nuclear spin relaxation time. In a system free of magnetic impurities this can exceed 8 hours. The Barodyn-100 pump appears to satisfy all our requirements. The design is potentially very compact and is compatible with the accelerator environment of the nuclear scattering experiments. It should also be useful for internal target experiments and may find application in the design of a neutron spin filter.



1. F.D. Colegrove, L.D. Schearer, and G.K. Walters, *Phys. Rev.* **132**, 2561 (1963).
2. G.C. Phillips, R.R. Perry, P.M. Windham, G.K. Walters, L.D. Schearer, and F.D. Colegrove, *Phys. Rev. Lett.* **2**, 502 (1962).
3. *Workshop on Polarized ^3He Beams and Targets*, AIP Conference Proceedings no. **131** (1985).
4. C. G. Aminoff, C. Larat, M. Leduc, and F. Laloe, *Revue de Physique Appl.* **24**, 827 (1989).
5. Padetha Tin and L.D. Schearer, *J. Appl. Phys.*, to be published, Aug (1990).
6. M. Leduc, S.B. Crampton, P.J. Nacher, and F. Laloe, *Nuc. Sci. Appl.* **2**, 1 (1984).
7. R.G. Milner, R.D. McKeown, and C.E. Woodward, *Nucl. Instr. Meth.* **A257**, 286 (1987).
8. R.S. Timsit, J.M. Daniels, E.I. Dennig, A.K.C. Kiang, and A.D. May, *Can. J. Phys.* **49**, 508 (1971).
9. G. Eckert, W. Heil, M. Myerhoff, E.W. Otten, and L.D. Schearer, work in progress, University-Mainz, Germany.

**PHOTON STATISTICS IN RESONANCE FLUORESCENCE:
RESULTS FROM AN ATOMIC BEAM DEFLECTION EXPERIMENT**

M.D. Hoogerland, M.N.J.H. Wijnands, H.A.J. Senhorst,
H.C.W. Beijerinck and K.A.H. van Leeuwen
Physics Department, Eindhoven University of Technology,
P.O. Box 513, 5600 MB Eindhoven, The Netherlands

The statistical properties of the spontaneous radiation emitted by a driven two-level atom have been extensively studied theoretically. Mandel¹ pointed out the sub-Poissonian character of the distribution of the number of photons emitted in a given time. He derived a formula giving the normalized second factorial moment Q as a function of interaction time T and driving field intensity. In the limit of long interaction time (T much larger than the natural lifetime τ of the upper level) a simple relation, $Q = -3s/(1+s)^2$, is obtained, with s the saturation parameter. The minimum value, $Q = -3/4$, is obtained at $s = 1$. This corresponds to a width of the photon number distribution equal to half the width of a Poissonian distribution. Since then the theory has been extended to include detuning of the driving field frequency, finite bandwidth effects and analytical expressions for the complete photon number distribution.

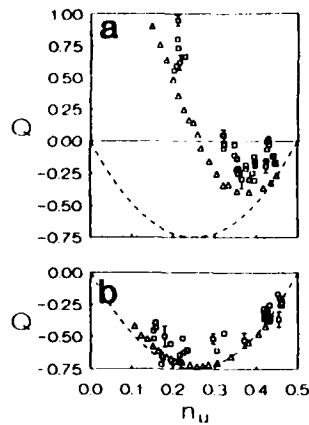
Experimentally, less information is available. After the first experimental result by Short and Mandel², so far the most extensive results from a photoncounting experiment have been reported for a transition between two levels in a three-level system prior to a quantum jump to the third level.³ The results confirmed Mandel's two-level formula. Cook⁴ suggested studying photon statistics by analyzing the radiation-pressure induced deflection of an atomic beam, using the simple relation between net momentum transfer and spontaneous emission.

We have performed an experiment along Cook's suggestion. A supersonic beam of ²⁰Ne atoms, partly excited in a discharge to the metastable $\{3s\}^3P_2$ state, is deflected by a laser beam (nearly resonant with the transition to the $\{3p\}^3D_3$ state ($\tau = 19.4$ ns) at 640 nm. This constitutes a closed-level system with only magnetic degeneracy. The atomic beam is collimated to $<10^{-4}$ rad. The beam profile after deflection is analyzed using a movable slit and an Auger type metastable atom detector. The atomic beam is chopped to enable time-of-flight velocity analysis of the deflected atoms. The laser beam, intersecting the atomic beam at right angles, has an approximate flat-top intensity profile over the 1.75 mm long interaction region.

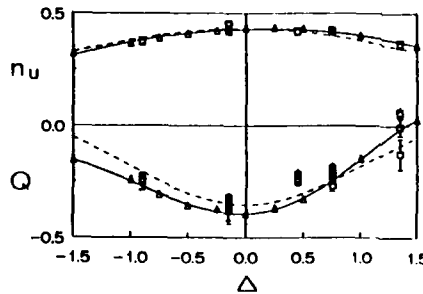
The Q -parameter is extracted from the atomic momentum spread of the deflected atomic beam in the direction of the laser beam using Eq. 2 from Ref. 4, which splits the momentum variance into contributions from the variance before deflection, from the variance of the photon number distribution and from the angular distribution of the spontaneous-emission induced recoils.

The comparison of experimental results with theory is complicated by the lack of a pure two-state system due to magnetic degeneracy. The atoms enter the interaction region in a statistical mixture of all substates of the metastable level. During the interaction time, the atomic ensemble evolves towards a steady state distribution which depends on the laser polarization. This evolution is easily calculated by density matrix techniques but the influence on the total photon number- and atomic momentum distributions is much more difficult to evaluate. The approach taken by us follows the Monte Carlo treatment of spontaneous emission and atomic momentum change for two-level atoms used by Blatt et al.⁵, extended to include magnetic degeneracy.

In Figs. 1^a and 1^b the on-resonance experimental results for the Q -parameter are shown together with the results of the Monte Carlo calculation for σ -polarization and π -polarization respectively. The Q -parameter is shown as a function of the average upper state population n_u , as determined from the average beam deflection. For a two-level system, the intensity dependence of the upper state population is given by $n_u = s/2(s+1)$ and Mandel's formula leads to the simple quadratic



1) Q as a function of upper state population n_u for a σ^+ and b π polarization. Squares: experiment. Triangles: Monte Carlo calculations. Dashed line: two level formula.



2) n_u (upper data) and Q (lower data) as a function of Δ . Squares: experiment. Triangles with full lines: Monte Carlo calculations. Dashed lines: two-level analytical formulae.

circular polarization, the differences are large

but agreement with experiment is still very good. expression $Q = 12 n_u (n_u - \frac{1}{2})$. Experimental results for both polarizations are seen to be in good agreement with the calculations, although the experimental results tend to be systematically somewhat too high. The agreement extends over the complete range of laser intensities (from $\approx 20 \mu\text{W}/\text{mm}^2$ to $\approx 800 \mu\text{W}/\text{mm}^2$). For linear polarization, the results are very close to the simple two-level, infinite interaction time Mandel formula (see the dashed lines in Fig. 1). However, for circular polarization Q is much higher. This is a direct consequence of the evolution from an equally populated statistical— towards a steady state substate distribution during the interaction time. Due to the small transition rates out of the negative M_j states under σ^+ excitation, the time scale of the evolution is of the same order as the interaction time. This produces an extra inhomogeneous broadening effect which drastically increases the width of the photon number and momentum distributions of the atomic ensemble.

The dependence of n_u and Q on the laser detuning $\delta\omega$ for linearly polarized light at fixed laser intensity ($\approx 400 \mu\text{W}/\text{mm}^2$) is shown in Fig. 2. Again, calculation and experiment are in excellent agreement, demonstrating the rapid increase in Q with increasing detuning. The asymmetry which is apparent in the curves is a consequence of the Doppler shift changing the effective laser detuning while the atomic beam is being deflected. In Fig. 3, Cook's analytical formula for Q as a function of detuning, $Q = -s(3 - \Delta^2)/(s + 1 + \Delta^2)^2$ for a two-level system is shown as well (with $\Delta = 2\tau\delta\omega$ the normalized laser detuning).

Summarizing, accurate measurements on photon number statistics using the atomic beam deflection technique have been performed. The predominantly sub-Poissonian character of the statistics has been confirmed. The Q -parameter has been measured for a wide range of driving field intensity and for a number of values of the laser detuning. The experimental dependency on these parameters is in good agreement with the results of calculations based on a Monte Carlo approach of spontaneous emission, which enables us to include in a simple way the effects of magnetic degeneracy in the neon $^3P_2 \rightarrow ^3D_3$ closed level system as well as those of finite interaction time and Doppler shift effects. For linear polarization, the results from the Monte Carlo calculation differ only slightly from the simple analytical formulae given by Cook and Mandel; for circular polarization, the differences are large

- 1) L. Mandel, *Optics Lett.* **4**, 205 (1979).
- 2) R. Short and L. Mandel, *Phys. Rev. Lett.* **51**, 384 (1983).
- 3) M.A. Finn, G.W. Greenlees, T.W. Hodapp and D.A. Lewis, *Phys. Rev. A* **40**, 1704 (1989).
- 4) R.J. Cook, *Optics Commun.* **35**, 347 (1980).
- 5) R. Blatt, W. Ertmer, P. Zoller and J.L. Hall, *Phys. Rev. A* **34**, 3022 (1986).

CALCULATIONS FOR THE HANLE EFFECT IN NON-MONOCROMATIC LASER LIGHT*

R. Ryan and T. Bergeman
 Physics Department, State University of New York
 Stony Brook, NY 11794 USA

Questions about the effects of non-monochromaticity in the excitation of atomic transitions by laser light have attracted growing interest. Recent experiments in this field have led to a renewed interest in models for light fields with phase and amplitude fluctuations and for the interaction of such fields with atoms. The Hanle effect represents the simplest example of an atomic transition between states with multiple sublevels. Experiments [1] have now demonstrated that an intense monochromatic laser field can preserve the coherence between the excited state sublevels and hence broaden the Hanle dip, and that this broadening decreases if the laser spectral bandwidth increases. However, the full range of possibilities was not evident because of the limited parameter range experimentally available at the time.

In this report, we solve the density matrix equations for a $J=0 \rightarrow J=1$ atomic transition in laser fields with phase or amplitude fluctuations using methods for stochastic differential equations developed by Dixit et al [2]. With phase fluctuations, the spectral profile varies between Lorentzian and Gaussian depending on the ratio of two parameters, β/b , where β is the cut-off of high-frequency fluctuations, and $2b$ is the laser FWHM in the Lorentz shape limit $\beta \rightarrow \infty$. Numerical simulations of the phase evolution for two extreme cases are shown for two typical realizations in Fig. 1. In the case of amplitude fluctuations [3], the bandwidth and rms amplitude vary, but the profile is always Lorentzian.

For a $J=0 \rightarrow J=1$ transition and the geometry often used for the Hanle effect (e.g., x-polarized excitation, y-polarized fluorescence, field in z direction) calculated signals for phase fluctuations and a laser bandwidth of 2.8Γ are shown in Fig. 2. Here $\Gamma=1/\tau$ is the radiative linewidth of the atomic transition and B_{H} is the Hanle HWHM for broadband excitation. At high fields, the fluorescence signal falls off because of detuning, and this fall-off is more rapid when the laser spectral shape is more nearly Gaussian (Fig. 2, top) than with a Lorentzian profile (Fig. 2, bottom). On the other hand, for a given FWHM, a Gaussian spectral profile concentrates more power within the half-height points, so the Hanle dip tends to broaden more rapidly with laser power than with a Lorentzian profile.

Also for phase fluctuations, the broadening of the Hanle dip as a function of laser intensity is shown in Figs. 3a and 3b. Fig. 3a shows the HWHM for purely Lorentz spectral profile ($\beta \rightarrow \infty$). Analogous curves for a more nearly Gaussian profile ($\beta/b = 0.01$ in each case) in Fig. 3b, show that over this range of intensity, laser spectral widths up to 10Γ give Hanle FWHM values very close to those from monochromatic excitation.

Hanle signals calculated for laser amplitude fluctuations exhibit much less power broadening for the same rms amplitude. Even in the monochromatic limit (long correlation time) there is a Gaussian distribution of field amplitudes, hence the averaging over amplitude produces a Hanle dip less than one-half as wide as that obtained for a monochromatic laser with no fluctuations. This may be seen by comparing the curve for a laser width of $10^{-3} \Gamma$ in Fig. 3c with the curve for

monochromatic excitation in Fig. 3a. Furthermore, Fig. 3c shows that Hanle widths for moderate laser bandwidths also tend to be less with amplitude fluctuations than with the phase diffusion model.

*Supported by the US NSF.

*Also at Grumman Corporate Research Center, Bethpage, NY 11714.

1. K. Arnett, S. Smith, R. Ryan, T. Bergeman, H. Metcalf, M. Hamilton, and J. Brandenberger, Phys. Rev. **A41**, 2580 (1990) and references cited.
2. S. Dixit, P. Zoller and P. Lambropoulos, Phys. Rev. **A21**, 1289 (1980).
3. A. T. Georges, Phys. Rev. **A21**, 2034 (1980).

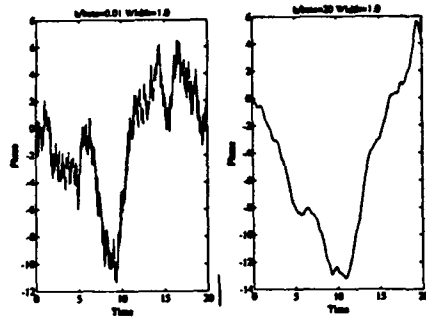


Fig. 1. Numerical simulation of phase noise for (left) Lorentzian profile - small b/β , and (right) Gaussian profile - small β/b .

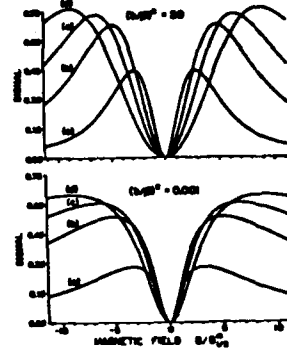


Fig. 2. Hanle signals calculated with laser bandwidth 2.8 times the atomic linewidth, with intensities a) 3.5, b) 18 c) 36, and d) 71 times the saturation value. Gaussian spectral profile at top, Lorentzian bottom.

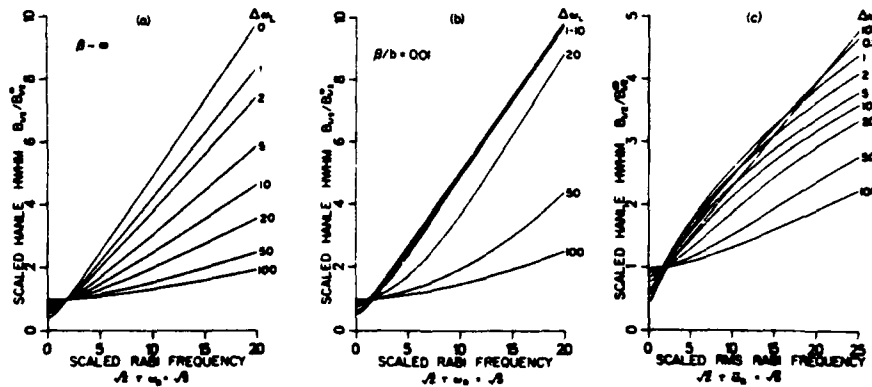


Fig. 3. Hanle HWHM (scaled) vs. scaled Rabi frequency for various laser spectral widths, for a) phase diffusion model, Lorentz lineshape; b) phase diffusion model, nearly Gaussian lineshape; c) amplitude fluctuation model.

RESONANCES IN 1D SCATTERING WITH ASYMPTOTICALLY LINEAR POTENTIALS:
A SIMPLIFIED MODEL OF ATOMS IN A QUADRUPOLE MAGNETOSTATIC TRAP

H. Sporn, T. Bergeman, and N. D. Balazs

Physics Department, SUNY, Stony Brook, NY 11794 USA

Cold atoms in a quadrupole magnetostatic trap [1] move in a potential that depends on the atom's magnetic sublevel and is linear to first order. Very near the zero of field at the origin, the atom can change its orientation with respect to the field, e.g., from a trapped to an untrapped state. This leads to a finite decay rate and hence a decay width for quantum levels of trapped atoms. [2] Although resonance energies and widths have been computed for $S=1/2$ atoms, certain questions remain. To shed light on various effects possible, we pose model problems of motion in two crossed linear potentials with a coupling element $\alpha(x)$:

$$V = \begin{pmatrix} x & \alpha(x) \\ \alpha(x) & -x \end{pmatrix}$$

We take $\alpha(x)$ to have the form either of a Gaussian or delta function. Similar potentials occur over small regions of internuclear distance in atomic collision phenomenon and in molecular curve-crossings, but here the interest is in resonant states in which the atom oscillates back and forth with minimum decay rate. Clearly, if $\alpha(x)$ for small x is large enough, very stable motion will occur over the "adiabatic" potential $V_{AD} = (x^2 + \alpha(x)^2)^{1/2}$.

Asymptotically, the potential is linear, hence the phase shift can be defined relative to a basis of Airy functions. Resonances occur where the derivative of the phase shift with energy is maximum, while the resonance width, $\Gamma = 2(d\delta/dE_{\max})^{-1}$. In Fig. 1, we plot the lowest odd and even parity resonance energies for $\alpha(x) = A \exp(-x/\gamma)^2$ for $\gamma=3.16$, as a function of the amplitude A , together with energy eigenvalues for adiabatic motion in the potential V_{AD} . It will be seen that as A increases, the resonance energies approach the adiabatic energy eigenvalues, as expected. Also, resonance widths decrease as A increases (not shown).

This type of problem generalizes previous discussion of one-dimensional scattering with one channel [3,4], in which resonances are often associated with maxima in the transmission coefficient, T . Normally $T=1$ at the resonance energy. The distinct feature of the resonances in Fig. 1 is that very near the resonance energy, an incoming wave from the left is reflected with unit probability, so that $T=0$ at this energy. This behavior is shown by comparing plots of $d\delta/dE$ (Fig. 2, bottom) with plots of the transmission coefficient, T (Fig. 2, top). We find also for certain simple two channel 1D problems with asymptotically constant potentials, $T=0$ very near a resonance. On the other hand, when $\alpha(x)$ approaches the $\gamma=0$ limit of a delta function, the more usual case of $T=1$ very near the resonance energy occurs, as shown in Fig. 3. Note also that for Gaussian coupling (Fig. 2), there is uniform spacing between successive resonances of odd and even parity, but for delta function coupling (Fig. 3) odd and even parity resonances are almost degenerate.

We hope to exploit these findings in further computations of quantum resonances in 3D magnetostatic traps.

*Supported by NSF and ONR grants to H. J. Metcalf.

1. A. Migdahl, J. Prodan, W. Phillips, T. Bergeman and H. Metcalf, Phys. Rev. Lett. 54, 2596 (1985).
2. T. Bergeman, P. McNicholl, J. Kycia, H. Metcalf, and N. Balazs, J. Opt. Soc. Am. 88, 2249 (1989).
3. A. Kahn, Am. J. Phys., 29, 77 (1961).
4. J. Eberly, Am. J. Phys., 33, 771 (1965).

Fig. 1. Resonance energies (solid line) for a particle in crossed linear potentials vs. the amplitude of the Gaussian coupling term compared with energy eigenvalues (dashed line) for the corresponding one channel adiabatic potential.

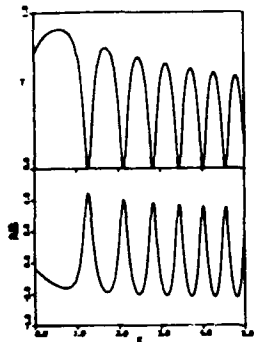
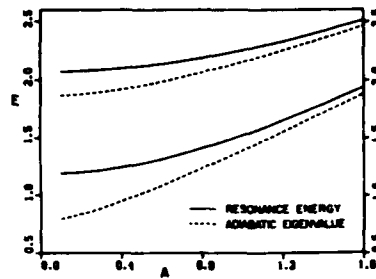


Fig. 2. Phase shift derivative (lower trace) and transmission coefficient, T, (upper trace) vs. energy for a particle in crossed linear potentials with a Gaussian coupling term. For this case, on resonance, $T=0$.

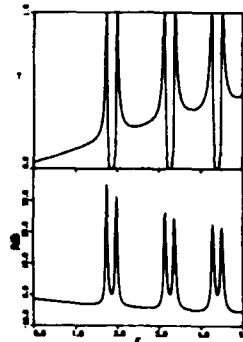


Fig. 3. Phase shift derivative (lower trace) and transmission coefficient (upper trace) vs. energy for a particle in crossed linear potentials with a delta function coupling term. Odd and even parity resonances are nearly degenerate, and for each, $T=1$.

MAGNETO-OPTICAL COMPRESSION OF SLOW ATOMIC BEAMS

J.Nellessen, G.Hennig, J.H.Müller, K.Sengstock, U.Spangenberg,
J.Werner and W.Ertmer
Institut für Angewandte Physik
Wegelerstr.8, D-5300 Bonn,FRG

Several schemes have been developed to decelerate, to cool and to deflect neutral atomic beams.

For many experiments with atomic beams, it is advantageous to reduce spatial spreading that is due to transverse diffusive heating during the deceleration process and to the initial beam divergence by further compression and simultaneous collimation of the deflected atomic beam. For this purpose the 2-D version [1,2] for the magneto-optical trap [3] seems to be an ideal tool. The feasibility of the scheme even for multilevel atoms is demonstrated by the compression of a slow monoenergetic sodium beam [1,4]. The scheme consists of two pairs of counterpropagating $\sigma^+ \sigma^-$ polarized laser beams irradiating the atomic beam at right angles within a superimposed transverse magnetic quadrupole field. Damping is accomplished by choosing a laser detuning of typically one-half of the natural linewidth to the red. The trapping mechanism is based on the circumstance that the linearly increasing magnetic field will shift that particular laser beam into resonance, which forces the atom back to the axis; in particular, on the symmetry axis of the magnetic field, the atomic velocities are damped out to zero (ordinary molasses). For an atom approaching the axis the difference between the radiation pressure forces is becoming weaker. Therefore, for optimum compression of an atomic beam, it is necessary to use a quadrupole magnetic field, the transverse field strength of which increases along the propagation direction of the atomic beam.

In our first experiments we used a quadrupole configuration with eight permanent magnets with a length of 40mm exhibiting field gradients starting starting from 50 to about 500G/cm on

axis. After laser deceleration of a sodium atomic beam by the chirp method [5] and subsequent deflection of the slow part of the beam the resulting monoenergetic beam with mean velocities ranging from 30 to 150m/s entered the transverse magneto-optical molasses region (MOM) with a diameter of several millimeters. Behind the MOM the beam was compressed down to $43\mu\text{m}$ at 50m/s in general agreement with Monte-Carlo simulations.

This beam is very attractive for many applications like e.g. cold collision experiments; at present we use this beam in experiments for atom interferometry.

Another interesting application will be a laser cooled magnesium beam. Magnesium has several interesting transitions, which are of great interest for optical or microwave atomic clocks [6]. It can be decelerated within about 11cm on its fast 285nm transition, using a tapered permanent magnet to compensate for the changing Dopplershift, as has been demonstrated in our lab recently [7]. To separate the cold part of this beam from the fast part and to recollimate the Mg-beam, we can use a MOM, which is tilted about 10° from the atomic beam axis, as has been confirmed by Monte-Carlo simulations.

- [1] J.Nellessen, J.Werner, W.Ertmer, Opt.Comm. in press
- [2] E.Riis, D.S.Weiss, K.A.Moler, S.Chu, Phys.Rev. Lett. 64,1658(1990)
- [3] E.L.Raab, M.Prentiss, A.Cable, S.Chu, D.E.Pritchard, Phys.Rev.Lett. 59,2631(1987)
- [4] J.Nellessen, J.H.Müller, K.Sengstock, W.Ertmer, J.Opt. Soc.Am. B6,2149(1989)
- [5] W.Ertmer, R.Blatt, M.Zhu, J.L.Hall, Phys.Rev. Lett. 54,996(1985)
- [6] W.Ertmer, R.Blatt, J.L.Hall, Prog.Quant.Electr. 8,249(1984)
- [7] G.Hennig, J.H.Müller, K.Sengstock, U.Spangenberg, W.Ertmer, to be published

**POLARIZATION GRADIENT COOLING: MULTIPOLE
INTERPRETATION OF LIGHT FORCES IN 3D-LASERFIELDS**

H.Wallis and W.Ertmer
Institut für Angewandte Physik, Universität Bonn
Wegelerstr.8, D-5300 Bonn, W.-Germany

Abstract:

Laser cooling of free atoms has been used to prepare extremely cold gases in the focus of three intersecting pairs of laser beams. At a very low atomic velocity new cooling mechanisms have been observed to result in temperatures below the standard "Doppler"-limit $k_B T = \Gamma/2$ of scattering force laser cooling. These mechanisms have been attributed to the lifting of the degeneracy of the magnetic sublevels of the ground state by the polarized laser fields¹. The modulation of the corresponding light shifts and/or the modulation of the atomic eigenstates produces a friction force, if the laser frequency is detuned red from the resonance. To analyze the spatial structure of the atomic eigenstates and levels in more detail also in 3D-fields, we investigate the dynamics of the atomic ground state in a low intensity approximation.

In this limit we can determine an effective ground state operator from an adiabatic elimination procedure:

$$H_{\text{eff}}(r) = \sum_{q,q'} \frac{d_q d_{q'}^\dagger E_q \cdot E_{q'}}{\hbar(\delta - i\Gamma/2)} = - \sum_{q,q'} \chi_{qq'} E_q \cdot E_{q'} \quad (1)$$

Here d and d^\dagger denote the lowering and raising atomic dipole operator, E and E^* the positive and negative frequency part of the laser electric field, δ the detuning from resonance and Γ the width of the excited state. The definition of the complex atomic susceptibility operator χ implied above

¹ J.Dalibard, C.Cohen-Tannoudji, *JOSA B* **6**, 2023 (1989); P.J.Ungar, D.S.Weiss, E.Riis, S.Chu, *JOSA B* **6**, 2058 (1989)

can be applied to arbitrary level schemes. (1) allows a simple description of light forces in arbitrarily polarized 3D-Laser-fields:

$$F = \sum_{q,q'} \chi'_{q,q'} \nabla(E_q \cdot E_{q'}) + i\chi''_{q,q'} (E_q \cdot \nabla E_{q'} - \nabla E_q \cdot \nabla E_{q'}) \quad (2)$$

Here χ' and $i\chi''$ represent the hermitian and anti-hermitian part of the susceptibility. For the atom at rest they are proportional to $\delta/(\delta^2 + \Gamma^2/4)$ and $\Gamma/(\delta^2 + \Gamma^2/4)$ respectively. The expectation values of the susceptibility are determined by the steady state of optical pumping in the ground state. We calculate the steady state density matrix from reduced Optical Bloch Equations for the ground state.

A straightforward interpretation of the results is provided by considering the multipole decomposition of the susceptibility dyade χ and the field dyade EE^* . A modulated ellipticity field can be described by a periodic modulation of dipole and quadrupole component of the field tensor respectively. The expectation values of the susceptibility for atoms at rest are modulated in an analogous manner. The motion of the atom induces a retarded extra-susceptibility proportional to velocity and gives rise to cooling. Simulations of the stochastic atomic motion are performed to study the instability of optical molasses near the recoil limit.

Effects of Quantum Noise on a Two-Level System in a Single-Mode Cavity

Linda Vahala
 Department of Electrical and Computer Engineering
 Old Dominion University, Norfolk, Virginia. 23529

Abstract

The effects of quantum noise on a two-level system in the bad cavity regime are considered perturbatively in the form of closure at the pair correlation level. It is found that pair correlation effects can reduce the level of semi-classical chaos. However, under the rotating wave approximation (RWA), quantum noise can lead to chaos if there is an initial population inversion, while the full RWA Hamiltonian system remains integrable.

One of the most standard problems considered in quantum optics¹⁻⁴ is the interaction of a two-level quantum system with a single mode radiation field. Here, we shall concentrate on laser fields with frequencies $\omega/2\pi$ in the optical range. In the Heisenberg representation, one obtains an infinite set of coupled nonlinear ordinary differential equations for expectation values. Some closure approximation must be made to turn this system into a tractable model. All previous Heisenberg studies^{2,3} have introduced the semi-classical^{5,6} factorization of the form [radiation field operator a]

$$\langle \sigma_z (a + a^\dagger) \rangle \approx \langle \sigma_z \rangle \langle (a + a^\dagger) \rangle \quad \text{where } \sigma \text{ are the Pauli spins}$$

and thereby achieving 5th order closure. This factorization leads to errors² of order $O(n^{-1/2})$, where n is the number of cavity photons [typically $10^{10} < n < 10^{18}$].

Under the rotating wave approximation the full Hamiltonian system yields an integrable and hence non-chaotic system but one notes that the RWA is valid provided $|\omega - \omega_0| \ll \omega_0$ and $\lambda/\omega_0 \ll 1$ [typically $\lambda \approx 2 \cdot 10^8 \text{ s}^{-1}$ and $\omega_0 \approx 10^{15} \text{ s}^{-1}$]. Hence both factorization and the RWA lead to comparable errors.

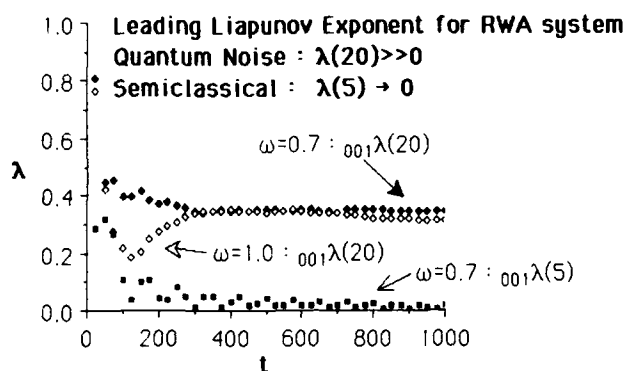
Here, we examine the comparable effects of the inclusion of quantum noise on the chaotic properties of this 2-level system with and without RWA. We consider the effects of quantum noise perturbatively by retaining all pair correlations between operators

$$\langle \sigma_z (a + a^\dagger) \rangle \approx \langle \sigma_z \rangle \langle (a + a^\dagger) \rangle + P_{2a}$$

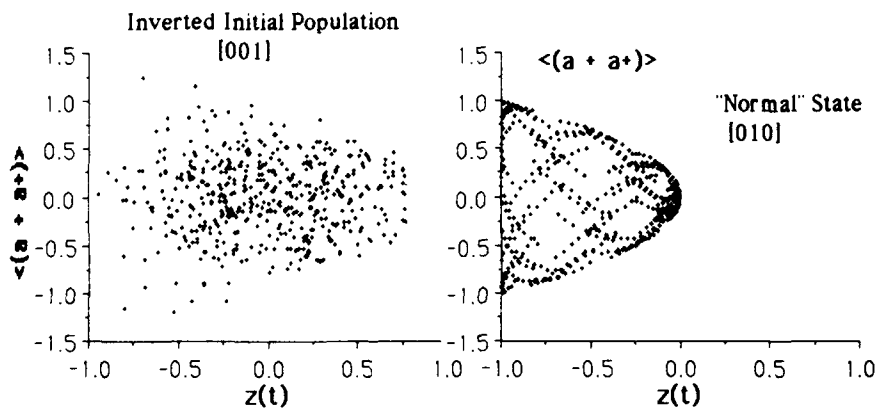
and achieve closure by ignoring all triple correlations. This approximation is also known as the "bad cavity" limit. One now obtains a 20th order nonlinear system for both the full and RWA Hamiltonians.

Two representative initial conditions are considered: either an initially inverted atomic population with $\langle \sigma_z \rangle = 1$, denoted by **[001]** and a normal initial state denoted by **[010]**. Quantum noise effects reduce the chaos for the non-RWA Hamiltonian for both inverted and non-inverted ("normal") initial states. However, for the RWA Hamiltonian we find

that the initially inverted atomic population can become chaotic in the "bad cavity" regime, but not in the semiclassical limit:



The corresponding Poincare plot for the 20th order RWA system (including quantum noise effects) are



¹ E. T. Jaynes and F. W. Cummings, Proc. IEEE **51**, 89 (1963).

²

R. F. Fox and J. Eidson, Phys. Rev. **A34**, 482 (1986), and references therein.

³ P. W. Milonni, J. R. Ackerhalt, and H. W. Galbraith, Phys. Rev. Lett. **50**, 966 (1983).

⁴ R. Graham and M. Hohnerbach, Phys. Lett. **101A**, 61 (1984).

⁵ P. D. Drummond and D. F. Walls, Phys. Rev. **A23**, 2563 (1981)

⁶ C. M. Savage, Phys. Rev. Lett. **60**, 1828 (1988)

PHOTODETACHMENT-THRESHOLD SHIFTS IN TWO-COLOR RADIATION FIELDS

L.A. Bloomfield

Department of Physics, University of Virginia
Charlottesville, Virginia 22901, USA

We have solved the one-dimensional Schrodinger equation numerically to observe the effects of a strong radiation field on the photodetachment-threshold behavior of a model negative ion. The negative ion is exposed to a near-threshold single-photon detaching radiation pulse while in the presence of a second, constant-intensity, low-frequency field. As the second field frequency is increased from zero to the photodetachment threshold, we observe a gradual transition from the interference effects found for detachment into a static field (dc limit) to the increased energy required to detach an electron into a strong oscillatory field (ac limit). The detachment-threshold shift occurs because the second field drags the temporarily detached low-energy electrons back across the potential, where they are reattached.

When the constant-intensity field is reduced to zero frequency, the calculation describes photodetachment into a static electric field (Fig. 1). As observed previously in both experiment[1] and theory[2], photodetachment appears below the zero-field threshold and interferences appear above the threshold between the electron partial waves starting out with and against the static field.

If the constant-intensity field is now allowed to oscillate in time, the dc regime of Fig. 1 transforms into a new ac regime in a continuous manner (Fig. 2). At low frequencies, the constant-intensity field produces an essentially dc effect. At high frequencies, it induces a shift of the photodetachment threshold by an amount U_p , the ponderomotive "potential" energy of a free electron in an oscillatory field. U_p is given by $e^2 E^2 / 4m\omega^2$.

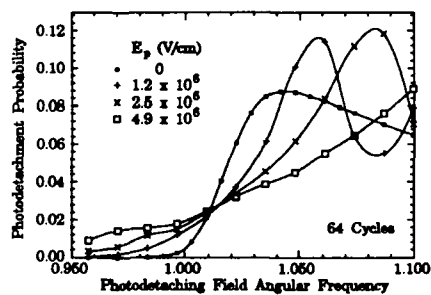
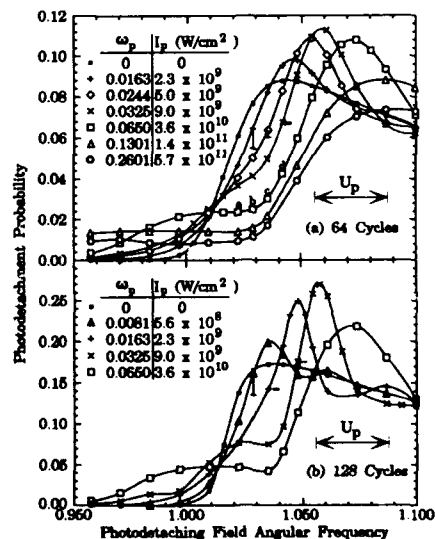


Fig. 1 Detachment probability versus detaching frequency for 64-cycle Gaussian detaching pulses (70 fsec) in the presence of several different static fields E_p . The detaching pulse peak intensity is 2.3×10^{10} W/cm². $\omega = 1.000$ is the photodetachment threshold.

Fig. 2 Detachment probability versus detaching frequency for (a) 64-cycle and (b) 128-cycle Gaussian detaching pulses in the presence of several different oscillatory fields with intensities I_p and angular frequencies ω_p as noted in the figure.



To understand the origins of the threshold shift and the reasons why it is only effective when the constant-intensity field oscillates at high frequency, we can look at the low energy continuum electron partial waves as a function of time. In Fig. 3, we present the electron partial waves corresponding to single photon detachment into a right drifting continuum state. Bound state and multiphoton detachment portions of the wavefunction have been removed. The wavepacket drifts to the right, oscillating 180° out of phase with the constant-intensity field. When the photodetaching field is below the shifted threshold (Fig. 3a, also point (a) in Fig. 2a), the wavepacket tries to leave but is mostly reattached to the well during its oscillations. Above the shifted threshold (Fig. 3b, also point (d) in Fig. 2a), the wavepacket does not return across the potential and is not reattached.

Thus, while a radiation field shifts the detachment threshold by an amount U_p , the electron is not aware of this shift until it has sampled the region surrounding the potential well. As soon as the photodetaching field exceeds the unshifted threshold, the electron begins to make excursions outside the potential. If it does not have enough energy to avoid the potential during its oscillations, it will be reattached to the potential. This is the origin of the threshold shift.

This detachment, excursion, and reattachment process is quite fragile, particularly in three dimensions, and will lead to leakage detachment below the shifted threshold. In one dimension, reattachment fails to occur if the detaching field is turned off before the wavepacket returns to the potential. This can be viewed as detachment due to the high frequency components of the detaching field pulse needed to give it a finite temporal width. However, in three dimensions, the wavepacket may miss the potential well in the two dimensions transverse to its oscillatory motion. Transverse momentum uncertainty, relativistic effects, photon recoil, and static electric or magnetic fields can all prevent the wavepacket from finding the potential for reattachment.

Thus it is not surprising that recent experiments with two color photodetachment of Cl^- ions[3] have observe less than the full threshold shift. Once the electron partial waves begin to explore the region around the potential, there are a great many reasons for those waves not to return to the potential.

REFERENCES

- [1] H. C. Bryant, et al., Phys. Rev. Lett. 58, 2412 (1987).
- [2] M. L. Du and J. B. Delos, Phys. Rev. A 38, 5609 (1988).
- [3] R. Trainham, G. D. Fletcher, N. B. Mansour, and D. J. Larson, Phys. Rev. Lett. 59, 2291 (1987); D.J. Larson, Bull. Am. Phys. Soc. 34, 1209 (1989); M. C. Baruch, T. F. Gallagher, and D. J. Larson, Bull. Am. Phys. Soc. 34, 1398 (1989).

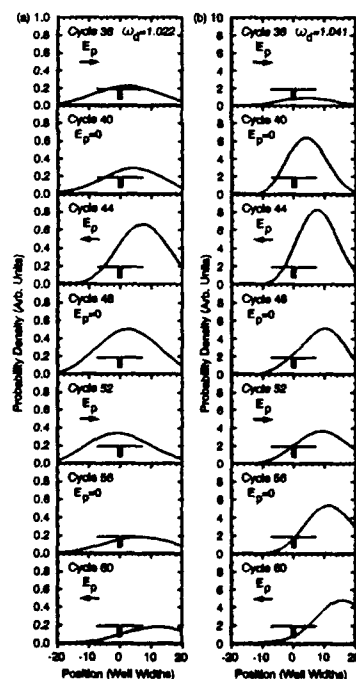


Fig. 3 Particle probability density versus distance from the potential well center during the trailing edge of a 64-cycle (70-fsec) below-shifted-threshold detaching pulse (a) and above-shifted-threshold detaching pulse (b). Note the scale difference between (a) and (b).

**OBSERVATION OF THE $^2S_{1/2} - ^2D_{5/2}$ TRANSITION IN LASER COOLED
TRAPPED Yb^+**

A.S. Bell, H.A. Klein, G.P. Barwood, P. Gill, A.P. Levick and W.R.C. Rowley

National Physical Laboratory
Teddington, Middlesex TW11 0LW, UK.

Narrow transitions in trapped ions offer potential for frequency standards both in the microwave and optical regions. At NPL, $^{172}Yb^+$ ions have been confined and laser cooled in an r.f. trap to temperatures below 2K [1]. Effective cooling over long periods requires 2.438 μm radiation to empty the $D_{3/2}$ metastable level, in addition to the 369.5 nm cooling radiation (fig.1).

The narrow $S_{1/2} - D_{5/2}$ transition in Yb^+ at 411 nm was driven for the first time using a Stilbene-1 dye ring laser [2]. As the blue radiation was tuned to the 411 nm transition, the 369.5 nm monitored fluorescence was extinguished. This fluorescence could be recovered by directing an electron beam into the trap. Our observations suggest that the $D_{5/2}$ state may be decaying into the $F_{7/2}$ state, whereas the $D_{3/2}$ state does not, under our operating conditions. Recent calculations [3] indicate a significant $D_{5/2} - F_{7/2}$ transition rate by means of configuration interaction mixing.

Loss of ions into the very long lived $F_{7/2}$ state is a significant constraint on the use of the $S_{1/2} - D_{5/2}$ 411 nm transition as an optical frequency standard. An alternative may be to drive the $S_{1/2} - F_{7/2}$ transition at 467 nm directly [4]. However, it may be difficult to locate the $S_{1/2} - F_{7/2}$ transition in a reasonable time, given the likely laser power and linewidth available. A better knowledge of the $S_{1/2} - F_{7/2}$ transition energy is desirable and one possible method for determining this will be discussed.

1. H A Klein, A S Bell, G P Barwood and P Gill, Appl. Phys B50, 13 (1990).
2. H A Klein, A S Bell, G P Barwood, P Gill and W R C Rowley, IEEE Trans. Instrum. Meas. (1990), submitted.
3. B C Fawcett and M Wilson, Atomic Data and Nuclear Data Tables (1990), to be published.
4. R Blatt, R Casdorff, V Enders, W Neuhauser and P E Toschek, Frequency Standards and Metrology, Proceedings of the 4th Symposium, Springer-Verlag, 306 (1989).

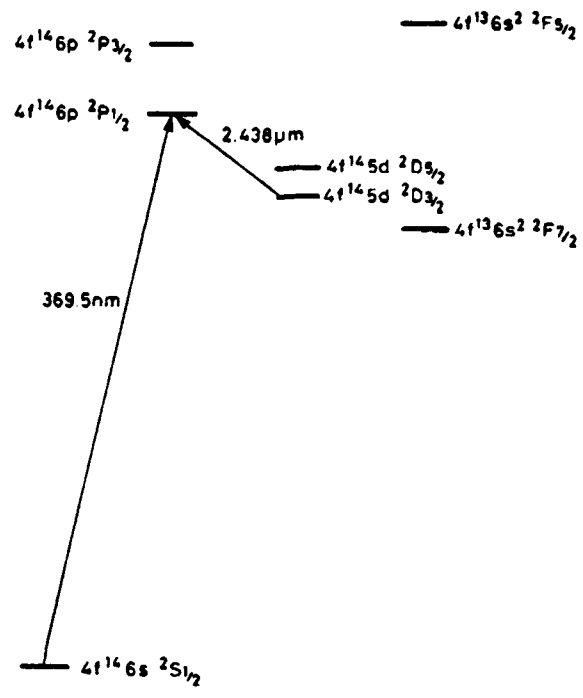


Figure 1. Partial energy level diagram of Yb⁺ showing the transitions necessary to cool the trapped ions.

LINEAR TRAP FOR HIGH ACCURACY SPECTROSCOPY OF STORED IONS*

M.G. Raizen, J.C. Bergquist, Wayne M. Itano and D.J. Wineland

Time and Frequency Division

National Institute of Standards and Technology

Boulder, CO 80303

High accuracy spectroscopy and realization of frequency standards with trapped ions has been one of the goals of the NIST ion storage group in recent years. Two possible limitations on accuracy are the uncertainty in the second order Doppler shift and the signal-to-noise ratio. With a single ion in an rf quadrupole trap, the uncertainty in the second order Doppler shift can be smaller than 1 part in 10^{18} . For good signal-to-noise ratio we would like to have the number of ions $N \gg 1$. However, in the rf quadrupole trap, as the number of ions increases so does the second order Doppler shift since ion-ion repulsion displaces the ions from the center of the trap causing the rf micromotion velocity to increase. This problem can be suppressed in a linear trap.⁽¹⁻⁵⁾

We are pursuing at NIST the development of a miniature linear rf trap which can store $N \gg 1$ ions with small second order Doppler shift.⁽⁴⁾ The trap consists of 4 rods to which an rf potential is applied between adjacent rods providing radial confinement. Each rod is split into three segments. A dc potential applied to the outer segments provides axial confinement. The size of the trap is 500 μm from the axis to the rods, and similar size in the axial direction. The small size is chosen to enable ion confinement near the Lamb-Dicke regime. Computer simulations show $N \sim 50$ ions will trap along the axis like "beads on a string".⁽⁴⁾ Each ion can then be individually imaged, providing N independent clocks. A microwave and an optical frequency standard based on $^{199}\text{Hg}^+$ ions are considered and possible atom-radiation field experiments are described.

*Supported by ONR and AFOSR.

1. D. A. Church, J. Appl. Phys. **40**, 3127 (1969).
2. H. G. Dehmelt, in Frequency Standards and Metrology. Proc. 4th Symposium, ed. by A. DeMarchi, Ancona, Italy (Springer-Verlag, Berlin, Heidelberg 1989) p. 286.

3. J. D. Prestage, G. J. Dick and L. Maleki, J. Appl. Phys. 66, 1013 (1989).
4. D. J. Wineland, J. C. Bergquist, J. J. Bollinger, W. M. Itano, D. J. Heinzen, S. L. Gilbert, C. H. Manney, and C. S. Weimer, Proc. 43rd Annual Symposium on Frequency Control, Denver, June, 1989, IEEE Catalog no. 89CH2690-6; D. J. Wineland, J. C. Bergquist, J. J. Bollinger, W. M. Itano, D. J. Heinzen, S.L. Gilbert, C. H. Manney, and M. G. Raizen, IEEE Trans. on Ultrasonics, Ferroelectrics, and Frequency Control, to be published.
5. H. Walther, private communication.

SUBHARMONIC EXCITATION OF TRAPPED ELECTRONS' CYCLOTRON RESONANCE[†]Carl S. Weimer^{*}, F. L. Moore, and D. J. Wineland

Time and Frequency Division

National Institute of Standards and Technology

Boulder, CO 80303

An experiment is being constructed to investigate the nonlinear dynamics of a single electron interacting with an electromagnetic field. The cyclotron motion of an electron in a Penning trap will nonlinearly couple to an externally applied electromagnetic field through the spatial dependence of the field. [1,2] This nonlinear coupling allows the cyclotron motion to be resonantly excited by the electromagnetic field when the field's frequency is a harmonic of the cyclotron frequency. By observing the response of the cyclotron motion, this subharmonic excitation process can be studied. This process may provide the mechanism for a frequency divider.[1,2]

A Penning trap for operation at cryogenic temperatures has been completed. The axial motion of trapped electrons is monitored by observing image currents induced in the trap endcaps. In preliminary experiments single electrons have been trapped and observed. This is done by driving one of the endcaps with a rf voltage and measuring the response of the axial motion with a phase sensitive detector.[3] This method allowed the axial resonant frequency ($\nu_z = 63$ MHz) to be measured to approximately ± 5 Hz.

By using a servo to lock the axial frequency to an rf synthesizer, the axial detection system can be used to detect excitations of the radial magnetron and cyclotron modes. This is possible because anharmonic terms in the trap potential and magnetic field inhomogeneities weakly couple the radial and axial modes [3] causing a change in the axial servo correction voltage when the radial modes are excited. This detection method allowed the magnetron frequency ($\nu_m = 726$ kHz) to be measured to ± 0.1 Hz, and the cyclotron frequency ($\nu_c = 2.8$ GHz) to ± 1 kHz. Magnetron sideband cooling [3] was used throughout to center the electrons in the trap. Cyclotron excitation was also observed by driving at $2\nu_c$.

With the cyclotron motion near thermal equilibrium (4°K), the $2\nu_c$ drive required approximately 75 db more power to initiate the same level of excitation.

Changes have recently been made in the experiment to increase the stability of the trap potential. Also phase sensitive cyclotron detection electronics have been completed. This should allow the cyclotron motion to be detected directly by induced currents in the split ring electrode.[4] By detecting the cyclotron motion directly, higher order subharmonic excitation will be investigated as well as the phase dynamics of that excitation.

† Supported by AFOSR and ONR

* Also Colorado State University, Ft. Collins, Colorado.

1. D.J. Wineland, J. Appl. Phys. 50(4), 2528 (1979).
2. A.E. Kaplan, Optics Letters 12(7), 489 (1987).
3. Robert S. Van Dyck, Jr., Paul B. Schwinberg, and Hans G. Dehmelt in New Frontiers in High Energy Physics, ed. B Kursunoglu, A. Perlmutter, and L. Scott. (Plenum Publishing Corp, 1978); Lowell S. Brown and Gerald Gabrielse, Rev. of Mod. Phys. 58(1) (1986).
4. Robert S. Van Dyck, Jr., Paul B. Schwinberg and Samuel H. Bailey, Atomic Masses and Fundamental Constants 6, ed. Jerry A. Nolen, Jr. and Walter Benenson (Plenum Publishing Corp, 1980).

IV-16
COUPLED TRAP SPECTROSCOPY†

D.J. Heinzen, J.J. Bollinger,
W.M. Itano, F. Moore, and D.J. Wineland
Time and Frequency Division,
National Institute of Standards and Technology
Boulder, CO 80303

Recently, a single trapped ion has been laser-cooled into its quantum ground state of motion [1]. Such a laser-cooled ion may be used to cool and detect oscillations of a second oscillator by coupling that oscillator to the ion trap's electrodes [2]. Cooling and detection at nearly the quantum limit may be achieved if the second oscillator's Q is sufficiently high.

An interesting application of this idea may be the cooling and detection of motions of a second ion (which cannot be directly laser-cooled) in a separate trap. We are currently developing such a "coupled trap" experiment, in which a single electron stored in a Penning trap will be coupled to the electrodes of a separate Penning trap with a single ${}^9\text{Be}^+$ ion. Using the technique of sideband cooling and detection in the ${}^9\text{Be}^+$ trap, together with inhomogeneous drive fields in the electron trap, it should be possible to cool the electron into its quantum ground state of motion, and to detect single-quantum excitations of any of its degrees of freedom [2].

This technique should dramatically reduce the energy-dependent perturbations to the electron's frequencies of motion, thereby opening up the possibility of improved electron mass and g-factor measurements. By extension, this technique may also find application to the measurement of mass or internal degrees of freedom of other elementary particles or atomic or molecular ions. Cooling and detection of vibrations of a quartz crystal mode also appear possible.

† Supported by ONR and AFOSR

1. F. Diedrich, J.C. Bergquist, W.M. Itano, and D.J. Wineland, Phys. Rev. Lett. **62**, 403 (1989).
2. D.J. Heinzen and D.J. Wineland, Phys. Rev. A, to be published.

DIODE LASER MEASUREMENTS OF RB OPTICAL PUMPING PARAMETERS*

M.E. Wagshul and T.E. Chupp
Lyman Laboratory of Physics, Harvard University
Cambridge, MA 02138

Recent interest in the use of Rb as a spin exchange partner for producing polarized ^3He samples has necessitated the determination of the relevant parameters which limit the Rb vapor polarization. We have developed a new technique, a variation of the Franzen¹ method for measuring spin decay "in the dark", to study transients in the optical pumping process. The optically thick vapor is pumped by up to 1W of D1 light from a Ti:Sapphire laser, while a low power diode laser, tuned off the D2 line to obtain optimal signal to noise, is used to probe the polarization. This procedure is especially geared toward studying optical pumping at very high densities where the on-resonant optical absorption length is several orders of magnitude smaller than the sample length. We have used this technique to measure the Rb spin destruction rates due to Rb-Rb, Rb-N₂ and Rb- ^3He collisions and due to diffusion of the spins to the walls of the cell.

*Supported by the National Science Foundation

¹ Phys. Rev. 115, 850 (1959)

**OBSERVATION OF THE CHANNELING OF ATOMS
IN THREE DIMENSIONAL OPTICAL INTERFERENCE PATTERNS**

N. P. Bigelow and M. Prentiss, A.T. & T. Bell Laboratories
Crawfords Corner Road, Holmdel, NJ 07733

Summary

We report on the observation of the channeling of sodium atoms in the three dimensional optical interference pattern of an optical trap. In contrast to previous channeling experiments, in our experiments the interaction time between the atom and the field was much longer than the time required for the atoms to reach equilibrium with the field. The channeling is shown to occur on length scales from $< 50\mu\text{m}$ up to several millimeters.

Observations

We have observed the channeling of cold sodium atoms cooled in a magneto-optical trap¹⁻³ by studying the fluorescence of the trapped atoms. The observations described here were made in a trap which used light nearly resonant with the $F=2$ (ground state) to $F'=3$ (excited state) and $F=1$ to $F'=2$ levels of the $3^2S_{1/2} \rightarrow 3^2P_{3/2}$ transition. Perhaps the most striking aspect of this work is the observation of channeling on a length scale of several millimeters, where striations (regular patterns of dark and light bars) in the fluorescence are readily apparent to the unaided eye. We observed the channeling on smaller length scales, by studying the trapped atom fluorescence using an optical microscope, and, at the smallest length scales, by studying distortions in the fluorescence lineshape due to the channeling. A discussion of the fluorescence lineshapes of the trapped atoms is presented in detail in a complementary paper.

We attribute the channeling to a repulsion of atoms from the intensity minima in the optical interference pattern of the trap and to a clustering of the atoms near the intensity maxima. For trapping light tuned below resonance, the ac stark shift produces a potential minima at the intensity maxima, and a potential maxima at the intensity minima.⁴ It is the localization of the atoms in this potential which gives rise to the channeling which we observe. This observation of channeling is important because, for a two-level atom in a one dimensional standing wave, it was predicted that channeling would not be significant in the case of long interaction times since the characteristic kinetic energy of the atoms was expected to be greater than the depth of the ac stark potential.⁵ Our observations show that this channeling does however occur. This observation may help explain the anomalously long lifetimes observed in optical traps, since the atoms may have to bounce many times off the channels as they walk out of the trap.

We discuss the large scale striations in terms of the confining effects of the potential created by the interference between two of the three sets of retroreflected light beams which formed the trap. The spacing of the striations in fluorescence pattern was observed to vary with the alignment of the trapping beams as predicted by our model. In Figure 1 we show the intensity profile of one such striated fluorescence pattern and its spatial Fourier transform. The overall shape of the striated fluorescence pattern was generally that of a two-dimensional disc with the striations in the plane of the disk. In comparison, in a trap where the alignment did not produce such large scale striations, the trapped atom fluorescence could be made to appear cloud-like with no particular orientation.

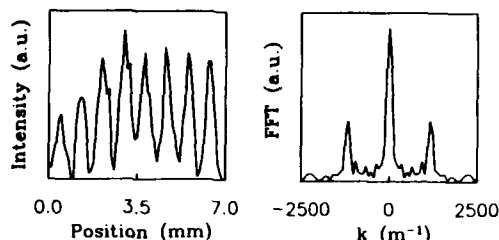


Figure 1 Left: Intensity profiles of the fluorescence from trapped atoms. Right: Magnitude of Fourier transform of the profiles to left showing $850 \mu\text{m}$ periodicity.

We have verified that there are no atoms present in the dark bars of the striated pattern by using an additional laser beam to push atoms out of the trap. When the beam was directed at the bright bars, the total trap fluorescence decreased, and a dark hole appeared where the probe beam intersected the trap. When viewed in the plane of the striations, a plume of fluorescing atoms could be seen leaving the trap. In contrast, when the probe was directed at a dark bar, there was little change in the total number of trapped atoms, and no plume was observed. The confinement of the atoms in the striations was also studied dynamically by modulating the striation pattern, and studying the frequency dependence of the total trapped atom fluorescence. Analysis of the changes in the total fluorescence in both the modulation and probe-pushing experiments indicate that the characteristic temperature of the trapped atoms is on the order of half the depth of the confining potential. We point out that as a result of the spatial dependence of the damping and heating which is introduced by the optical interference pattern, the concept of a characteristic temperature may in fact not be very well defined. We suggest that 1) the true multi-level structure of the atoms and 2) the mixture of standing and traveling wave fields introduced by the interference may both contribute to the dramatic difference between the theoretical predictions for the two-level atom in a 1-d standing wave and our observations.

We have further examined the fluorescence pattern on smaller length scales using an optical microscope (resolution $\sim 10 \mu\text{m}$). The microscope revealed a rich variety of three dimensional patterns which often resembled a nest of intertwined filaments. Such structure suggests that the paths which a given atom follows as it wanders through the trap may be more aptly treated as a percolation problem than as a diffusive random walk, thus giving rise to an enhancement of the trap lifetime.

¹E. L. Raab, M. G. Prentiss, A. E. Cable, S. Chu and D. E. Pritchard, *Phys. Rev. Lett.* **59**, 2631 (1987).

²N. P. Bigelow and M. G. Prentiss, *Phys. Rev. Lett.*, to be published, 2 July 1990. The reader is also directed to the references therein.

³The authors note that a complementary observation of the effects of channeling of trapped atoms was made concurrently by workers at NIST (C. Westbrook et. al., *ibid*).

⁴A. Ashkin, *Phys. Rev. Lett.* **40**, 729 (1978).

⁵J. P. Gordon and A. Ashkin, *Phys. Rev. A* **21**, 1606 (1980).

**OBSERVATIONS OF DISTORTIONS IN THE FLUORESCENCE LINESHAPES
OF COLD ATOMS IN 3-D OPTICAL INTERFERENCE PATTERNS**

N.P. Bigelow and M. Prentiss A.T. & T. Bell Laboratories
Crawfords Corner Road, Holmdel, NJ 07733

We have measured the fluorescence of cold Na atoms as a function of probe frequency. The source of the cold atoms was a magnetic molasses trap, which is composed of three orthogonal pairs of counterpropagating fields at frequency ω_{trap} , centered on the zero of a magnetic quadrupole field¹. The fluorescence spectrum was measured by turning off the trapping light for a 10 μ s interval, during which the atoms were exposed to weak light at a frequency ω . The probe light passed through the same optical fiber as the trapping light, so the position and polarization of the probe light is the same as that of the trapping light, though the probe light was much weaker than the trapping light. The lineshapes were normalized to the probe intensity. We found that the fluorescence as a function of ω is not simply a Lorentzian, but is considerably distorted. In this paper, we will discuss the fluorescence lineshapes as functions of trap parameters, and make some suggestions about the physics which may underly this behavior, including the exciting possibility that much of the distortion can be attributed to channeling of the cold atoms in the potential formed by the interference pattern of the trapping fields.

The trapping light was nearly resonant with the $3^2S_{1/2} \rightarrow 3^2P_{3/2}$ transition in Na, which has a natural linewidth, Γ of 10 MHz. The data discussed here was taken with trapping fields which contained light nearly resonant with each of the sublevels of the groundstate(GS) two different levels in the excited state (ES). We used two different tunings: Type I which was nearly resonant with the F=2 GS to F=3 ES and the F=1 GS to F=2 ES; Type II which was nearly resonant with the F=2 GS to F=2 ES and the F=1 GS to F=0 ES.² At type I tuning, the trap size was of the order of 100 μ m. When we measured the absorption from a single traveling wave field which was pulsed on for 10 μ s while the trapping light was entirely off, we obtained symmetric lineshape approximately 11 MHz when the magnetic field gradient was approximately 10 Gauss/cm. In contrast, at type II tuning, the trap size was \sim 2 mm and the absorption linewidth was again symmetric, but with a width of approximately 14 MHz at 10 Gauss/cm. The measured linewidth increased with increasing field gradient.

For both Type I and type II detunings, the fluorescence at $\omega > \omega_{max}$ is suppressed below that of a Lorentzian with linewidth Γ , and the fluorescence at $\omega < \omega_{max}$ is enhanced above that for a Lorentzian with linewidth Γ . The FWHM on both sides increases and the asymmetry decreases as ω_{trap} approaches resonance. The asymmetries are more marked at 8 mW/cm² per beam than at 16 mW/cm² per beam. In some of the lineshapes it was possible to distinguish additional fluorescence peaks which we attribute to a transitions between magnetic sublevels.

The fluorescence linewidth for type I tuning are somewhat broader than Γ . The fluorescence maximum occurred at a frequency, ω_{max} which was approximately the resonance frequency. At Type II detunings, the fluorescent linewidths were approximately Γ and ω_{max} varied somewhat more from resonance. In particular, at intensities \sim 15 mW/cm² there was some indication that $\omega_{max} - \omega_{trap} \sim \Gamma$ for $-12 < \omega_{trap} < -5$ MHz. It is important to note that the single traveling wave probe beam produced symmetrical lineshapes, suggesting that more than one field is required to produce the asymmetry.

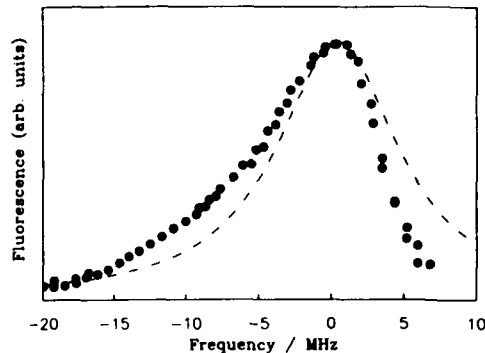


Figure 1 Fluorescence lineshape for $\omega_{trap} = -7\text{MHz}$, with $8\text{mW}/\text{cm}^2$ per beam type I tuning. The dash-dot line is a Lorentzian with $\text{FWHM}=\Gamma$.

We attribute the lineshape asymmetries to channeling in the potentials formed by the optical interference pattern of the trapping fields.³ : when the probe field is detuned below resonance atoms are attracted to the intensity maximum, so the total fluorescence will be greater than that for a uniform distribution; in contrast, if the probe field is detuned above resonance, then the atoms will be attracted to the potential minima, and the total fluorescence will be less than that for a uniform distribution. When the probe field is detuned far from resonance, the potential become very small, and the lineshapes should return to the Lorentzian lineshape that would be expected for an unperturbed distribution. The behavior is demonstrated by the fluorescence lineshape shown in figure 1. Since the atoms were able to redistribute themselves within the interference pattern in a time $< 10\mu\text{s}$ and the acceleration due to the interference pattern is $\ll 10^6 \text{ m/s}^2$, the scale of the interference pattern must have been $\ll 50\mu\text{m}$. In fact, the length scale may have been of the order of the optical wavelength since the interference patterns between the counterpropagating fields were on that length scale. This suggestion is supported by separate experiments done by another group.

The displacement of the fluorescence maximum from resonance in the case of type I detuning we attribute to the atoms sitting in a non-zero magnetic field, where ω_{trap} was detuned from the Zeeman shifted resonance by $\sim -\Gamma$. This accords with the observation that the trap center moved with frequency and field. In contrast, for type II tuning the trap remained stationary, and the center frequency occurs approximately on resonance. The increase in linewidth associated with tuning ω_{trap} closer to resonance may be attributed to a decrease in cooling due to mechanisms which transfer kinetic energy to internal energy and then radiate the energy into the vacuum field (e.g. polarization gradient cooling)⁵. The associated decrease in asymmetry may result from the increase in kinetic energy with respect to the potential energy of the interference potential, since the potential decreases with decreasing detuning.

References

- ¹E. L. Raab, *et. al.*, Phys. Rev. Lett. **59**, 2631 (1987).
- ²M. G. Prentiss, *et. al.*, Opt. Lett. **13**, 452 (1988).
- ³M. G. Prentiss and S. Ezekiel, Phys. Rev. Lett. **56**, 46 (1986).
- ⁴C. Westbrook *et. al.*, Phys. Rev. Lett., to be published, 2 July 1990.
- ⁵J. Dalibard, *et. al.*, Proc. 11th Int'l Conf. Atomic Phys., S. Harosche, J. C. Gay and G. Grynberg, eds. (World Scientific, New Jersey, 1989); S. Chu, *et. al.*, (*ibid*); B. Sheehy, *et. al.*, Phys. Rev. Lett. **64**, 858 (1990).

STUDIES OF A SINGLE LASER COOLED, TRAPPED STRONTIUM ION

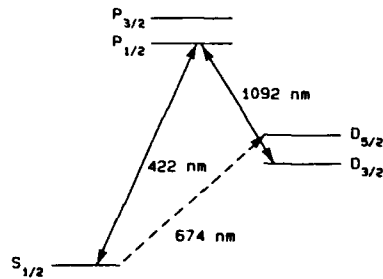
A. A. Madej, M. Houssin^{*}, and J.D. Sankey
 Time and Frequency Standards
 Institute for National Measurement Standards
 National Research Council of Canada
 Ottawa, Canada K1A 0R6

1. Introduction:

A single ion held in an electrodynamic trap under high vacuum conditions (10^{-8} Pa) and laser cooled by near resonant laser light provides an excellent approximation to an atomic system at rest and essentially free from external perturbation. Recent work in this area has provided insights into single atom quantum phenomena [1-3], collisional quenching and molecular association at the single atom regime [3], photon antibunching and coherence effects [4], and high resolution spectroscopy [1,2]. Also, such ions could form the basis of an optical frequency standard with stability and precision superior to that of the Cs beam standard. Unfortunately, the lack of available continuous-wave laser sources for laser cooling, optical pumping, and excitation of the dipole forbidden, narrow-linewidth transitions of interest has been a restricting factor in the number and versatility of single ion systems studied. The energy level structure of Sr^+ (see Fig.1) possesses transition frequencies compatible with systems composed entirely of tunable solid state lasers.

2. Experiment and Results :

A description of the experimental arrangement and preliminary results has recently been reported [5]. Briefly, a Strontium ion was contained in a radio frequency (Paul) trap whose characteristic dimensions are $r_0 = 1.4$ mm and $z_0 = 1.0$ mm. Cooling and detection of Sr^+ is achieved via excitation on the 422nm $5p \ ^2P_{1/2} - 5s \ ^2S_{1/2}$ transition using dye laser light of 1 MHz linewidth. The $^2P_{1/2}$ level can decay to the metastable $4d \ ^2D_{3/2}$ level with 1:13 branching hence optical pumping at 1092 nm is necessary to ensure efficient laser cooling and detection. A tunable, frequency narrowed Nd^{3+} doped fiber laser [6] provides the required radiation for excitation on the $5p \ ^2P_{1/2} - 4d \ ^2D_{3/2}$ transition. Incident powers into the trap were 10-50 μW for the 422nm radiation and 400 μW for the 1092nm light using excitation beams of 100 μm diameter. Detection of the ion was obtained by blocking all but the desired 422nm S-P fluorescence with a narrow band filter and by imaging the trap center on a pinhole aperture located in front of a photon counting photomultiplier system.

Fig. 1 Energy Level Diagram of Sr^+

By controlling the ion loading rate into the trap, it was possible to load and subsequently cool a single Sr^+ atom. Initial lineshape scans showed strong frequency modulation of the absorber lineshape due to micromotion induced Doppler broadening. The origin of the micromotion probably arises from the fact that the DC and RF defined centers of the trap are not coincident. By applying a DC voltage of

1V between the trap endcap electrodes, this micromotion effect was substantially reduced resulting in observed single ion temperatures below 500 mK. Confirmation that the observed fluorescence originated from a single trapped ion was achieved by observing the quantum jumps in the 422nm fluorescence as the ion was excited into the $4d \ ^2D_{5/2}$ metastable level. Initially this was achieved using a Sr^+ hollow cathode lamp light emitting on the $5p \ ^2P_{3/2} - 5s \ ^2S_{1/2}$ line. The ion could then decay into the $4d \ ^2D_{5/2}$ level. Later direct laser excitation into the metastable level was achieved on the electric quadrupole allowed $4d \ ^2D_{5/2} - 5s \ ^2S_{1/2}$ transition using a 1 MHz linewidth dye laser operating with incident powers in the region of 100mW with an incident beam diameter of 100 μ m. The observed quantum jumps in fluorescence followed the exponential distribution of times in the metastable level as expected [7]. From these studies, an improved value of the metastable $4d \ ^2D_{5/2}$ lifetime was obtained of 372 ± 25 ms implying an ultimate linewidth for the transition being below 0.5 Hz. Initial results using alternate illumination by the cooling-detection lasers and probing laser show a linewidth on the S-D transition limited by residual micromotion due most probably to residual stray fields in the radial direction resulting in ion heating during the S-D probing interval to 10 K. Work is proceeding toward the reduction of this effect using compensating electrodes.

Another area of research has been the development of solid state laser systems for the necessary radiations at 422, 1092, and 674 nm. Operation of the 1092nm fiber laser has been demonstrated using a 100 mW diode laser as the pump source yielding an output power of 0.6 mW. Radiation at 422nm has been obtained by direct doubling of 843nm diode laser light in $KNbO_3$ with temperature tuned phase matching. With incident diode powers of 75 mW, single pass second harmonic powers of 40 μ W have been obtained. Experiments are now underway to narrow the linewidth of the diode radiation using optical feedback techniques such that the generated 422nm linewidth is below the 22 MHz width of the S-P transition. Finally, radiation at 674nm in resonance with the Sr^+ S-D transition has been obtained using the recently developed visible laser diodes. Although the initial linewidth from the diode is of moderate width (200 MHz), the diode output had sufficient spectral brightness to excite the strontium S-D transition that quantum jumps into the metastable state were observed. Linewidth reductions of these diodes using external cavity feedback are being examined. Progress in these areas will be reported at the conference.

* CRNS/NRC exchange scientist, Present address: Laboratoire de l'Horloge Atomique, Equipe de Recherche du CNRS associee a l'Universite de Paris Sud, Bat. 221, 91405 Orsay, France.

References:

- 1) J. C. Bergquist, F. Diedrich, W. M. Itano, and D. J. Wineland, in *Laser Spectroscopy IX*, M.S. Feld, J.E. Thomas, and A. Mooradian, eds. (Academic, San Diego Calif., 1989), p.274, and references therein.
- 2) W. Nagourney, N. Yu, and H. Dehmelt, in *Frequency Standards and Metrology*, A. DeMarchi, ed. (Springer-Verlag, Berlin, 1989), and references therein.
- 3) A.A. Madej and J.D. Sankey, *Phys. Rev. A* **41**, 2621 (1990).
- 4) G. Janik, W. Nagourney and H. Dehmelt, *J. Opt. Soc. Am. B* **2**, 1251 (1985).
- 5) A.A. Madej and J.D. Sankey, *Opt. Lett.* **15**, 634 (1990).
- 6) A.A. Madej, W.E. Berger, G.R. Hanes, and M.S. O'Sullivan, *Opt. Comm.* **73**, 147 (1989).
- 7) R. Blatt and P. Zoller, *Eur. J. Phys.* **9**, 250 (1988).

VELOCITY- SELECTIVE COHERENT POPULATION TRAPPING FOR LASER
COOLING IN TWO AND THREE DIMENSIONS

F. Mauri ⁽⁰⁾ and E. Arimondo ^(*)

⁽⁰⁾ Scuola Normale Superiore, Piazza dei Cavalieri 2, I-56100 Pisa, Italy

^(*) Dipartimento di Fisica, Università di Pisa, I-56100 Pisa, Italy

In laser cooling based on velocity selective coherent population trapping an atom by spontaneous emission falls into a coherent superposition of ground state where remains trapped. A previous experiment on a ^4He beam and a theoretical analysis have shown the feasibility for one dimension scheme⁽¹⁾.

We have investigated theoretically, on the basis of the solution of the density matrix equations and of optical Hamiltonian eigenstates, the feasibility and efficiency of laser cooling schemes based on velocity coherent trapping in higher dimensions, for different atomic configurations.

We have determined the general conditions on the laser configurations and the atomic transitions for the realization of coherent trapping in two or three dimensions.

Thus in the $J_g = 1 \rightarrow J_e = 0,1$ transitions, three planar light beams at $2\pi/3$ angle produce a 2D trapped state. For the $J_g = 3/2 \rightarrow J_e = 3/2$ transition in presence of an external magnetic field, three collinear σ light beams and three planar π beams at $2\pi/3$ angle give rise to a 3D trapped state.

A numerical solution of the density matrix equations has been used to determine the efficiency of the pumping rate in a single stationary uncoupled ground state. By combining the velocity selective coherent population trapping to a Doppler force a high efficiency of pumping rate may be realized.

An heuristic model based on the solution of diffusion-like equation has been used to provide good estimate of the pumping rate efficiencies.

(1) A. Aspect, E. Arimondo, R. Kaiser, N. Vansteenkiste and C. Cohen-Tannoudji, Phys. Rev. Lett. 61, 826 (1988); J. Opt. Soc. Amer. B6, 2112 (1989)

Excitation of a Single Trapped Electron by Squeezed Back-Action

Peter B. Lerner* and P. Tombesi

Dipartimento di Fisica, Università di Roma "La Sapienza",
P.le A. Moro 2, 00185, Roma, ITALY

The hysteresis curve of the bistable cyclotron motion of a single electron in a magnetic field driven by an external microwave radiation is obtained exclusively by variation of the squeezing parameter. Thus, the steady-state solution of the electron motion includes two branches which could be governed by the phase of squeezing.

It is well known that a medium with macroscopic nonlinear properties may provide bistable behavior. One of the best examples is optical bistability in nonlinear dispersive media. The first experimental demonstration of optical bistability was achieved as early as 1976. Since then a great amount of theoretical work has been performed. In the last decade considerable interest has been devoted to a single electron in a Penning trap (Dehmelt et al. 1979-1987). In particular, Kaplan (1982) showed that, due to relativistic correction of the mass, the cyclotron motion of the electron in a magnetic field shows a bistable behavior when its motion is driven by an external field. Thus, even the simplest of macroscopic objects interacting with an electromagnetic field is already intrinsically bistable. Gabrielse, Dehmelt and Kells, by varying the frequency of the driving field, observed the bistable hysteresis in the cyclotron motion of the electron. This hysteresis results entirely from a relativistic correction to the mass. Recently, a new radiation source with non-classical properties of the emission, called squeezing, has been demonstrated. Some recent work has pointed out that the interaction of matter with this type of radiation can result in surprising effects, such as the inhibition of an atomic phase relaxation (Gardiner, 1985), or the suppression of one of the sidebands in the resonance fluorescence spectrum. Furthermore, it was shown that in optical bistability, imbedded in a squeezed bath, the bistable curve can be influenced by variation of the phase of a squeezing parameter (Tombesi et al. 1989). Using parametric down-conversion techniques, La Porta, Slusher and Yurke were able to perform a back-action evading measurement, and the development of such techniques can be applicable for a wide range of measurements in quantum systems. In this paper we demonstrate that implementation of the back-action evading techniques can result in the possibility of control over the bistability by the variation of the squeezing phase and very sophisticated properties of the electron excitation.

* Present address: Dept. of Electrical Eng., University of Michigan,
Ann Arbor, MI 48109-2122

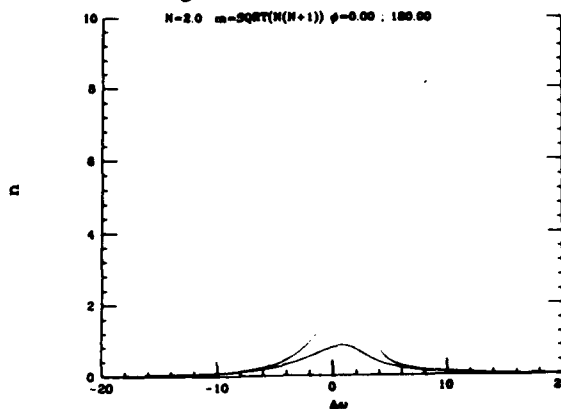
Namely, the monitoring of the cyclotron motion of the electron in the Penning trap is provided by the measurement performed on the axial degree of freedom (i.e., the oscillatory motion along the direction of the magnetic field). The shift of the axial resonance is related to the properties of a cyclotron motion.

Recently, some experimental schemes were developed, in which the back-action of the measurement device can be controlled on the quantum level. It means that the excitation of the probe system by the measuring apparatus could be considered to be equivalent to the penetration of the squeezed vacuum from the output port or, equivalently, the action of squeezed oscillator along axial direction. The abovementioned wide separation of the characteristic frequencies in the cyclotron micromaser, ensures that degrees of freedom other than axial are not directly effected by the back-action of the measurement.

We have demonstrated that a hysteresis curve may be obtained just by varying the phase angle of the squeezing parameter ϕ . For a sufficiently high squeezing ($N \approx 2$, for a squeezed vacuum pushed by back-action), the resonance line shape of the anharmonic oscillator could be modified or even suppressed for a particular value of the angle ϕ .

The Fig.1 shows that for a fixed value of the driving amplitude E , which can be chosen as real, and for a given detuning, satisfying the relation the switching from one branch of a bistable curve to another can be realized by varying the phase of the squeezing parameter. The switching can also be performed by change in the frequency of the driving field. However, this result can be considered as an example of transition induced by a squeezed noise.

Fig.1 Excitation of the single electron, $n = \langle a^\dagger a \rangle$, arb. units



EFFECTS OF RADIATION TRAPPING ON OPTICALLY TRAPPED ATOMS

T. Walker, D. Sesko, and C. Wieman

Joint Institute for Laboratory Astrophysics, University of Colorado and National Institute for Science and Technology, and Department of Physics, University of Colorado, Boulder, CO 80309-0440

Optically trapped and cooled atoms are of great interest for many experiments because of the promise of providing a dense, cold source of atoms. Such a source would reduce or eliminate many limitations of conventional spectroscopic experiments, such as Doppler shifts and transit-time broadening. For many experiments the reduction of these effects is in vain if the signal-to-noise ratio is insufficient, i.e. if the number or density of the trapped atoms is too small. We have therefore done experiments¹ on atoms trapped in the popular Zeeman-shift spontaneous-force trap to determine their properties when large numbers of atoms are loaded into it. We find that when the cloud of trapped atoms begins to become optically thick, repulsive forces between the atoms due to radiation trapping cause the cloud to expand. Radiation trapping limits the *density* of the trapped atoms. The maximum number of atoms which can be trapped (in our case 5×10^8) is reached when the cloud of atoms fills the intersection region of the trapping laser beams.

Radiation trapping also manifests itself by affecting the dynamics of the trapped atoms. In particular, we have observed that when the trapping lasers are aligned to put a vortex-type force on the cloud of atoms (in addition to the trapping force) the spatial distribution of the cloud can abruptly change from a roughly constant-density sphere to a ring of atoms orbiting a smaller cloud. In some cases the ring is actually an orbiting clump of atoms. Thus the atoms have become strongly coupled by their radiation fields and can behave as a collective unit.

A simple model of the radiation trapping force explains most of the above observations. Two atoms a distance r apart in a laser field of intensity I experience a force $f = \sigma_R \sigma_L I / 4\pi c r^2$ between them due to the absorption of the radiated photons. Here σ_L and σ_R are the absorption cross-sections for the laser light and the radiated light, respectively. Thus the atoms behave as if they have acquired a net charge $q = \sqrt{\sigma_R \sigma_L I / 4\pi c} \sim 10^{-4} e$. In analogy to electrostatics we then can write for the force field on a cloud of atoms $\nabla \cdot \mathbf{F}_R = \sigma_R \sigma_L I n / c$ where n is the atom density. Dalibard² has shown that there is also a force on the cloud which arises from the attenuation of the laser beams by the atoms; this obeys $\nabla \cdot \mathbf{F}_A = -\sigma_L^2 I n / c$. At zero temperature these two forces must cancel the trapping force, which we take to be $-kr$. Then the density of the cloud of the cloud is fixed at the value $n_{max} = 3ck / (\sigma_R - \sigma_L) \sigma_L c$. At non-zero temperature the maximum density the cloud can attain is n_{max} .

¹T. Walker, D. Sesko, and C. Wieman, Phys. Rev. Lett. 64, 408 (1990).

²J. Dalibard, Optics Commun. 68, 203 (1988).

Key to this model is the notion that since the polarization, coherence, and the frequency distribution properties of the reradiated light are different from the properties of the laser light, the cross-sections σ_R and σ_L are not the same. We have calculated these cross-sections for a two-level atom,³ and find $\sigma_R/\sigma_L = 1.2$; the radiation trapping force is about 20% stronger than the attenuation force. Figure 1 shows how this comes about. The emission profile is the familiar Mollow triplet in addition to the usual Rayleigh peak at the laser frequency. The absorption profile is quite different. Convoluting the two profiles, we find that the cross-section for absorbing the reradiated light is larger than the cross-section for absorbing the laser light.

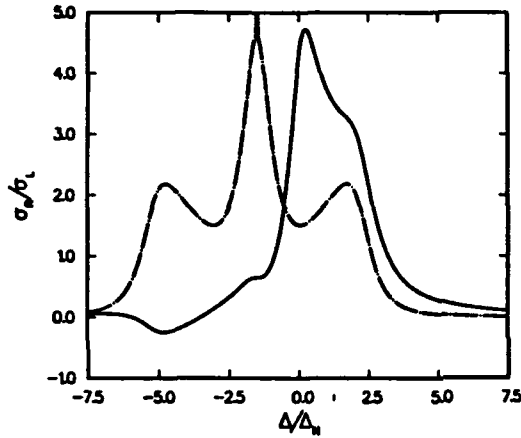


Figure 1: The absorption (solid line) and emission (dashed line) profiles calculated for a two-level atom. The zero-width elastic peak (which comprises about 50% of the total) is represented by the spike at $-1.5\Delta_N$.

We can also explain the existence and stability of the observed orbiting rings by considering the motion of an atom in a trap with misaligned beams. The vortex force due to the misalignment is taken to be $\mathbf{F} = k'\hat{z} \times \mathbf{r}$. If we neglect radiation trapping, unstable circular orbits exist with frequency $\omega = k'/\gamma$. Including the radiation trapping force $\alpha N/r^2\hat{r}$ from the other atoms, we find stable circular orbits exist only for the special orbit radius

$$R = \left(\frac{\alpha N}{k - m\omega^2} \right)^{1/3}. \quad (1)$$

The predictions of the model are in reasonable agreement with our observations.

We have trapped as many as 5×10^8 atoms in a volume of about 1mm^3 , limited by the repulsion due to radiation trapping. This sample scatters about 10^{18} photons per second, making it very attractive for many experiments.

³D. Sesko, T. Walker, and C. Wieman, submitted to JOSA B.

COOPERATIVE STIMULATED RADIATION : COHERENCE IN
 ATOMIC REACTION INDUCED BY LASER

K. T. Lu

Atomic Engineering Corp., P. O. Box 3342, Gaithersburg, Md., 20878

ABSTRACTS

Cooperative stimulated radiation is based on cooperation of stimulated radiation among an ensemble of exciplexes (excimer complexes). The exciplexes are formed by atomic reactions induced by laser pumping. The stimulated radiation originates from the upper stable exciplex state to the repulsive ground state.

The frequency spectrum of the cooperative stimulated radiation process is the 4-dimensional Fourier transform of the correlation function of the macroscopic transition moment, M , of the system (= laser + atoms) in space and time,

$$C(\omega, 2\omega, \dots, n\omega; \omega', 2\omega', \dots, n\omega') = \langle M(0)M(X) \rangle_{\omega} \text{-----} (1)$$

where $n\omega$ and $n\omega'$ represents the incident photon frequency and the scattered photon frequency respectively. $\langle \rangle_{\omega}$ represents average over the entire volume and time. X is the four vector, $X=(r,t)$. The conditions of physical observation that satisfy the gauge invariance in space and time (1) requires that the correlation functions remain unchanged under space-time displacement $X' \rightarrow X+X''$. The correlation function would vanish unless the system simultaneously conserves energy, momentum and angular momentum. That is, the phase factor of the laser and particle operators in the correlation function commute with the Hamiltonian of the system. Consequently, the non-integrable phase factor $\int \omega dX$ is quantized, such that the scalar product of four vectors belonging to each phase factor of the system superimposed coherently. The expression in eq. 1 after reduction of the correlation function by integration over time leads to the form,

$$C(n\omega, n\omega') = \text{Tr} \{ P \langle e^{iK \cdot X} X(K) \rangle_{\omega} P \langle e^{-iK \cdot X} X^*(K) \rangle_{\omega} P \} \text{----} (2)$$

where $X(K)$ is the susceptibility function of the system and the phase-factor is expressed in terms of scalar product of the collective wave vector K of the photon and the particles and the collective coordinate X of the radiator. P is the projection operator projecting on the photon space. The expression in the $\langle \rangle$ can be identified as the macroscopic transition moment M which has the characteristic of running waves of Bloch state distributed uniformly over the medium of the cooperative mode. The condition of coherent process is determined by the requirement that the total phase of the system satisfies

$$\sum K_{1\alpha} \cdot X_1 = \sum [(k'_1 - k_1) + p_{\alpha}] \cdot X_1 = n\pi \quad (3)$$

where k' , k and p are the wave vectors of the scattered photon, incident photon and the particle respectively. The macroscopic moment can also be expressed in terms of the localized coordinates of the particles r_1 and the corresponding amplitude $S_1(r)$

$$M = \langle (\sum S_{1-}(r_{1-}) \exp(iK \cdot r_{1-})) \times (\sum S_{1+}(r_{1+}) \exp(iK \cdot r_{1+})) \times (\sum S_{10}(r_{10}) \exp(iK \cdot r_{10})) \rangle \quad (4)$$

where r_{1-} , r_{1+} and r_{10} are the coordinate of the electron, ion and atom respectively. The symbol \times stands for correlated product. The expression in each of the $()$ satisfies the Bloch state. Comparing eqs. 2, 3 and 4, we can identify the collective coordinate X as the sum of the localized coordinates r_1 . This result suggests that the scattering process with the electron, ion and atom is coherent and the scattering amplitudes are superimposed linearly. Thus, the coherent process in the macroscopic moment is proportional to $N \cdot N \cdot N_0$ which is in turn proportional to the cubic of the number density of the atom, N^3 . One can view that the electron, ion and atom are coupled by the laser field to form an excimer A^*_2 . The coherent scattering conditions can be best satisfied for forward scattering with small angle. This result in an elongated polarization along the optical axis. In the process a phase-coherent polarization is produced through the medium. The inelastically scattered photon induced by the atomic reaction to form the excimer is in cooperation with its neighbor. The general expression of the ensuing cooperative radiation with reaction has the form,

$$C(n\omega, n\omega') = \sum \langle I \rangle_n N^n, \quad n=1,2,3,\dots \quad (5)$$

The linear term corresponds to in-coherent n-photon scattering. The quadratic term corresponds to n-photon off-resonance harmonic generation and superradiance without reactions. The fourth and sixth power terms correspond to cooperative processes with reactions. The odd power terms correspond to interference scattering. The detailed discussion and comparison with recent experimental results (2,3) will be presented.

1. T. T. Wu and C. N. Yang, Phys. Rev. D. 12, 3845 (1975).
2. J. Y. Zhang, H. Zhou and K. T. Lu, to be published.
3. C. C. Gomez, J. Tsee, J. Mack, H. H. Hsu and K. T. Lu, 1990-1991 SPIE, Los Angeles, to be published in conference proceedings.

V. PHOTOIONIZATION PROCESSES

PCI IN THE ANGULAR DISTRIBUTION OF AUGER-ELECTRONS
FOR THE INNER-SHELL ATOMIC PHOTOIONIZATION

M.Yu.Kuchiev, S.A.Sheinerman

A.F.Ioffe Physical-Technical Institute
of the Academy of Sciences, Leningrad, 194021 USSR

The process of the inner shell ionization followed by Auger-decay of the created vacancy is considered. There are three particles in the final state of the process: photoelectron, Auger-electron and double-charged ion. Their Coulomb interaction (known as Post Collision Interaction) substantially influences the angular and energy distribution of the electrons. PCI is well-studied for the case when the velocities of both electrons are known in the final state [1]. The purpose of this thesis is to consider the case when only Auger-electron is registered in the final state. The PCI is shown to influence on the angular distribution of Auger-electrons. The effect manifests itself in the usual non-coincidence experiments.

The consideration is based on the eikonal theory [2] which is valid when photoelectron velocity V_{ph} satisfies the condition $V_{ph} \gg \Gamma^{1/3}$.

It is natural to consider three kinematical regions. In the near threshold region $V_{ph} \ll V_A$, V_A is the Auger-electron velocity, PCI is caused mainly by the interaction of low-energy photoelectron with the ion. The high-energy Auger-electron is not affected by PCI. When the velocities are comparable, $V_{ph} \sim V_A$, PCI essentially distorts the angular distribution of Auger-electrons. The numerical methods are developed to calculate the angular and the energy distributions. In the asymptotical region $V_{ph} \gg V_A$ the problem is solved in the analytical form. The formula

for the most simple case of $(n-1)s - ns^2$ Auger transition has the form:

$$\frac{d^3 \sigma}{dE_A d\Omega_A} = \frac{2 \sigma(E_{ph}) \Gamma_A}{\epsilon^2 + \Gamma^2/4} \left(1 + \alpha P_2(\cos \theta_A) \right) \quad (1)$$

$$\alpha = \frac{2}{5} \beta_{(n-1)s} \frac{v_A^2}{v_{ph}^3} \operatorname{arctg} \frac{2\epsilon}{\Gamma} \quad (2)$$

Here $\sigma(E_{ph})$ - is the photoionization cross section; Γ_A - the partial width of the considered Auger-decay, Γ is the total width of the vacancy $(n-1)s$; $\beta_{(n-1)s}$ - the parameter of the angular distribution of the photoelectrons; ϵ is the energy of Auger-electron relative to its non-perturbed value; P_2 - the Legendre polinomial.

The shift of the maximum of Auger line caused by PCI depends on the velocities v_{ph} , v_A and the angle θ_A of the Auger electron:

$$\Delta \epsilon = \frac{\Gamma}{2} \left(\frac{1}{5} \frac{v_A^2}{v_{ph}^3} \beta_{(n-1)s} P_2(\cos \theta_A) \right) \quad (3)$$

The obtained results in the regions of high and low energies of photoelectrons are in agreement with the formulas of the approximated approach developed in [3] for the angular distribution.

1. M.Yu.Kuchiev, S.A.Sheinerman, Sov.Phys.Usp. 32, 569 (1989)
2. M.Yu.Kuchiev, S.A.Sheinerman, Sov.Phys. - JETP 63, 986 (1986)
3. P.Van der Straten, R.Morgenstern, and A.Niehaus, Z. Phys. D 8, 35 (1988)

THE RADIATIVE SELF-FORCES IN SEMICLASSICAL THEORY
AND THE ANOMALOUSLY SMALL LUMINESCENCE OF ATOMIC SYSTEMS

N.N.Bezuglov, E.N.Borisov, V.P.Proshihin

Department of Optics & Spectroscopy, Institute of Physics,
Leningrad State University, USSR.

The reasons for suppressing photoionization processes observed for some alkali metals atoms are discussed in [1]. The Seaton's arguments concerning a small recovery of the wave functions involved in optical $l \rightarrow l'$ transitions are well known: the difference $\Delta\mu_1 = \mu_1 - \mu_{1'}$ between quantum defects (μ) for l - and l' -series must be close to a half-integer value. In this paper the reduction of the radiative processes efficiency is interpreted by means of the classical motion trajectories.

Sommerfeld notions [2] allow to find the classical analogues for the difference $\Delta\mu_1 (n \rightarrow 0)$: $2\pi\Delta\mu = \Delta\theta_r$. Here θ_r is the Rydberg optical electron rotational angle within the period T_r of the electron radial motion. When the final l' -state belongs to the continuum ($\varepsilon' > 0$, $\varepsilon' \rightarrow 0$) the value $\theta_r = \Delta\theta_r - \pi$ becomes the scattering angle of the slow l' -electron by the ionic core. So, if $\Delta\mu$ is a half-integer, then $\theta_r = 2\pi n$ ($n=0,1,\dots$). There is no classical scattering, consequently no radiation occurs and the probability of the photon absorption is small.

The exclusion of classical factors from radiative processes also results in anomalously small values of the natural line-width A_k . The Feynman concept of quantum electrodynamics was used in [3] to quantize the A_k values. The radiative decay total probability A_k of k -level may be divided into two components

$$(\text{atomic units}): A_k = A_k^{(cl)} + A_k^{(qu)}; \quad A_k^{(qu)} = \langle \hat{\Delta}^2 U(r) \rangle_{ce} / (3c^3); \quad (1)$$

$$A_k^{(cl)} = A_k^{(r)} + A_k^{(l)}; \quad A_k^{(l)} = -2 \langle L \cdot r^{-1} dU/dr \rangle_{ce} / (3c^3). \quad (2)$$

The $A_k^{(cl)}$ -component appears to be analogue to the radiative damping forces for an electron moving in potential $U(r)$. The component $A_k^{(qu)}$ has a quantum mechanical nature. The term $A_k^{(cl)}$

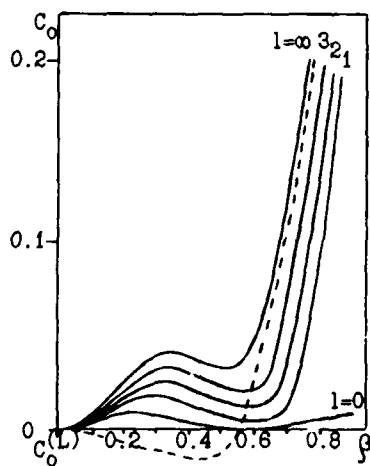
itself consists of two parts, corresponding to the optical electron radial ($A_k^{(r)}$) and angular ($A_k^{(L)}$) motions. The part $A_k^{(L)}$ coincides with the L angular momentum changing rate averaged (symbol $\langle \rangle_{c1}$) along the classical orbit: $A_k^{(L)} = -\Delta L / \Delta t$. In the $\hbar \rightarrow 0$ limit L is given by the orbital quantum number l: $L = l + 0.5$.

The figure represents the results of radiative width A_k calculations for Sommerfeld potential $U_S(r)$ [2]:

$$U_S(r) = -1/r + \alpha / (2r^2); \quad \Delta \theta_r / (2\hbar) \equiv \beta = L / \sqrt{L^2 + \alpha} \quad (3)$$

$$A_k = \frac{8}{\sqrt{3} \cdot c^3} \frac{1}{T_r} \frac{C_0}{L^2}; \quad C_0^{(L)} = \frac{\hbar}{2\sqrt{3}} \beta^3 [1 + 1.5(\beta^2 - 1)] \quad (4)$$

where α is a parameter. The rotational angle $\Delta \theta_r$ (3) is found to be independent upon the energy \mathcal{E} of l-electron. The case of highly excited levels is discussed, so the principal part of A_k asymptotical form [3] has been kept here only. Coefficient C_0 (solid curves) from (4) defines the effectivity of Rydberg l-levels luminescence. For hydrogen atom ($\alpha=0$) $C_0=1$ always, except s-series where $C_0=0.0125$ [3]. Coefficient $C_0^{(L)}$ mentioned in (4) (broken curve) corresponds with the angular component $A_k^{(L)}$. One can see that the appearance of the minimum in the radiative decay probability correlates with the zero value ($A_k^{(L)}=0$ when $\beta=\beta_0=1/\sqrt{3}=0.577$) of the angular momentum change rate dL/dt .



It should be noted that the scattering angle $\theta_r^{(0)} = 2\hbar \beta_0 - \hbar = 0.077 \cdot \hbar$ ($\mathcal{E} \rightarrow 0$) in the region of curves minimum is quite small.

Thus the quantum mechanical probability of radiative processes is mainly controlled by the classical radiation theory factors.

1. Fano U. - Rev. Mod. Phys., 1968, v.40, p.431.
2. Sommerfeld A. Atomic Structure and Spectral Lines, 1931, London.
3. Bezuglov N.N. - Sov. Opt. & Spectr. v.65, p.772. (1988)

SPIN-ORBIT PERTURBATION IN ATOMIC RUBIDIUM
THROUGH PHOTO-ELECTRON ANGULAR DISTRIBUTIONS

Yi-Yian Yin, Ce Chen and D. S. Elliott
School of Electrical Engineering, Purdue University
West Lafayette, IN 47907 USA

We have measured the angular distribution of photo-electrons ejected from atomic rubidium through photo-ionization by light of wavelength 280 nm and by light of wavelength 560 nm. The former has sufficient photon energy to ionize the rubidium atoms through a linear absorption process, while two photons at 560 nm are required. From this data we derive the spin-orbit coupling strength of the continuum states. This same perturbation leads to an asymmetry in the ionization rate of a polarized atom beam using left or right circularly polarized light¹. Our results disagree somewhat with those derived from these measurements.

The photo-electron angular distributions are measured using familiar techniques. The laser beam intersects an atomic rubidium beam inside a vacuum system maintained at a pressure of $\sim 5 \times 10^{-8}$ torr. The interaction region is free of electric and magnetic fields by virtue of a pair of grounded parallel conducting plates and three pairs of Helmholtz coils. An electron lens and a channeltron detector are located behind a 2 mm diameter hole in one of the conducting plates. The angular distributions are measured by counting the fraction of laser shots which produce an electron with momentum in the direction towards the aperture, as a function of the orientation of the laser polarization. The polarization is rotated using a half-wave plate (uv beam) or a half-wave Fresnel rhomb (visible beam). Angular distribution data and their fits (solid line) are shown in figure 1.

Current activities on this project are directed toward measurement of the photo-electron angular distribution when both fields (560 nm and 280 nm) are incident on the atom concurrently. In this case we expect an interference between the different ionization channels, such that the angular distribution is sensitive to the relative phase of the two fields.

This work is supported by an award from the National Science Foundation.

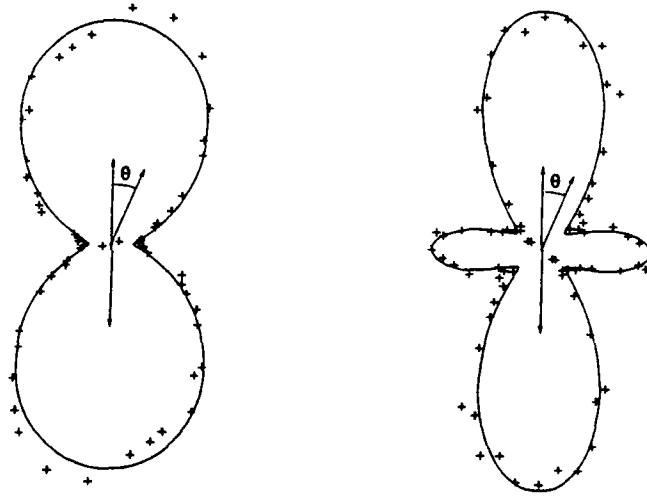


Figure 1: Photo-electron angular distributions for one-photon ionization (left) using light of wavelength 280 nm, and for two-photon ionization (right) using light of wavelength 560 nm. Theta is the angle between the laser polarization and the direction of the electron momentum. The solid line is the result of a least squares fit to the data.

References

- ¹ G. Baum, M. S. Lubell and W. Raith, Phys. Rev. Lett. **25**, 267 (1970).

PHASE SENSITIVE MULTI-PHOTON IONIZATION

Ce Chen, Yi-Yian Yin and D. S. Elliott
School of Electrical Engineering, Purdue University
West Lafayette, IN 47907 USA

We have demonstrated¹ an interference between multi-photon ionization processes which results in a phase-sensitive enhancement or inhibition of the net ionization rate. We focus two laser beams, either of which can induce an atomic transition between the same two states, into a cell containing atomic mercury. One of the fields is at a wavelength of 185 nm, and can induce the $6s\ ^1S_0 \rightarrow 6p\ ^1P_1$ transition in mercury linearly. The other field is at a wavelength precisely three times as long, and can excite the 6p resonance by a three-photon process. The absorption of two additional visible photons ionizes the mercury. In the presence of both fields, the transition amplitudes interfere, and their relative phase is very important. Their phases can be controlled by controlling the phase of the optical fields inducing the transitions. Coherence between the two fields, vital for the interference, is ensured by generating one field from the other using a non-linear third harmonic process. The experimental cell is shown in figure 1. Light at 554 nm from a pulsed dye laser is focussed into a high density mercury vapor cell in order to generate its third harmonic at 185 nm. The two beams diverge collinearly, are collimated and refocussed using spherical mirrors into a low-density mercury cell where the ionization rate is determined. In the region between the third-harmonic generation cell and the mercury ionization cell, the relative phase of the two optical fields is controlled by varying the density of an argon gas. The total ionization rate as a function of argon pressure is shown in figure 2. The solid line is a fit to the data.

We have further demonstrated² the effect of spatial phase variations of the two fields on the local photo-ionization rate. We have used an array of parallel linear collection electrodes to determine the photo-ionization rate at various distances along the laser beam axis from the focus. As the argon gas density is varied, each electrode measures a sinusoidally varying ionization signal, but the phase of each signal varies from one electrode to the next. This shift is due to the phase shift of a focussed Gaussian beam from one side of the focus to the other. The measured spatial dependence of the phase variation agrees very well with results calculated for the

laser beam geometry of our experiment.

This work is supported by the National Science Foundation and a David Ross Grant from Purdue University.

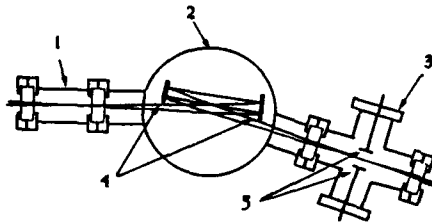


Figure 1: The three chamber cell. The labels indicate (1) the third-harmonic generation cell, (2) the phase-delay cell, (3) the ionization cell, (4) the spherical mirrors, and (5) a pair of biased collection plates.

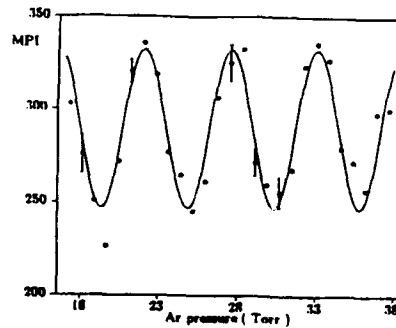


Figure 2: Ionization signal measured as a function of argon pressure of argon pressure in second chamber. Solid line indicates a best fit to the data. Error bars showing one standard deviation of the mean are shown for a few data points.

References

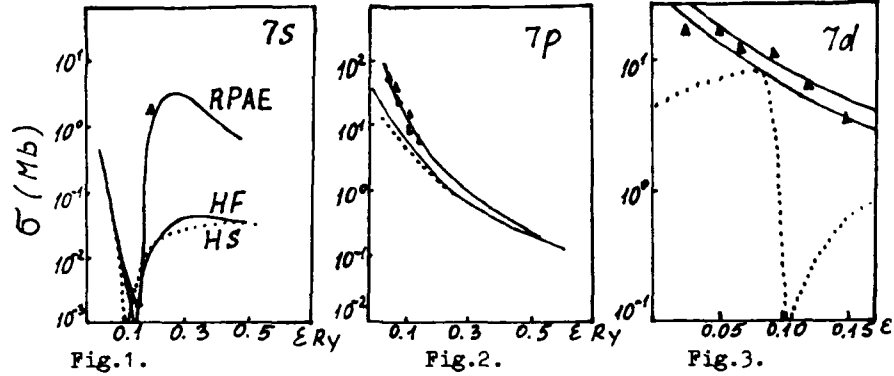
- 1 Ce Chen, Yi-Yian Yin, and D. S. Elliott, Phys. Rev. Lett. **64**, 507 (1990).
- 2 Ce Chen and D. S. Elliott, submitted to Phys. Rev. Lett.

THE CALCULATION OF THE PHOTOIONIZATION CROSS SECTIONS
OF THE 7^2L EXCITED STATES OF Cs.

N.B.Avdonina and M.Ya.Amusia
Technological Institute of Refrigeration Industry,
Lomonosov st.9 SU 191002 Leningrad, USSR.
A.F.Ioffe Physical-technical Institute, Leningrad,
198904 USSR.

The photoionization of the preliminary excited $7s$, $7p$ and $7d$ states of Cs is considered. The calculation of the cross sections are carried out both in the Hartree-Fock approximation and with inclusion of the many electron correlations in the random-phase approximation with exchange (RPAE). It is demonstrated that our results obtained in RPAE are in a good agreement with experimental measurements. In recent years, laser technique has advanced to such a degree that experimental work on excited atomic states becomes quite possible. A few years ago experiment for the photoionization of the Cs 7^2P state was carried out /1/. The cross section for the 7^2S state have been measured at 540-nm wavelength /2/ and recently the absolute data for the 7^2D Cs state have been reported /3/. Thus at present we have the possibility to test the different theoretical calculations for the excited states of Cs atom.

The good test of the accuracy of the approximation used in the calculation is the comparison the theoretical photoionization results with the experimental data for the $7s$ excited state in the Cooper minimum region where cross section has a very strong dependence on energy (Fig.1). The interaction with $5s$ and $5p$ subshells is taken into account within framework of RPAE. One can see that the effect of the intershell interaction on photoionization of $7s$ state in excited Cs is very strong. Hartree-Fock and Hartree-Slater approximations /4/ predict a values about one half of the experimental data /2/.



We also find rather good agreement between RPAE theory and experiment /1/ for the photoionization cross section of the 7p excited state. The interaction of the $7p \rightarrow \epsilon s$ and $7p \rightarrow \epsilon d$ transitions leads to the increasing of the total cross section. RPAE smooth curve obtained in a such way describes the experimental data quite well (Fig.2). Hartry-Fock and Hartry-Slater curves lie considerably lower then the RPAE one. The results of measurements for 7d excited states of Cs /3/ and our calculations are presented in Fig.3. The minimum predicted for 7d state in the Hartry-Slater approximation /4/ is not confirmed by the measurement in the investigated spectral region. RPAE predicts those minima at much higher energy and our results, taking into account the interaction with 5p subshell of Cs are in good agreement with the experimental cross section.

Thus we note that the results of RPAE appear to be in better agreement with measurements then the Hartry-Fock results for all considered excited states.

1. K. Gerwert and K. G. Kollath, J. Phys. B16 (1983) L217.
2. S. L. Gilbert, M. C. Noecker and C. E. Wieman, Phys. Rev. A29 (1984) 3150.
3. K. D. Bonin, M. Gatzke, C. L. Collins and M. A. Kadar-Kallen, Phys. Rev. A39 (1989) 5626.
4. J. Lahiri and S. T. Manson, Phys. Rev. A33 (1986) 3151.

A NEW METHOD TO COMPUTE ATOMIC AND MOLECULAR
PHOTOIONIZATION CROSS SECTIONS BY USE OF BASIS SETS

L. Veseth

Department of Physics, University of Oslo,
0316 Oslo 3, Norway.

The development of efficient and accurate methods to compute atomic and molecular photoionization cross sections by use of basis sets (algebraic approximation) has been a longstanding problem in atomic and molecular physics. Sophisticated numerical techniques of current use in the atomic case are very problematic for molecules due to the difficulties involved in obtaining accurate continuum orbitals for multicenter systems.

A new approach to the problem of computing atomic- and molecular photoionization cross sections by use of basis sets will be presented. The first step is to compute complex dynamic polarizabilities. Many-body perturbation theory is used for that purpose, and the perturbation expansion is complete to second order in the Coulomb interaction. Hence, the amount of correlation included in the calculations is higher than what is normal in current photoionization work.

Finally, the photoionization cross section is derived by inverting a simple integral equation which relates this quantity to the (real) polarizability on the imaginary frequency axis. The real part of the polarizability on the real frequency axis (index of refraction) is then in turn computed from the Kramers-Kronig dispersion relations.

Computed results will be presented for the atoms neon and argon as test cases. Applications to molecules are, however, the main objective of the present method, and results will be given for the diatomics HF and CO.

PHOTODETACHMENT CROSS SECTIONS FOR Ca^- , Sr^- and Ba^- G.F.Gribakin[†], B.V.Gul'tsev[†], V.K.Ivanov[†], M.Yu.Kuchiev[‡][†] M.I.Kalinin Polytechnical Institute, 195251 Leningrad, USSR[‡] A.F.Ioffe Physical Technical Institute of the Academy of Sciences of the USSR, 194021 Leningrad, USSR

The Dyson equation method, recently suggested in /1/, is applied to the negative ions of Ca^-4s^24p , Sr^-5s^25p and Ba^-6s^26p . Binding energies and wavefunctions of the outer electrons and their photodetachment cross sections are calculated.

The wavefunction $\Psi_0(\vec{r})$ and energy ε_0 for the outer electron in the negative ion are obtained from the equation:

$$\hat{H}^{(0)}\Psi_0(\vec{r}) + \int \Sigma_{\varepsilon}(\vec{r},\vec{r}')\Psi_0(\vec{r}')d\vec{r}' = \varepsilon_0\Psi_0(\vec{r}) \quad (1)$$

where $\hat{H}^{(0)}$ is the static Hartree-Fock Hamiltonian of the neutral atom, $\Sigma_{\varepsilon}(\vec{r},\vec{r}')$ is the energy dependent polarisational potential. The latter is calculated by means of the diagrammatic expansion in powers of the residual interelectron interaction. The values for the binding energies of the outer electron are $|\varepsilon_0| = 0.058$ eV, $|\varepsilon_0| = 0.129$ eV and $|\varepsilon_0| = 0.144$ eV for Ca^- , Sr^- and Ba^- correspondingly (/2/).

The outer electron wavefunction is used to calculate photodetachment amplitudes:

$$D_{\ell\pm 1}(\omega) = \int \Psi_{\ell\pm 1}^{(\omega)*}(\vec{r}) \hat{d} \Psi_0(\vec{r}) d\vec{r} \quad (2)$$

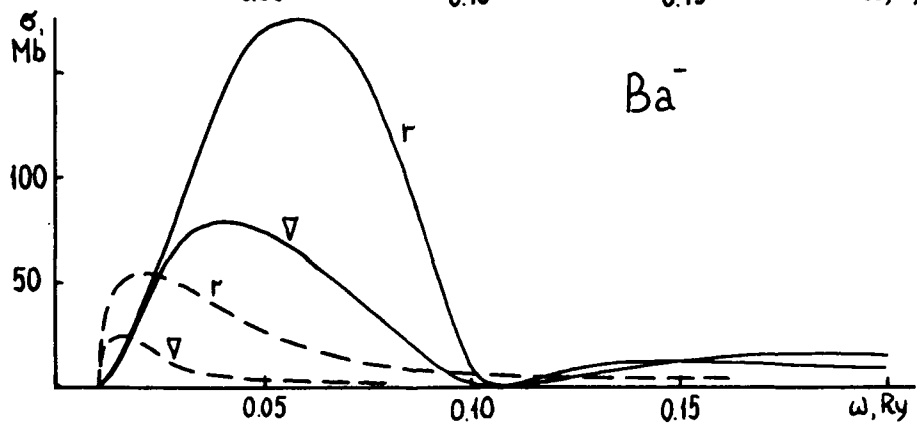
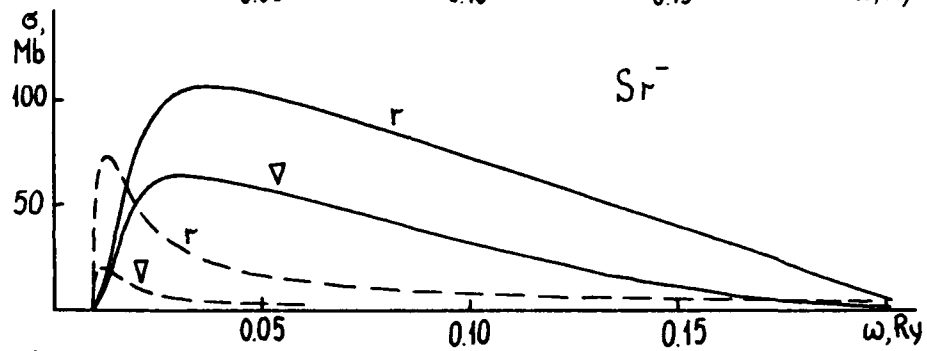
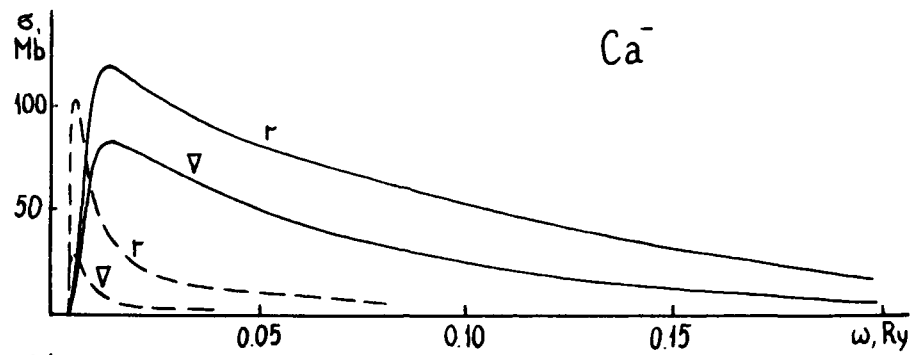
Here \hat{d} is the dipole operator of the electron-photon interaction, and $\Psi_{\ell\pm 1}^{(\omega)}$ is the Hartree-Fock wavefunction for the photoelectron of energy $\varepsilon = \omega + \varepsilon_0$ and $\ell \pm 1$ orbital momentum. The amplitudes and the cross sections for p-electron detachment of Ca^- , Sr^- and Ba^- were calculated with \hat{d} in r and ∇ forms. The cross sections are presented in the figure (solid line is the p-d channel, dashed line - p-s channel). We suppose that they may be changed strongly by the action of $\Sigma_{\varepsilon}(\vec{r},\vec{r}')$ onto the photoelectron d and s waves.

1. Chernysheva L.V., Gribakin G.F., Ivanov V.K., Kuchiev M.Yu.

J.Phys.B: At.Mol.Opt.Phys. 21, L419-L425 (1988).

2. Gribakin G.F., Gul'tsev B.V., Ivanov V.K., Kuchiev M.Yu.

submitted to J.Phys.B: At.Mol.Opt.Phys. (1990).



NEAR-THRESHOLD PHOTODETACHMENT OF H^- IONS IN PARALLEL AND CROSSED
ELECTRIC AND MAGNETIC FIELDS

I. I. Fabrikant
 Department of Physics and Astronomy
 University of Nebraska, Lincoln, NE 68588, USA

The cross section for photodetachment of atomic negative ions in external static electric and magnetic fields is known to have an oscillatory dependence on the light frequency. In the case of a pure electric field this structure is due to interference effects and in the case of a pure magnetic field due to the Landau thresholds. Combination of these two structures can be observed for photodetachment in parallel or crossed fields.

In the present paper we consider this process for the H^- ions with the inclusion of the final-state interaction between the electron and the H atom in the framework of the zero-range potential approximation. The frame transformation approach is used for the treatment of the problem. The case of linear photon polarization parallel to the electric field is studied since in this case the interference effects caused by the electric field are more pronounced.

The importance of the final-state interaction is controlled by the parameter

$$n = \frac{a\omega_B}{(2E)^{1/3}} \quad (\text{a.u.})$$

where a is the scattering length, ω_B is the cyclotron frequency and E is the

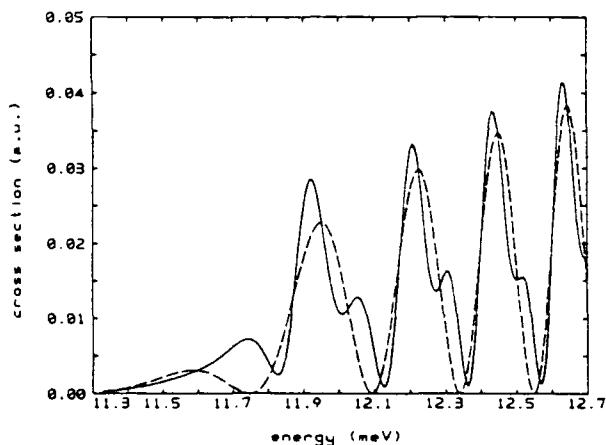


Fig. 1. Photodetachment cross section in parallel electric ($E = 100\text{V/cm}$) and magnetic ($B = 200\text{T}$) fields as a function of the electron energy in the final state. Solid curve and dashed curve, with and without the account of e-H interaction in the final state, respectively.

electric field strength. An example illustrating the importance of the final-state interaction (the rescattering effect) is presented in Fig. 1. A noticeable rescattering effect requires a very high magnetic field. However, deep modulations of the cross section presented in Fig. 1 can be observed also for moderate fields between the first and second Landau thresholds if

$$\frac{\omega B}{(2E)^{2/3}} \geq 1$$

An example of the structure for perpendicular fields is presented in Fig. 2. In both cases the magnetic field increases the modulations induced by the electric field but in the case of parallel fields the modulations are deeper corresponding to the quasi-one-dimensional character of the problem.

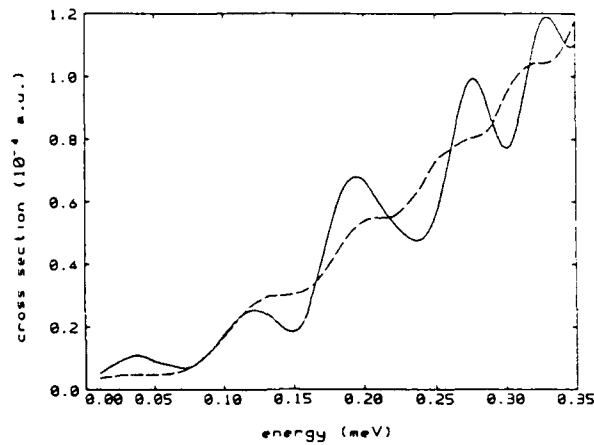


Fig. 2. Photodetachment cross section in an electric field of 15V/cm (dashed curve) and in crossed fields of E = 15V/cm and B = 1T (solid curve).

SPIN AND CHANNEL COUPLING IN PHOTOIONIZATION OF Na

Alfred Z. Msezane and Francis Nyandeh
Clark Atlanta University, Atlanta, Georgia 30314 U.S.A.

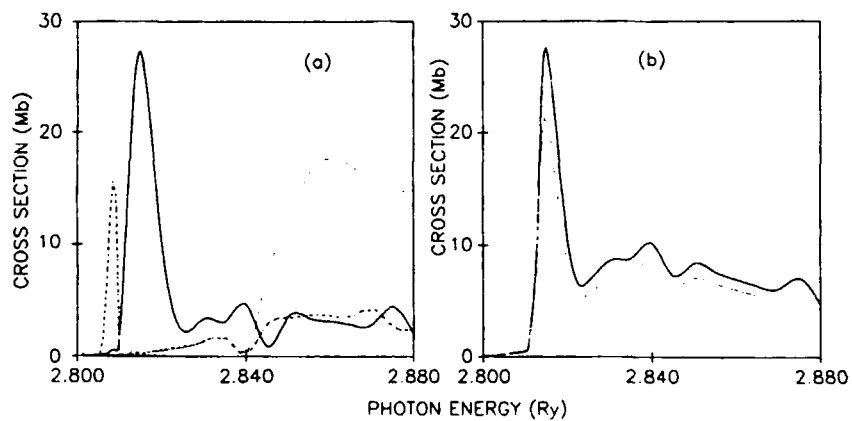
Spin exchange interactions and channel coupling in ground state photoionization of Na, leaving the residual Na⁺ ions in the 2p⁵3s ³P^o and ¹P^o excited states are investigated in the R-matrix method¹ coupling the lowest 15, 3 and 2 extensive CI target states. The appropriate combination of states is selected from: 2p⁶ ¹S, 2p⁵3s ^{3,1}P^o, 2p⁵3p ^{3,1}S, ^{3,1}P, ^{3,1}D; and 2p⁵3d ^{3,1}P^o, ^{3,1}D^o and ^{3,1}F^o. The states and their corresponding energy splittings were generated using Program CIV3 of Hibbert², the latter are all within 5% of the experimental values.

Four sets of cross sections were evaluated for leaving the Na⁺ ions in the 2p⁵3s ³P^o states coupling: (a) 2p⁶ ¹S and 2p⁵3s ³P^o; (b) 2p⁶ ¹S and 2p⁵3s ¹P^o; (c) 2p⁶ ¹S and 2p⁵3s ^{3,1}P^o; and (d) all the 15 states. (a) and (b) represent "spin-uncoupled" 2CC calculations, while (c) corresponds to 3CC "spin-coupled" computations. The results from (d) give a 15CC spin and channel coupled cross sections. Comparison of the 15CC, 3CC, and 2CC results will indicate the extent of importance of spin and channel coupling.

FIG. (a) presents the photoionization cross sections of Na, leaving the Na⁺ ion in the 2p⁵3s ³P^o state: —, 15CC; - - - -, 3CC and ·····, 2CC. The addition of the 2p⁵3s ¹P^o state dramatically throws the 2CC peak close to threshold, and narrows it while preserving its magnitude. The major effect of adding the states of the n=3 (l=1 and 2) manifolds is to enhance the magnitude of, broaden and shift away from threshold the 3CC resonance. At higher photon energy, the 3CC is a reasonable approximation to the 15CC calculation. FIG. (b) gives the total length (—) and velocity (·····) photoionization cross sections of Na 3s in the 15CC approximation. The dominant enhancement near threshold is due to the triplet component as previously predicted.³ The additional enhancement at higher energy is due mainly to the 2p⁵3s ¹P^o contribution. Strong correlations are also evident in the results.

We conclude that the most important coupling is between the 2p⁵3s ^{3,1}P^o spin states. The near threshold behavior of the triplet cross section is consistent with that observed in Be photoionization.⁴ The details of the calculations will be presented.

*Work was supported by DOE, Basic Energy Sciences, Division of Chemical Sciences and NSF. We are grateful for generous computer time on the NMFEECC Crays provided by DOE, Office of Basic Energy Sciences Division of Chemical Sciences and Office of Fusion Energy through Oak Ridge National Laboratory.



REFERENCES

- ¹ K.A. Berrington et. al., *Comput. Phys. Commun.* **14**, 367 (1978).
- ² A. Hibbert, *Comput. Phys. Commun.* **9**, 141 (1975).
- ³ A. Z. Msezane, W. Armstrong-Mensah and J. Niles, *Phys. Rev. A* **xx**, to appear (1990).
- ⁴ M. O. Krause and C. D. Caldwell, *Phys. Rev. Lett.* **59**, 2736 (1987).

HIGHER RETARDATION AND MULTIPOLE CORRECTIONS TO THE DIPOLE ANGULAR
DISTRIBUTION OF INNER SHELL PHOTOELECTRONS

A. Bechler* and R. H. Pratt
Department of Physics and Astronomy, University of Pittsburgh
Pittsburgh, PA 15260

We present results of a calculation of the corrections to the dipole angular distributions of the photoelectrons ejected from K and L shells in low to medium Z atoms. The calculations were performed nonrelativistically in the independent particle approximation. We used an expansion of the photon plane wave up to and including terms linear in the photon momentum k , $\exp(ik \cdot r) \approx 1 + ik \cdot r$, obtaining the following expression for the transition matrix element:

$$M = -i \int d^3x \psi_p^* \epsilon \nabla \psi_{nl} - i \int d^3x \psi_p^* (\epsilon \nabla)(ik \cdot r) \psi_{nl}, \quad (1)$$

with obvious notations. The first term corresponds to the dipole approximation and the second term is called the first retardation correction.¹ For the initial electron in an s-state the angular distribution of the photoelectrons ejected by polarized photons with polarization vector ϵ has the form

$$\frac{d\sigma}{d\Omega} \sim |\epsilon \cdot \hat{p}|^2 (1 + \kappa \cos\theta), \quad (2)$$

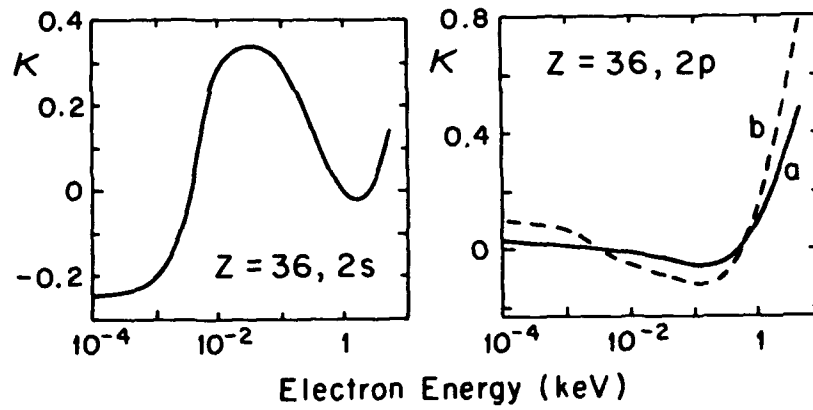
where $\cos\theta = k \cdot p / kp$; p is the momentum of the final electron and κ , which measures the retardation correction, is proportional to $|k|$. For a p-subshell the angular distribution has the form

$$\frac{d\sigma}{d\Omega} \sim 1 + \beta P_2(|\epsilon \cdot \hat{p}|) + (\hat{p} \cdot \hat{k}) [a + b P_2(|\epsilon \cdot \hat{p}|)], \quad (3)$$

where β is the asymmetry parameter and a, b characterize the retardation corrections to the dipole differential cross section. As can be seen, these first retardation corrections vanish upon integration over angles and do not contribute to the total cross-section. The first nonvanishing correction to the dipole term in the total cross-section is therefore of the same order of magnitude as relativistic corrections, whereas in the angular distribution it is at low energies much bigger [of the order $Z\alpha$ rather than $(Z\alpha)^2$], and it can be consistently calculated in the nonrelativistic framework.

The retardation correction factor κ can be as large as 0.2 even for energies of the final electron of the order of 10 eV. Its sign at threshold depends on the sign of $\cos(\delta_1 - \delta_2)$, to which κ is proportional, and this sign changes several times as Z increases from 6 to 40. For 2p-subshells the retardation effects in the angular distribution are in general smaller at low energies than in the 1s or 2s cases.

The graphs below show the retardation corrections for photoeffect from 2s and 2p initial electrons ejected from Krypton ($Z = 36$) at energies ranging from threshold to a few keV.



References

*Permanent address: Institute of Physics, University of Szczecin, Szczecin, Poland.

1. A. Bechler, and R. H. Pratt, Phys. Rev. A 39, 1774 (1989).

THEORETICAL INVESTIGATIONS OF PHOTON-ELECTRON POLARIZATION
CORRELATIONS IN ns-SUBSHELL PHOTOIONIZATION OF URANIUM

Y. S. Kim,[†] I. B. Goldberg,^{*} and R. H. Pratt[‡]

[†]Department of Physics, Myong Ji University, Yong-In 449-728 Korea
Racah Institute of Physics, Hebrew University of Jerusalem
Jerusalem 91904 Israel

[‡]Department of Physics and Astronomy, University of Pittsburgh
Pittsburgh, PA 15260 USA

We have made a comprehensive survey of the behavior of all possible correlations between the polarization of the incoming photon and the spin of the outgoing photoelectron, ejected from all subshell of uranium, for photon energies from 1 eV to 300 keV. The correlations for ns-subshell photoionization will be reported here. The numerical results for these polarization correlations are obtained within independent particle approximation in a relativistic self-consistent atomic field (Dirac-Slater type), including all significant multipole contributions. We characterize the polarization correlations as the functions of energy and angle C_{ij} such that

$$\frac{d\sigma}{d\Omega}(\vec{\xi}, \vec{\zeta}) = \left(\frac{d\sigma}{d\Omega}\right)_{\text{unpol}} \left[\frac{1}{2} \sum_{i,j=0}^{\infty} \xi_i \zeta_j C_{ij} \right],$$

where the photon polarization is described by the Stokes parameters ξ_i , and the spin of the ejected electron in its rest system is given as the direction $\vec{\zeta}$, with $\xi_0 = \zeta_0 = C_{00} = 1$.

The general expressions for C_{ij} in terms of relativistic multipole transition matrix elements¹ are fairly complicated. We have obtained their dipole reductions in the coordinate system in which the \hat{z} -axis is along the incoming photon momentum \hat{k} and \hat{y} is along $\hat{k} \times \hat{p}$, so that the production plane is the \hat{x} - \hat{z} plane and the momentum \hat{p} of the photoelectron makes an angle θ with \hat{z} . The spin polarization of the ejected electron is specified by its spin direction $\hat{\zeta}$ in its rest system, with $\zeta_1 = \vec{\zeta} \cdot (\hat{y} \times \hat{p})$, $\zeta_2 = \vec{\zeta} \cdot \hat{y}$, and $\zeta_3 = \vec{\zeta} \cdot \hat{p}$. The dipole expressions for the C_{ij} of the ns-photoionization in the long-wavelength limit are

$$C_{02} = -3 \sin\theta \cos\theta R_1 R_3 \sin\delta / (16\pi D_{00}),$$

$$C_{10} = 3 \sin^2 \theta (R_2^2 + 2R_1 R_3 \cos \delta) / (32\pi D_{00}),$$

$$C_{12} = C_{02} ,$$

$$C_{21} = 3 \sin \theta R_1 R_3 \sin \delta / (16\pi D_{00}) ,$$

$$C_{23} = 0 ,$$

$$C_{31} = \sin \theta (R_1^2 - 2R_3^2 + R_1 R_3 \cos \delta) / (16\pi D_{00}) ,$$

$$C_{33} = \cos \theta (R_1^2 + R_3^2 - 2R_1 R_3 \cos \delta) / (16\pi D_{00}) ,$$

where R_1 and R_3 are the radial dipole matrix elements for the transitions from ns to $\epsilon p_{1/2}$ and $\epsilon p_{3/2}$ states respectively, (apart from the factor $e^{i\delta_j}$), $\delta = \delta_{1/2} - \delta_{3/2}$, and

$$D_{00} = \frac{k}{16\pi p E \alpha} \left(\frac{d\sigma}{d\Omega} \right)_{\text{unpol}} = \frac{1}{16\pi} [(R_1^2 + 2R_3^2) - (R_3^2 + 2R_1 R_3 \cos \delta) P_2(\cos \theta)] .$$

We confirm that at low photon energies (up to $T \sim 1$ keV), which means low kinetic energy T of the photoelectron ejected from a subshell of high n , the dipole predictions are generally valid, accurately reproducing the full numerical results including the abrupt changes in the shape of the C_{ij} curves as functions of θ for low T and high n .

As photon energy increases, the correlation coefficients become complicated functions of the ejection angle θ , losing symmetry around $\theta = 90^\circ$. For higher T , the correlation coefficients of different n tends to merge into a common curve as a function of θ , though the shape of the curve keeps changing as T increases, as we have previously reported for angular distributions.²

References

1. R. H. Pratt, Akiva Ron and H. K. Tseng, Rev. Mod. Phys. 45, 273 (1973).
2. Y. S. Kim, R. H. Pratt, Akiva Ron and H. K. Tseng, Phys. Rev. A 22, 567 (1980).

ENERGY- AND ANGULAR DISTRIBUTION OF SHAKE-OFF ELECTRONS OF HE NEAR THRESHOLD

R. Wehlitz, O. Hemmers, B. Langer, A. Menzel and U. Becker*
Institut für Strahlungs- und Kernphysik, Technische Universität Berlin,
Hardenbergstr. 36, D-1000 Berlin 12, West Germany

The simultaneous emission of two electrons in an ionization process is an example of the three body Coulomb problem [e. g. 1]. One theoretical prediction on this problem is that, near threshold, the excess energy is shared randomly between the two electrons; that is, the energy distribution $P_E(E_r)$ where E_r is a residual energy, is uniform. This is not the case at high energies where the distribution curve generally shows marked curvature with a minimum at the mid-point due to screening between the two electrons. What is still controversial on this problem is the range over which the random partitioning holds.

Another prediction particularly for double ionization of rare gases refers to the angular distribution of the two emitted electrons with respect to the electric vector of the ionizing radiation. The prediction is that in each of the rare gases the asymmetry parameter approaches the "unfavored value" $\beta \rightarrow -1$ near the double escape threshold [2]. We have used angle resolved time-of-flight photoelectron spectroscopy to investigate these two predictions. The results are shown in fig. 1 and 2.

The prediction on the uniform energy distribution is well proven up to an unexpectedly high value of approximately 5 eV. The second prediction concerning the angular distribution is not verified, instead of approaching $\beta \rightarrow -1$ the angular distribution seems to retain more isotropic character even near threshold.

References:

1. J. M. Feagin, J. Phys. B 17, 2433 (1984)
2. C. H. Green, J. Phys. B 20, L 357 (1987)

This work was supported by the Bundesminister für Forschung und Technologie under contract No. 05414 CAB7

*Present address: Fritz-Haber-Institut der Max-Planck-Gesellschaft, Faradayweg 4 - 6,

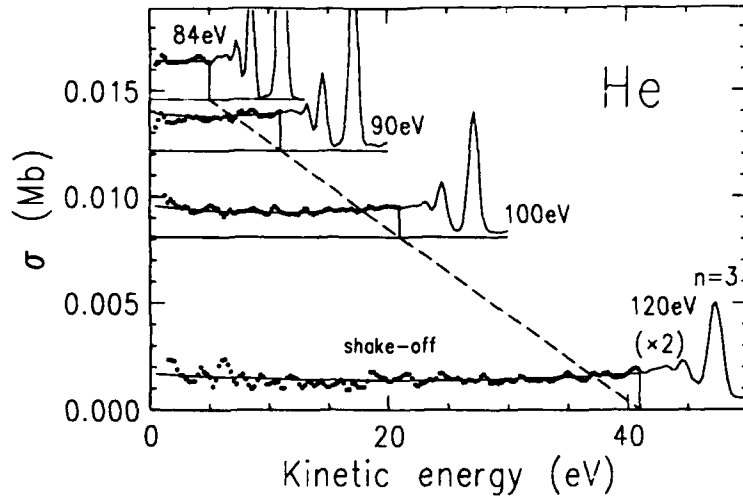


Fig. 1: Photoelectron spectra of He above the double ionization threshold. The solid lines in the shake-off interval represent semiempirical symmetric distributions.

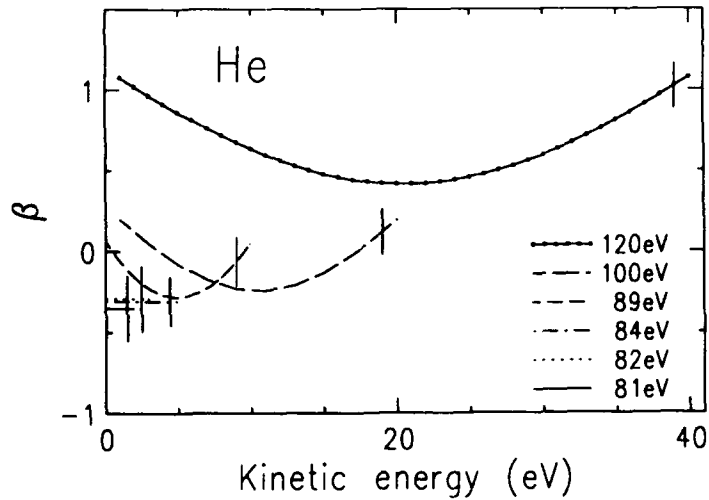


Fig. 2: Angular distribution asymmetry-parameters of shake-off electrons for different photon energies. The lines are derived from fitted energy distributions under different angles, they represent the corresponding average values.

DECAY OF THE AR 2p'nd CORE RESONANCES:

AN AUGER SPECTRUM DOMINATED BY SHAKE PROCESSES

J.E. Hansen

Zeeman Laboratory, University of Amsterdam, Plantage Muidergracht 4,
NL-1018 TV Amsterdam, The Netherlands

M. Meyer, E. v. Raven and B. Sonntag

II. Institut für Experimentalphysik, Universität Hamburg,
Luruper Chaussee 149, D-2000 Hamburg, W.Germany

The autoionization of the Ar 2p'nd resonances has been studied both experimentally and theoretically. The resonances have been studied experimentally at the FLIPPER I-Wiggler/undulator beamline at the Hamburger Synchrotronstrahlungslabor HASYLAB [1]. An atomic beam of argon crossed the monochromatized synchrotron radiation in the source volume of a cylindrical mirror analyzer. The photoelectrons were detected close to the magic angle. The resolution of the mirror analyzer was improved by retarding the fast electrons by a constant electric field. The resolution thus achieved is given by $\Delta E_{kin} = 0.01*(E_{kin} - eU_{ret})$. The bandwidth of the monochromator was about 0.6 eV. An example of a spectrum is given in the figure which shows the decay of the 3d resonance.

If the nd electron is considered as being interacting weakly with the inner electrons, the Auger spectrum should resemble the electron spectrum following decay of a 2p hole in Ar. This spectrum is also shown in the figure. We have already studied the decay of the 4s resonance [2] and found that the above picture is a reasonable description of the decay process although deviations were found due to the fact that the interaction between 4s and in particular 3p in the final ionic state is non-negligible. In contrast, the figure shows that the 3d decay bears no resemblance to the 2p hole decay. However, Ar lies just before the transition metals in the periodic system at a point where the 3d electron is very sensitive to the environment. One consequence is that while the 3d orbital is far from being collapsed in the presence of a 2p hole, the presence of two 3p holes does lead to an appreciable collapse of the 3d function and consequently to a large 3d \leftrightarrow 3p interaction. These facts leads to a unprecedented amount of shake-up and shake-down in the Auger decay from the initial state (with the 2p hole) to the final state (with the two 3p holes).

The effect of the partial collapse of the 3d wavefunction between the initial and the final state has been studied with regard to shake probabilities as well as to the structure of the final ionic configuration. The decay probabilities depend strongly on the principal quantum number both of the core excited Ar* 2p'nd state and of the Ar* 3p'n'd final state. The 2p'nd \rightarrow 3p'nd ϵ l decay is almost completely forbidden for n=4. This is the first time such a case has been observed. The measured and calculated branching ratios are given in the table.

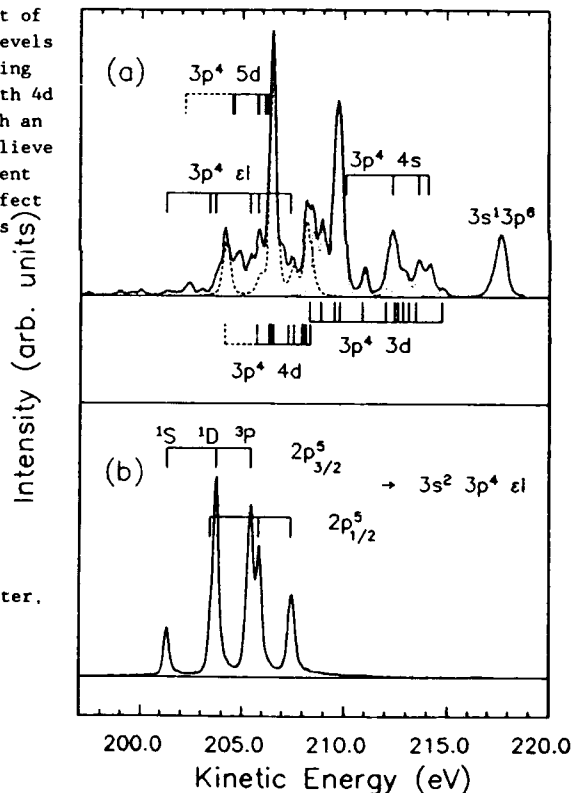
Observed and calculated intensities for the decay channel
 $\text{Ar}^* 2p^3s^3p^4d \rightarrow \text{Ar}^* 2p^3s^3p^4d$.

initial state	Intensity of final states [%]									
	3p' nd									
	n = 3		n = 4		n = 5		n = 6		n = 7	
Ar*	exp.	calc.	exp.	calc.	exp.	calc.	exp.	calc.	exp.	calc.
2p'4d	13	12	9	0.04	46	63	32	24	-	0.2

The small calculated value shows that the 4d orbitals in the initial and final states are close to being orthogonal. We believe that the disagreement with observation is less than the numbers indicate. We have found that there is a mixing between 3p'nd configurations which has the effect of directing shake-up to 5d back to levels identified as 4d as well as directing shake-down to 3d back to levels with 4d labels. This is the first time such an effect has been observed and we believe that a large part of the disagreement with observation is due to this effect because the detailed analysis shows that the discrepancies occurs primarily for levels which we find to be mixed.

References

- [1] F. Senf, K. Berens v. Rautenfeld, S. Gramm, C. Kunz, J. Lamp, V. Saile, J. Schmidt-May and J. Voss, Nucl. Instr. Meth. A246, 314 (1986)
- [2] M. Meyer, E. v. Raven, M. Richter, B. Sonntag and J.E. Hansen, J. Electron Spectrosc. Related Phenom. 51, 407 (1990)



STUDY OF DIELECTRONIC AND RADIATIVE RECOMBINATION OF
FEW-ELECTRON IONS IN THE HEAVY-ION STORAGE RING TSR

A. Wolf^a, J. Berger^a, M. Bock^a, D. Habs^a, B. Hochadel^a, G. Kilgus^a, A. Müller^c,
M. Music^a, G. Neureither^a, U. Schramm^a, R. Schuch^b, D. Schwalm^a and M. Wagner^c
^aPhysikalisches Institut der Universität and Max-Planck-Institut für Kernphysik, Heidelberg,
Fed. Rep. of Germany; ^bManne-Siegbahn Institute, Stockholm, Sweden;
^cInstitut für Kernphysik, Universität Giessen, Fed. Rep. of Germany

In the heavy-ion storage ring TSR in Heidelberg [1] inelastic interactions of bare and few-electron ions with free electrons are studied in the overlap region of an intense, cold electron beam with the circulating ion beam. This experimental arrangement has been used to measure radiative and dielectronic recombination rates with a high resolution in center-of-mass electron energy. In particular, the dielectronic recombination of hydrogen-like ions via helium-like doubly excited states could be studied for the first time with high energy resolution [2]. The state-resolved dielectronic-recombination measurements provide a sensitive probe for the energies, autoionization rates, and radiative decay rates of these doubly excited states. The properties of these resonances are of interest in the study of the correlated motion in two-electron systems and also important for understanding atomic processes in thin, high temperature plasmas. In this environment, dielectronic recombination often is the dominant recombination process. Similarly, the electron-impact excitation and ionization of few-electron ions proceeds to a considerable fraction via resonant intermediate states.

State-resolved measurements of the dielectronic recombination rates involving changes $\Delta N \geq 1$ of the core principal quantum number N were performed for the hydrogen-like ions O^{7+} and C^{5+} and for the helium-like C^{4+} . These ions were accumulated in the TSR storage ring at a beam current of the order of $100 \mu A$ and at a relatively high energy between 6 and 10 MeV/u. First, the intense electron beam of the electron cooling device of the TSR was used to reduce the ion beam size to about 3 mm and to maintain an ion momentum spread of the order of 10^{-4} . During this electron cooling process the velocities of the overlapping ion and electron beams were matched to each other (typical electron energy 5 keV). After this preparation the electron energy was detuned to typical values between 7 and 9 keV in order to measure resonant recombination. The energy of the electrons (e) in the ion rest-frame then corresponded to the $2l n l'$ doubly excited states in the systems $O^{7+} + e$ and $C^{5+} + e$, and to the $1s 2l n l'$ states in $C^{4+} + e$. The recombined ions were separated from the stored ion beam in the bending magnet downstream of the electron cooling device and then counted by a channelplate detector.

The observed dielectronic recombination cross-section as a function of the rest-frame electron energy (Fig. 1) shows strong contributions from highly excited states $2l n l'$, which could be resolved up to $n \approx 7$. The rest-frame energy resolution and the error of the absolute rest-frame energy presently are of the order of ± 1 eV. Energy differences between the levels in the $2l n l'$ configuration could be measured to about ± 0.2 eV. Small but significant differences were found in comparing the energies of the helium-like doubly excited states ($O^{7+} + e$) with available calculations. For the hydrogen-like ions (Fig. 1a, 1b) the structure below the $N = 2$ threshold can be explained by a scaling $\propto n^3$ of the resonant recombination cross section. For the helium-like ion (Fig. 1c) the strongest resonances are those converging to the $1s 2p(^1P)$ threshold; the resonance strengths below this threshold are

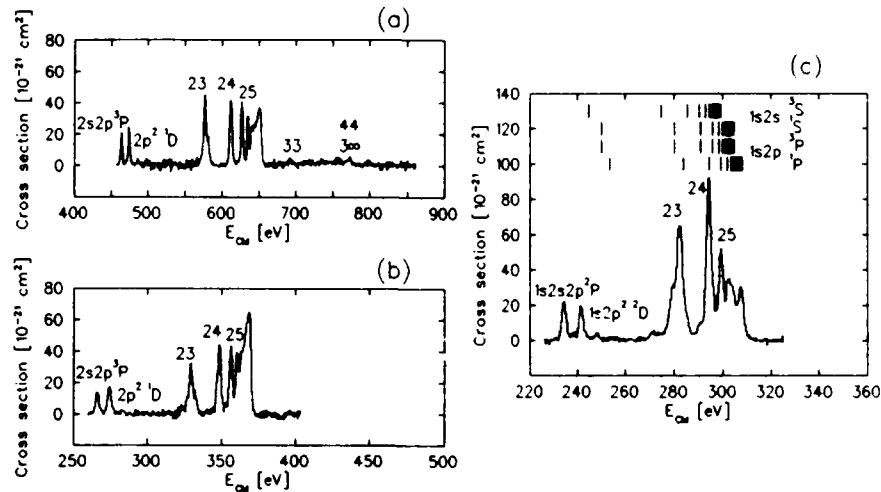


Figure 1: Dielectronic recombination cross section as a function of the center-of-mass electron energy for 8.9 MeV/u O^{7+} ions (a), 9.4 MeV/u C^{5+} ions (b), and 6.0 MeV/u C^{4+} ions (c) stored in the TSR. Configuration and term designations are given for the prominent low-lying resonances; principal quantum numbers Nn are given for the higher resonances. Bars in diagram (c) indicate one-electron Rydberg ladders.

additionally influenced by the autoionization into the open channels of the lower-lying 2^3P , 2^1S , and 2^3S thresholds.

The measurements of the dielectronic resonance strengths for hydrogen-like ions triggered theoretical calculations [3], which show good but not perfect agreement. Theoretical predictions of the helium-like spectra below the 2^1P threshold should be very sensitive to the 2^3S - 2^1P energy difference since the $1s2p(^1P)5l$ resonance lies very close to the $1s2p(^3S)$ threshold.

For future experiments, also studies of highly excited resonances $Nlnl'$ with $N, n \gg 1$ are intended. Besides these resonant processes, also the recombination of highly charged ions with free electrons at low rest-frame energy (≈ 0.1 eV) and laser-induced recombination are presently studied in the merged-beam arrangement at the TSR [4].

This work has been funded by the German Federal Minister for Research and Technology (Bundesministerium für Forschung und Technologie) under contract No. 06 HD 938 I.

1. D. Krämer *et al.*, Nucl. Instrum. Methods **A287**, 268 (1990).
2. G. Kilgus *et al.*, Phys. Rev. Lett. **64**, 737 (1990).
3. M.S. Pindzola, N.R. Badnell and D.C. Griffin, submitted to Phys. Rev. A.
4. D. Habs *et al.*, Nucl. Instrum. Methods **B43**, 390 (1989).

PHOTODETACHMENT IN INFRARED AND MICROWAVE FIELDS

D. J. Larson, P. S. Armstrong, M. C. Baruch,
W. G. Sturru, N. D. Gibson, and L. P. Ratliff
Department of Physics, University of Virginia
Charlottesville, Virginia 22901

Photodetachment from negative ions near the single photon threshold has been studied in the presence of strong infrared and microwave fields. The experiments raise interesting questions about detachment or ionization in strong oscillating fields.

In the experiments using infrared fields a strong infrared beam (up to 10^{11} W/cm²) overlaps a weak tunable ultraviolet probe beam in a Penning ion trap containing Cl⁻ ions. The experiments have been done at two infrared wavelengths, the fundamental of a Nd:YAG laser at 1.06 μ m and its first-Stokes, Raman-shifted output in H₂ at 1.91 μ m. The data are fitted to a model which includes a threshold shift and two-color, two-photon detachment, both proportional to the infrared intensity. The apparent threshold shifts are smaller than the ponderomotive energy of the electron in the infrared field.^{1,2}

Photodetachment from Cl⁻ and from S⁻ in a strong microwave field was studied using ion beams with energies near 1 KeV. Detachment in a 2.6 GHz field was measured using time-of-flight spectroscopy of the resulting neutrals. Field values of up to 3 KV/cm were investigated using a pulsed dye laser beam collinear with the ion beam passing through a microwave cavity. Below threshold detachment and oscillations on the cross section above threshold were observed near the Cl⁻ threshold at 29138 cm⁻¹, and near the ³P_{3/2}-³P₂ and ²P_{1/2}-³P₂ thresholds in S⁻ at 16754 cm⁻¹ and 16272 cm⁻¹, respectively. The observed effects are consistent with detachment in a static electric field.³⁻⁶

This work was supported in part by the National Science Foundation.

1. R. Trainham, G. D. Fletcher, N. B. Mansour, and D. J. Larson, Phys. Rev. Lett. **59**, 2291 (1987).
2. M. Kutzner, H. P. Kelly, D. J. Larson, and Z. Altun, Phys. Rev. A **38**, 5107 (1988).
3. J. E. Stewart et al., Phys. Rev. A **38**, 5628 (1988).
4. H.-Y. Wong, R. R. Rau, and C. H. Greene, Phys. Rev. A **37**, 2393 (1988).
5. M. L. Du and J. B. Delos, Phys. Rev. A **38**, 5609 (1988).

PHOTODISSOCIATION OF H_2 VERY NEAR THRESHOLD-
HALF-COLLISIONS AT VERY LOW ENERGY

E.E. Eyler
Department of Physics and Astronomy
University of Delaware, Newark, DE 19716

E. McCormack
Argonne National Laboratory
Argonne, IL 60439

Using optical double resonance through the E,F ${}^1\Sigma_u^+$ state of H_2 , we have investigated the region of the second dissociation limit, converging to $H(1s) + H(2\ell)$. Both bound and continuum levels of the B , B' and C states can be excited from the $\nu=6$ level of the E,F state using a pulse-amplified cw dye laser. Figure 1 shows the potential curves of the states involved.

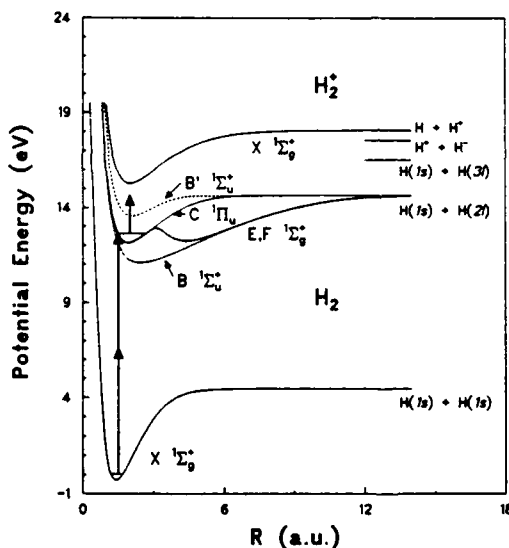


Fig. 1 Potential curves involved in near-threshold dissociation

We have been particularly successful in investigating the highest bound levels just below the dissociation threshold, where resonant multiphoton ionization provides an efficient detection scheme. The resonant $1/R^2$ potential of the $B \ ^1\Sigma_u^+$ state supports a dense series of high vibrational levels near the limit, and we have been able to observe levels with outer turning points at $R > 100$ bohr. The physics of such weakly bound levels is intermediate between ordinary molecular physics and long-range atomic physics. In a completely adiabatic picture, Stwalley and others have shown that the vibrational levels would follow a simple asymp-

otic pattern.¹ Very near threshold more complicated behavior is expected because fine structure mixing becomes important.

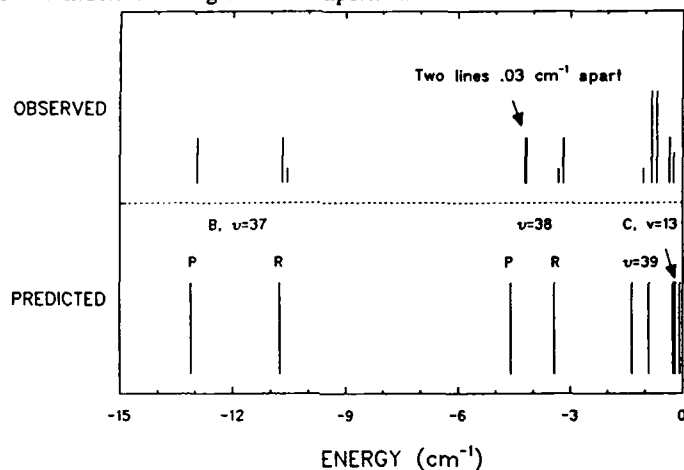


Fig. 2. Stick diagram showing observed and predicted levels excited from $v=6, N=1$ of the E,F state.

Surprisingly, our experimental results to date indicate that the level structure becomes quite complicated as far as 30-40 cm^{-1} below threshold, where unexpected doublings of some lines begin to occur as shown in Fig. 2. In the last 1 cm^{-1} the regular vibrational spacing is lost completely because of extensive level mixing. The details of this spectrum are not yet fully understood, but Paul Julienne has pointed out that a likely explanation is *gerade-ungerade* mixing induced by the hyperfine interaction in the ground-state H atom. Similar effects are expected to be important in neutral atom traps, where experimental evidence has recently been observed for bound molecular levels formed in ultracold atomic collisions.² A more thorough investigation of these levels in the H_2 , D_2 , and HD molecules using a much-improved excitation scheme is currently underway.

This research was supported by the National Science Foundation, grant number PHY90-00375.

¹W.C. Stwalley, Chem. Phys. Lett. 6, 241 (1970).

²P. Jeunhomme, F. Mies, and J. Lett, private communication.

**THEORETICAL EVALUATION OF CROSS-SECTIONS
FOR COMPTON SCATTERING FROM INNER SHELL ATOMIC
ELECTRONS**

T. Surić¹, P. M. Bergstrom², K. Pisk¹ and R. H. Pratt²

**¹Ruđer Bošković Institute
Bijenička 54
41000 Zagreb
Yugoslavia**

**²Department of Physics and Astronomy
University of Pittsburgh
Pittsburgh, Pa 15260**

We have developed a computer program to calculate the cross-section for photons scattering incoherently from electrons bound in atoms. Initially, we calculate the cross-section doubly differential in the scattered photon energy and angles. Our approach is exact within the independent particle approximation to second order external field quantum electrodynamics. Our calculations may use any realistic spherically symmetric potential. Our calculations include all necessary photon multipoles.

We compare our results with more approximate calculations in order to examine the validity of these approaches. We report disagreement with the commonly used "A²" approaches in some cases. We present comparisons with recent experiments. We also present, for the first time, calculations of Compton scattering within this framework with a screened atomic potential. We observe an infrared divergence in our calculations as predicted by Gavrilin in his Coulombic non-relativistic dipole approximation calculations. This divergence has not been observed unambiguously in experiments. We do not find agreement with the Coulombic calculations of Whittingham.

**EXACT CALCULATION OF MULTI-PHOTON PROCESSES BY
A SINGLE LONGITUDINAL MODE PULSED LASER**

Edward S. Fry, ShiFang Li, Feng Gao, and XingFu Li

Department of Physics, Texas A&M University
College Station, TX 77843

Resonant multi-photon excitation and ionization processes have ultra high selectivity and sensitivity, and thus have been used for detection of trace elements and small numbers of atoms. Previous work with multi-photon processes has generally involved high intensity broad band pulsed lasers. However, when a metastable state acts as a resonant intermediate state, a single longitudinal mode laser is even more efficient.

It is suggested here that a larger fraction of atoms can be excited to an intermediate metastable state or ionized by using a single mode pulsed laser, and that the possible Rabi oscillation may be employed to measure the multi-photon coupling constant. This constant has been difficult to calculate because of the infinite sums involved^[1]; and difficult to measure because of variable laser line shapes and spatial distributions^[2]. In the absence of a resonant intermediate state, the high fluence required necessitates the use of a pulsed laser. The extent of noise and chirp in laser pulses on multi-photon processes is the major concern of this paper.

The effect of colored noise on the multi-photon process has been an interesting subject for a long time. However, the effect of a single longitudinal mode laser including some fraction of colored noise is a new and practical problem. In such a case, the coherent dynamical process is perturbed by this colored noise. G.Vemuri et.al.^[3] considered resonance fluorescence from a two level system with colored noise by directly integrating the master equation, and the exact behavior was obtained. A similar method is described here for studying multi-photon processes.

The present calculation is for two photon resonant excitation and three photon ionization. It is based on direct numerical integration of the matrix equation. A Gaussian temporal profile with 8.3 ns at FWHM is assumed. Both the resonance excitation and ionization probabilities have been calculated as a function of pulse fluence and center frequency. The two photon Rabi frequency, a.c. Stark

shift and ionization cross section, are chosen in such a way that in the absence of chirp and noise, the population of the two photon resonantly excited state oscillates several times before it is ionized.

It is found that pulse chirp tends to wash out the minima in the excitation probability, but slightly increases the ionization fraction at a specific pulse fluence, as shown in figure 1.

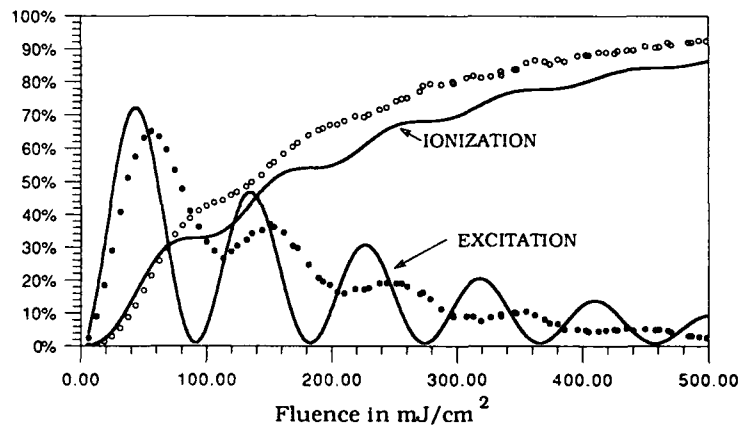


Figure 1. Solid line: excitation and ionization probability vs. pulse fluence at zero detuning without chirp and noise; circles: with a chirp parameter of 0.5 and with 9.1% of the fluence being colored noise whose Lorentzian of linewidth is 12 GHz (FWHM)

Finally, we would like to mention here that our results agree very well with the experimental data of S. W. Downey for hydrogen atoms^[3] with the laser parameters of their experiment and the same atomic parameters of figure 1. It is anticipated that, the two photon coupling constant of hydrogen atoms will be determined accurately in future experiments by using a single longitudinal mode pulsed laser, and the extensive disagreement between experimental data and theoretical calculations^[4] can be clarified.

[1] Yves Justum, Phys. Rev. **A41**, No.5, 2791(1990).

[2] S. W. Downey and R. S. Hozack, Opt. Lett. **14**, No.1, 15(1989).

[3] Gautam Vemuri and Rajarshi Roy, Phys. Rev. **A41**, No.5, 2749(1990).

[4] ShiFang Li and Edward S. Fry - to be published.

RETARDATION EFFECTS IN RAYLEIGH SCATTERING BY K SHELL ELECTRONS

A. Costescu^{*}, P. M. Bergstrom, and R. H. Pratt
Department of Physics and Astronomy
University of Pittsburgh
Pittsburgh, Pa 15260

An expression for the non-relativistic matrix element for photons scattering coherently from a K shell electron bound in a hydrogenic atomic system has been given¹ in the form

$$M = (\vec{S}_1 \cdot \vec{S}_2) M + (\vec{S}_1 \cdot \vec{v}_2) (\vec{S}_2 \cdot \vec{v}_1) N,$$

where

$$M = O \cdot P(\Omega_1) - P(\Omega_2),$$

$$N = -[Q(\Omega_1) + Q(\Omega_2)],$$

and S_i, v_i are photon polarization and momentum direction vectors respectively. The quantities P and Q are expressed in terms of Appell functions.

Although it is possible to numerically calculate this matrix element, we have developed expressions that express the matrix element directly in terms of dipole approximation results,² in order to make clear the effects of retardation on this fundamental atomic process and when such effects are important. We develop different expressions for different energy regimes and make comparisons of our forward scattering results with the non-retarded result, with the relativistic dipole approximation and with the full multipole relativistic result.³ We discuss the relative importance of retardation effects versus the effects of relativity in the energy regimes considered.

*Permanent address: Department of Physics, Bucharest
University, Bucharest, Romania.

References:

1 M. Gavrila and A Costescu, Phys. Rev. A **2**, 1752 (1970).

2 M. Gavrila, Phys. Rev. **163**, 147 (1967).

3 See for example: L. D. Kissel, R. H. Pratt and S. C. Roy, Phys.
Rev. A **22**, 1970 (1980).

STUDY OF Mg 3pnd AND 3pns (J=1) AUTOIONIZATION SPECTRA

G.W. Schinn, C.J. Dai, and T.F. Gallagher
 Department of Physics, University of Virginia
 Charlottesville, VA 22901, U.S.A.

We report an experimental and computational study of the Mg 3pnd ($n=9-40$) and 3pns ($n=9-18$) $J=1$ autoionization spectra resulting from isolated-core excitation. Mg atoms in an effusive beam are excited with three frequency-doubled and -mixed laser beams from three pulsed dye lasers. The linearly-polarized radiation from two of the lasers, with wavelengths of 285.3 nm and ~385 nm respectively, are used to stepwise excite one valence electron to the $3sn\ell$ Rydberg state. A third laser beam, polarized in the same direction, is scanned across what are effectively the ~280 nm $3s-3p$ ion transitions to produce a doubly-excited $3pn\ell$ state. The ions resulting from the autoionizing decay of this doubly-excited state are detected by a charged-particle detector as a function of third-laser wavelength. With this excitation scheme, the $3pn\ell$ final state is restricted to 3pns ($J=1$) and 3pnd ($J=1$ and $J=3$).

We have calculated the $J=1$ spectra using reaction-matrices supplied to us by Greene¹, in conjunction with the multichannel quantum defect method of Cooke and Cromer.² For 3pnd final states, these calculations have been combined with our previously-calculated $J=3$ spectra³ to yield computed spectra in very good agreement with experiment (Fig.1). The synthesized 3pns spectra are also in excellent accord with the measurements. A simple physical model accounts for the 3pnd $J=1$ features being generally narrower than the $J=3$ features.

This work has been supported by the U.S. Department of Energy, Division of Chemical Sciences, Office of Basic Energy Sciences.

1. C.H. Greene, private communication
2. W.E. Cooke and C.L. Cromer, Phys.Rev. A 32, 2725 (1985)
3. C.J. Dai, G.W. Schinn, and T.F. Gallagher, Phys. Rev. A (in press)

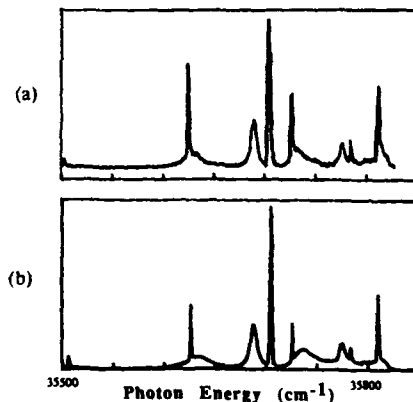


Fig. 1. (a) Measured and (b) calculated spectra corresponding to excitation of the 3p14d state with linearly-polarized light.

IONIZATION OF RYDBERG ATOMS BY A CIRCULARLY
POLARIZED MICROWAVE FIELD

J.M. Hetteema, C.Y. Lee, Panming Fu, T.J. Scholz, T.F. Gallagher
Department of Physics, University of Virginia
Charlottesville, Virginia 22901

We report the first observation of the ionization of Rydberg atoms by a circularly polarized 8.5 GHz microwave field. The observed threshold field for ionization is $E = 1/16n^4$, a value higher than that required for ionization by a linearly polarized microwave field. The origin of this threshold may be understood by transforming to a frame rotating at the microwave frequency. In the rotating frame no transitions occur, and level mixings alone are responsible for the ionization. Measurements at higher frequencies are currently in progress. This work has been supported by the AFOSR.

COLLECTIVE EFFECTS ON IONIZATION OF RYDBERG SODIUM ATOMS BY
BLACKBODY RADIATION.

F. Fuso, M. Allegrini, R. Dygdala*, F. Giammanco and E. Arimondo
Dipartimento di Fisica, Universita' di Pisa, Piazza Torricelli, 2 - 56100 PISA, Italy

We have investigated the ion production in an effusive beam of sodium atoms excited to Rydberg levels by a two-step laser process. The experimental parameters, such as atom density and intensity of the two lasers, vary in a range where the blackbody photoionization is the predominant source of ions. The ejected electrons are very cold and they may be strongly affected by collective interactions with the ion bunch when escaping from the production region. During the laser pulse, Rydberg atoms are also ionized well above the continuum limit by absorption of an additional laser photon; the electrons produced by this ionization channel have large kinetic energy, approximatively the laser photon energy. Although the cross section for this process is small, its rate may become comparable to the blackbody photoionization rate, depending on the laser intensity.

During the collection phase, the time-space behaviour of the produced charges may differ noticeably from that of non interacting charged particles[1]. Trapping occurs when the electron kinetic energy is not sufficient to overcome the self generated electric field. Collective effects have been thoroughly investigated in three-photon ionization experiments of sodium atoms [2], where electrons were produced with an initial kinetic energy of about 1.5eV. Here we report the results of an ionization experiment which produces both slow (at threshold) and fast ($\approx 2+3eV$) electrons and indicates a collective behaviour of the produced charges.

Ground state sodium atoms in an effusive beam were excited to Rydberg states by a two-step excitation process $3s \rightarrow 3p \rightarrow ns$ or $3s \rightarrow 3p \rightarrow nd$, using the light from two pulsed, yellow and blue, dye lasers, pumped by the same excimer laser. The yellow laser had a pulse duration of ≈ 13 ns and a power sufficient to saturate the sodium resonance transition $3S \rightarrow 3P_{3/2}$. The blue laser had a pulse duration of ≈ 15 ns and, when focussed into the atomic beam, provided an intensity up to $10 MW cm^{-2}$, which allowed us to reach saturation for the transitions $3p \rightarrow ns$ or nd . For the detection system ions were collected with electrostatic focusing lenses, analyzed by a time-of-flight drift tube and detected with a multichannel plate, while electrons were collected by a plate kept at a fixed positive potential. Ion and electron signals were analyzed by a boxcar integrator and/or a gate counter.

Several processes, radiative or reactive (collisional), contribute to the ion formation. For every Rydberg level we have investigated, we have found a linear dependence of the total ion yield as a function of the atom density, indicating that photoionization is the dominant ionization process. Ionization by photon absorption is the result of various processes. However, in the present experimental conditions, non-resonant processes as three (yellow or blue)-photon ionization from ground state are negligible compared to multi-step excitation to a Rydberg level followed by one of these ionization processes: (1) absorption of a blackbody photon or (2) absorption of a yellow or blue photon. The most

important difference between processes (1) and (2), is that electrons produced by (1) are slow electrons, while those coming from (2) have considerable kinetic energy ($\sim 2\text{eV}$ or $\sim 3\text{eV}$, respectively). Since the blackbody radiation is always present in the laser-vapor interaction volume, process (1) acts for a time given by the Rydberg atoms survival time, of the order of microseconds, or longer, if we consider collisional-mixing. Process (2) is on the contrary dominated by the 15ns blue laser pulse duration and the number of charges it produces, although not negligible, occurs only within this short time interval.

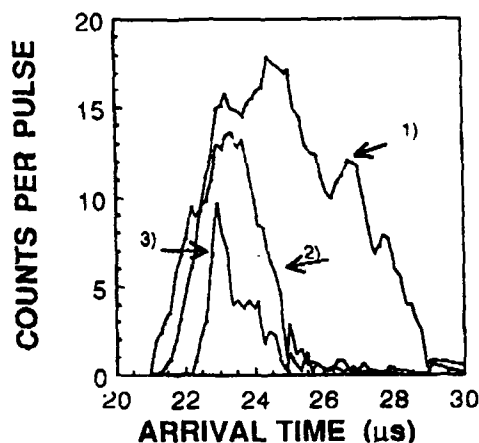


Fig.1 Ion counts vs arrival time at the detector. $[\text{Na}] = 2 \times 10^{11} \text{cm}^{-3}$ and different blue laser intensities: 750kW/cm^2 for curve 1), 500kW/cm^2 for curve 2) and 130kW/cm^2 for curve 3).

By studying the ion yield and the electron current behaviour as a function of the blue laser intensity, we have obtained evidence of the influence of collective effects on charge motion. Fig. 1 reports results for blue laser tuned to the 20d Rydberg state. The number of ions per pulse, gated in a 150ns temporal window, is reported as a function of the ion arrival time to the detector, at fixed $[\text{Na}]$ density and for three different intensities of blue laser. It is clear that the ratios between the peaks of the three curves, that is the maximum ion counts per pulse, are different from the ratios between the areas under the three curves, that is the total collected ions. The peak is shifted towards higher values of the arrival time when the laser intensity was increased. As proved in the theoretical analyses [1] and observed previously in the three-photon ionization [2], this is the typical behaviour of charges which do not move independently, but are trapped in a collective motion. The study of the electron current signal has provided a complementary information of the influence of collective phenomena. A threshold value, $\sim 10^8 + 10^9 \text{charges cm}^{-3}$ has been determined for the occurrence of these collective phenomena, comparable with the value determined in previous three-photon ionization experiments.

* Fellow International Center for Theoretical Physics, Trieste, Italy. Permanent address: Institut of Physics, University of Torun, Poland

[1] F. Giammanco, Phys. Rev. A36 (1987) 5658; A40 (1989) 5160

[2] E. Arimondo, C.E. Burkhardt, F. Giammanco, L.J. Qin and A. Vellante, Opt. Commun. 71 (1989) 52; F. Giammanco, Phys. Rev. A40 (1989) 5171; F. Giammanco and E. Arimondo Europhys. Lett. 11 (1990) 31

VI. PLASMA PHYSICS

FAST ELECTRON RELAXATION ON LANGMUIR OSCILLATIONS
IN COLLISIONAL LOW-TEMPERATURE PLASMA

V.I. Demidov, T.V. Rudakova and V.Y. Simonov
Department of Physics, Mining Institute,
2 Line 21, 199026, Leningrad, USSR.

The study of different species of a low-temperature plasma with fast electron sources is of great interest for the gas discharge physics and its applications /1/. In particular, the non-equilibrium of such plasmas is connected, as a rule, to the presence of one or several groups of the fast electrons, the energies of which are significantly greater than the mean energy of all electron energy distribution. The theoretical and experimental study of the influence of electron-electron and electron-atom collisions, the walls of a plasma volume and wall potential layers on the electron energy distribution function formation has been carried out in recent years for the plasma with fast electrons /2/. However, the influence of the Langmuir oscillations (electrostatic ones) on the electron energy distributions, particularly in a collisional plasma, has been investigated so far insufficiently. Therefore, the aim of the present paper is to study the diffusion non-equilibrium plasma with the fast electrons, where the relaxation on the Langmuir oscillations may play the dominant role. This corresponds to the plasma conditions, when the fast electron free path λ is significantly less than the characteristic dimensions of the plasma volume, that enables to obtain the theoretical criterion for the diffusion plasma and to compare it with the experimental one obtained for collisional plasma /3/.

Let us analyse the simple one-dimensional case, when the fast electrons arise in the plane with the coordinate $X = 0$ (for example, near the cathode), move to the anode in the plasma (in the positive direction of X axis) and annihilate in the plane $X = L$ (at the anode). As the fast electron energy ϵ_f is significantly higher than the mean energy of all the electrons $\langle \epsilon \rangle$, their motion is usually the free diffusion to the tube walls (the potential difference in plasma has an order of magnitude $\langle \epsilon \rangle / e$, where e is the electron density flux in the X direction may be written in the form

$$\Gamma_f = \frac{1}{3} \lambda v_f \frac{N_f(0) - N_f(L)}{L} \approx \frac{\lambda v_f N_f(0)}{3L} \quad (1)$$

where v_f is the mean velocity of the fast electrons; $N_f(0)$ and $N_f(L)$ are the concentrations of the fast electrons near the cathode and anode respectively. The last approximate equality belongs to the case of the full absorptive anode. Note, that this theoretical model is the very good approximation for the description of the phenomena, for example, in a low-voltage beam noble gas discharge. In this case, due to the locking electron potential on the tube walls the fast electrons move practically in the one-dimensional diffusion regime along the tube axis and carry out mainly the current-transfer in the plasma /2/.

On the basis of the quasi-linear theory /4/ for the fast electron energy relaxation path l one may write the following expression:

$$l \approx R_D \Lambda \frac{N_t v_t}{T_f} \quad (2)$$

Here R_D is the Debye screening distance; Λ is the Coulomb logarithm; N_t and v_t are the concentration and the mean velocity of the thermal electrons of a plasma respectively. Substituting (1) into (2), one may obtain

$$l \approx \frac{1}{2\pi} \frac{\lambda_x}{\lambda} \Lambda \frac{E_t}{E_f} \frac{N_t}{N_f} L \quad (3)$$

where

$$\lambda_x = \frac{2\pi v_f}{\omega_p} R_D = \frac{2\pi v_f}{\omega_p} \quad (4)$$

is the Langmuir wave length; ω_p is the Langmuir frequency; E_t is the mean energy of the thermal electrons; L is the discharge gap.

It is evident that the fast electron energy relaxation on the Langmuir oscillations turns out to be essential if the corresponding relaxation length (3) is less than the dimensions of the discharge gap. Hence, the relaxation condition may be written as

$$\lambda/\lambda_x \geq \frac{1}{2\pi} \Lambda \frac{N_t}{N_f} \frac{E_t}{E_f} \quad (5)$$

When the inequality (5) is valid, the examined mechanism of the fast electron relaxation on the Langmuir oscillations is appeared to be essential for the given conditions, particularly for the collisional plasma.

The experimental proof of the efficiency of the theoretical criterion (5) has been performed actually in /3/, where the propagation of the fast electron beam was observed in the helium plasma of the low-voltage beam discharge. For the studied conditions the relaxation on the Langmuir oscillations is shown to be essential at $\lambda/\lambda_x \approx 5$. This result is in rather good agreement with the expression (5) using the corresponding experimental values of the concentrations and mean energies of the electrons.

In conclusion, the theoretical criterion obtained in the present paper is in rather good agreement with the experimental results obtained in /3/.

References

1. L.M. Biberman, V.S. Vorob'ev and I.T. Yakubov, Kinetics of Non-equilibrium Low-temperature Plasma (1982).
2. V.I. Demidov, N.B. Kolokolov and O.G. Toronov, Sov. J. Plasma Phys. 12 402 (1986).
3. A.S. Mustafaev and A.P. Mezentssev, J. Phys. D: Appl. Phys. 19 L 69 (1986).
4. A.A. Ivanov, Physics of Highly Non-equilibrium Plasma (1977).

COINCIDENCE STUDY OF HEAVY NOBLE GAS EXCITATION
BY ELECTRON IMPACT IN THE REGIME OF LARGE IMPACT PARAMETERS

K.E. Martus, S.H. Zheng and K. Becker
Dept. of Physics, City College of New York
Convent Avenue and 138th Street, New York, NY 10031

Electron-polarized photon coincidence experiments provide a very sensitive tool to study the finer details of the electron impact excitation of atoms and molecules [1,2]. In this type of experiment inelastically scattered electrons that have excited a particular target state are detected in coincidence with the subsequently emitted decay photons whose polarization is also determined. Typically, one measures two linear (P_1, P_2) and one circular (P_3) coherence or polarization correlation parameter perpendicular to the scattering plane and one additional linear parameter (P_4) in the scattering plane. Heavy noble gas atoms present a challenging subject for coincidence studies, both from an experimental and a theoretical view point. Exchange, deviation from the Russell-Saunders angular momentum coupling scheme in the excited target states and spin-orbit effects involving the continuum electron can all be present simultaneously. The experimental challenge lies in the fact that the resonance lines of the heavy noble gases are in the VUV where reflection-type polarization analyzers rather than the standard transmission-type analyzers have to be used for polarization analysis.

Theory and experiment of heavy noble gas excitation have been dealing primarily with the excitation of the first excited states, the spin-orbit coupled $ns'[1/2]_1$ (" 1P_1 ") and $ns[3/2]_1$ (" 3P_1 ") states ($n = 3, 4, 5, 6$ for Ne, Ar, Kr, and Xe). Both excited states are often pictured as linear combinations of LS-coupled singlet and triplet states. The previous emphasis of our work was on a systematic measurement of the P_1 parameter for " 1P_1 ", excitation in Ne and Ar in forward scattering [3]. A value of $P_1 = +1$ demonstrated that the excitation process under those conditions, i.e. at large impact parameters, is dominated by the direct excitation of the LS-coupled singlet component of the excited states as predicted by theory.

We report measurements which extend the previous results in two directions:

1. P_1 measurements were carried out in forward scattering for excitation of the " 1P_1 " and " 3P_1 " states of Kr in the energy range 30-100 eV. The measurements

resulted again in P_1 values consistent with +1 confirming the previous notion that scattering at very large impact parameters is dominated by direct excitation.

2. P_1 and P_2 measurements were carried out at 50 eV and small scattering angles. Results for the alignment angle γ extracted from P_1 and P_2 are shown in figure 1 for the Kr " 3P_1 " state. The solid line is the DWBA calculation of Bartschat and Madison [4]. Excellent agreement between theory and experiment was found for scattering angles up to 15° . Also shown is the first Born Approximation. The FBA description of γ is adequate only for very small scattering angles (less than 10°) in contrast to He, where the FBA was found to describe γ adequately up to about 40° . Additional results will be presented and discussed at the Conference.

This work was supported by the NSF (Grant Nos. PHY-8819510 and PHY-8910360).

References

1. K. Blum and H. Kleinpoppen, Phys. Rep. 52, 203 (1979).
2. K. Anderson, J.W. Gallagher and I.V. Hertel, Phys. Rep. 165, 1 (1988).
3. K.E. Martus and K. Becker, J. Phys. B 22, 2497 (1989).
4. K. Bartschat and D.H. Madison, J. Phys. B 20, 5839 (1987).

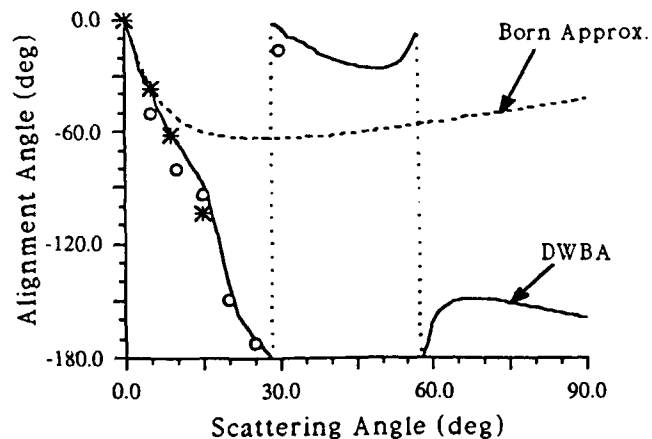


Fig. 1: Alignm. angle as a function of scattering angle for Kr " 3P_1 " at 50 eV. Crosses, present results; circles, angular correlations of Danjo et al.

VII. ATOMIC SPECTROSCOPY AND STRUCTURE
- THEORY

SPLINE SOLUTIONS OF THE HELIUM PAIR EQUATION ¹

Charlotte Froese Fischer
 Vanderbilt University, Box 6035B
 Nashville, TN 37235 USA

Schrödinger's equation for an atom with m electrons is a partial differential equation with $3m$ space variables. Because of the complexity of this problem, general purpose atomic structure methods approximate the wave function using angular momentum theory and apply the variational principle for finding radial distributions that are functions of m variables. The goal of this research was to develop algorithms for the helium problem appropriate for concurrent vector processors, such as the Cray with multiple processors or the Intel RX with many vector nodes. These algorithms may be the basis for a many-electron pair correlation theory.

In spherical coordinates, the spin-independent, nonrelativistic Schrödinger equation for two electrons in an atom with nuclear charge Z is

$$\left[-\frac{1}{2}\nabla_1^2 - \frac{1}{2}\nabla_2^2 - \frac{Z}{r_1} - \frac{Z}{r_2} + \frac{1}{r_{12}} - E \right] \Psi(\mathbf{r}_1, \mathbf{r}_2) = 0, \quad (1)$$

where r_{12} is the distance between the two electrons. In the present work, the multipole expansion is used, for expanding $1/r_{12}$. At the same time, the eigenfunction is expanded in terms of partial waves in which the radial factor is a function of two variables, (r_1, r_2) . Several cases are considered:

$$\Psi(^1S) = 1/(r_1 r_2) \sum_l p_l(r_1, r_2) |l l^1 S\rangle \quad (2)$$

$$\Psi(^{2S+1}P) = \frac{1}{\sqrt{2} r_1 r_2} \sum_l (1 - \mathcal{P}_{12}) p_l(r_1, r_2) |l l'^{2S+1} P\rangle, \quad l' = l + 1. \quad (3)$$

In the above, $|l l'^{2S+1} L\rangle$ is a function of the angular and spin coordinates of the two electrons and \mathcal{P}_{12} is the permutation operator that interchanges the coordinates of the two electrons both in the radial and spin-angular factor. For the 1S solutions, the permutation operator can be omitted, provided symmetry conditions are imposed on the radial factors of the partial waves. In a spline approximation, each pair function is represented as

$$p_l(r_1, r_2) \approx \sum_i \sum_j p_{ijl} B_i(r_1) B_j(r_2), \quad (4)$$

where $B_i(r)$ is a spline of order k defined on a grid [1]. The coefficients p_{ijl} were obtained by applying the Galerkin method to Schrödinger's equation, leading to a generalized eigenvalue problem that was solved iteratively.

Calculations were performed for $l = 0, \dots, 7$ for the five states, $1s^2\ ^1S$, $1s2s\ ^1S$, and $1s2p\ ^1P$. The same grid was used in all cases with splines of order $k = 5$. Results are reported in Table 1. along with results extrapolated with respect to l . The latter are compared with values reported by Accad *et al.* [2] and, in the case of the ground state, with recently reported data by Salomonson and Öster [3]. Grid extrapolation has not been used in this work which accounts for the reduced accuracy for the ground state.

¹Research supported by the National Science Foundation, grant No. ASC-8810885.

VII-1

Table 1. Total energies (in a.u.) for 1^3S and 1^3P states as a function of l . All calculations were for grid parameters $h = 1/8$ and $k = 5$. For the ground state, r_{\max} was 15 bohr radii; for all others had r_{\max} was 50 bohr radii.

l	$1s^2 \ ^1S$	$1s2s \ ^1S$	$1s2s \ ^3S$	$1s2p \ ^1P$	$1s2p \ ^3P$
0	-2.8790287574	-2.1442153138	-2.1742648560	-2.1225967720	-2.1323713798
1	-2.9005162155	-2.1457670280	-2.1751719819	-2.1236901854	-2.1331149317
2	-2.9027667894	-2.1459148161	-2.1752204362	-2.1237970194	-2.1331558584
3	-2.9033209853	-2.1459495114	-2.1752271248	-2.1238232078	-2.1331619337
4	-2.9035184623	-2.1459616191	-2.1752286204	-2.1238327044	-2.1331633869
5	-2.9036055328	-2.1459669023	-2.1752290698	-2.1238369793	-2.1331638484
6	-2.9036496662	-2.1459695644	-2.1752292344	-2.1238391882	-2.1331640253
7	-2.9036743530	-2.1459710562	-2.1752293040	-2.1238404449	-2.1331641030
∞	-2.903724025	-2.145974019	-2.175229378	-2.123843076	-2.133164189
Ref. [2]	-2.9037243536	-2.1459740437	-2.1752293782	-2.1238430846	-2.1331641904
Ref. [3]	-2.90372439				

Table 2. Performance when autotasking the calculations of each partial wave on the Cray Y-MP/8. NCPUS is the number of CPU's requested and Av. CPU's the average number allocated.

l	NCPUS	Av. CPU's	Total CPU time (s)	User CPU time (s)
1	2	1.97	20.80	19.86
2	3	2.72	40.42	37.21
3	4	3.43	70.22	59.66
4	5	3.59	187.06	166.80
5	6	4.16	268.61	231.36

To assess the vectorization capabilities, the 3P calculations were also performed on a Cray Y-MP/8. The total time required, using vectorization only, was 3.3 minutes. The Mflop rate was about 82 for the larger l values and would be even higher for a problem with a larger grid since the present vector length was only 52. Autotasking was also considered. The strategy most appropriate for a distributed computing environment, would be one where each processor updates its own partial wave. In this strategy, the ideal number of processors would equal the number of partial waves. Table 2. presents data for this strategy on the Y-MP/8. The results show an increase in the average number of CPU's although, as NCPUS increases the average begins to differ more and more from the theoretical maximum. At the same time, if the average CPU is inversely related to turnaround time, there has been a significant decrease in this time.

1. C. Froese Fischer and M. Idrees, *Computers in Physics* **3** 53 (1989).
2. S. Salomonson and P. Öster, *Phys. Rev. A* **40** 5559 (1989).
3. Y. Accad, C.L. Pekeris, and B. Schiff, *B. Phys. Rev. A* **4** 516 (1971).

VII-2

CURRENT STATUS OF ATOMIC SPECTROSCOPIC DATA COMPILATIONS AT NIST

W. L. Wiese, J. R. Fuhr, W. C. Martin, A. Musgrove and J. Sugar
National Institute of Standards and Technology
Gaithersburg, MD 20899 USA

Two data centers at the National Institute of Standards and Technology (NIST) are engaged in the critical evaluation and compilation of atomic spectroscopic data-- the Atomic Energy Levels Data Center and the Data Center on Atomic Transition Probabilities. Both centers perform comprehensive literature searches and critically evaluate and compile the data on their respective subjects. Several major compilations have been recently completed, centered on the iron-group elements. A comprehensive publication of atomic energy levels contains about 20,000 energy levels for the 235 spectra of potassium through nickel in all stages of ionization [1]; two volumes on atomic transition probabilities contain about 18,000 transitions for the neutral atoms and most stages of ionization of the elements scandium through nickel [2,3]. Work has also been completed or is in progress on many lighter elements [4-8] and selected heavier elements through molybdenum [9,10], and a general numerical data base is being developed which will ultimately include evaluated reference data on all principal spectroscopic data quantities associated with observed spectral transitions. A listing of current spectroscopic compilations published by NIST, as well as sample pages of the tables and the data base will be presented.

References

- [1] Sugar, J., and Corliss, C., "Atomic Energy Levels of the Iron Period Elements: Potassium through Nickel," J. Phys. Chem. Ref. Data 14, Supplement No. 2 (1985).
- [2] G. A. Martin, J. R. Fuhr and W. L. Wiese, "Atomic Transition Probabilities- Scandium through Manganese," J. Phys. Chem. Ref. Data 17, Supplement No. 3 (1988).
- [3] J. R. Fuhr, G. A. Martin, and W. L. Wiese, "Atomic Transition Probabilities- Iron through Nickel," J. Phys. Chem. Ref. Data 17, Supplement No. 4 (1988).
- [4] Martin, W. C., and Zalubas, R., "Energy Levels of Magnesium, Mg I through Mg XIII," J. Phys. Chem. Ref. Data 9, 1-58 (1980).
- [5] Martin, W. C., and Zalubas, R., "Energy Levels of Sodium, Na I through Na XI," J. Phys. Chem. Ref. Data 10, 153-195 (1981).
- [6] Martin, W. C. and Zalubas, R., "Energy Levels of Silicon, Si I through Si XIV," J. Phys. Chem. Ref. Data 12, 323-380 (1983).
- [7] Martin, W. C., Zalubas, R., and Musgrove, A., "Energy Levels of Phosphorus, P I through P XV," J. Phys. Chem. Ref. Data 14, 751-802 (1985). (ACS)

VII-2

- [8] Martin, W. C., Zalubas, R., and Musgrove, A., "Energy Levels of Sulfur, S I through S XVI," J. Phys. Chem. Ref. Data, Vol. 19, (1990) (in press).
- [9] Sugar, J., and Musgrove, A., "Energy Levels of Copper, Cu I through Cu XXIX," J. Phys. Chem. Ref. Data, Vol. 19, (1990) (in press).
- [10] 10. Sugar, J., and Musgrove, A., "Energy Levels of Molybdenum, Mo I through Mo XLII," J. Phys. Chem. Ref. Data 17, 155 (1988).

ANALYTICAL EXACTNESS OF ESTIMATING EIGENQUANTUM DEFECTS
FROM LU-FANO PLOTS

Liu Xuewen and Yu Gengsun

Department of Physics, Northwest Normal University, Lanzhou, China

Starting from the compatibility equation in the multichannel quantum-defect theory, we have examined the analytical exactness of estimating eigenquantum defects from Lu-Fano plots in the two-dimensional projecting planes. The results indicate that it is analytically untenable to estimate the eigenquantum defects from any two-dimensional Lu-Fano plot if more than two ionization thresholds are involved in the multichannel quantum-defect theory models, while the Lu and Fano's original two-limit recipe is regoriously valid.

References

1. U. Fano and A.R.P. Rau, Atomic Collisions and Spectra (Academic, New York, 1986).
2. K.T. Lu and U. Fano, Phys. Rev. A 2, 81(1970).
3. J.A. Armstrong, P. Esherick and J.J. Wynne, Phys. Rev. A 15, 180(1977).

MULTICHANNEL QUANTUM DEFECT THEORY OF LIFETIMES
FOR HIGHLY EXCITED STATES OF ATOMS:
CALCULATION OF Yb LIFETIMES IN THE PERTURBED $6sns$ S SEQUENCE

Liu Xuewen

Department of Physics, Northwest Normal University, Lanzhou, China

Z.-W. Wang

China Center of Advanced Science and Technology (World Laboratory),
P.O. Box 8730, Beijing, China

and

Institute of Atomic and Molecular Physics, Jilin University,
Changchun, China

Using the multichannel quantum-defect theory of lifetimes for highly excited states of atoms, we have evaluated the lifetimes for the perturbed $6sns$ S ($n=8, 11-32$) Rydberg levels as well as $6p$ S and $4f$ $5d6s6pA$ perturbing level for neutral ytterbium atom. We have not only obtained excellent results which are perfectly in agreement with the recent measurements, but also predicted for the first time the lifetimes of 10 other highly excited levels ($n=23-32$). The results indicate that the dramatic variation of lifetimes of Rydberg series in the vicinity of perturbing states is due to the channel interaction.

In the framework of multichannel quantum-defect theory of lifetimes for highly excited states of atoms, we have taken account of all channel interaction and the cancellation interference effects on radiative transition probability by expressing the wavefunction as a superposition of all dissociation channels, including the contributions from either long-lived Rydberg series or short-lived perturbing channels. All these enable us to reproduce the relative variation of observed lifetimes of Yb in the $6sns$ S Rydberg levels exactly and to predict the lifetimes of other highly excited states reasonably (see Fig.1). These predicted lifetimes remain to be examined by new measurements.

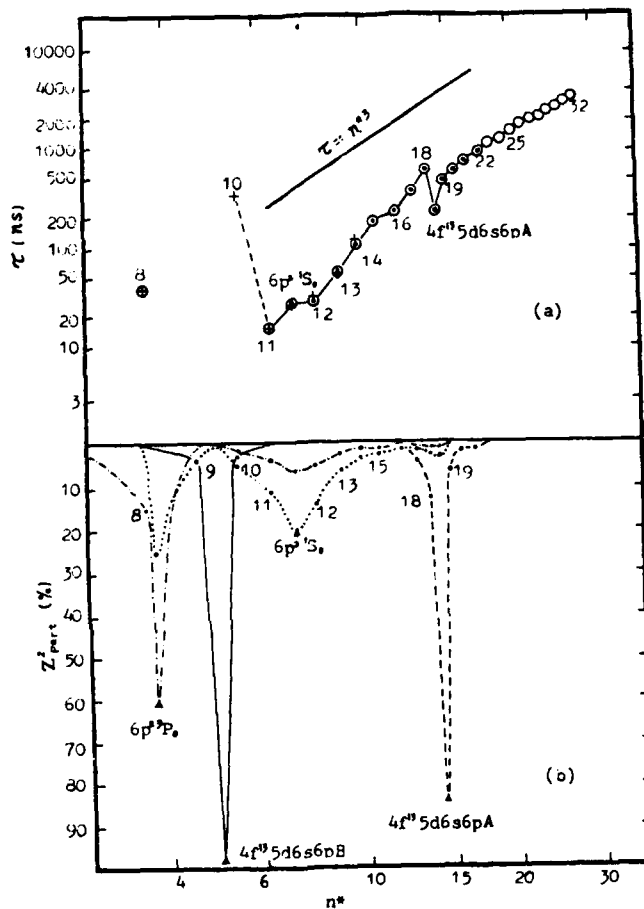


Fig.1 (a) Lifetime values of Yb J=0 levels plotted against the effective principal quantum number n^* on a ln-ln scale. The symbols are + for observed values from Ref.2, • for observed values from Ref.3, and o for the theoretical values of this work. (b) Fractional admixture of the perturbing channels in $6sns S$.

References

1. X.-W. Liu and Z.-W. Wang, Phys. Rev. A 40, 1838(1989).
2. M. Baumann et al, Z. Phys. D 6, 275(1987).
3. Wang Dadi et al, J. Phys. B 20, L555(1987).
4. M. Aymar et al, J. Phys. B 13, 1089(1980).

VARIATIONAL PRINCIPLE WITH NONDIFFERENTIABLE FUNCTIONS
FOR EQUIVALENT ELECTRONS

I. L. Beigman
P.N. Lebedev Physical Institute, USSR Academy of Sciences
Leninsky pr., 53, Moscow, 117924, USSR

The Hartree-Fock approach is widely used for obtaining approximate wavefunctions for many-electron atoms. Usually equivalent electrons are described with one radial function (1). Multi-configuration Hartree-Fock (MCHF) or Extended Hartree-Fock (EHF) methods give better description with the linear combination of products of the different radial functions. These methods lead to the rather complicated equations. The main difficulty is due to a large number of products arising from the symmetrization procedure.

The description of the equivalent electrons with the radial functions of variable of type $r_<$, $r_>$ is proposed in /2/. The functions are symmetric with respect to an interchange of radial coordinates, but they are nondifferentiable in the points of coincidence of radial coordinates. This (NDHF) method yields the more complicated radial equations, than usual HF equations, but simpler, than the EHF or MCHF ones.

In the special case of two equivalent s - electrons, the wavefunction is

$$\Phi(r_1, r_2) = \frac{\Phi(r_1, r_2)}{r_1 r_2} ; \Phi(r_1, r_2) = \begin{cases} P_1(r_1)P_2(r_2), & r_1 \leq r_2 \\ P_1(r_2)P_2(r_1), & r_2 \leq r_1 \end{cases}$$

This function is continuous for all values of r_1, r_2 , but the first derivative has a jump at $r_1 = r_2$. The second derivative is proportional to the δ -function

$$\frac{\partial^2}{\partial r_1^2} \Phi(r_1, r_2) = (P_1'P_2 - P_1P_2') \cdot \delta(r_1 - r_2) .$$

The variational principle gives the system of equations for P_1, P_2 . If r_1, r_2 tend to infinity, the functions P_1, P_2 are proportional to $\exp(-\alpha_1 r)$, $\exp(-\alpha_2 r)$. The functions P_1, P_2 are proportional to r at $r_1, r_2 \rightarrow 0$. If the nuclear charge tends to infinity, P_1, P_2 tend to the exact solution - the hydrogen functions.

The wavefunctions and energies for ground state of HeI and BeIII are calculated. The function P_1 is close the usual HF function P_0 at small r , and the function P_2 is close the HF function P_0 at large r . The calculated energies (in Z^2Ry units) are tabulated in the table:

Energy for the $1s^2$ state of He and BeIII (Z^2Ry units)

	NDHF /2/	HF	EHF /1/ /1/	EX /3/
He	1.4371	1.4308	1.4390	1.4519
BeIII	1.7028	1.7014	1.7032	1.7071

For comparison the HF, EHF and (EX) energies are presented too. The EX energies are obtained by the variational method with nonseparated variables /3/, where errors are negligible in comparison to those of the HF-type methods. The radial correlation energy is equal to $E' - E(\text{HF})$, where E' is energy of state $1s^2$ with taking into account the interaction with configurations ns^2 ($n>1$). Analysis /1/ shows that this value equals a 41% - fraction of the total correlation energy $E(\text{EX}) - E(\text{HF})$. Methods EHF and NDHF take into account 95% and 74% of the radial correlation energy, respectively.

Also, the variation principle with nondifferentiable functions of the type $r_{<}r$, takes into account the radial correlation considerably simpler, than EHF, and is perspective for complex atoms. For example, the configuration with p equivalent electrons may be described with one product of the type (1) with p radial functions.

References

1. C.Froese Fisher, The Hartree Fock method for atoms. (1977)
2. I.L.Beigman, Sov.Phys.-Lebedev Inst. Reports, N^o1, 27 (1990)
3. C.L.Pekeris, Phys.Rev., 112, 1649, 1948

An analytical approach to the calculation of the electron energy levels for a many electron atom.

SEBASTIANO TOSTO

ENEA C.R.E. CASACCIA, s.p. Anaguillarese 301, 00060 Roma Italy

ABSTRACT

The paper describes an analytical approach to the solution of a wave equation for a many electron atom in presence of a coulombian interaction field. The approach is non relativistic. The basic idea is to replace the coordinates of the electrons in the equation of the total energy with space ranges where the electrons themselves are delocalized; then, corresponding ranges for the respective momenta are associated to this space delocalization. The Heisenberg's principle is utilized thus to calculate the numbers of quantum states allowed to the electrons in correspondence to these ranges. This assumption is treated as a boundary condition imposed on the wave equation for the energy of the electrons. The results obtained through such a procedure have been first verified in the well known case of hydrogenoid atoms and then extended to the case of many electron atoms. In the first case, it is found that the total energy results as a sum of three terms expressing the kinetic, quantum rotational and electronic contributions; it shows the possibility to obtain in a natural way all the forms of non relativistic energies characterizing the atom. These terms appear of course also in presence of several electrons; in the latter case, the equation allows to calculate also the energy levels of neutral and variously ionized atoms in a systematic and conceptually simple way, without the necessity of any numerical approximation; the calculated energies are in a good agreement with the experimental spectroscopic data.

CONFIGURATION INTERACTION BETWEEN RYDBERG SERIES IN Cl

L. BUREYEVA

Council on Spectroscopy of the USSR Academy of Sciences
Pr.Sapunova, 13/15, Moscow, 103012, USSR

As far as a cold interstellar medium is concerned the radio emission lines of heavy elements are a subject of special interest. There is a widely discussed opinion that the observed lines are radiated by Cl atoms. However, modern methods of radio spectroscopy do not permit to distinguish these lines from the lines irradiated by the N- and O- atoms. Therefore one needs additional confirmation for their origin.

In the present paper the possibility is considered for the identification of the Cl lines based on the interaction of two Rydberg series with the different ionization potentials.

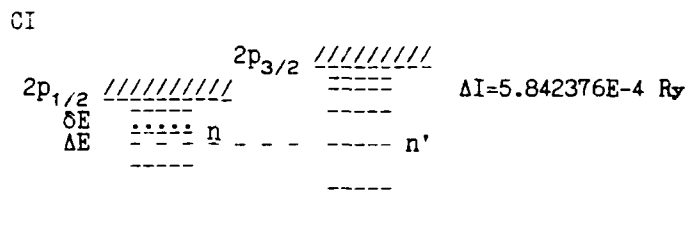


Fig. 1

The Cl atom "identification mark" could be the presence of such pairs of levels from different Rydberg series which have almost the same energies shifted on a specific for each elements value due to quasiresonance electrostatic interaction.

For the Cl atom levels these pairs n and n' are:

Table

ΔE	3,182E-6	-2,482E-7	-2,006E-9
n	20	38	293
n'	18	28	41

The shift δE could be written in the form [1]

$$\delta E = \frac{1}{4} \frac{2l+1}{n^2} \frac{|M|^2}{\Delta E_{nn'}} \quad (1)$$

where $M = \langle l_0 s_0 j_0 | [k l s] | l' s' j' \rangle \langle l' s' j' | [k' l' s'] | l_0 s_0 j_0 \rangle$. The angular and radial parts in this matrix element are factorized $M = \sum_{\alpha} U_{\alpha} R_{\alpha}$. The analysis shows that for highly excited levels n region of large coordinate r provides the main contribution to the radial integral R_{α} and R_{α} may be written as $R_{\alpha} = R_{n_0 l_0}^{n' l'} * R_{n l}^{n' l'}$. The integral $R_{n_0 l_0}^{n' l'}$ is calculated numerically, the integral $R_{n l}^{n' l'}$ is calculated analytically in the quasiclassical approximation. Expanding the method developed for the calculation of radial dipole matrix element [2] on the case of arbitrary multipoles α obtain

$$R_{n l}^{n' l'} = \frac{1}{\pi} \frac{(\omega_0 \omega'_0)^{1/2}}{\omega_0^*} \left[\frac{Z}{n^* \bar{z}} \right]^{\alpha+1} \int_0^{\pi} (1-\epsilon \cos \eta)^{-\alpha} (\cos[-\Delta n(\eta - \epsilon \sin \eta)] + \epsilon + 2\Delta l \arctg[(1+\epsilon)/(1-\epsilon)]^{1/2} \operatorname{tg} \frac{\eta}{2}) d\eta \quad (2)$$

where $\epsilon = (1 - (2l+1)^2 / 4n^{*2})^{1/2}$, $\Delta n = n - n'$, $n^* = 2nn' / (n+n')$, $\omega_0 = -\frac{Ry}{n^3}$.

In the case of our interest values $\alpha=2$, $\Delta l=0, \pm 2$. The value $\delta E_n / \Delta E_{n, n+1}$ was analytically estimated for n given in the Table. The author is grateful to I.L. Beigman for the discussion and help.

References

1. I.I. Sobelman, Introduction in the theory of atomic spectra, Springer, 1982
2. L.A. Minaeva (Bureyeva), Sov. Astr. J, 45, 578, 1968

INVESTIGATION ON THE BOUND EVEN-PARITY $J=0,2$ SPECTRA OF NEUTRAL TIN

Mingxing Jin, Dajun Ding, Hang Liu, and Shoufu Pan

Institute of Atomic and Molecular Physics, Jilin University,
Changchun 130023, P.R.China

Even-parity highly excited np and nf Rydberg series of atomic tin converging to the $^2P_{1/2}$ ground state of Sn^+ have been investigated recently using two-photon resonant excitation starting from the ground state $5s^2 5p^2 (1/2, 1/2)_0$ and the metastable $5s^2 5p^2 (1/2, 3/2)_1$ level. Five Rydberg series np and nf with J values ranging from 0 to 3 have been observed. Two autoionizing Rydberg series have also been observed by two-photon resonance from the metastable $5s^2 5p^2 (3/2, 3/2)_2$ level. The n values was as high as 46 in some case. Most of the Rydberg series observed belonged to $J=0,2$ Rydberg series. They are $5pnp(1/2, 1/2)_0$, $5pnp(1/2, 3/2)_2$, $5pnf 1/2[5/2]_2$, $5pnp(3/2, 3/2)_2$ and $5pnf 3/2[5/2]_2$ ^[1]. The aim of this paper is to analyse the new data on the highly excited np and nf $J=0,2$ levels. The techniques of MQDT have been used to analyse the even-parity $J=0,2$ bound Rydberg series of atomic tin quantitatively in this work. We adopte two-channel model and six-channel model for analysis the $J=0$ and 2 even-parity Rydberg series of atomic tin respectively. The optimized values of MQDT parameters $U_{i\alpha}$ and μ_α are determined by minimizing the $(\sum_{n=1}^N F_n^2 / N_n)^{1/2}$ to make the plot of $F(\nu_1, \nu_2)=0$ pass as close as possible to the points that represent the experimental energies. Where $F_n = F(\nu_{1,n}, \nu_{2,n})$ and N_n is the number of energy levels that considered in the fitting procedure. Using the parameters we calculate the level position with $J=0,2$ and even-parity. Comparison of these calculated values with measured values shows an excellent agreement. For the values with $n > 10$ the rms error between them is about 0.23 cm^{-1} . The calculation was extended to some high-lying levels which were unmeasured. The strong perturbations among Rydberg series can be illustrated graphically, namely, by a method of Lu-Fano plot^[2]. The Lu-Fano plots have been shown in Fig.1 and Fig.2 for

even-parity $J=0,2$ levels of tin. The effective quantum number ν_i is no longer a smooth function of energy in the perturbed Rydberg series, therefore the curve bends obviously in the perturbed Rydberg series. In this case the wave function for a given state can be expressed as a superposition of i -channels^[3]

$$\psi_n = \sum_i P_i^{(n)} Z_i^{(n)}$$

The mixing coefficients $Z_i^{(n)}$ for given state in i -channel can be calculated from the MQDT parameters μ_a and U_{ia} . A quantitative analysis of the perturbation is performed with the wave function and the mixing coefficients $Z_i^{(n)}$ for each level is calculated.

1. Jin Mingxing, Ding Dajun, Liu Hang, and Pan Shoufu, J.Phys. B. to be published.
2. K.T.Lu and U.Fano, Phys. Rev. A2, 81(1970).
3. C.N.Lee and K.T.Lu, Phys. Rev. A8, 1241(1973).

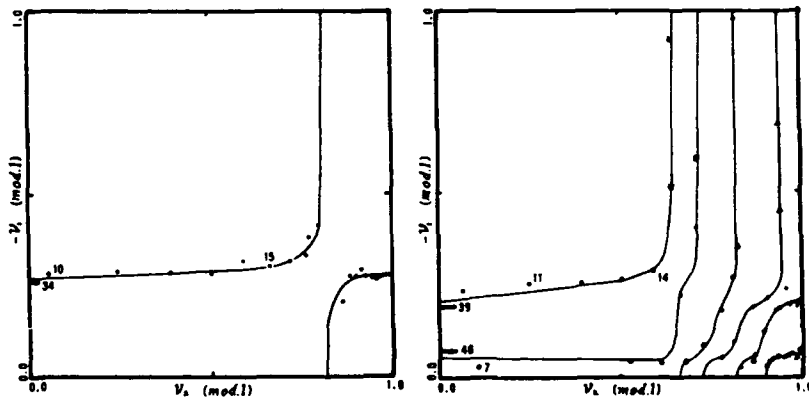


Fig. 1. Lu-Fano plot for the even-parity $J=0$ bound energy levels $5pnp$ $(1/2, 1/2)_0$ in tin. \bullet : observed levels.

Fig. 2. Lu-Fano plot for the even-parity $J=2$ bound energy levels $5pnp$ $(1/2, 3/2)_2$ and $5pnf$ $1/2[5/2]_2$ in tin. \bullet : $5pnp$ $(1/2, 3/2)_2$. \circ : $5pnf$ $1/2[5/2]_2$. Δ : $5pnf$ $3/2[5/2]_2$. \square : $5pnf$ $(3/2, 3/2)_2$. \blacktriangle : $5pnf$ $3/2[3/2]_2$. \blacksquare : $5pnf$ $(3/2, 1/2)_2$.

HIGHER ORDER EFFECTS IN THE HYPERFINESTRUCTURE AND ISOTOPE SHIFT IN HEAVY ELEMENTS

G. Klemz and H.-D. Kronfeldt

Optisches Institut, Technische Universität Berlin
Straße des 17. Juni 135, 1000 Berlin 12, Germany (FRG)

For the determination of fundamental atomic effects in optical transitions, such as hyperfine-structure splitting (hfs) or isotope shift (IS), new high resolution laserspectroscopical techniques have been developed. With these refined methods in the last few years it was possible to study even higher order effects in the hfs and IS also in the complex spectra of heavy elements. E.g. with two-photon measurements in Eu I, we recently investigated the hfs in the e^6D term of $4f^76s6d$. Here for a theoretical interpretation the necessity arises, to introduce also off-diagonal hfs splitting constants $A(J, J')$ and $B(J, J')$ considering second order hfs, besides the common magnetic dipole hfs constants $A(J)$ and the electric quadrupole hfs constants $B(J)$. In Fig. 1 the hfs interactions, generated by off-diagonal $A(J, J')$ matrix elements in the case of single hfs levels are sketched as an example for the $e^6D_{3/2}$ level. The experimental energy positions of each hfs level are fully explainable [1]. We discuss preconditions and aspects of further measurements in Eu (e.g. $4f^76s7d f^6D$) and in other heavy elements leading to a refined theoretical interpretation with higher order hfs constants.

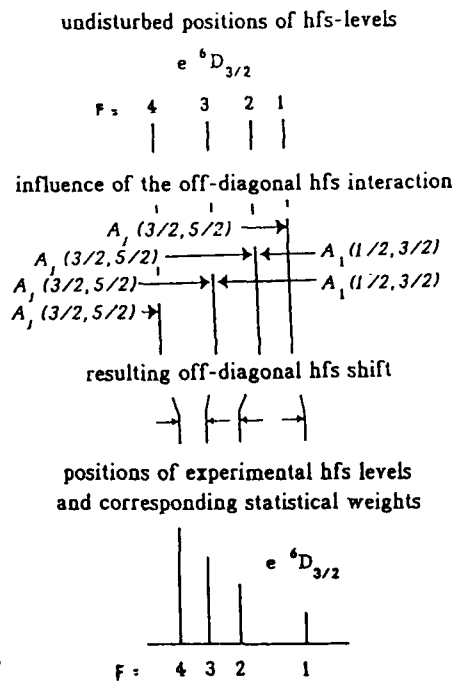


Fig. 1: Schematic example of the off-diagonal hfs interaction $A(J, J')$ in the hfs levels of the finestructure levels $e^6D_{3/2}$ of $4f^76s6d$

In this review also the situation of the higher order IS effects in the series of 5d-elements as well

as in the lanthanides will be presented. Especially the parametric description of these higher order, i.e. mainly crossed-second-order (CSO) [2], effects will be discussed. For special CSO-parameters systematics extending over entire series are obtainable, e.g. in the case of the J-dependence in the lanthanides, represented by the parameter z_{4f} , (Fig. 2a) [3]. However in other series the corresponding parameter (z_{5d}) in the 5d-elements show only a statistical scattering without correlation to the finestructure radial integrals (see Fig. 2b) [4].

Fig. 2a: $z_{4f}/\delta\langle r^2 \rangle$ and ζ_{4f} versus the charge number in the lanthanides

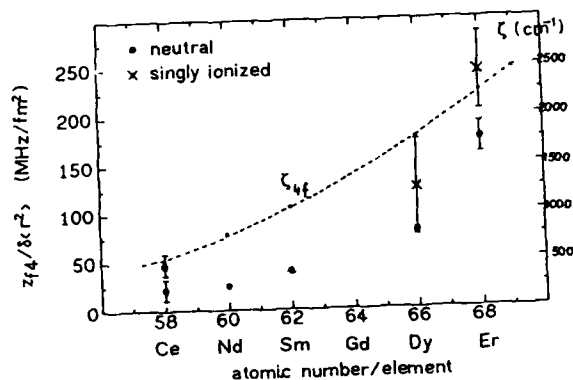
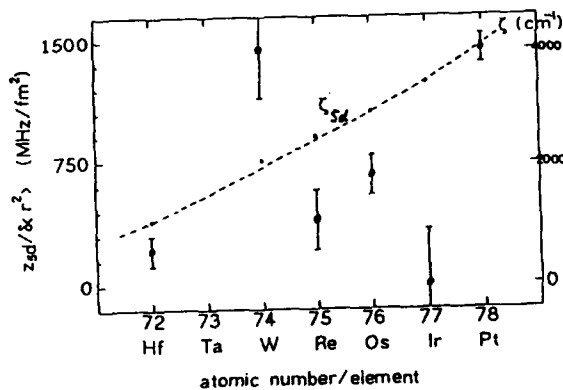


Fig. 2b: same as in Fig. 2a for the 5d-elements



References

1. H.-D. Kronfeldt, D.-J. Weber, in preparation; D.-J. Weber, Thesis, D 83, (1989)
2. J. Bauche, R.-J. Champeau, Adv. At. Mol. Phys. **12**, 39 (1976)
3. H.-D. Kronfeldt, G. Sinn, Z. Phys. D - Atoms, Molecules and Clusters **14**, 205 (1989)
4. G. Sawatzky, R. Winkler, Z. Phys. D - Atoms, Molecules and Clusters **14**, 9 (1989)

SPECTROSCOPIC DATA FOR HIGHLY CHARGED IONS

Shichang Li Yongsheng Sun
Guoxing Han and Hanyang Yang
Institute of Applied Physics and Computational Mathematics

Yonglu Yang and Lixian Chen
Chinese Research Association for Atomic and Molecular Data
(P.O. Box 8009, Beijing, China)

The purpose of the present work is to provide the immense amount of atomic data needed for applications to the ICF and X-ray laser research work in our institute and for the compilation-evaluation work in Chinese Research Association for Atomic and Molecular Data.

Using the non-relativistic Hartree-Fock self-consistent field method including the relativistic mass-velocity and Darwin terms in the Hamiltonian(HFR) proposed by Dr. R. Cowan^[1] we have calculated atomic structure data and spectroscopic data for the Neon-like Fe XII, Cu XX, Ge XXIII and Se XXV ions. In the calculations the configuration-interaction effects were taken into account and the following 15 configurations were included: $1s^2 2s^2 2p^6$, $1s^2 2s^2 2p^5 3s$, $1s^2 2s^2 2p^5 3p$, $1s^2 2s^2 2p^5 3d$, $1s^2 2s^2 2p^5 4s$, $1s^2 2s^2 2p^5 4p$, $1s^2 2s^2 2p^5 4d$, $1s^2 2s^2 2p^5 4f$, $1s^2 2s 2p^6 3s$, $1s^2 2s 2p^6 3p$, $1s^2 2s 2p^6 3d$, $1s^2 2s 2p^6 4s$, $1s^2 2s 2p^6 4p$, $1s^2 2s 2p^6 4d$, and $1s^2 2s 2p^6 4f$.

The configuration average energies, 88 energy levels, all possible electric dipole transition wavelengths, oscillator strengths and spontaneous radiative decay rates will be presented.

The same method was applied to Na-like Fe XIV, Cu XIX, Ge XXII, and Se XXIV ions and 12 configurations were included: $1s^2 2s^2 2p^6 3s$, $1s^2 2s^2 2p^6 3p$, $1s^2 2s^2 2p^6 3d$, $1s^2 2s^2 2p^6 4s$, $1s^2 2s^2 2p^6 4p$, $1s^2 2s^2 2p^6 4d$, $1s^2 2s^2 2p^6 4f$, $1s^2 2s^2 2p^6 5s$, $1s^2 2s^2 2p^6 5p$, $1s^2 2s^2 2p^6 5d$, $1s^2 2s^2 2p^6 5f$, and $1s^2 2s^2 2p^6 5g$. The spectroscopic data will be also presented.

In order to discuss the accuracy of the present results we have compared them with other works^[2].

- [1] R.D. Cowan, Theory of Atomic Structure and Spectra(Univ. of California Press, Berkeley,1981)
- [2] Hong Lin Zhang and D.H. Sampson, Atomic Data and Nuclear Data Tables,41, 1(1989), 43, 1(1989)

CALCULATION OF $2p^4(^3P)nl(l=s,d)$ RYDBERG SPECTRA OF
THE FLUORINE ISOELECTRONIC SEQUENCE*

Z.-W. Wang and X.-Z. Qian

Institute of Atomic and Molecular Physics, Jilin University
Changchun 130023, The People's Republic of China

We report a calculation of the basic structure parameters of $2p^4(^3P)ns$ and $2p^4(^3P)nd$ Rydberg spectra of the fluorine isoelectronic sequence by using eigenchannel quantum defect theory (EQDT)^{1,2}. These results should provide an aid to the understanding of systematic features of the spectra for this sequence and basic atomic data for magnetic fusion and laser programs.

Photoabsorption of a fluorine-like system from its ground state, $2p^5^2P_{3/2}$, leads to $2p^4(^3P)ns$ and $2p^4(^3P)nd$ Rydberg series with $J=1/2, 3/2$ and $5/2$ and even parity, and thence to 18 series (5 ns-channels and 13 nd-channels) in the final states. We can decouple the ns-channels from the nd-channels because the interactions between them are very weak, and consider the ns-channels and the nd-channels separately. Since the channels with different total angular momenta J do not interact, five ns-channels may be divided into three groups: two two-channel problems, $2p^4(^3P_1)ns$ and $2p^4(^3P_0)ns'$ with $J=1/2$, and $2p^4(^3P_2)ns$ and $2p^4(^3P_1)ns'$ with $J=3/2$, and one single-channel problem, $2p^4(^3P_2)ns$ with $J=5/2$, thirteen nd-channels may be also divided into three groups: one three-channel (two-ionizing limit) problem, $2p^4(^3P_2)nd$, $2p^4(^3P_2)nd'$ and $2p^4(^3P_1)nd$ with $J=1/2$, two five-channel (three-ionizing limit) problems, $2p^4(^3P_2)nd$, $2p^4(^3P_2)nd'$, $2p^4(^3P_1)nd$, $2p^4(^3P_1)nd'$ and $2p^4(^3P_0)nd$ with $J=3/2$, and $2p^4(^3P_2)nd$, $2p^4(^3P_2)nd'$, $2p^4(^3P_1)nd$, $2p^4(^3P_1)nd'$ and $2p^4(^3P_0)nd$ with $J=5/2$. According to EQDT, the whole eigenvalue problem is completely determined by the structure parameters (EQDT parameters) and the separation of ionizing limits^{1,2}. These parameters

consist of the eigen-quantum defects $\mu_{i\alpha}$ and the orthogonal transformation matrix $U_{i\alpha}$.

The structure parameters of each F-like system are calculated, as functions of the effective nuclear charge, by using the EQDT method, which establishes the relationship between the parameters and the radial integrals^{2,3}. The separation of ionizing limits are obtained from available data. The results indicate that the channel interactions gradually diminishes with the increasing value of effective nuclear charge. This behaviour can be interpreted in terms of the competition between electrostatic and spin-orbit interactions along this isoelectronic sequence.

The energy levels and the mixing coefficients of all Rydberg states and the autoionizing structures of these 18 channels for each F-like ion are evaluated from the structure parameters.⁴ A vast amount of basic atomic data can be obtained with little CPU time.

*Work performed under the auspices of the National Natural Science Foundation of China and the China Research Union on Atomic and Molecular Data.

1. Z.-W.Wang and K.T.Lu, Phys. Rev. A31, 1515(1985).
2. Z.-W.Wang and K.T.Lu, Phys. Rev. A31, 1521(1985).
3. Z.-W.Wang and K.T.Lu, Phys. Rev. A37, 2941(1988).
4. Z.-W.Wang and X.-Z.Qian, to be published.

QUANTUM ELECTRODYNAMIC PERTURBATION THEORY
FOR HIGH-Z FEW-ELECTRON ATOMS

V.M. Shabaev

Department of Physics, North-Western Extra-Mural Polytechnical
Institute, Leningrad, USSR

The quantum electrodynamic perturbation theory in the Rayleigh-Schrödinger form for the calculation of the high-Z few-electron atoms is constructed.

The proposed approach is based on the B.Sr.-Nagy and T.Kato formalism [1] for the relativistic renormalized few-electron Green functions, integrated over the relative energies and projected on the space of the considered states [2].

A series of the perturbation theory in the Rayleigh-Schrödinger form for the determination of the energy levels of the relativistic atom is constructed. The proposed method is applied to the determination of the electron interaction corrections due to the two-photon exchange diagrams to the energy levels of the two-electron multicharged ion.

The reduction formulae are derived for the amplitudes of the following processes: the photon emission by an atom, the auto-ionization, the photon scattering on the atom, the electron scattering on the atom, the photoeffect.

In order to study the natural spectral line shape in the framework of quantum electrodynamics the resonance photon scattering on the few-electron atom is considered. The general case of the few overlapping levels is studied. In the resonance approximation the calculation formulae for the differential and total scattering cross-sections are obtained. The equations allowing to improve the resonance approximation are also derived.

1. T.Kato, Perturbation theory for linear operators (Springer, Berlin, 1966).
2. V.M.Shabaev, Teor. y mat. fis. 82,83 (1990).

DETERMINATION OF CONFIGURATION MIXING COEFFICIENTS
FROM FINE STRUCTURE DATA

Edward S. Chang
Department of Physics and Astronomy
University of Massachusetts
Amherst, MA 01003

Abstract

From basic theory, we have proved Edlen's conjecture that the sum of fine structure (FS) intervals in a perturbed series is equal to the FS interval of the unperturbed interloper under certain circumstance. Further, the admixture coefficient P_n of a level is then simply the quotient of its FS over the summed FS. Therefore P_n can be determined experimentally to the precision of spectroscopic data.

Column two of Table I shows the FS data [1] in A II. The experimentally determined P_n (labeled E) are found to be in very good agreement with those calculated by Chang [2] and by Froese Fisher [3]. However some P_n calculated by Weiss [4] are in discrepancy by as much as a factor of three. Similarly the admixture coefficients are calculated for the same series in Si III, P IV, and S V.

Table I. Magnetic Fine Structure and the Perturber Admixture

State	ES(cm ⁻¹) 3F ₄ ^o - 3F ₂ ^o	Admixture P _n (%)			
		E	C	F	W
3s 4f	4.88	3.4		3	1.0
3s 5f	12.36	8.6		10	3.1
3s 6f	40.4	28.1	28	34	30
3p 3d	58.2	40.6	36	34	32
3s 7f	17.92	12.5	12	11	29
3s 8f	5.82	4.1		4	3.3
3s 9f	2.57	1.8			1.2
3s 10f	1.36	0.9			0.74
sum σ	143.5				

C Ref. 2

F Ref. 3

W Ref. 4

1. W.C. Martin and R. Zalubas, Phys. Chem Ref. Data **8**, 817 (1979).

2. T.N. Chang, Phys. Rev. **A36**, 3535 (1987)

3. C. Froese Fischer, Physica Scripta **21**, 466 (1980).

4. Q.W. Weiss, Phys. Rev. **A9**, 1524 (1974).

STARK EFFECT IN THE HIGH-L RYDBERG LINES OF MAGNESIUM IN THE SOLAR
INFRARED SPECTRUM

William G. Schoenfeld and Edward S. Chang
Department of Physics and Astronomy
University of Massachusetts
Amherst, MA 01003

Abstract

For a Rydberg atom with principal and orbital quantum numbers n and l ($l > 3$), we have found that the scalar dipole polarizability is given by

$$\alpha = \frac{n^7 l(l+1) a_0^6}{\alpha_c} \left[\frac{n^2 - (l+1)^2}{5n^2 - l(l+2)} (l - 1/2) (l + 1/2) (l + 2) (l + 5/2) \right. \\ \left. - \frac{n^2 - l^2}{5n^2 - (l-1)(l+1)} (l - 3/2) (l - 1) (l - 1/2) (l + 3/2) \right]. \quad (1)$$

In Eq. (1), α_c is the polarizability of the core and a_0 the Bohr radius. For magnesium, the value for α_c has been found [1] to be $34.7 a_0^3$. The above expression assumes the quadratic Stark effect, which is valid provided that the electric field strength ϵ is substantially less than the critical value estimated to be 10^5 V/cm for $n = 7$ in Mg.

In the Solar spectrum features at 7, 11, and 12 μm have already been identified [1] as high l Rydberg-Rydberg transitions in Mg I. Fig. 1 shows the 6h-7i transition in the Solar spectrum obtained from the Earth-orbiting satellite, SPACE-LAB III. We have fitted the spectrum to the sum of an emission and an absorption Lorentzian shape. Our fitting program evaluates the widths to be 0.0177 and 0.1000 cm^{-1} respectively, with the line centers displaced by 0.0046 cm^{-1} . We interpret this as a Stark shift on the absorption trough, which yields a value of 147 V/cm for ϵ .

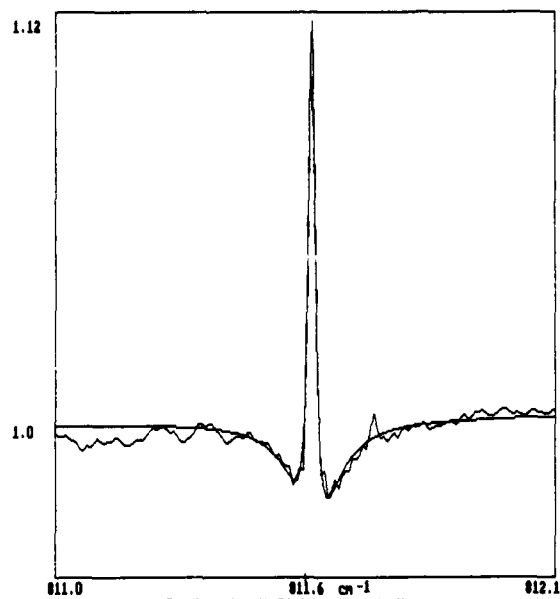


Fig.1 The 6r-7i transition in Mg.

In total 6 lines produce electric fields ranging from 70 to 440 V/cm. According to the Holtzmark theory [2], these fields imply electron densities of 3 to $50 \times 10^{12}/\text{cc}$ which in turn imply heights h of from 140 down to 25 km. Since the Solar photosphere is defined [3] as between $h = 0$ (optical depth at 500 nm = 1) to $h = 320$ km at the base of the chromosphere, we have confirmed that the absorption troughs are produced in the photosphere, while the emission peaks are chromospheric as originally suggested [4]. We will discuss line widths and what they reveal about the Solar atmosphere.

1. E.S. Chang, *Physica Scripta* **35**, 792 (1987).
2. C.R. Cowley, *The Theory of Stellar Spectra*, Gordon and Breach (1970) p. 158.
3. C.W. Allen, *Astrophysical Quantities*, Clowes and Sons, (1973) p. 165.
4. J. Brault and R. Noyes, *Astrophys. J.* **269**, L61 (1983).

Reanalysis of the Isotope Shift and Nuclear Charge Radii in Radioactive Potassium Isotopes

A-M Mårtensson-Pendrill¹, L Pendrill², S Salomonson¹, A Ynnerman¹ and H Warston¹

1) Dept. of Physics, Chalmers University of Technology, S-412 96 Göteborg, Sweden

2) National Testing Institute, P O Box 857, S-501 15 Borås, Sweden

Laser spectroscopic studies of chains of radioactive nuclei can reveal systematics of nuclear properties and have been performed in particular at CERN and GSI. One important goal of these experiments is to determine changes in nuclear charge radii. The experimentally observed shift is a sum of several terms. Subtracting the normal mass shift leads to the "residual isotope shift" (RIS) given for the case of K by

$$\delta v_{\text{RIS}}^{A,39} = \delta v_{\text{FS}}^{A,39} + \delta v_{\text{SMS}}^{A,39} = F \delta \langle r^2 \rangle^{A,39} + k_{\text{SMS}} (M_A - M_{39}) / ((M_{39} + m_e) M_A)$$

The specific mass shift (SMS) constant, k_{SMS} , is the expectation value of $\sum_{i>j} \mathbf{p}_i \cdot \mathbf{p}_j$ for the lower state minus that for the upper state of the transition. It involves a correlation between two electronic momenta and is difficult to evaluate. The electronic factor for the field shift, $F = -4\pi\Delta|\Psi(0)|^2 Z/6 (e^2 a_0^3 / 4\pi\epsilon_0)$, is determined by the electron density at the nucleus, $|\Psi(0)|^2$, for the lower state minus that in the upper state of the transition. Being a scalar one-body operator, the field shift is much less sensitive than the SMS to correlation effects.

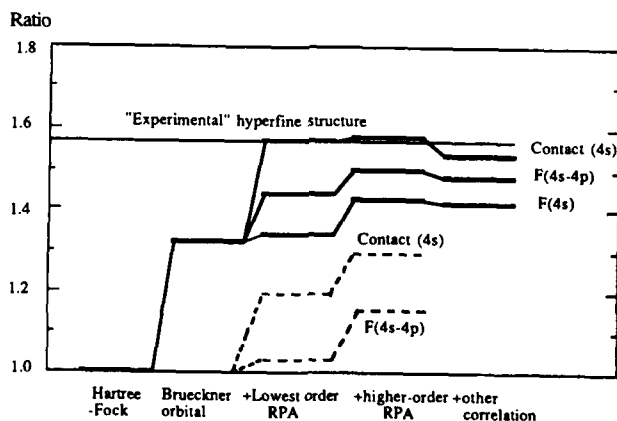


Figure 1. Comparison between the many-body effects on the contact hyperfine interaction in the 4s states in K and on the field shift factor. The results are normalized to the HF value for the respective quantities.

In the absence of reliable *ab initio* values, the field shift constant F in an s - p transition, such as the resonance transition in K , is estimated from the hfs of the s state, which depends on the spin density at the nucleus. In this work, described in more detail in /1/ we analyse (Fig. 1) how the ratio between these two properties is changed by many-body effects. Our final field shift constant is found to be $F = -110(3) \text{ MHz/fm}^2$, significantly smaller than the value, $F = -128 \text{ MHz/fm}^2$ used by Touchard *et al.* /2/ to interpret their experimental data for a series of radioactive K isotopes. Combining our value with muonic data leads to the shifts in nuclear charge radii shown in Fig. 2

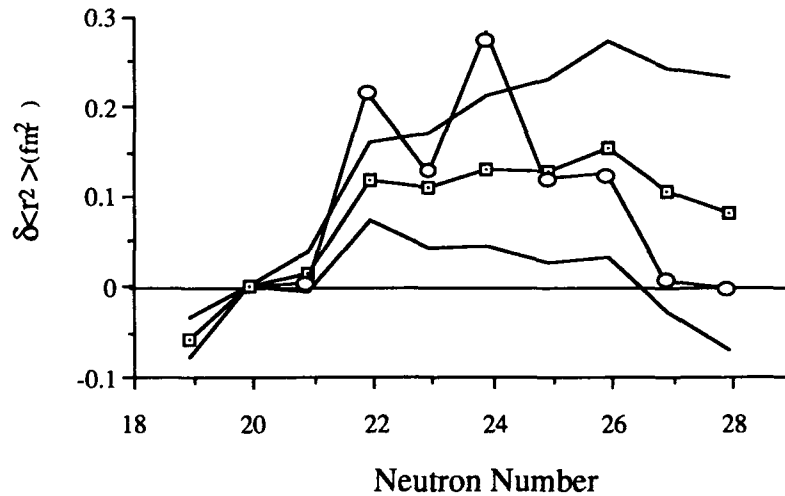


Figure 2 Comparison between the changes in nuclear charge radii for K (squares) and for the isotones of Ca (circles). The uncertainty for the K charge radii due to the uncertainty in muonic data is marked by the two curves without symbols.

In spite of the large uncertainties we can see that the addition of eight neutrons to the ^{39}K nucleus gives a surprisingly small increase in nuclear charge radius – within the error bars the result is compatible with identical charge radii for the two isotopes ^{39}K and ^{47}K , with the magic neutron numbers $N=20$ and $N=28$, respectively. This is another example of the nuclear $1f_{7/2}$ shell closure effect that leads to nearly identical charge radii for the doubly magic nuclei ^{40}Ca and ^{48}Ca /3/.

1. A-M Mårtensson-Pendrill *et al.* J. Phys. B, in print
2. F Touchard *et al.* Phys. Lett. **108B** 169 (1982)
3. E Bergmann *et al.* Z. Phys. **A294** 319 (1980), F Träger, *ibid.* **A299** 33 (1981)

VII-16

VARIATIONAL METHOD FOR THE MANY-PARTICLE DIRAC EQUATION

K. Aashamar

Institute of Physics, University of Oslo, Oslo, Norway

J.D. Talman

Departments of Applied Mathematics and Physics and Centre for Chemical Physics,
University of Western Ontario, London, Ontario, Canada

The variational method for atomic ground state wave functions is based on the fact that the ground state energy is the minimum of the expectation value of the Hamiltonian. If the Schroedinger kinetic energy operator is replaced by the Dirac operator, this is no longer the case since the latter is not bounded from below, and there is a continuum of negative energy eigenvalues. Therefore, the usual variational method of minimizing the expectation value for the energy cannot be expected to work for the Dirac equation. Although there is no upper bound property for the Dirac equation, it can be shown¹ that, for the single-particle problem, the ground state energy and wave function are the solution of the variational problem

$$e = \min_{\phi_1, \phi_2} \left[\max_{\phi_3, \phi_4} \langle H_D \rangle \right] \quad (1)$$

where ϕ_1 and ϕ_2 are the 'large' components of the Dirac spinor, ϕ_3 and ϕ_4 are the 'small' components, and $\langle H_D \rangle$ is the expectation value of the Dirac Hamiltonian. The variational derivative with respect to each component yields one of the four Dirac equations.

We have considered the generalization of (1) to the case of more than one particle. The Dirac wave function then has 4^N components, each of which is either large or small for each particle. It can be argued that the generalization of (1) is that the $\langle H_D \rangle$ should be maximized on all the components that are small for any of the particles, and then minimized on the 2^N components that are large for all N particles. That is,

$$e = \min_{\phi_{i_1} \dots i_N} \left[\max_{\phi_{j_1} \dots j_N} \langle H_D \rangle \right] \quad (2)$$

where $i_k = 1$ or 2 , and at least one of the j 's is 3 or 4 .

It is easy to see that this variational problem gives the 4^N Dirac equations for the system, but it is less clear that this particular variational formulation leads to the ground state of the system if it exists. In particular, the Brown-Ravenhall problem² may render the identification of the N -particle ground state ambiguous. It can be seen, however, that eq. (2) gives the correct result in the case of N non-interacting particles, each bound in a static potential. If eq. (2) has a solution, that solution also satisfies the N -particle non-interacting Dirac equation which then separates so that $\phi_{i_1 \dots i_N}(\mathbf{r}_1, \mathbf{r}_2, \dots, \mathbf{r}_N) = \prod \phi_{k, i_k}(\mathbf{r}_k)$. The solution of (2) can therefore be found over the subspace of such product wave functions. Since H_D is the sum of N independent Hamiltonians, it can be seen that (2) reduces to N copies of eq. (1), and therefore that e is the sum of the N ground state energies.

This variational principle for the Dirac equation should permit high accuracy variational calculations for two-electron ions at large Z values for which the usual technique of including relativistic corrections to the Schroedinger equation may not be suitable.

Results of a number of preliminary calculations for two-electron ions of large Z will be presented for both the non-interacting and interacting cases.

1. J.D. Talman, Phys. Rev. Lett. **57**, 1091(1986).

2. G.E. Brown and D.G. Ravenhall, Proc. Roy. Soc. London, **A208**, 552(1951).

EFFECTIVE MULTICONFIGURATION POTENTIAL
FOR MANY-BODY PERTURBATION CALCULATIONS

Z. W. Liu and H. P. Kelly

Department of Physics, University of Virginia
Charlottesville, VA 22901, USA

For open-shell atoms, especially for those with quasi-degenerate or strongly-mixed configurations, it is appropriate to start many-body perturbation theory (MBPT) calculations from the multiconfiguration Hartree-Fock (MCHF) wave functions, or its relativistic version of the multiconfiguration Dirac-Fock (MCDF) wave functions, because a significant portion of the correlation effects have been included in the lowest-order approximation. We report here an approach for MBPT calculations of open-shell systems based on the MCDF approximation. Considering that the different configuration states are weighted by configuration mixing coefficients in the MCDF scheme and using projection operators, we construct an effective multiconfiguration potential to generate an optimized complete set in the relativistic framework. The low-lying bound states in the orthogonal complete set are approximately the MCDF core and valence orbitals. This complete set provides a convenient basis to implement multi-reference (MR) MBPT calculations. By using the coupled-cluster approach in the MR model space spanned by the configuration state functions, an infinite subset of MBPT expansion terms, i.e. single- and pair-excitation amplitudes, is evaluated.

As an example, the calculation is performed for the correlation energy of ground-state beryllium. Its MR model space consists of the $1s^2 2s^2$, $1s^2 2p_{1/2}^2$ and $1s^2 2p_{3/2}^2$ configurations with a total angular momentum $J = 0$. The convergence of MBPT series starting from different mean fields is discussed, and the comparison of the present work with Salomonson *et al*'s MR-MBPT result¹, Morrison and Froese Fischer's MCHF+MBPT result², Millack, Dietz and Hess's *g*-Hartree results³, and an V^N -HF potential MBPT result is presented. Our calculation is relativistic, so the method reported here can readily be extended to the high-accuracy calculation for heavy atoms.

1. S. Salomonson, I. Lindgren and A.-M. Mårtensson, Phys. Scr. **21**, 351(1980).
2. J. Morrison, Phys. Scr. **34**, 423(1986); J. Morrison and C. Froese Fischer, Phys. Rev. A **35**, 2429(1987); J. Morrison, J. Phys. B **21**, 2915(1988).
3. T. Millack, Phys. Rev. A **40**, 6188(1989); K. Dietz and B. A. Hess, Bonn preprint AM-89-07, 1989.

**ANOMALOUS DOUBLET SPLITTINGS OF BINDING ENERGIES
IN DIRAC-FOCK CALCULATIONS**

Chien-Tsun Chen and Keh-Ning Huang

Institute of Atomic and Molecular Sciences, Academia Sinica

P.O. Box 23-166, Taipei, Taiwan 10764, ROC

and

Department of Physics, National Taiwan University

Taipei, Taiwan 10764, ROC

Recently Misra *et al.*¹ reported negative Sommerfeld screening parameters σ_2 of spin doublets in neutral atoms. The binding energies adopted in the calculation were Dirac-Fock(DF) energies evaluated with Dirac-Fock-Slater(DFS) wave functions;² to this approach we refer as DF(S). To investigate the negative σ_2 anomaly, we consider specifically the splitting of $3p$ -electron binding energies in neutral atoms of Sc through Zn in the Dirac-Fock formulation. Physically the spin-doublet splitting is of relativistic origin and should vanish in the nonrelativistic limit. However the nonrelativistic splittings ΔE_{DF-NR} do not vanish in the DF calculations. If we neglect the slight difference in orbital wave functions from the two configurations and take $3p_{1/2} = 3p_{3/2} = 3p$, $3d_{3/2} = 3d_{5/2} = 3d$, we express the energy expression of the doublet splitting in the nonrelativistic limit approximately by

$$\Delta E_{DF-NR}^{approx} = \frac{1}{20} (3m - 2n) \left[G^1(3p \ 3d) - \frac{3}{7} G^3(3p \ 3d) \right]$$

where m and n are the occupation numbers of $3d_{3/2}$ and $3d_{5/2}$ subshells, respectively. Unless $\left[G^1(3p \ 3d) - \frac{3}{7} G^3(3p \ 3d) \right]$ is negligibly small, the above expression vanishes only for empty $3d$ subshells $m=0, n=0$ and for completely filled $3d$ subshells $m=4, n=6$. The $\Delta E_{DF-NR}^{approx}$ and ΔE_{DF-NR} are in close agreement from the results of practical calculations. Hence, we conclude that the anomalous doublet splittings which remain in the nonrelativistic limit come from the nonvanishing energy expression. The anomalous doublet splittings in the nonrelativistic limit should therefore be removed from the relativistic calculations, and the resulting doublet splittings are referred to as those of the corrected Dirac-Fock(CDF).

The doublet splittings of DF(S) and DF are similar and contain spurious contributions because they were both obtained from the same DF energy expressions. There is reasonable agreement between the CDF and experiment. The $3p$ doublet splittings of DF and CDF are plotted in Fig. 1.

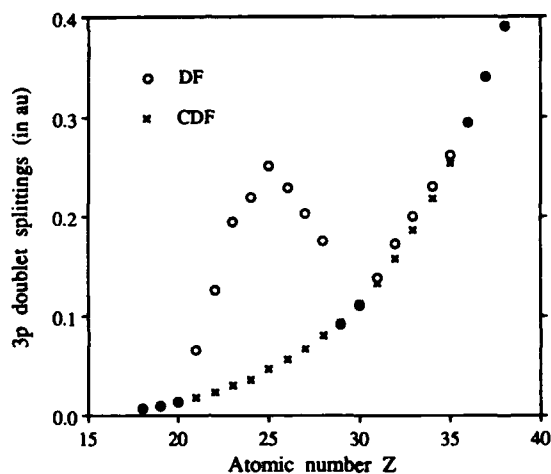


FIG. 1. Comparison of 3p doublet splittings of DF and CDF for neutral Ar through Sr

There is an apparent anomaly in the DF results for $Z=21-28$, whereas the CDF results form a smooth function of the atomic number Z . The screening parameters σ_2 derived from the CDF values also form a smooth function of the atomic number Z , in contrast to the DF values, which show negative screening parameters for $Z=22-25$. We have elucidated the anomalous doublet splittings of 3p-electron binding energies in the DF formulation for atoms with partially filled 3d subshells. A similar condition exists when there are partially filled 4p subshells. This corresponds to the slight anomaly of the DF results for $Z=31-35$ in Fig. 1. Spin doublet splittings for other subshells, such as 3d, 4p, 4d, etc. can be analyzed similarly.

This work was supported in part by the National Science Council of the Republic of China.

REFERENCES

1. U. D. Misra, M. Sah, and B. G. Gokhale, *J. Phys. B* **22**, 1505 (1989).
2. K.-N. Huang, M. Aoyagi, M. H. Chen, B. Crasemann, and H. Mark, *At. Data and Nucl. Data Tables* **18**, 243-291 (1976).
3. A. Liberman, D. T. Cromer, and J. T. Waber, *Comput. Phys. Commun.* **2**, 107 (1971).
4. J. P. Desclaux, *Comput. Phys. Commun.* **9**, 31 (1975).
5. J. C. Fuggle and N. Mårtensson, *J. Electron Spectrosc. Related Phenom.* **21**, 275-281 (1980).

A THEORETICAL SURVEY OF THE NEON ISOELECTRONIC SEQUENCE

E. Biémont (*)
 Institut d'Astrophysique, Université de Liège
 B-4200 Cointe-Liège, Belgique.

Abstract

The coherence of experimental values of energy levels and wavelengths available along the neon isoelectronic sequence has been tested by comparison with theoretical results calculated for the ions Na II - Eu LIV ($11 \leq Z \leq 63$).

The calculations of energy levels and wavelengths have been performed with a fully relativistic MCDP method [1]. Breit contributions and QED corrections have been introduced in the calculations.

Configuration interaction was considered among the configurations

$$2s^2 2p^6 + 2s 2p^6 3s + 2s 2p^6 3d + 2s^2 2p^5 3p + 2p^6 3s^2 + 2p^6 3p^2 + 2p^6 3d^2$$

and $2s^2 2p^5 3s + 2s^2 2p^5 3d + 2s 2p^6 3p$, which correspond to 32 and 20 relativistic configurations respectively.

Some inconsistencies between theoretical and observed energy levels have been obtained particularly for the $3s 3p^6 nl$ configurations where further experimental investigations are needed.

(*) Senior Research Associate of the Belgian National Fund for Scientific Research (FNRS).

[1] I.P. Grant, B.J. McKenzie, P.H. Norrington, D.F. Mayers, N.C. Pyper, *Comput. Phys. Comm.* 21, 207 (1980)

A THEORETICAL INVESTIGATION OF TRANSITION RATES
AND WAVELENGTHS IN THE X-RAY SPECTRA OF NICKEL-
LIKE IONS (Ge V - Pb LV)

P. Quinet (§)	and	E. Biémont (*)
Faculté des Sciences		Institut d'Astrophysique
Université de Mons		Université de Liège
Belgique		Belgique

Abstract

The strong 3d - 4p and 3d - 4f resonance transitions in nickel-like ions have been observed recently in hot plasmas up to very high electric charges. The $n=4$ $\Delta n=0$ transitions might be also responsible of amplified emission of radiation in relation with population inversion and, consequently, of laser effect in the X-ray region. This effect has been observed effectively in ions like Gd, Sm and Ta.

The $n = 3-4$ transitions which appear in the X-ray spectra of nickel-like ions (Ge V - Pb LV) have been investigated theoretically by the multiconfigurational Dirac-Fock approach. For that purpose, Grant's code was used in the extended average level (EAL) option. Configuration interaction was retained among the configurations $3p^6 3d^{10}$, $3p^6 3d^9 4s$, $3p^6 3d^9 4d$, $3p^5 3d^{10} 4p$, $3p^5 3d^{10} 4f$ and $3p^6 3d^9 4p$, $3p^6 3d^9 4f$, $3p^5 3d^{10} 4s$ and $3p^5 3d^{10} 4d$ for even and odd parity, respectively.

The effect of the level crossings on the transition rates of low excitation depopulation transitions has been considered both for forbidden and for allowed transitions. A comparison of the ab initio wavelengths with the available observations shows that some experimental data could be refined.

(§) Holder of an IRSIA Fellowship.

(*) Senior Research Associate of the Belgian National Fund for Scientific Research (FNRS).

COMPARISON OF THE SADDLE-POINT METHOD AND THE FESHBACH-TYPE PROJECTION METHOD

Kwong T. Chung*

Institute of Atomic and Molecular Sciences, Academia Sinica, Rep. of China
and

Department of Physics, North Carolina State University, Raleigh, N. C. 27695

In a recent paper[1], Bylicki uses the Feshbach-type projection operator method to solve triply-excited three-electron systems. His method is interesting because the traditional Feshbach projection method can not solve these problems easily. He obtained for the closed channel wave function

$$Q\psi = \prod_{i=1}^3 (1 - P_i)\Psi \quad \text{where} \quad P_i = |\varphi_{1s}(\vec{r}_i)\rangle\langle\varphi_{1s}(\vec{r}_i)|. \quad (1)$$

φ_{1s} is the ground state wave function of the hydrogenic ion. Two important points are made by Bylicki: Q is completely symmetric with respect to the electron coordinates; and it takes the same form as the projection operator of the saddle-point method[2]. He also mentioned that the same situation occurs in doubly excited two electron systems. He believes that the successful applications of the saddle-point method to triply-excited resonances in He^- , Li and Be^+ justify his approach.

For $(2l2l'2l'')$ resonances, Eq.(1) does take the same form as the projection operator of the saddle-point method[2]. The only difference is that the φ in [2] is parametrized. That is

$$\varphi_{1s}(q) = (1/\sqrt{\pi}) q^{3/2} e^{-qr}. \quad (2)$$

This parameter is determined by maximizing the energy with respect to q. This implies the energy obtained using Eq.(2) is necessarily higher than that from Eq.(1). In the case where Eq.(1) is applicable, it guarantees that variational breakdown will never occur in a saddle-point calculation.

In this work, we compare the two similar methods to determine which gives a better approximation to the true resonance energy. For two electron systems in the elastic scattering region, the method derived by Bylicki is identical to the usual Feshbach projection operator method. If we assume the eigenvalues from the QHQ operator is E_n^{Ft} and the true resonance position is E_n^{res} , we can define a Feshbach shift as

$$\Delta_n^{\text{Ft}} = E_n^{\text{res}} - E_n^{\text{Ft}} \quad (3)$$

Bhatia and Temkin[3] have calculated the Feshbach shifts for twenty two resonances of helium. Only two shifts are negative. One can also define a saddle-point shift Δ_n^{sp} by subtracting the saddle-point energy from E_n^{res} . A compari-

son of these two shifts using the available data in the literature show that in most cases, the saddle-point energies give significant improvement over the eigenvalues of QHQ.

For resonances in the inelastic region such as $3s3p^1P$, the operator of Bylicki can not remove the open channels (2skp), (2pks) or (2pkd). Therefore, variational breakdown will always occur in the computation. It is, however, possible to construct Feshbach type projection operators for these resonances. One can also compare saddle-point results with Feshbach type QHQ calculation. If we compare the calculated results with the most precise experiment, the saddle-point results give significant improvement over that of the Feshbach-type calculation again. These comparison will be presented.

For triply-excited three-electron resonances such as (2s2s2p), the projection operator of Eq.(1) resembles that of the saddle-point method. However, for (2sn ℓ n' ℓ') resonances with n, n' \geq 3, the two methods are completely different. For example, for the [(2s3s) 1S , 3p] $^2P^0$ resonance, the saddle-point method gives for the two major partial waves [(0,0) 10,1] and [(1,1) 10,1]

$$Q\bar{Q} = A (1-P_{1s}(1))(1-P_{1s}(2))(1-P_{2s}(2))(1-P_{2p}(3))\bar{\phi}(r_1, r_2, r_3)[(0,0)^10,1] \\ + A (1-P_{2p}(2))(1-P_{2p}(3))\bar{\phi}'(r_1, r_2, r_3)[(1,1)^10,1] \quad (4)$$

whereas Eq.(1) gives

$$Q\bar{Q} = (1-P_{1s}(1))(1-P_{1s}(2))(1-P_{1s}(3)) A (\bar{\phi}(r_1, r_2, r_3)[(0,0)^10,1] + \\ \bar{\phi}'(r_1, r_2, r_3)[(1,1)^10,1]) \quad (5)$$

In the wave function of Eq.(5), all states of the symmetry (2s2snp), (2s2pns), (2s2pnd), (2p2pnp) and the corresponding continua will be present. This implies that in the computation of this resonance variational breakdown can not be avoided. It is not clear how one can improve the Q operator in Eq.(5) to overcome this difficulty. This serious problem indicates that the method of Bylicki can not be used for general triply-excited three-electron systems.

* Supported by the National Science Foundation Grant No. PHY87-15238 and by the National Research Council of the Republic of China.

Reference:

1. M. Bylicki, Phys. Rev. A39,3316(1989);A40,1748(1989).
2. K. T. Chung, Phys. Rev. A20, 1743(1979);K. T. Chung and B. F. Davis, in "Autoionization-Recent Developments and Applications", Ed. by A. Temkin (Plenum, New York, 1985). Chapter 3.
3. A. K. Bhatia and A. Temkin, Phys. Rev. A11,2016(1975).

IDENTIFICATION OF HIGH RESOLUTION AUGER SPECTRUM OF BERYLLIUM

Kwong T. Chung*

Institute of Atomic and Molecular Sciences, Academia Sinica, Rep. of China
and

Department of Physics, North Carolina State University, Raleigh, N. C. 27695

The Auger spectrum of beryllium has been studied by Rødbro et al.[1] using 100 to 500 Be^+ on CH_4 and on He. Singly- and doubly-core-excited states are abundantly populated. High resolution is obtained using a small observation angle (6.4°). Of the twenty-one reported line positions within the range of 96 to 120 eV, twelve are shown to be the decay of lithiumlike resonances[2]. The identifications of the other nine spectral lines remained uncertain.

In this work, a saddle-point method is used to calculate the energies of the $1s2\ell'2\ell''$ states of BeI in order to identify the observed lines in the spectrum. A multiconfiguration interaction wave function is used. The 1s

Table I. Energies of $1s2\ell'2\ell''$ states of BeI (in a.u., L is the No. of partial waves used, N is the No. of terms, energies in parentheses indicate the corresponding Auger channel is not favored by symmetry.)

state	L	N	q	$-E_{\text{non-rel}}$	$-\text{Relat. Corr.}$	$-E_{\text{total}}$	Auger	Ele. energy(eV)	
								1s1s2p	1s1s2s
$1s2s^2 3p^0$	29	260	3.46	10.462737	.002048	10.464785		101.10	105.07
$1s2s^2 1p^0$	29	286	3.36	10.420905	.002051	10.422956		102.24	106.20
$1s2s2p^2 5p$	14	134		10.422510	.001969	10.424488		102.20	106.16
$1s2s2p^2 3p(1)$	25	246	3.40	10.322790	.001919	10.324709		104.91	(108.88)
$1s2s2p^2 3p(2)$	28	327	3.52	10.195611	.001909	10.197720		108.37	(112.33)
$1s2s2p^2 1p$	20	197	3.16	10.172185	.001934	10.174119		109.01	(112.98)
$1s2s2p^2 3d$	28	327	3.30	10.310631	.001975	10.312606		105.24	109.21
$1s2s2p^2 1d$	23	272	3.45	10.234599	.001884	10.236483		107.31	111.28
$1s2s2p^2 3s$	25	298	3.32	10.254758	.001975	10.256733		106.76	110.73
$1s2s2p^2 1s$	19	236	3.46	10.156460	.001937	10.158397		109.44	113.40
$1s2p^3 5s^0$	11	89		10.184155	.001886	10.185941		108.69	(112.65)
$1s2p^3 3s^0$	18	197		10.116261	.001788	10.118049		(110.54)	(114.50)
$1s2p^3 3d^0$	29	318	3.25	10.157500	.001864	10.159364		109.41	(113.38)

vacancy orbital is built into the wave function with a parameter q . The results of this calculation is given in Table I. In this table, L is the number of orbital and spin angular partial waves used in the wave function. N is the number of linear parameters. The relativistic corrections are calculated using first-order perturbation theory. They include correction to the kinetic energy, Darwin terms, electron-electron contact terms and orbit-orbit interaction. The mass polarization correction is also included. To calculate the energies of the Auger electrons, we need $1s1s2s$ and $1s1s2p$ energies. The energies used in Table I are -14.325852 a.u. for $1s1s2s$ and -14.180132 a.u. for $1s1s2p$, respectively.

The intensities of the four-electron spectral lines in [1] are all very weak in comparing to the intensities of the lithium-like lines. If we compare the four-electron lines between them-

self, the lines with the most intensities are line #8 and #14. Our results show that line #8 comes from the symmetry preferred decay of $1s2s2p^2 \ ^3P(1) \rightarrow 1s^22p,e$. In Ref.[1], line #14 and #15 are reported to be 108.96 ± 0.2 eV and 109.26 ± 0.2 eV. Our results show that four possible Auger lines lie in the range of 109.01 eV to 109.44 eV. The nine previously unidentified lines are all shown to have come from BeI $1s2\ell 2\ell' 2\ell''$ four-electron resonances.

Table II. Identifications of BEI Auger spectrum (in eV).

	This work Energy Identification	Experiment[1] line No. Energy
	101.10 $1s2s^22p \ ^3P^0 \rightarrow 1s^22p,e$	#4 101.02 \pm 0.1
	102.20 $1s2s2p^2 \ ^5P \rightarrow 1s^22p,e$	#5 102.12 \pm 0.1
	102.24 $1s2s^22p \ ^1P^0 \rightarrow 1s^22p,e$	
	104.91 $1s2s2p^2 \ ^3P(1) \rightarrow 1s^22p,e$	#8 104.88 \pm 0.1
	105.24 $1s2s2p^2 \ ^3D \rightarrow 1s^22p,e$	#9 105.5 \pm 0.2
	106.16 $1s2s2p^2 \ ^5P \rightarrow 1s^22s,e$	#10 106.0 \pm 0.2
	106.20 $1s2s^22p \ ^1P^0 \rightarrow 1s^22s,e$	
	106.76 $1s2s2p^2 \ ^3S \rightarrow 1s^22p,e$	#11 107.02 \pm 0.2
	107.31 $1s2s2p^2 \ ^1D \rightarrow 1s^22p,e$	
	108.37 $1s2s2p^2 \ ^3P(2) \rightarrow 1s^22p,e$	#13 108.15 \pm 0.2
	109.01 $1s2s2p^2 \ ^1P \rightarrow 1s^22p,e$	#14 108.96 \pm 0.2
	109.21 $1s2s2p^2 \ ^3D \rightarrow 1s^22s,e$	#15 109.26 \pm 0.2
	109.41 $1s2p^3 \ ^3D^0 \rightarrow 1s^22p,e$	
	109.44 $1s2s2p^2 \ ^1S \rightarrow 1s^22p,e$	

* This work was supported by the National Science Foundation, Grant No. PHY87-15238 and by the National Science Council of the Republic of China.

Reference

1. M. Rødbro, R. Bruch and P. Bisgaard, J. Phys. B12, 2413(1979).
2. B. F. Davis and K. T. Chung, J. Phys. B15 3113(1982).
3. K. T. Chung, Phys. Rev. A20, 1743(1979).

FINITE ELEMENT ANALYSIS OF THE THREE-BODY COULOMB SYSTEM

J. Shertzer*

*Institute for Theoretical Atomic and Molecular Physics
Harvard-Smithsonian Center for Astrophysics
Cambridge, MA 02138 USA*

In atomic and molecular physics, the standard approach to solving few-body systems is the variational method. This method yields highly accurate values for the energy by optimizing the wavefunction in the region of space where the contribution to the Hamiltonian is large. There is no reason to expect the wavefunction to be equally well determined in other regions of space and localized error in the wavefunction can lead to inaccurate values for physical observables.

The finite element method (FEM) offers an alternate approach to solving the Schrödinger equation for few-body systems¹ which eliminates the problems that arise from using globally defined basis functions. In FEM, the space is discretized into small regions called elements. The Schrödinger equation is solved in each element and the unknown wavefunction is approximated locally using polynomial interpolation functions. These functions are smoothly joined at the element boundaries to obtain the complete wavefunction. As the number of elements is systematically increased the approximate energy and wavefunction converge to the exact Schrödinger solution. The advantage of this method is clear: the use of local basis functions guarantees that the wavefunction is accurate over the entire space. It is possible to "fine tune" the wavefunction in a particular region of space by locally increasing the number of elements, without reducing the accuracy of the wavefunction in other regions. Consequently, the FEM wavefunctions are well suited for calculating expectation values of physical observables.

A FEM code has been developed to solve the Schrödinger equation for the three-body Coulomb system with arbitrary charges and masses. For the ground state of helium (with finite nuclear mass), five digit accuracy has been obtained for the energy and geometry using only 245 elements. The results are stable with respect to minor variations in the discretization. Work is in progress to obtain the energy and wavefunctions for the muonic molecular ions. The most recent results for the energy and geometry of $dd\mu^+(J=0, \nu=0)$ are converged to four significant digits.

*Permanent address: Department of Physics, Holy Cross College, Worcester, MA 01610.

¹F. S. Levin and J. Shertzer, *Phys. Rev. A* **32**, 3285 (1985); F.S. Levin and J. Shertzer, *Phys. Rev. Lett.* **61**, 1089 (1988); J. Shertzer, *Phys. Rev. A* **39**, 3833 (1989); J. Shertzer, L.R. Ram-Mohan and D.Dossa, *Phys. Rev. A* **40**, 4777 (1989); L.R. Ram-Mohan, S. Saigal, D. Dossa and J. Shertzer, *Comput. in Phys.* **4**, 50 (1990); J. Shertzer and L.R. Ram-Mohan, *Phys. Rev. B*, **41**, 9994 (1990).

THE SPECTRUM OF PHOTOEXCITED Nd³⁺ IONS IN LaCl₃

J. Shertzer*

*Institute for Theoretical Atomic and Molecular Physics
Harvard-Smithsonian Center for Astrophysics
Cambridge, MA 02138 USA*

N. Pelletier-Allard and R. Pelletier

*Laboratoire Aime Cotton, Centre National de la Recherche Scientifique
en association avec l'Universite Paris XI, Bat. 505
Campus d'Orsay, 91405 Orsay Cedex, France*

Although the spectrum of Nd³⁺:LaCl₃ has been widely studied,^{1,2} many of the crystal field components are still unknown, particularly the $\mu = 5/2$ levels for which absorption transitions from the ground level are forbidden by the selection rules. Through absorption experiments on photoexcited ions, nine new levels have been identified.³ A least squares fit has been carried out for the 127 known levels.

The lowest levels of the ${}^4I_{11/2}(\mu = 3/2)$, ${}^4I_{13/2}(\mu = 1/2)$ and ${}^4I_{15/2}(\mu = 1/2)$ multiplets are metastable and can be populated for further absorption. In this experiment, the Nd³⁺ ions were photoexcited by two methods. First, the sample was illuminated using an iodine lamp with an IR filter; the metastable levels were then populated through radiative and non-radiative processes. In the second approach, photoexcitation occurred without any additional source of energy when the laser radiation was coincident with vibronic side bands;⁴ the same deexcitation processes populated the metastable levels.

All data were obtained by monochromatic laser excitation of the fluorescence; the spectrometer was fixed at a particular wavelength and the laser frequency was scanned over the investigated spectral range. Changes in the emitted fluorescence intensity indicated the presence of absorption lines. For lines that did not correspond to known transitions, the starting level was determined by considering the relative intensities of the various fluorescence lines. The crystal quantum number of the excited level was assigned based on the polarization.

A least squares fit was carried out for the known levels of Nd³⁺:LaCl₃ using a Hamiltonian¹ which includes operators for the two- and three-body electrostatic interactions; spin-orbit interaction; spin-other-orbit and spin-spin interactions; pseudomagnetic configuration mixing interactions; and the crystal field interaction. Using 20 free parameters, 127 levels were fit with a mean error of 9.4 cm⁻¹.

*Permanent address: Department of Physics, Holy Cross College, Worcester, MA 01610

¹H.M. Crosswhite, H. Crosswhite, F.W. Kaseta, and R. Sarup, *J. Chem. Phys.* **64**, 1981 (1976).

²R.S. Rana, F.W. Kaseta and R.H. Garvey, *J. Chem. Phys.* **77**, 4400 (1982).

³N. Pelletier-Allard, R. Pelletier and J. Shertzer, *J. Chem. Phys.*, to appear (1990).

⁴N. Pelletier-Allard and R. Pelletier, *J. Luminesc.* **46**, 217 (1990).

FINE STRUCTURE OF THE ALKALINE EARTH NEGATIVE IONS

V.A.Dzuba[†], V.V.Flambaum[†], G.F.Gribakin[‡], O.P.Sushkov[†][†] Institute of Nuclear Physics, 630090 Novosibirsk, USSR[‡] M.I.Kalinin Polytechnical Institute, 195251 Leningrad, USSR

The number of recent calculations have confirmed the existence of Ca^-4s^24p negative ion, which was discovered earlier experimentally. They have predicted also the formation of stable negative ions of Sr^-5s^25p , Ba^-6s^26p (see, e.g. /1/) and Ra^-7s^27p (/2/). The binding energy for the outer p electron in these ions is very small (~ 0.1 eV). Therefore, in order to calculate it accurately, it is necessary to take into account relativistic corrections, in particular, the spin-orbit interaction. The latter splits the ns^2np 2P ionic state into two levels: the ground $^2P_{1/2}$ with $J = 1/2$ total angular momentum, and the excited $^2P_{3/2}$ with $J = 3/2$. The energy interval ΔE_{fs} between these states is proportional to $(\alpha Z)^2$, where $\alpha = 1/137$ is the fine structure constant and Z is the nuclear charge. However, even for the lightest Ca^- ion with $Z = 20$ ΔE_{fs} makes 10% of the 4p electron binding energy (see the table).

Ion	Binding energy, eV		ΔE_{fs} , cm^{-1}
	$np_{1/2}$	$np_{3/2}$	
Ca^-4s^24p	0.071	0.064	55.9
Sr^-5s^25p	-	-	200 *)
Ba^-6s^26p	-	-	400 *)
Ra^-7s^27p	-	-	1000 *)

*) extrapolated values

The calculations are performed by means of the many-body perturbation theory, which gives good accuracy in the atomic calculations /3/. The outer electron orbital Ψ_a is obtained from the equation:

$$(H_0 + \hat{Z})\Psi_a = E_a\Psi_a. \quad (1)$$

Here H_0 is the relativistic Hartree-Fock Hamiltonian for the neutral atom, $\hat{\Sigma}$ is the nonlocal polarisational potential. The equation (1) is analogous to the nonrelativistic Dyson equation, applied to negative ions in /1/.

$\hat{\Sigma}$ is calculated using the technique of Green's functions and Feynman diagrams (/3/). The role of $\hat{\Sigma}$ in (1) is different for atoms and negative ions. For atoms it is nearly equivalent to the calculation of the first order correction $\langle 0|\hat{\Sigma}|0\rangle$ to the relativistic Hartree-Fock energy of the 0 level. On the contrary, in the negative ions $\hat{\Sigma}$ can not be treated by perturbations, because it is the polarisational potential, which accounts for the binding of the extra electron to the atom. Besides that, $\hat{\Sigma}$ itself is considerably greater for the outer electron in the negative ion, than for the external atomic electron, in accordance with the fact that the polarisability of the atom exceeds that of the positive ion by an order. Therefore, the calculation of the negative ion binding energy with 10% accuracy needs the 1% accuracy in the calculation of $\hat{\Sigma}$. The value of ΔE_{fs} is less sensitive to $\hat{\Sigma}$, because ΔE_{fs} is determined essentially by the behaviour of the electron wavefunction at small distances from the nucleus, which depends weakly on $\hat{\Sigma}$ for p electron.

For Ra^- ion the magnitude of ΔE_{fs} reaches 1000 cm^{-1} , that is comparable to the binding energy. Hence, the $Ra^- 2P_{1/2}$ either has an extremely small binding energy, or is not bound at all, being a resonance in the continuum.

$2P_{1/2}$ ionic states are metastable against M1 or E2 transitions to the ground $2P_{1/2}$ state of the ions. The M1 transition dominates over E2 for small Z systems, resulting in the $6.3 \cdot 10^5 \text{ s}$ lifetime for $Ca^- 2P_{1/2}$. For heavier alkaline earth negative ions the E2 transition is enhanced by the greater value of the quadrupole moment of the outer electron and the fact that ΔE_{fs} is comparable with the binding energy.

1. Gribakin G.F., Gul'tsev B.V., Ivanov V.K., Kuchiev M.Yu. ZhTF, Pis'ma 15, no.12, 32-36 (1989).
2. Vosko S.H., Lagowski J.B., Mayer I.L. Phys.Rev.A 39, 446-449(1989)
3. Dzuba V.A., Flambaum V.V., Silvestrov P.G., Sushkov O.P. Phys. Lett.A 131, 461 (1988); 140, 493 (1989).

Dirac-Fock Basis set calculations for Atoms and Molecules

Ajaya K. Mohanty and E. Clementi

IBM Corporation
Center for Scientific & Engineering Computations
Department 48B/428
Neighborhood Road
Kingston, NY 12401 USA

Abstract

We present Dirac-Hartree-Fock (DHF) atomic structure calculations¹⁻³ of many-electron atoms ($Z = 2-86$) using kinetically balanced geometric basis sets of Gaussian functions. It is seen that "variational collapse" or bound failure does not occur if we impose the condition of kinetic balance between the large and the small component spinors along with proper boundary conditions for bound state orbitals. Furthermore, with a finite size nucleus model the DHF total energy for atoms converges more rapidly to the numerical Dirac-Fock (DF) limit with a fewer number basis functions than in those calculations where point nucleus is assumed. By systematically extending the geometric basis sets, we have obtained¹⁻³ the DHF total energies for all atoms (upto $Z = 86$) within a few millihartrees of the numerical (DF) limit⁴, with smooth convergence from above.

We also demonstrate⁵ the use of kinetically- balanced geometric Gaussian basis functions in DHF molecular structure calculations. The molecular spinors are expanded as a linear combinations of atomic spinors with the large component related to the small component by kinetic balance. As a result, all the multi-center integrals involving small components can be related to corresponding integrals involving the large component. Furthermore, because of geometric nature of the basis functions, one has to evaluate only the nonrelativistic-type integrals, permitting this way, extensive pretabulations which would render significant time saving. Finally, the effect of finite nucleus size is readily incorporated⁵ in the one- and multi-center integrals following the approach of Matsuoka. A status report on our DF molecular program to study molecules containing heavy atoms will be discussed.

References

1. A.K. Mohanty and E. Clementi, *Chem. Phys. Letters*, **157**, 348 (1989).
2. A.K. Mohanty and E. Clementi, *Modern Techniques in Computational Chemistry (MOTTECC-89)*, edited by E. Clementi, ESCOM Science Publishers B. V., Lieden 1989 Chapter 4.
3. A.K. Mohanty and E. Clementi, "Kinetically Balanced Geometric Gaussian Basis Sets for Relativistic Atoms", *J. Chem. Phys.* (To appear in 8/90)
4. I.P. Grant, B.J. McKenzie, P.H. Norrington, D.F. Mayers and N.C. Pyper, *Comput. Phys. Communication*, **21**, 207 (1980).
5. A.K. Mohanty and E. Clementi, "Dirac-Fock Self-Consistent Field Calculations for Closed-Shell Molecules with Kinetic Balance and Finite Nuclear Size, *Int. J. Quant. Chem.* (submitted)

The EXACT BORN-OPPENHEIMER OSCILLATOR STRENGTH DISTRIBUTION MOMENTS
in the CONTINUUM for $H_2^+(1s\sigma_g)$

J. W. Liu

Division of Electrical Engineering, National Research Council,
Ottawa, Canada K1A 0R6

Abstract

The exact Born-Oppenheimer oscillator strength moments¹ $S_i(\mu)$ and $L_i(\mu)$, where μ is an integer, in the continuum for $H_2^+(1s\sigma_g)$ for various internuclear distances R are calculated according to the previous calculational method². The value is calculated by subtracting the value of total excitations from the sum of all discrete excitations. In this calculation the moment for all discrete excitations includes the quantum state $[n \ell m]$ with values of quantum numbers (Q.Ns.) $n \leq 13$, $\ell \leq 9$ and $m \leq 1$, where $[1 0 0]$ denotes for the state of $1s\sigma_g$. It is found that the values of $L_i(\mu)$ for $\mu > 0$ estimated from the reported³ photoionization cross sections given for some states with $\ell \leq 5$ and the photoelectron energy ≤ 20 a.u are not accurate as compared to the present values. The accurate values of the moments for $L_i(\mu)$ and $S_i(\mu)$ for comparison with the values estimated³ and reported by others⁴ are shown in Table 1. The values of L sums for H calculated according to Eqs.49 and 46 given in Ref 2 are in good agreement with the values reported by Inokuti⁵, but it is not found for He^+ . It is very interesting to learn that all the moments in the continuum for $H_2^+(1s\sigma_g)$ smoothly approach to the the values of atomic limits. According to the previous work² the vibrational averaged values over the Frank-Condon (FC) factor⁶ for the moments are also calculated and given in Table 1.

1. M. Inokuti Rev. Mod. Phys. **43** 297 (1971)

2. J. W. Liu J. Phys.B: **22** 2605 (1989)

3. J.A. Richards and F. P. Larkins, J. Phys. **B19** 1949 (1986)

4. M. Kimura, Phys. Rev. **A35** 4101 (1987)

5. M. Inokuti, Argonne National Laboratory, Report No. ALN 6769 p. 7 (1963)

6. F. von Busch and G.H. Dunn Phys. Rev. **A5** 1726 (1972)

		Table 1 ^a							
μR	0 ^b	1.0	2.0	2.0 ^c	5.0	10.0	∞	VIB ^d	
S	-2	0.01307	0.0128	0.0125	0.011	0.0566	0.108	0.20919 ^b	0.0179
L	-2	0.02157	0.0109	0.00778	0.013	0.0340	0.0429	0.05515	0.0126
S	-1	0.0708	0.0483	0.0365	0.036	0.107	0.172	0.28348 ^b	0.0450
L	-1	0.1232	0.0678	0.0427	0.043	0.0726	0.0894	0.09991	0.0468
S	0	0.4350	0.198	0.120	0.119	0.226	0.312	0.435 ^b	0.135
			0.216 ^e	0.133 ^e					
L	0	0.83195	0.291	0.152	0.14	0.188	0.217	0.22892	0.158
S	+1	3.53588	0.992	0.516	0.39	0.612	0.748	0.884 ^b	0.526
L	+1	8.34969	1.79	0.886	0.5	0.759	0.843	0.8604	0.852
								0.86198 ^b	
S	+2	79.5598	11.26	5.583	1.3	4.294	4.801	4.9725 ^b	5.232
L	+2	366.18	42.92	21.19	1.6	14.83	16.31	16.40	19.53
								15.993 ^b	

a - All the values in a.u. The values of moments for small R are more accurate than the ones reported in Ref 2 .

b - Values from Ref.5.

c - Best estimated using Ref.3.

d - Vibrational average using Ref.6.

e - The value taken from Ref.4.

BRILLOUIN'S THEOREM AND THE ROLE OF SINGLE EXCITATIONS IN MULTICONFIGURATION
HARTREE-FOCK CALCULATIONS

T.M. Luke and J.D. Talman

Departments of Applied Mathematics and Physics and Centre for Chemical Physics,
University of Western Ontario, London, Ontario, Canada

It is well-known¹⁻⁴ that under many circumstances the Hamiltonian matrix elements connecting a Hartree-Fock ground state to singly-excited states vanish. It appears to be an accepted practice for this reason to omit singly excited states from multiconfiguration Hartree-Fock calculations (MCHF). It is therefore of interest to observe that despite Brillouin's theorem, the inclusion of singly-excited states can make a significant improvement in the results of a MCHF calculation.

We have carried out calculations very similar to MCHF calculations for the ground state of the Ne atom within the framework of the multiconfiguration optimized potential model (MCOPM)⁵. The basis of this approach is quite similar to the MCHF method except that the orbitals are not varied individually to minimize the expectation value of the energy, but are derived from an effective central potential which is variationally optimized.

Although the form of the wave function is more restricted in the MCOPM approach than in the MCHF approach, the results in single-configuration calculations are virtually the same as the results of Hartree-Fock results⁶. For example, in the Ne ground state calculation considered here, the ground state energy is -257.0916 Ry compared with -257.0942 Ry in the Hartree-Fock method⁴. The difference of 0.0026 Ry is very small compared with the total error in the Hartree-Fock approximation which is estimated to be about 0.78 Ry⁷. Since the single-configuration MCOPM wave function is essentially the same as the corresponding MCHF wave function, Brillouin's theorem should apply in the former case. In fact, when the CI calculation is carried out including the $2p^5 3p$ and $2s 2p^6 3s$ single excitation configurations in the single configuration optimized potential, it is found that their amplitudes are -0.00033 and -0.00101 respectively so that they contribute essentially zero to the energy.

When the potential is optimized, however, for these three configurations, it is found that the total energy is reduced to -257.2182 Ry, or by 0.1266 Ry which is a substantial fraction of the total correlation energy. The amplitudes for the

single excitations become very substantial: -0.438 for the $2p \rightarrow 3p$ excitation and 0.134 for the $2s \rightarrow 3s$ excitation. If the $2p \rightarrow 3p$ excitation alone is included, the energy energy reduction is 0.0589 Ry. The energy gain within a full MCHF calculation would probably be at least as great as that obtained here, since the single-configuration OPM and HF results are essentially the same.

Introducing these single excitations effectively introduces radial correlations between electrons in the same orbital. It is to be expected that this might decrease the angular correlations represented by pair excitations. We have carried out calculations including the $2p^6$, $2p^43s^2$, $2p^43p^2$ and $2p^43d^2$ configurations. In the ground state potential, these have very small amplitudes and contribute very little to the correlation energy. When the potential is optimized, the energy is -257.1487 Ry corresponding to a correlation energy of 0.0571 Ry. The amplitudes of the pair configurations are 0.014 , 0.097 and 0.044 respectively.

The MCOPM calculation including both the $2p \rightarrow 3p$ and $2s \rightarrow 3s$ single excitations and the three pair excitation configurations gives an energy of -257.2797 Ry or a correlation energy of 0.1881 Ry. Thus the pair excitations contribute 0.0615 Ry to the correlation energy in this case, so that their contribution is somewhat enhanced. The amplitudes of the pair excitations are 0.020 , 0.079 and 0.078 for the $3s^2$, $3p^2$ and $3d^2$ configurations respectively; the amplitude for the $3d^2$ configuration is therefore substantially increased by the single excitation configurations while the $3p^2$ amplitude is somewhat reduced.

-
1. L. Brillouin, *J.Phys.*3,373(1933).
 2. J. Bauche and M. Klapisch, *J.Phys.*B5,29(1972).
 3. M. Godefroid, J. Lievin and J.Y. Metz, *J.Phys.*B20,3283(1987).
 4. C. Froese Fischer, *The Hartree-Fock Method for Atoms* (Wiley-Interscience, New York, 1977).
 5. K. Ashamar, T.M. Luke and J.D. Talman, *J.Phys* B12,3455(1979).
 6. K. Ashamar, T.M. Luke and J.D. Talman, *Phys. Rev* A19,6(1979).
 7. T. Lee, N.C. Dutta and T.P. Das, *Phys. Rev.* A4,1410(1971).

SPECTROSCOPIC FACTORS OF SUBVALENT ELECTRONS IN ARGON AND XENON

M.Ya. Amusia and A.S. Kheifets

A.F. Ioffe Physical-Technical Institute, Academy of Sciences of the USSR
Leningrad 194021, USSR

We present new results of calculation of relative intensities of number of satellite lines in Ar and Xe. The existence of the difference between corresponding values derived from (e,2e) and (γ ,e) experiments is explained, being entirely attributed to the effect of ground state correlations in the considered atoms. Good agreement with recent experimental data is achieved.

Improving of experimental accuracy and increase of incoming electron and photon energies demonstrates a systematic difference in spectroscopic factors or intensity of line values derived from (e,2e) and (γ ,e) experiments for Ar [1,2] and, in somewhat smaller degree, for Xe [3,4]. As it was shown in our paper [5], this difference is inherited in the different contributions of the atomic ground state correlations in both reactions. In the (e,2e) reaction on condition of small momentum transferred to the ion the ground state correlations are negligible and the "true" spectroscopic factor Z is measurable which defines the contribution of the pure one-hole state to the exact state $|N-1, \alpha\rangle$ of the ion. Otherwise, in (γ ,e) reaction these correlations are of importance and another quantity \tilde{Z} determines the relative line intensity. In the limit of the high energy transferred to the atom to be ionized the following expression can be derived:

$$\tilde{Z}_\alpha = Z_\alpha \cdot [1 + (\epsilon_\alpha - E_0)/\Delta]^2 \quad (1)$$

Here ϵ_α and E_0 are exact and Hartree-Fock energies of the ion $|N-1, \alpha\rangle$ state, respectively. $\alpha=0$ defines the ion ground state, $\alpha=1$ refers to the first excited state and so on. $\Delta = |E_1|$ is a parameter to be calculated numerically. So, we can look upon \tilde{Z}_α as a structural characteristic of the ion, although it is more complicated than Z_α .

Expression (1) enables us to make some qualitative predictions which are in agreement with experiment. As it was shown in [6], $\epsilon_\alpha > E_0$ and $\epsilon_\alpha < E_0$. It means that $\tilde{Z}_\alpha > Z_\alpha$ and $\tilde{Z}_\alpha < Z_\alpha$, i.e. the main line is more intensive in (γ ,e) reaction, while the satellites are stronger in (e,2e) reaction. The difference between \tilde{Z}_α and Z_α increase with the distance between the main and corresponding satellite line. Therefore, the broader satellite spectrum, the larger difference of the line intensities in (γ ,e) and (e,2e) reactions. This is the case of Ar as compared with Xe.

We have performed *ab initio* calculation of the spectroscopic factors Z_α and \tilde{Z}_α of the main and the strongest satellite lines in Ar. These results in the form of normalized line intensities are presented in the table along with corresponding experimental data. Details of calculation are presented in our earlier work [5]. As compared with it, more extensive basis set consisted of 5 excited states $3s^2 3p^4 ({}^1D) nd^2 s, n=3+7$ were taken into account. Our results seem to be in rather good agreement both with (γ ,e) [1] and (e,2e) [2] experiments.

Analogous calculation for Xe, as it was demonstrated by assignment of experimental lines, needs more extensive basis set of the ion states. In particular, not only s, but also p and p ion states should be taken into

account. It requires relativistic calculation which is beyond our abilities at present. However, we have compared the ratio of corresponding line intensities measured in (γ, e) and $(e, 2e)$ reactions with the value Z^2/Z_0 given by expression (1). In spite of complex structure of the ion states, we have managed to describe experimental data rather well using Δ as a fitting parameter. The obtained value $\Delta=3.4$ Ry turned out to be close enough to the Hartree-Fock energy of the first strongest satellite $E = E_{5p^4, 1D, 3d}^2 S = 1.98$ Ry.

It is noteworthy that argon has broader satellite spectrum than xenon has. Indeed, energy gap between the main and the strongest satellite lines is of 9.36 eV and 5.68 eV for Ar and Xe, respectively. According to expression (1), it explains more diverging line intensities in (γ, e) and $(e, 2e)$ reactions for Ar as compared with Xe.

SATELLITE LINES INTENSITIES OF ARGON AND XENON

Main ion configuration	Energy, eV		Normalized line intensity, %			
	Exper.	Calcul.	(γ, e)		$(e, 2e)$	
	Exper.	Calcul.	Exper.	Calcul.	Exper.	Calcul.
ARGON						
	[1]	[1]	[1]	[2]		
$3s3p^6 2S_{1/2}$	29.24	29.27	100	100	100	100
$3s^2 3p^4 (1D) 3d^2 S$	38.60	38.63	18.6	18.6	33.0	36.0
4d	41.21	41.14	9.4	8.1	17.0	19.3
5d	42.67	42.55	4.1	2.8	9.6	7.6
6d	43.43	43.38	1.5	1.3	8.1	6.3
7d	44.00	43.87	0.5	0.8		
XENON						
	[3]	[3]	[4]			
$5s5p^6 2S_{1/2}$	23.40		100			1
$5s^2 5p^4 (1S) 6s^2 S$	27.35		3.6			
$(1D) 5d^2 P$	27.82		11.7		31	0.81
?	28.22		9.8			
?	28.71		13.9		67	0.69
$(1D) 5d^2 S$	29.08		22.0			
$(1D) 6d^4 P$	29.44		10.3			0.78
?	30.67		3.1		28	0.69
$(1D) 6d^2 S, 2P$	31.44		13.2			
$(3P) 8s^4 P$	31.9		3			0.70
?						
$(1D) 7d^2 S, 2P$	32.81		5		31	0.23
$(1S) 7s^2 S$						
$(1D) 8d^2 S, 2P$	33.5		2			0.37

1. I.E. McCarthy, R. Pascual, P. Storey and E. Weigold, Phys. Rev. **A10** (1989) 3041.
2. S. Svensson, K. Helenelund and U. Gelius, Phys. Rev. Lett. **58** (1987) 1624.
3. J.P. Cook, I.E. McCarthy, J. Mitroy and E. Weigold, Phys. Rev. **A33** (1986) 211.
4. S. Svensson, B. Ericsson, N. Martensson et al., J. Electr. Spectr. **47** (1988) 327.
5. M. Ya. Amusia and A.S. Kheifets, J. Phys. **18B** (1985) L679.
6. A.S. Kheifets, Sov. Phys. -JETP, **62** (1985) 260.

POSITIVENESS OF FREE-FREE COULOMB DIPOLE MATRIX ELEMENTS

Sung Dahm Oh* and R. H. Pratt
 Department of Physics and Astronomy, University of Pittsburgh
 Pittsburgh, PA 15260

We wish to report a proof that nonrelativistic Coulomb free-free dipole matrix elements are always positive. We have presented similar demonstrations earlier that a major class of Coulomb dipole matrix elements (CDME), namely those connecting a bound state to a state of greater energy, never vanish¹ and decrease monotonically as the transition energies increase.² These transition matrix elements are related to the free-free elements through an analytic continuation on the bound state energy. Explicit expressions for all the CDME of the nonrelativistic hydrogen atom have been given by Gordan;³ the analytic structure of the exact free-free CDME are fairly complex:

$$D_{k k'}^{\ell, \ell-1} = \frac{\pi \left| \frac{1}{k} - \frac{1}{k'} \right|}{4kk' \Gamma(2\ell)} \left[\frac{\prod_{s=1}^{\ell} \left(s^2 + \frac{1}{k^2} \right) \prod_{s=1}^{\ell-1} \left(s'^2 + \frac{1}{k'^2} \right)}{kk' \sinh \frac{\pi}{k} \sinh \frac{\pi}{k'}} \right]^{1/2} S,$$

$$\text{with } S = \text{Im} \left| \frac{k-k'}{k+k'} \right|^{1/k-1/k'} F(\ell-1+i/k, \ell-i/k'; 2\ell; 4kk'/(k+k')^2).$$

In recent years semiclassical formulae for free-free CDME have been derived which have a simpler analytic structure; these provide checks on the validity and accuracy of features deduced from Gordan's complete expressions.

As in our previous work,^{1,2} we use the recursion relations of Infeld and Hull,⁴ for fixed initial and final momenta k and k' ,

$$2\ell A_k^{\ell} D_{k, k'}^{\ell-1, \ell} = (2\ell+1) A_{k'}^{\ell+1} D_{k, k'}^{\ell, \ell+1} + A_k^{\ell+1} D_{k, k'}^{\ell+1, \ell},$$

$$2\ell A_{k'}^{\ell} D_{k, k'}^{\ell, \ell-1} = A_{k'}^{\ell+1} D_{k, k'}^{\ell, \ell+1} + (2\ell+1) A_k^{\ell+1} D_{k, k'}^{\ell+1, \ell},$$

connecting successive pairs of dipole matrix elements, $D_{k, k'}^{\ell, \ell'}$, where

$$D_{k, k'}^{\ell, \ell'} = \int_0^{\infty} R_{k', \ell}^* r^3 R_{k, \ell} dr.$$

Here we use the linear momentum, k , instead of the energy, ϵ , ($\epsilon = k^2$) to characterize the quantum states in the continuum. In the case of CDME from a bound state we obtained^{1,2} an explicit proof that all CDME are positive by showing that the top CDME of a sequence for fixed energies, with $\ell = n-1$, is positive.

It does not look possible at first glance to show in the same way that free-free CDME are always positive, since there is no definite top matrix element in the chains, specified by the angular momentum of the lower energy state. However what we can do is to consider the CDME for the asymptotic large ℓ case for specified energies and recur down. If we can show that the asymptotic large ℓ case of the free-free CDME for the transition from a state

(k, ℓ) to $(k', \ell-1)$ are positive, then each pair of free-free CDME are also positive since the coefficients A_k of the recursion relations are always positive.

The sign of $D_{k, k'}^{\ell, \ell-1}$ is completely determined by the sign of S . The asymptotic large k, k' result can be directly obtained from the study of asymptotic expansion of hypergeometric functions;⁶

$$S = \frac{8}{k} \text{ if } k > k'$$

$$= \frac{4k}{k'^2(1-k^2/k'^2)} \text{ if } k < k'$$

For zero transition energies ($k = k'$), S is simply

$$S = \frac{4k\Gamma(2\ell)}{(\ell^2 + \frac{1}{k^2})|\Gamma(\ell + \frac{1}{k})|^2} \lim_{k \rightarrow k'} \frac{1}{(k-k')^2}$$

We conclude that the free-free CDME are always positive, including the case of a positive singularity for zero transition energy, while the bound-bound CDME are negative at zero transition energy.

Research supported in part by the Korea Science and Engineering Foundation and the U.S. National Science Foundation, under INT-8719835.

References

*Permanent address: Department of Physics, Sookmyung Women's University, Seoul, Korea.

1. Sung Dahm Oh and R. H. Pratt, Phys. Rev. A 34, 2486 (1986).
2. Sung Dahm Oh and R. H. Pratt, Phys. Rev. A 37, 1524 (1988).
3. W. Gordan, Ann. Phys. 2, 1031 (1929).
4. L. Infeld and T. E. Hull, Rev. Mod. Phys. 23, 31 (1951).
5. G. N. Watson, Trans. Cambridge Phi. Soc. 22, 277 (1918).

Ab Initio CALCULATIONS OF ORTHOGONAL PARAMETERS FOR COMPLEX

CONFIGURATIONS USING B-SPLINES

Yu-Tang Shen, Milco Landtman and Jørgen E Hansen
Zeeman-Laboratory, University of Amsterdam, Plantage Muidergracht 4
NL-1018 TV Amsterdam, The Netherlands

In general many-body calculations of atomic structure have consisted of calculating the properties of each term or level separately. For simple configurations this approach is the natural one. For more complex configurations the amount of work involved grows rapidly. The introduction of orthogonal operators [1] has made it possible to define a set of effective operators which can describe the structure of a complex configuration to infinite order in perturbation theory. Thus to determine the energy, say, of all levels of a particular configuration it is "only" necessary to obtain values for the set of parameters associated with the orthogonal set. Thus for configurations with many levels, the use of orthogonal operators can lead to a considerable reduction in the work necessary to calculate the structure and properties of a configuration. However, the basic difficulties associated with the calculation of atomic properties, for example, the necessity to sum over infinite sets including the necessity to consider excitations to the continuum remains.

In principle it is easy to obtain experimental values for the parameters because these have been introduced so that their extraction from the observed energy level structure can be performed with maximum precision using least-squares fitting [2]. In practice, non-linear fitting is usually required because the set of operators is complete and this gives rise to difficulties.

Orthogonal operator sets for the $p'd$ configurations have recently been published [3] and a first ab initio calculation has been carried out [4] in which Hartree-Fock values were used to define the zero-order values of the parameters and second-order corrections were determined from a Hartree-Fock basis which included a number of the lowest configurations which can be reached by excitations from $2p^3d$ configurations in III, IV and V spectra in the first period. In some cases rather good agreement was obtained and in other cases the agreement was bad. The worst case was, unexpectedly, the simplest, the $2p3d$ configuration in O III (the agreement for the $2p^3d$ configuration in Mg III for example was much better). At the time it was not possible to decide whether the reason for the disagreement was the neglect of third- and higher-order contributions, because the second-order calculations were not complete.

We are therefore engaged in carrying out "complete" second order calculations for, in the first instance O III $2p3d$ (the worst case), using B-splines to allow us to sum over a complete set of excitations (including the continuum). The work is in progress but first results have recently been reported [5]. This work showed that there are

rather large contributions from the continuum but also that the eight excitations, which were considered in ref. [4], are insufficient to give a good description of the $1s^2s^2p3d$ configuration.

We found that some excitations involving an inner 2s electron not only have large second-order effects but also sometimes large higher-order effects. This can happen for example if the perturbing configuration has a 2s2p subconfiguration with a very large splitting due to the large 2s \leftrightarrow 2p interaction. If this splitting is large relative to the distance to 2p3d, the second-order approach can be expected to fail. However, the number of configurations of this type is not so large and it is therefore possible to include the perturbation in these cases to infinite order by diagonalizing the interaction matrix. In the course of doing this we noted that it is possible to include a large part of the higher order effects if instead of summing the second order expressions over all states we sum, in the case of the above example, over all states built on each of the 2s2p SL parent states. This technique we are now applying to all configurations of this type except the lowest one(s) for which direct diagonalization is more accurate. Latest results will be reported at the conference but the present situation is indicated in the table below.

Parameter	HF	HF+CI	Fitted	Previous [4]	[5]
p_1	890.9	682.6	770.0 \pm 0.3	648.9	457.6
p_2	369.4	623.6	595.0 \pm 0.2	383.3	571.2
p_3	-369.4	-248.5	-348.6 \pm 0.1	-281.6	-354.2
p_4	243.5	213.4	180.9 \pm 0.1	265.9	237.7
p_5	180.0	134.1	154.4 \pm 0.1	154.2	149.5

References

1. B.R. Judd, J.E. Hansen, and A.J.J. Raassen, *J. Phys. B* **15**, 1457 (1982)
2. J.E. Hansen, P.H.M. Uylings and A.J.J. Raassen, *Phys. Scripta*, **37**, 664 (1988).
3. H. Dothe, J.E. Hansen, B.R. Judd, and G.M.S Lister, *J. Phys. B* **18**, 1061 (1985)
4. J.E. Hansen, B.R. Judd, and G.M.S. Lister, *J. Phys. B* **21**, 1437 (1988)
5. Y.-T. Shen, M. Landtman and J.E. Hansen, *J. Phys. B* **23**, L121 (1990)

**A RELATIVISTIC MANY-BODY STUDY OF THE ENERGY LEVELS
OF THE Hg I $6p^2$ RESONANCES**

Ziyong Cai and Donald R. Beck
Physics Department
and
Warren F. Perger
Departments of Electrical Engineering & Physics

Michigan Technological University
Houghton, MI 49931

ABSTRACT

Fully *ab initio* relativistic many body calculations are made for the $6p^2$ resonances of Hg, using the Dirac-Breit Hamiltonian. Projection operators are used to separate the localized portion of the wavefunction and the open channels, à la Nicolaides¹. The localized portion is treated by a relativistic variational CI method just introduced by Beck and Cai² in which the virtual spinors are represented by energy variational principle optimized screened hydrogenic functions (this prevents variational collapses). The continuum functions are generated from a new relativistic frozen core procedure introduced by Perger³ in which all aspects of exchange, normalization, and orthogonality are handled properly. The open channels are then allowed to interact with the localized wavefunction, using the methods of Fano and Altick,^{4,5} to provide a shift of the localized energy, as well as resonance lifetimes.

Our calculations include the effects of $5d$ correlations, and are the most thorough to date⁶ undertaken on this system. The results should help in completing the identification of the 1S_0 and 1D_2 resonances⁷.

1. C. A. Nicolaides, Phys. Rev. A **6**, 2078 (1972).
2. D. R. Beck and Z. Cai, Phys. Rev. A **41**, 301 (1990).
3. W. F. Perger and V. S. Karighattam, Submitted to Comp. Phys. Commun., 1990.
4. U. Fano, Phys. Rev. **124**, 1866 (1961).
5. P. L. Altick, Phys. Rev. **169**, 21 (1968).
6. M. Wilson, Phys. Lett. **111**, 363 (1985).
7. L. F. Forrest, J. Phys. B **18**, 4519 (1985).

NON-VARIATIONAL SERIES SOLUTION TO THE NON-RELATIVISTIC HELIUM
PROBLEM USING A STANDARD ANGULAR MOMENTUM DECOMPOSITION

by

Douglas McColm and Glen Erickson
University of California, Davis, CA 95616

The purpose of this study was to formulate a series solution to the non-relativistic helium problem using the standard theory of angular momentum. No variations on the energy were to be used; the differential equation was to be solved directly.

Previously we reported [1] that the radial coordinates r_1 , r_2 and the interelectron distance, r_{12} , could not be used for this purpose. And because the multipole expansion is expressed in terms of $r_<$ and $r_>$, we chose these as radial coordinates. The interelectron coordinate, r_{12} , was not used, a choice which simplified the formalism but undoubtedly worsened the convergence of the series obtained.

The series employed then had the form,

$$\psi = \sum_{\Lambda} |\Lambda\rangle F_{\Lambda}(r_<, r_>)$$

where $|\Lambda\rangle$ is just a vector-coupled function of spin and orbit, having orbital angular momentum ℓ' for the first electron and ℓ'' for the second. The functions F_{Λ} are partial waves.

The logarithmic terms introduced by Fock [2] are necessary if a normalizable solution is to be obtained. The logarithmic terms contain powers of the logarithm of $r_<^2 + r_>^2$. But, since

$$\ln(r_<^2 + r_>^2)^{\frac{1}{2}} = \ln r_> + \ln(1 + x^2)^{\frac{1}{2}}$$

where

$$x = r_</r_>$$

and since the second term on the right-hand side is itself expandable in powers of x , the residual logarithmic factors are just powers of $\ln r_>$. Thus the partial waves, F_{Λ} , have the form,

$$F_{\Lambda}(r_<, r_>) = \sum a_{\beta\gamma\eta\Lambda}^{(<)} r_<^{\beta} x^{\gamma} (\ln r_>)^{\eta} e^{-(\alpha' r_< + \alpha'' r_>)}$$

The Pauli principle connects $a^{(1)}$ and $a^{(2)}$.

When substituted into the differential equation, this equation results in a recursion formula for the coefficients, $a^{(i)}$. However, iteration of this recursion relation does not determine all these coefficients. Those with $\gamma = \ell' - \beta$ are undetermined by this procedure. To determine their value, the matching conditions occurring at $r_< = r_>$ and the normalization condition must be employed.

Because the coefficients $a^{(i)}$ determined by the recursion formula depend linearly on those which are undetermined, we renamed the undetermined coefficients u_{ω} . (ω standing

for the values of β , η and Λ associated with the undetermined coefficient in question). The remaining coefficients then satisfy,

$$a_{\beta\eta\Lambda}^{(i)} = \sum_{\omega} c_{\beta\eta\Lambda\omega}^{(i)} u_{\omega}$$

The matching conditions lead to a series of linear equations in the u_{ω} .

However, in every fourth linear equation the terms possessing the value of η associated with the diagonal value of ω cancel. As a result, these equations determine the u_{ω} associated with higher values of η , thereby bringing the logarithmic terms into the solution. Of course the range of the η index is $(0, \infty)$, but to obtain a solution the range is truncated to $(0, \eta_{max})$. Such a truncation causes every fourth η_{max} equation to be empty. The empty equations are then deleted.

The removal of these equations leaves room for the introduction of equations defining a set of parameters, k_{σ} , whose value must be determined by the normalization procedure. Without adjustment of the k_{σ} the different partial waves were found to approach zero at large radius at different values of the energy, making normalization impossible. Preliminary results show that a suitable adjustment of the k_{σ} can cause the different partial waves to approach zero at large radius at the same energy.

-
1. D. W. McColm and G. W. Erickson, Bull. Am. Phys. Soc. **35**, 1188 (1990)
 2. V. Fock, D. Kngl. Norske Videnskab. Selsk. Forh. **31**, 145 (1958)

WIDTHS OF THE nl' AUTOIONISATION RESONANCES IN THE RARE GAS ATOMS

M.Ya. Amusia, V.L. Tsemekhan, K.L. Tsemekhan
 A.F. Ioffe Physical-Technical Institute, Academy of the Sciences of the USSR
 Leningrad, USSR

Autoionisation resonances which occur in the interval between $np_{1/2}^5$ and $np_{3/2}^5$ thresholds in the rare gases Rg = Ne, Ar, Kr, Xe were first observed Beutler and their shapes were analyzed by Fano. Last high precision measurements [1] provided exact values of widths of these resonances. The behavior of the width appeared to be nontrivial and it is the purpose of this paper to report results of an *ab initio* calculation of the widths of Beutler-Fano resonances in Ne, Ar, Kr and Xe, explaining this behavior.

As in experiment [1], we studied Rg ($np_{1/2}^5 2p_{1/2} ns', nd'$) autoionisation resonances with different total angular momentum J . All results of calculations are marked in Tables 1 and 2 by the letter (a). The wave functions used in all matrix elements were calculated in nonrelativistic Hartree-Fock approximation. The methods of many-body perturbation theory are used in this work. In agreement with the experiment, the reduced width $\tilde{\Gamma} = \Gamma_n / (n^*)^3$, Γ_n being the width of ns' or nd' level, n^* - effective principal quantum number, does not depend on n^* with the 3% accuracy for $n \geq 10$. This can be explained by the fact that all matrix elements describing the decay processes are determined by the quadrupole and dipole parts of Coulomb interaction, thus being governed by short distances $r \ll n$ (in atomic units).

1). For Rg ($ns', J=0$) resonances the matrix elements corresponding to the direct $ns' - sd$ interaction provides the nonmonotonic behavior of the width from Ne to Xe in agreement with experiment, but overestimates the absolute values of width by a factor of 2+3. We obtained correct results taking into account higher order corrections. They describe screening of the core potential by the excitations of outer shell electrons ("two-hole-two-electron" excitations) and decay through the excitations from ns -shell. Moreover, some of the former processes are known to be important due to the super-Koster-Kronig transition $ns^2 np^5 \rightarrow nsnp^5 md$ in the intermediate state.

2). For Rg ($nd', J=1$) mainly one term contributes to the width, namely direct $nd' - sd$ interaction. In Ar, Kr and Xe its value is significantly larger than the corresponding $ns' - cd$ direct matrix element for Rg($ns', J=0$) resonance. Therefore, the nd' resonance is much wider than the ns' one. On the contrary, Ne ($nd', J=1$) resonance appeared to be narrower than Ne ($ns', J=0$).

3). Some problems arise while studying Rg ($ns', J=1$) resonances. Compared to $J=0$, the Ne ($ns', J=1$) resonance turned out to be three times wider. Two reasons cause alteration of the width. On the one hand, the exchange interaction $ns' - cd$ existing only for $J=1$ resonance noticeably decreases the probability of decay into sd continuum. On the other hand, the probability of the autoionization into open for $J=1$ cs -channel is not small even in the first order, being significantly increased while taking into account higher order corrections. Thus the contribution of this channel is important ($\approx 70\%$) enlarging the width. Both of these two factors do not play any essential role in Ar, Kr, Xe (ns' ,

$J=1$) resonances. Narrowing of these resonances compared to $Rg(ns', J=0)$ can be understood while considering only the first order terms of MBPT. The states of investigated atoms are described by the following quantum numbers: $j, l', K,$ and J , where j and J are the total angular momenta of the core and of the atom respectively, l' - the angular momentum of the outer electron, $\vec{K} = \vec{j} + \vec{l}'$. It is evident that the atomic angular momentum L and the atomic spin S are not good quantum numbers and, therefore, the wave functions of these states can be reproduced as certain linear combinations of LS-term wave functions with different L and S . Only 3P term contributes into $ns', J=0$ states, so the matrix element $V_{J=0}$ of $Rg(ns', J=0)$ decay is equal to $V_{L=1, S=1}$. Another situation takes

place in $Rg(ns', J=1)$ state for it is a mixture of two terms: 3P and 1P . So the matrix element corresponding to its decay is in fact the linear combination of $V_{L=1, S=1}$ and $V_{L=1, S=0}$: $V_{J=1} = \frac{2}{3} V_{L=1, S=1} + \frac{1}{3} V_{L=1, S=0}$. However, the wave function of the outer electron depends on term this electron belongs to. For two terms with different S these wave functions appeared to be essentially different at short distances, so that in Ar, Kr, and Xe the matrix elements $V_{L=1, S=0}$ are much smaller than $V_{L=1, S=1}$ and, hence, $V_{J=1}$ is smaller than $V_{J=0}$.

At the conclusion we would like to discuss the following problem. One can derive both from experimental and theoretical data that for Ar, Kr, and Xe $Rg(ns', J=1)$ and $Rg(nd', J=1)$ resonances overlap due to the large width of the latter one. It is naturally to suppose them interacting so that the broad nd' resonance affects upon the narrow ns' one, changing its width. However, the interaction between two resonances is small in this case. This becomes clear if one takes into account that ns' and nd' autoionisation states decay with the overwhelming probability into different continuum channels.

Table 1. Reduced widths Γ of the $Rg(ns', J=0, 1)$ resonances (in cm^{-1}).

	Ne	Ar	Kr	Xe
J=0	135 (a)	940 (a)	2490 (a)	1410 (a)
	121 (1)	790 (1)	2248 (1)	1105 (1)
J=1	330 (a)	610 (a)	1390 (a)	1070 (a)
	372 (1)	510 (1)	1185 (1)	848 (1)
	730 (2)			

Table 2. Reduced widths Γ of the $Rg(nd', J=1)$ resonances (in cm^{-1}).

	Ne	Ar	Kr	Xe
J=1	190 (a)	28400 (a)	23700 (a)	31600 (a)
	160 (1)	30600 (1)	21600 (1)	35000 (1)

1. H. Hotop, Invited Papers at Workshop "Today and Tomorrow of Photoionisation", Leningrad, 1990, to be published.
2. W.R. Johnson and M. Le Dourneuf. J. Phys. B 13(1980)L13-L18.

**AN EXTENDED RELATIVISTIC HAMILTONIAN
FOR SPIN 1/2 PARTICLES**

S. P. Goldman

*Department of Physics, The University of Western Ontario
London, Ontario, Canada N6A 3K7*

The Dirac hamiltonian is extended non-trivially to include simultaneously the electron and positron states in the presence of a Coulomb potential. Exact solutions are presented. It is found that the new hamiltonian predicts shifts in the Dirac energy levels. The new energy levels are given by $E^2 = E_D^2 \cos^2 \xi + m^2 c^4 \sin^2 \xi$, where E_D is the Dirac energy and ξ an arbitrary angle. An upper bound on ξ is estimated from the experimental and theoretical values of the g-factor. The requirement of charge conservation leads to a concise five-dimensional formalism and the introduction of a phase factor given by the classical action of the fermion. The projector over positive-energy states is derived and assumes a simple analytic form. Moreover, unlike the Dirac case, the set of positive-energy radial functions is complete.

Interesting results are also obtained if the formalism is applied to finite basis-set variational representations of the Dirac-Coulomb hamiltonian extended to include simultaneously the electron and positron states with the same value of the Dirac quantum number κ (equivalent to the simultaneous description of *all* electron states with the same value of the total angular momentum quantum number j). The spurious root previously obtained using finite basis sets for states with $\kappa > 0$ is now clearly identified as the ground state of the fermion with opposite charge. By imposing a mild boundary condition at the origin, the resulting variational spectrum is symmetric around $E=0$ and *free of spurious roots*. Moreover, an *absolute criterion* for the accuracy of the variational results is obtained.

**RELATIVISTIC VARIATIONAL CALCULATIONS FOR
HYDROGENIC ATOMS IN STRONG MAGNETIC FIELDS****Z. Chen and S. P. Goldman***Department of Physics, The University of Western Ontario
London, Ontario, Canada N6A 3K7*

A Relativistic finite-basis-set method is used to calculate the ground-state energy of Hydrogenic atoms in a strong magnetic field with $10^9\text{G} \leq B \leq 10^{12}\text{G}$, for several values of the nuclear charge Z . A modified Slater-type basis set with different values of the total angular momentum is used. Even though an upper bound on the energy can not be obtained with this basis set, good convergence is achieved. For example, the relativistic correction to the ground-state energy of hydrogen ($Z = 1$) is found to be of the order of 4×10^{-6} a.u. for $B = 4.7 \times 10^9\text{G}$, and the convergence achieved is 10^{-7} a.u. with one nonlinear parameter, 15 powers and 15 eigenstates of total angular momentum in the basis set. With magnetic field B fixed, the convergence is better for larger nuclear charge Z where relativistic effects are more important. For very strong B and small Z , a modified Landau-type basis set is required.

RELATIVISTIC FINITE BASIS SET CALCULATIONS FOR ATOMS

H.M.Quiney and I.P.Grant
Department of Theoretical Chemistry
5, South Parks Road, Oxford OX1 3UB
UNITED KINGDOM

The use of a finite basis set of square-integrable functions is a convenient technique for the evaluation of the sum-over-states expressions which are found in relativistic many-body perturbation theory. The finite-dimensional representation of Dirac single-particle states is complicated by the constraints which must be imposed on allowable trial functions [1]. Unlike the finite-difference method, which is employed in the Oxford GRASP² computer code [2], negative-energy states form an explicit part of the spectrum in the finite-basis approach and must be incorporated within an approximate formulation of quantum-electrodynamics based on finite-dimensional spectral expansions.

Calculations are presented which illustrate the use of two related analytic basis sets; S- and L-spinors. The S-spinor functions, which are defined as a special case of the L-spinor prescription, form the computational basis of a new computer program, SWIRLES, designed to evaluate relativistic and many-body effects in atoms. Recurrence relations associated with S-spinor functions allow the routine evaluation of many-body corrections in atoms, including contributions from Coulomb and low-frequency Breit photon interactions, at modest computational cost [3]. The L-spinor basis, which exploits the recurrence and orthogonality relations of generalized Laguerre polynomials, has been developed for high-precision calculations on few-electron systems, where a richly detailed discrete spectrum is required [1,4]. We present recent work, which aims to evaluate relativistic, many-body and quantum electrodynamical energy corrections in few-electron atoms within a unified computational framework.

1. I.P.Grant and H.M.Quiney, *Adv.At.Mol.Phys.*, **23**, 37 (1988)
2. F.A.Parpia, I.P.Grant and C.Froese-Fischer, in preparation (1990)
3. H.M.Quiney, I.P.Grant and S.Wilson, *J.Phys.B*, (1990) in press
4. H.M.Quiney, *The Effects of Relativity in Atoms, Molecules and the Solid State*, Plenum Press, (in press, 1990)

SOFTWARE FOR
RELATIVISTIC ATOMIC STRUCTURE THEORY:
THE GRASP PROJECT AT OXFORD

F. A. PARPIA and I. P. GRANT

Oxford University, Department of Theoretical Chemistry,
5 South Parks Road, Oxford OX1 3UB, United Kingdom

GRASP is an acronym for General-purpose Relativistic Atomic Structure Program. The objective of the GRASP project at Oxford is to produce user-friendly state-of-the-art multiconfiguration Dirac-Fock (MCDF) software packages for relativistic atomic structure theory.

Modules for the computation of angular coefficients (all based upon Racah techniques), the generation and manipulation of radial functions (based exclusively on finite-difference methods), and utility modules, have been assembled under an interface to produce the Oxford MCDF package. The three extant versions of the Oxford MCDF software, MCDF+MCBP/BENA [1,2], GRASP [3], and GRASP² [4], are described.

Planned improvements to GRASP² include extending the capabilities of the package so that systems involving continuum electrons can be modelled, and the development of a new generation of algorithms optimised for shared-memory vector processors operating in parallel. Future versions of the Oxford MCDF program are likely to make use of basis set methods, ideally suited to the use of multi-reference many-body perturbation theory, for the improvement of MCDF estimates of atomic properties.

References

1. I. P. Grant, B. J. McKenzie, P. H. Norrington, D. F. Mayers and N. C. Pyper, *Comput. Phys. Commun.* **21** (1980) 207.
2. B. J. McKenzie, I. P. Grant and P. H. Norrington, *Comput. Phys. Commun.* **21** (1980) 233.
3. K. G. Dyall, I. P. Grant, C. T. Johnson, F. A. Parpia and E. P. Plummer, *Comput. Phys. Commun.* **55** (1989) 425.
4. F. A. Parpia, I. P. Grant, and C. F. Fischer, in preparation.

AN EFFICIENT METHOD FOR COMPUTING RELATIVISTIC MIXING IN COMPLEX SPECTRA

K.Aashamar

Institute of Physics, University of Oslo, Oslo, Norway

T.M.Luke and J.D.Talman

Departments of Applied Mathematics and Physics and Centre for Chemical Physics
University of Western Ontario, London, Canada.

We present a method of achieving a very considerable reduction in the amount of algebra that arises in a relativistic calculation of complex atomic spectra. The method is demonstrated using the example of the $3d^4 4p$ $^6D^0$, $^6P^0$ and $^4P^0$ levels of Cr II which are strongly mixed by relativistic interactions.

A serious practical difficulty in such relativistic calculations is that a very large number of levels results when one includes enough configurations to account adequately for correlation. The resulting calculations of algebraic coefficients become very demanding in terms of both CPU time and storage.

The key to the modified approach that we have developed is very simple: It is to reduce to a minimum the proliferation of levels by choosing a "natural parentage" scheme for constructing the algebraic states in which the physical states are expanded. Though we describe the method in terms of the codes we use, the analogous problem will arise and the same idea can presumably be adapted to other atomic structure calculations.

Briefly, the context of our calculations is this. We perform a nonrelativistic variational calculation of the energies of the terms of interest and thereby determine a set of orbitals. This is done using the Multiconfiguration Optimized Potential Model (MCOPM)¹. These orbitals are then used to construct wave functions for a large scale CI calculation in which the Breit-Pauli hamiltonian is diagonalized. The code SUPERSTRUCTURE² is used for this relativistic calculation of level wave functions and energies.

Normally, in SUPERSTRUCTURE, an algebraic basis is constructed with no particular parentage in terms of Slater states and the physical states are expanded in terms of this basis. To see an important source of level proliferation consider the important correlation configuration $3d^3 4p4d$ in our example above. This configuration has 19 $^4P^0$ terms leading to 57 levels. There is no way of knowing a priori which of these 19 terms are important and which could be cut from the calculation. They are all constructed from the same set of Slater states and all of them will make some contribution.

One approach to cutting back on included terms is to make a preliminary non-relativistic calculation which is relatively inexpensive and cut terms from these 19 whose mixing coefficients fall below a certain value. This is unsatisfactory because of the arbitrariness of the cutoff and because there may remain a large number of the 19 that are still required for accuracy.

Our alternative approach is to perform the same preliminary nonrelativistic calculation and use it to discover the exact linear combination of the 19 terms that appears in the physical term of interest - i.e. in the eigenvector of the non-relativistic hamiltonian. We then perform an orthogonal transformation in the 19

dimensional subspace to construct that combination of the Slater states that actually appears - in this case, in the nonrelativistic $3d^4 4p^4 p^0$ eigenvector of interest. We retain only that single combination and cut the remaining 18 from the calculation.

We emphasize that the choice of this "natural parentage" scheme results in essentially no loss of accuracy. The nonrelativistic terms are of course identical in the full and modified calculations and the relativistic levels resulting from mixing by spin-orbit and other couplings have only negligible differences.

The following tables compare some parameters of a full and a modified 7 configuration calculation and give comparisons of the resulting energies. Further results on level mixing and oscillator strengths will be provided at the conference.

1. Aashamar, K., Luke, T.M., and Talman, J.D. J.Phys.B:Atom.Molec.Phys. **12**, 3455 (1979).
2. Eissner, W., Jones, M., and Nussbaumer, H. Comput.Phys.Comm. **8**, 270 (1974).

Table 1. Comparison of some parameters of a 7 configuration calculation of the energy levels resulting from relativistic calculation of the $^4D^0$, $^4P^0$, $^4P^0$ terms in Cr II. (a) denotes the full calculation and (b) denotes the modified calculation.

Parameter	(a)	(b)
# terms retained	70	21
# levels retained	238	77
# nonrel. coefficients	10670	1305
# spin-orbit coefficients	4986	317
CPU time [†] (sec)	9000*	900*

[†] ETA Piper.

* Relativistic calculation only. (b) also used 1850 sec for the nonrelativistic calculation required for the natural parentage transformation.

Table 2. Comparison of energies (cm^{-1}) for levels in the calculations described above.

Level	(a)	(b)
$z^4 P^0$	0	0
$z^4 P^0 3/2$	100	102
$z^4 P^0 5/2$	262	259
$z^4 P^0 7/2$	688	692
$z^4 P^0 1/2$	903	906
$z^4 D^0 3/2$	1183	1183
$z^4 D^0 5/2$	1306	1308
$z^4 D^0 1/2$	1409	1409
$z^4 D^0 3/2$	1430	1427
$z^4 D^0 7/2$	1636	1634
$z^4 P^0 5/2$	1651	1648
$z^4 D^0 9/2$		

RELATIVISTIC CONFIGURATION INTERACTION METHOD FOR ATOMIC SYSTEMS

Takashi Kagawa and Shuji Kiyokawa
 Department of Physics, Nara Women's University
 Nara 630, Japan

In the variational calculation for energy levels in relativistic many-electron systems, one often encounters a difficulty of obtaining an appropriate positive-energy solution for the relativistic wave equation without the contamination of the negative-energy states. One of ways to remove the difficulty is that one uses a modified relativistic Hamiltonian whose energy spectrum is bounded from below, where a projection operator which projects the positive-energy states is introduced into the Hamiltonian^{1,2,3}. This treatment of the Hamiltonian leads to the no-pair approximation for the relativistic wave equation.

In the present work, the relativistic configuration interaction (RCI) method based on the no-pair approximation is presented, where a variational one-electron potential $v(r)$ is introduced into a Hamiltonian. In this method both a projection operator and a RCI wavefunction are constructed from the eigenfunctions for the one-electron Hamiltonian involving $v(r)$.

The wave equation for an atomic system is given by

$$H_+ \psi = E \psi, \quad (1)$$

where

$$H_+ = \sum_i H_0(i) + \Lambda_+ \left\{ \sum_{i < j} \frac{1}{r_{ij}} - \sum_i v(i) \right\} \Lambda_+. \quad (2)$$

and

$$H_0(i) = H_D(i) + v(i). \quad (3)$$

$H_D(i)$ and $v(i)$ are the Dirac Hamiltonian and a variational potential, respectively, and Λ_+ is a projection operator onto the positive-energy states. Λ_+ is expressed as a product of single-electron projection operators $\Lambda_+(i)$ given by

$$\Lambda_+(i) = \sum_m |\psi_m^{(+)}(i)\rangle \langle \psi_m^{(+)}(i)|. \quad (4)$$

Here, $\psi_m^{(+)}(i)$ denotes an eigenfunction belonging to the m th

positive-energy eigenstate for $H_0(i)$ in eq.(3).

We write a total configuration interaction (CI) wavefunction $\Psi(\Gamma)$ in the following,

$$\Psi(\Gamma) = \sum_n c_n \phi_n(\Gamma), \quad (5)$$

where c_n is an expansion coefficient and each CSF is constructed as a product of the basis functions $\{\psi_m^{(+)}(i)\}$.

By using some types of variational potentials having a few variational parameters such as Green's potential⁴ and the Coulombic one, numerical calculations for the ground and some lower excited states in helium-like systems with $Z=2, 10, 50$ and 100 are carried out. The RCI energy values for the ground state in these systems are almost the same as the DHF ones. So the RCI method hardly yields the correlation energy because of the slow convergence. However, it could be used to calculate the various physical quantities in heavier atomic systems with Z more than 50 since the relativistic effects can be taken into account sufficiently with the method.

Table. Comparison of calculated and experimental energies for the ground state (1^1S_0) in helium-like systems in atomic units.

Method	Z=2	Z=10	Z=50	Z=100
RCI(GSZ)	-2.8622159	-93.981550	-2556.4516	-11796.863
RCI(Coul.)	-2.858563	-93.97651	-2556.444	-11796.84
NRCI(Coul.)	-2.859822	-93.85582	-2468.855	-9937.605
DHF	-2.861813	-93.98279	-2556.452	-11796.86
NRHF ^{a)}	-2.86168	-93.86111		
Exact(NR) ^{b)}	-2.9037244	-93.906805		
Exp. ^{c)}	-2.9037844	-94.008358		

a) C.Froese-Fisher(1967). b) C.L.Pekeris(1958). c) C.E.Moor(1970).

1. G.E.Brown and D.G.Ravenhall: Proc. R. Soc. London Ser. A208, 552 (1951).
2. M.Mittleman: Phys. Rev. A5, 2395 (1972), *ibid.*, A24, 1167 (1981).
3. J.Sucher: Phys. Rev. A22, 348 (1980).
4. A.E.S.Green, D.L.Sellin and A.S.Zachor, Phys. Rev. 184, 1 (1969).

POTENTIAL ENERGY SURFACE FOR H_3^+
 VIA Z-DEPENDENT PERTURBATION THEORY-
 A THIRD-ORDER STUDY

Moh'd Abu-Jafar, Frank C. Sanders, and Donald H. Galvan
 Department of Physics
 Southern Illinois University - Carbondale

Potential energy surfaces for polyatomic molecules are expensive and time-consuming to calculate, even on modern computational equipment. We discuss a perturbative approach to such calculations which has the advantage of simplicity and efficiency. In Z -dependent perturbation theory, the lowest-order wave functions for a polyatomic molecule are not only independent of the nuclear charges, but are also independent of the total number of nuclear centers and electrons for the molecule. Thus the complexity of the problem can be restricted to a manageable level determined by the highest order of the calculation.

Making the simplest possible choice, we describe an N -electron, M -center polyatomic molecule as N "hydrogenic" electrons on a single center perturbed by electron-electron and electron-nucleus Coulomb interactions. In charge-scaled atomic units, this Hamiltonian is written as $H = H_0 + Z^{-1}H_1$ where

$$H_0 = \sum_{i=1}^N \left[-\frac{1}{2} \Delta_i - \frac{1}{r_{iA}} \right],$$

$$H_1 = \sum_{i=1}^N \left[\sum_{j>i}^N \frac{1}{r_{ij}} - \sum_{\sigma=A}^M \frac{Z_{\sigma}}{r_{i\sigma}} - \frac{\sigma}{r_{iA}} \right].$$

$Z = Z_A - \sigma$ is a "screened" nuclear charge with Z_A the charge on which the electrons are centered. With this choice of H_0 it is easy to show that the first-order wave function for any polyatomic molecule will consist entirely of two-electron, one-center (atomic) and one-electron, two-center (molecular) first-order wave functions. These are separately obtained from calculations on He -like and H_2^+ -like systems. More generally, the n th-order wave function for a polyatomic molecule will decouple into a sum of n th-order wave functions for all p -electron, q -center subsystems ($p + q = n + 2$) that are contained within the molecule of interest.

We illustrate application of this method with some results, complete through third order in the energy, for two-electron, three-center (H_3^+ -like) polyatomic molecules. For such systems, $\psi_0 = 1s(1)1s(2)$, $\epsilon_0 = -1$, and the first-order energy

coefficient is

$$\epsilon_1 = \epsilon_1^{1S} + 2Z_B \epsilon_1^{1s\sigma}(R_B) + 2Z_C \epsilon_1^{1s\sigma}(R_C) + 2\sigma \epsilon_1^S.$$

Here $\epsilon_1^{1S} = \frac{5}{8}$ is the first-order correction to the ground state energy of a two-electron atom. Similarly $\epsilon_1^{1s\sigma}(R)$ is the first-order correction to the ground state energy of a one-electron diatomic molecule with internuclear distance R . R_B and R_C are the internuclear distances of the two perturbing centers. Finally, $\epsilon_1^S = -1$ is the first-order correction to the energy of a 1s hydrogenic orbital due to the screening of the nuclear charge.

The first-order correction to the wave function is then given by

$$\begin{aligned} \psi_1 = & \psi_1^{1S}(12) + Z_B[\psi_1^{1s\sigma}(R_B, 1)1s(2) + 1s(1)\psi_1^{1s\sigma}(R_B, 2)] + Z_C[\psi_1^{1s\sigma}(R_C, 1)1s(2) \\ & + 1s(1)\psi_1^{1s\sigma}(R_C, 2)] + \sigma[\psi_1^S(1)1s(2) + 1s(1)\psi_1^S(2)], \end{aligned}$$

ψ_1^{1S} is available from highly accurate, variational perturbation calculations and $\psi_1^{1s\sigma}$ and ψ_1^S are available in closed form. With this wave function, one can calculate the second- and third-order energy coefficients. These coefficients will also incorporate results from simpler sub-systems, simplifying the calculation.

The total energy through third order for the molecule, in ordinary atomic units, is then given by

$$E = \sum_{m=0}^3 Z^{2-m} \epsilon_m + \frac{Z_A Z_B}{R_B} + \frac{Z_A Z_C}{R_C} + \frac{Z_B Z_C}{R}.$$

Results of these partial sums for the total energy of H_3^+ are presented in this paper, where they are compared with accurate, variationally obtained energies.

SECOND-ORDER CONTRIBUTION TO THE WIDTH AND SHIFT
OF AUTOIONIZING STATES OF TWO-ELECTRON ATOMS
BELOW THE $n=2$ THRESHOLD

Lonnie W. Manning and Frank C. Sanders
Department of Physics, Southern Illinois University-Carbondale
Carbondale, IL 62901-4401

A combined Complex Rotation and Feshbach Projection method is implemented within Z -dependent perturbation theory to obtain the lowest-order contribution to the width and shift of autoionizing states of two-electron atoms below the $n=2$ threshold. Under the complex rotation transformation, the resonant state has a complex energy, ω . This is expanded in a power series in $1/Z$,

$$\omega = \sum_n \omega_n Z^{-n}.$$

Application of the complex rotation method removes the degeneracy with the continuum in zeroth order, resulting in a bound zero-order wave function. This in turn means that the lowest-order contributions to the total energy, ω_0 and ω_1 , are purely real. Hence the lowest-order contribution to the width occurs in second order. Expressing the first-order wave function in terms of the Feshbach projection operators, P and Q , the expression for the second-order coefficient becomes,

$$\omega_2 = \langle (P + Q)\Psi_1^* | \frac{\epsilon^{-i\theta}}{r_{12}} - \omega_1 | (P + Q)\Psi_0 \rangle.$$

The usual choice of projector, $P = P_1 + P_2$ with $P_1 = |1s(i)\rangle\langle 1s(i)|$, results in $P\Psi_0 = 0$ and a $P\Psi_1$ of the form:

$$P\Psi_1 = \frac{1}{\sqrt{2}}(1s(1)\phi(2) \pm \phi(1)1s(2)),$$

where ϕ is an one-electron function. ω_2 can be divided into a purely real part,

$$\omega_2^Q = \langle Q\Psi_1^* | \frac{\epsilon^{-i\theta}}{r_{12}} - \omega_1 | Q\Psi_0 \rangle,$$

and a complex part containing the lowest-order contributions to the shift, Δ_2 , and the width, Γ_2 :

$$\omega_2^P = \langle P\Psi_1^* | \frac{\epsilon^{-i\theta}}{r_{12}} | Q\Psi_0 \rangle = \Delta_2 - i\frac{\Gamma_2}{2}.$$

The object of this work is to calculate ω_2^P . The problem requires the solution

of a single-electron differential equation for ϕ :

$$\left(-\frac{\epsilon^{-2i\theta}}{2}\nabla^2 - \frac{\epsilon^{-i\theta}}{r} - \epsilon_0 + \frac{1}{2}\right)\phi + Y_1 = 0,$$

where Y_1 is just the 1s component of the inhomogeneous part of the first-order perturbation equation,

$$Y_1 = \langle 1s^* | P \frac{\epsilon^{-i\theta}}{r_{12}} Q | \Psi_0 \rangle.$$

Use of the complex rotation method simplifies this calculation by making ϕ a square-integrable function, and by removing the degeneracy in zero order with the continuum. The function ϕ , and hence Δ_2 and Γ_2 , can then be obtained essentially exactly with the use of simple variational basis sets.

Results obtained here with this approach for the 2s2p 1P and 3P states are in perfect agreement with exact results[1]. Similar results for the 50 lowest doubly-excited P states below the $n = 2$ threshold will be reported. The present results represent the limiting values of the shift and width for high Z in the non-relativistic approximation. Comparisons to accurate theoretical values of the total widths for the isoelectronic series indicate that these lowest-order results can yield useful estimates of the total width for even relatively low values of Z . This approach is particularly useful for states with extremely narrow widths. These are difficult to calculate accurately in a straightforward application of the complex rotation method, so that these lowest-order estimates give useful information for such states, even for small values of Z .

1. Z.J. Horak and M.N. Lewis, Czech. J. Phys. B 26, 1088 (1976), and J.M. Seminario and F.C. Sanders, to appear in Phys. Rev. A.

RELATIVISTIC COUPLED-CLUSTER CALCULATIONS

I Lindgren, E.Lindroth, H.Persson, S.Salomonson and P.Öster

Department of Physics, Chalmers University of Technology/University of Gothenburg, S-412 96 Göteborg, Sweden

The method of discretization for generating a single-particle basis set, described in the previous abstract, is well suited for relativistic many-body calculations, and a corresponding coupled-cluster program has been developed and applied to He and He-like systems [1]. In the so-called *no-virtual-pair approximation* projection operators are required in order to prevent the electrons from falling into the negative-energy sea. With a discrete basis set of single-particle states the inclusion of such projection operators is much easier than with the differential-equation technique we employed earlier [2]. By carefully comparing the relativistic and non-relativistic results, it has been demonstrated that the partial-wave expansion of the relativistic contribution has a much slower rate of convergence, for neutral helium close to $(1+1/2)^{-2}$, compared to the non-relativistic contribution, $(1+1/2)^{-4}$. By extrapolating the two components separately, an accuracy of 10^{-8} Hartree has been achieved.

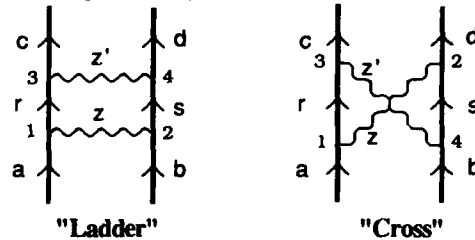
The relativistic pair program has also been applied to evaluate the transition rate and transition energy for the $2^3S_1 - 1^1S_0$ transition for He-like argon [3]. The exchange of virtual photons (the Breit interaction) is here included together with the Coulomb interaction to all orders in the no-virtual-pair approximation.

The problem of finding the most suitable form of the electron-electron interaction has recently been approached by several authors [4-6]. Straight-forward application of QED in first order (single-photon exchange) leads to

$$V_{12}^F = \frac{e^2}{4\pi\epsilon_0} (1 - \alpha_1 \cdot \alpha_2) \frac{e^{i|q|r_{12}}}{r_{12}}$$

$$V_{12}^C = \frac{e^2}{4\pi\epsilon_0} \left\{ \frac{1}{r_{12}} - \alpha_1 \cdot \alpha_2 \frac{e^{i|q|r_{12}}}{r_{12}} + [\alpha_1 \cdot \nabla_1, [\alpha_2 \cdot \nabla_2, \frac{e^{i|q|r_{12}} - 1}{q^2 r_{12}}]] \right\}$$

in the Feynman and Coulomb gauges, respectively (q is here the energy transfer over c). Gorcex and Indelicato [4] have demonstrated that these potentials lead to significantly different results in SCF calculations, even when the orbitals are generated in a *local* potential. They conclude that the ambiguity is not related to the use of SCF wave functions. Lindroth and Mårtensson-Pendrill [6] find that the discrepancy remains on the level $O(\alpha^2$ Hartree), even if one goes beyond the no(-virtual)-pair approximation. The explanation, however, lies *within* that approximation, as is found from an analysis of the complete two-photon exchange [7].



In a standard MBPT or SCF treatment only the *reducible (ladder)* part of the two-photon exchange is included. The *irreducible (crossed)* diagram, however, contributes to $O(\alpha^2$ Hartree) in the Feynman gauge, but *not* in the Coulomb gauge. This part corresponds exactly to the discrepancy found in the analyses of Gorcex and Indelicato and of Lindroth and Mårtensson-Pendrill. It should be noted that this contribution appears with intermediate states of *positive* energy. The result can be generalized to an arbitrary number of photons.

The discretized eigenvector basis also makes it possible to go *beyond the no-virtual-pair approximation* and to evaluate numerically the effect of negative-energy states (virtual electron-positron-pair creation) as well as radiative corrections of Lamb-shift type. Also the *renormalization* will in the latter case be made numerically. Calculations of this kind are in progress.

1. S.Salomonsen and P.Öster, Phys. Rev. A40, 5548 (1989)
2. E.Lindroth, Phys. Rev. A37, 316 (1988)
3. E.Lindroth and S.Salomonsen, Phys. Rev. A41, 4659 (1990)
- 4a. O.Gorci, P.Indelicato and J-P.Desclaux 1987 J.Phys. B20 639
- 4b. O.Gorciex and P.Indelicato P, Phys. Rev. A37 1087 (1988)
5. J.Sucher, J Phys. B21 L585 (1988)
6. E.Lindroth and A-M.Mårtensson-Pendrill, Phys.Rev. A39 3794 (1989)
7. I.Lindgren, J. Phys. B23, 1085 (1990)

COUPLED-CLUSTER CALCULATIONS FOR ATOMS

I. Lindgren, A.-M. Mårtensson-Pendrill, S. Salomonson, A. Ynnerman
and P. Öster

Department of Physics, Chalmers University of Technology/University of
Gothenburg, S-412 96 Göteborg, Sweden

To perform accurate calculations one has to go beyond the central field models and study effects of the correlation between the electrons. We use the *Coupled-Cluster* formulation of *many-body perturbation theory* to study the effects of *Single* and *Double* excitations clusters, operating on a central-field wave function used as a first approximation (the CCSD method). With this approach, important three- and four-particle excitations that are products of single and double excitations clusters are included. The CCSD method has now been implemented without any further approximations [1]. With the CCSD wave functions, very accurate results can be obtained for energies of small systems, as well as for the hyperfine structure and electric dipole transition rates for the lighter alkalis [2]. For Be and Li⁻ the CCSD method accounts for more than 99 % of the correlation energy (the energy not accounted for by the central field model).

Until recently, the single and double excitations were obtained in our work as solutions to inhomogeneous differential equations. By solving the equations iteratively, important effects are summed to all orders. During the last year a new method has been developed, involving a direct summation over a discrete set of numerical orbitals [3]. These orbitals are eigenvectors of a symmetric discretized one-particle Hamiltonian, obtained by representing the radial parts on a finite radial lattice. Through their construction, they form a complete orthogonal basis set on the discrete radial lattice chosen. The new solution method has been tested on He an accuracy of about 10^{-8} a.u. was achieved [3].

So far, our calculations have been based on *the intermediate normalization (IN)*, which leads to an "asymmetry" of the effects included at a specific truncation, such as the pair-correlation approximation. This can be remedied by a "*Hermitian formulation*" of the coupled-cluster approach [4]. In this procedure a number of diagrams, which in IN require inclusion of three-body (S_3) effects, are included at the pair correlation ($S_1 \times S_2$) level. This procedure has the additional advantage that it leads to *connectivity* also for an incomplete model space, in contrast to IN.

The access to a complete spectrum makes the evaluation of correlation effects very flexible and has also opened the possibility to study *genuine* three-body effects. As an example we take the ionization energy of sodium [5]. The CCSD approximation accounts for only 95% of the correlation energy in IN (see Table 1). The remaining 5% of the correlation energy then has to be due mainly to three-body effects. A part of these can be accounted for by the S_1 and S_2 clusters in the Hermitian formulation, as mentioned, e.g. the diagram in Fig. 1a, which accounts for $-273\mu\text{H}$. However, there are large cancellations among these diagrams for sodium, and they sum to $69\mu\text{H}$ [6]. The genuine three-body effects (not included in the Hermitian $S_1 \times S_2$ formulation), are here more important. Typical diagrams are shown in Fig 1b,c. The largest contribution comes from Fig 1b which contributes $306\mu\text{H}$.

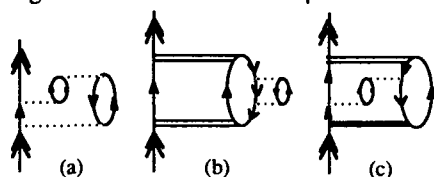


Fig 1 Examples of diagrams corresponding to S_3 effects.

Table 1. Ionization energy of sodium 3s in Hartree atomic units (μH)

Dirac-Fock	182 033	
Correlation		
CCSD [5]		6428
Relativistic effects [5,6]		30
Effects of S_3 in third order [6]		69
Genuine S_3 effects [5]		313
Total	188 873	6840
Experiment	188 858	6825

1. S. Salomonson and P. Öster, Phys. Rev. A **41**, 4670 (1990)
2. A.-M. Pendrill and A. Ynnerman, Physica Scripta **41**, 329 (1990)
3. S. Salomonson and P. Öster, Phys. Rev. A **40**, 5559 (1989)
4. I. Lindgren, J. Phys. B (submitted)
5. S. Salomonson and A. Ynnerman, (in manuscript)
6. S. Blundell, private communication

**Analyse of the Nonlinear Dichroic Voigt Effect and Its Relation
with Nonlinear Faraday Effect and Nonlinear Hanle Effect**

X.Chen

That variant of the resonant Faraday effect, where the light propagates perpendicularly to an external magnetic field B is known as the Voigt effect [1]. There have been already several experimental investigations, by modern laser techniques, of the nonlinear (i.e. power dependent) Voigt effect in the neighborhood of a resonance line [2,3]. In the Reference [2], a theory for a 1-0 transition to lowest, i.e. E^3 , order in the incident electric field was developed and the result was obtained numerically. In the present work, we report an analytical result for both 1-0 and 0-1 transitions and physical interpretation of different contributions to this effect.

One of the simplest experimental configuration is to have 45° between the B field and the polarization of the beam, with some experimental technique, one can measure only the absorptive effect (dichroism) [3]. The analyse is carried out for this configuration. For 1-0 and 0-1 transitions, the density matrix ρ_{mn} in stationary regime was computed explicitly to the third order; from it, the susceptibilities and hence the "Voigt angle" follow readily. With Doppler integration over the atomic velocities, we arrive to an analytical formula.

At the level of the density matrix computing, enlightened by the perturbative theory, we found out the close relationship between nonlinear Voigt effect, Faraday effect, and Hanle effect.

References

- [1] W.Voigt : Magneto- und Elektrooptik, Teubner, Leipzig 1908
- [2] K.H.Drake, W.Lange, and J.Mlynek. Opt.Comm., 66,315 (1988)
- [3] X.Chen, V.L.Telegdi, and A.Weis. Submitted to Opt.Comm.

PHOTOIONIZATION CALCULATIONS FOR THE 3D SUBSHELL OF BARIUM

M. Kutzner, D. Winn, V. Radojević*, and H. P. Kelly*

Department of Physics, Andrews University
Berrien Springs, Michigan, USA*Department of Physics, University of Virginia
Charlottesville, Virginia, USA

Photoionization studies of the 4d subshells of xenon and barium have added much to our understanding of electron correlation. In particular, the effects of interchannel coupling, relaxation, and core-polarization have been found to have strong influences on the photoionization cross section above the 4d threshold.^{1,2} Recent work has extended the calculations to energies above the 3d threshold of xenon and found significant many-body effects there also.³

The present work was undertaken to determine the extent to which interchannel coupling and relaxation effects influence the barium photoionization cross section and angular distribution above the 3d threshold. The threshold energies used were the Dirac-Fock eigenvalues ($\epsilon_{5/2} = 808.50$ eV and $\epsilon_{3/2} = 824.45$ eV) and the ΔE_{scf} energies ($\Delta E_{\text{scf}5/2} = 789.89$ eV and $\Delta E_{\text{scf}3/2} = 805.55$ eV) for the unrelaxed and relaxed calculations, respectively.

The effects of interchannel coupling were investigated by performing calculations within the relativistic random-phase approximation (RRPA).⁴ Calculations were first performed which include coupling between only the six jj-coupled 3d channels. RRPA calculations including nineteen jj-coupled interacting channels arising from dipole excitations of 3d, 4s, 4p, and 4d electrons were then carried out to determine the effects of interchannel coupling on the cross section.

Relaxation of the 3d shells was also taken into account in the present work. The effect was included in our RRPA-type calculation by computing the excited state orbitals in the V^{N-1} potential of a relaxed ionic core.² Overlap integrals between the ground state orbitals and the orbitals of the ionic core reduce the calculated cross section by 25.4% (this compares to about 20% for the 4d subshell of barium).^{1,2} The large reduction of the partial 3d cross section due to the overlap integrals indicates that double photoionization and photoionization with excitation channels are important here.

The calculations of cross sections and beta parameters in the various approximations are compared and contrasted. Of particular interest is the partitioning of the total photoionization cross section into various singly- and doubly-excited channels. Singly-

excited cross sections are obtained explicitly in the RRPA method and in the RRPA with relaxation. The contributions of doubly-excited cross sections are estimated from the overlap integrals resulting from the relaxed calculations. To our knowledge, experimental work has yet to be performed in the 3d threshold region of the barium spectrum. It is hoped that the present work and a new generation of synchrotron sources will stimulate such experimental work.

1. M. Kutzner, Z. Altun, and H. P. Kelly, Phys. Rev. A 41, 3612 (1990).
2. V. Radojević, M. Kutzner, and H. P. Kelly, Phys. Rev. A 40, 727 (1989).
3. M. Kutzner, V. Radojević, and H. P. Kelly, Phys. Rev. A 40, 5052 (1989).
4. W.R. Johnson and C.D. Lin, Phys. Rev. A 20, 964 (1979).

HYDROGEN-LIKE ATOM IN A STRONG MAGNETIC FIELD

N. N. Abyazov, M. Yu. Kuchiev

A. F. Ioffe Physical Technical Institute, Leningrad, USSR

The ground state energy of the hydrogen-like atom in a strong magnetic field is calculated. It's assumed that there exists a core potential, which strongly modifies the Coulomb potential in a short-range region $r < r_0$. The radius of core potential, the Bohr radius a_0 and the magnetic length $\lambda = (\hbar c/eH)^{1/2}$ are supposed to obey the following inequality

$$r_0 \ll \lambda \ll a_0 \quad (1)$$

Our main result is the equation for the ionization potential

$$\phi(k) = 2 \ln(a_0/\sqrt{2}\lambda) - la_0/\lambda^2 \quad (2)$$

where the left-hand side is

$$\phi(k) = k + 2 \ln k + 2\psi(1 - k^{-1}) + 3C$$

$k^2 = E(H)/E_0$ is the ionization potential in a Bohr units, $C=0.577$ is the Euler constant, $\psi(x)$ is the logarithmic derivative of the gamma-function and l is the scattering length for core potential.

When the core is insignificant, $l = 0$, then equation (2) is reduced to the well-known result [1]. In this case the ionization potential increases with the magnetic field as $\ln^2(a_0/\lambda)$.

The short range potential changes the result drastically. For the attractive core, $l < 0$, the bond energy increases like H . An even more intriguing situation occurs for the repulsive core case, $l > 0$. The bond energy has a maximum when $la_0/\lambda^2 \sim 1$ and asymptotically approaches the value in the high field region.

The influence of the core potential on the energy spectrum is significant when the condition

$$la_0/\lambda^2 \sim 1 \quad (3)$$

is fulfilled.

This model of the hydrogen-like atom with a core potential is widely used in semiconductor physics for shallow impurities. Here the Bohr radius greatly exceeds the lattice constant. The potential inside the impurity plays the role of the core potential, so condition (1) may be fulfilled [2]. Rydberg atomic states in a strong magnetic field may also be considered using the above approach.

- 1 H. Hasegawa and R. E. Howard, J. Phys. Chem. Solids, 1961, vol. 21, n. 1, p. 179-193.
2. N. N. Ablyazov and M. Kuchiev, Yu. Fizika Tverd. Tela, 1988, vol. 30, no. 6.

A DATA MANAGEMENT SYSTEM FOR HIGH PRECISION UV LASER
SPECTROSCOPY BASED ON RELATIVISTIC QUANTUM DEFECT THEORY

K. T. Lu , Dennis T. Baba and Keri Carpenter

Atomic Engineering Corp., P. O. Box 3342, Gaithersbury, Md., 20878

ABSTRACTS

A user-friendly software program for high precision UV laser spectroscopy of extremely high Rydberg states is being developed. The program is based on relativistic quantum defect theory (RQDT). The isotope shifts and hyperfine structures (hfs) of the Rydberg states are parametrized in terms of RQDT (1-4). The main features of this theory are:

- o It factorizes the fine structure due to electron's coupling with the ion core from the hfs and isotope shifts due to the electron's coupling with the nucleus.
- o It includes both the electron correlation effects and the relativistic effects.

The specific results and output are:

- o improved hfs splitted ionization limits with accuracy in order of MHz.
- o new hfs structures and autoionizing resonances induced by nucleus.
- o Grottrian diagram for laser spectroscopy.
- o potential applications in predicting the most efficient laser isotope separation scheme.

The software program allows researchers to evaluate data, generate new data, generate graphs and tables. This program is based on the manu-driven Atomic Engineering Data Base (5) and the entire program is written in the C language.

The data processed are:

- o Energy levels
- o Frequencies
- o Isotope shifts
- o hfs A and B coefficients

This system will be useful in:

- o laser spectroscopy
- o laser isotope separation
- o nuclear waste management
- o environmental studies in chemical engineering

Example of alkaline earth data will be presented.

1. K. T. Lu, J. Q. Sun and R. Beigang, Phys. Rev. A 37, 2220, (1988).
2. J. Q. Sun and K. T. Lu, J. Phys B : At. Mol. Opt. Phys. 21, 1957, (1988).
3. J. Q. Sun, K. T. Lu and R. Beigang, J. Phys. B: At. Mol. Opt. Phys. 22, 2887, (1989).
4. J. Q. Sun and K. T. Lu, J. Phys. B: At. Mol. Opt. Phys. 22, 2963, (1989).
5. Atomic Engineering Data Base, 3, Atomic Engineering Corp., P. O. Box 3342, Gaithersbury, Md., 20878, U. S. copyright, 1990.

VIII. ATOMIC SPECTROSCOPY AND STRUCTURE
- EXPERIMENT

SUPERFLUORESCENT TRANSITIONS BETWEEN HIGH-LYING ATOMIC LEVELS IN AN
ELECTRIC FIELD

T. Becker, R.-H. Rinkleff

Institut für Atom- u. Molekülphysik, Abteilung Spektroskopie
Universität Hannover, Appelstr. 2, D3000 Hannover, Fed. Rep. Germany

Superfluorescence [1] is a coherent spontaneous emission of an ensemble of atoms or molecules. Due to the long wavelengths and large dipole moments of transitions between high lying levels, the decaying atoms may act cooperatively as a result of being strongly coupled to each other by their common near radiation field. The intensity distribution of the superfluorescent pulse, which results from this strong coupling is given by a hyperbolic secant function [2-4]. A possible way to influence superfluorescence is to excite the atoms in a tunable cavity. The collective emission can then be controlled or even eliminated [5,6]. The aim of the present work is to show that it is also possible to eliminate the superfluorescent transitions by an external electric field. The experiments were performed with Sr, Ba and Na atoms.

The experimental set up was described in [7]. An atomic beam flew perpendicularly to the direction of the electric field. The atomic beam density was chosen to be about 10^{10} cm^{-3} . The alkaline earth atoms were excited stepwise via the $n s n p \ ^1P_1$ level into the $n s n' s \ ^1S_0$ or $n s n' d \ ^1D_2$ levels by two short dye laser pulses. The Na atoms were excited into $n' p \ ^2P_{3/2}$ levels.

The excited levels decay by superfluorescence into nearby levels. The fluorescence from these superfluorescently populated levels was detected by means of a monochromator and a fast photomultiplier. The single shot signal was recorded time resolved by a transient digitizer and stored by a computer. About 500 single decay curves were then averaged to enhance the signal to noise ratio. The measurements were performed at various electric field strengths and different atomic densities.

VIII-1

The superfluorescent transitions react very sensitive to the external electric field. The intensity of the signal decreases with the increase of the electric field. Thus it is possible to influence or to suppress completely the superfluorescent transitions. The experiments demonstrate that in a superfluorescent cascade the second transition or one transition in a superfluorescent branching can be suppressed and that the square root of the maximum of the intensity of a superfluorescent pulse decreases with the second power of the electric field. Calculations were carried out and confirm the experimental results qualitatively.

This work was supported by the Deutsche Forschungsgemeinschaft

References:

- 1) R. H. Dicke, Phys. Rev. 93, 99 (1954)
- 2) N. E. Rehler, J. H. Eberly, Phys. Rev. A3, 1735 (1971)
- 3) R. Bonifatio, L. A. Lugiato, Phys. Rev. A11, 1507 (1975)
- 4) A. T. Rosenberger, S. J. Petuchowski, T. A. DeTemple, Coh. Quant. Optics 4,555 (1978)
- 5) S. Haroche, J. M. Raimond: Adv. in At. a. Mol. Phys., ed. by D. Bates, B. Bederson (Academic Press, New York 1985) Vol. 20
- 6) P. Kulina, C. Leonard, R.-H. Rinkleff, Phys. Rev. A34, 227 (1986)
- 7) T. Becker, R.-H. Rinkleff, A. Steudel, Appl. Phys. B49, 257 (1989)

EXPERIMENTAL STUDY OF HEAVY ATOMIC SPECTROSCOPY USING DISCHARGE SPUTTERING

Fucheng Lin

Shanghai Institute of Optics and Fine Mechanics, Academia Sinica.

P.O.Box 800-211, Shanghai 201800, China.

Laser spectroscopy of heavy atoms has been an interesting area in theoretical, experimental, and application study. Most heavy elements are refractory metals, some isotopes are radioactive. Usually, laser spectroscopy measurements of these atoms are performed in an atomic beam device. We report here that using discharge sputtering, almost all the laser spectroscopy measurements including hfs structure of the high-lying levels and resonant photoionization via autoionization states can be studied in a much easier and safer way.

Hyperfine structure of ^{139}LaI

A La-Kr cylinder cathode lamp was used the source and a Spectra-Physics 380D ring laser was used to performed intermodulated optogalvanic or fluorescence spectroscopic measurement. A typical spectrum is shown in Fig.1. The transition corresponds to $3010 - 20083 \text{ cm}^{-1}$ and wavelength is 585.724 nm . Mark "X" is the cross-over peak. Using discharge the numerous low-lying levels can be populated enough to obtain strong signal. In our experiment, the intermodulated fluorescence has a greater signal/noise ratio than the optogalvanic spectroscopy. We measured the A and B constants for 10 levels of LaI using this Doppler-free technique and A constant for 10 levels of LaI where the signal is too weak to perform a Doppler-free measurement. Table 1 gives these results [1].

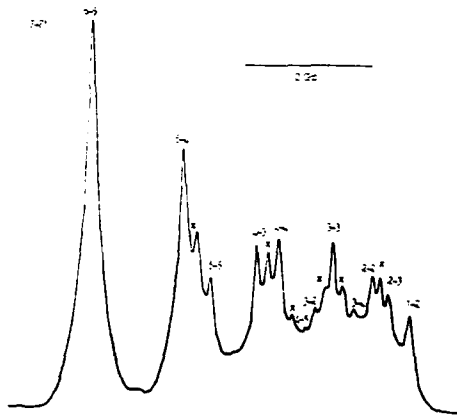


Fig.1 hfs of 585.724 nm transition of LaI.
"X" marks the cross-over peak.

VIII-2

Table 1

levels(/cm)	2668	3010	3494	4122	20019	20083	20197	20972	20763	21448
A(MHz)	-480	300	472	473	-40.7	90.2	131.5	-65.2	192.5	121.5
B(MHz)	15	8.2	21.5	25.7	-2.4	-3.4	0	31.5	-1.2	-35.7
	1053	2668	3010	7490	7680	19379	18157	20083	24409	24910
	199	-498	315	931	796	-58.7	662	91.1	183	-339

Hyperfine structure of $^{235}\text{U I}$ [2].

Using two ring lasers one can excited a certain velocity group of ^{235}U atom to its first excited state and then perform the Doppler-free measurement from this state to a high-lying state. Tuning both lasers properly, one can obtain hfs data of the high-lying levels. For example, the A and B constants of 33625 cm^{-1} level was measured to be $A=-97\text{ MHz}$, $B=1326\text{ MHz}$.

Resonant photoionization spectroscopy of U I [3].

Using three tunable pulse lasers and pulse discharge of the lamp synchronized with these lasers, one can use this lamp as a source of the neutral atoms first and then the collector of the photo-ion. Fig.2 shows such a spectrum for the first excited wavelength 605.68nm, the second excited wavelength 609.80nm, and the third laser scanned from 579.8 to 582.3nm.

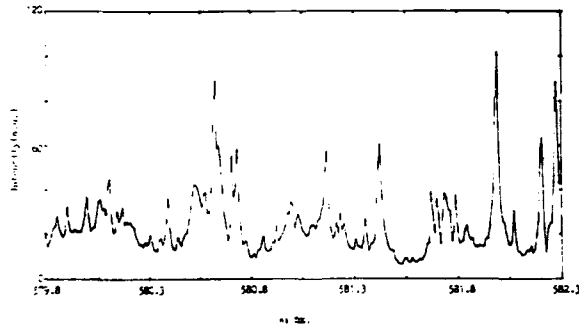


Fig.2 Photoionization spectroscopy of U I.

1. C.Luo, J.Qu, L.Zhou, and F.Lin, to be published on J.Opt.Soc.Am.B.
2. Fucheng Lin et al., CLEO'89, Baltimore, 1989.
3. Yin Lifeng, Wu Li, Zhang Shaofeng, and Lin Fucheng, unpublished.

HYPERFINE STRUCTURES OF STABLE TERMS IN ^{14}N -IONS

H. Winter

Inst. f. Kernphysik der Universität Münster, D-4400 Münster

A. Schirmacher

Physikalisch Technische Bundesanstalt, D-3300 Braunschweig

On the 11th ICAP-meeting (Paris, 1988) we presented first results of a new technique to resolve hyperfine (hf)-splittings in stable terms of atoms and ions. With this method we have measured hf-splittings of stable terms in ^{14}N I, II, III with good precision where the data for the ions have been determined for the first time (for NI $2p^3\ ^2D$ the precision of our data is about one order of magnitude higher than earlier measurements [1], furthermore these former data show an inconsistency with respect to one splitting). Our measurements allow to evaluate the nuclear quadrupole moment of ^{14}N $Q(^{14}\text{N})$ and the quadrupole coupling constant for a single electron in the $2p^3$ -configuration. The analysis of data is based on CI-calculations by the code of Glass and Hibbert [2].

In brief, grazing scattering of fast ions (about 100 keV) at a highly polished surface results in a well defined reflected beam and a large orientation of orbital angular momenta of terms in atoms and ions. Via hyperfine (hf)-interaction this anisotropy is partially transferred into the nuclear spin ensemble which is detected by a "beam-foil"-method [3].

By a rf-magnetic field we induce NI-transitions between hyperfine-levels with $\Delta F = \pm 1$ and $\Delta M_F = \pm 1$ so that the atomic anisotropy is slightly modified which also affects the nuclear polarization. Recording the nuclear polarization of the fast beam in dependence on rf-frequency allows to determine the hf-splittings in stable terms of atoms and ions.

We have measured the hf-splittings of most stable terms in ^{14}N I, II, III with linewidths due to transition broadening of about 260-500 kHz. The precision of the hf-splittings is 10 to 30 kHz. From CI-calculations we evaluate from results for three different configurations in NII and NIII the quadrupole moment $Q(^{14}\text{N})$ and find consistent data within $3 \cdot 10^{-3}$. At the current level of analysis we conclude $Q(^{14}\text{N}) = (20.0 \pm 0.2)$ mb which significantly improves the knowledge of this quantity with respect to accuracy and reliability. The same holds for the quadrupole coupling constant for the $2p^3$ -configuration of the neutral atom. From an extrapolation based on calculated electric field gradients we obtain $e^2 Q q_{at} = (11.2 \pm 0.2)$ MHz.

[1] H.E. Radford and K.H. Evenson, Phys. Rev. 168, 70 (1968)

[2] R. Glass and A. Hibbert, Comp. Phys. Comm. 11, 125 (1976)

[3] H.J. Andrä, H.J. Plöhn, R. Fröhling, and A. Gaupp, Z. Phys. A281, 15 (1977)

ON-LINE COLLINEAR FAST BEAM LASER SPECTROSCOPY OF ^{88}Kr AND ^{90}Kr TO STUDY
NUCLEAR CHARGE RADII BEYOND THE N=50 SHELL CLOSURE

H. A. Schuessler, R. M. Evans, M. Brieger, and Y. F. Li
Department of Physics, Texas A&M University, College Station, TX 77843

and

A. Alousi and F. Buchinger
Foster Radiation Laboratory, McGill University, H3A2B2, Montreal

Optical isotope shifts have been measured in the $5s[3/2]_2^0 - 5p[3/2]_2$ transition in atomic krypton at $\lambda=760$ nm. The short-lived isotopes, which have half-lives of $T_{1/2}(^{88}\text{Kr})=2.84$ h and $T_{1/2}(^{90}\text{Kr})=32.3$ sec, were produced on-line in the TRISTAN isotope separator at the 60 MW High Flux Beam Reactor at Brookhaven National Laboratory. A thermal neutron beam of 3×10^{10} n/(cm²sec) intensity induces fission in a ^{235}U target located inside a high temperature plasma ion source. The fission products are ionized, extracted from the source at an energy of 43 keV, and injected into the collinear fast beam laser spectroscopy apparatus. The frequency of the tunable dye laser is locked to a 300 MHz confocal Fabry-Perot etalon which in turn is locked to a Zeeman stabilized He-Ne laser. The ion beam is converted into a fast neutral beam after passing through a charge exchange cell containing alkali vapor. The atomic transition is detected by laser induced fluorescence. The laser frequency is kept fixed while the absorption frequency of the atoms in the beam is Doppler-tuned through resonance. This is achieved by applying a variable potential to the charge exchange cell. A solenoid, placed between the charge exchange cell and the observation region, provides a magnetic field along the beam axis and reduces optical pumping of the atoms before they reach the observation region. Suitably located apertures reduce the laser stray light to about 30 counts per sec per mW of laser power.

Isotope shifts were determined for the short-lived neutron-rich isotopes ^{88}Kr and ^{90}Kr as well as for all the stable isotopes between A=78 and A=86, thus extending the data in this element beyond the N=50 shell closure. Changes in the nuclear mean-square charge radii were deduced and are depicted in Fig. 1. They indicate a slow decrease of the charge radius with increasing neutron number below N=50 and a much more rapid increase above it. This corroborates the characteristic discontinuity that is usually observed at major shell closures.

For a first interpretation of the results, measured changes in the charge radii can be compared to the predictions of the droplet model [1]. In this model, a change in the nuclear charge distribution is accounted for by changes in: (i) volume, (ii) quadrupole deformation, and (iii) Coulomb repulsion. Information on the quadrupole deformation was obtained from experimental B(E2) values tabulated for the stable isotopes [2], and predictions of the B(E2) values for the neutron-rich isotopes [3]. These predictions are based on an empirical relation between

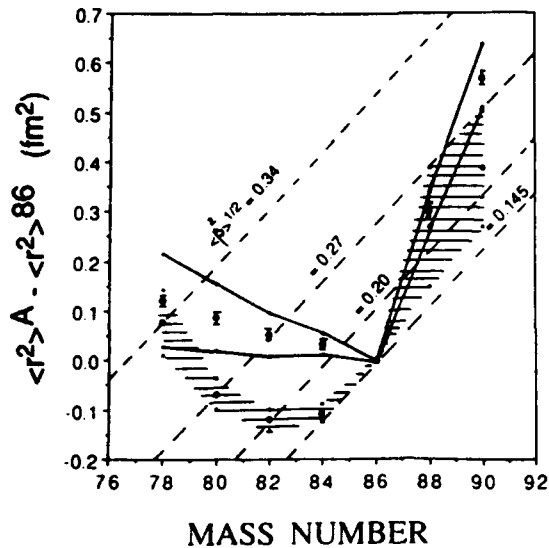


Fig. 1. Comparison between the experimental changes of mean-square charge radii of Kr isotopes (full dots) with predictions from the droplet model (shaded area) adjusted for quadrupole deformation. The solid lines indicate the systematic error in the evaluation of the experimental data when the calibration factor $F(760 \text{ nm})$ and the specific mass shift are varied by one error interval. The errors indicated for the droplet values are due to the uncertainties of the $B(E2)$ values used to evaluate the ground state deformation. Droplet model isodeformation lines are indicated as dashed lines.

the $E2$ and $B(E2)$ values [4]. The isotope shifts of all stable isotopes were also measured off-line in seven additional optical transitions making possible the use of extensive King plot procedures to evaluate the electronic factors.

This work was supported by DOE under contract #DE-AS05-80ER10578, the Texas Advanced Research Program, the Center of Energy and Mineral Resources of TAMU, and the Natural Sciences and Engineering Research Council of Canada.

1. W. D. Myers and K. H. Schmidt, Nucl. Phys. **A410**, 61 (1983).
2. S. Raman, C. H. Malarkey, W. T. Milner, C. W. Nestor, and P. H. Stelson, At. Data Nucl. Data Tables **36**, 1 (1987).
3. S. Raman, C. W. Nestor, S. Kahane, and K. H. Bhatt, At. Data Nucl. Data Tables **42**, 1 (1989).
4. L. Grodzins, Phys. Lett. **2**, 88 (1962).

**PERTURBATION OF THE $2D$ SERIES IN ALUMINUM;
an old problem solved with new measurements.**

A. Dönszelmann, M. Davidson, E.P. Buurman, Zeeman-laboratorium,
Plantage Muidergracht 4, 1018 TV Amsterdam, The Netherlands.

Aluminum is one of those elements that demonstrates strong configuration interaction effects, particularly in the $nd\ 2D$ series, perturbed by the $3s3p^2(1D)\ 2D$ term. The pure perturber is situated between the states $n=3$ and $n=5$. The perturbation is smeared out over the whole series[1]. However, it was believed that the influence was restricted to the lowest few terms. This perturbation changes the lifetime values, the finestructure (fs), the level positions etc. not only in the lowest part of the series, but effects are still observable at the high n values [2].

New measurements were taken of the fs[2], the quantum defects[2], and the lifetimes[3] were taken with improved accuracy in order to detect the influence of the perturbation especially at higher n values. Atoms in an atomic beam are excited by laser beams at right angles. The experimental arrangement used in these experiments is straightforward. For the lifetime experiments a frequency doubled (β -BBO) dye laser is used. The fluorescence light is detected by a fast photomultiplier, coupled to a fast multichannel analyser. For the quantum defect and the fs measurements we use 3-step excitation with two dye lasers. Excited atoms are detected by field ionization and recorded by a fast gated integrator. Averaging over many laser pulses is used in both cases.

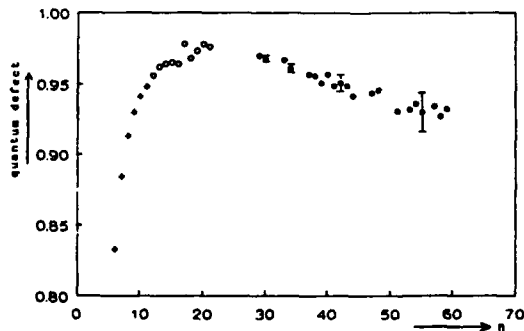


Fig. 1: The quantum defect as a function of the principal quantum number; \bullet , \circ lit. values.

In this experiment we investigated the level positions (i.e. the quantum defects) of the series $2D$ between $n=28$ and $n=60$. Figure 1 shows the quantum defects plotted as a function of n . For small n values the influence of the core electrons disturbs the straight line. The quantum defects of the $2D$ series have the opposite sign as those of the unperturbed $2P$ and $2S$ series, probably due to the perturbation. Between $n=10$ and $n=20$ the quantum defects tends to go to a straight line; the influence of the core is decreasing faster than the influence of the perturbation and the effects compensate each other. Beyond $n=20$ one can expect to see the influence of the perturbation alone, repelling from the straight line and forming a flat maximum.

Together with the level positions we investigated the fs of a few members of the $2D$ series. Figure 2 shows the fs as a function of n . In an unperturbed Rydberg series the fs should be proportional to n^{-3} .

Apart from the values at low n , this proportionality is observed. However, the values are about two orders of magnitude too large. Perturbation by the $3s3p^2\ ^2D$ term alone does not seem to be able to account for the fs in the series, since it is based on a 1D parent and

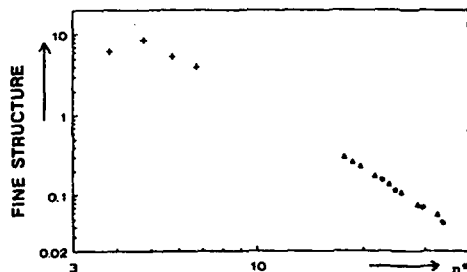


Fig. 2: The fine structure as a function of the effective quantum number; +, Δ literature values.

does not exhibit first order fs . The $3s$ electron also does not contribute to a sizeable fs . It should be clear that there must be another source of fs in the perturber. The extended theory of spin-orbit interaction [4] explains this. The wavefunctions are mixed with continuum wave functions. With this ($sp^2 + \text{continuum}$) 2D perturber the calculated fs in the 2D series is of the same order of magnitude as the experimental results.

The lifetimes of the 2D series were measured very accurately together with the branching ratios. We obtained values well within the error limits of literature values [5]. In an unperturbed series the lifetimes are proportional to n^{-3} . As expected, the largest deviations are found around $n=4$. For large values of n , the lifetimes tend to follow the line n^{-3} line. According to the theory developed by Uylings [4] and the measurements of the other observables discussed above, this trend is not expected. A deviation between $n=15$ and $n=20$ should be present. However, the errors in that

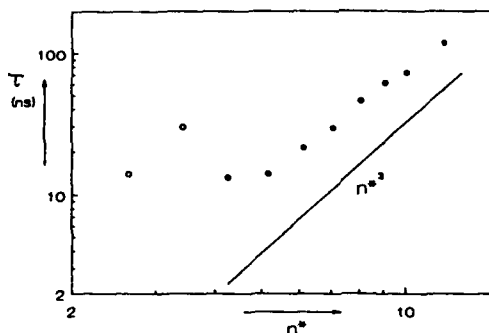


Fig. 3: The lifetime values as a function of n^3 .

region are large and observing this effect will be very difficult. The signal-to-noise ratio becomes small, mainly due to the numerous decay channels. Also, the two fs transitions from the groundstate to the excited levels for different n and l values will mix, making the determination of the spectral lines complex.

- 1) A.W. Weiss, Phys. Rev. A9, 1524, (1974)
- 2) E.P. Buurman O.J. Koning, A. Dönszelmann, J.Phys. B22, 3965, (1989).
E.P. Buurman, M.D. Davidson, P.H.M. Uylings, A. Dönszelmann,
J. Phys. B. in press
- 3) M.D. Davidson, H. Volten, A. Dönszelmann, Astron. Astrophys. accepted
- 4) P.H.M. Uylings, J. Phys. B in press
- 5) G. Jönsson, H. Lundberg, Zeitschr. Phys. A313, 151, (1983)

ONE-PHOTON RESONANT TWO-PHOTON IONIZATION PROCESSES OF ATOMIC LEAD

Dajun Ding, Mingxing Jin, Hang Liu

Institute of Atomic and Molecular Physics, Jilin University,

Changchun 130023, P.R.China

and

K.T.Lu

Atomic Engineering Corporation, P.O.Box 3342, Gaithersburg, MD 20878

The resonant enhanced effect of multiphoton ionization (MPI) can be reduced significantly by some competing processes, both coherent and incoherent^(1,2). It is worth concentrating on the influence of these competing processes on MPI for understanding of fundamental atomic dynamics and selecting MPI scheme in various applications. These competing processes can deplete the population of atoms in the resonant intermediate state, resulting in the overall resonant enhancement to be rather limited. A proper investigation for MPI and relevant processes involves the simultaneous observations of both photons and ionizing products under specific conditions of laser intensity and atomic density.

This experiment is performed on Pb one-photon resonant two-photon ionization. A dye laser-frequency-doubled system pumped by a YAG laser is used to produce a 2833 Å UV laser beam with a 5×10^{-9} s pulse duration at a 10Hz repetition rate for exciting Pb $6p^2P_0 - 6p7s^3P_1^0$ resonance. The laser intensity is from 1μJ/pulse to 6mJ/pulse. The UV laser crosses a Pb beam of 10^{10} atoms/cm³ density at right angles in a 10^{-6} torr vacuum chamber with a TOF-mass spectrometry and a fluorescent collecting and detecting system. This apparatus provides a possibility for the simultaneous observation of the channels both going into and out of the resonant MPI in a collisionless condition.

Several interesting features emerging from the observation are the

following:

a) Far from the resonant wavelength 2833 Å, Pb undergoes a non-resonant two-photon ionization from the ground state $6p^2 \ ^3P_0$ into the ionization continuum. The signal intensity grows rapidly with increasing laser intensity, having an order of non-linearity 2 in log-log plot.

b) The signal intensity of resonant ionization displays a more slow increase rate than the one in non-resonant ionization. Also the saturation of resonant ionization appears at high laser intensity under both focused (having a 0.4 mm diameter) and unfocused (having a 4 mm diameter) conditions.

c) Resonant ionization is accompanied by fluorescences corresponding to the decay channels of the resonant intermediate state. The saturation of a fluorescence (4059 Å, $6p7s \ ^3P_1 - 6p^2 \ ^3P_2$) appears at low laser intensity (about several micro-joule/pulse).

d) The line shape of resonant ionization has a broadening with increasing laser intensity, much more severely than the accompanying fluorescence, which remains practically unchanged over the range of laser intensity used in the experiment. No apparent shift of the resonant position has been observed in both the ionization and the fluorescence.

e) A dip at the ionization peak, which is the result of the sharp decrease of the resonant intermediate state population, is observed at different laser intensity with the UV laser scanning. The position of the ion-signal dip is exactly resonant and corresponds to the peak of the fluorescence spectra. At low laser intensity, the depth of the ion-signal dip is about a half of the ionization peak. We have noted the widths of dip slightly narrow than the linewidths of fluorescence.

1. Rainer Wunderlich, N.G. Payne, and V.R. Garrett, Resonant Ionization Spectroscopy, Inst. Phys. Conf. Ser. No. 84: Section 7, P. 269(1986).

2. J.C. Miller and R.N. Compton, Phys. Rev. A25(4), 2056(1982).

BEAM-FOIL STUDY OF TWO-ELECTRON TRANSITIONS IN CU-LIKE IONS
OF SOFT-X-RAY LASER INTEREST

E. Träbert

Harvard College Observatory, 60 Garden Street, Cambridge, MA 02138, U.S.A.

J. Sugar

NIST, Gaithersburg, MD 20899, U.S.A.

G. Möller, P.H. Heckmann,

Experimentalphysik III, Ruhr-Universität, D-4630 Bochum 1, F.R. Germany

Among the decisive elements of working schemes for XUV lasers are high-lying excited levels (to obtain lasing at short wavelengths) which must be sufficiently long-lived so that they can be populated substantially by whatever processes envisaged before they decay. One of the proposed schemes, by Morley and Sugar [1], suggests to employ the $3d^{10} 4p^2 P^o - 3d^9 4s^2 {}^2D$ transitions in Cu-like ions. These transitions occur because of some weak mixing of the upper level with the $3d^9 4p^2 {}^2D$ levels and the associated Rydberg series. A particular attractive pair of elements to use in such a laser applied to the study of biological specimens would be Pd ($Z=46$) and Ag ($Z=47$), which would provide laser radiation on either side of the K absorption edge of carbon.

Calculations of the wavelengths and the transition rates have been done using Cowan's Hartree-Fock code. Some of the results are included in table 1. After the first experiments it became apparent that the levels of interest are not the only long-lived high-lying levels, but are repopulated by cascades from $3d^9 4s4p {}^{2,4}L^o$ levels. Among these are the lowest-lying quartet levels in the Cu I isoelectronic sequence, and many of them have lifetimes in the same range as those of the levels of primary interest, some even exceeding them by up to a factor of about six.

The experiment was done at the Bochum 4 MV Dynamitron tandem accelerator laboratory using the beam-foil method [2]. Two 2.2 m grazing-incidence spectrometers were alternatively employed to analyze the light emitted by the foil-excited ion beam. Spectra were recorded near to the foil and at distances of up to one centimeter downstream of the foil, corresponding to a time of up to 2 ns after excitation. The "prompt" spectra showed lines known from other light sources as well as a number of as yet unidentified lines.

It was hoped that some of the lines measured near the foil would survive for sufficiently long distances downstream so that they could be used as wavelength references in the downstream spectra. The only suitable in-beam reference lines for the downstream spectra turned out to be the Cu-like 4f-5g yrast lines which show extended tails due to the cascades along the yrast chain of levels and which therefore appear clearly at all delay times. The wavelengths of these 4-5 transitions, however, exceed those of the lines of interest by about a factor of 2.5. Therefore the candidate lines of interest were observed in first and second diffraction order, as far as the gratings allowed to do so. Clearly, long-lived transitions appear in the spectrum near the predicted positions of the $3d^{10} 4p^2 P^o - 3d^9 4s^2 {}^2D$ transitions. In case of Nb, all three expected lines are being seen; in case of Ag only the long-wavelength component of the multiplet is not blended (with an as yet unidentified line).

The decay curves recorded on the candidate lines feature a fast component attributed to blending lines and their cascade tails, and a fairly intense slow component. The lifetime of the latter typically exceeds the predicted lifetime of the $3d^9 4s^2 {}^2D$ levels by about a factor of

four. Simulations of the expected decay curves, allowing for cascade repopulation from the $3d^9 4s4p$ levels, indicate that, indeed, such a curve with such an apparent lifetime has to be expected. Thus the general time scale is confirmed by the decay curve measurements, but the simulations tell that it will not be possible to measure the lifetime of the principal decay component unless all $4s^2 - 4s4p$ cascades can be measured individually.

The present experimental data nevertheless corroborate the validity of the calculations and assumptions on atomic structure used for the soft-x-ray laser scheme suggested by Morley and Sugar [1]. The observed prominent slow cascades do not disturb the working principle of this laser scheme, and their long-lived levels of origin might even be beneficial as high-lying energy storage bins, repopulating the lasing levels.

The dominant slow decay component which we ascribe to cascades is also compatible with the decay constant observed in a beam-foil study of iodine by Cocke et al. [3]: Those authors expected the $3d^9 4s^2 {}^2D_{3/2}$ level to decay to the $3d^{10} 4s {}^2S$ level by electric quadrupole decay (E2). They observed the experimental lifetime to be shorter than the (E2 only) prediction, and they suggested that the previously unsuspected E1 transition to $3d^{10} 4p {}^2P^o$ might be the reason for this. The lifetime they measured was about four times the value of the Morley and Sugar (E1 only) prediction for the $3d^9 4s^2 {}^2D$ levels [1]. The conclusion from the present study is that their decay curves - as in our case - rather represent the somewhat slower cascades from $3d^9 4s4p$ levels than the primary decays.

Acknowledgement: This study has been supported by NATO research grant CRG 900094. E.T. gratefully acknowledges financial support by the Max Kade Foundation (New York) and the Alexander von Humboldt Foundation (Bonn, Feodor Lynen Program).

1. P.D. Morley and J. Sugar, Phys. Rev. A38, 3139 (1988)
2. E. Träbert et al., J. Opt. Soc. Am. B5, 2173 (1988)
3. C.L. Cocke et al., Phys. Rev. A12, 2413 (1975)

Table 1: $3d^{10} 4p - 3d^9 4s^2$ transitions: Wavelengths, transition probabilities and lifetimes

Ion	Transition	Wavelength		Transition probability		Lifetime
		Theory λ / nm	Experiment λ / nm	Theory gA/s^{-1}	Theory τ / ns	
Nb ¹²⁺	${}^2P^o_{3/2} - {}^2D_{5/2}$	8.278	8.269±0.002	1.45 E9	4.10	
	${}^2P^o_{3/2} - {}^2D_{3/2}$	8.124	8.16 ±0.01	1.73 E8	3.14	
	${}^2P^o_{1/2} - {}^2D_{3/2}$	7.961	7.938±0.004	1.09 E9	3.14	
Ag ¹⁸⁺	${}^2P^o_{3/2} - {}^2D_{5/2}$	4.220	4.247±0.03	3.52 E9	1.66	
	${}^2P^o_{3/2} - {}^2D_{3/2}$	4.131		4.24 E8		
	${}^2P^o_{1/2} - {}^2D_{3/2}$	4.027	(4.03±0.04) (blend)	3.11 E9	1.13	

VIII-8

LIFETIME OF THE 2^3S_1 STATE OF HELIUM-LIKE $^{79}\text{Br}^{33+}$

R. W. Dunford, C. J. Liu, H. G. Berry, M. L. A. Raphaelian,*
R. C. Vondrasek, and B. J. Zabransky
Physics Division, Argonne National Laboratory, Argonne Illinois 60439

M. Hass†
NSRL, University of Rochester, Rochester, NY 14627

L. J. Curtis
Department of Physics and Astronomy, University of Toledo, Toledo, OH 43606

D. A. Church
Physics Department, Texas A&M University, College Station, Texas 77843

New measurements of forbidden lifetimes in one- and two-electron ions [1-3] are providing sensitive tests of relativistic quantum mechanics. We report here a measurement of the lifetime of the 2^3S_1 level in helium-like $^{79}\text{Br}^{33+}$. This level decays to the 1^1S_0 ground state by a forbidden M1 transition. Bromine-79 is a good choice for the measurement of the lifetime of the helium-like 2^3S_1 level because, in this isotope, all of the other $n=2$ levels which decay by single-photon emission are much shorter lived and so there is a minimum of complication from the decay of other levels.

Our experiment utilizes the beam foil time-of-flight technique. The beam which is provided by the Argonne Tandem-Linac (ATLAS) is incident on a $200 \mu\text{g}/\text{cm}^2$ foil and the helium-like $33+$ charge state is magnetically analyzed and directed to the experimental area. The beam velocity is measured with a time-of-flight velocity analyzer. In the interaction region a thin carbon foil ($30 \mu\text{g}/\text{cm}^2$) is moved relative to two fixed Si(Li) X-ray detectors by a precision translation stage. The detectors are collimated so that they observe a region 2 mm along the beam. A lower resolution silicon X-ray detector attached to the target holder observes the X-ray intensity at a fixed foil-detector distance and was used for normalization.

At each foil-detector separation, peaks near 12 keV in the Si(Li) detectors are fitted to a Gaussian. We then divide the peak areas by the number of counts in the normalization detector. The normalized counts are fitted to a decay curve to obtain the lifetime. We will discuss our method for handling cascade effects which are the major source of systematic error in our measurement. Our final result [4] is $\tau(2^3S_1) = 224.1(7.1)$ ps, which agrees with the theoretical calculations [5].

This work was supported by the U.S. Department of Energy, Office of Basic Energy Sciences, under Contracts No. W-31-109-ENG-38 and No. DE-FG05-88ER13958 (University of Toledo) and by the NSF (University of Rochester).

VIII-8

References

*Permanent address: The University of Illinois, Chicago, IL.

†Permanent address: Weizmann Institute of Science, Rehovot, Israel.

1. R. Marrus, V. San Vicente, P. Charles, J. P. Briand, F. Bosch, D. Liesen and I. Varga, Phys. Rev. Lett. 56, 1683 (1986).
2. R. Marrus, P. Charles, P. Indelicato, L. de Billy, C. Tazi, J. P. Briand, A. Simionovici, D. D. Dietrich, F. Bosch and D. Liesen, Phys. Rev. A 39, 3725 (1989).
3. R. W. Dunford, M. Hass, E. Bakke, H. G. Berry, C. J. Liu, M. L. A. Raphaelian and L. J. Curtis, Phys. Rev. Lett. 62, 2809 (1989).
4. R. W. Dunford, D. A. Church, C. J. Liu, H. G. Berry, M. L. A. Raphaelian, M. Hass, L. J. Curtis and Phys. Rev. A 41, 4109 (1990).
5. G. W. F. Drake, Phys. Rev. A 3, 908 (1971); G. W. F. Drake (private communication); W. R. Johnson and C. P. Lin, Phys. Rev. A 9, 1486 (1974).

**MAGNETIC FIELD DECOUPLING OF ALKALI EXCITED STATE
HYPERFINE STRUCTURE**

W. A. van Wijngaarden and J. Sagle

Department of Physics, York University

Toronto, Ontario M3J 1P3, Canada.

We describe how sub-Doppler excited state hyperfine splittings can be measured using a magnetic field to decouple the nuclear and electronic spins. This method is particularly easy to use for nuclei having a zero electric quadrupole moment as is the case when the nuclear spin is less than one. To illustrate the method, we measured the hyperfine splitting of the $8D_{3/2}$ state which has a very small electric quadrupole moment.¹

In our experiment, cesium atoms were contained in an evacuated cell that was heated to about 100°C. A Nd:YAG pumped pulse dye laser, having a repetition rate of 10 Hz., excited the $6S_{1/2}$ cesium ground state to the $8D_{3/2}$ via a two photon excitation. The quantization axis was defined to be along the linear polarization direction of the dye laser. Hence, cesium atoms were excited into the $m = \pm \frac{1}{2}$ Zeeman sublevels of the $8D_{3/2}$ state.

Alkali atoms can be modelled as hydrogenic systems since all but one of their electrons are in fully occupied shells. The time evolution of the excited state wavefunction is governed by the Schrodinger equation, where the Hamiltonian is given by

$$H = H_0 + ah\vec{I} \cdot \vec{J} + g_J\mu_B\vec{J} \cdot \vec{B}$$

H_0 represents the Coulomb and fine structure interactions. The second term is the magnetic dipole hyperfine interaction where a is the magnetic dipole constant, h is Planck's constant, while \vec{I} and \vec{J} are the nuclear and electronic angular momenta respectively. The last term represents the interaction of the electron with the external magnetic field \vec{B} applied along the quantization axis while μ_B is the Bohr magneton and g_J is the gyro-magnetic ratio of the electron. The Zeeman sublevels $|Jm_J\rangle$ are not eigenstates of the Hamiltonian. One may think of the hyperfine interaction as shuffling the atoms among

¹ P. Buck et al, Phys. Rev. 104, 553 (1956).

the four Zeeman sublevels of the $8D_{3/2}$ state. The populations of the $m = \pm\frac{1}{2}$ sublevels relative to the $m = \pm\frac{3}{2}$ sublevels can be monitored by measuring the polarization intensity of the fluorescence produced when the $8D_{3/2}$ state decays to the $6P_{1/2}$ state. We detected fluorescence linearly polarized parallel to the quantization axis which results from a $\Delta m = 0$ transition, and fluorescence polarized perpendicular to the quantization axis which is produced by a $\Delta m = \pm 1$ transition.

Fluorescent light that is emitted transverse to both the laser propagation and polarization directions was measured. Detected light traverses a linear polarizer followed by an interference filter before reaching a photomultiplier. The time decaying photomultiplier signal is electronically integrated by a boxcar integrator for a time interval greatly exceeding the radiative lifetime of the $8D_{3/2}$ state. Finally, a computer calculates the ratio of the integrated fluorescent intensities polarized parallel and perpendicular to the quantization axis, and takes the average of data generated by typically 300 laser shots. This ratio is plotted as a function of the magnetic field generated by a Helmholtz coil. The resulting plot is known as a decoupling curve. The shape of the theoretically computed decoupling curve very closely resembles a Lorentzian function centered at zero magnetic field. A Lorentzian curve was therefore fit to the data using a least squares fit. The hyperfine magnetic dipole constant a is determined by the magnetic field halfwidth of this decoupling curve. It can be shown that the field halfwidth is independent of the excited state lifetime τ provided $2\pi a\tau \gg 1$. Furthermore, the shape of the decoupling curve is unaffected by the excited state number density and hence the laser energy, since a ratio of time integrated intensities is measured. The resulting value of $a = 4.0 \pm 0.10$ MHz. agrees with that obtained by a Quantum Beats experiment.²

² J. S. Deech et al, J. Phys. B **8** No. 9, 1406 (1975).

HYPERFINE STRUCTURE STUDIES OF ^{93}Nb USING
LASER OPTOGALVANIC SPECTROSCOPY

Ranjit Singh and G.N.Rao
Department of Physics, Indian Institute of Technology,
Kanpur 208016, India.

Hyperfine structure of seven transitions of niobium in the wavelength range 570-600 nm have been studied using Doppler limited high resolution optogalvanic spectroscopy. The sample was prepared by sputtering technique employing a Nb/Ne hollow cathode lamp. A frequency stabilized single mode ring dye laser was used for excitation and optogalvanic spectroscopy techniques for detection. Magnetic dipole and electric quadrupole hyperfine coupling constants were evaluated from the observed well resolved hyperfine components. We report the hyperfine coupling constants for twelve levels out of which values for four levels are reported for the first time. Recently, we reported¹⁾ the hyperfine structure measurements of 12 levels in the configurations $4d^45s$, $4d^35s^2$, $4d^35s5p$ and $4d^45p$. As extension of this work, we report here the hyperfine structure of twelve more levels.

The stability and the linewidth of the dye laser was better than 1 MHz. The dye laser can be scanned electronically over a range of 30 GHz. Transition of interest was selected by using a wavemeter (Burleigh WA20) which reads vacuum wavelength to an accuracy of 0.001 nm. The laser beam was chopped at a frequency in the range 300-600 Hz using a mechanical chopper. Changes in the impedance of the discharge were monitored by picking up the signals across a ballast resistor using a dc blocking capacitor. These signals were fed to a lock-in amplifier through a fast over voltage protection circuit. Frequency calibration was achieved by recording the transition signals of a 300 MHz FSR, confocal Fabry-Perot interferometer (Coherent 216).

VIII-10

Measured hyperfine coupling constants A and B. The uncertainties in A are given parenthatically. The uncertainties in the values of B are ≈ 35 MHz.

Level	Energy	This work		Others ^(a)	
		A(MHz)	B(MHz)	A(MHz)	B(MHz)
$4d^3 5s^2 - a^4 P_{3/2}$	5297.92	495.5(6)	30	497.7569(16)	59.902(1.4)
$4d^4 5s - a^4 D_{3/2}$	8705.32	-136.9(6)	-69	-143.3225(217)	- 10.761(178)
$4d^4 5s - a^4 D_{7/2}$	9497.52	-474.4(2)	90	-477.0373(35)	126.899(81)
$4d^5 - a^6 S_{5/2}$	11344.70	-645.0(7)	-	-639.3786(79)	- 0.061(92)
$4d^4 5s - b^4 D_{7/2}$	15282.35	957.3(5)	---	---	---
$4d^4 5p - z^4 P_{1/2}^0$	22006.74	-273.7(13)	---	-267.3(3)	---
$4d^4 5p - y^4 F_{5/2}^0$	26060.65	261.1(3)	---	266.7(3)	46.1(48)
$4d^4 5p - y^4 F_{9/2}^0$	26440.33	325(2)	120	337.61(20)	88.6(81)
$4d^3 5s 5p - y^6 P_{3/2}^0$	28278.25	743.2(6)	19	747.1(8)	14.7(76)
$4d^3 5s 5p - y^6 P_{5/2}^0$	28652.66	746.2(6)	-154	---	---
$4d^4 5p - v^4 F_{9/2}^0$	32605.39	264.7(4)	---	---	---
$4d^4 5p - w^4 G_{9/2}^0$	32802.44	632.5(3)	16.5	---	---

(a) L.Fraenkel, C.Bengtsson, D.Hanstorp, A.Nyberg and J.Persson, Z.Phys. D8, 171 (1988).

¹⁾ Ranjit Singh and G.N.Rao, Phys. Scripta, 40,170 (1989).

CASCADE-CORRECTED LIFETIME MEASUREMENTS FOR THE
 $3s3p^2\ ^2S$, 2P and 2D LEVELS OF TiX, FeXIV AND NiXVI

E.H. Pinnington, A. Tauheed and W. Ansbacher
 Department of Physics, University of Alberta,
 Edmonton, Alberta T6G 2J1, Canada.

E. Träbert
 Harvard College Observatory
 60 Garden St.,
 Cambridge, Mass. 02138, U.S.A.

P.H. Heckmann and G. Möller
 Experimentalphysik III, Ruhr-Universität
 4630 Bochum 1, Fed. Rep. Germany

Spectra emitted by laser-produced plasmas have been analyzed recently by Redfors and Litzen [1] to establish the doublet levels belonging to the configurations $3p^3$ and $3s3p^3d$ for the Al-like ions from Ca VIII to NiXVI. Using foil excitation of ion beams produced at the Bochum Dynamitron Tandem Laboratory, we have recorded intensity decay curves for transitions from all the $3s3p^2$ doublet levels for TiX, FeXIV and NiXVI. We have also made use of the analysis by Redfors and Litzen to record decay curves for transitions into the $3s3p^2$ levels from the doublet levels belonging to the $3p^3$ and $3s3p^3d$ configurations in these ions. We list here the lifetimes obtained from our decay curves for the $3s3p^2$ doublet levels using both multi-exponential curve-fitting and the ANDC method [2]. We compare these results with the semi-empirical Hartree-Fock calculations by Fawcett [3]. This work was supported financially by NSERC and the Alexander von Humboldt Stiftung.

Level	Method	Lifetimes of the $3s3p^2$ Doublet Levels (in ps)		
		TiX	FeXIV	NiXVI
$^2S_{1/2}$	M-E Fit	115±5	77±4	51±2
	ANDC	109±10	61±6	38±4
	Theory	100	50	37
$^2P_{1/2}$	M-E Fit	60±4	45±2	36±2
	ANDC	43±5	35±7	24±4
	Theory	39	29	26
$^2P_{3/2}$	M-E Fit	56±8	46±3	28±2
	ANDC	34±5	34±7	21±2
	Theory	37	24	20
$^2D_{3/2}$	M-E Fit	890±40	550±20	340±20
	ANDC	850±60	340±60	290±20
	Theory	830	450	330
$^2D_{5/2}$	M-E Fit	970±30	700±20	500±20
	ANDC	950±50	530±40	400±30
	Theory	930	540	450

1. A. Redfors and U. Litzen, J. Opt. Soc. Am. B6, 1447 (1989).
2. L.J. Curtis et al, Phys. Scripta 2, 216 (1970).
3. B.C. Fawcett, At. Data Nucl. Data Tables 28, 557 (1983).

LASER SPECTROSCOPY ON COPPER AND SILVER ATOMS

J. Bengtsson, J. Carlsson, P. Jönsson, J. Larsson,
L. Sturesson and S. Svanberg

Department of Physics, Lund Institute of Technology, Lund, Sweden

Lifetimes and hyperfine structures of copper and silver atoms have been studied with different laser spectroscopic techniques.

Using the delayed coincidence technique with a continuous mode-locked dye laser as the source of the excitation light, accurate determinations of lifetimes and hyperfine structures of the copper $3d^{10}4p \ ^2P$ and silver $4d^{10}5p \ ^2P$ states have been made. [1,2]

For the higher-lying $3d^{10}5p \ ^2P_{3/2}$ state in copper and the $4d^{10}6p \ ^2P$ and $4d^{10}7p \ ^2P$ states in silver, short UV or VUV excitation is demanded. A pulsed Nd:YAG pumped system was therefore used to investigate these states. For the lifetime studies both time-resolved techniques and the Hanle effect were employed. The high-resolution spectroscopy was performed with either level crossing or optical double resonance techniques or by observing quantum beats in the time-resolved recordings. [3,4]

In addition to these experiments, theoretical calculations have been performed using multi-configuration Hartree-Fock methods. These calculations can be used to explain many of the experimental results. They particularly describe the dominating effects of the $3d^{10}nl - 3d^94s4p$ configuration interaction in copper and the polarization of the 4d shell in silver. [5]

1. J. Carlsson, L. Sturesson and S. Svanberg, *Z. Phys.* D11, 287 (1989).
2. J. Carlsson, P. Jönsson and L. Sturesson, to be published in *Z. Phys.* D.
3. J. Bengtsson, J. Larsson, S. Svanberg and C.-G. Wahlström, *Phys. Rev.* A41, 233 (1990).
4. J. Bengtsson, J. Larsson and S. Svanberg, to be published in *Phys. Rev.* A.
5. J. Carlsson, *Phys. Rev.* A38, 1702 (1988).

LASER SPECTROSCOPY OF ATOMIC HYDROGEN

C. D. Thompson, G. H. Woodman, C. J. Foot, P. Hannaford*,
D. N. Stacey, P. E. G. Baird, J. B. Swan† and G. K. Woodgate

Clarendon Laboratory, Parks Road, Oxford, OX1 3PU, United Kingdom

* CSIRO, Division of Materials Science and Engineering,
Clayton, Victoria 3168, Australia

† Department of Physics, University of Western Australia, Nedlands,
Western Australia 6009, Australia

We are studying the $1S_{1/2} - 2S_{1/2}$ transition in atomic hydrogen using the technique of two-photon Doppler-free spectroscopy in order to measure the ground state Lamb shift. The natural linewidth of this transition is only 1.3 Hz giving the potential for a more stringent test of quantum electrodynamics than is possible with r.f. spectroscopy of the $2S_{1/2} - 2P_{1/2}$ interval [1].

The transition is excited with continuous wave 243nm radiation produced by intra-cavity second harmonic generation in a ring dye laser, using beta-barium borate as the frequency doubling material. The 243nm radiation is mode-matched into a servo-controlled enhancement cavity which increases the power density in the interaction region by about an order of magnitude.

In a preliminary experiment [2,3], the transition was excited in a gas cell, and calibrated with respect to a molecular tellurium reference. Results were obtained for the $1S_{1/2}$ Lamb shift in hydrogen and deuterium with an accuracy of better than 1 MHz.

We have recently reported the excitation of the $1S_{1/2} - 2S_{1/2}$ transition in an atomic beam [4]. The metastables are Stark quenched at a distance of 8 cm downstream. The resulting Lyman- α fluorescence is monitored with a photomultiplier. A typical scan is shown in Fig. 1.

The present stage of the experiment is to excite the metastable atoms in the beam to $n = 4$ states by transverse illumination with a second 486nm c.w. dye laser. This follows the approach developed by Hänsch and his co-workers [5]: a direct measurement of the frequency difference of the two lasers allows a determination of the $1S_{1/2}$ Lamb shift without the need for an absolute frequency standard or a precise value of the Rydberg constant. Progress will be reported at the conference.

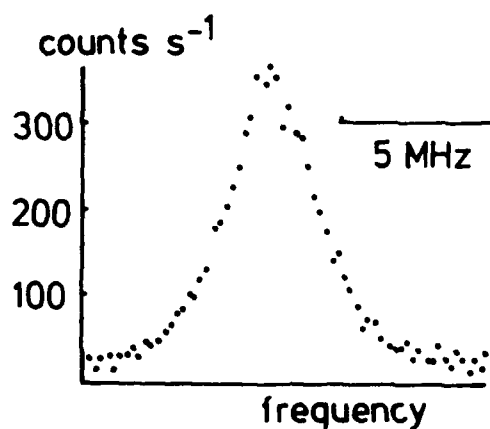


Figure 1. Quench signal as a function of laser frequency (measured at 486 nm).

1. See, for example, "The Hydrogen Atom", ed. G. F. Bassani, M. Inguscio and T. W. Hänsch, Springer Verlag Berlin, Heidelberg 1989; "The Spectrum of Atomic Hydrogen-Advances", ed. G. W. Series, World Scientific Publishing 1988.
2. M. G. Boshier, P. E. G. Baird, C. J. Foot, E. A. Hinds, M. D. Plimmer, D. N. Stacey, J. B. Swan, D. A. Tate, D. M. Warrington and G. K. Woodgate, *Nature* **330** 463 (1987).
3. M. G. Boshier, P. E. G. Baird, C. J. Foot, E. A. Hinds, M. D. Plimmer, D. N. Stacey, J. B. Swan, D. A. Tate, D. M. Warrington and G. K. Woodgate, *Phys. Rev.* **A40**, 6169 (1989).
4. C. J. Foot, P. Hannaford, D. N. Stacey, C. D. Thompson, G. H. Woodman, P.E.G. Baird, J. B. Swan and G. K. Woodgate, *J. Phys. B.* **23**, L203 (1990)
5. C. Wieman and T. W. Hänsch, *Phys. Rev.* **A22**, 192 (1980).

CIRCULAR-METASTABLE DI-EXCITED STATES OF BARIUM

L.CHEN, G.SPIESS, F.ROUSSEL, M.CHERET, T.BOLZINGER
Service de Physique des Atomes et des Surfaces
CEN-Saclay 91191 Gif sur Yvette cedex France

J.HARE and M.GROSS
Département de Physique de l'Ecole Normale Supérieure
Laboratoire de Spectroscopie Hertzienn^e
24, rue Lhomond 75231 Paris cedex 05 France
*Laboratoire associé au CNRS et à l'Université Pierre et Marie Curie

Di-excited Rydberg states play an important role in the study of the correlation effects in atomic systems. Several researches have shown that di-excited atoms, lying above the first ionization limit, autoionize rapidly into an ejected electron and an ion, via the Coulomb type interaction between the two excited electrons[1][2]. The autoionization rate decreases rapidly when the angular momentum of the outer electron increases[3]. We present here the first investigation[4] of circular di-excited long-lived Ba atoms with one of the excited electrons in the 5d metastable state and the other in the 21c state (c stands for circular and means here $l=m=n-1=20$). We have observed very long autoionization lifetimes which are different for the two fine-structure components of the inner electron: $t \sim 1\mu\text{s}$ for Ba ($5d_{5/2}, 21c$) and $t > 400\mu\text{s}$ for Ba ($5d_{3/2}, 21c$).

Barium circular atoms with $n=21$ are initially created using the adiabatic crossed-field method, proposed by Delande and Gay[5] and realized in lithium[6] and Barium[7]. According to the Isolated Core Excitation method (ICE)[8], the $6s_{1/2}$ inner electron is then excited either to the $6p_{1/2}$ or to the $6p_{3/2}$ states by a laser adjusted to the corresponding resonance of the Ba^+ ion. The Ba($5d, 21c$) levels are finally populated by spontaneous emission from the inner $6p_i$ electron according to the following branching ratio: $6p_{1/2} \rightarrow 5d_{3/2}$, 30%; $6p_{3/2} \rightarrow 5d_{5/2}$, 24% and $6p_{3/2} \rightarrow 5d_{3/2}$, 3%. The atoms in different atomic states are then detected selectively by the method of electric field ionization according to their ionization thresholds. It has been found that the field-ionization threshold depends mainly on the outer electron, the metastable-circular Ba($5d_i, 21c$) atoms ionize at the same threshold field as the initial Ba($6s_{1/2}, 21c$) circular atoms.

It has been observed that the properties of the metastable circular atoms depend strongly on the fine structure component of the inner electron.

- Ba($5d_{3/2}, 21c$) atoms are very stable against the following decay processes: radiative decay of both electrons and autoionization to the Ba^+ ($6s_{1/2}$) ground state continuum, the lifetime of the latter process has been estimated to be longer than 400 μs . The overall lifetime of the atoms (100 μs) is limited by the blackbody radiative transition of the outer circular electron[7].

- Ba($5d_{5/2}, 21c$) level lies just 0.07eV above the threshold of the Ba^+ ($5d_{3/2}$) second continuum, which is favorable for the autoionization process. It has been confirmed that the dominant decay mechanism for these atoms is the near-threshold autoionization to the Ba^+ ($5d_{3/2}$), leading to a lifetime of 1 μs . A direct time analysis technique has been used for this low rate decay measurement.

REFERENCES

- [1] P. Camus, T.F. Gallagher, J.M. Lecomte, P. Pillet, L. Pruvost and J. Boulmer Phys. Rev. Lett. 62, 2365, (1989).
- [2] U. Eichmann, V. Lange and W. Sandner Phys. Rev. Lett. 64, 274 (1990).
- [3] R.R. Jones and T.F. Gallagher Phys. Rev. A 38, 2846, (1988).
- [4] F. Roussel, M. Chéret, L. Chen, T. Bolzinger, G. Spiess, J. Hare and M. Gross submitted to Phys. Rev. Lett.
- [5] D. Delande and J.C. Gay Europhys. Lett. 5, 4, (1988).
- [6] J. Hare, M. Gross and P. Goy Phys. Rev. Lett. 61, 1938, (1988).
- [7] M. Chéret, F. Roussel, T. Bolzinger, G. Spiess, J. Hare and M. Gross Europhys. Lett. 9, 3, (1989).
- [8] W.E. Cooke, T.F. Gallagher, S.A. Edelstein and R.M. Hill Phys. Rev. Lett. 40, 178, (1978).

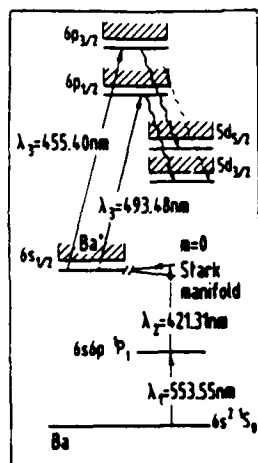


FIG.1

Energy diagram (for $n=21$) of the relevant Ba levels and Ba^+ continua. The first electron, excited by L1 and L2, is transferred to $21c$ (circular state) in crossed-fields. The second electron, excited to $6p_{1/2}$ or $6p_{3/2}$ by L3, decays spontaneously to the fundamental state $6s_{1/2}$ or to a metastable state $5d_{1/2}$. Finally di-excited metastable atoms $Ba(5d_{1/2}21c)$ are prepared.

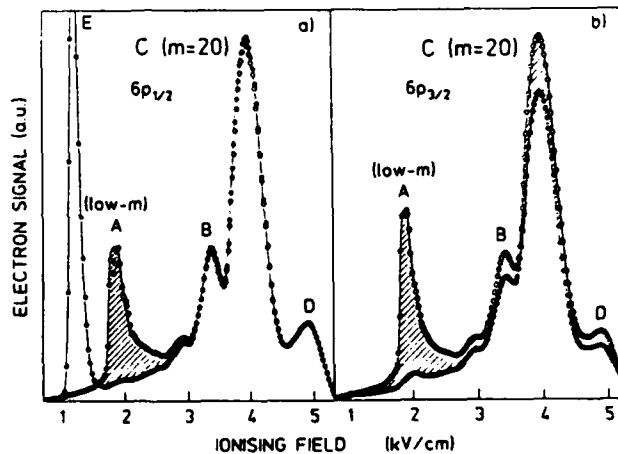


FIG.2 Field-ionization signals.

Open circles: without excitation of the inner electron

peak A: low- m states, $n=21$

peak C: main circular state $Ba(6s_{1/2}21c)$, $m=20$

peak B(D): neighboring circular state $n=22(20)$

Filled circles: with excitation of the inner electron

a) to the $6p_{1/2}$ level.

b) to the $6p_{3/2}$ level.

peak C: $Ba(6s_{1/2}21c)$ and $Ba(5d_{3/2}21c)$, signal losses of peak C in b) according to the autoionization of $Ba(5d_{3/2}21c)$

peak E: saturated electron signal of autoionization

Hatched areas: signal losses due to autoionization

HIGH PRECISION ISOTOPE SHIFT MEASUREMENT IN HELIUM

Ping Zhao, J.R. Lawall, and F.M. Pipkin
 Department of Physics, Harvard University, Cambridge, MA 02138

We report a high precision isotope shift measurement between ^3He and ^4He of the transition $2^3\text{S} \rightarrow 2^3\text{P}$ with a laser-microwave spectroscopy technique. Our result is by far the most precise isotope shift measurement ever made for a multi-electron system.

As a three body system, helium has attracted the attention of both mathematicians and physicists for many years. A recent new variational technique by Drake [1] gives very high precision calculations for both energy levels and wave functions for this atom. Precision measurement of the isotope shift provides a good test of the theory. This is especially true for the low-lying states, where the specific mass shift, $(P_1 \cdot P_2)\mu/M$, is large. The specific mass shift, which is generally difficult to calculate and requires a good knowledge of the wave functions, is very sensitive to any configuration interaction.

The isotope shift is about 33668 MHz for this helium transition. Based on previous experimental results [2-4], the ^3He : $2^3\text{S}_{1, F=3/2} \rightarrow 2^3\text{P}_{0, F=1/2}$ line should fall in between the ^4He : $2^3\text{S}_1 \rightarrow 2^3\text{P}_{1,2}$ lines. Our experiment measures these gaps with a new technique and thereby obtains a high precision value of the isotope shift for this transition.

The standard method to measure the isotope shift is to scan the laser across the spectral lines and use the frequency markers produced by a Fabry-Perot etalon to measure the separation. Due to the difficulty of finding the precise line center, the precision of this method is limited to several MHz. We have developed a new way to make the isotope shift measurement, which we call "laser-microwave spectroscopy". A single mode laser with frequency ν is passed through an EOM frequency shifter that is driven by a controlled microwave frequency f . The EOM generates two sidebands on the laser light of frequencies $\nu \pm f$. The carrier ν is tuned to one isotope transition and f is adjusted so that the sideband $(\nu+f)$ or $(\nu-f)$ is on the other isotope transition. Then f is fixed and the laser is scanned across the two isotope transitions simultaneously. The scan is slow and narrow ranged so the line centers can be located precisely. This new technique overcomes the shortcomings of the old method and can improve the precision by two orders of magnitude. The only requirement for employing this technique is that the two isotopes must not be in the same sample. In addition, we have developed a technique we call "Doppler-shifted saturation spectroscopy". When the laser beam contains two frequencies with a fixed separation and a transition falls in the exact center of the two frequencies, there will be a signal peak. This is due to one frequency burning a hole on one side of the Doppler profile (rather than at the center) and the other frequency coming from the opposite direction probing it. With this method, we can use the carrier to saturate the transition and use the sideband to probe, which may be advantageous if the sideband power is too low. Thus the signal to noise ratio can be increased significantly.

The ^3He and ^4He metastable states 2^3S_1 are prepared in two separate low pressure rf discharge cells. The cells are magnetically shielded by mu-metal tubes. The LNA ($\text{La}_{1-x}\text{Nd}_x\text{MgAl}_{11}\text{O}_{19}$) laser, whose output is at $1.083\ \mu\text{m}$, is a home made ring laser stabilized to an external cavity. Pumped by the 4 W green line (514 nm) from an Ar^+ laser, it puts out 100 mW single mode with a bandwidth of 200 kHz. A LiTaO_3 crystal EOM generates the sideband frequency which can be precisely tuned by a synthesizer. The laser is then scanned so the carrier and sidebands cross the ^3He and ^4He transitions, and the saturated absorption signals are detected and recorded simultaneously. The scan is repeated for different sideband frequency settings. To avoid systematic shifts, care has been taken to use cells with different pressures, and to use different laser powers, microwave powers, and rf discharge levels.

The results are: $\nu_0 - \nu_2 = 810.61(10)\ \text{MHz}$
 $\nu_1 - \nu_0 = 1480.68(10)\ \text{MHz}$

where $\nu_0 = ^3\text{He}: 2^3\text{S}_1, F=3/2 \rightarrow 2^3\text{P}_0, F=1/2$ and $\nu_{1,2} = ^4\text{He}: 2^3\text{S}_1 \rightarrow 2^3\text{P}_{1,2}$. The result for $\nu_0 - \nu_2$ agrees with the previous less precise measurement [4] of 811(3) MHz. To test the reliability of our results, the ^4He fine structure $2^3\text{P}_2 - 2^3\text{P}_1$ deduced from our data, 2291.29(14) MHz, is compared with the known high precision measurement [2] of this splitting, which is 2291.196(5) MHz. The agreement is good. The isotope shifts are as follows:

Transition	This work	Theory [1]
$2^3\text{S}_1 - 2^3\text{P}_0$	33667.96(10) MHz	33667.86(5) MHz
$2^3\text{S}_1 - 2^3\text{P}_1$	33667.67(10) MHz	33667.57(5) MHz
$2^3\text{S}_1 - 2^3\text{P}_2$	33668.66(10) MHz	33668.56(5) MHz

The results agree with theory within the quoted uncertainty.

In conclusion, the isotope shift between ^3He and ^4He of the $2^3\text{S} \rightarrow 2^3\text{P}$ transition has been measured to a precision of 3 ppm, or 100 kHz, with yet further improvement expected. Our result is 30 times more precise than the previous measurement and is by far the most precise isotope shift measurement ever made for a multi-electron system. It provides, for the first time, not only a check for the specific mass shift, but also for small corrections such as the nuclear volume shift, the relativistic corrections involving the coupling between electrons, and the QED contributions. The laser-microwave spectroscopy technique (including the Doppler-shifted saturation spectroscopy) is generally applicable and should be a very useful experimental method.

We would like to thank G.W.F. Drake for communicating his results before publication. This research is supported by NSF Grant PHY-87-04527.

- G.W.F. Drake et al., Nucl. Instrum. Methods Phys. Res. B 31, 7 (1988), J. Opt. Soc. Am. B 5, 2207 (1988), and private communications.
- V.W. Hughes et al., Phys. Rev. 169, 55 (1968), Phys. Rev. A 2, 86 (1970), Phys. Rev. A 24, 264 (1981), Phys. Rev. A 24, 279 (1981).
- E.A. Hinds et al., Phys. Rev. Lett. 50, 828 (1983), Phys. Rev. A 32, 2615 (1985), and Phys. Rev. A 32, 2712 (1985).
- D. Bloch et al., J. Phys. B 18, 1093 (1985).

STERNHEIMER FREE DETERMINATION OF THE ^{47}Ti NUCLEAR QUADRUPOLE MOMENT FROM HYPERFINE STRUCTURE MEASUREMENTS

E. Stachowska*, J. Dembczyński*, W. Ertmer
Institut für Angewandte Physik der Universität Bonn, FRG
*Instytut Fizyki, Politechnika Poznańska, Poznań, Poland

In order to determine the nuclear quadrupole moment $Q(^{47}\text{Ti})$ free of Sternheimer corrections the hyperfine splitting of 12 metastable states of ^{47}Ti has been measured and the parametrization method for the hyperfine structure analysis of 3d-shell atoms [1] has been used.

The hfs-splittings of the states: $3d^2 4s^2 a^3 P_{1,2}$, $3d^3 (^4F) 4s a^5 F_{2,3,4,5}$, $b^3 F_{2,3,4}$, $3d^3 (^2G) 4s a^3 G_{4,5}$, $3d^3 (^4F) 4s a^5 F_1$, have been measured by laser induced fluorescence. The first 11 of these states have been measured additionally very precisely by a laser-rf double resonance method. The ABMR-LJRF (atomic beam magnetic resonance-detected by laser induced resonance fluorescence) detection scheme consists of two interaction regions of an atomic beam with a single mode continuous wave dye laser beam crossing the atomic beam twice orthogonally. In the first region one of the hfs states is depleted selectively by optical pumping. In the second interaction region the residual population of this depleted level is probed by the laser induced fluorescence signal. If radio frequency (rf) transitions from a neighbouring hfs level to the depleted level are induced in an rf loop between the two interaction regions, the resulting repopulation of the depleted level can be detected very efficiently. The linewidth of this rf resonance signal does not depend on the spectral width of the laser light. This permits to measure hfs-splittings of the ^{47}Ti levels very precisely, with an accuracy of several kHz. The corresponding hyperfine structure constants A_{exp} and B_{exp} are given in Table 1. More details of the experimental set-up is given elsewhere [2,3].

Taking into account the results given in Table 1 and earlier hfs measurements [4,5] the hfs of altogether 17 fine structure states has been analysed by the parametrization of the one- and two-body interactions in the atomic hfs for the model space $(3d+4s)^{N+2}$ ($N=2$). This parametrization method allows the evaluation of SL- and N-dependent contributions to the observed hfs splitting, which arise from the mixing of far configurations via Coulomb interaction. For the "real" fine structure states ψ written in SL-basis the hfs magnetic dipole interaction constant A and the hfs electric quadrupole interaction constant B are determined as [1]:

$$A = \sum_{n_1} \alpha_{n_1}^{jk}(\psi) a_{n_1}^{jk} + \sum \alpha(\psi)_i a_i \quad (1)$$

$$B = \sum_{n_1} \beta_{n_1}^{jk}(\psi) b_{n_1}^{jk} + \sum \beta(\psi)_i b_i \quad (2)$$

$\kappa\kappa = 01, 12, 10$, $n_1 = 3d, 4s$, $i = 1, \dots, 11$

$\kappa\kappa = 02, 13, 11$, $n_1 = 3d$, $i = 1, \dots, 8$

where $a_{n_i}^{st}$ and $b_{n_i}^{st}$ are hfs one-body radial parameters and $\alpha_{n_i}^{st}$ and $\beta_{n_i}^{st}$ are their corresponding angular coefficients in intermediate coupling scheme. The terms $\alpha_i(\psi)a_i$ and $\beta_i(\psi)b_i$ represent the contributions of the hfs two-body interactions. For each contribution the radial part is common for all states of the whole model space $(3d+4s)^4$, whereas the corresponding angular parts depend on the individual fine structure state. The angular part can be calculated exactly from the formulae given in [1], if precise wavefunctions in intermediate coupling scheme will be available. The radial parameters $a_{n_i}^{st}$, a_i , $b_{n_i}^{st}$ and b_i have been fitted to the experimental hfs constants A and B (corrected for the off-diagonal second order perturbation) using the expressions (1) and (2). For such linear equation systems the values of hfs one- and two-body radial parameters have been obtained and the SL- and N-dependent contributions have been separated. This permits the determination of the nuclear quadrupole moment Q free from Sternheimer corrections up to second order from the independent set of two-body hfs parameters [1]:

$$Q_i = (2\mu_B/e^2) b_i/a_i \quad i=1,\dots,8 \quad (3)$$

The preliminary value of $Q(^{47}\text{Ti})$ free of Sternheimer corrections obtained from (3) is 0.303 b [6].

Table 1. The experimental values of hfs constants A und B.

State	J	A [MHz]	B [MHz]
$3d^24s^2 a^3P$	1	2.6646(1)	23.897(1)
	2	-25.2147(1)	-47.822(1)
$3d^3(^4F)4s a^5F$	1	31.6(5)	-6.8(1.0)
	2	-43.8818(25)	-5.088(20)
	3	-62.8456(30)	-9.290(38)
	4	-70.6106(23)	-17.395(30)
	5	-74.8450(25)	-28.674(53)
$3d^3(^4F)4s b^3F$	2	-120.758(1)	-20.828(8)
	3	-25.3916(4)	-22.865(5)
	4	10.1520(3)	-29.224(5)
$3d^3(^2G)4s ^3G$	4	-58.386(1)	22.478(8)
	5	-90.284(1)	26.110(8)

Part of this work were performed under project CPBP 1.06.1.04.

Thanks are due to the Deutsche Forschungsgemeinschaft for financial support.

1. J. Dembczyński, W. Ertmer, U. Johann, P. Unkel, Z. Phys. A-Atoms und Nuclei 321, 1 (1986).
2. J. Dembczyński, W. Ertmer, U. Johann, S. Pensein, P. Stinner, Z. Phys. A-Atoms und Nuclei 291, 207 (1979).
3. W. Ertmer, U. Johann, J. Dembczyński, Z. Michalski, Z. Phys. D 2, 67 (1986).
4. K.H. Channappa, J.M. Perlebury, Proc. Phys. Soc. 88, 1145 (1966)
5. W.J. Childs, private communication.
6. R. Aydin, E. Stachowska, U. Johann, J. Dembczyński, P. Unkel, W. Ertmer, Z. Phys. D 15, 281 (1990).

**THE SODIUM D-LINES IN MAGNETIC FIELDS
UP TO 1 TESLA**

M. Musso, L. Windholz, H. Jäger
Institut für Experimentalphysik
Technische Universität Graz
Petersgasse 16
A-8010 Graz / Austria

Continuing our investigations on the behaviour of the hyperfine components of the alkali D-lines in external fields [1,2,3,4,5,6,7], we present results concerning the splitting of the sodium D-lines in a magnetic field of strength between 0.08 T and 1 T (800 to 10000 Gauss) [8,9,10,11]. This investigation is a continuation of the measurements described in [2,3], where the maximum magnetic field amounted to about 280 Gauss.

The measurements were performed by laser-atomic beam-spectroscopy using a cw ring-dye-laser with 1 MHz linewidth. Due to the very large splitting of the lines at high field strengths we had to take several scans at each fixed field strength. The frequency of the laser at the beginning of each scan was determined with a precision of ± 6 MHz with the help of a lambda-meter [12]. During the scan the transmission maxima of a marker etalon with 197.5974(3) MHz free spectral range were recorded together with the spectra. The magnetic field strength was measured with a NMR-Gaussmeter to an accuracy of 1 Gauss.

We determined the distance between the center of gravity of the D_1 - and D_2 -line to 515523(4) MHz, compared to 515523(30) MHz as given in [13].

Our measurements in presence of the magnetic field were compared with calculations based on the assumption that the two fine structure levels do not interfere with each other. That means that we assumed J to be a good quantum number and g_J to be constant. We observe a deviation of the experimental position of the hyperfine components belonging to the states

$M_J = \pm 1/2$ of the upper levels ${}^2P_{1/2}$ and ${}^2P_{3/2}$ from the calculated position. This deviation closely fits the relation [14,8,9,15]:

$$\Delta E({}^2P_{3/2, M_J=\pm 1/2}) = \frac{2}{9} \frac{\mu_B^2 B^2}{(E({}^2P_{3/2}) - E({}^2P_{1/2}))}$$

$$\Delta E({}^2P_{1/2, M_J=\pm 1/2}) = -\Delta E({}^2P_{3/2, M_J=\pm 1/2})$$

which describes the repulsion between the states with $M_J = \pm 1/2$ of the two fine structure levels ${}^2P_{3/2}$ and ${}^2P_{1/2}$.

1. L. Windholz and C. Neureiter, Phys. Lett. **109A** (4), 155 (1985)
2. L. Windholz, Z. Phys. A **322**, 203 (1985)
3. L. Windholz and M. Musso, Z. Phys. D **8**, 239 (1988)
4. L. Windholz and M. Musso, Phys. Rev. A **39** (5), 2472 (1989)
5. L. Windholz, Z. Phys. D **14**, 361 (1989)
6. L. Windholz, Z. Phys. D **15**, 87 (1990)
7. L. Windholz, H. Jäger, M. Musso and G. Zerza, Z. Phys. D **16**, 361 (1989)
8. H. Ackermann, Z. Phys. **194**, 253 (1966)
9. W. Hartmann, Z. Phys. **240**, 323 (1970)
10. H. Hori, M. Miki, M. Date, J. Phys. Soc. Jap. **51** (5), 1566 (1982)
11. M. Musso, Ph. D. Thesis, (1990)
12. H. Jäger, M. Musso, C. Neureiter and L. Windholz, Opt. Eng. **29** (1), 42 (1990)
13. W. C. Martin and R. Zalubas, J. Phys. Chem. Ref. Data, **10** (1), 153 (1981)
14. H. Kopfermann, Kernmomente, Akademische Verlagsgesellschaft (1956)
15. I. I. Sobelman, Atomic Spectra and Radiative Transitions, Springer Verlag (1979)

SPECTROSCOPY OF HIGH ANGULAR MOMENTUM RYDBERG STATES IN Si^{10+} A.E. Livingston, F.G. Serpa, and E.J. Galvez¹

Department of Physics, Notre Dame University, Notre Dame, Indiana 46556 USA

¹ Department of Physics and Astronomy, Colgate University, Hamilton, New York 13346 USA

High angular momentum Rydberg states in beryllium-like ions are sensitive to strong polarization effects due to the large polarizabilities of their lithium-like atomic cores. This results in resolvable L-structure splittings through the spectroscopic observation of emission from $\Delta n \neq 0$ transitions involving the $1s^2 2snL$ states. In addition to providing basic spectroscopic data for an unexplored class of high Z berylliumlike transitions, wavelength measurements for such transitions are also valuable in determining the ionization energy of the ion as well as the electrostatic polarizability of the next ionization stage, represented by the ionic core. However, these high L Rydberg states represent perhaps the most poorly understood simple atomic structures at high Z, both experimentally and theoretically. First, there are few details available concerning the accurate description of the associated complete polarization structure¹. Second, the presence of the displaced (or doubly-excited) $1s^2 2pnL$ Rydberg series of levels that partially overlaps the normal $1s^2 2snL$ levels causes strong Z-dependent configuration interaction effects that have not been studied. Third, very few observations of transitions involving these high L states exist. Several years ago we performed the first measurements and analysis of such structures at high Z for the $n=7$ transition in S XIII² using foil excited fast ions (beam-foil excitation). There we demonstrated that the complexities of atomic core polarization effects and configuration interaction contributions must be considered to begin to provide correct interpretations of these transition structures. We have subsequently extended these initial studies to include selected states from $n=5$ to $n=8$ in S XIII and Cl XIV³. Very recently, the observation of Rydberg transitions in highly-ionized silicon was reported for the first time in a different excitation source, a high temperature theta-pinch plasma⁴.

We have undertaken a new spectroscopic study of high angular momentum Rydberg states in highly ionized silicon using fast ion excitation at the Notre Dame Accelerator Laboratory. A primary goal of this work is to extend detailed observations to states with $L > 8$ in berylliumlike Si XI. The first result of these studies is our measurement of the structure of the $n = 9 - 10$ transition in Si XI. This measurement can be compared with the discussions in ref. 4, which proposed using a simple scaled hydrogenlike analysis of this transition structure to associate observed relative line intensities with relative excited state population densities in the plasma. Although that analysis represents a promising method for utilizing high L Rydberg state transitions as a plasma diagnostic, we have pointed out in a recent Comment⁵ that the interpretations of the atomic structure in ref. 4 are highly oversimplified. Our measured partial structure of the $n = 9 - 10$ transition is shown in Fig. 1, where we also present comparison with our multiconfiguration Dirac Fock calculations for the high angular momentum structure. The Si^{10+} ions were obtained by exciting a beam of 42 MeV silicon ions with a $20 \mu\text{g}/\text{cm}^2$ carbon foil. The fluorescent emission from the $n = 10$ state in Si XI was observed using a vacuum ultraviolet monochromator and a UV sensitive photon counting photomultiplier. In Fig. 1, the substantial wavelength shifts displayed by all but the two highest angular momentum components result from perturbations of the lower state $2s9L$ levels by nearby $2p6L$ levels. The $2s10L$ upper state levels are essentially unperturbed.

Further details of our measurements and calculations of the $n = 9 - 10$ transition structure in Si XI will be presented. Also, new results will be reported for the $n = 8 - 9$ transition structure, which also reflects the effects of perturbations of the $2s9L$ levels. Additional complexities in the structures of high L Rydberg states in berylliumlike ions will be discussed.

1. L.J. Curtis, Phys. Scripta 39, 447 (1989).
2. A.J. Mazure et al, Phys. Rev. A 32,3775 (1985).
3. Y.N. Lu et al, Nucl. Instrum. Meth. B 31,157 (1988).
4. R. König et al, Phys. Rev. Lett. 62, 1750 (1989).
5. A.E. Livingston et al, Phys. Rev. Lett. 64, 2335 (1990).

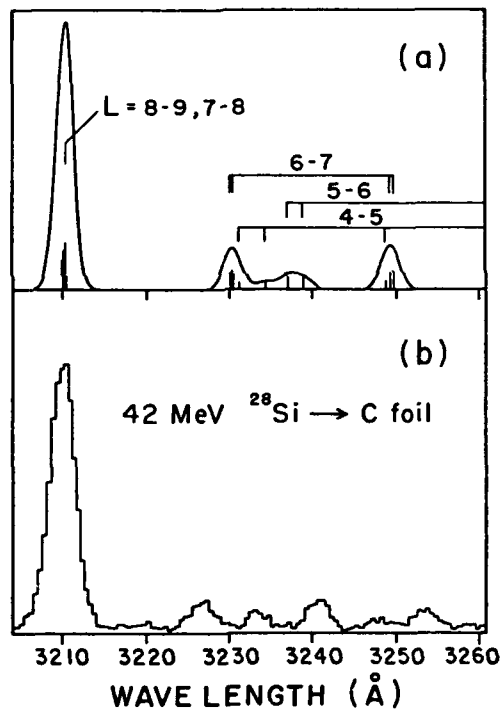


Fig.1 High angular momentum structure of the $n = 9 - 10$ transition in berylliumlike Si XI:
 (a) MCDF calculations with instrumental linewidths applied, (b) fast-ion measurements.

**DOUBLY-EXCITED $6p_{1/2,3/2}np$ $J=1$ AND $4f_{5/2,7/2}nf$ $J=5,6$
AUTOIONIZING RYDBERG SERIES IN BARIUM**

R.J. de Graaff, M. Abutaleb*, W. Ubachs and W. Hogervorst
Laser Centre Free University Amsterdam
De Boelelaan 1018, 1081 HV Amsterdam, The Netherlands
* Department of Physics, Cairo University, Giza, Egypt

Two classes of relatively long-lived autoionizing states in a two-electron system are known. First, when one of the electrons is in a Rydberg state with high orbital momentum and the one-electron orbitals have only small overlap, the autoionization rates are low as e.g. in $6pnh$ series in Ba [1]. In a second class of states autoionization is inhibited by coincidental interference effects between different interacting states, as e.g. is the case for $5d_{3/2}26d_{3/2}$ $J=0$ [2]. Here we report on a Rydberg series of extremely narrow widths, the $6p_{1/2,3/2}np$ $J=1$ series in barium, that does not fit into these categories. We also present results of an experiment in which we observed $4f_{5/2,7/2}nf_{5/2,7/2}$ ($J=5,6$) states at an energy of approximately 90000 cm^{-1} , about 48000 cm^{-1} above the first ionization limit ($6s_{1/2}$). These states were excited via an isolated core excitation scheme using $5dnf$ levels as intermediate states.

The $6pnp$ $J=1$ states were excited in a two-laser experiment. In an atomic beam containing $6s5d$ 3D_1 metastables, produced in a discharge near the source, the $5d6p$ 3P_0 state was populated with a first pulsed dye laser at $\lambda=602\text{ nm}$. A second laser in the wavelength range $\lambda=260-280\text{ nm}$ further excited the atoms into the four $6p_{1/2,3/2}np_{1/2,3/2}$ $J=1$ Rydberg states. Moreover the $6p_{3/2}nf_{5/2}$ $J=1$ series was excited, which is the only series observed above the Ba^+ $6p_{1/2}$ ionization limit (at 62296.46 cm^{-1}). It should be noted that $6p_{1/2}np$ states cannot be excited from a pure $5d_{3/2}6p_{3/2}$ 3P_0 intermediate state. It is the $6s_{1/2}6p_{1/2}$ configuration mixed into the $5d6p$ 3P_0 state that was probed in this experiment. In Fig. 1 the observed spectrum as a function of energy in the range $61500-62300\text{ cm}^{-1}$ (above the $6s^2$ 1S_0 ground state) is shown. Two $6p_{1/2}np_{1/2,3/2}$ $J=1$ Rydberg series converging to the $6p_{1/2}$ -limit appear. Both series interact in this energy range with the $6p_{3/2}7f$, $6p_{3/2}8f$ and $6p_{3/2}11p$ states, which belong to series converging to the higher $6p_{3/2}$ -limit. The interactions between the five $J=1$ bound Rydberg series observed were parametrized in a seven-channel quantum-defect analysis, where it was assumed that the four $6pnp$ series are coupled to one and the $6pnf$ to a second continuum. Without going into the details we only present here the calculated oscillator strength distribution dS/dE resulting after optimization in this seven-channel quantum-defect model (see Fig. 1). All spectral features could be reproduced very well. An important result of this study is the fact that the scaled linewidth of the $6p_{1/2}np_{3/2}$ $J=1$ series is $n^3\Gamma=0.0024$ (FWHM in a.u.). This is much smaller than expected from earlier experiments on the $6p_{3/2}np$ series [3] and even smaller than the linewidth reported for the $6p_{1/2}nh$ series [1]. Thusfar this effect has not yet been explained satisfactorily. Possibly a cancellation in the contribution of direct and exchange autoionization amplitudes occurs.

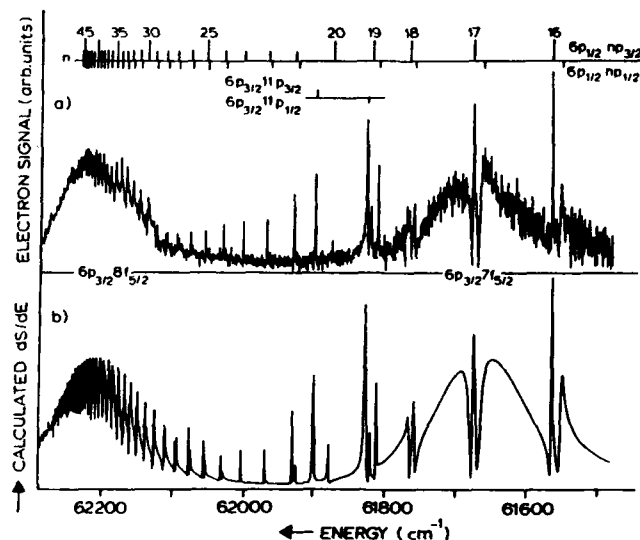


Fig. 1: Observed spectrum of the $6p_{1/2}np$ $J=1$ series with $6p_{3/2}7f$, $6p_{3/2}8f$ and $6p_{3/2}11p$ perturbers. The lower part shows the calculated oscillator strength distribution dS/dE .

The $4fnf$ states were excited with the use of the $5d^2\ ^1G_4$ and the $5d^2\ ^3F_3$ metastable states, also populated in the discharge. The first dye laser ($\lambda \sim 460\text{nm}$ or 390nm resp.) excited the known $5dnf$ ($J=4,5$) states. A second laser ($\lambda \sim 230\text{nm}$) was tuned around the $5d-4f$ ionic resonances, exciting $4fn'f$ states with $n'-n$. Excitation from two different metastable states was necessary to be able to determine the J -value of the excited $4fnf$ states. By detecting electrons ($>4\text{eV}$) we observed $4f_{5/2,7/2}nf_{5/2,7/2}$ states ($J=5,6$ and $8 < n < 44$). Interesting is the strong channel interaction between one of the two $4f_{7/2}nf$ ($J=6$) channels and the $4f_{5/2}nf_{7/2}$ ($J=6$) channel, resulting from a quantum-defect analysis. In progress is an experiment to excite the $n'gnf$ states with the use of a third UV laser followed by photoionization to Ba^{2+} . In these states correlation effects between the two electrons will be strong [4].

- [1] E. A. J. M. Bente and W. Hogervorst, *J. Phys. B: At. Mol-Opt. Phys.* **23** (1990) 1403.
- [2] L. v. Woerkom, J.G. Story and W.E. Cooke, *Phys. Rev. A* **34** (1986) 3457
- [3] J.G. Story, E.G. Yap and W.E. Cooke, *Phys. Rev. A* **39** (1989) 5127
- [4] U. Eichmann, V. Lange and W. Sandner, *Phys. Rev. Lett.* **64** (1990) 274

HIGH-RESOLUTION STUDY OF THE $B^2\Sigma_u^+ - X^2\Sigma_g^+$ SYSTEM OF $^{16}\text{N}_2^+$

T.J. Scholl, A.W. Taylor, R.A. Holt, and S.D. Rosner
 Department of Physics, University of Western Ontario
 London, Ontario N6A 3K7, Canada.

The molecular ion N_2^+ has been studied for many years [1], both as a fundamental system and because of its presence in auroras and comet-tails. The $B^2\Sigma_u^+ - X^2\Sigma_g^+$ system, which is observed in both these sources, is also interesting as an example of strong rotational perturbations, here between the $B^2\Sigma_u^+$ state and the long-lived $A^2\Pi_u$ state. Much of the spectroscopy of this ion has used the classical method of a hollow-cathode discharge viewed with a grating monochromator. With data obtained in this way, Gottscho *et al.* [2] performed a complete deperturbation of several bands of the B-X system of $^{14}\text{N}_2^+$, obtaining spectroscopic constants for the A and B states and the interactions which mix them. The advent of laser spectroscopic techniques coupled with fast ion beams has given Doppler linewidths that are kinematically suppressed by over an order of magnitude. Using a fixed laser frequency and Doppler tuning, we were able to fully resolve the fine and hyperfine structure of $^{14}\text{N}_2^+$ in the (0,1) band of the $B^2\Sigma_u^+ - X^2\Sigma_g^+$ system and obtain the related constants to a few per cent [3].

In the case of $^{16}\text{N}_2^+$, there has been far less work. The most recent is that of Reddy and Prasad [4], who made a conventional measurement of several bands of the $B^2\Sigma_u^+ - X^2\Sigma_g^+$ system. Although establishing that rotational levels with N' in the range $\sim 19-32$ of $v'=0$ level are strongly perturbed by $v'=10$ of the $A^2\Pi_u$ state, they fit their data to a simple model in which the effects of the perturbing A-state vibrational levels are not explicitly represented. These effects then appear approximately in the fit values of the spin-doubling constants γ' and γ'' , and produce values of these constants which can be quite different from their values in a more exact model.

In the present work, we have measured over 40 rotational lines in the (0,1) band by detecting the laser-induced fluorescence produced by the collinear overlap of a fast $^{16}\text{N}_2^+$ beam and a single-mode dye laser beam. The optical detection system consists of two lenses, a mirror, a 391.4 Å interference filter and a photomultiplier viewing a 5 cm-long post-acceleration region. As the laser is scanned, Fabry-Perot fringes are observed for interpolation purposes and Te_2 absorption lines from a vapour cell provide absolute frequency calibration.

A sample spectrum is shown in Fig.1 along with the Fabry-Perot and Te_2 calibration spectra. The large Doppler shift ($\sim 18 \text{ cm}^{-1}$ for 8 keV ions) is accounted for experimentally by observing the LAB-frame frequencies ν_a and ν_p of a given $^{16}\text{N}_2^+$ line with the collinear beams anti-parallel and parallel. The Doppler free transition frequency ν_0 is given by $\nu_0 = \sqrt{\nu_a \nu_p}$. Because the conversion from the LAB frame to the ion rest frame of a relatively small frequency offset can be done accurately with only a crude value of the ion beam energy, the determination of ν_0 values was done for only a few lines across the spectrum. These ν_0 values together with frequency offsets produced an overdetermined set of linear equations for the absolute transition frequencies which were solved for the best fit using singular value decomposition. From this adjustment of the data, we estimate that the relative position of any two lines measured is known to $< 0.002 \text{ cm}^{-1}$, while the absolute frequencies are limited by the accuracy of the Te_2 Atlas [5], which is $\sim 0.003 \text{ cm}^{-1}$.

In the region of large rotational perturbations, we observed eight 'extra' lines representing transitions to states of mixed $A^2\Pi_u$ and $B^2\Sigma_u^+$ character which would go adiabatically to pure $A^2\Pi_u$ as the perturbation goes to zero. The admixture of the relatively short-lived $B^2\Sigma_u^+$ state to the long-lived $A^2\Pi_u$ state makes these lines visible under our experimental conditions. The frequencies and intensities of these lines are sensitive to the relative positions of the $A^2\Pi_u$ and $B^2\Sigma_u^+$ states and the magnitudes of the spin-orbit and rotational-electronic interactions which mix

the two Born-Oppenheimer states. The triplet hyperfine splitting in the extra lines of even N' is much smaller than that of the pure B-state and can be used to derive an estimate of the A-state hyperfine coupling.

A table of rotational line frequencies for the (0,1) band, and spectroscopic constants obtained by least-squares fitting to a model hamiltonian will be presented and compared with theory and other experimental work.

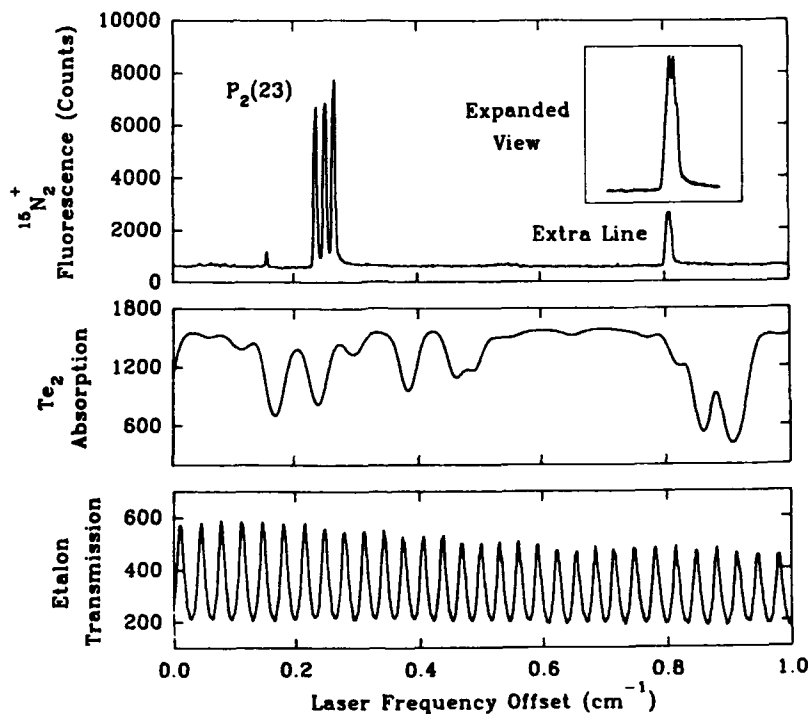


FIG.1. Laser-induced fluorescence signal from $^{15}\text{N}_2^*$ along with Te_2 and étalon frequency calibration spectra.

References:

1. A. Lofthus and P.H. Krupenie, *J. Phys. Chem. Ref. Data* 6, 113-307 (1977).
2. R.A. Gottscho, R.W. Field, K.A. Dick, and W. Benesch, *J. Mol. Spectrosc.* 74, 435-455 (1979).
3. S.D. Rosner, T.D. Gaily, and R.A. Holt, *J. Mol. Spectrosc.* 109, 73-84 (1985).
4. S.P. Reddy and C.V.V. Prasad, *Ap. J.* 331, 572-582 (1988) and Errata, *Ap. J.* 337, 579 (1989).
5. J. Cariou and P. Luc, *Atlas du spectre d'absorption de la molécule de tellure*. Laboratoire Aimé-Cotton CNRS II 91405 Orsay (France).

LASERSPECTROSCOPY INVESTIGATIONS OF THE EU-I LINE 5765 Å

W. Pietsch, M. Musso, L. Windholz

Institut für Experimentalphysik, Technische Universität Graz,
Petersgasse 16, A-8010 Graz / Austria

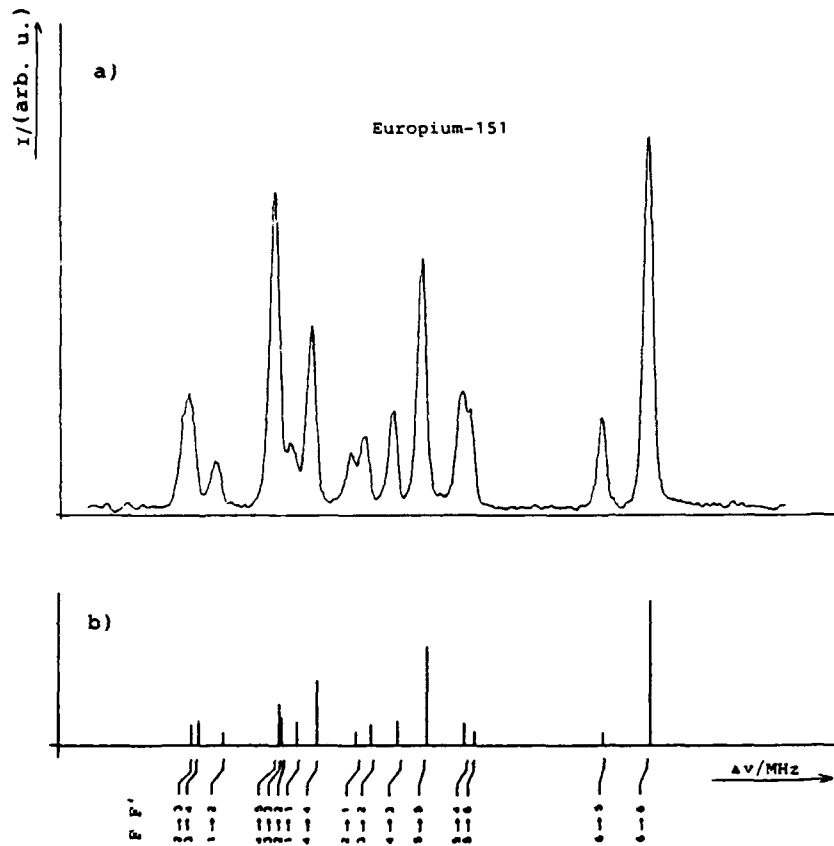
The investigations were performed by means of laser-atomic-beam-spectroscopy using a stabilized ring dye laser. The Europium line was excited from the ground level $4f^7 6s^2 {}^8S_{7/2}$ to the upper level $4f^7 6s6p {}^6P_{7/2}$ of the atom. There are two stable isotopes, ${}^{151}\text{Eu}$ and ${}^{153}\text{Eu}$, of nearly equal abundance and the nuclear spin of both is $5/2$. The value of g_J for the ground state ${}^8S_{7/2}$ is about 2. Both levels split in zero field in six hyperfine levels labelled by $F = 6, \dots, 1$. By the application of a magnetic field, they are further split into 48 states. The selection rules $\Delta F = 0, \pm 1$, $\Delta m = \pm 1$ (σ transition) and $\Delta F = \pm 1$, $\Delta m = 0$ (π transition) allow the observation of electric dipole transitions between these states. At high fields the levels are labelled by the quantum numbers m_J , m_I and allowed transitions, in which $\Delta m_J = 0, \pm 1$, $\Delta m_I = 0$, may be observed.

The transition at 5765.20 Å shows a very small hyperfine splitting; the isotopes ${}^{151}\text{Eu}$ and ${}^{153}\text{Eu}$ generate two structures respectively, each structure having 16 components in a frequency region of about 350 MHz. The HFS-constants: A, the magnetic dipole interval factor, and B, the electric quadrupole constant of the upper level $z^6P_{7/2}$ and the isotope shift were determined with high accuracy and compared with those of other authors /1/. The behaviour of the Europium line in magnetic fields was studied up to field strengths of 0.01 Tesla. The magnetic spectra could be compared with theoretical calculations /2/ of the splitting and the intensity behaviour of the Zeeman components, even in the case of Europium with its complicated hyperfine structure.

If an atomic beam passes through a field arrangement, which consists of a homogeneous magnetic, a crossed magnetic and electric and finally a homogeneous electric field in tandem arrangement, we expect a change in the population density of the HF-levels of the line (e.g. 5765.20 Å) excited from the ground state in a field-free region.

/1/ E.R. Eliel, K.A.H. van Leeuwen, W. Hogervorst; Phys. Rev. A 22, 1491 (1980)

/2/ M. Musso, Dissertation; Technische Universität Graz (1990)



a) Measured profile, b) line intensities and - positions $1/$ of the isotope ^{151}Eu for the transition 5765.20 \AA ; F' upper level, F lower level.

LYMAN ALPHA STARK BEATS

J F Williams

Department of Physics, The University of Western Australia
Nedlands, Perth 6009, Australia

The Lyman-alpha 'Stark beats' produced by the coherent decay of the perturbed $2s$ and $2p$ states has been studied by the simultaneous detection of the scattered electron and radiated photon from the same scattering event. Previous work [1,2] using a coincidence timing resolution of 0.47 nsec observed well-defined 'Stark beats' in the circularly polarized radiation which changed its direction of rotation when the mixing electric field of 250 V/cm was reversed and when the mixed s-p state evolved with time in a negative field. Coincidence measurements of the total intensity and the linear polarizations led to the determination of the scattering amplitudes and their relative phases for an incident energy of 350 eV and an electron scattering angle of 3 degrees.

This paper presents an extension of that work to a larger scattering angle of 10 degrees for which the scattering plane is better defined and where the angular momentum transfer is larger than in earlier work. Similar phenomena to those observed previously are observed. The beat pattern contains large oscillations near the Stark-shifted $2s_{1/2} - 2p_{1/2}$ frequency (about 1000 MHz) and the envelope of these oscillations is modulated at the hyperfine splitting of the $2s_{1/2}$ state (about 180 MHz). The experimental uncertainty is not small but adequate to show the hyperfine modulation. The more rapid oscillations from the $2p_{1/2} - 2p_{3/2}$ frequency (about 10^4 MHz) are not seen because of the coincidence resolving time of 0.47 nsec. The observed quantum beats in the Stokes' parameters can be described approximately by a simple model which includes only a $S_{1/2} - P_{1/2}$ ($m_j = \pm 1/2$) superposition state [1,2] but are described better, as expected, by the accurate model which also includes $S_{1/2} - P_{3/2}$ ($m_j = 1/2$) coupling [3]. A complete set of excited state multipoles are determined with an accuracy sufficient to distinguish between existing theoretical models. The data clearly indicate the inadequacy of the first Born approximation and are fairly well described by the most recent close coupling theory.

1. E.L. Heck and J.F. Williams, *J. Phys. B: At. Mol. Opt. Phys.* **20**, 2871 (1987).
2. J.F. Williams and E.L. Heck, *J. Phys. B: At. Mol. Opt. Phys.* **21**, 1627 (1988).
3. S. Chwirot, S. Legowski, J. Slevin and J. Zaremba, *J. Phys. B: At. Mol. Opt. Phys.* **22**, 1411 (1989).

MEASUREMENT OF THE LAMB SHIFT IN LITHIUMLIKE URANIUM (U^{89+})*

J. Schweppe, A. Belkacem, L. Blumenfeld, Nelson Claytor, B. Feinberg, Harvey Gould, V.E. Kostroun, L. Levy, S. Misawa, R. Mowat, and M. Prior
Materials and Chemical Sciences Division, Lawrence Berkeley Laboratory,
University of California, Berkeley, CA 94720

We have measured the energy of the $1s^2 2p\ 2^2P_{1/2} - 1s^2 2s\ 2^2S_{1/2}$ (first-excited state to ground state) transition in lithiumlike uranium (U^{89+}) to be 280.41 ± 0.13 eV. This is sufficiently accurate to determine the self-energy contribution to the one-electron Lamb shift in uranium ($Z=92$) to 0.15% - a factor of 60 improvement over the only other measurement [1] at this high Z .

Our measurement tests new relativistic many-body calculations [2] and multi-configurational Dirac-Fock calculations [3] and is sensitive to the nuclear polarizability [4] and to higher-order QED radiative corrections which explicitly involve more than one electron in a relativistic system. These radiative corrections have not yet been calculated and present estimates of their size [2] have large (0.6 eV) uncertainties.

Lithiumlike uranium (U^{89+}) was produced at the LBL Bevalac accelerator by stripping a beam of ~ 95 MeV/u U^{40+} and magnetically selecting the U^{89+} fraction. The $2^2P_{1/2}$ state was populated by collisional excitation in a 1.7 mg/cm² Al foil. The state has a lifetime of 50 ps and we observe its decay in vacuum, 1 cm downstream from the target.

We measured the 280-eV transition energy with a Doppler-tuned spectrometer using the $L_{2,3}$ photo-absorption edge, and in particular the $2p-4s$ resonance [5], in argon gas as our reference. The photons were detected by six position-sensitive, multiwire-proportional-counters arranged in pairs in a ring around the beam. In front of each detector was a tapered Soller-slit collimator and a gas cell holding ~ 7 Torr of argon gas.

The beam velocity was measured by time of flight between two thin scintillators 19 m apart. An elaborate but highly reproducible series of optical and x-ray measurements determined the angle between the beam and the detectors. The alignment withstood a major earth quake. We measured at the two beam velocities of $\beta = 0.4136$ and 0.4228 . The average of the 6 independent measurements, each with a pair of detectors, is 280.41 eV with a sample standard deviation of 0.10 eV. Our estimate of the total experimental uncertainty for each of the three pairs of x-ray detectors is 0.13 eV.

Calculations of the energy of the $2^2P_{1/2} - 2^2S_{1/2}$ transition in lithiumlike uranium have been made by S.A. Blundell, W.R. Johnson, and J. Sapirstein [2] based on relativistic many-body perturbation theory (RMBPT) and by P. Indelicato and J.P. Desclaux [3] based on a multi-configurational Dirac Fock method (MCDF). Their results are shown in Table I.

Table I. Contributions to $2^2P_{1/2} - 2^2S_{1/2}$ transition in lithiumlike uranium (eV)

	RMBPT [2]	MCDF [3]
Relativistic energy	322.374 (0.035)	322.794 ($\pm?$)
Self energy [6]	-56.732 (0.015)	-56.732 (0.015)
Vacuum polarization [7]	14.314 (0.0)	14.314 (0.0)
Second-order radiative corr. [4]	1.193 (0.57)	1.318 ($\pm?$)
Nuclear polarization [4]	-0.126 (0.013)	-0.126 (0.013)

Total Theory	281.02 (0.57)	281.57 ($\pm?$)
This Experiment	280.41 (0.13)	280.41 (0.13)

The theoretical calculations are presently in agreement with our experimental result, but their uncertainty is a factor of 4 greater. More accurate calculations of the radiative corrections are clearly required.

* This work was supported by the Director: Office of Energy Research, Office of Basic Energy Science, Chemical Sciences Division; of the U.S. Department of Energy under contract No. DE AC03 76SF00098.

1. C. Munger and H. Gould, *Phys. Rev. Lett.* **57**, 2927 (1986).
2. W.R. Johnson, S.A. Blundell, and J. Sapirstein, *Phys. Rev. A* **37**, 2764 (1988); S.A. Blundell, W.R. Johnson, and J. Sapirstein, *Phys. Rev. A* **41**, 1698 (1990).
3. P. Indelicato and J.P. Desclaux, *MCFD Calculations of Transition Energies with QED Corrections in Three-Electron Ions*, submitted to *Phys. Rev. A* (1989).
4. G. Plunien, B. Müller, W. Greiner, and G. Soff, *Phys. Rev. A* **39**, 5428 (1989).
5. G.C. King *et al.*, *J. Phys. B* **10**, 2479 (1977); M. Nakamura *et al.*, *Phys. Rev. Lett.* **21**, 1303 (1968); R.D. Deslattes, *Phys. Rev.* **186**, 1 (1969); T. Hayaishi *et al.*, *J. Phys. B* **17**, 3511 (1984).
6. P.J. Mohr, *Ann. Phys. (N.Y.)* **88**, 26 (1974); *Ann. Phys. (N.Y.)* **88**, 52 (1974); *Phys. Rev. Lett.* **34**, 1050 (1975); *Phys. Rev. A* **26**, 2338 (1982).
7. W.R. Johnson and G. Soff, *ADNDT* **33**, 405 (1985); G. Soff and P.J. Mohr, *Phys. Rev. A* **38**, 5066 (1988).

FIRST TWO PHOTON SPECTROSCOPY OF SINGLET HELIUM

W. Lichten, D. Shiner and Zhi-Xiang Zhou
Physics Department, Yale University,
Box 6666, New Haven, CT 06511-8167

We present preliminary, absolute wavelength measurements of the two photon transitions $2^1S_0 - n^1D_2$ ($7 \leq n \leq 20$). These have a precision of $0.000\ 01\ \text{cm}^{-1}$ or better. The measurements provide a test of our understanding of the D levels. This, in turn, leads to a more precise value for the ionization potential of the 2^1S state, which provides a timely test of theoretical calculations of this energy level.

The experiment is done with an atomic beam of helium, bombarded by electrons to excite the metastable 2^1S state, which is detected by secondary electron emission. The metastables are quenched in a buildup cavity by two photon transitions to the n^1D levels. The effective laser power density is of the order of $60\ \text{kW/cm}^2$. The resulting change in metastable beam intensity produces the observable signal.

The laser frequency measurements are as by Zhao et al.¹, with a relative precision of one part in 10^{10} or better. The absolute accuracy of wavelength measurement is limited by the realization of the meter (1.6 parts in 10^{10}). We have followed the method of exact fractions, with corrections for the mirror coating phase shifts.² These measurements, given in the table, are subject to later verification by the method of virtual mirrors.

The results for the relative position of the D levels agrees within the errors (generally $0.000\ 01\ \text{cm}^{-1}$) with semi-empirical fits, based on radiofrequency spectroscopy by Farley, MacAdam, Wing, Cok, and Lundeen; and on theoretical calculations by Drachman and Drake.³ On the basis of this agreement, and assuming the precision of the fitted expressions improves for higher values of the principal quantum number n , we have a preliminary value for the binding energy 2^1S level, $32\ 033.228\ 817(5)\ \text{cm}^{-1}$, with a substantially smaller error than previous values.³

VIII-24

PRELIMINARY RESULTS FOR TWO PHOTON TRANSITIONS IN HELIUM FROM 2^1S

Upper Level	Laser λ (nm)	Binding Energy (cm^{-1})		difference
		Our value*	Previous value ³	
2S	-----	32 033.228 817(5)	32 033.230 3(30)	.001 5(3)
			32 033.232 1 [†]	-.003 3
7D	671.3	2 240.540 42(7)	2 240.540 539 4(3)	-.000 12(7)
8D	659.7	1 715.294 87(5)	1 715.294 884 0(2)	.000 00(5)
9D	651.9	1 355.220 22(4)	1 355.220 23(2)	.000 00(5)
10D	646.5	1 097.679 45(3)	1 097.679 44(2)	.000 02(4)
11D	642.5	907.139 70(2)	907.139 68(1)	.000 02(2)
12D	639.6	762.225 77(2)	762.225 77(1)	.000 00(2)
13D	637.3	649.453 40(1)	649.453 388	.000 01(1)
14D	635.5	559.975 200(8)	559.975 193	.000 007(8)
15D	634.0	487.791 013(7)	487.791 010	.000 004(7)
16D	632.8	428.715 162(7)	428.715 162	.000 000(7)
17D	631.8	379.755 722(7)	379.755 727	-.000 004(7)
18D	631.0	338.728 118(8)	338.728 123	-.000 006(8)
19D	630.3	304.007 11(1)	304.007 130	-.000 02(1)
20D	629.7	274.363 40(2)	274.363 421	-.000 02(2)

*We adjusted the 2^1S energy to get the best fit of the currently measured wavelengths to the data of reference 3; that is, with tabulated energy levels and with the empirical formulae for the D states.

[†]Theoretical calculation by G. W. F. Drake, Nucl. Instr. and Meth. B31, 7 (1988).

1. P. Zhao, W. Lichten, Zhi-Xiang Zhou, H.P. Layer and J. Bergquist, Phys. Rev. A39, 2888 (1989).
2. W. Lichten, J. Opt. Soc. Am. A3, 909 (1986).
3. See G.W.F. Drake, Phys. Rev. Letters 59, 1549 (1987) for theoretical calculations of 7D and 8D levels; for the other levels, see reviews of calculations, experiments and semi-empirical fits by W.C. Martin, Phys. Rev. A29, 1883 (1984); A36, 3575 (1987) and E.S. Chang, Phys. Rev. A35, 2777 (1987).

LINESHAPES OF IONIZING STARK RESONANCES IN HELIUM

E.E. Eyler
 Department of Physics and Astronomy
 University of Delaware, Newark, DE 19716

A. Nussenzweig
 Laboratoire Hertzienne de l'ENS.
 24 rue L'homond 75231 Paris Cedex 05, France

T. Bergeman
 Department of Physics, State University of New York at Stony Brook
 Stony Brook, NY 11794

E. Pollack
 Department of Physics, University of Connecticut, Storrs, CT 06269

At the last ICAP meeting we presented preliminary results of a high-resolution study of ionizing Stark levels in helium. Here we present the final results from this project, which is also described in a very recent publication.¹ Selected diabatic levels of the $n=32$ and $n=40$ manifolds have been measured, all the way from the classical saddle point field where ionization first becomes possible, to the high-field limit where the levels broaden rapidly and disappear into the continuum. Figure 1 shows a Stark map for a portion of the $n=32, m=0$ manifold.

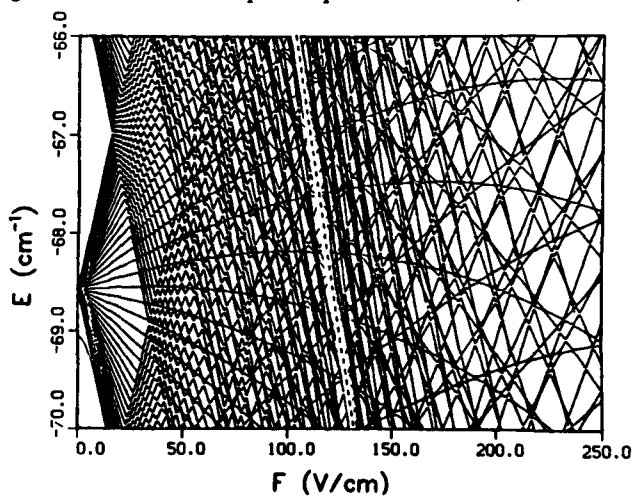


Fig. 1 Stark map of $n=32$ manifold in helium, for region near the classical saddle-point threshold (dotted line).

Energies, intensities, widths, and lineshapes have been studied for a wide range of electric field strengths and compared with detailed theoretical predictions obtained using the WKB quantum-defect method first developed by Harmin.³ Careful experimental design allows very accurate determination of the lineshapes, including linewidths and asymmetry parameters accurate to 6% in the best cases. Figure 2 shows a comparison of experimental and theoretical results for the $n = 32$, $n_1 = 31$, $n_2 = 0$, $m = 0$ level over the full range of electric fields. The field values chosen for these measurements were intentionally selected to avoid the immediate vicinity of level crossings, so overall trends are observed rather than the effects of local interactions. Excellent agreement between experiment and theory is found for all the cases we have studied. A simpler autoionization model produces similar results, although less accurately than the WKB-QD theory.

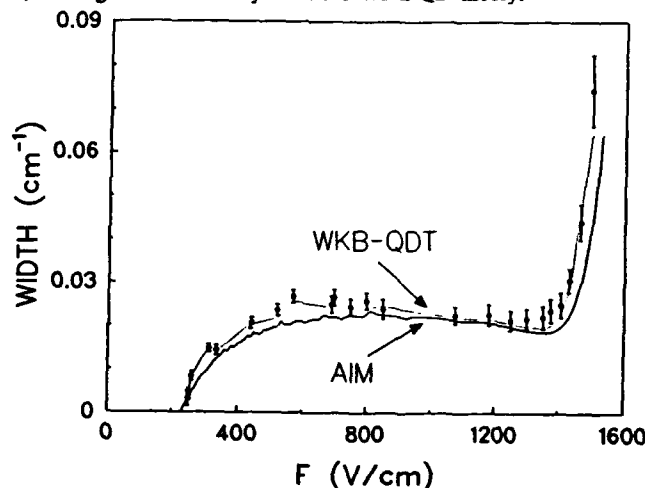


Fig. 2. Experimental results for the linewidth parameter Γ , with predictions of MQDT-WKB theory and the autoionization model (AIM).

Energy level spacings were investigated for a closely spaced group of 8 lines. Calculated and measured energy levels agree with an average deviation of 0.001 cm^{-1} when the electric field value is adjusted to give the best match. This determines the electric field to about 50 parts per million, considerably more accurate than other techniques. It should be possible in future experiments to investigate the limits of theoretical accuracy by measuring line positions more accurately, and by investigating the regions near avoided crossings.

This research was supported by the National Science Foundation, grants PHY87-17051 and PHY90-00375.

¹A. Nussenzweig, E.E. Eyler, T. Bergeman, and E. Pollack, *Phys. Rev. A* 41, 4944 (1990).

³D.A. Harmin, *Phys. Rev. A* 26, 2656 (1982); *Phys. Rev. A* 30, 2413 (1984).

PRECISION WAVELENGTH MEASUREMENT OF THE $1s2s\ ^3S - 1s2p\ ^3P^*$
TRANSITIONS IN HELIUM-LIKE BORON

T. P. Dinneen,* N. B. Mansour, H. G. Berry, L. Young and R. C. Pardo
Physics Division, Argonne National Laboratory, Argonne, IL 60439

We have made laser-induced fluorescence measurements of the wavelengths of the $1s2s\ ^3S - 1s2p\ ^3P^*$ transitions at 282 nm in helium-like Boron. We are able to compare our measurements of fine structures, hyperfine structures, and absolute wavelengths with the latest relativistic theory, including two-electron QED corrections.¹

Ions in the $1s2s$ metastable state were extracted from the ECR ion source injector of the Argonne ATLAS accelerator. The resulting 36 keV B^{3+} ion beam was mass-analyzed, and interacted in a voltage cell with a collinear, frequency-doubled cw laser beam. The 282 nm wavelength was generated by intracavity frequency-doubling of a Coherent 699 ring dye laser. We obtained 5mW of 282 nm radiation, while pumping Rhodamine 110 with 7 watts from an argon-ion laser. The collinear geometry allowed us to measure the resonances in both parallel and antiparallel laser excitation, thus eliminating the doppler shift of the fast beam from the results. The resonance wavelengths were measured relative to wavelengths observed simultaneously from a standard iodine absorption cell. The hyperfine structures were scanned by varying the observation cell voltage, keeping the exciting laser wavelength fixed. This technique eliminates the need to scan the laser, and was necessary since the hyperfine multiplet of each fine structure component spans frequency ranges of up to 100 GHz.

From the hyperfine structures, we are able to deduce magnetic dipole interaction constants for these levels. These are the first hyperfine structure measurements in B III. Preliminary values are:

$1s2s\ ^3S_1$	A = 31.084(40)	GHz
$1s2p\ ^3P_1$	A = 14.788(40)	GHz
$1s2p\ ^3P_2$	A = 14.366(20)	GHz

The measured fine structures are compared with the theory of Accad et al.². Preliminary values in wavenumbers are:

	Experiment	Theory (ref. 2)
$^3P\ J=1\ \text{to}\ J=2$	52.660(5)	52.3959 (excludes singlet-triplet mixing)
$^3P\ J=2\ \text{to}\ J=0$	36.453(5)	36.4162

The submitted manuscript has been authored by a contractor of the U. S. Government under contract No. W-31-109-ENG-38. Accordingly, the U. S. Government retains a nonexclusive, royalty-free license to publish or reproduce the published form of this contribution, or allow others to do so, for U. S. Government purposes.

The absolute wavelengths (Table 1) give direct measurements of the sum of the non-relativistic and the QED contributions to these transition energies. Previous measurements in Li II³ are limited by the precision of the calculation of the non-relativistic energy difference. At higher nuclear charge, no measurements to this precision exist, and all measurements have poorer precision than the best calculations.¹ We see from Table 1 that, in all these transitions, we differ from theory by greater than five standard deviations. Note, however, that the deviations are of differing sign for the different fine structure transitions. These indicate that the discrepancies must be relativistic in origin (an error in the non-relativistic energies² would affect all three transitions equally). Since the sum of discrepancies is near zero, the disagreements may be attributed to the leading, uncalculated spin-dependent terms of order $\alpha^4 Z^4$ a.u. arising from relativistic QED correlation terms.

Table 1: Transition energies in cm^{-1} . (Preliminary values)

Transition	This Experiment	Theory (ref. 1)	Expt.-Theory
$^3S_1 + ^3P_2$	35430.084(3)	35430.023	0.061
$^3S_1 + ^3P_0$	35393.631(5)	35393.703	-0.071
$^3S_1 + ^3P_1$	35377.424(5)	35377.399	0.025

References

1. G. W. F. Drake, Can. J. Phys. **66**, 586 (1988).
2. Y. Accad, C. L. Pekeris and B. Schiff, Phys. Rev. **A4**, 516 (1971).
3. E. Riis, H. G. Berry, O. Poulsen, S. Lee, S. Y. Tang, Phys. Rev. **A33**, 3023 (1986).

*Graduate Student, University of Chicago.

IX. MOLECULAR SPECTROSCOPY, AND STRUCTURE,
SURFACES AND CLUSTERS

DV-X α CALCULATION OF X-RAY ABSORPTION SPECTRA OF RESONANCES FOR SF₆

Hirohide Nakamatsu†, Takeshi Mukoyama† and Hirohiko Adachi‡

† *Institute for Chemical Research, Kyoto University,*

Uji, Kyoto 611, Japan

‡ *Hyogo University of Teacher Education,*

Shimokume, Yashiro-cho, Kato-gun, Hyogo 673-14, Japan

Introduction

The X-ray absorption spectra of SF₆ have been studied with special attention because of very weak Rydberg series and the presence of extremely strong peaks near the K and L absorption edges. These peaks are referred as resonances. We have reported that the theoretical energies for the resonances near the X-ray absorption edges for sulfur atom are in good agreement with the experimental results, derived from discrete-variational (DV)-X α calculation[1]. The character of the wavefunctions has also been illustrated.

In the present work, we have performed the DV-X α calculations of cross section for the X-ray absorption spectra of the sulfur in SF₆. The main advantage of the DV-X α method is that a realistic molecular potential can be used instead of the muffin-tin approximation in the MS-X α method. The calculated spectra are compared with the experimental data. It is shown that the potential in the interatomic region is influential in determining the wavefunctions for the resonances.

Computation

The computational details of the DV-X α method used in the present work have been described elsewhere [1]. Numerical atomic orbitals were used as a basis set for the MO calculations, which consisted of atomic orbitals of 1s to 5d without 4f for S atom and 1s to 5d without 4f and 5s for F atoms. The Slater exchange parameter was chosen to be $\alpha = 0.7$ for all calculations.

Results and discussion

The calculated and experimental spectra are shown in Fig. 1. The intense peaks are attributed to the molecular orbitals which contain large components of sulfur atomic orbitals. The wavefunctions for the K and the L shells of sulfur atom are localized in a small volume of the central part of the sulfur atom. Therefore, the components of sulfur atomic orbitals contribute predominantly to the X-ray absorption cross section. Cross sections were obtained under the dipole approximation. The peak width (fwhm) of each level was set to 2.7eV for the spectra in Fig. 1b. The spectra calculated by DV-X α method are fairly in good agreement with the experimental results from -10eV to +25eV.

As a comparison, a smaller basis set is also examined. A better spectrum is derived from the calculation with the larger basis set. The peak at about 25eV may become broader, when the basis set is further enlarged. This peak may correspond to the small and broad

peak in the experimental spectrum.

Many weak peaks form a base line which increases with the energy (Fig. 1b). For the experimental spectrum of sulfur L absorption in Fig. 1a, the background which slopes down to high energy has not been subtracted. Therefore, the increasing base line is contained in the experimental spectra and depicted by the calculation.

A comparison between the wavefunctions in low energy and high energy are shown in Fig. 2. For the excited electron in high energy, the molecule can be divided into two regions: atomic and interatomic regions. For the interatomic region, the excited electron can be considered as a free electron, which is schematically illustrated in Fig. 2b. On the contrary, the potential even in the interatomic volume should be taken as a superposition of the atomic potentials. Especially, as the resonances have large components of sulfur atom, the main feature of their wavefunctions is determined predominantly by the potential of sulfur atom. The boundary condition is governed by the potential of fluorine atoms.

[1] H. Nakamatsu, T. Mukoyama and H. Adachi, Chem. Phys. 143 (1990) in press.

[2] T.M. Zimkina and A.S. Vinogradov, J. Phys. Paris Colloq. 32, C4-3 (1971).

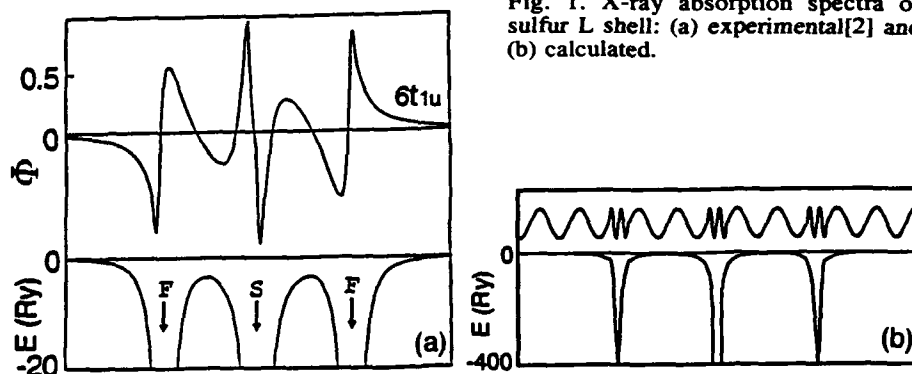


Fig. 1. X-ray absorption spectra of sulfur L shell: (a) experimental[2] and (b) calculated.

Fig. 2 Schematic diagram for comparison between the wavefunctions in: (a) low energy and (b) high energy (t_{1u} resonance). Potential is also shown.

SOLUTION OF THE INTERFACE PROBLEM BETWEEN TWO CHAINS
USING A GREEN'S MATRIX METHOD

M. A. ABDEL-RAOUF

Chair for Theoretical Chemistry, University of Erlangen-Nürnberg,
Egerlandstr. 3, 8520 Erlangen, FRG.

The interfacial interaction between various one, two and three dimensional macromolecular structures is one of the most interesting problems of condensed matter physics (1). Effects of this interaction on the band structure of the considered systems, especially of different conductivity, gain extreme industrial and scientific interest (2). In this paper, the Green matrix technique utilized for solving this problem is explained (3). Its application to quasi-one dimensional systems is discussed. Particularly, the interface states arising among polyacetylene, polyethylene and various fluorinated ethylenes are investigated. Implication of the results for industrial devices as well as the appearance of the bending bands phenomenon are discussed in detail.

-
- (1) S. M. Sze, Physics of Semiconductor Devices, (Wiley Interscience, New York-1969).
- (2) See for example: Semiconductors and Semimetals, Ed. R. K. Willert, sen. & A.C. Beer) Vol. 11, (H. J. Horel, Solar Cells) (Academic Press, New York-1975).
- (3) M. A. Abdel-Raouf, P. Otto, J. Ladik and M. Seel, Phys. Rev. B40, 1450 (1989); M. A. Abdel-Raouf and J. Ladik, Solid State Commun. 71, 1019 (1989).

RECOMBINATION SPECTROSCOPY OF ALKALI AND ALKALI-LIKE IONS IN SUPERFLUID HELIUM

H. Bauer, M. Beau, J. Fischer, H.J. Reyher*, J. Rosenkranz and K. Venter

Physikalisches Institut der Univ. Heidelberg, Philosophenweg 12, 6900 Heidelberg, F.R.G.

*Fachbereich Physik der Universität Osnabrück, Barbarastr. 7, 4500 Osnabrück, F.R.G.

Recombination spectroscopy of impurity ions in liquid helium has developed as a powerful tool to investigate the microscopic structure of these defects /1/. The light emitted after the recombination into excited atomic states yields valuable insight into the recombination process itself, the initial population of the excited states and the relaxation of the helium environment due to the neutralization of the ion.

Recent work was focussed on the alkaline earth ions (Be, Mg, Ca, Sr, Ba) as well as Zn and Cd ions forming bubble states in liquid helium /2/. A model describing the recombination as a tunneling process of the electron from his own bubble into the bubble of the defect ion was developed. It explains the experimental observation that only atomic states with an energy of more than 1.5 eV below the ionisation energy are populated during the recombination. The small line shifts indicates that the atoms are only slightly disturbed by the surrounding helium.

In contrast to the alkaline earth ions, alkali ions are expected to form defects like the He^+ ion in liquid helium. Therefore, the recombination of a snowball type structure with the electron bubble can be studied.

The ions used in our experiment are sputtered from a metal probe a few millimeters above the liquid helium surface with an N_2 laser (Fig. 1). This offers the possibility to investigate a variety of elements and to exchange targets quickly during the same measurement. The electrons are produced with a tip emission in the liquid /3/. The ions and electrons drift in the electrical field between the grid and the tip and recombine in the helium. The recombination light emitted in the optical volume is analysed with a monochromator and detected with a photomultiplier.

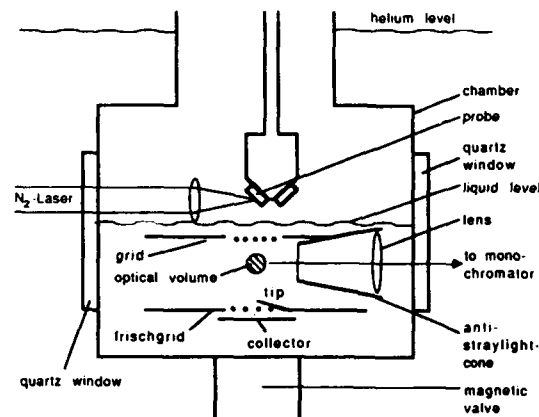


Fig. 1: Experimental chamber

For all alkali ions studied so far (Li, Na, K, Rb) no recombination light could be observed in the range from 250 to 800 nm. The presence of the ions was checked independantly by measuring the ion mobilities in the liquid. To explain the absence of any recombination light one may assume that the atoms are formed in their ground state only. However, the modification of the recombination modell to snowball structures predicts that the first excited states of the alkali ions are populated. An other possible explanation would be that the atoms are formed in excited levels but that the emission of light is suppressed by radiationless transitions to the ground state. For sodium, our measurements imply that these transitions have to be at

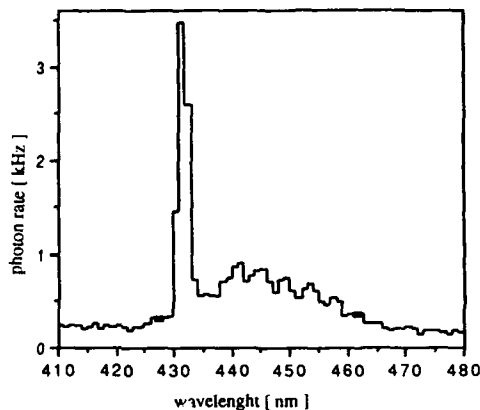


Fig. 2: The recombination band of Ag_2^+ clusters observed in liquid helium

least a factor of 1000 faster than the corresponding optical deexcitation.

Experiments carried out with the transition metals Cu, Ag and Au having the same valence electron structure support the idea that radiationless transitions may play an important role to understand the behaviour of alkali atoms in liquid helium. For these elements, many optical transitions have been detected which can unambiguously be attributed to the corresponding atom. However, several transitions were not observed even though the excited levels were populated. The presence of radiationless transitions, well known from matrix spectroscopy in noble gases /4/, could be demonstrated for Cu, Ag and Au in liquid helium for the first time.

In addition, two emission bands ranging from 430 to 460 nm and 370 to 410 nm were detected in the recombination spectrum of Ag (Fig. 2). From comparison with molecular beam /5/ /6/ and matrix spectroscopy experiments /7/, there is strong evidence that the observed bands are caused by recombination of Ag_2^+ and Ag_3^+ clusters in the liquid.

This offers the possibility to investigate these clusters and cluster ions in the "soft matrix" liquid helium.

This work has been supported by the Deutsche Forschungsgemeinschaft.

- /1/ H. Bauer, M. Beau, A. Bernhardt, B. Friedl and H.J. Reyher, Phys. Lett. **A137** (1989) 217
- /2/ H. Bauer, M. Beau, B. Friedl, C. Marchand, K. Miltner and H.J. Reyher, accepted for publication in Phys. Lett. A
- /3/ P.V.E. McClintock, J. Low Temp. Phys. **11** (1973) 15
- /4/ H. Wiggerhauser, D.M. Kolb, H.H. Rotermund, W. Schrittenlacher and W. Schroeder, Chem. Phys. Lett. **122** (1985) 71
- /5/ M.D. Morse, Chem. Rev. **86** (1986) 1049
- /6/ P.Y. Cheng and M.A. Duncan, Chem. Phys. Lett. **152** (1988) 341
- /7/ P.S. Bechthold, U. Kettler and W. Krasser, Surf. Science **156** (1985) 875

IX-4
NEUTRAL MASS-SELECTED LEAD CLUSTER BEAMS

M. Abshagen, J. Kowalski, M. Meyberg, G. zu Putlitz, J. Slaby, and F. Träger*
Physikalisches Institut der Universität Heidelberg
Philosophenweg 12, D-6900 Heidelberg, Federal Republic of Germany

In order to generate neutral, mass-separated lead cluster beams, Pb_n^+ ions (with $3 \leq n \leq 12$) were neutralized by means of charge transfer reactions in sodium vapor,



ΔE is the energy defect of the reaction. Na has been chosen because its ionization potential of $E = 5.14$ eV equals the ionization potentials of small lead clusters with $n \geq 4$ within a few tenths of an eV. Therefore, the charge exchange is "near-resonant", i.e. $\Delta E \approx 0$, and the cluster ions can be neutralized

- (a) with high efficiency because of large cross sections
- (b) without extensive fragmentation because the electron is captured preferably in the ground state of the neutralized cluster, thus minimizing transfer of internal energy. To induce dissociation at least 1.5 eV would be required, the experimentally determined value for the cohesive energy of small lead clusters.

Neutralization cross sections σ_N as a function of cluster size have been determined with Beer's law from measurements of the flux of generated neutrals in the beam as a function of the target gas density. The result is displayed in Fig. 1. The variation of σ_N reflects the different values of ΔE for different cluster sizes as well as the change of the electron affinity.

Fragmentation possibly associated with the charge transfer has been investigated by translational spectroscopy. This method presently allows us to exclude dissociation with a release of kinetic energy of ≤ 100 meV. Thermal evaporation of the clusters with even smaller kinetic energies of the dissociation products, however, is highly unlikely because of resonant charge transfer into the electronic ground state of the neutralized cluster. It is therefore concluded, that neutral monodisperse lead

clusters have been produced. The neutralization rates being as high as 30%, very intense neutral size-selected beams of metal clusters have become available for future experiments that measure cluster properties unambiguously as a function of size.

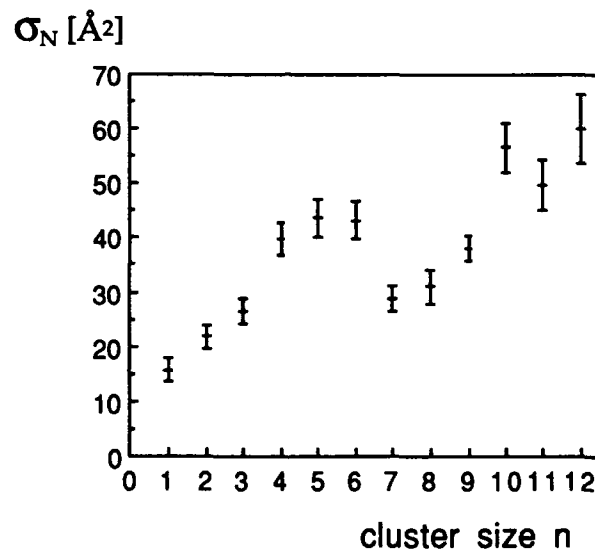


FIGURE 1: Measured cluster size dependent cross sections σ_N for the neutralization of singly charged lead cluster ions in sodium vapor. The ion energy was 2,450 eV.

This work was supported by the Deutsche Forschungsgemeinschaft.

* Present address: Fachbereich Physik der Universität Kassel,
Heinrich-Plett-Str. 40, D-3500 Kassel, Federal Republic of Germany

THE EXPERIMENTAL DETERMINATION OF THE ELECTRON CHARGE DENSITY OF DIATOMIC MOLECULES BY ELECTRON DIFFRACTION

Y. Zhang, A. W. Ross, and M. Fink

Physics Department, The University of Texas at Austin, Austin TX 78712

Elastic differential cross sections were recorded for H_2 , N_2 , and O_2 . After subtracting out the kinematic contribution to the diffraction pattern by the constituent atoms, the resulting difference functions reveal the rotationally averaged Fourier transform of the distortion of the atomic charge densities due to either binding or correlation effects. These functions are sensitive to the first and second order densities because the elastic and inelastic scattering intensities are available individually. For all cases studied to date, the Hartree-Fock predictions of the elastic scattering intensity agree well with the data, with the exception of N_2 . At present, no theory, including all CI efforts, can reproduce the N_2 experimental data. For inelastic scattering, nearly all theories fail, with the exception of H_2 , for which agreement is found between the rotationally averaged results of Kolos *et al*¹, and our measurements. Moments derived from the smallest angle data agree well with the diamagnetic susceptibility and other measurements.

Electron charge density maps have been obtained for these molecules by fitting the experimental elastic cross section data to a functional form whose inverse Fourier transform is known². As a check of this procedure, the reverse operation has been performed on a theoretical charge density map of H_2 ³ to obtain an elastic scattering cross section which agrees well with the the experimental measurement.

¹ W. Kolos, H. J. Monkhorst, and K. Szalewicz, *J. Chem. Phys.* **77**, 1323 (1982).

² D. A. Kohl and L. S. Bartell, *J. Chem. Phys.* **51**, 2891 (1969) and *J. Chem. Phys.* **51**, 2896 (1969).

³ R. Moszyński and K. Szalewicz, *J. Phys. B: At. Mol. Phys.* **20**, 4347 (1987).

THE SPECTROSCOPIC INVESTIGATION OF EXCITED DISSOCIATION PRODUCTS OF
CLUSTER IONS DESORBED BY ELECTRONS.

I.P. Bogdanova, V.A. Vladimirov, V.I. Yakovleva

State University, Leningrad, USSR

The rare gas luminescence of Ar, Kr and their mixtures with He and Ne in tubes with electron guns were investigated. The Ar and Kr pressures were tenths of mtorr, He and Ne pressures < 100 mtorr. The spectra of above mentioned gases by dc and pulsed electron current $/T = 10 - 50$ ns/ were observed.

Besides the conditions when the metal grid of electrode A_2 was bombarded by the electrons of $/30 - 200$ eV energy and that they are retarded by electrode A_3 with $V_3 = V_4 = /100 - 150/$ V were obtained. In this case the cluster ions desorbed by electrons from the grid A were penetrated into the equipotential volume $A_3 - A_4$.

Spectroscopic time-resolved investigations was used. The electron interaction with adsorbed atoms on the A_2 grid leads to desorption of excited longlived cluster ions. The dissociation of these cluster ions in volume $A_3 - A_4$ $/l = 10$ mm/ causes the appearance of selective excited atoms or atomic ions¹. Time-of-flight measurements of the m/ne of metastable cluster ions were carried out. In Ne gas only one type of cluster ions with $m/ne = 40$ $/Ne_2^{+*}$, $\tau > 300$ ns/ was detected. Dissociation of these ions leads to formation of the atoms in 3p states. In Ar gas the ions with $m/ne = 80$ and 40 $/Ar_2^{+*}$ and Ar_2^{2+*} / were registered. In Kr gas the cluster ions with $m/ne = 252, 168, 84$ and 56 $/Kr_3^{+*}, Kr_2^{+*}, Kr_2^{2+*}$ / were discovered. The ions with $m/ne = 56$ are difficult to identify. Dissociation of excited Kr cluster ions causes mainly the formation of excited atomic Kr ions in quadric states.

In Kr - He mixture /1:2/ the time-of-flight measurements based on luminescens of spectral lines of atomic Kr ions gave $m/ne = 8$ mass. This phenomenon may be explained by collisional dissociation with energy transfer from ions He_2^{+*} to Kr atoms. In He mass-spectrum on the atomic lines only one maximum was detected with $m/ne = 8$. In the Kr - Ne mixture / 1:3/ the collisional dissociation leads energy transfer from Ne_2^{+*} to Kr atoms. The desorbed long- lived excited cluster ions are dissociating accompanied by formation of Ar and Kr atomic excited ions in the laser generating states. Therefore the desorption by electrons of excited cluster ions from surface of metal grid and their dissociation to atomic excited fragments may lead to laser generation.

In the table some cluster ions parameters are given

Gas	P, mtorr	Cluster ion	m/ne	E,eV threshold	τ , ns eff
He	25	He_2^{+*}	8	45	120
Ne	90	Ne_2^{+*}	40	40	>300
Ar	40	Ar_2^{2+*}	40	55	140
	-	Ar_2^{+*}	80	40	300
Kr	40	Kr_2^{2+*}	84	55	220
	-	Kr_2^{+*}	168	35	270

I.P. Bogdanova, S.V. Ryazantseva, V.E. Yakhontova
Opt. & Spectrosc./USA/ 49, 465, /1980/.

**ZN₂ POTENTIAL CURVES:
A SIMPLE THEORETICAL TREATMENT OF INTERSHELL EFFECTS**

M. Couty, G. Chambaud and W. E. Baylis*

Groupe de Chimie Quantique, LPCR Bat. 337, 91405-Orsay, France

*Department of Physics, University of Windsor, Ontario, Canada N9B 3P4

Potential-energy curves of the first 60 electronic states of Zn₂ (in the symmetries Σ , Π and Δ) have been calculated. The calculational method consists of a limited CI with an empirical correction via an effective Hamiltonian. The correction accounts, in a very simple way, for the various intershell effects which are not taken into account by the CI calculation, in which the inner electrons of the system are frozen. The curves permit a first interpretation of spectroscopic data available for the Zn₂ states (Czajkowski *et al.* 1990; Kedzierski *et al.* 1989 and 1990).

Correlation effects are very important in theoretical determinations of the electronic states of Zn₂ (Hay *et al.* 1976; Bender *et al.* 1979; Tatewaki *et al.* 1985) mainly because the core-valence correlation differs in the various excited states. A simple method has already been proposed for the study of such effects in the interaction of Ca and H (Chambaud and Levy 1989) and in the HgZn system.

The present calculation proceeds in five steps:

- The first step consists of an SCF calculation of the ground state $X^1\Sigma_g^+$ and of the triplet state $^3\Sigma_u^+$ correlated asymptotically to the lowest Zn(³P) + Zn(¹S) atomic states. We also performed calculations of the first Rydberg states of the Zn atom to deduce Rydberg orbitals. The orbitals obtained by all these calculations are then put together into a set to be used in the CI calculation. All the electrons of the Zn are taken into account in this step. The basis set used for each Zn is a (15s, 12p, 7d/7s, 7p, 3d) basis of gaussian functions: the contraction is made in such a way that the core is described by a mono-zeta basis (Huzinaga 1977) and the more diffuse orbitals are left uncontracted to allow sufficient flexibility. The total basis set contains 86 atomic functions.

- The second step is a CI calculation of the ground state and of the first-excited states using the optimized set of virtual orbitals (64 molecular orbitals) from step one. The CI consists of a variational part (about 200 configurations of each symmetry) plus a perturbative part with all single and double excited configurations that can be built from the reduced space using the set of virtual orbitals (about 10⁶ configurations).

- The third step consists of the construction of an effective Hamiltonian by projecting the CI wave functions onto an effective basis of small dimension (typically 20 configurations), corresponding to the asymptotic configurations. The effective basis set is orthonormalized at each distance where the calculations are made.

- The fourth step involves adjusting this effective Hamiltonian by comparing calculated energies with experimental values for the separated atoms and then diagonalizing the adjusted effective Hamiltonian matrix in order to provide a new adiabatic representation.

- The fifth step performs a final calculation the spin-orbit interactions between the new adiabatic states.

Transition dipole moments have been calculated between all the states, and spectroscopic constants of the bound states have been determined.

W. E. Baylis, *J. Phys. B: Atom. Mol. Phys.* **10**, L583 (1977)

C. F. Bender, T. N. Rescigno, H. F. Schaefer III and A. E. Orel, *J. Chem. Phys.* **71**, 1122 (1979).

G. Chambaud and B. Levy, *J. Phys. B: Atom. Mol. Opt. Phys.* **22**, 3155 (1989).

M. Czajkowski, R. Bobkowski and L. Krause, *Phys. Rev. A* **41**, 277 (1990).

P. J. Hay, T. H. Dunning and R. C. Raffanetti, *J. Chem. Phys.* **65**, 2679 (1976).

S. Huzinaga, *J. Chem. Phys.* **66**, 4245 (1977).

W. Kedzierski, J. B. Atkinson and L. Krause, *Optics Letters* **14**, 607 (1989).

W. Kedzierski, J. Supranowicz, J. B. Atkinson and L. Krause, *Chem. Phys. Letters* (to appear).

H. Tatekawi, M. Tomonari and T. Nakamura, *J. Chem. Phys.* **82**, 5608 (1985).

X. ATOMIC, IONIC AND MOLECULAR COLLISIONS

**RECENT DEVELOPMENTS IN COLLISION INDUCED
INTRAMULTIPLY MIXING WITH $\text{Ne}^{**}\{(2p)^5(3p)\}$ ATOMS**

W.Boom, J.P.H.Sanders, H.C.W.Beijerinck and B.J.Verhaar
Physics Department, Eindhoven University of Technology, P.O.Box 513
5600 MB Eindhoven, The Netherlands

Absolute total cross sections $Q_{ik}^{|M_k|}$ for intramultiplet mixing collisions of short-lived electronically excited $\text{Ne}^{**}\{(2p)^5(3p)\}=\{\alpha\}$ atoms with groundstate atoms, like He, Ne or Ar, can be measured accurately for the various $\alpha_k \rightarrow \alpha_1$ transitions [1]. The magnetic quantum number M_k of the electronic angular momentum J of the initial α_k state with respect to the asymptotic relative velocity specifies the initial polarization of the atoms, produced with a polarized laser. Narrow-band interference filters are used to detect the fluorescence radiation from the short-lived α_k and α_1 states.

Insight in the collision dynamics can be obtained by comparing the experimental results with both quantum-mechanical coupled-channels calculations and semiclassical calculations [2,3,4,5]. Avoided crossings between the adiabatic potentials and rotational coupling between the different $\Omega=|M_k|$ molecular states play a dominant role. Currently both the magnitude of the measured cross sections as well as the observed polarization effect can be understood quantitatively in most cases, thereby clearly demonstrating the validity of the model-potentials used [6,7]. Possible symmetry effects for the $\text{Ne}^{**}\text{-Ne}$ system [5] and the competition between intramultiplet mixing and Penning ionization for the $\text{Ne}^{**}\text{-Ar}$ system [8] are still to be revealed.

Recently, a hollow cathode arc beam source for $\text{Ne}(^3P_0, ^3P_2)$ atoms has been installed, resulting in a wide range of collision energies (300-3000 meV). Also, in the future, application of laser cooling techniques [9] should enable us to study ultra cold collisions (0.01-10 meV).

In Figure 1 preliminary quantum calculations are presented for the exothermal $\alpha_4 \rightarrow \alpha_3$ transition of the $\text{Ne}^{**}\text{-He}$ system, with the collision energy varying over seven orders of magnitude. In the low energy limit the cross section is determined by a single scattering matrix element (*s-wave scattering*) and is proportional to the De Broglie wavelength. In the high energy limit many partial waves contribute to the cross section, and a semiclassical Landau-Zener model is appropriate for this case. An oscillatory quantum structure interconnects the two extremes.

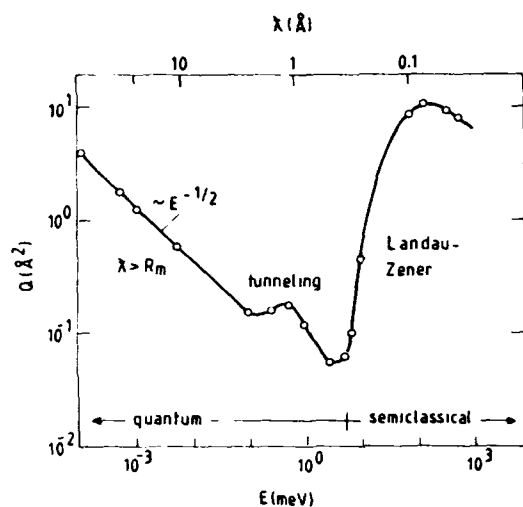


Fig.1 Calculated cross section for the exothermal process of collision induced intramultiplet mixing for the $\alpha_4 \rightarrow \alpha_5$ transition in $\text{Ne}^{**}\{(2p)^5(3p)\}$ in collisions with He as a function of the collision energy.

Preliminary high energy quantum calculations reveal many interesting new features, yet to be studied in further detail. The $\alpha_5 \rightarrow \alpha_7$ transition, for example, displays a clear asymmetry in polarization effect: at 1 eV the ratio $Q^0/Q^1 \approx 1$ for the $\alpha_5 \rightarrow \alpha_7$ transition, but $Q^0/Q^1 \approx 2$ for the reverse $\alpha_7 \rightarrow \alpha_5$ transition. Another example is the large impact parameter behaviour of the $\alpha_4 \rightarrow \alpha_5$ and $\alpha_7 \rightarrow \alpha_6$ transition. A considerable part of the cross section originates from an impact parameter range far beyond the crossing radius of the relevant avoided crossing, and is not accounted for in the current semiclassical model.

1. M.P.I.Manders, W.M.Ruyten, F.v.d.Beucken, J.P.J.Driessen, W.J.T.Veuglers, P.H.Kramer, E.J.D.Vredendregt, W.B.M.van Hoek, G.J.Sandker, H.C.W.Beijerinck and B.J.Verhaar, *J.Chem.Phys.* **89**(1988)4777
2. M.P.I.Manders, J.P.J.Driessen, H.C.W.Beijerinck and B.J.Verhaar, *Phys.Rev.Lett.* **57**(1986)1577, *ibid.* **57**(1986)2472
3. M.P.I.Manders, J.P.J.Driessen, H.C.W.Beijerinck and B.J.Verhaar, *Phys.Rev.A* **37**(1988)3237
4. M.P.I.Manders, W.B.M.van Hoek, E.J.D.Vredendregt, G.J.Sandker, H.C.W.Beijerinck and B.J.Verhaar, *Phys.Rev.A* **39**(1989)4467
5. M.P.I.Manders, W.Boom, H.C.W.Beijerinck and B.J.Verhaar, *Phys.Rev.A* **39**(1989)5021
6. D.Hennecart and F.Masnou-Seeuws, *J.Phys.B* **18**(1985)657
7. H.Kucal, D.Hennecart and F.Masnou-Seeuws, *J.Chem.Phys.* (accepted for publication)
8. J.P.J.Driessen, F.J.M.v.d.Weijer, M.J.Zonneveld, L.M.T.Somers, M.F.M.Janssens, H.C.W.Beijerinck and B.J.Verhaar, *Phys.Rev.Lett.* **62**(1989)2369
9. P.S.Julienne and F.H.Mies, *J.Opt.Soc.Am B* **6**(1989)2257

COLLISIONAL ION DRIFT SELFALIGNMENT AS A TOOL FOR
ELECTRIC FIELD DETERMINATION IN IONIZED GAS

S.A.Kazantsev, A.G.Petraashen, N.T.Polezhaeva, V.N.Rebane,
T.K.Rebane
Institute of Physics, Leningrad State University, 199034
Leningrad, U S S R

Anisotropic collisional relaxation of close fine structure levels caused by the drift motion of ions in an ionized gas gives rise to the polarization effects on ion spectral lines /1/. The ion drift self-alignment was used in this work for the determination of electric field variation in a plasma and the ion drift velocity profile.

Experimental measurements were performed in the argon discharge plasma maintained in the cylindrical hollow cathode (1 cm diameter) for the pressure range 0.01-0.5 Torr and the discharge current 20-25 mA. The optical emission was observed along OX direction parallel to the axis of the hollow cathode from different radial small parts of the discharge with z-coordinate. The studied spectral lines 3819 and 3883 Å correspond to the transitions from fine structure levels of Ar⁺ doublet 4d¹ 2 P^{1/2, 3/2} with the fine structure splitting of 0.01 eV to the same lower level 4p¹ 2 D^{3/2}. The radial profiles of the first and second Stokes parameters (I, P) which were measured by means of the Hanle polarization spectrometer /2/ (Fig.1) indicated that the drift selfalignment of 4d¹ 2 P^{3/2} level was responsible for the linear polarization of the line 3819 Å emission.

Making use of the equation for the polarization moments of ionic doublets under the anisotropic collisional relaxation due to Ar⁺ drift in the atmosphere of argon atoms and the expressions of Stokes parameters of a spectral line in terms of polarization moments of the upper level for the dipole transition /3,4/ we have

$$A(p, v_0, z) = \frac{12,5(I_y - I_z)^{3/2}}{5(I_y + \frac{1}{2}I_z)^{3/2} - (I_y + \frac{1}{2}I_z)^{1/2}} = \frac{\sqrt{2} R_0^{02}(1/2, 3/2)}{\Gamma_0 - R_0^{22}(3/2, 3/2)}$$

where I_y, I_z are the spectral line intensities with the linear polarizations directed along OY and OZ axes (OZ is the radial drift direction), 1/2, 3/2 denote the spectral transitions 3883 and 3819 Å respectively, R_{0⁰²}(1/2, 3/2) - matrix elements of the anisotropic collision relaxation matrix of Ar⁺ excited states for Ar⁺-Ar collisions. These matrix elements are dependent on the radial drift velocity v₀ of Ar⁺ ions in the plasma electric field E(z), Γ₀ - radiative decay constant.

The function A(p, v₀, z) is composed of observable linear polarizations I_y, I_z for two spectral lines originating from 4d¹ 2 P^{1/2, 3/2} Ar⁺ doublet. This quantity is a function of the gas pressure, the position of the studied part of the discharge and the locale drift

velocity of argon ions. The left hand side of this equation was determined experimentally as a function of z -coordinate and the gas pressure p on a basis of the spectropolarimetric data. The relaxation matrix elements R_0 on the right hand side are in turn dependent on the drift velocity v_0 . These matrix elements were calculated numerically considering the drift velocity v_0 as a variable parameter and using the technique devised in the paper /4/.

The drift velocities for every z -coordinate were determined as a result of the comparison of the calculated function $\Lambda(p, v_0)$ with the experimental one. The final $v_0(z)$ values provided the best fit of the calculated dependence $\Lambda(p, z)$ to the experimental data. The radial profile of the drift velocity is presented in Fig.2 for different gas pressures. Using the mobility coefficients of Ar^+ ions in the own gas the radial profile of the electric field $E(z)$ was determined for different gas pressures (Fig.3). The comparison of $E(z=5\text{mm})$ values (*Fig. 3) with independent electric measurements showed good agreement.

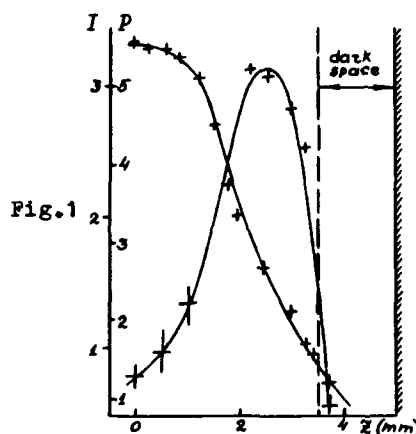


Fig.1

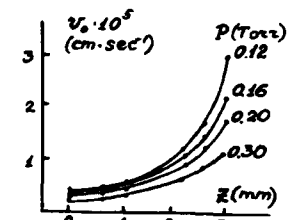


Fig.2

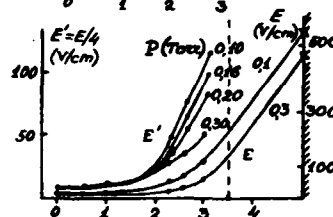


Fig.3

Fig.1 Radial variation of the first (I) and the second (P) Stokes parameters of the Ar^+ 3819 Å line emitted by the hollow cathode (1 cm diameter, $i = 20$ mA, $p = 0.25$ Torr)

Fig.2 Radial profile of Ar^+ ion drift velocity $v_0(z)$ for different argon pressures ($i = 20$ mA)

Fig.3 Radial profile of electric field in the ionized gas of the hollow cathode argon discharge ($i = 20$ mA).

1. S.A.Kazantsev, A.G.Petrashen, N.T.Polezhaeva, V.N.Rebane, T.K.Rebane - Europhys. Confer. Abstracts 1987, 11E, C3-12
2. S.A.Kazantsev, A.V.Subbotenko - J. Phys. D 1987, 20, 741
3. S.A.Kazantsev, A.G.Petrashen, N.T.Polezhaeva, V.N.Rebane, T.K.Rebane - Abstr.Contrib.Papers ELICAP(Paris) 1988, p. XI-54
4. A.G.Petrashen, V.N.Rebane, T.K.Rebane-Sov. JETP 1984, 87, 147.

FREE PARTICLE MODEL FOR CHARGE-CHANGING PROCESS AT RELATIVISTIC VELOCITY COLLISION

S. Karashima
 Department of Electrical Engineering, Science University of Tokyo
 Kagurazaka 1-3, Shinjuku-ku, Tokyo 162, Japan

Calculations are made for charge state distribution of U-ions at energies of 200-, 437- and 962- MeV/amu passing through low and high atomic number (Z_T) targets. An approximation is made on the target atom in the charge-changing processes between electron loss and capture ones. The target consists of a free electron gas - a target nucleus. This free particle model (FP model) is equivalent to a free plasma model.

The interaction potentials consists of a Coulomb potential V_{Te} of an ejected electron with a target nucleus and V_{ee} of an ejected electron with a free target electron. Following the FP model and the first Born approximation with some relativistic modifications, the transition probability of an electron loss induced by a Coulomb potential V_{Te} is nearly Z_T times larger than that by a Coulomb potential V_{ee} . Hence the total electron loss transition probability roughly depends on $Z_T(Z_T + 1)$, provided it is given as a sum of respective probabilities. Such a Z_T -dependence might not be always valid and is reduced in reality, because an ejected electron feels only effective charges screened by inner shell electrons and a target nucleus due to outer electrons. However, this FP assumption is almost justified in the case of collision system dealt with in the present calculation.

The kinematics in the collision system is shown in Fig.1. We adopt the projectile frame and neglect the recoil of a projectile nucleus. The momentum conservation requires $q_T + p = q_T' + k$; q_T and q_T' are the initial and final momenta of a target nucleus (T); the momentum transfer $q = q_T - q_T'$, and k is the momentum of an ejected electron (e). Here p denotes the initial momentum of the projectile-electron and follows the distribution $|\tilde{\phi}_{pe}(p)|^2$ with $\tilde{\phi}_{pe}(p)$ describing the Fourier transform of the bound-state wave function $\phi_{pe}(r)$. From the energy conservation in collision process, we obtain the following relation in the projectile frame:

$$M_p + \epsilon_0 + E_T = M_p + \epsilon_k + E_T' \quad (1)$$

where M_p is the projectile mass; E_T and E_T' are the initial and final energies of a target nucleus (T): $E_T = (M_T^2 + q_T^2)^{1/2}$ and $E_T' = (M_T^2 + q_T'^2)^{1/2}$; ϵ_0 is the energy of the projectile electron given by $\epsilon_0 = m \epsilon_p$ with $\epsilon_p = [1 - (Z_p \alpha)^2]^{1/2}$ (α is the fine structure constant); ϵ_k is the energy of an ejected electron: $\epsilon_k = (m^2 + k^2)^{1/2}$. Using the projectile frame as a reference, q_T reads

$$q_T = -M_T \gamma v. \quad (2)$$

with the Lorentz contraction factor $\gamma = (1 - v^2)^{-1/2}$ and the initial velocity v . Consequently, from eq.(2) and the momentum transfer q , the energy transfer under the condition $M_T \gg |q_T|$ is given by

$$E_T - E_T' = -\gamma v \cdot q, \quad (3)$$

where we have employed $E_T \approx M_T + q_T^2 / (2M_T)$ and $E_T' \approx M_T + (q_T - q)^2 / (2M_T)$.

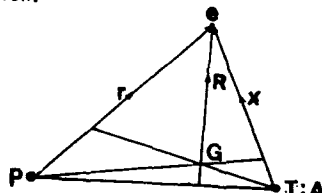


Fig.1 Electron loss system consists of a target atom A (target nucleus T), a projectile ion core P and an ejected electron e. The position vectors with respect to P, T and the center-of-mass G of the system are r, x , and R .

Here we consider the Rutherford scattering of T under the interaction V_{Te} between the projectile and electron. It is well known that this process is most probable in the forward direction, i.e. $(q_T \cdot q_T^i)/(q_T q_T^i) = 1$. Thus $q \cdot v = -1$. Combining eqs.(1), (3) and $q \cdot v$, we obtain

$$\gamma q v = \epsilon_k - \epsilon_0 \quad (4)$$

By the form factor $F(k, q) = \langle \psi_{pe}^{(-)}(k, r) | e^{iq \cdot r} | \psi_{pe}^{(-)}(r) \rangle$; $\psi_{pe}^{(-)}$ is continuum-state wave function, $|F(k, q)|^2$, the initial momentum distribution is approximately expressed by

$$\phi_{pe}(p) \propto \frac{1}{[p^2 + (Z_p a m)^2]^4} \quad (5)$$

Since eq.(5) has a sharp peak at $p \approx k - q \approx 0$, i.e. $k \approx q$, eq.(4) has the form

$$\gamma q v + \epsilon_0 = (m^2 + q^2)^{1/2} \quad (6)$$

Solving the quadratic equation (6), we obtain

$$q \approx \frac{m(1 - \epsilon_p)}{\gamma v}$$

in the relativistic region $\gamma v \gg 1$. The quantity $1/q$ is the effective range of the potential between e and T. Thus we put this effective range $\langle r \rangle$ as

$$\langle r \rangle \approx \frac{\gamma v}{m(1 - \epsilon_p)} \quad (7)$$

On the other hand, the non-relativistic orbital radius of the hydrogenic target is in the order of

$$\bar{r}_n \approx \frac{\bar{n}}{Z_T a m} \quad (8)$$

where \bar{n} is the effective principle quantum number and Z_T is the atomic number of the target atom. The effective atomic radius of the target for the electron loss process is at most up to $\bar{r}_n \approx \langle r \rangle$. We can estimate the effective principle quantum number from eqs.(7) and (8) as

$$\bar{n} \approx \frac{Z_T a \gamma v}{1 - \epsilon_p} \quad (9)$$

If the collision system is quite asymmetric, i.e. $Z_p \gg Z_T$, \bar{n} is much smaller than unity. Then the effective range of V_{Te} is very closed to a target nucleus. This means that the electron loss process takes place the close collision and electron screening is negligible. This is favorable to the assumption of the FP model.

On occasion of 200 MeV/amu- and 962 MeV/amu- U^{91+} bombardment on mylar ($Z=6.6$), \bar{n} becomes 0.12 and 0.32, respectively. Moreover, when 437 MeV/amu- and 962 MeV/amu U^{91+} on Ta ($Z_T=73$), we obtain $\bar{n}=2.19$ and $\bar{n}=3.62$. Even in this case, the effective atomic orbital is no more than the N-shell and hence the electronic screening contributions are almost neglected. Therefore, bound electrons are safely replaced with free ones.

1) S. Ichimaru, S. Mitake, S. Tanaka and X. Z. Yan, Phys. Rev. **A32**, 1768(1985).

COLLISIONAL MULTIPOLE RELAXATION IN THE 7F GROUND TERM OF SAMARIUM

P. Hannaford, R.M. Lowe and R.J. McLean
CSIRO Division of Materials Science and Technology
Clayton, Victoria 3168, Australia.

Collisional depolarization in the $4f^6 6s^2 {}^7F_{1-6}$ ground-term levels of Sm I by rare-gas perturbers has been studied using a technique based on the detection of Zeeman quantum beats in transmission geometry [1,2]. With this technique a sharp, broad-band pump pulse of resonant laser radiation generates coherence between non-degenerate Zeeman states of the lower level of an atomic transition by absorption and stimulated (or spontaneous) emission processes, and the time evolution of this coherence is monitored by the transmission of a weak cw probe laser through nearly-crossed polarizers. With the pump laser chosen to be either circularly polarized or linearly polarized at 45° to the magnetic field direction, the technique yields individual relaxation rates for the destruction of either orientation or alignment, respectively [2].

The 7F ground term of samarium has proven to be a useful test case for studying the nature of the collision interaction. Depolarization cross sections measured for the ${}^7F_{1-6}$ levels in the case of argon perturbers are summarized in Table 1. The magnitudes of the cross sections are unusually small and vary greatly from level to level within the 7F term. In the case of the 7F_1 level, the ratios of the cross sections for destruction of orientation and alignment are unexpectedly high ($\sigma_1/\sigma_2 \approx 1.6$ for each of the rare-gas perturbers) compared with the ratios for other $J=1$ levels studied previously and with the detailed numerical calculations of Berman and Lamb ($\sigma_1/\sigma_2 = 1.12 \pm 0.02$ [3]). By contrast the ratios for the ${}^7F_{2-6}$ levels are very low (σ_1/σ_2 in the range 0.39-0.46).

In the impact approximation the cross section for collisional relaxation of the 2^k -multipole can be expressed in the following form [4]:

$$\sigma_k = \sigma_0 + \sum_{\chi=1}^{2J} \left[[2J+1]^{-1} - (-)^{2J+k+\chi} \left\{ \begin{matrix} J & J & k \\ J & J & \chi \end{matrix} \right\} \right] B_\chi \quad (1)$$

where χ is the multipolarity of the collision interaction, B_χ are velocity-averaged and impact parameter-averaged coefficients that depend on irreducible components of rank χ of the collision S-matrix, and σ_0 is the cross section for depopulating collisions which is taken to be zero on the basis of our experimental results. Comparison of the ratios σ_1/σ_2 calculated from Eq. 1 with the experimental ratios (Table 1) shows remarkable agreement for all J levels of the Sm 7F term if just a single value of $\chi=2$ (corresponding to a pure quadrupole interaction) is used in the multipole expansion, in which case the theoretical expression for the ratio is given simply by

$$\sigma_1/\sigma_2 = [2J-1](2J+3)/3[4J(J+1)-7] \quad (2)$$

Also, the J-dependence of the geometrical factor in square brackets in Eq. 1 is found to account for much (factor of 30 for $k=1$) of the large decrease in the experimental σ_1 and σ_2 values as J increases from 1 to 4 (Table 1).

The occurrence of an essentially pure even-x collision interaction implies that during the collision the interaction commutes with itself at all times and the atomic levels remain pure J levels [5]. Such behavior is characteristic of a weak collision interaction. The weak nature of the interaction between the samarium $4f^6 6s^2 \ ^7F_{1-6}$ atoms and rare-gas perturbers indicated by these results is likely to be a consequence of the strong shielding of the 4f valence electrons by the symmetric charge distribution of the closed outer 6s shell, together with the relatively large separation of the fine-structure levels in the 7F term. Similar behavior could be expected in ground-term levels of other rare-earth atoms.

The observed depolarization cross sections for the Sm 7F_1 level in collisions with rare-gas atoms appear to be the first experimental realization of the simple theoretical result $\sigma_1/\sigma_2=5/3$, initially obtained by Omont in 1965 [6].

Table 1 Cross sections (\AA^2) for destruction of orientation (σ_1) and alignment (σ_2) in the $4f^6 6s^2 \ ^7F_J$ ground-term levels of samarium by argon perturbers.

Level J	Energy (cm^{-1})	Experiment			Theory ^a
		σ_1	σ_2	σ_1/σ_2	σ_1/σ_2
1	293	16.1(8)	10.3(5)	1.56(11)	1.67
2	812	2.2(2)	5.2(5)	0.42(4)	0.41
3	1490	0.19(2)	0.48(5)	0.39(5)	0.37
4	2273	0.10(1)	0.22(2)	0.46(5)	0.35
5	3125	0.77(9)	1.8(2)	0.42(7)	0.35
6	4021	1.7(3)	4.3(6)	0.39(9)	0.34

^acalculated from Eq. 2.

1. W. Lange and J. Mlynek, Phys. Rev. Lett. **40**, 1373 (1978).
J. Mlynek and W. Lange, Optics Comm. **30**, 337 (1979).
2. R.M. Lowe, D.S. Gough, R.J. McLean and P. Hannaford,
Phys. Rev. A, **36**, 5490 (1987);
R.J. McLean, P. Hannaford and R.M. Lowe,
(submitted to Phys. Rev. A).
3. P.R. Berman and W.E. Lamb, Phys. Rev. **187**, 221 (1969).
4. A. Omont, Prog. Quantum Electronics **5**, 69 (1977).
5. E. Lewis, Phys. Reports **58**, 1 (1980).
6. A. Omont, J. Phys. (Paris) **26**, 26 (1965).

RELATIVISTIC COUPLED-CHANNEL CALCULATIONS WITH COULOMB BOUNDARY
CONDITIONS

Nobuyuki Toshima

Institute of Applied Physics, University of Tsukuba, Tsukuba, Ibaraki 305, Japan

and

Jörg Eichler

Bereich Schwerionenphysik, Hahn-Meitner-Institut Berlin, D-1000 Berlin 39, Germany

Coupled-channel calculations constitute an appropriate method for simultaneously deriving excitation, ionization, and charge transfer cross sections in cases where the collision velocity is comparable to the speed of the active electron. In previous publications[1], we have worked out and applied this approach for relativistic projectile and electron velocities. In our analysis, we discovered the existence of anomalous long-range couplings in excitation processes which are absent in nonrelativistic collisions. While in the latter case the coupling between states has the characteristic dipole behavior with an R^{-2} dependence on the internuclear separation R , the coupling for relativistic collisions decreases as R^{-1} suggesting the influence of a monopole contribution.

The target nucleus is considered as a classical point charge Z_T fixed at the origin of the laboratory system, while the point charge Z_P representing the projectile moves with a relativistic velocity v along a classical rectilinear trajectory $\mathbf{R}(t) = \mathbf{b} + \mathbf{v}t$, where \mathbf{b} is the impact parameter. We seek to construct the solution $\Psi(\mathbf{r}_T, t)$ of the exact time-dependent Dirac equation

$$i \frac{\partial}{\partial t} \Psi(\mathbf{r}_T, t) = \left(-i c \boldsymbol{\alpha} \cdot \nabla_T - \frac{Z_T}{r_T} - S^2 \frac{Z_P}{r_P} + \gamma_4 c^2 \right) \Psi(\mathbf{r}_T, t) \quad (1)$$

where \mathbf{r}_T, t and \mathbf{r}'_P, t' are the electronic space-time coordinates with respect to the target nucleus in the target frame and with respect to the projectile nucleus in the projectile frame. The Lorentz transformation into the projectile frame of an eigenfunction ψ defined in the target frame is mediated by the spinor transformation S . Usually [1], Eq.(1) is solved approximately by expanding

$$\Psi(\mathbf{r}_T, t) = \sum_k a_k(t) \psi_k(\mathbf{r}_T, t) + \sum_{k'} a_{k'}(t) S^{-1} \psi_{k'}(\mathbf{r}'_P, t'). \quad (2)$$

However, even at asymptotically large projectile-target separations, the presence of one collision partner results in a distortion of the atomic states at the other collision partner. This effect is taken into account by a phase factors multiplying the atomic eigenfunctions. Such modified states are denoted as 'boundary-corrected' wave functions satisfying the asymptotic Dirac equation. Modifying the expansion (2) and denoting target and projectile states by labels k and k' , respectively, we write

$$\Psi(\mathbf{r}_T, t) = \sum_k a_k(t) e^{-i\nu_P \ln(R'-vt')} \psi_k(\mathbf{r}_T, t) + \sum_{k'} a_{k'}(t) e^{i\nu_T \ln(R-vt)} S^{-1} \psi_{k'}(\mathbf{r}'_P, t'). \quad (3)$$

where $R' = \sqrt{b^2 + v^2 t'^2}$, and the Sommerfeld parameters are $\nu_T = Z_T/v$ and $\nu_P = Z_P/v$.

Owing to the Lorentz transformation $t' = \gamma(t - vz_T/c^2)$ with $\gamma = (1 - v^2/c^2)^{-1/2}$, the additional phase factors in (3) not only depend on time but also on space coordinates and hence cannot be absorbed into the expansion coefficients. This is different from the nonrelativistic case. With the expansion (3), the long-range couplings [1] disappear from the coupled equations.

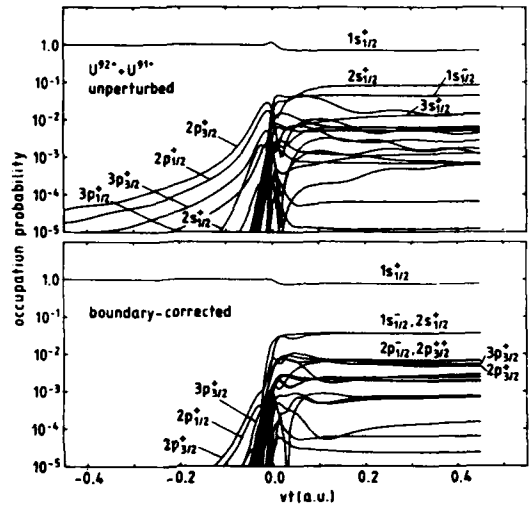


Figure 1: Time evolution of occupation probabilities in 36-state two-center coupled-channel calculations

Figure 1 shows the time evolution of the occupation probabilities of various target states populated from an initial $1s_{1/2}$ state in a $U^{92+} + U^{91+}$ collision at 0.5 GeV/u. The probabilities are calculated at $b = 0.01 a.u.$ which is approximately equal to the K-shell radius a_K of uranium. The upper part of the figure corresponds to the expansion (2) in terms of unperturbed basis states while the lower part of the figure is calculated with the boundary-corrected expansion (3).

We show that in relativistic Born calculations for excitation, owing to the simple unidirectional two-state coupling, proper boundary conditions are automatically satisfied whether or not the additional phase factors are included. However, for multi-state coupled-channel calculations it is vital to explicitly include Coulomb boundary conditions. As is seen in figure 1 this not only affects the distance over which the couplings prevail but also completely changes the final transition probabilities.

1. N. Toshima and J. Eichler, Phys. Rev. Lett. 60,573(1988); Phys. Rev A 38,2305(1988); Phys. Rev A 40,125(1989)

ATOMIC POLARIZATION PRODUCED IN NA-AR AND NA-XE OPTICAL COLLISIONS

D. Olsgaard and M. Havey
 Physics Department
 Old Dominion University
 Norfolk, Virginia 23529

Atomic state distributions produced in simultaneous collisional and radiative processes are sensitive to both the pertinent molecular potentials and the nonadiabatic couplings among the adiabatic terms of a system. These distributions are important in many elastic and inelastic collisions processes, including electronic quenching and collisional depolarization in excited atomic states. In this paper, experimental results on Na-Ar and Na-Xe optical collisions are reported. Excitation of atomic Na $3p^2P_{3/2}$ is achieved with linearly polarized radiation tuned from about 600 cm^{-1} blue to 150 cm^{-1} red of the Na resonance transitions. The experiments determine both the fine structure branching and the alignment of the $j = 3/2$ level as a function of detuning from resonant excitation.

A short pulse, pump-probe technique is used for the alignment measurements. Excitation during the collision is achieved by a 0.5 ns laser pulse tuned in the vicinity of the Na resonance transitions. The alignment is determined by probing the $j = 3/2$ level on the $3p^2P_{3/2} - 5s^2S_{1/2}$ transition with a second laser whose polarization is alternately parallel and perpendicular to that of the pump laser. The ultraviolet cascade fluorescence from the $4p^2P_{3/2}$ to the $3s^2S_{1/2}$ ground state is detected; the relative signal size in the parallel and perpendicular channels is proportional to the alignment. This approach eliminates depolarizing effects due to hyperfine precession, subsequent collisions, and radiative trapping. Two-photon, two-color measurements of the relative (collision free) polarization dependence of the $3s - 5s$ transition rate are used to illustrate the effectiveness of this technique. Data illustrating this effect in the vicinity of the resonance transitions is presented in Figure 1.

The dependence of the atomic polarization as a function of detuning for Na - Xe optical collisions is illustrated in Figure 2. The polarization is defined as the signal difference in the parallel and perpendicular channels normalized to the sum of the signals. The polarization of the $j = 1/2$ level was determined to be zero within a measurement uncertainty of about 2 percent; this is consistent with an alignment of zero expected for a $j = 1/2$ state. Resonant excitation of the $j = 3/2$ level produced a polarization of 59 (2) percent; in the absence of any depolarizing mechanisms, a value of 60 percent is expected. For red detunings the polarization is seen to be zero within the measurement uncertainties. This arises partly from curvature of the collision trajectories associated with the strongly bound molecular states excited for red detunings. Coherent excitation of the two, nearly degenerate Π electronic states also leads, through the spin-orbit coupling, to strong depolarization for red detunings when a characteristic collision

time is longer than the spin-orbit precession time; this is the case for Na -Xe collisions. For large blue detunings excitation is primarily to a strongly repulsive Σ state. The consequently reduced curvature of the trajectories is a primary determinant of the higher polarization of about 7.5(2) percent seen for these detunings.

Figure 1.

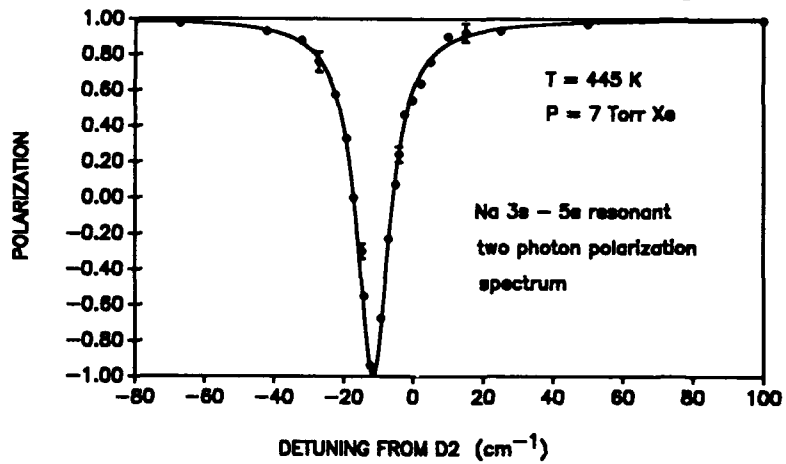
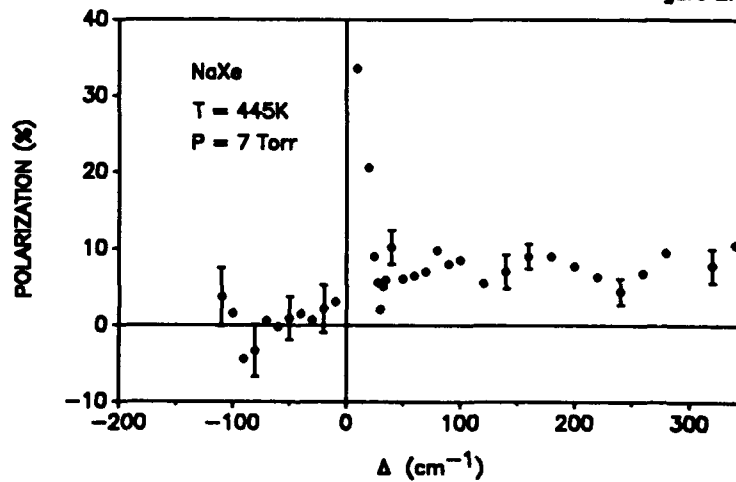


Figure 2.



**POLARIZED N^{4+} ION BEAM FORMED BY ELECTRON
CAPTURE IN A POLARIZED SODIUM TARGET**

C.J. Liu, R.W. Dunford, Y. Azuma, N.B. Mansour and H.G. Berry

Physics Division, Argonne National Laboratory, Argonne, IL 60439

D.A. Church

Physics Department, Texas A&M University, College Station, TX 77843

We have obtained a beam of electron polarized N^{4+} ions by charge exchange of a beam of N^{3+} in an optically-pumped sodium target. This experiment demonstrates the general applicability of the optical pumping technique for producing beams of polarized highly-charged ions [1].

Experiments with beams of polarized atoms/nuclei have long been of interest in atomic, nuclear, and high-energy physics. In atomic physics, ions with significant electronic polarization can be used for fundamental experiments such as tests of parity nonconservation [2] and in the study of spin-dependent effects in the scattering of polarized electrons by polarized ions. Also, measurement of the polarization of the photons emitted after charge exchange by a polarized ion in an atomic target is a means of testing the theory of charge-exchange excitation [3]. Use of nuclear-spin polarized beams allows the study of spin-dependent interactions and of symmetries and invariances in nuclear and particle physics.

The N^{3+} ion beam comes from the Argonne PII ECR ion source at the ATLAS heavy-ion linac. The sodium beam is formed by a two-stage oven [4]. It is optically pumped by a CR699-21 ring dye laser with both frequency and noise modulation on the laser spectral-density distribution to cover both the ground-state hyperfine levels and the complete Doppler profile [1]. The polarization of the ions was detected by measuring the circular polarization of radiation from the $NV\ 2s\ ^3S - 2p\ ^3P^0$ (124 nm) transition taking place after the electron capture. A circular polarization (S/I) of $(5.7 \pm 0.7)\%$ was observed. Based on the observed circular polarization, we estimate that electron and nuclear polarizations of approximately 4% were obtained in our experiments for ions which reached the ground state via the 2s-2p transition.

Our calculations [5] indicate that the maximum expected electron and nuclear polarization for N^{4+} using our schemes is 10%. A maximum electron-spin polarization of 25% for N^{4+} is possible with a magnetic field in the capture region strong enough to decouple the nuclear spin. The reasons for lower than expected polarization of the N^{4+} beam will be discussed. An experiment to produce electron-spin polarized $^{12}C^{3+}$ ions (nuclear spin zero) is being planned. In this experiment, the circular polarization of the radiation from the $C\ IV\ 2s\ ^2S - 2p\ ^2P^0$ (154.8 nm) transition taking place after the electron capture will be measured.

This work is supported by the U. S. Department of Energy, Office of Basic Energy Sciences, under Contract W-31-109-ENG-38.

References

- [1] C.J. Liu, N.R. Mansour, Y. Azuma, H.G. Berry, D.A. Church and R.W. Dunford, *Phys. Rev. Lett.* **64**, 1354 (1990); R.W. Dunford, C.J. Liu, N.B. Mansour, Y. Azuma, H.G. Berry, D.A. Church, T.P. Dinneen, L. Young and B.J. Zabransky, *Nucl. Instrum. Methods* **B43**, 459 (1989); R.W. Dunford, H.G. Berry, C.J. Liu, M. Hass, R.C. Pardo and M.L.A. Raphaelian, *Nucl. Instrum. Methods* **B40/41**, 9 (1989).
- [2] R.W. Dunford and R.R. Lewis, *Phys. Rev. A* **23**, 10 (1981).
- [3] S.M. Khalid and H. Kleinpoppen, *Z. Phys. A* **311**, 57 (1983).
- [4] C.J. Liu, R.W. Dunford and N. Mansour, *Bull. Am. Phys. Soc.* **34**, 1372 (1989).
- [5] C.J. Liu and R.W. Dunford, submitted for publication.

DETERMINING THE ABSOLUTE SCALE FOR Mg^+ + He DIFFERENTIAL SCATTERING CROSS SECTIONS
AT 30-, 66.7-, AND 150-keV Mg^+ ENERGIES

E. Redd, Industrial Technology Department
Southwest Missouri State University, Springfield, MO 65804 USA

Introduction

These differential cross sections were first reported in 1988 [1]. In that publication only the cross section at 66.7 keV was on an absolute scale. The cross sections at 30- and 150-keV were reported on a relative scale. Alternate methods have since been developed to make these latter two cross sections absolute.

This paper reports these cross sections. In addition, the zero-angle method developed for 150-keV was applied to the other energies. Its results are in acceptable agreement with the truncated method used at 30 keV. At 66.7 keV the zero-angle method's results agree so poorly with the original results that it calls into question the zero-angle method's validity. However, at present, there is no other way to obtain an absolute cross section for 150 keV.

Original Normalizing Method

The Mg^+ ions were accelerated and collimated, and traversed a differentially pumped He target. The scattered beam entered an analyzing magnet which separated the ions and neutrals. The deflected ions were measured with one detector. The undeflected neutrals were measured with another. As the accelerator rotated about the scattering center, data from both detectors were collected as a function of angle. Relative cross sections were obtained from these two angular distributions through the proper mathematical operations, including deconvolution[2]. They are relative because the detectors' efficiencies were unknown.

But by turning off the analyzing magnet, auxiliary measurements were made as both ions and neutrals struck the same detector. The still unknown ion and neutral detection efficiencies of this detector were assumed equal[1]. This assumption, coupled with measuring the whole non-negligible angular range of both the ion and neutral signals, gave the absolute total cross section at 66.7 keV. The relative differential cross section was then normalized to this absolute total cross section.

At 150 keV, an auxiliary measurement was made only at zero angle. At 30 keV, the auxiliary measurements were made out to an angle of 5.6 mrad. Measurements at such small angles are not sufficient to give absolute total cross sections.

Truncated Normalizing Method

At 30 keV, then, the auxiliary measurements could only give a "partial" total cross section, that is, a differential cross section integrated out to 5.6 mrad. Therefore, the 30 keV relative differential cross section was truncated to 5.6 mrad and was normalized to the "partial" total cross section. The relative differential cross section at angles greater than 5.6 mrad was then brought to the same scale. These results are shown in Fig. 1. Since the differential cross section in Fig. 1 is non-negligible and still rising at 28 mrad, a total cross section can not be determined. But integration of these results gives a lower bound to the total cross section at 30 keV of $(1.2 \pm 0.4) \times 10^{-17} \text{ cm}^2$.

Zero-Angle Normalizing Method

Since auxiliary measurement angular distributions did not exist at 150 keV, the relative ion angular distribution was scaled to make its zero-angle result equal to the zero-angle auxiliary ion measurement. The relative neutral angular distribution was similarly scaled to the zero-angle auxiliary neutral measurement. Both angular distributions were therefore scaled to the same detector. Absolute total and differential cross sections could then be calculated. The total cross section is $(2.0 \pm 0.7) \times 10^{-17} \text{ cm}^2$. The differential cross section is shown in Fig. 2.

Method Comparison

Since the auxiliary measurements for 30- and 66.7-keV included zero angle, their data can be subjected to the zero-angle method. At 30 keV this method obtained an integrated (out to 28 mrad, as above) cross section of $(1.9 \pm 0.7) \times 10^{-17} \text{ cm}^2$. This result contains, within its error, the lower bound given above.

At 66.7 keV the zero-angle method gives a value of $(1.1 \pm 0.6) \times 10^{-16} \text{ cm}^2$ for the total cross section. This is 6 times as large as the $(1.8 \pm 0.4) \times 10^{-17} \text{ cm}^2$ result from the original method given in Ref. 1.

The agreement at 30 keV and the variance at 66.7 keV occur because the zero-angle method is very susceptible to noise in the measurements at zero angle. However, this method is the only presently available means to calculate an absolute cross section at 150 keV.

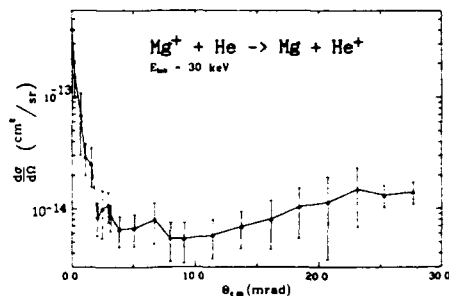


Figure 1. Angular differential cross section $\text{Mg}^+ + \text{He} \rightarrow \text{Mg} + \text{He}^+$ at 30-keV.

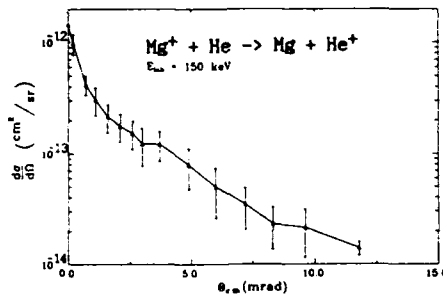


Figure 2. Angular differential cross section $\text{Mg}^+ + \text{He} \rightarrow \text{Mg} + \text{He}^+$ at 150-keV.

1. T.J. Gay, E. Redd, D.M. Blankenship, J.T. Park, J.L. Peacher, and D.G. Seely, J. Phys. B21, L467 (1988).

2. J.T. Park, J.M. George, J.L. Peacher, and J.E. Aldag, Phys. Rev. A18, 857 (1978).

Thanks go to Aron Gaus for preparing the Figures.

STATE-SELECTIVE *KLL* RTEA MEASUREMENTS FOR COLLISIONS OF
0.25–2 MeV/u F^{7+} WITH H_2 AND He TARGETS.[†]

D.H. Lee, P. Richard, T.J.M. Zouros*, J.M. Sanders, and J.L. Shipaugh
J.R. Macdonald Laboratory and Physics Department, Kansas State University
Manhattan, Kansas 66506, USA

Absolute *KLL* Auger production cross sections were measured for collisions of 0.25–2 MeV/u $F^{7+}(1s^2\ ^1S, 1s2s\ ^3S)$ with H_2 and He at 0° with respect to the beam direction. Fig. 1 shows a sample *KLL* Auger electron spectrum for $1\frac{1}{8}$ MeV/u F^{7+} incident on He and consists of the Auger decay of $[1s2l2l']\ (2S+1)L$ excited states to the $1s^2\ ^1S$ ground state. The absolute cross sections were obtained by normalizing to binary encounter electron production calculated in the impulse approximation (IA) for 0.5–2 MeV/u $F^{9+} + H_2$ collisions.¹

The mechanisms for forming the excited states include transfer excitation from the projectile $1s^2\ ^1S$ ground state and either electron capture or transfer excitation from the projectile metastable $1s2s\ ^3S$ state.² The projectile energy dependence of the Auger production cross section reflects the various mechanisms as shown in Fig. 2, where only the 2D and $^2P_+$ are shown. These two states exhibit strong signatures of resonant transfer-excitation followed by Auger decay (RTEA) around 20 MeV. RTE is possible only from the $1s^2\ ^1S$ ground state.

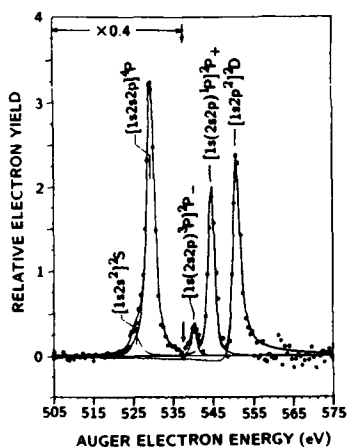


Fig. 1. 0° Auger electron spectrum produced in $1\frac{1}{8}$ MeV/u $F^{7+}(1s^2\ ^1S, 1s2s\ ^3S) + He$ collisions.

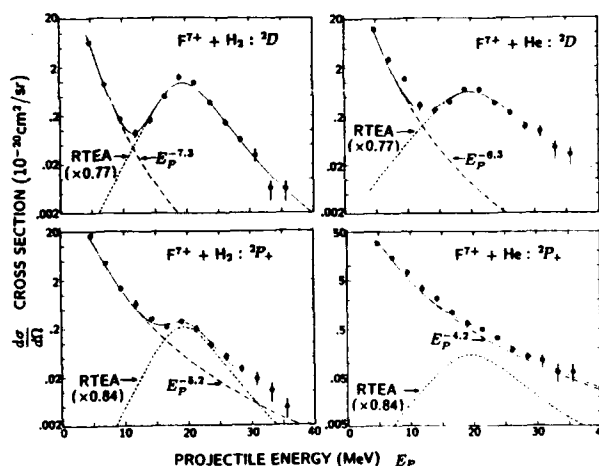


Fig. 2. Absolute 0° Auger electron production cross sections for 2D and $^2P_+$ states produced in $F^{7+}(1s^2\ ^1S, 1s2s\ ^3S) + He$ and H_2 collisions versus projectile energy.

We attribute the monotonically decreasing cross section (see dashed lines) for the 2D and $^2P_+$ states to non-resonant transfer excitation (NTE) and electron capture, respectively, from the $1s2s\ ^3S$ metastable state. The NTE from the metastable state is much larger than that from the ground state due to the large $2s \rightarrow 2p$ excitation probability relative to the $1s \rightarrow 2p$ excitation

probability which explains the large NTE cross section for the 2D state compared to the negligible NTE cross section for $[1s2s2p^2]^3D$, 1D states in $F^{6+}(1s^22s) + H_2$ collisions.³ The projectile energy dependence of the $^2P_+$ state is consistent with that of the 4P state (not shown here). The 4P state is found to be produced primarily by electron capture by the metastable $1s2s^3S$ state.²

The data are fit to an E_p^{-n} dependence (as shown in Fig. 2) which reflects the NTE and capture mechanisms from the metastable beam component, and to the RTEA energy dependence. The dot-dashed line is the RTEA calculation using the IA with an improved treatment¹ and the RTE alignment factor.⁴

In the following Table, we present calculated and measured resonance excitation-scattering (RES) strengths (in units of $10^{-19} \text{ cm}^2 \text{ eV}$) for the production of all $F^{6+}[1s2l2l']$ states. $\Omega_{RES} = \xi \cdot \Omega_{RC}$, where ξ is Auger yield and Ω_{RC} is radiationless capture strength and its expression is given in Ref. 3. E_A (eV) are from Ref. 5. Auger rate Γ_A ($10^{13}/\text{sec}$) and yield ξ were taken from Ref. 6. Quoted experimental error of $\Omega_{RES}[\text{expt}]$ is only relative. Absolute error is $\sim 15\%$.

State	E_A	$E_A[\text{expt}]$	Γ_A	ξ	Ω_{RES}	$\Omega_{RES}[\text{expt}]$
$[1s2s^2]^2S$	525.9	526.1	7.97	.997	7.48	-
$[1s2s2p]^4P$	529.8	529.8	< .001	.895	0.00	-
$[1s(2s2p)^3P]^2P_-$	540.3	540.1	0.579	.618	1.10	$1. \pm .4$
$[1s(2s2p)^1P]^2P_+$	545.6	545.2	6.18	.990	16.7	14 ± 2
$[1s(2p^2)^3P]^4P$	544.9	-	$\sim .001$.975	0.01	-
$[1s(2p^2)^1D]^2D$	551.1	551.2	10.13	.979	45.5	35 ± 2
$[1s(2p^2)^3P]^2P$	553.1	-	.0085	.013	6.00	-
$[1s(2p^2)^1S]^2S$	561.2	-	1.23	.857	0.93	-

In conclusion, the absolute 0° RTEA cross sections were measured and compared with the results of an RTEA-IA treatment leading to a good agreement. RES strengths for these states were extracted from the measured Auger cross sections and compared with the theoretical values resulting in good agreement within the experimental and theoretical uncertainties. This simultaneous agreement for both 2D and $^2P_+$ states confirms the selection rule for the formation of an excited state by RTE and the preferential population of the $M_L=0$ magnetic substate.⁴

† Supported by the Division of Chemical Sciences, Office of Basic Energy Sciences, Office of Energy Research, U.S. Department of Energy.

* Present address: University of Crete and Research Center of Crete, Department of Physics, Iraklion, Greece.

¹ D.H. Lee, P. Richard, T.J.M. Zouros, J.M. Sanders, J.L. Shinpaugh and H. Hidmi, Phys. Rev. A41 4816 (1990).

² M. Terasawa, T.J. Gray, S. Hagmann, J. Hall, J. Newcomb, P. Pepmiller, and P. Richard, Phys. Rev. A27, 2868 (1983).

³ T.J.M. Zouros, C.P. Bhalla, D.H. Lee and P. Richard to be published in Phys. Rev. A 1990.

⁴ C.P. Bhalla Phys. Rev. Lett. 64, 1103 (1990); N.R. Badnell Phys. Rev. A41, 3555 (1990).

⁵ K.T. Chung and B.F. Davis, private communications (1988).

⁶ C. Can, T.W. Tunnell, and C.P. Bhalla, J. Elec. Spectr. and Related Phenom. 27, 75 (1982); T.W. Tunnell, C. Can, and C.P. Bhalla, IEEE Trans. NS-26 No.1, 1124 (1979); M.H. Chen and B. Crasemann, Phys. Rev. A27, 544 (1983); E. Träbert, Nucl. Instrum. & Meth. in Phys. Res. B23, 287 (1987).

MOLECULE LIKE BEHAVIORS OF H⁻ IN COLLISION DYNAMICS

Michio Matsuzawa*, Naoto Koyama[†], Motoi Maeda* and Tokuichi Ishihara*
 Department of Applied Physics and Chemistry*, Division of Affairs of Foreign Students[†],
 The University of Electro-Communications,
 Chofu-shi, Tokyo 182, Japan

We report our theoretical study on double photoexcitation and Ar-impact double excitation of H⁻ in the strongly correlated doubly excited states. We have calculated the energy levels and the wavefunctions of H⁻ using the hyperspherical coordinates^{1,2,3}. We have evaluated optical oscillator strengths of H⁻ between strongly correlated doubly excited states and the excitation cross sections of H⁻ in the doubly excited states by Ar impact. To investigate the Ar-impact excitation, we employ the impulse approximation. In the present treatment, we have assumed that the coupling of the doubly excited states with the continuum can be neglected. In other words, for example, we discuss only the dipole matrix element to the discrete part of the resonant wavefunction, in photodetachment of H⁻ in the ground state. In the Ar-impact excitation processes, we study the energy ranges of an incident particle in which their collision times are much shorter compared with the life times of the doubly excited states against autoionization.

To interpret the results obtained, we employ the classification scheme of the doubly excited states, ie. $[N(K,T)A_n]^{2S+1L^{\pi}}$ proposed by Lin⁴ and rely on the rovibrator model proposed by Kellman and Herrick⁵, in which H⁻ is viewed as a floppy "e-H⁺-e" linear triatomic molecule. Here N(n) is a principal quantum number of an inner (outer) electron, K and T are angular correlation quantum numbers, while A is a radial correlation quantum number. It is convenient for understanding the character of the excitation processes studied here to introduce the vibrational quantum number $v=N-K-1$ of doubly degenerate bending modes of the "floppy linear molecule" and the radial bending quantum number $n_2=(v-T)/2$.

We have found some systematic trends, ie. a set of simple propensity rules for the excitation processes studied here, ie. the radial propensity rule $\Delta A=0$ and the angular propensity rules $\Delta v=\Delta T=0$ for the ¹Se-¹Se and ¹Se-¹D^e Ar-impact excitation. The latter leads to the propensity rules $\Delta n_2=0$. Namely, the excitation processes specified by these propensity rules is most likely to occur within the manifold of excitation processes from the same initial excited state. This is interpreted as a result of isomorphism of the correlation pattern in the surface density plot of the squared hyperspherical channel functions between the initial and final states. According to the rovibrator model, this indicates that H⁻ in the doubly excited states tends to conserve its internal state as the "floppy triatomic molecule" during these excitation processes.

For ¹Se-¹Po excitation processes, the radial propensity rule $\Delta A=0$ is incompatible with the angular propensity rules $\Delta v=\Delta T=0$ because of the Pauli exclusion principle for two atomic electrons. Tables 1 and 2 list the excitation processes in the decreasing order of the magnitudes of the optical oscillator strengths

Table 1. Double photoexcitation of H⁻

Initial States	Final States	ΔN	ΔA	Δv	ΔT	Δn_2	Δn
3(2,0)+3 ¹ Se	3(1,1)+3 ¹ Po	0	0	1	1	0	0
	3(2,0)+4 ¹ Po	0	x	0	0	0	1
	4(2,1)+4 ¹ Po	1	0	1	1	0	1
	4(3,0)+5 ¹ Po	1	x	0	0	0	2

Table 2. Ar-impact excitation of H⁻

Initial States	Final States	ΔN	ΔA	Δv	ΔT	Δn_2	Δn
3(2,0)+3 1S ^e	3(2,0)-4 1p ^o	0	x	0	0	0	1
	3(1,1)+3 1p ^o	0	0	1	1	0	0
	4(2,1)+4 1p ^o	1	0	1	1	0	1
	4(3,0)-5 1p ^o	1	x	0	0	0	2

and Ar-impact excitation cross sections for 1S^e-1p^o transitions. In these tables, we also give the changes of the quantum numbers N, A, v, T, n₂ and n. This enables us to understand easily the character of the excitation processes based on the rovibrator model.

For double photoexcitation, the radial propensity rule prevails over the angular propensity rules. The latter are modified into $\Delta v = \Delta T = 1$ though n₂ tends to be conserved. On the other hand, for the Ar-impact excitation processes, the angular propensity rules $\Delta v = \Delta T = 0$ dominate over the radial propensity rule $\Delta A = 0$. The latter is changed into $\Delta A \neq 0$. This difference is considered to arise from the short rangeness of Ar-H⁻ interaction. However, in these propensity rules, the selectivities become weaker for H⁻ than those for electron-impact excitation of He excitation^{6,7,8}. The results obtained will be discussed in more details in comparison with those for electron-impact excitation of He^{6,7,8} and Ar-impact excitation of He⁹.

- 1 N. Koyama, H. Fukuda, T. Motoyama and M. Matsuzawa, *J. Phys.* B19, L331(1987).
- 2 H. Fukuda, N. Koyama and M. Matsuzawa, *J. Phys.* B20, 2959(1986).
- 3 N. Koyama, A. Takafuji and M. Matsuzawa, *J. Phys.* B22, 553(1989).
- 4 C.D. Lin, *Adv. At. Mol. Phys.* 22, 77 (1986) and references therein.
- 5 a) M.E. Kellman and D.R. Herrick, *Phys. Rev.* A22, 1536(1980).
b) D.R. Herrick, *Ad. Chem. Phys.* 52 1(1983) and references therein.
- 6 M. Matsuzawa, T. Motoyama, H. Fukuda and N. Koyama, *Phys. Rev.* A34, 1793(1986).
- 7 T. Motoyama, N. Koyama and M. Matsuzawa, *Phys. Rev.* A38, 670(1988).
- 8 M. Matsuzawa, T. Atsumi and N. Koyama, *Phys. Rev.* A41, 3596 (1990).
- 9 a) A. Takafuji, N. Koyama and M. Matsuzawa, Abstracts of Papers 16th ICPEAC, New York, 26 July - 1 August 1989, p703.
b) N. Koyama, A. Takafuji and M. Matsuzawa, *Chinese J. Phys.* 27, 323 (1989).

RESONANCE SCATTERING INVOLVING
TRI-ATOMIC SYSTEMS

Sung-Ho Salk (Suck)

Department of Physics
Pohang Institute of Science and Technology
Pohang, Kyungbuk Korea 790-600

and

C. K. Lutrus

Department of Physics
University of Missouri-Rolla
Rolla, Missouri, U.S.A.

A generalized theory of treating resonance scattering involving three-body systems is introduced. The original Feshbach's theory of resonance was concerned with elastic and inelastic collisions. In the present theory reactive (rearrangement) resonance scattering processes are treated by resorting to three-body interaction. It is shown that in a limit the present theory leads to the Feshbach's effective two-body resonance scattering theory. In addition, computed results of electron-diatom systems are discussed using an effective two-body treatment¹. Unlike the claims of other researchers, the contribution of resonant reactive (rearrangement) scattering in some electron-diatom collisions is seen to be negligible compared to that of direct scattering, thus requiring caution in the interpretation of experimental cross sections.

1. Sung-Ho Salk and C.K. Lutrus, Phys. Rev. A 35, 3388 (1988)

**SCALING OF RYDBERG CHARGE-TRANSFER CROSS SECTIONS:
INITIAL MEASUREMENTS WITH A NEW DETECTOR**

S. B. Hansen, ** K. B. MacAdam and L. G. Gray
Department of Physics and Astronomy, University of Kentucky
Lexington, KY 40506-0055

In earlier measurements of charge-transfer cross sections for collisions between ions and Rydberg atoms the final state distribution was the main objective, and data was obtained at only a few ion velocities [1,2]. Now we have initiated a new experiment where the relative total charge-transfer cross section in $\text{Na}^+ + \text{Na}(nl)$ collisions (i.e. encompassing all final states) is measured with high precision as a function of velocity for selected initial Rydberg target-states. To accomplish this, a new detector has been constructed that can efficiently detect Rydberg atoms in a beam, independent of the incoming kinetic energy (for energies less than about 2 keV) and independent of the specific Rydberg state.

Fig. 1 shows a schematic diagram of the new detector, which is placed a few cm downstream from the crossed-beam interaction region. Rydberg atoms entering from the left will undergo field ionization in an intense electric field defined by two grids at different potential, $V_1 - V_2 = 10$ kV. Just behind the second grid is

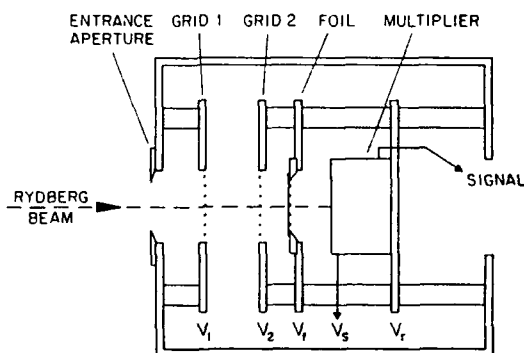


Fig. 1. Total charge-transfer detector.

a thin carbon foil ($1.5 - 2 \mu\text{g}/\text{cm}^2$) supported by a nickel grid at the same potential as grid 2 ($V_f = V_2$). Singly charged positive ions resulting from the field ionization will be accelerated between grid 1 and 2 to an energy of 10 keV plus the original energy of the ion beam, will with high probability penetrate the carbon foil, and will be detected in a particle multiplier behind the foil. Atoms

in lower states ($n \leq 15$) created by charge-transfer from ground-state rest-gas atoms will not be ionized in the strong field between the grids and will therefore not gain enough energy to penetrate the foil and be detected.

Selected data from our first measurements between 50 and 900 eV are shown in Fig. 2. We have compared our results with charge-transfer cross sections from $p + H(1s)$ collisions [3] by matching the two data sets at $\bar{v} = 1.4$ and scaling the Rydberg cross sections by a factor n^4 . At low reduced velocity \bar{v} the Rydberg data lies about a factor three above the $H(1s)$ data. This difference has been suggested as a fundamentally different dynamical response of the three-body system in the case of charge-transfer from a Rydberg state as compared with capture from $H(1s)$ [4]. Also the initial data indicate a small difference in velocity dependence for s states and d states. This might be interpreted as due to a different momentum distribution in the initial s or d state.

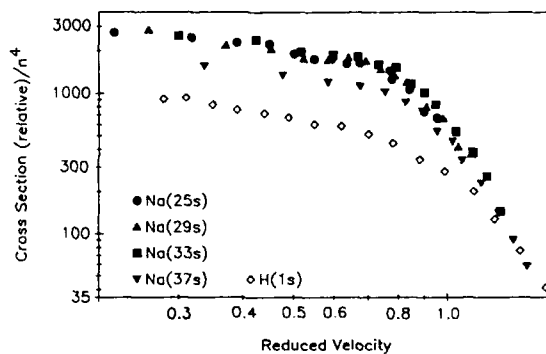


Fig. 2. Scaled charge-transfer cross sections as a function of reduced velocity $\bar{v} = v_{ion}/v_{Bohr}$.

* This work was supported in part by NSF Grant PHY-8808022.

** Permanent address: Institute of Physics, University of Aarhus, DK-8000 Aarhus C., Denmark

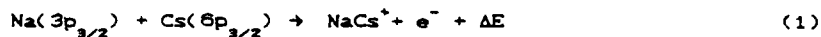
1. K. B. MacAdam, L. G. Gray and R. G. Rolfes (submitted to Phys. Rev. A).
2. K. B. MacAdam and R. G. Rolfes, Rev. Sci. Instrum. 53, 592 (1982).
3. G. W. McClure, Phys. Rev. 148, 47 (1966).
4. K. B. MacAdam, Phys. Rev. A 34, 2767 (1986).

ASSOCIATIVE IONIZATION BETWEEN SODIUM AND CESIUM

M. Biagini, C. Gabbanini, S. Gozzini, A. Lucchesini and L. Moi
Istituto di Fisica Atomica e Molecolare del C.N.R.
Via del Giardino 7, 56100 Pisa Italy

The study of collisional processes in vapors and atomic beams is far from being complete even for simple atomic elements, like the alkali atoms. In particular, the process of associative ionization between the first excited states $A^* + B^* \rightarrow AB^+ + e^-$ has been studied for homonuclear collisions, but not at all for the heteronuclear case. The reason is due to the major difficulties raised by an heteronuclear sample of alkali atoms: these have quite different vapor pressures at a given temperature, more than one resonant laser is needed and many more parameters have to be measured and controlled. In our laboratory we made a systematic study of heteronuclear samples in the vapor regime, measuring several cross sections for the energy-pooling process in different alkali mixtures¹⁾; the energy-pooling process, in which a highly excited atom is produced, is just a different output channel of the collision between two excited atoms. In the case of energy-pooling, the analysis of the fluorescence spectrum may be sufficient to monitor the reaction, while for the associative ionization ions have to be collected and analyzed. To this aim we builded up an apparatus with crossed atomic beams in which ion detection and mass spectroscopy by a quadrupole filter is possible. Two ovens were filled with sodium and cesium metals, independently heated and the two atomic beams crossed in a collision cell. One c.w. dye laser tuned to the D_2 transition of sodium and a monomode diode laser tuned to the D_2 line of cesium, intersected the two atomic beams. The produced ions were collected by electrostatic lenses and mass analyzed; a typical mass spectrum is shown in fig.1. A side hole in the collision cell allowed a fluorescence monitoring.

The studied process is then:



where ΔE is determined by the energy difference between the final and the initial state; that depends on the dissociation energy D_0 of the molecular ion NaCs^+ for which only theoretical calculations exist^{2,3}. The D_0 value of ref.2 would imply an endothermic reaction while the value of ref.3 would carry to an exothermic reaction. A measurement of the cross section for process (1) is underway and it should keep clearness in the potential calculations. The experimental procedure adopted allows a cross section measurement through the known homonuclear associative ionization cross section of sodium.

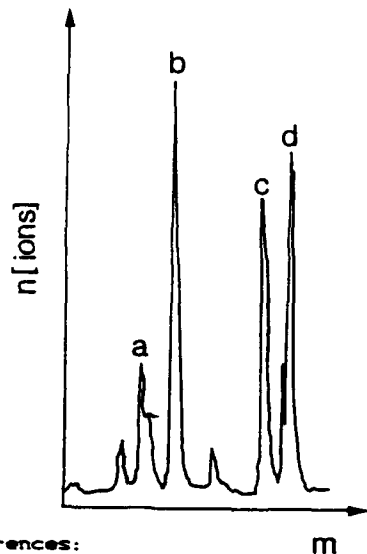


Fig.1:
Typical mass spectrum of ions produced by Na and Cs D_2 laser excitation; peaks a), b), c), d) correspond respectively to Na^+ , Na_2^+ , Cs^+ and NaCs^+ .

References:

- 1) C. Gabbanini, S. Gozzini, G. Squadrito, M. Allegrini and L. Moi
Phys. Rev. A 39, 6148 (1989)
- 2) A. Valence J. Chem. Phys. 69, 355 (1978)
- 3) L. Von Szentpaly, P. Fuentealba, H. Preuss and H. Stoll
Chem. Phys. Lett. 93, 555 (1982)

A STUDY OF H^0+H_2 COLLISIONS

E. J. Quintana, J.A. Lozano, and E. Pollack
 Dept. of Physics, Univ. of Connecticut
 Storrs, CT 06269-3046

An investigation of collisions between low keV energy H^0 atoms and H_2 is in progress. The goal of this work is to provide tests of calculations on H_3 , the most fundamental triatomic molecule. The three collision channels resulting in H^0 (direct scattering), H^+ (stripping), and H^- (electron capture) are studied differentially at small scattering angles. Time-of-flight techniques are used for measurements of energy loss in the direct scattering and electrostatic energy analysis for the capture and stripping channels. The basic experimental arrangement is outlined in Ref. 1.

A typical energy loss spectrum for the direct scattering is shown in Fig. 1. The peaks labelled A and B correspond to elastic and direct inelastic scattering respectively. Figure 2 is a plot of P, the probability of elastic scattering in the direct collision channel as a function of angle. It is clearly seen that the inelastic processes dominate the collision beyond the smallest scattering angles.

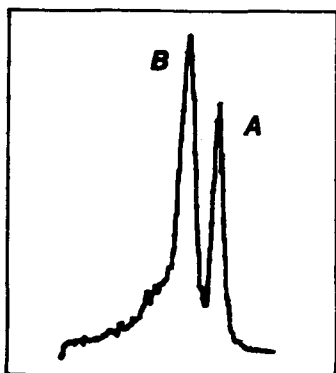


Fig. 1. An energy loss spectrum at $\theta=0.3$ deg. in 1.0 keV H^0+H_2 . Peak A results from elastic scattering and B is due to inelastic collisions. The energy between A and B is 10.6 eV.

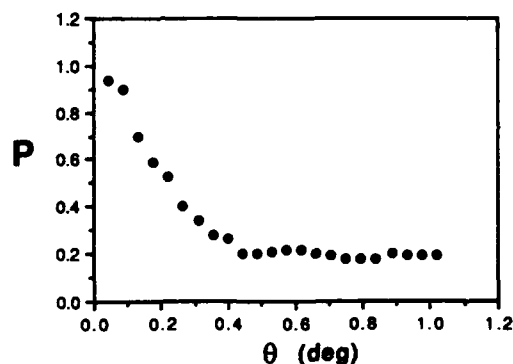


Fig. 2. The probability of elastic scattering at 1.0 keV. It is clearly seen that electronically inelastic channels dominate the collision for $\theta > 0.2$ deg.

To date we have determined the differential cross section for small angle electronically elastic scattering at an energy $E=1.0$ keV. These elastic collisions primarily involve the repulsive H_3 ground state surface. The cross section was found by multiplying the "summed" direct scattering ($H^0+H_2 \rightarrow H^0+H_2$, $H_0^+ + H_2$, $H^0 + H_2^+$, and $H^{0+} + H_2^+$) cross section by the probability in Fig. 2. Our summed cross sections are found to be in agreement with

the results of Johnson et al.² Figure 3 is a plot showing the differential cross section for elastic scattering in 1.0 keV H^0+H_2 collisions.

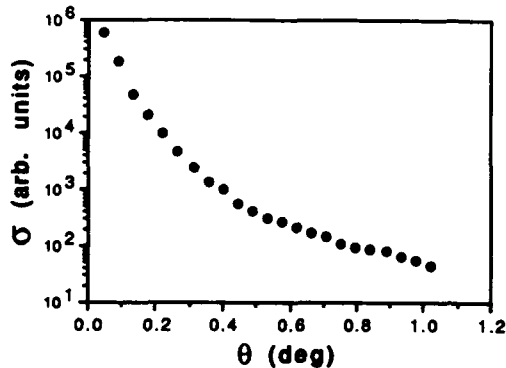


Fig. 3. The differential cross section for elastic scattering in H^0+H_2 collisions at $E=1.0$ keV.

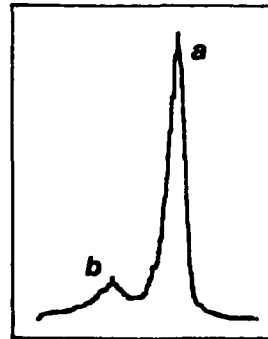


Fig. 4. A typical energy spectrum for $E=1.0$ keV, $\theta=0.5$ deg $H^0+H_2 \rightarrow H^+$. The peaks are separated by 10 eV.

Figure 4 is a typical spectrum from $H^0+H_2 \rightarrow H^+$ collisions. Since the scattered projectile has a different charge state the incident beam cannot provide the usual energy reference. In this work the necessary reference is obtained from $H^0+Ar \rightarrow H^++Ar+e^-$ collisions. The two processes a and b are separated by 10 eV and correspond to H^++H_2 and $H^++H_2^*$ final channels. The stripping is seen to primarily result in ground state H_2 in the angular range studied. The probability of exciting the $H^++H_2^*$ channel increases from a value of 0.1 at $\theta=0.1$ deg to 0.2 at $\theta=1.0$ deg.

We are also studying the $H^0+H_2 \rightarrow H^-$ collision using $H^0+Ar \rightarrow H^-+Ar^+$ collisions as an energy reference. We find that the electron capture generates both the ground and excited H_2^+ states.

This work was supported by the University of Connecticut Research Foundation.

1. E.J. Quintana, A. Andriamasy, and E. Pollack, Phys. Rev. A **39**, 5045 (1989).
2. L.K. Johnson, R.S. Gao, K.A. Smith, and R.F. Stebbings, Phys. Rev. A **38**, 2794 (1988).

DOUBLE IONIZATION OF HELIUM BY FAST HE⁺ PROJECTILES*

J.L. Forest, J.A. Tanis, M.W. Clark, S.M. Ferguson, K. Lifrieri
Department of Physics, Western Michigan University
Kalamazoo, Michigan 49008

V.L. Plano
Kalamazoo College, Kalamazoo, Michigan 49007

The double ionization of helium by charged projectiles is a problem of fundamental interest [1] as it samples the electron correlation in the initial state of the helium atom. At intermediate to high projectile velocities (i.e., $v_{ion} \geq 10v_{Bohr}$), double ionization is attributed to two mechanisms [2]: (1) direct, in which both target electrons are removed in separate interactions with the projectile, and (2) shakeoff, in which the first electron is removed in a direct interaction with the projectile while the second electron is ejected when the resulting ion relaxes to a continuum state. In the high velocity limit ($v_{ion} \gg v_{Bohr}$), the ratio of double- to single-ionization is predicted [2] to be independent of the incident projectile charge and velocity.

In order to investigate double ionization for different ranges of impact parameters, and the relative importance of the direct and shakeoff mechanisms in these different ranges, we have measured the single and double ionization of a helium target associated with capture, loss, and no charge change by incident singly-charged helium projectiles with energies 0.125 to 3.0 MeV/u. This work was done at Western Michigan University using the tandem Van de Graaff accelerator. Singly- and doubly-charged recoiling target ions were detected in coincidence with projectiles undergoing capture, loss, or no charge change using a recoil time-of-flight spectrometer. Ratios of double-to-single target ionization were determined for each outgoing projectile charge state as shown in Fig. 1. The measured ratios are compared to previous studies and to theoretical predictions.

For the lowest energies investigated in the present work, the ratios are consistent with the direct mechanism for double ionization. The present results extend to the high-velocity limit as evidenced by the fact the ratio reaches constant values for the highest energies investigated. At these high energies, however, the ratios are all higher than the value predicted by the empirical equation of Knudsen *et al* [3]. Furthermore, the constant ratios in the high-velocity limit are strongly dependent on the outgoing projectile charge state indicating differing amounts of electron correlation being responsible for double

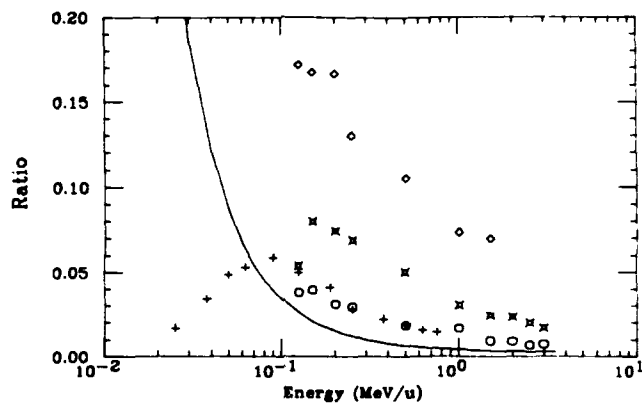


Fig. 1. Ratio of double-to-single ionization in helium by He^+ projectiles vs E (MeV/u). Symbols represent target ionization associated with outgoing projectile charge states as follows:

- electron capture
- × electron loss
- ◻ no charge change
- + no charge change from Wood et al. [4]

The solid line is the empirical prediction of Knudsen et al. [3]

ionization associated with projectile capture, loss, and no charge change, respectively. These high-velocity ratios differ significantly from previous results [3] for H^+ and He^{2+} projectiles contrary to theoretical expectations [2]. The connection of the present results to double ionization by high-energy photons will be considered.

* Supported in part by the U.S. Department of Energy, Office of Basic Energy Sciences, Division of Chemical Sciences.

References

1. M.H. Mittleman, Phys. Rev. Lett. **16**, 498 (1966); F.W. Byron, Jr., and C.J. Joachain, Phys. Rev. Lett. **16**, 1139 (1966)
2. J.H. McGuire, Phys. Rev. Lett. **49**, 1153 (1982)
3. H. Knudsen, L.H. Andersen, P. Hvelplund, G. Astner, H. Cederquist, H. Danared, L. Liljeby and K.-G. Rensfelt, J. Phys. B: At. Mol. Phys. **17**, 3545 (1984)
4. R.M. Wood, A.K. Edwards, R.L. Ezell, Phys. Rev. A **34**, 4415 (1986)

**IMPACT-PARAMETER TREATMENT OF ATOMIC COLLISIONS
INCLUDING NONINERTIAL NUCLEAR-ELECTRONIC TERMS**

Gabriel Hose
The James Franck Institute
The University of Chicago
Chicago Illinois, 60637

Recently [1,2] we proposed a quantum formulation of the perturbed-stationary-state method for atomic collisions including noninertial nuclear-electronic interactions. Here we discuss an analogous derivation within the semiclassical impact-parameter framework. An application of the method to charge-exchange in collisions of He^{++} and H is presented.

In the semiclassical eikonal approximation, the time-dependent Schrodinger equation for the electronic Hamiltonian of the system is solved for a given impact parameter along a rectilinear classical trajectory of the internuclear vector. During a collision the electronic Hamiltonian is implicitly time dependent, which requires the electronic basis to be so as well. The atomic expansion method uses traveling atomic states to expand the electronic wave function whereas in the perturbed-stationary-state approach the basis is the molecular adiabatic states.

To express explicitly the time-derivative operation on the basis functions the chain rule can be applied once a collision vector is defined. The latter is traditionally equated with the internuclear vector. This choice is known to lead to problematic derivative couplings of the basis functions that are origin dependent and may be of infinite range. To overcome these difficulties the basis functions are usually modified by phenomenological electron translation factors. We suggest a different approach and apply the chain rule using the real collision vector which is the vector separating the atomic centers of mass. This gives two coupling contributions. The first is the usual non-adiabatic term while the second arises from the coupling of the electronic and nuclear momenta. The separate coupling types are

both origin dependent and of infinite range. However, the combined coupling is translationally invariant and vanishes asymptotically as is required for scattering boundary conditions. Note that for an atomic expansion the radial dynamical non-adiabatic and nuclear-electronic couplings cancel precisely at all internuclear distances.

For charge exchange processes the coupling matrix is not necessarily hermitian. When an atomic traveling basis is employed, this is because the perturbation potential differs between the charge exchange channels. For a molecular adiabatic expansion the dynamical coupling is channel specific since the real collision coordinate is dependent on the charge-exchange (rearrangement) channel. Time evolution under a nonhermitian Hamiltonian spans a biorthogonal space. That is, beginning from the same initial state the Hamiltonian and its nonidentical hermitian conjugate propagate, respectively, a "right" and a "left" vector. Though the norms of the right and left vectors may vary during the propagation, the biorthogonal norm between the two remains constant. In the biorthogonal space therefore probability is conserved and detailed balance is maintained. We demonstrate this fact in our calculations. At intermediate energies our results are in good agreement with experiment. For example, at center-of-mass energy of 3.02 keV the total cross section for $\text{He}^{++} + \text{H} \Rightarrow \text{He}^+ + \text{H}^+$ calculated with a basis comprising only the five lowest molecular adiabatic states is 38.8 bohr². The interpolated experimental value [3] is 36.6 bohr². At 1.01 keV the theoretical and experimental cross sections are 14.7 and 14.2 bohr², respectively.

[1] G. Hose, Comments Atom. Mol. Phys. 22 , 307 (1989).

[2] G. Hose, J. Phys. Colloq. France 50 , C1-111 (1989).

[3] M.B. Shah and H.B. Gilbody, J. Phys. B 11 , 121,1457 (1978).

ON THE TRANSITION TIME IN
LANDAU-ZENER MODEL

S.V. Bobashev, V.A. Kharchenko *

A.F. Ioffe Physico-Technical Institute of the Academy of
Sciences of the USSR, Leningrad

* Politechnical Institute, Leningrad.

Now the Landau-Zener Model for interaction between two states of physical system gives rise to special interest due to fast progress in studying mesoscopic characteristics in solid states and superconductivity. In these problems not only transition probability values are going to be essential but also a detal knowledge of phase correlation between the scattering amplitudes in the area of interaction.

Mullen et.al. [1] drew attention to the transition time t_z in this problem and found two expressions for t_z in adiabatic (t_z^a) and sudden (t_z^s) limits of interaction region passing.

In this work we found analytical expression for transition time t_z which are going to be valid in all range of model characteristic parameters

$$t_z = \left[\left(\frac{\hbar}{2\alpha} \right)^2 + \left(\frac{\Delta}{\alpha} \right)^4 \right]^{1/4} \quad (1)$$

In (1) 2Δ is minimum splitting between interacted terms, α is a velocity of system energy changing ($\alpha \equiv 2 \lim_{\Delta \rightarrow 0} dE/dt$). Exp.(1) is not approximation and gives correct description of transition probability time profile for all values of $\gamma \equiv \Delta^2/\hbar\alpha$. (1) transforms to the expressions proposed in 1 in adiabatic limit to $t_z^a = \Delta/\alpha$ at $\gamma \gg 1$ and in sudden limit to $t_z^s = (\hbar/2\alpha)^{1/2}$ at $\gamma \ll 1$.

References.

[1] Mullen K., Ben-Jacob E., Gefer Y., Schuss I., Phys.Rev.Lett, 1989, 62, 21, 2543.

ABSOLUTE L -MIXING CROSS SECTIONS FOR SLOW $K^+ + Na$
RYDBERG ATOM COLLISIONS*

W. W. Smith

Department of Physics, University of Connecticut, Storrs, CT 06269

T. F. Gallagher

Department of Physics, University of Virginia, Charlottesville, VA 22901

P. Pillet*, R. Kachru and N. H. Tran**

Molecular Physics Laboratory, SRI International, Menlo Park, CA 94025

We have calibrated some previous measurements [1] to determine the approximate absolute cross sections for loss from a beam containing $Na(nd)$ Rydberg states due to l -mixing collisions with a crossed beam of 300 and 630 eV K^+ ions. Selective field ionization (SFI) was used in the manner of Gallagher *et al.* [2] to monitor the number of $Na(nd)$ atoms in the interaction region as a function of ion beam current I times the interaction time t . The cross sections are determined from the formula $S = S_0 \exp(-\sigma I t / e A_{eff})$, where S is the size of the SFI signal jump [1] that characterizes excitation of the nd Rydberg state with $m_l = 0$, I is the K^+ ion beam current, t the time of exposure to the ions, e the electronic charge, A_{eff} the measured effective overlap area of the ion and Rydberg atom beams, and σ the loss cross section of the nd state to $n'l'$ ($l' > 2$) states. Both dipole-allowed and dipole-forbidden contributions are included.

Cross sections have been determined at K^+ beam energies of 300 and 630 eV for loss from $n = 16 - 27$. We believe the absolute values at 630 eV are accurate to $\sim 30 - 40\%$. They are ~ 1000 times the geometric cross sections, ranging from 1.8×10^{-8} ($n = 16$) to 21.7×10^{-8} cm^2 ($n = 27$) at 630 eV. Cross sections at 300 eV agree fairly well at the same $v_{ion}/v_e (= 0.41)$. For the 300 eV data, we find that σ scales with principal quantum number n approximately as $n^{4.5}$, whereas for 630 eV σ scales approximately as $n^{5.5}$, in agreement with the trend previously found by MacAdam *et al.* [3] using Na^+ projectiles. The highest v_{ion}/v_e we have measured (630 eV K^+) is 0.69 for $n = 27$. If we use $n^{5.5}$ scaling to extrapolate our cross section at this velocity to $n = 28$, we obtain 26.6×10^{-8} cm^2 compared to a lower limit of approximately 17×10^{-8} cm^2 , computed from Fig. 11 of MacAdam *et al.* [4]. The shapes of our SFI signals vs. ionizing field make it quite clear that in the ion velocity and n range of our experiments, the ion collisions produce $nd \rightarrow n'l'$ states with $l' \gg 2$ and going essentially up to $l' = n-1$.

*The original experimental work was done at SRI, International under grants from ONR and NSF. Partial travel support has been provided by the U. of CT Research Foundation.

*Permanent address: Laboratoire Aimé Cotton, CNRS II, Batiment 505, F-91405 Orsay Cedex, France.

**Permanent address: Photometrics, Inc., Woburn, MA 01801.

1. W. W. Smith, P. Pillet, R. Kachru, N. H. Tran and T. F. Gallagher, "Collisional Angular Momentum Mixing of Na Rydberg States by a K^+ Ion Beam", *Abstracts, XIII ICPEAC, J. Eichler, et al., Editors (Berlin, 1983) p. 668*. This reference contains a simple "maximum collisional electric field" argument as to why σ should scale approximately as n^5 .
2. T. F. Gallagher, S. A. Edelstein and R. M. Hill, *Phys. Rev. A* **15**, 1945 (1977).
3. K. B. MacAdam *et al.*, *Abstracts XV ICPEAC, Brighton, U.K. (1987) p. 763*.
4. K. B. MacAdam, R. Rolles and D. A. Crosby, *Phys. Rev. A* **24**, 1286 (1981). See also ref. 3.

XI. ELECTRON AND POSITRON COLLISIONS

THE FINAL STATE INTERACTION IN THE INTERVAL IONIZATION
FOLLOWING β -DECAYS

E.G. Drukarev
Leningrad Nuclear Physics Institute
Gatchina, Leningrad 188350, USSR

It is well known that the ionization of the internal electrons during the nuclear β -decay takes place mainly due to the sudden change of the nuclear charge - the shake-off (SO). This mechanism was considered in a number of works. The other possibility is the final state interaction (f.s.i.). The role of the latter was discussed in a number of papers partially in connection with the discrepancy between the experimental data and selfconsistent field calculation of SO [1].

Here we calculate the contribution of the f.s.i. in the lowest order of perturbation theory. We show it to be rather large and to diminish strongly the disagreement between the experimental and the theoretical data. We base our calculations on the general equation taking into account the lowest order f.s.i. contribution [2]

$$|F|^2 = |P^{(0)}|^2 + 2\text{Re}P^{(1)}P^{(0)} + |\text{Im}P^{(1)}|^2 + 2\text{Re}P^{(2)}P^{(0)}, \quad (1)$$

where $P^{(l)}$ denotes the amplitude of the l -th order of the f.s.i. which causes the transition of the atomic electrons. The last term of eq.(1) was not taken into account in the previous works.

We use the explicit expressions for the amplitudes $P^{(l)}$ [2,3] and calculate the probability of creating the vacancy in the atomic shell through the closure condition. The f.s.i. contribution is thus expressed through the expectation values averaged over the ground state. For the internal ionization of the $1s$ states we obtain the approximate explicit equation describing these states by the nonrelativistic Coulomb functions. The f.s.i. contribution to spectrum is

$$1/w \frac{dw}{dT} = 2.8 \frac{\pi(\alpha z)^2}{2T} \quad (2)$$

with w - the probability of the β -decay, T - the kinetic energy of the β -electron, z - the charge of the daughter nucleus. The calculations with the Hartree-Fock-Slater wave functions [4] gave the results close to those given by eq. (2).

After the integration over T we obtain the total contributions of the f.s.i. to the internal ionization of the K -shell. Being added to the SO values [1] they either remove or strongly diminish the discrepancy between the theoretical and experimental data. The case

of the decay of calcium-45 can be an illustration. The SO contributes $1.2 \cdot 10^{-3}$, the f.s.i. gives $1.1 \cdot 10^{-3}$. Thus the sum is $2.3 \cdot 10^{-3}$ while the experimental data is $(2.4 \pm 0.4) \cdot 10^{-3}$.

References

1. T. Isozumi, S. Shimizu, T. Mukoyama, Nuovo Cim. 41A, 366 (1977).
2. E.G. Drukarev, M.I. Strikman, Sov. Phys. JETP 24, 686 (1986).
3. E.G. Drukarev, J. Nucl. Phys. 22, 876 (1986).
4. E.G. Drukarev, M.B. Trzhaskovskaya, Nucl. Phys. A (to be published).

THEORY OF POSITRON-ATOM AND POSITRON-ION COLLISIONS

M. A. ABDEL-RAOUF

CHAIR FOR THEORETICAL CHEMISTRY, UNIVERSITY OF
ERLANGEN-NÜRNBERG, EGERLANDSTR. 3, 8520 ERLANGEN, FRG.

The theory of positron-atom and positron-ion collisions is reviewed. A special attention is given to inelastic processes in which the positronium channel is open and to excitation and ionisation processes. We comment upon the recent discussions of the existence of positron-atom bound-states and appearance of resonances in scattering problems involving positrons {1}.

Two new problems are treated for the first time, namely:

i) Collisions of positrons with ions contained in molecular crystals.

ii) Production of Auger-spectra in positron-atom and positron-ion collisions.

In case i), we are interested in the collisions of positrons with alkaline-earth positive ions and their resemblances produced from the third group of the periodic table, (especially Sc^{2+} , Y^{2+} and La^{2+}), which are involved in high T_c superconducting materials. Particularly, we would like to investigate the effect of the surrounding field of the ion on the resultant cross sections, annihilation rates, etc., a problem of great interest for people working in this field {2}.

In case ii), the physics of an annihilating or escaping positron and a flying Auger-electron is investigated in detail, a problem which has been treated very recently experimentally and opens new prospects for people working in Auger-spectra, (see e.g. {3}). We expect that our studies in both cases will be further developed so that we will be able to present preliminary results in the Conference.

{1} S.J. Ward et al, J. Phys. B22, 3763 (1989); Y.K. Ho, Phys. Rev. A38, 6424 (1988); M.A. Abdel-Raouf and R.F. Wood, Phys. Rev. A (in press).

{2} A. Bansil et al, Phys. Rev. Lett. 61, 2480 (1988).

{3} D. Mehl et al, Phys. Rev. B41, 799 (1990).

ELECTRON IMPACT EXCITATION OF THE 3^1P STATE IN MAGNESIUM

Rajesh Srivastava
Department of Physics, University of Roorkee,
Roorkee - 247667, U.P., India

For electron impact resonant excitation (3^1S-3^1P) in magnesium, Brunger et al (1,2) have recently reported experimentally measured differential cross sections (DCS) and angular correlation parameters (3) at 20 and 40 eV of incident electron energies. A number of calculations (see for example reference 4-5) have also been performed for 3^1S-3^1P transition in magnesium. However, it is interesting to note that none of the performed calculations has been able to explain the experimentally measured DCS results at 40 eV, in particular, as well as the ACP results, in general. I therefore reexamined (6) theoretically the study of electron impact 3^1P excitation in magnesium and tried to find if there can be any suitable other theoretical description for this excitation.

Since considerable work (7-8) on electron-atom scattering indicate that reasonable agreement between theory and experiment can be obtained by using either the close-coupling approach at low energies or perturbative approach like the distorted-wave approximation (DWA) at high energies. Especially, the "first-order" form of the DWA method with an appropriate choice of distortion potential for the projectile wave has been very attractive, as in general it yields reasonably reliable results at the intermediate incident electron energies for a minimum of effort.

In the present conference, I present the work where I explored the suitability of DWA for 3^1S-3^1P excitation in magnesium. Three different versions of DWA have been used for the calculations and results for the DCS and ACP are obtained. These results are compared with the available experimental and other theoretical results. The comparison of the present calculations with experiment suggests the suitability of the DWA to describe the 3^1S-3^1P transition in magnesium at 40 eV.

The details of the DWA method along with complete results will be presented in the conference.

Reference

1. M.J. Brunger et al, J. Phys. B, 21, 1639 (1988)
2. M.J. Brunger et al, J. Phys. B 22, 1431 (1989)

3. N.Andersen et.al, Phys. Rept. 165, 1(1988)
4. J.Mitroy and I.E.McCarthy J. Phys. B 22, 641 (1989)
5. I.E.McCarthy et.al, J. Phys. B 22, 2597 (1989)
6. R.Srivastava, Physical Review A (submitted)
7. Y.Itikawa Phys. Rept. 143, 69 (1986)
8. J.A.Slevin and S.Chwirot J. Phys. B 23, 165 (1990).

ELECTRON SCATTERING BY ATOMIC HYDROGEN

S.N. Tiwary*

Department of Physics, L.S. College
Bihar University, Muzaffarour, Bihar

The study of the scattering by the atomic hydrogen has been of growing interest in atomic collision physics, especially from the theoretical point of view, because the hydrogen atom provides an excellent testing ground for a theoretical model as the wave functions of both discrete and continuum states are exactly known. Consequently, the collision problem is not complicated by the atomic structure problem. The electron scattering by the atomic hydrogen is a three-body Coulomb problem consisting of a proton and two electrons. Although two-body Coulomb can be solved exactly, the exact solutions to three-body Coulombic system are impossible to obtain. A number of approximate theoretical methods to electron-atom scattering problems have been introduced in the literature which are applicable in different incident energy ranges (low, intermediate and high). The success or failure of these methods leads us to a better understanding of the problems that are encountered in other complex collision systems.

In the low bombarding energy region, the close-coupling¹ and the R-matrix² methods yield reliable results. In our present work, we have employed the R-matrix method with the basis functions (1s-2s-2p) exactly in the same way as in our earlier work³ to calculate the electron impact angular differential cross sections for the excitation $1s^2s^e \rightarrow 2s^2s^e$ optically forbidden transition in the hydrogen atom at a low incident energy 1 Rydberg.

For the first time, our present very careful theoretical investigation clearly demonstrates (i) a deep minimum at around the scattering angle $\theta = 52^\circ$, (ii) a broad maximum at around $\theta = 70^\circ$ and (iii) a shallow minimum at around $\theta = 94^\circ$ in the differential cross sections curve.

*This work was done while the author was Research Director, CNRS Laboratory, and Invited Professor at the University of Paris-Sud, France, Associate Member of ICTP, Trieste, Italy.

1. P.G. Burke and J.F. Williams, Phys.Rev. **34**, 325(1977).
2. P.G. Burke, A Hirbert and W.D. Robb, J.Phys. B: **4**, 153(1971).
3. S.N. Tiwary, J.Phys. B: **16**, L459(1983).

MEASUREMENTS OF ELECTRON-IMPACT EXCITATION CROSS SECTIONS
AND OSCILLATOR STRENGTHS IN RARE GAS ATOMS

Y.Sakai, T.Suzuki, G.P.Li, T.Takayanagi, K.Wakiya and H.Suzuki
Department of Physics, Sophia University, Chiyoda-ku, Tokyo 102 Japan

T.Inaba, S.S.Kano and H.Takuma
Institute for Laser Science, University of Electro-Communications
Chofu-shi, Tokyo 182 Japan

For the purpose of providing standard data for excitation cross sections and oscillator strengths, we measured differential cross sections (DCS) for the following excitation processes in rare gas atoms by means of the electron-energy-loss spectroscopy (EELS):



where n corresponds to 2 for Ne, 3 for Ar, 4 for Kr, and 5 for Xe.

We measure the EELS at impact energies from 300 to 500 eV and for scattering angles from 1.5 to 10 degrees. We determine the absolute DCS from the scattering intensity ratio relative to the elastic scattering by multiplying the absolute elastic scattering cross section, which are obtained with the fitting calculation based on the experimental data by Bromberg[1], Jansen et al.[2], and Wagenaar et al. [3].

When the impact electron energy is high enough to ensure the validity of the Born approximation, one can deduce the generalized oscillator strength (GOS) $F(K)$ from the DCS, $d\sigma/d\Omega$, using the following relation (in a.u.) [4]:

$$F(K) = \frac{W}{2} \frac{k_i}{k_f} K^2 \left(\frac{d\sigma}{d\Omega} \right),$$

where W stands for the excitation energy, k_i and k_f for the incident and scattered momenta, respectively, and K for the momentum transfer. Under the assumption of the Born approximation, $F(K)$ depends only on K. The optical oscillator strength (OOS) is determined by extrapolating the GOS to the limit $K = 0$ [5].

Results of the GOS for Xe and Ne are illustrated in Figure 1 and 2, respectively, as functions of the squared momentum transfer K^2 . Solid lines in the figures are calculated by fitting the present experimental data to the expansion formula of $F(K)$ by Klump and Lassettre [5]. The intercepts of the curves with the ordinate present the corresponding OOS. The results for Ar [6] and Kr [7] are already published.

The results for the OOS in Xe, Kr, Ar, and Ne are tabulated in Table I. Data for Ne are still tentative.

We will make comparisons of the present results with previous experimental works and theoretical calculations on the occasion of the poster session.

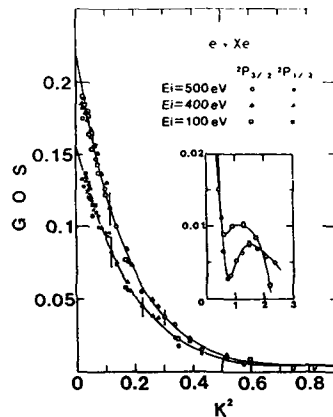


Fig.1. The generalized oscillator strengths for the $5p^2 (^2P_{1/2})6s$ and $5p^3 (^2P_{3/2})6s$ states in Xe as a function of the squared momentum transfer K^2 .

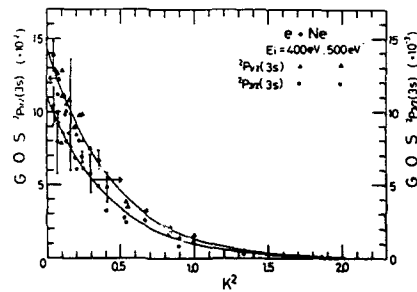


Fig.2. The generalized oscillator strengths for the $2p^2 (^2P_{1/2})3s$ and $2p^1 (^2P_{3/2})3s$ states in Ne as a function of the squared momentum transfer K^2 .

TABLE I. Present results for the Optical Oscillator Strengths.

	$1S_0 + np^5 (^2P_{1/2})(n+1)s$	$1S_0 + np^5 (^2P_{3/2})(n+1)s$
Xe (n = 5)	0.158 \pm 0.024	0.222 \pm 0.033
Kr (n = 4)	0.127 \pm 0.015	0.143 \pm 0.015
Ar (n = 3)	0.222 \pm 0.02 - 0.03	0.058 \pm 0.005 - 0.008
Ne (n = 2) tentative	0.144 \pm 0.019	0.0111 \pm 0.0014

1. J.P.Bromberg, J.Chem.Phys. 61,963(1974).
2. R.H.Jansen, F.J.deHeer, H.J.Luyken, B.vanWingerden, and H.J.Blaauw, J.Phys. B9,185(1976). R.H.Jansen and F.J.de Heer, J.Phys.B9,213(1976).
3. R.W.Wagenaar, A.de Boer, T.van Tubergen, J.Los and F.J.de Heer, J.Phys.B19, 3121(1986).
4. H.Bethe, Ann.Phys. 5,325(1930).
5. K.N.Klump and E.N.Lassettre, J.Chem.Phys.68,886(1978).
6. G.P.Li, T.Takayanagi, K.Wakiya, H.Suzuki, T.Ajiro, S.Yagi, S.S.Kano, and H.Takuma, Phys.Rev.A38,1240(1988).
7. T.Takayanagi, G.P.Li, K.Wakiya, H.Suzuki, T.Ajiro, T.Inaba, S.S.Kano, and H.Takuma, Phys.REV.A in press(1990).

CROSS SECTIONS AND SPIN POLARIZATIONS FOR e^{\pm} SCATTERING FROM CADMIUM

Sultana N. Nahar
 Department of Physics and Astronomy, Georgia State University
 Atlanta, GA 30303, USA

Recently a few experiments^{1,2} and one nonrelativistic theoretical calculation³ have been carried out for the elastic scattering of electrons from cadmium and the same theoretical investigators³ have calculated the cross sections for the elastic scattering of positrons from cadmium to investigate the scattering features of this comparatively heavy atom ($Z = 48$).

In the present work, relativistic calculation has been carried out by solving the Dirac equation to obtain the various scattering cross sections such as, differential, integrated elastic, momentum transfer and total integrated cross sections, and the spin polarization parameters for both the elastic and the total scatterings of electrons and positrons from cadmium in the impact energy range of 6.4 - 300 eV. Since both the electrons and the positrons are spin 1/2 particles, their orbital angular momenta can interact with the spins and orient the spins in a preferred direction causing a net polarization in the scattered beam. For the pure elastic scattering, the total projectile-target interaction has been represented by the real model potential, $V_R(r)$, which consists of the static potential (attractive), a parameter-free polarization potential (attractive) and an electron exchange potential for the electrons scattering, and the static potential (repulsive) and a parameter-free polarization potential (attractive) different from that of electron scattering for the positrons scattering from cadmium. For the total scattering which includes both the elastic scattering and the inelastic scattering processes such as excitation, ionization, recombination etc. causing an absorption in the scattered beam, the total projectile-target interaction has been represented by a complex potential, $V_R(r) + iV_A(r)$, where a model absorption potential, $V_A(r)$, has been added as its imaginary part.

The shapes and features of the calculated differential cross section (DCS) curves obtained using potentials without and with inclusion of the absorption potential for the elastic scattering of electrons from cadmium are found to be in good agreement with the recent measured DCS values while the agreement with the previously measured values of DCS is reasonable as can be seen in Fig. 1 next page at few electron impact energies. However, the values of the recently measured cross sections, both the differential and integrated elastic, are much lower than the present calculated values. While the features of the present DCS curves agree with the measured values of Ref. 2, they as well as the values of the integrated elastic cross sections differ with those of the only other available calculation. Inclusion of absorption potential show consistent results for both the elastic and the total scattering of electrons from cadmium in the present work. The present results show significant amount of spin polarization in the scattered beam for the elastic scattering of electrons from cadmium.

The DCS curves for positrons scattering from cadmium show less features, especially those obtained using the real model potential, than the DCS curves for electrons scattering. This is in general to be expected since positron-target interaction is weaker than the electron-target interaction and with positrons there is no exchange during scattering. Inclusion of the absorption potential show more consistent results for elastic scattering of positrons at lower energies than at higher energies. The spin polarization is found to be negligible for positrons scattering from cadmium.

1. J. C. Nogueira, W. R. Newell and W. M. Johnstone, *J. Phys. B* **20**, L537 (1987).
2. B. Marinkovic, V. Pejcev, D. Filipovic and L. Vuskovic, in Abstracts of the Contributed Papers, Fifteenth International Conference on the Physics of Electronic and Atomic Collisions, Brighton, 1987, edited by J. Geddes, M. B. Gillbody, A. E. Kingston, and C. J. Latimer (Queen's University, Belfast, 1978), p.186; B. Marinkovic, Ph.D. thesis, University of Belgrade, 1988 (private communication).
3. A. W. Pangantiwar and R. Srivastava, *Phys. Rev A* **40**, 2346 (1989).

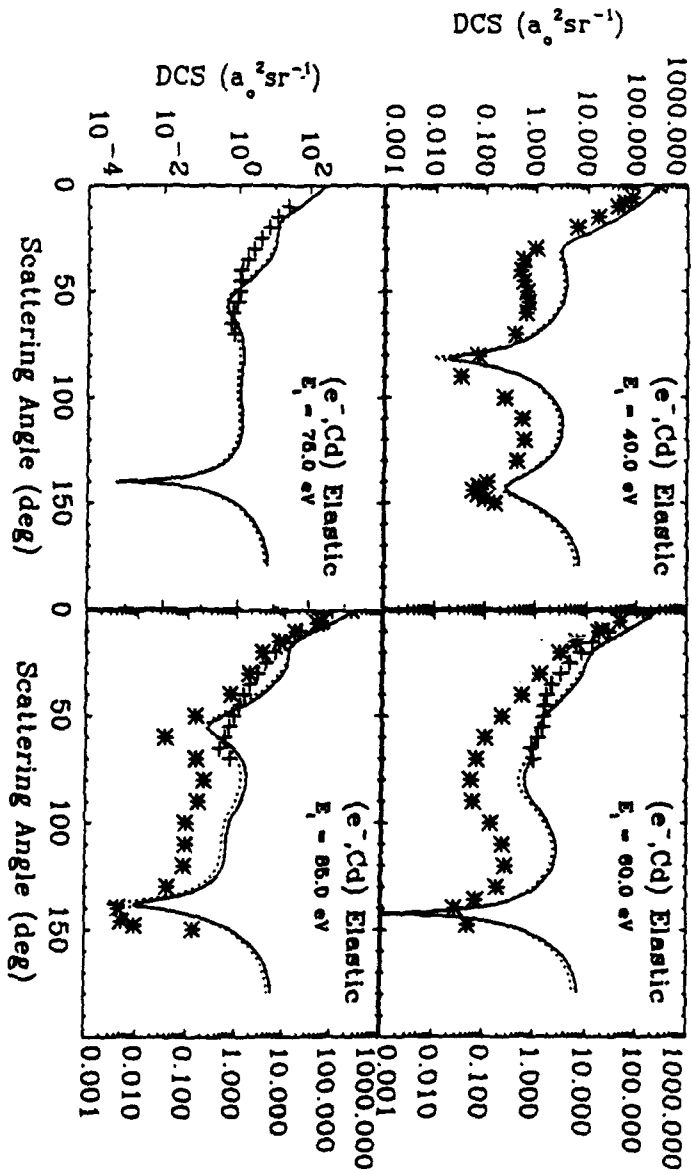


Fig. 1. The differential cross sections (DCS) for the elastic scattering of electrons from cadmium. The solid curves correspond to the DCS values obtained using the real potential and the dotted curves to those obtained using the complex potential. The experimental values are of Ref. 1 (plus) and of Ref. 2 (asterisk).

WANNIER'S THRESHOLD LAW AND ADIABATIC REPRESENTATION

S. Watanabe
 Department of Applied Physics and Chemistry
 University of Electro-Communications
 1-5-1, Chofugaoka, Chofu-shi, Tokyo 182 Japan

In 1953, Wannier[1] deduced his famous electron-impact ionization threshold law $\sigma \approx E^{1.1269}$. Since his work was entirely based on classical mechanics, Rau[2] and Peterkop[3] investigated the problem using quantum mechanics and arrived at a pair of solutions of the local Schrödinger equation. They concluded that the cross section scales as above. In the 1971 paper[2], however, Rau questioned what would be the possible connection between his quantum mechanical treatment and Macek's[4] adiabatic expansion method for dealing with doubly-excited states of He. This is an important question since nonseparable problems are often solved by integrating coupled adiabatic or diabatic equations. The present work elucidates the connection for a particular subset of adiabatic channels[5].

Near threshold, ionization is expected to proceed by way of the unstable configuration, $\vec{r}_1 \approx -\vec{r}_2$, of the outgoing two electrons. Expansion of the two-electron Hamiltonian near $\vec{r}_1 \approx -\vec{r}_2$ leads to

$$H \approx -\frac{1}{2} \frac{\partial^2}{\partial R^2} - \frac{Z_0}{R} - \frac{1}{2R^2} \left[\frac{\partial^2}{\partial \beta^2} + \nu_1^2 R \beta^2 + \frac{\partial^2}{\partial \gamma^2} + \nu_2^2 R \gamma^2 \right] \quad (1)$$

where $R = (r_1^2 + r_2^2)^{1/2}$, $\beta = \frac{\pi}{4} - \arctan \frac{r_2}{r_1}$, $\gamma = \frac{1}{2}(\pi - \theta_{12})$, and $Z_0 = \frac{(4z-1)}{\sqrt{2}}$, $\nu_1^2 = \frac{(1-12z)}{\sqrt{2}}$, $\nu_2^2 = \frac{1}{\sqrt{2}}$. For revealing the gist of the problem, we consider the following two-variable equation,

$$\left(-\frac{1}{2} \frac{\partial^2}{\partial R^2} - \frac{1}{2R^2} \left[\frac{\partial^2}{\partial x^2} + \nu^2 R x^2 \right] \right) \Psi(R, x) = E \Psi(R, x) \quad (2)$$

where x and ν represent either β and ν_1 or γ and ν_2 .

Let us define the adiabatic channel functions $\Phi_n(R; x)$ and the potential energies $U_n(R)$ through

$$-\frac{1}{2R^2} \left[\frac{\partial^2}{\partial x^2} + \nu^2 R x^2 \right] \Phi_n(R; x) = U_n(R) \Phi_n(R; x). \quad (3)$$

A solution $\Psi(R, x)$ of the local Schrödinger equation is expanded in terms of the adiabatic channel functions as

$$\Psi(R, x) = \sum_n F_n(R) \Phi_n(R; x) \quad (4)$$

so that the radial functions $F_n(R)$ satisfy the coupled ordinary differential equations,

$$\sum_{n'} \left(\delta_{nn'} \left[\frac{1}{2} \frac{d^2}{dR^2} + \frac{Z_0}{R} + \frac{\nu}{R^{3/2}} \left(n' + \frac{1}{2} \right) - E \right] + [P_{nn'} \frac{d}{dR} + \frac{1}{2} \sum_{n''} P_{r,n''} P_{n''n'}] \right) F_{n'} = 0 \quad (5)$$

where $P_{nn'}(R) = \int dx \Phi_n^*(R; x) \frac{\partial}{\partial R} \Phi_{n'}(R; x)$. It is easy to put down the matrix element of $P_{nn'}$,

$$P_{nn'}(R) = \frac{1}{8R} (n|aa - a^\dagger a^\dagger|n') \quad (6)$$

where a^\dagger and a are the creation and annihilation operators of the harmonic/antiharmonic oscillator.

Let us now employ the WKB representation of $\tilde{F}_j(R)$, namely

$$\frac{d \ln \tilde{F}_j(R)}{dR} = +i\sqrt{2E + \frac{2Z_0}{R} - 2\tilde{U}_j(R)}. \quad (7)$$

Substituting Eq. (7) into Eq.(5) and keeping terms to order $\frac{1}{R^{3/2}}$ lead, in the range $R \ll \frac{Z_0}{R}$, to the eigenvalue problem

$$\tilde{U}(R) = \frac{1}{8R^{3/2}} \left[8\nu \left(aa^\dagger - \frac{1}{2} \right) + i\sqrt{2Z_0} (aa - a^\dagger a^\dagger) \right]. \quad (8)$$

The *post adiabatic* type potential energy and the corresponding channel functions are thus obtained to order $R^{-3/2}$ by diagonalization of \tilde{U} using the Bogoliubov transformation. Hence,

$$R^{3/2} \tilde{U}_j(R) = \tilde{\nu} \left(j + \frac{1}{2} \right) \quad (j = 0, 1, 2, \dots) \quad (9)$$

where $\tilde{\nu} = \frac{1}{8} \sqrt{(8\nu)^2 - 8Z_0}$. Moreover since $\frac{Z_0}{R} \gg E$ and $R \gg 1$,

$$\text{WKB phase integral} \simeq \int dR \sqrt{2E + \frac{2Z_0}{R} - 2\tilde{U}_j(R)} \sqrt{\frac{R}{2Z_0}}. \quad (10)$$

The flux loss from the ridge region continues up to about $R_0 \approx \frac{Z_0}{E}$. The threshold law stems from the second term of the WKB phase integral integrated up to R_0 , yielding $\sigma \simeq E^{1.1269}$ for $j = 0$, $\sigma \simeq E^{3.88}$ for $j = 1$, etc.

References

1. G. H. Wannier, Phys. Rev **90**, 817 (1953).
2. A. R. P. Rau, Phys. Rev. A **4**, 207 (1971).
3. R. Peterkop, J. Phys. B **4**, 513 (1971).
4. J. H. Macek, J. Phys. B **1**, 831 (1968).
5. S. Watanabe, submitted to Physical Review Letters (1990).

POSITRON COLLISION WITH RUBIDIUM*

T. T. Gien

Department of Physics, Memorial University of Newfoundland,
St. John's, Newfoundland A1B 3X7, Canada.

The total cross sections for positron and electron collisions with rubidium are calculated, using the modified Glauber (MG) approximation [1]. Both the inert-core and frozen-core approximations are employed in the calculation. As usual, the amplitude in the two-potential scattering is given by

$$f = f^{\text{core}} + f^{\text{CC}}$$

where

$$f^{\text{core}} = -\frac{1}{2\pi} \langle \phi_f | V_c | \chi_1^{(+)} \rangle$$

and

$$f^{\text{CC}} = -\frac{1}{2\pi} \langle \chi_f^{(-)} | V_a | \psi_1^{(+)} \rangle$$

V_a is the scattering potential of the valence-electron atom. V_c is the scattering potential of the core of the rubidium atom. In the frozen-core approximation, V_c is represented by the frozen-core potential. Within the inert-core approximation, the scattering from the core potential is neglected.

f^{core} is calculated "exactly" by employing the partial wave analysis. The second term, f^{CC} , is the scattering amplitude of the valence-electron atom, in which the scattering wave has been distorted by the presence of the core potential. In the modified Glauber approximation [2], the amplitude for this part of scattering is

$$f_{\text{MG}}^{\text{CC}} = f_G^{\text{CC}} + f_{\text{B2}}^{\text{CC}} - f_{\text{G2}}^{\text{CC}}$$

f_G^{CC} , $f_{\text{G2}}^{\text{CC}}$, and $f_{\text{B2}}^{\text{CC}}$ are, respectively, the core-corrected Glauber amplitude of scattering from the valence-electron atom, its second-order eikonal term, and the second-Born counterpart.

The MG total cross sections below 30 eV were found to be consistent with the values calculated by McEachran et al. [3] who used the close-coupling calculation. The modified Glauber total cross sections for positron collision with rubidium were also found to agree with experimental data [4] (available, at present, at energies below 100 eV) reasonably well, if one takes into consideration the possible uncertainty in experimental data due to the inability of discriminating against the elastically scattered positrons (electrons) near the forward direction. The MG total cross sections for positron and electron scatterings were found to merge (within less than 5 per cent) at a rather low energy. Detailed derivations of the relevant formulae and complete results of this work will be reported at the conference.

*Research work supported by the Natural Science and Engineering Research Council of Canada.

1. T. T. Gien, Phys. Repts. 160, 123-187 (1988).

2. T. T. Gien, Chem. Phys. Lett. 139, 23 (1987) (Erratum 142, 575); J. Phys. B 22, L129 (1989), *ibid*, L463 (1989).
3. R. P. McEachran et al., in Proc. NASA Workshop on Annihilation in Gases and Galaxies, p. 1 (1990); R. P. McEachran et al., *ibid*, p. 45.
4. T. S. Stein et al., in Proc. NASA Workshop on Annihilation in Gases and Galaxies, p. 13 (1990)

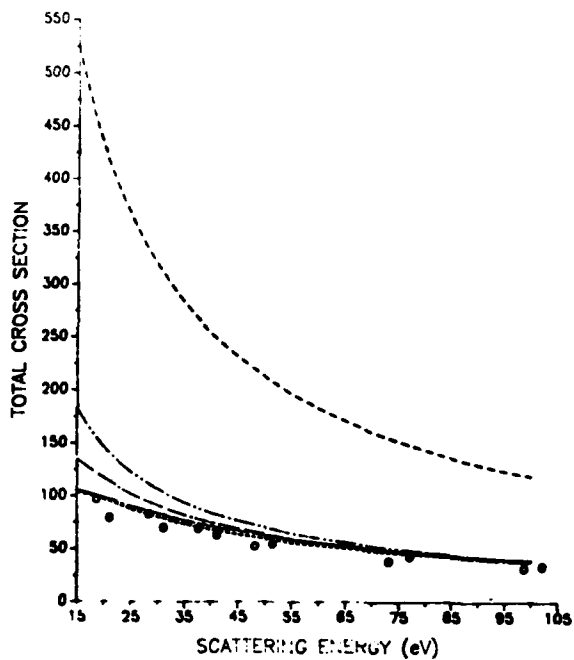


Figure 1

Figure 1. Total cross sections for positron and electron collision with rubidium in 10^{-20} units. — : modified Glauber, positron scattering; — : modified Glauber, electron scattering; - - - : VMG, modified Glauber in the inert-core approximation, positron and electron scattering; ····· : B2, second-Born approximation; - · - · - : VB2, second-Born in the inert-core approximation; o : experimental data [4] of positron scattering; ● : experimental data of electron scattering.

WALLACE APPROXIMATION FOR $e\pm$ SCATTERING*

T. T. Gien and Z. C. Yan
 Department of Physics, Memorial University of Newfoundland,
 St. John's, Newfoundland, Canada A1B 3X7.

Both the Glauber and Wallace approximations [1] have been used to study electron and positron scattering from hydrogen for some time. While the employment of the Glauber approximation has been extended to analyze scatterings by more complex targets [1], the application of the Wallace approximation has, so far, been limited only to scattering from hydrogen, and even with hydrogen as target, only some Wallace calculations for simple processes such as elastic, and 2s and 2p inelastic scatterings [2] from its ground state have been reported in the literature. To our knowledge, no Wallace calculation has been carried out for any of the elastic and/or inelastic scattering metastable processes of hydrogen.

In this work, we have analyzed the elastic and inelastic scatterings of both electron and positron by the 2s metastable state of hydrogen in the framework of the Wallace approximation, with the main purpose of comparing these results with the similar ones obtained in the Glauber approximation. The most general expression for the Wallace amplitude, which is valid for any s-s and s-p process of $e\pm$ scattering from hydrogen-like atom, was obtained for the calculation.

The Glauber amplitude in its closed form [3] has been used in the calculation. For the Wallace amplitude, we calculated the correction term of these various processes by employing both its four-dimensional and three-dimensional integral forms. The general expressions for this term, in their three-dimensional integral form, are:

$$F_{s,s}^{corr.} = \frac{ik_1}{\pi} \int_{\mu}^{\infty} D \int_{\mu}^{\infty} dx_1 \int_{\mu}^{\infty} dx_2 x_2^{1+2i\eta} \int_0^{\pi} d\phi [A_{5+\mu} - C_{5+\mu}^{(0)}] (1+x_1^2+x_2^2+2x_2 \cos\phi)^{\mu/2}$$

and

$$F_{s,pt}^{corr.} = ie^{i\phi} \sqrt{3/2} \frac{k_1}{\pi} \int_{\mu}^{\infty} D \int_{\mu}^{\infty} dx_1 \int_{\mu}^{\infty} dx_2 x_2^{1+2i\eta} \int_0^{\pi} d\phi (1+x_2 \cos\phi) (B_{6+\mu} - C_{6+\mu}^{(1)}) \times (1+x_1^2+x_2^2+2x_2 \cos\phi)^{\mu/2}$$

$C_{5+\mu}^{(0)}$ and $C_{6+\mu}^{(1)}$ are expressed in terms of the derivatives of the product of the Bessel functions J and K. The meaning of the notations used here will be given in more detail at the conference.

In order to compare the characteristics of the DCS obtained for scattering from the metastable state with those obtained for scattering from the ground state, we have also recalculated the DCS for scatterings from ground state. A sample of the results of DCS are presented in Table 1. Detailed derivations of the relevant formulae and complete results of this work will be reported, with discussion, at the conference.

*Research work supported by NSERC (Grant No. A-3962).

- [1] T. T. Gien, Phys. Rept. 160, 123-187 (1988).
- [2] F. W. Byron Jr. et al., J. Phys. B 14, 2429 (1981), *ibid* 15, 3915 (1982).
 V. Franco and Z. Iwinski, Phys. Rev. A 25, 1900 (1982). F. W. Byron Jr. et al.,

J. Phys. B 18, 1637 (1985).

[3] B. K. Thomas and E. Gerjuoy, J. Math. Phys. 12, 1567 (1971).

Table 1 Differential cross sections in $a_0^2 \text{sr}^{-1}$ of electron and positron scatterings from hydrogen at 200 eV.

Angles (degree)	Glauber e±	Wallace e-	Wallace e+	Glauber e±	Wallace e-	Wallace e+
		<u>2s-2s</u>			<u>2s-3s</u>	
5.00	0.887+2 ⁶	0.928+2	0.847+2	0.851+1	0.847+1	0.853+1
35.00	0.122+0	0.125+0	0.117+0	0.216-2	0.215-2	0.209-2
70.00	0.929-2	0.924-2	0.861-2	0.193-3	0.187-3	0.182-3
140.00	0.129-2	0.124-2	0.115-2	0.274-4	0.253-4	0.253-4
		<u>2s-2p</u>			<u>2s-3p</u>	
5.00	0.950+2	0.909+2	0.991+2	0.108+1	0.908+0	0.127+1
35.00	0.974-3	0.244-2	0.337-2	0.175-4	0.195-3	0.676-4
70.00	0.123-4	0.496-3	0.537-3	0.129-8	0.340-4	0.334-4
140.00	0.581-6	0.180-3	0.183-3	0.450-9	0.125-4	0.125-4
		<u>1s-2s</u>			<u>1s-3s</u>	
5.00	0.743+0	0.784+0	0.702+0	0.125+0	0.133+0	0.117+0
35.00	0.180-2	0.182-2	0.165-2	0.440-3	0.436-3	0.411-3
70.00	0.196-3	0.203-3	0.166-3	0.467-4	0.486-4	0.393-4
140.00	0.284-4	0.272-4	0.241-4	0.680-5	0.654-5	0.575-5
		<u>1s-2p</u>			<u>1s-3p</u>	
5.00	0.126+2	0.124+2	0.128+2	0.231+1	0.227+1	0.234+1
35.00	0.992-3	0.382-3	0.271-2	0.293-3	0.104-3	0.738-3
70.00	0.258-4	0.123-3	0.229-3	0.737-5	0.287-4	0.554-4
140.00	0.136-5	0.505-4	0.598-4	0.389-6	0.116-4	0.139-4
		<u>1s-1s</u>				
5.00	0.145+1	0.164+1	0.131+1	⁶ The last two digits indicate power of ten.		
35.00	0.783-1	0.910-1	0.649-1			
70.00	0.831-2	0.930-2	0.675-2			
140.00	0.123-2	0.132-2	0.975-3			

CROSS-SECTIONS AND ELECTRON COLLISION EXCITATION
FUNCTIONS OF SOME $5p^56p$ Xe LEVELS.

I.P.Bogdanova, S.V.Yurgenson

Department of Optics, Leningrad State University, USSR

In [1] we have described the method of electron impact excitation cross-sections measuring by using a pulsed electron beam. In the method spectral lines intensities are being measured in 10-20 ns after beginning of exciting pulses. In this case the influence of the cascade population was shown to be decreased, with the degree of decreasing being dependant on the relation between the lifetime of the cascade level and the effective duration of exciting pulses and practically independent of the lifetime of the emitting level.

We have measured excitation cross-sections of four Xe levels. Xenon was excited by the pulsed electron beam (pulse duration 20 ns, repeating frequency 500 kHz). The target gas pressure was 50 mTorr. The radiation was registered by the photo-electrical multiplier, operating in the photon count regime and was scanned in time by the multichannel delayed coincidence method. Excitation cross-sections were calculated from the spectral line intensity on the back front of exciting pulses, namely in 20 ns after the excitation start. It is seen from the estimation, that cascade transitions part in cross-sections is 5-10 times decreased as compared with continious electron beam measurements.

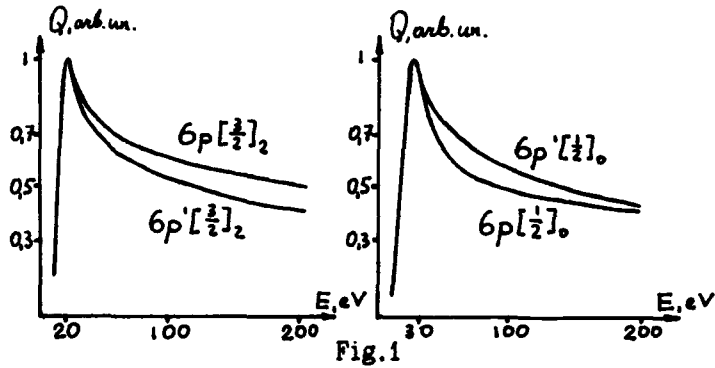
For the absolute calibration the He 728,1 nm line was used. Obtained cross-sections and excitation functions of the Xe level are represented in table 1 and fig.1. The error of absolute measurements is 25%.

Comparison with the results of [2,3], where cross-sections were also measured by optical methods but without consideration of

the cascade contribution, demonstrate our data to be 2-8 times less, there appeared to be no structure in the excitation function, which in [2] was attributed to the cascade population from d-levels.

Table 1

Levels	Q max, 10^{-20} cm ²	[3]
$6p'[\frac{1}{2}]_0$	82	275
$6p'[\frac{3}{2}]_2$	115	334
$6p[\frac{1}{2}]_0$	415	807
$6p[\frac{3}{2}]_2$	121	1000



1. I.P.Bogdanova, S.V.Yurgenson , Opt.Spektrosk. 61, 241, 1988
[Opt. Spectrosc. (USA) 61, 156, 1988]
2. P.V.Feltsan, I.P.Zapesochnyi, Ukr.Fiz.Zh.(Russ.Ed), 13, 205, 1989
3. I.P.Zapesochnyi, P.V.Feltsan, Opt.Spektrosk. 20, 512, 1988

COHERENT EXCITATION OF THE HEAVY RARE GASES BY ELECTRON IMPACT

J.J. Corr, P.J.M. van der Burgt, and J.W. McConkey
 Department of Physics, University of Windsor
 Windsor, Ontario N9B 3P4, Canada.

Electron-photon coincidence experiments have provided a fruitful testing ground for theories of electron-atom scattering and much progress has been made, particularly for L-S coupled targets. This has been detailed in recent reviews by Andersen et al.¹ and Slevin and Chwirot.²

In our laboratory we have carried out a series of polarization correlation Stokes parameter measurements. These relate in a rather straight-forward way to the parameters which define the excited state of the target¹ and in particular, data collected using an in-plane polarization analyser have enabled the so-called "height" of the excited state charge cloud to be studied in detail. A search has been carried out for any effects which might be caused by a breakdown in the reflection symmetry of the excitation process caused, for example, by a spin-flip of the exciting electron. Such an effect would result in a non-zero ρ_{00} (height) parameter.

In making these measurements particular care must be taken to minimize experimental effects which might cause a lack of definition of the scattering plane and thus lead to spurious measured Stokes parameters. We have carried out a careful analysis of these problems³ and will present a detailed report at the Conference. Our basic findings are that such effects are only likely to be significant at very small electron scattering angles ($<5^\circ$) and at angles where the P_1 parameter approaches -1.

We have also carefully investigated the depolarizing effect of hyperfine interactions. These are important for Kr and Xe targets where 11.5 and 47.6 percent respectively of the target atoms have non-zero nuclear spin. In both cases the natural lifetimes of the excited states are sufficiently long for complete hyperfine relaxation to occur prior to photon decay. As an example of the importance of these effects we show in the Figure our measured P_1 and P_4 Stokes parameters for electron scattering from Xe at 30 eV incident energy. Also shown are the Distorted Wave Born Approximation calculations of Bartschat and Madison.⁴ It is clear that when finite interaction volume and, particularly, hyperfine interaction effects are taken into account, good agreement between experiment and theory is obtained.

ρ_{00} parameters, which are appropriate to the nascent excited state charge cloud immediately following the original collision, have been evaluated for a range of incident electron energies and electron scattering angles. Within experimental error we find no deviation of ρ_{00} from zero. This resolves a previously reported⁵ discrepancy between measured and calculated ρ_{00} parameters.

-
1. N. Andersen, J.W. Gallagher and I.V. Hertel, Phys. Repts. **165**, 1 (1988).
 2. J. Slevin and S. Chwirot, J. Phys. B **23**, 165 (1990).
 3. P.J.M. van der Burgt, J.J. Corr and J.W. McConkey, J. Phys. B (submitted) (1990). J.J. Corr, P.J.M. van der Burgt, P. Plessis, M.A. Khakoo, P. Hammond and J.W. McConkey, J. Phys. B (submitted) (1990).
 4. K. Bartschat and D.H. Madison, J. Phys. B **20**, 5839 (1987).
 5. P. Plessis, M.A. Khakoo, P. Hammond and J.W. McConkey, J. Phys. B **21**, L483 (1988).

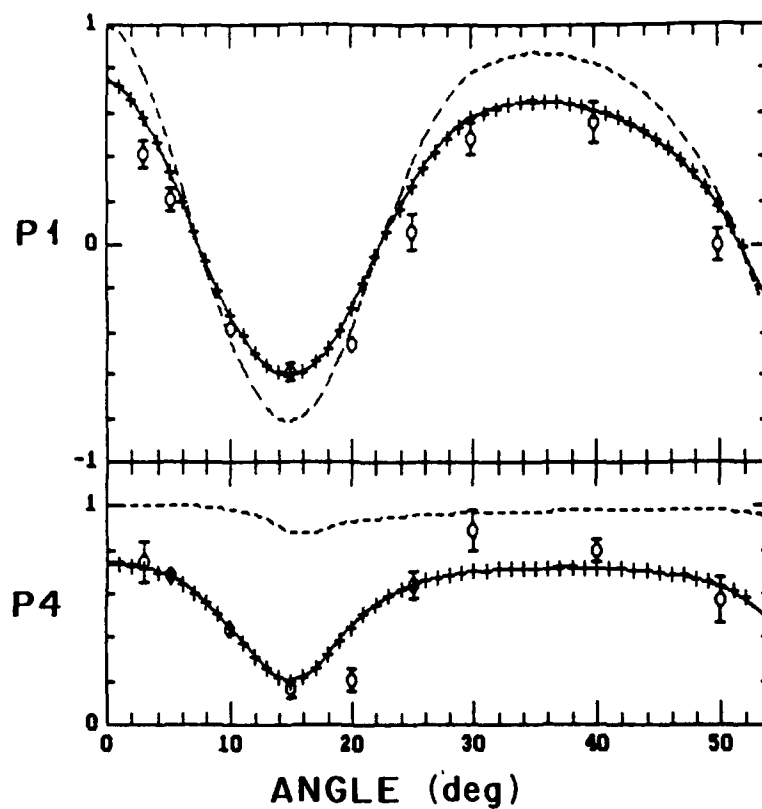


Fig. 1 P_1 and P_4 Stokes parameters as a function of electron scattering angle for electron impact excitation of the $[3/2]_0^o 6s$ state of Xe at 30 eV. Open circles, present data; dashed curve, DWBA results before correction for hyperfine interaction and finite volume effects; solid line, DWBA data corrected for hyperfine effects; crosses, DWBA data corrected for both hyperfine and finite volume effects.

COLLISION DATA FOR ELECTRIC QUADRUPOLE TRANSITIONS IN Ca⁺

A. Burgess¹, M. C. Chidichimo² and J. A. Tully³

¹ D.A.M.T.P., Silver Street Cambridge CB3 9EW, U.K.

² Department of Applied Mathematics, University of Waterloo, Waterloo, Ontario N2L 3G1.

³ Observatoire de Nice, B.P. 139, 06003 Nice Cédex, France.

We report on a research programme whose aim is to provide collision strengths for electron impact excitation of astrophysically important heavy ions. At present we are studying singly ionised calcium and strontium for which reliable atomic data is required in order to understand the abundances of these elements in peculiar A-type stars [1]. In this poster we present results for six optically forbidden E2 type transitions in Ca⁺ (see figure 1).

We use Chidichimo's non-exchange Coulomb distorted wave approximation CDW II, which is discussed in [2] and [3]. The target valence orbitals $P_n(r)$ are solutions of a one electron Schrödinger equation with observed binding energies; this approximation is described in [4]. The collision approximation assumes LS coupling and takes into account all open channels based on the lowest 7 states of Ca⁺ shown in figure 1. The calculation was performed at 12 impact energies ranging from 0.2368 to 23.09 Ryd. A sample of results is given in table 1, including values at $E_{4s} = \infty$ obtained by Born's approximation.

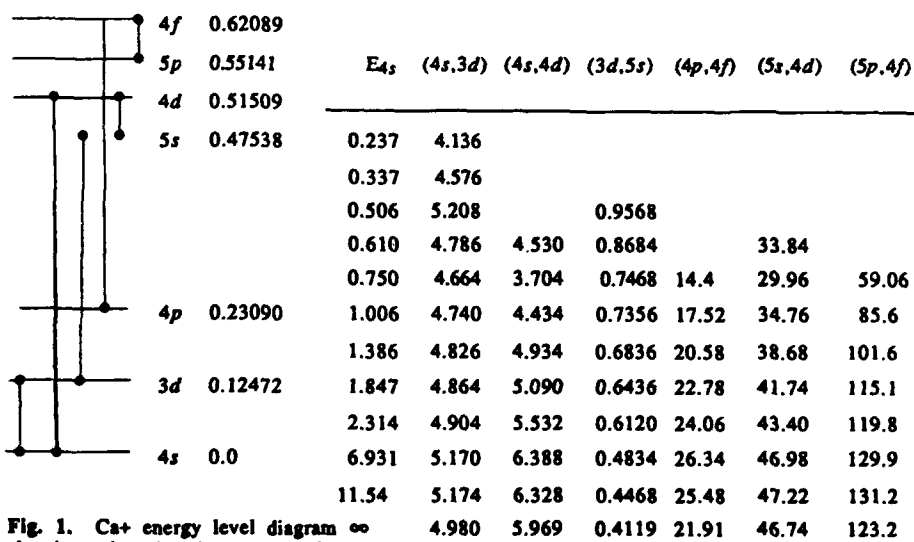


Fig. 1. Ca⁺ energy level diagram showing six electric quadrupole transitions amongst the lowest 7 states included in the present calculation. Energies are in Ryd; 1 Ryd = 109737.32 cm⁻¹.

E_{4s}	(4s,3d)	(4s,4d)	(3d,5s)	(4p,4f)	(5s,4d)	(5p,4f)
0.237	4.136					
0.337	4.576					
0.506	5.208		0.9568			
0.610	4.786	4.530	0.8684		33.84	
0.750	4.664	3.704	0.7468	14.4	29.96	59.06
1.006	4.740	4.434	0.7356	17.52	34.76	85.6
1.386	4.826	4.934	0.6836	20.58	38.68	101.6
1.847	4.864	5.090	0.6436	22.78	41.74	115.1
2.314	4.904	5.532	0.6120	24.06	43.40	119.8
6.931	5.170	6.388	0.4834	26.34	46.98	129.9
11.54	5.174	6.328	0.4468	25.48	47.22	131.2
∞	4.980	5.969	0.4119	21.91	46.74	123.2

Table 1. CDW II total collision strengths $\Omega(n'l, n'l')$.

E_{4s} = energy (in Ryd) of free electron relative to Ca⁺ (4s).

In order to interpolate the data in table 1 we make use of the interactive graphics program OME-UPS which is based on the method by Burgess and Tully [6] for interpolating and compacting collision strengths. Summaries of the method and the program are given in [4] and [5]. OME-UPS is in BBC BASIC and was written by one of us (A.B.) for use on the ARCHIMEDES and other ACORN micros. By using an emulator it runs on MACINTOSH and IBM microcomputers. Figure 2 is an example produced by an IBM PS/2. In this case $\Omega_{red} = \Omega(5s,4d)$ and $E_{red} = (E_{4d}/E_{5s,4d})(E_{4d}/E_{5s,4d} + C)$, where $E_{5s,4d} = E_{5s} - E_{4d}$ is the transition energy. C is an adjustable parameter. The value $C = 13$ optimises the least squares spline fit to this particular set of data points. The spline curve is defined by its values at the five equally spaced knots; these are listed to the right of the graph. A short program for the spline interpolation is given in appendix C of reference [4]. Further examples, as well as details of the program OMEUPS, will be available at the conference.

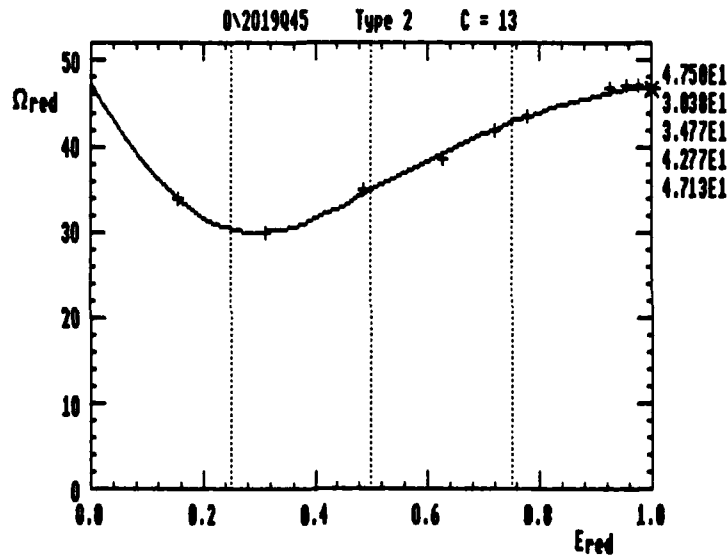


Fig. 2. Plot of reduced data for the transition $5s \rightarrow 4d$.

1. J. Borsenberger, G. Michaud and F. Praderie *Ap. J.* 243, 533 (1981).
2. M.C. Chidichimo, *Phys. Rev. A* 37, 4097 (1988).
3. M.C. Chidichimo, *Phys. Rev. A* 38, 6107 (1988).
4. A. Burgess, H.E. Mason and J.A. Tully, *Astron. Astrophys.* 217, 319 (1989).
5. A. Burgess, M.C. Chidichimo and J.A. Tully, *Phys. Rev. A* 40, 451 (1989).
6. A. Burgess and J.A. Tully, *Prod. R. Soc. Lond. A*, to be submitted (1990).

ELASTIC SCATTERING OF LOW-ENERGY ELECTRONS BY Ca, Sr AND Ba ATOMS

G.F.Gribakin⁺, B.V.Gul'tsev⁺, V.K.Ivanov⁺, M.Yu.Kuchiev[‡]⁺ M.I.Kalinin Polytechnical Institute, 195251 Leningrad, USSR[‡] A.F.Ioffe Physical Technical Institute of the Academy of Sciences of the USSR, 194021 Leningrad, USSR

The cross sections for the elastic scattering of low-energy ($\epsilon \leq 1$ eV) electrons by Ca, Sr and Ba atoms are calculated. In this problem the attractive electron-atom polarisational potential manifests itself strongly due to the large values of the dipole polarisabilities of the alkaline earth atoms. Taking into account the polarisational potential, the cross sections are completely changed in comparison with static Hartree-Fock approximation.

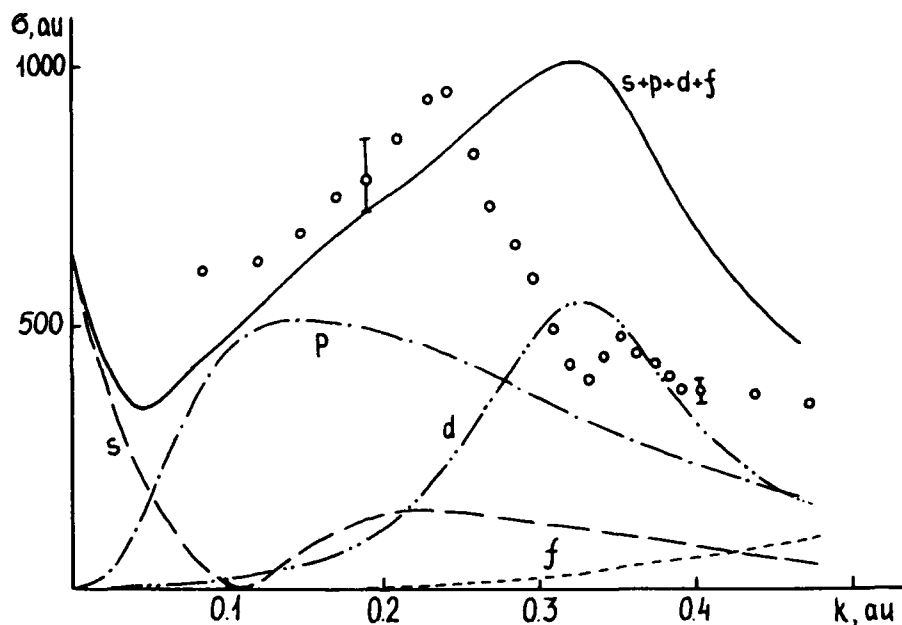
As is known, the polarisational potential results in the formation of Ca^- , Sr^- and Ba^- negative ions by binding of the p electron to the atom (see the experiment on Ca^- /1/ and the calculations, e.g. /2/). According to the Levinson's theorem, the arising of the new bound state increases p phaseshift by π at low energy, and the p scattering becomes of non-resonant behaviour.

As for the s wave, the polarisational potential changes the sign and the magnitude of the scattering length (e.g., for Ca $Q^{n^f+p^l} = -7.1$ au contrary to $Q^{HF} = 6.1$ au). Therefore the Ramsauer minimum appears in the s wave cross section and in the total cross section as well.

The d wave scattering has an explicit resonant character. The position and the width of the resonance depend strongly on the polarisational. In Ca the resonance, being located at $\epsilon \approx 4$ eV within Hartree-Fock approximation, is narrowed and shifted to $\epsilon = 1.45$ eV. In Sr and Ba the d resonance is shifted to even smaller energies, which leads to much greater maximal values of the cross sections.

The contribution of f wave and higher partial waves to the cross section is small. Their magnitude is determined mainly by the polarisational potential. In the figure the s, p, d, f partial cross sections and the total cross section for the elastic scattering by Ca are presented together with the experimental data from /3/.

The calculations were performed by means of the method /4/.



The scattering phaseshifts are obtained from the integral equation. the polarisational potential is taken into account by calculating the matrix elements for the self-energy operator of the "atom+electron" Green function. The self-energy operator is calculated by means of the perturbation technique in powers of electron-atom interaction, just as it was done for Ca^- , Sr^- , Ba^- negative ions /5/.

1. Pegg D.J., Thompson J.S., Compton R.N., Alton G.D. Phys.Rev.Lett. 59, 2267-2270 (1987).
2. Gribakin G.F., Gul'tsev B.V., Ivanov V.K., Kuchiev M.Yu. ZhTF, Pis'ma 15, no.12, 32-36 (1989) (in Russian).
3. Roman'uk N.I., Shpenik O.B., Zapesochny I.P. ZhETF, Pis'ma 32, 472-475 (1980) (in Russian).
4. Amusia M.Ya., Cherepkov N.A., Chernysheva L.V., Davidovic D.M., Radojevic V. Phys.Rev.A 25, 219-225 (1982).
5. Gribakin G.F., Gul'tsev B.V., Ivanov V.K., Kuchiev M.Yu. Submitted to J.Phys.B: At.Mol.Opt.Phys. (1990).

LOW ENERGY ELECTRON IMPACT EXCITATION IN H AND He⁺: n≤5 STATE CALCULATIONS

K.M. Aggarwal, K.A. Berrington, P.G. Burke, A.E. Kingston and A. Pathak

Department of Applied Mathematics and Theoretical Physics
The Queen's University of Belfast, Belfast BT7 1NN, Northern Ireland, U.K.

With a sophisticated exploitation of the most powerful computer available to us, the four-processor Cray X-MP/416 at the Atlas Centre, we have been able to carry out some of the largest close-coupling calculations in the world. An example is in electron scattering from hydrogen, where we have been able to include states up to a principal quantum number n=5 in an R-matrix calculation (Pathak et al. 1989).

Collision strengths Ω have been calculated for all transitions of H and He⁺ among the fifteen lowest physical states. These are done in the LS coupling scheme using the R-matrix code of Berrington et al.(1978) for all partial waves with angular momentum $L \leq 9$. For $L=10-45$, the no exchange program developed by Burke et al.(1990) has been used as exchange effects are not considered to be very important for this range of partial waves. For optically allowed and semi forbidden transitions, the contribution of partial waves with $L > 45$ has also been added using the Burgess(1974) sum rules. However, for the elastic transitions this range of partial waves is still insufficient to have convergence in Ω .

The calculations have been made over a fine mesh of impact energy (particularly close to the inelastic thresholds) in order to elucidate the resonances which contribute significantly to the excitation and deexcitation rate coefficients, especially at lower temperatures. In total, calculations have been done at 569 number of impact energies in the range 0 to 1.96 Ry for H and at 255 energies in the range 0 to 7.0 Ry for He⁺. Tabulated results for the total collision strengths Ω and effective collision strengths Υ at a number of energies/temperatures will be available during the conference and here we show in Figure 1 our Ω for the 1s-2s transition in the energy range below 1 Ry. Compared in the same figure are the Ω s of Callaway(1982) and Scholz et al.(1990). For this and 1s-2p transitions, it may be noted that these authors have included psuedo states in the expansion of their wavefunctions whereas we have not. For this reason, our present Ω are slightly overestimated in comparison to those from these authors. However, ours are the most comprehensive close coupling results available to date for all transitions up to n=5 levels in H and He⁺. In Figure 2, we show for the first time our Ω for the 1s-4s and 1s-4p transitions for H, and in Table 1, we list our Υ for both H and He⁺ at a few representative temperatures for transitions from the ground state to n=3 levels.

Table 1. Effective collision strengths for transitions from ground state to excited states up to n=3 levels in H and He⁺.

T (K)	H					He ⁺				
	1s-2s	1s-2p	1s-3s	1s-3p	1s-3d	1s-2s	1s-2p	1s-3s	1s-3p	1s-3d
5000	0.2781	0.4602	0.0680	0.1210	0.0638	0.1540	0.3272	0.0342	0.0521	0.0400
7500	0.2939	0.4919	0.0709	0.1267	0.0665	0.1554	0.3382	0.0370	0.0568	0.0394
10000	0.3054	0.5277	0.0737	0.1349	0.0691	0.1557	0.3462	0.0388	0.0608	0.0396
15000	0.3195	0.5991	0.0806	0.1589	0.0749	0.1553	0.3589	0.0404	0.0659	0.0399
20000	0.3284	0.6723	0.0879	0.1886	0.0803	0.1547	0.3699	0.0410	0.0694	0.0399
30000	0.3439	0.8330	0.1008	0.2522	0.0909	0.1534	0.3894	0.0413	0.0757	0.0397
40000	0.3597	1.0080	0.1105	0.3129	0.0986	0.1520	0.4061	0.0413	0.0820	0.0395
50000	0.3749	1.1870	0.1174	0.3675	0.1043	0.1506	0.4207	0.0412	0.0880	0.0393

Fig.1: (1s-2s) — Present Results, Callaway (1982),
 - - - - Scholz et al (1990).

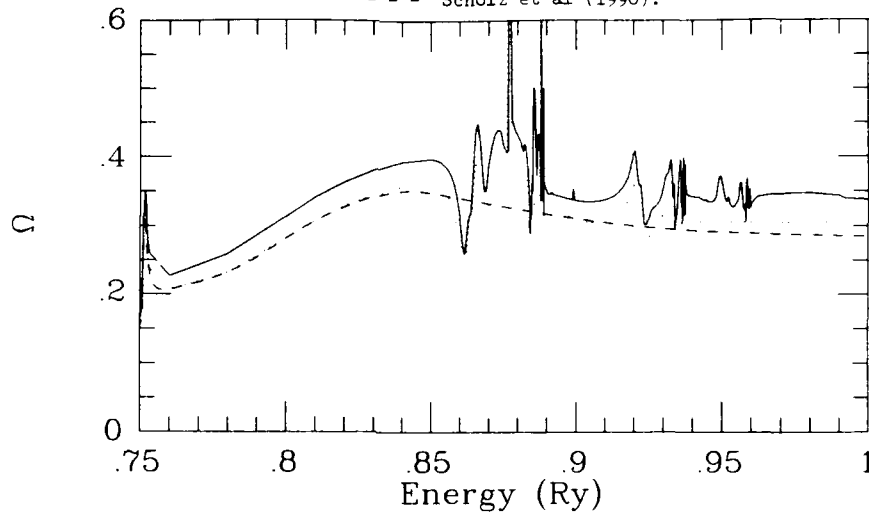
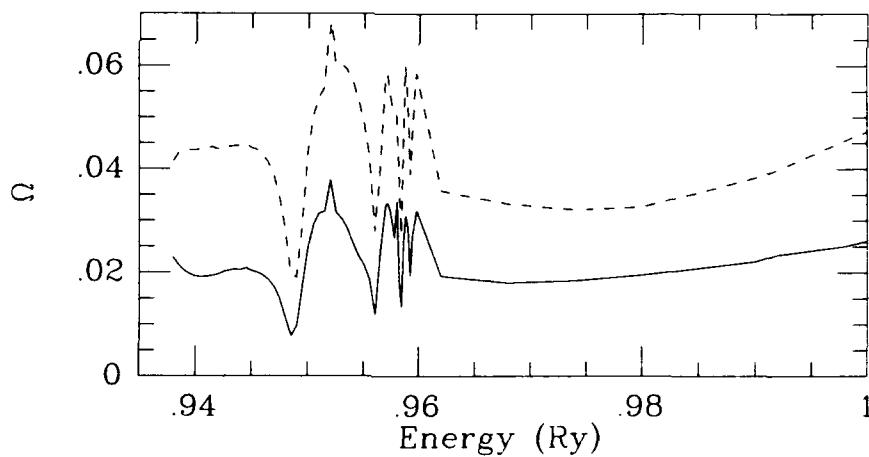


Fig.2: 1s-4s (---) and 1s-4p (- - -)



References

Berrington KA, Burke PG, LeDourneuf M, Robb WD, Taylor KT and Vo Ky Lan (1978) *Comput. Phys. Commun.* **14**, 367.
 Burgess A (1974) *J. Phys. B: At. Mol. Phys.* **7**, L364.
 Burke VM, Burke PG and Scott NS (1990) *Comput. Phys. Commun.* - submitted.
 Callaway J (1982) *Phys. Rev. A* **26** 199.
 Pathak A, Burke PG and Berrington KA (1989) *J. Phys. B: At. Mol. Opt. Phys.* **22**, 2759.
 Scholz TT, Walters HRJ, Burke PG and Scott MP (1990) *MNRAS* **242** 692.

ELECTRON IMPACT EXCITATION WITH Ca XV and Fe XXI

K.M. Aggarwal, K.A. Berrington, W.B. Eissner and P.H. Norrington

Department of Applied Mathematics and Theoretical Physics
The Queen's University of Belfast, Belfast BT7 1NN, Northern Ireland, U.K.

For over a decade electron impact excitation with ions in the Carbon sequence is being studied in The Queen's University of Belfast. But, in our recent paper (Aggarwal et al, 1990) a big *discrepancy* arose between two independent calculations viz. R- matrix and Distorted Wave (DW) of electron impact excitation with Ca XV. Both calculations excluded explicit configuration interaction (CI) with pseudo orbitals and included the contribution of *relativistic effects* in the *same* way through the JAJOM program of Saraph (1978) using *term coupling coefficients* (TCC). Yet the collision strengths Ω from the R- matrix program were *higher* by up to two orders of magnitude in comparison to those from the DW calculation of Dere et al. (1979), at least, for a few transitions, particularly the spin changing ones like $^3P_0 - ^1P_1^o$. Therefore, a need was emphasized for another independent calculation to investigate this discrepancy and to check the validity of the available results. To do that, we have now performed fully relativistic Dirac R- matrix calculations, as implemented by Norrington and Grant (1987), including all the relativistic effects in the target wavefunctions.

We are happy to report that our present Dirac R- matrix calculations are in *excellent agreement* with those of Dere et al. for almost all transitions except a few, for which the disagreements are within a factor of two only. The magnitude of Ω for these transitions is, however, very small, in general. The differences noted in our earlier paper appear to be due to inaccuracies in the description of TCC which particularly affect the spin changing transitions like $^3P_0 - ^1P_1^o$.

The calculations for Ω have been done for all the 190 inelastic fine structure transitions arising from the 20 fine structure levels among the $1s^22s^22p^2$, $1s^22s2p^3$, and $1s^22p^4$ configurations. The Ω s have been computed in the *jj* coupling scheme at three energies only viz. 15, 30 and 45 Ry and in Table 1 we compare our present Ω with those of Dere et al. and our previous R- matrix calculations (Aggarwal et al, 1990) at two energies. The results are compared here for a few transitions only, especially for those for which the *discrepancy* was quite large in our previous calculation. However, tabulations of Ω for all the transitions at these three energies will be available during the conference.

Similar calculations have also been done for another astrophysically important ion in the Carbon series viz. Fe XXI. Full tabulation of Ω at three impact energies i.e. 20, 50 and 100 Ry will be available during the conference and here in Table 2 we compare our Ω with those available from the DW calculations of Mason et al. (1979) for 10 fine structure transitions arising from the levels within the $1s^22s^22p^2$ configuration only. The agreement between the two independent sets of calculations is highly *satisfactory*.

The results of Ω for both Ca XV and Fe XXI at a greater number and in a wider range of impact energies will be available soon when the resonance structure will be studied in detail in order to calculate the excitation and deexcitation rate coefficients which are needed for the temperature and density diagnostics of the line intensity ratios observed in various astrophysical objects.

References

- Aggarwal KM, Berrington KA and Keenan FP (1990) *Astrophys. J. Suppl.* **72** 815.
 Dere KP, Mason HE, Widing KG and Bhatia AK (1979) *Astrophys. J. Suppl.* **40** 341.
 Mason HE, Doschek GA, Feldman U and Bhatia AK (1979) *Astron. Astrophys.* **73** 74.
 Norrington PH and Grant IP (1987) *J. Phys.* **B** 4869.
 Saraph HE (1978) *Comput. Phys. Commun.* **15** 247.

Table 1. Comparison of collision strengths between present relativistic Dirac R- matrix; [RM(D)], earlier R- matrix; [RM(TCC)] and DW calculations of Dere et al. (1979) for Ca XV.

Transition		E = 15 Ry			E = 45 Ry		
I	J	RM(TCC)	RM(D)	DW	RM(TCC)	RM(D)	DW
3P_0	3P_1	2.71-2	2.86-2	2.81-2	1.55-2	1.65-2	1.60-2
	3P_2	1.92-2	2.08-2	2.02-2	1.48-2	1.71-2	1.62-2
	1D_2	1.46-2	1.09-2	1.11-2	9.20-3	5.94-3	6.10-3
	1S_0	2.35-2	1.42-3	1.50-3	1.12-3	6.93-4	7.00-4
	$^3P_2^o$	2.32-4	9.19-4	1.00-3	4.94-5	5.67-4	6.00-4
3P_1	$^1P_1^o$	3.28-2	4.84-4	5.00-4	4.03-2	3.21-4	3.00-4
	3P_2	7.68-2	7.79-2	7.60-2	5.46-2	5.50-2	5.24-2
	1D_2	4.25-2	4.26-2	4.25-2	2.33-2	2.38-2	2.36-2
	1S_0	7.58-3	6.38-3	6.40-3	3.70-3	3.17-3	3.20-3
	3P_2	8.54-2	8.87-2	8.70-2	4.94-2	5.31-2	5.12-2
3P_2	1D_2	1.22-2	1.17-2	1.19-2	7.62-3	6.17-3	6.30-3
	1S_0	3.44-2	3.80-2	3.79-2	3.81-2	4.12-2	3.92-2
	$^3S_1^o$	1.53-3	9.77-4	7.00-4	1.41-3	6.30-4	4.00-4
1D_2	1S_0	9.54-4	2.01-4	1.58-4	5.90-4	1.17-4	9.59-5
	$^3D_2^o$	1.29-2	3.54-3	1.90-3	2.23-3	4.13-3	1.30-3
	$^3S_1^o$	2.95-2	5.32-3	5.20-3	4.12-2	6.47-3	6.20-3
$^3D_1^o$	1S_0	1.12-2	2.04-4	1.80-4	1.31-2	2.05-4	1.89-4
$^1P_1^o$	3P_0	5.93-2	2.37-3	2.76-3	1.03-1	1.67-3	1.67-3

Table 2. Comparison of collision strengths between present relativistic Dirac R- matrix and earlier DW calculations of Mason et al. (1979) for Fe XXI.

Transition		DW			R-matrix		
I	J	E=20 Ry	E=50 Ry	E=100 Ry	E=20 Ry	E=50 Ry	E=100 Ry
3P_0	3P_1	1.51-2	1.08-2	6.90-3	1.53-2	1.10-2	7.03-3
	3P_2	1.47-2	1.25-2	1.06-2	1.50-2	1.30-2	1.14-2
	1D_2	3.00-3	2.10-3	1.30-3	2.82-3	1.97-3	1.20-3
3P_1	1S_0	4.00-4	3.00-4	2.00-4	4.31-4	2.85-4	1.61-4
	3P_2	4.24-2	3.30-2	2.45-2	4.31-2	3.39-2	2.58-2
	1D_2	2.41-2	1.77-2	1.19-2	2.45-2	1.81-2	1.25-2
3P_2	1S_0	4.00-3	2.70-3	1.60-3	4.14-3	2.82-3	1.67-3
	1D_2	5.49-2	4.33-2	3.29-2	5.61-2	4.49-2	3.55-2
	1S_0	7.40-3	5.70-3	4.30-3	7.44-3	5.81-3	4.52-3
1D_2	1S_0	2.05-2	2.01-2	1.99-2	2.04-2	2.04-2	2.12-2

THEORETICAL DIFFERENTIAL CROSS SECTIONS AND SPIN POLARIZATIONS
FOR ELASTIC ELECTRON SCATTERING FROM XE ATOMS

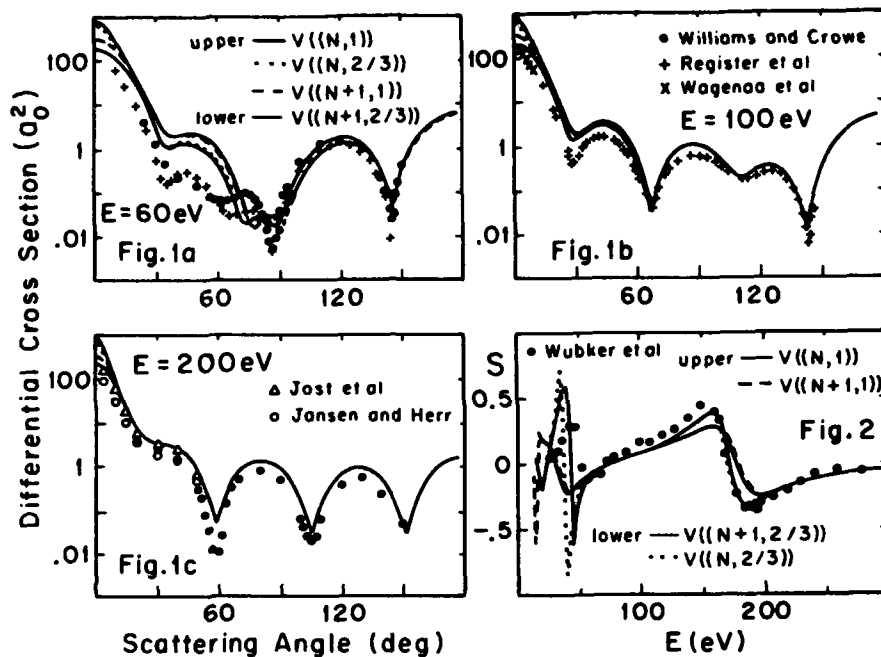
Qing Hou, * Jia-Ming Li * and R. H. Pratt **

* Institute of Physics, Academia Sinica, Beijing, China

** Department of Physics and Astronomy, University of Pittsburgh,
Pittsburgh, PA 15260 U.S.A.

Recent advances in experimental techniques have enabled experimentalists to perform so-called complete scattering experiments.¹⁻³ The simplest situation is that an electron with well defined spin polarization is elastically scattered from a spinless atom. Through the measurements of the spin polarization parameters (S, T, U) of scattered electrons at various scattering angles, in conjunction with absolute measurements of differential cross sections,⁴⁻⁷ all the available information about the scattering process, namely the moduli and relative phases of the scattering amplitudes, can be determined. Thus the validity of various theoretical methods can be tested in more detail. Here we present our theoretical results for the differential cross sections and spin polarization parameters for electrons elastically scattered from Xe atoms. In such processes, the incident electron is treated as moving relativistically in an effective central potential $V(r)$, which is calculated by relativistic self-consistent-field methods with the Slater local exchange approximation (i.e., Dirac-Slater SCF).⁸⁻⁹ Elastic scattering amplitudes are then calculated with the relativistic partial wave expansion method. In the Dirac-Slater SCF method with the local exchange parameter α , taking N (=54) electrons in the target-atom ground-state configuration without the Latter's approximation,¹⁰ we can obtain an effective potential $V(r;N,\alpha)$, where $V(r;N,1)$ is the Slater potential and $V(r;N,2/3)$ the Kohn-Sham potential. Taking the incident electron and the N bound electrons together in a specific configuration, (Xe)6s, with the Latter approximation, we then obtain an effective potential $V(r;N+1,\alpha)$.

Based on such types of potentials, we have calculated the differential cross sections and the spin polarization parameters. Figure 1 displays the differential cross sections for three incident energies; 60, 100 and 200 eV. At high energy (e.g., 200 eV), all four types of potentials give similarly good descriptions. At intermediate energy (e.g. 100 eV), the potential $V((N+1,2/3))$ is more appropriate. However, at lower energy (e.g., 60 eV), none of the four potentials can give an adequate description, because electron correlations became important. The electron correlations which have not been taken into account in our Dirac-Slater SCF potentials, require further theoretical improvements, as in a multichannel theoretical method.¹¹ In Fig. 2, we show our calculated spin polarization parameters (e.g., S parameter at the scattering angle $\theta = 60^\circ$). This also confirms the validity of the potentials. Based on our relativistic partial wave expansion method, the validity of Born approximation will also be discussed.



References

1. R. Mollenkamp, W. Wubker, O. Berger, et al., *J. Phys. B* **17**, 1107 (1984).
2. O. Berger and J. Kessler, *J. Phys. B* **19**, 3539 (1986).
3. W. Wubker, R. Mollenkamp, J. Kessler, *Phys. Rev. Lett.* **49**, 272 (1982).
4. J. F. Williams and A. Crowe, *J. Phys. B* **8**, 2233 (1975).
5. R. H. J. Jansen and F. J. de Heer, *J. Phys. B* **9**, 213 (1976).
6. D. F. Register, L. Vuskovic, S. Trajmar, *J. Phys. B* **19**, 1685 (1986).
7. R. W. Wagenaa, A. de Boer et al., *J. Phys. B* **19**, 3121 (1986).
8. Zong-Xin Zhao and Jia-Ming Li, *Acta Physica Sinica* **30**, 105 (1981).
9. D. A. Liberman, J. T. Waber, and D. T. Cromer, *Phys. Rev.* **137**, A27 (1965);
D. A. Liberman, D. T. Cromer and J. T. Waber, *Comp. Phys. Comm.* **2**, 107 (1965).
10. R. D. Cowan, *The Theory of Atomic Structure and Spectra*, (University of California Press, California, 1981).
11. Jia-Ming Li, Ying-Jian Wu and R. H. Pratt, *Phys. Rev.* **40**, 3036 (1986).

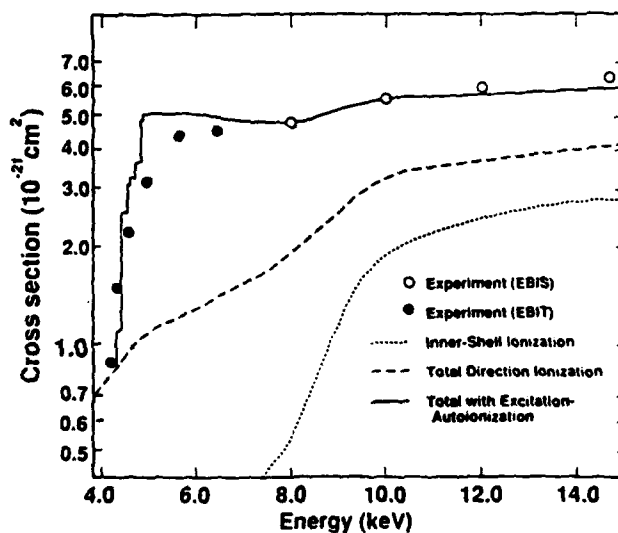
ELECTRON IMPACT IONIZATION OF HIGHLY CHARGED Na-LIKE IONS

K. J. Reed and M. H. Chen
 High Temperature Plasma Division
 Lawrence Livermore National Laboratory
 Livermore, CA 94550

D. L. Moores
 Department of Physics and Astronomy
 University College London
 Gower Street, London, WC1E 6 BT, England

We report relativistic calculations of electron impact ionization cross sections for highly charged sodium-like ions. The cross sections for direct ionization of the 3s electron and the n=2 inner-shell electrons were computed using a relativistic distorted wave code. A multi-configuration relativistic distorted wave method¹ was used to calculate electron impact excitation cross sections for transitions from the n=2 subshells to the n=3 and n=4 subshells of the ions. Detailed radiative and Auger rates for the intermediate excited states were obtained using a Multi-Configuration Dirac Fock model (MCDF).² These rates were used to determine the excitation-autoionization and resonant excitation double autoionization (REDA) contributions to the ionization cross sections.

Ionization Cross Sections For Na-like Xe



Earlier theoretical and experimental studies have shown that excitation-autoionization

enhances the direct ionization cross section by about a factor of 4 in light sodium-like ions with $Z \leq 28$. Until recently it has generally been assumed that contributions from indirect processes should be negligible in high Z ions because of radiative decay. But our investigations indicate that excitation-autoionization enhances the direct ionization cross sections by about a factor of 4 in high Z sodium-like ions with $26 \leq Z \leq 92$. The REDA process contributes about 30% to the average total cross section for Fe^{15+} and about 20% of the total cross section for Xe^{44+} . For sodium-like ions with $Z \geq 79$, the REDA contribution is less than 5%.

Our results are in very good agreement with measured cross sections in those cases where experimental data is available. In particular, recent experiments using the Electron Beam Ion Trap show a steep increase in the ionization cross section for Xe^{43+} in the energy region where the excitation-autoionization thresholds occur.

This work was performed under the auspices of the U.S. Department of Energy by Lawrence Livermore National Laboratory under Contract # W-7405-ENG-48.

1. P.L. Hagelstein and R. K. Jung, At. Data Nucl. Data Tables 37, 17 (1987).
2. M. H. Chen, Phys. Rev. A 31, 1449 (1985).

ABSOLUTE ELECTRON SCATTERING CROSS SECTIONS FOR THE $^2S \rightarrow ^2P$
TRANSITION IN Zn^+ USING ENERGY-LOSS AND MERGED-BEAMS METHODS

Steven J. Smith*, K-F. Man*, R.J. Mawhorter⁺,
I.D. Williams⁺⁺, and A. Chutjian*

* Jet Propulsion Laboratory, Caltech, Pasadena, CA 91109

⁺ Dept. Physics and Astronomy, Pomona College, Claremont, CA 91711

⁺⁺ Dept. Pure and Applied Physics, Queens Univ., Belfast, N. Ireland BT7 1NN

Using the electron energy-loss method[1-2] in a merged electron-ion beams geometry[3-4] absolute, cascade-free excitation cross sections have been measured for the resonance $^2S \rightarrow ^2P$ transition in Zn^+ . Measurements were carried out at electron energies of below threshold (threshold at 6.011 eV) to 40 eV. Results are in excellent agreement with close-coupling calculations[5] and, away from threshold, lie below absolute line-emission cross sections[6] which include effects of cascade into the 2P state from higher levels.

The apparatus used in these measurements has been described earlier[3]. Briefly, a beam of electrons is merged with a beam of ions in a uniform, stable solenoidal magnetic field through the use of trochoidal deflection plates and $\vec{E} \times \vec{B}$ fields. Inelastically-scattered electrons are demerged from the interaction region through trochoidal plates, and dispersed according to their final energy. Merging and analyzing electric fields are chosen to minimize beam-shear effects, while having only a small deflection effect upon the 4 keV ion beam. The merged interaction length is 20 cm. The resulting energy-loss feature is detected using a microchannel-plate array and 2-dimensional resistive anode as a position-sensitive detector (PSD) oriented along the beams directions. A PC/CAMAC data acquisition system is used for computer interface and control. Data are stored in a histogramming memory at the output of the PSD. The cross section $\sigma(E)$ at the center-of-mass (CM) energy E is related to the experimental parameters by the relation

$$\sigma(E) = \frac{Re^2F}{\epsilon I_e I_i L} \left| \frac{v_e v_i}{v_e - v_i} \right| \quad (1)$$

where R is the signal rate (sec^{-1}), e the electron charge, I_e and I_i the electron and ion currents (A), respectively, L the merged pathlength (cm), v_e and v_i the electron and ion velocities (cm/sec), respectively, ϵ the detection efficiency of the PSD (dimensionless), and F the overlap factor between the electron and ion beams (cm^2) as measured at four positions along the merged length.

Present absolute electron excitation cross sections for the $^2S \rightarrow ^2P$ transition in Zn^+ are shown in Fig. 1. These data have not been corrected for the backward-scattered portion of the inelastic cross section. This correction raises the cross sections at 15 and 20 eV by factors of 1.045 and 1.025, respectively[7], with slightly larger factors expected at threshold. Because of the kinematic effect of electrons and ions moving in the same direction, one is able to carry out measurements below the inelastic threshold (to ensure zero cross section, and the absence of metastable ions in the beam), while the electrons still have ~ 2 eV energy in the laboratory frame. Also given in Fig. 1 are line-emission cross sections[6], and theoretical, close-coupling calculations both with and without cascade into the 2P level[5]. The Gaunt-factor approximation (divided by three, with $f=0.732$) is given as the solid line[8]. One finds excellent agreement between present results and calculations-without-cascade, while present data (cascade-free), as expected, lie below line-emission results at energies above threshold where cascade effects become significant.

This work was carried out at JPL/Caltech through support from NASA and the Lawrence Livermore Nat. Lab. Collaboration with the Queen's Univ. was made possible through a NATO International Collaborative Research Grant. Several of us (SJS, KM, RJM and IDW) acknowledge support from the

NASA-National Research Council for Resident Research Associateships at JPL. We are grateful to R.J.W. Henry for results of the backward-scattered cross section prior to publication.

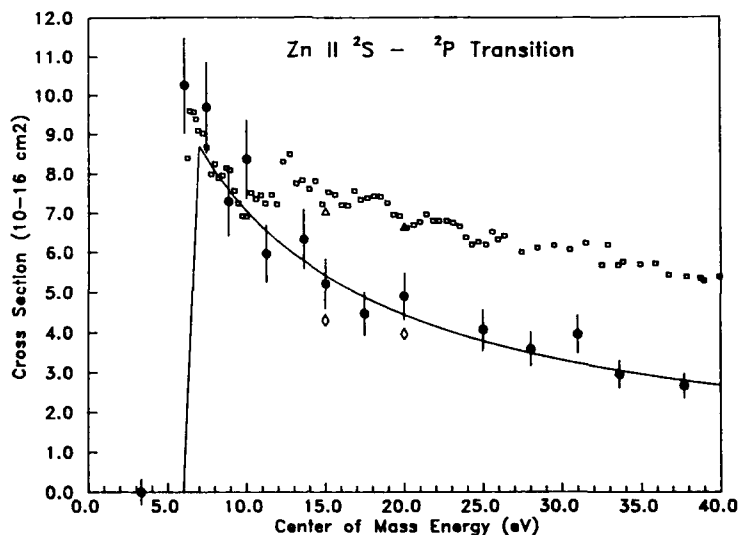


Figure 1: Absolute cross sections for excitation of the $2S \rightarrow 2P$ transition in Zn^+ . Present, cascade-free results are given as \bullet , and line emission cross sections[6] as \square . Calculations are from Ref. 5, with (Δ) and without (\circ) cascade. The Gaunt factor approximation, divided by three, is given by the solid line. Present data are not corrected for the backward-scattered electrons (see text).

1. A. Chutjian, A.Z. Msezane, and R.J.W. Henry, *Phys. Rev. Letters* 50, 1357 (1983).
2. I.D. Williams, A. Chutjian and R.J. Mawhorter, *J. Phys. B* 19, 2189 (1986).
3. R.J. Mawhorter, I.D. Williams, B.F. Lewis and A. Chutjian, *Bull. Am. Phys. Soc.* 32, 1273 (1987); and XVth Int. Conf. Phys. Elect. Atom. Coll. (Brighton, UK 1987).
4. C. Timmer, E. Wählin, B. DePaola, K. Rinn, D.R. Swenson, D.S. Belić, and G.H. Dunn, XVth Int. Conf. Phys. Electron. Atom. Coll. (Brighton, UK 1987) Abstracts p. 805; E. Wählin, C. Timmer, L. Forand, D. Swenson, B. DePaola, R. Phaneuf, D. Belić, K. Rinn, A. Müller, and G. Dunn, XVIth Int. Conf. Phys. Electron. Atom. Coll. (New York, NY 1989) Abstracts p. 368.
5. A.Z. Msezane and R.J.W. Henry, *Phys. Rev. A* 26, 692 (1982).
6. W.T. Rogers, G.H. Dunn, J.O. Olsen, M. Reading, and G. Stefani, *Phys. Rev. A* 25, 681 (1984).
7. R.J.W. Henry, private communication (1990).
8. R. Mewe, *Astron. Astrophys.* 20, 215 (1972).

**ELECTRON SCATTERING BY NEON-LIKE SELENIUM
USING THE DIRAC R-MATRIX THEORY**

W. P. WIJESUNDERA, I. P. GRANT, F. A. PARPIA

Oxford University, Department of Theoretical Chemistry,
5 South Parks Road, Oxford OX1 3UB, United Kingdom

and P. H. NORRINGTON

The Queen's University of Belfast,
Department of Applied Mathematics and Theoretical Physics
Belfast BT7 1NN, United Kingdom

Collision strengths for the scattering of electrons with kinetic energy 0-300 Ryd by neon-like selenium (Se^{24+}) have been calculated using the Dirac R-matrix method [1,2]. In these calculations the 27 *jj*-coupled levels arising from the configurations $1s^2 2s^2 2p^6$, $1s^2 2s^2 2p^5 3s$, $1s^2 2s^2 2p^5 3p$ and $1s^2 2s^2 2p^5 3d$ are included. Collision strengths converged to within 5% are obtained with twenty-four $N + 1$ -particle collision symmetries (partial waves). The rates for radiative transitions between the 27 levels have also been calculated. Our results are compared with previous calculations [3].

References

1. J. J. Chang, *J. Phys. B: At. Mol. Phys.* **8** (1975) 2327.
2. P. H. Norrington and I. P. Grant, *J. Phys. B: At. Mol. Phys.* **14** (1981) L261.
3. G. P. Gupta, K. A. Berrington and A. E. Kingston, *J. Phys. B: At. Mol. Phys.* **22** (1989) 3289 and references therein.

**ELECTRON SCATTERING BY OXYGEN-LIKE KRYPTON
USING THE DIRAC R-MATRIX THEORY**

W. P. WIJESUNDERA, F. A. PARPIA, I. P. GRANT

Oxford University, Department of Theoretical Chemistry,
5 South Parks Road, Oxford OX1 3UB, United Kingdom

and P. H. NORRINGTON

The Queen's University of Belfast,
Department of Applied Mathematics and Theoretical Physics,
Belfast BT7 1NN, United Kingdom

Cross sections for the scattering of electrons with kinetic energy 0-90 Ryd by oxygen-like krypton (Kr^{28+}) have been calculated using the Dirac R-matrix method [1,2].

The GRASP² [3] multiconfiguration Dirac-Fock (MCDF) program has been used to obtain wavefunctions and level energies of the target. In these calculations the 10 *jj*-coupled levels arising from the configurations $1s^2 2s^2 2p^4$, $1s^2 2s 2p^5$ and $1s^2 2p^6$ are included. Our calculated level intervals are very different from those obtained from a non-relativistic approach [4]. We compare the MCDF level intervals and wavelengths with experiment [5].

Cross sections converged to within 5% are obtained with thirty $N + 1$ -particle collision symmetries (partial waves). We have computed the profiles of, and identified, resonances in the cross sections at selected incident energies.

References

1. J. J. Chang, *J. Phys. B: At. Mol. Phys.* **8** (1975) 2327.
2. P. H. Norrington and I. P. Grant, *J. Phys. B: At. Mol. Phys.* **14** (1981) L261.
3. F. A. Parpia, I. P. Grant and C. F. Fischer (1990), *in preparation*.
4. K. J. Reed and R. J. W. Henry, *Phys. Rev. A* **40** (1989) 1823.
5. D. D. Dietrich, R. E. Stewart, and R. J. Fortner, R. J. Dukart, *Phys. Rev. A* **34** (1986) 1912.

EIKONAL EVALUATION OF CROSS SECTION ASYMMETRY IN ATOMIC
BREAK-UP PROCESS BY POLARIZED ELECTRONS

T. Onaga(*) and H. Narumi(**)

Department of Physics, Hiroshima University, Hiroshima 730, Japan

In the last two decades, as is well-known, the eikonal theories have experienced a remarkable applicability for atomic scattering as well as nuclear scattering even in the intermediate energy region[1].

Moreover the recent polarization measurements for the hydrogen system by polarized electrons are of considerable interest[2], since these experiments with cross section asymmetry allow for us to examine the validity of various approximation methods. In particular the exchange amplitude g in ionization process is closely related to the direct amplitude f through the relation $g(\underline{k}_2, \underline{k}_1) = f(\underline{k}_1, \underline{k}_2)$, where \underline{k}_1 and \underline{k}_2 are the momenta of scattered and ejected electrons.

In the Born approximation the exchange amplitude can be evaluated by the above formula. In the Glauber approximation, however, an abridged method, which is extremely conventional, was taken in an evaluation of the ionization amplitude[3].

In this paper we evaluate an eikonal exchange amplitude for the cross section asymmetry as well as the integrated ionization cross section of hydrogen atoms[4], where a new formulation is given for the evaluation of the exchange amplitude up to relatively higher partial Coulomb waves.

The results of integrated ionization cross sections and cross section asymmetries are illustrated in Fig.1 and Fig.2, respectively. The eikonal integrated cross sections with exchange amplitudes, as we can see, can reproduce the experimental ones especially in the region giving the maximum cross section as well as the high energy side.

On the contrary, regarding the cross section asymmetry, the eikonal approximation with exchange amplitudes does not always give experimental values in the intermediate energy region. Such an appearance can be seen in the Born exchange approximation, where the results strongly depend on the phase or interference factor, for example.

In the eikonal approach the above exchange relation can not be used in exact form, but the Born-Oppenheimer type approximation will be applicable.

Finally it is suggested from the above consideration that the cross section asymmetry will give an important criterion or validity of the high energy scattering theories in the intermediate energy region.

* Permanent Address: Kyoto Junior College of Culture, Kameoka 621, Japan

** Present Address: Fukuyama University, Fukuyama 729-02, Japan

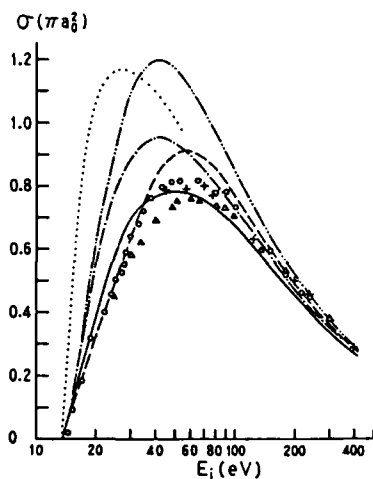


Fig.1 Integrated cross section of hydrogen ionization. The results of the Born-Oppenheimer(dotted line)[5], the Born(two dot-dashed line), the Born-exchange(dot-dashed line)[5], the Glauber(dashed line)[6] and the present Glauber-exchange(solid line) values are given.

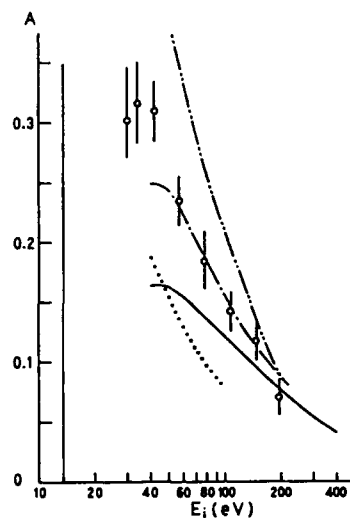


Fig.2 Ionization cross section asymmetry. The results of the Born-exchange with the maximum interference(two dot-dashed line)[7], the Born-exchange with the same phase as that in our eikonal approach(dot-dashed line)[5], the Glauber-exchange(dotted line)[3], which includes a serious problem, and the present Glauber-exchange(solid line) values are shown in comparison with experimental values[2].

References

1. for example, H. Narumi, KURRI-TR-332, Kyoto University (1990), 13
2. G.D. Fletcher et al., Phys. Rev. A31 (1985), 2854
3. J.E. Golden and J.H. McGuire, Phys. Rev. Lett. 32 (1974), 1218
4. T. Sekimura and H. Narumi, Prog. Theor. Phys. 63 (1980), 1797;
T. Sekimura, ibid. 64 (1980), 28
5. S. Geltman, M.R.H. Rudge and M.J. Seaton, Proc. Phys. Soc. London 81 (1963), 375
6. H. Narumi, A. Tsuji and A. Miyamoto, Prog. Theor. Phys. 54 (1975), 740
7. M.R.H. Rudge and M.J. Seaton, Proc. R. Soc. London, Ser. A283 (1965), 262

COMPLETE ELECTRON IMPACT EXCITATION PARAMETERS
FOR THE 3^3D STATE OF HELIUM

H J Beyer and H Kleinpoppen

Unit of Atomic and Molecular Physics
University of Stirling, Stirling, Scotland FK9 4LA

Considerable progress has been made recently to extend complete measurements of the electron impact excitation parameters in He to D states. For P states only 2 independent parameters have to be measured (apart from the total cross section), and these are commonly derived from the linear and circular polarisation Stokes parameters P_1 - P_3 of the decay light observed at right angles to the scattering plane and measured in coincidence with scattered electrons which have lost the energy corresponding to the excitation of the state. For D states a fourth independent coincidence measurement is required and this may be the linear polarisation Stokes parameter $P_4 = (I(0) - I(90)) / (I(0) + I(90))$ of light emitted in the scattering plane (where 0, 90 corresponds to the polariser angle with respect to the scattering plane). The Stokes parameters P_1 - P_4 may be translated into other complete parameter sets as discussed in detail in the review of Andersen et al.⁽¹⁾. The parameters commonly used for D states are the alignment angle of the charge cloud, γ , and the linear polarisation, P_2 , which are derived from P_1 and P_2 and the height of the charge cloud out of the scattering plane, φ_{00} , and the angular momentum transfer perpendicular to the scattering plane, L_1 , which require P_3 and P_4 as well.

We report measurements of P_4 for the 3^3D state of He to complete our earlier measurements of P_1 - P_3 ^(2,3) for 40 eV. The substantial depolarisation of the light as a result of fine structure coupling of the 3^3D states has been taken into account and the values of P_4 are shown in Fig.1 together with the derived parameters φ_{00} and L_1 . These measurements may be compared directly with recent results of the Belfast group^(4,5) also shown in Fig.1. The agreement of the 2 sets of data is encouraging. Calculations have been carried out for the 3^3D state by Bartschat and Madison⁽⁶⁾ and by Cartwright and Csanak⁽⁷⁾. Both calculations are restricted to P_1 - P_3 and thus do not predict out of plane effects like $\varphi_{00} \neq 0$ which are found to be substantial in the experiments.

References

1. N Andersen, J W Gallagher and I V Hertel, Phys.Rep. 165, 1-188 (1988).
2. H Kleinpoppen, H-J Beyer and M A Chaudhry in "Atomic Physics 11", Ed. S Haroche, J C Gay and G Grynberg, 1989 (Singapore: World Scientific), p650-2.
3. H-J Beyer, H A Siliu and H Kleinpoppen, XVI ICPEAC New York, 1989, Book of Abstracts, p165.
4. B P Donnelly and A Crowe, J.Phys.B 21, L697-L702 (1988).
5. B P Donnelly, D T McLaughlin and A Crowe, preprint (1990).
6. K Bartschat and D H Madison, J.Phys.B 21, 153-170 (1988) and private communication.
7. D C Cartwright and G Csanak, J.Phys.B 20, L603-L610 (1987) and private communication Oct. 1988.

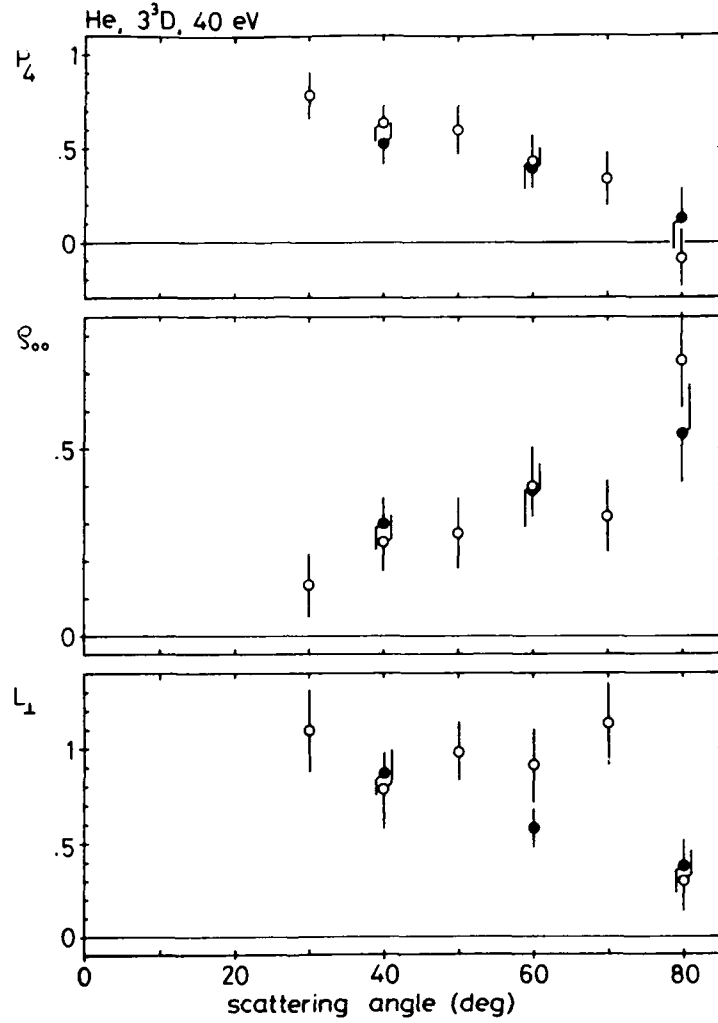


Fig.1. Top: Measured values of the Stokes parameter P_4 (corrected for fine structure depolarisation) for 3³D state excitation of He as a function of the scattering angle.

Below: Height parameter, S_{00} , of the charge cloud and angular momentum transfer, L_1 , derived from P_1-P_4 (3).
 o current results, ● Donnelly et al. (5)

PHOTON STOKES PARAMETERS OF ALKALI RESONANCE LINES IN
ELECTRON IMPACT EXCITATION OF SPIN-POLARISED ALKALI ATOMS

M A H Bukhari*, H J Beyer and H Kleinpoppen

Unit of Atomic and Molecular Physics,
University of Stirling, Stirling, Scotland, U.K.

*On leave from: Physics Dept., Umm Al-Qura University, Makkah, Saudi Arabia.

A beam of unpolarised electrons is crossed at right angles with a beam of partially polarised alkali atoms. The resonance radiation from the excited $^2P_{3/2,1/2}$ states is observed in a direction perpendicular to both beams, and the Stokes parameters P_1 , P_2 , P_3 of the emitted photons are measured.

$$P_1 = \frac{I(0) - I(90)}{I(0) + I(90)}, \quad P_2 = \frac{I(45) - I(135)}{I(45) + I(135)}, \quad P_3 = \frac{I(RHC) - I(LHC)}{I(RHC) + I(LHC)}$$

where 0, 45, 90, 135 corresponds to the polariser angle measured from the electron beam direction and RHC, LHC to right and left hand circular polarisation in the spectroscopic definition.

Because of reflection symmetries, only P_1 is expected to be non-zero for unpolarised atoms. If polarised atoms are used with their spins parallel to the direction of the observed photons, P_3 should also become non-zero (in addition to P_1), while P_2 remains zero. Such an experiment was originally proposed by Kleinpoppen¹⁾ and recently carried out for the lowest excited state of Na²⁾. We report independent data on the Na transition and new results on the KI($5^2P_{3/2,1/2} \rightarrow 4^2S_{1/2}$) transition ($\lambda = 4044, 4047 \text{ \AA}$).

The experimental set-up is similar to that of Jitschin et al.²⁾. Polarised atoms were produced by means of a hexapole spin-state selector which achieved about 21% spin polarisation for the Na and K atom beams. Small and only slowly varying magnetic guiding fields were used to maintain the spin polarisation of the atoms and to provide the orientation of the atoms in the interaction region. Reversing the magnetic field in the interaction region also reverses the spin polarisation of the ground state atoms and the handedness of the observed circular polarisation of the resonance radiation as shown in Fig.1. Using a guiding field close to the turning point into a constant spin orientation and thus a constant value of P_3 in Fig.1, P_3 was measured as a function of the electron energy as shown in Fig.2.

The complete data for Na and K will be presented and their relation to contributions from exchange and direct excitation channels will be discussed.

References

- 1) H Kleinpoppen, Phys.Rev.A 3, 2015 (1971)
- 2) W Jitschin, S Osimitsch, H Reihl, H Kleinpoppen and H O Lutz, J.Phys.B 17, 1899-1912 (1984).

XI-23

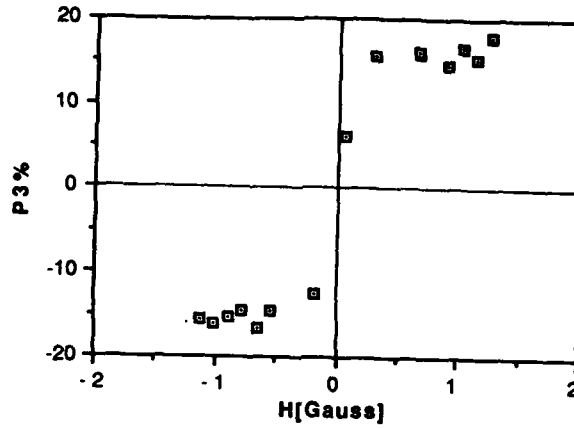


Fig.1

Circular polarisation of the KI($5^2P_{3/2,1/2} \rightarrow 4^2S_{1/2}$) resonance transition as a function of the guiding magnetic field. Electron impact energy $E_e = 25\text{eV}$.

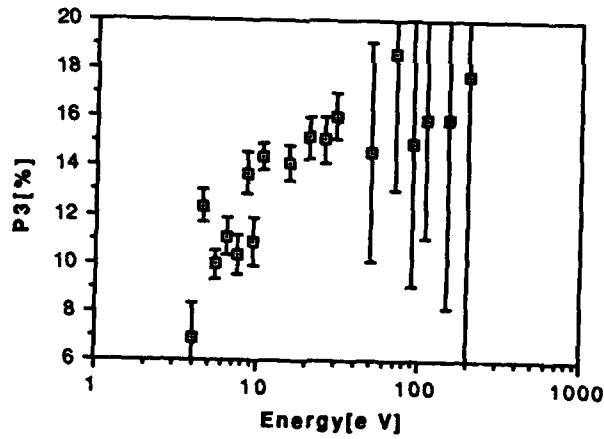


Fig.2

Circular polarisation of the KI($5^2P_{3/2,1/2} \rightarrow 4^2S_{1/2}$) resonance transition as a function of the electron impact energy.

SUPERELASTIC 3P→3S CROSS SECTIONS FOR 3 eV ELECTRONS
SCATTERED BY SODIUM*T.Y. Jiang,[†] M. Zuo,[‡] L. Vušković,[§] and B. Bederson
Physics Department, New York University, New York, NY 10003

Unpolarized 3 eV electron superelastic scattering by $3^2P_{3/2}$ sodium has been measured and absolute differential cross sections (DCS) in the range of 1° to 30° determined without normalization. The atoms are initially prepared by circularly polarized laser light which results in unequal initial excited hyperfine state populations. Accordingly detailed balancing cannot be directly invoked to compare the inverse reaction $3S \rightarrow 3P$, which normally corresponds to electron scattering with all atomic sublevels of initial and final states equally populated.

We have derived [1] exact equations that relate scattered electron and atom spatial distributions in order to take full advantage of the atom recoil technique [2] used in the present experiment, which involves observation of the scattered atom beam after being crossed-fired by an electron beam, in the presence of a mutually perpendicular laser beam tuned to the resonant $3S \rightarrow 3P$ transition. A standing wave bidirectional laser field is used, thereby minimizing the effects of photon recoil, although the atom beam spatial distribution is widened somewhat by spontaneous emission and statistical effects.

Small angle superelastic collisions are distinguished by observing the atom deflection in the detector plane caused by electron scattering, since these result in momentum transfer to the atom beam counter to the initial electron momentum. The deflection signature is unique and the analysis of experimental data [3] taking into account all relevant beam and apparatus parameters, including the atom velocity distribution, the electron energy distribution, the spatial distribution of the atom beam, and slit and detector geometries, generate the absolute DCS curve as the only unknown parameter. The recoil analyses for small angle scattering require accurate knowledge of the atom beam velocity distribution. For this purpose we employ laser-induced Doppler shifted fluorescence measurements. We determine the velocity distribution at several different points within the atom

beam cross sectional area since it is affected by the radial dependence of the velocity selection property of the atom beam focussing hexapole magnet, which is part of the experimental setup.

In the Table below are shown several examples of the present data and a recent six state close coupling calculation by Norcross and coworkers [4], performed to compare with our results, in the units $10^{-16} \text{ cm}^2\text{sr}^{-1}$.

θ°	present	Ref. 4
2	97.4	42.0
6	71.1	37.5
10	30.8	29.6
20	9.1	9.8
30	3.1	2.9

Agreement at larger angles is excellent, while discrepancies exceed experimental error at angles of 6° and less. The measured points are more forward peaked than the computed values, although the partial integral cross sections do not differ significantly.

* Research supported by U.S. National Science Foundation.

† Present address: Department of Physics, University of Rhode Island, Kingston, RI 02881-0817.

‡ Present address: Department of Chemistry, University of Chicago, Chicago, IL 60637.

§ Permanent address: Institute of Physics, P.O. Box 57, 11001 Belgrade, Yugoslavia.

1. L. Vušković, M. Zuo, G.F. Shen, B. Stumpf, and B. Bederson, Phys. Rev. A **40**, 133 (1989).

2. B. Jaduszliwer, P. Weiss, A. Tino, and B. Bederson, Phys. Rev. A **30**, 1255 (1984).

3. T.Y. Jiang, C.H. Ying, L. Vušković, and B. Bederson, submitted to Phys. Rev. A (1990).

4. H.L. Zhuo, D.W. Norcross, G. Snitchler, and A.D. Stauffer, Bulletin of the American Physical Society **35**, 1170 (1990) and private communication.

DIELECTRONIC RECOMBINATION IN HELIUM-LIKE HEAVY IONS*

R. Ali, C.P. Bhalla, C.L. Cocke, P. Richard, and M.P. Stockli
 J.R. Macdonald Laboratory, Kansas State University
 Manhattan, KS 66506-2604 USA

Helium-like ions are produced inside the KSU-CRYEBIS using an electron beam with an energy below the K-ionization threshold. The equilibrium charge state distribution between the helium-like and the lithium-like heavy ions is given by the electron beam-induced ionization rate of the lithium-like ions and the electron capture rate of the helium-like ions. If the energy of the electron beam is in resonance with a double-excited lithium-like state, the capture rate of the helium-like ions is dominated by the dielectronic recombination process. Off resonance, the electron capture is determined by the radiative recombination and by the capture of electrons from the residual gas, both of which vary slowly with the electron beam energy. Therefore, the dielectronic recombination cross section can be obtained from the ratio of the lithium-like ion yield divided by the helium-like ion yield, after subtracting the nonresonant background and multiplying the result by the electron-induced ionization cross section for the lithium-like ions. The ion yields of the different charge states are measured by extracting the ions after they reach the equilibrium distribution as a function of the electron beam energy. The results for helium-like Argon¹ shown in the figure are in excellent agreement with the theoretical calculations. Measurements on helium-like Neon are under way.

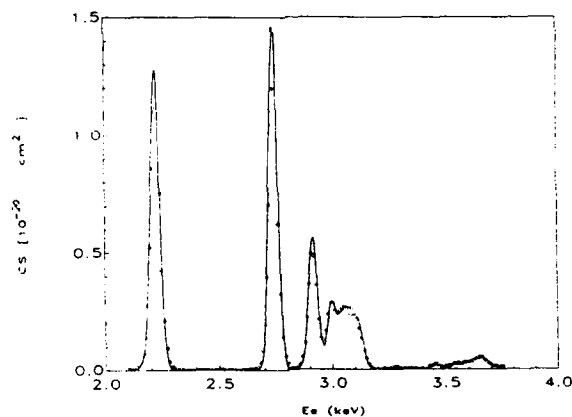


Figure: Dielectronic recombination cross section as a function of electron energy for helium-like Argon. The circles represent the measured data, whereas the curve shows the theory.

* This work supported by the Division of Chemical Sciences, Office of Basic Energy Science, Office of Energy Research, U.S. Department of Energy.

1. R. Ali, C.P. Bhalla, C.L. Cocke, and M. Stockli, Phys. Rev. Lett. **64**, 633 (1990), and to be published.

**ELASTIC SCATTERING OF POSITRONS ON MERCURY:
A NEGATIVE-ENERGY DIRAC-FOCK TREATMENT**

J. E. Sienkiewicz* and W. E. Baylis

Department of Physics, University of Windsor
Windsor, Ontario, Canada N9B 3P4

Dirac-Fock calculations have been performed on mercury plus one continuum electron of negative energy $< -m c^2$. The asymptotic form of the numerical wave function of the negative-energy electron determines the phase shifts for the elastic scattering of positrons on Hg. The self-consistent field (SCF) calculations include the usual exchange interaction between electrons. As discussed previously[1], the exchange between the bound Hg electrons and the negative-energy continuum electron represents the positron-electron annihilation/creation process. Such quantum electrodynamic (QED) effects are usually computed to some order of approximation in a perturbation expansion. We believe ours is the first SCF calculation of this QED effect.

The equivalence of the exchange and annihilation/creation diagrams can be seen by the CPT crossing method common in the relation of Möller ($e^- e^-$) to Bhabha ($e^+ e^-$) scattering. As the incident positron annihilates a bound electron, a new electron-positron pair is created. The effect is much smaller than the usual exchange between positive-energy electrons because in the CPT crossing, the roles of the "small" and "large" components of the Dirac bispinor are interchanged. As a result, the amplitude for the annihilation/creation process is down by a factor of the fine-structure constant at low incident positron energies.

To test the influence of pair annihilation/creation on positron scattering, we have chosen the heavy target atom mercury. Both differential and total cross sections for elastic scattering, as well as positron polarization parameters have been calculated. We treat the target atom as a frozen core to which correlation corrections have been added in the form of a model core-polarization potential[2]. A modified version of the Desclaux code[3,4] has been used for the computations. Analogous calculations have been successfully carried out for electron scattering on noble-gas targets.[4,5]

When the "exchange" interaction between the negative-energy continuum electron and the bound target electrons is omitted, calculated results reproduce those found by the more common procedure[6] of treating the positron as a positively charged, distinguishable particle. When "exchange" (the pair annihilation/creation process) is added, the changes are minimal. Spin polarization effects generally remain at or below the 10^{-4} level and are hence very difficult to observe experimentally. The polarization effects arise from the difference in phase shifts $\Delta\delta_l = \delta_l^+ - \delta_l^-$ for the relativistic scattering wave functions for a given orbital angular

momentum quantum number l and for $j = l \pm \frac{1}{2}$. Table 1 shows these phase-shift differences for $l = 1$ to 5 and for two energies of the incident positron. As may be seen, the differences increase with increasing incident energy. The results agree well with recent calculations of Hasenburger[7], who used a non-relativistic scattering calculation with a Dirac-Fock Hg charge density, a spin-orbit potential and a distinct polarization potential. To the accuracy shown, our results are independent of whether or not the pair annihilation/creation process is included.

Table 1. Phase shift differences $\Delta\delta_l = \delta_l^+ - \delta_l^-$ for positron scattering on mercury atoms in units of 10^{-5} rad.

l	$E = 150$ eV		$E = 800$ eV	
	(a)	(b)	(a)	(b)
1	9.99	9.92	44.20	44.23
2	10.49	10.97	55.04	52.91
3	7.86	8.97	49.89	49.88
4	5.63	6.29	38.47	42.25
5	3.86	4.10	29.31	34.05

(a) Present calculations

(b) Hasenburger [7]

This work has been supported by the Natural Science and Engineering Research Council of Canada and the Polish Ministry of National Education.

* Permanent address: Institute of Theoretical Physics and Astrophysics, University of Gdansk, 80-952 Gdansk, Poland

1. W. E. Baylis and J. E. Sienkiewicz, *Eleventh International Conference on Atomic Physics, Abstracts of Contributed Posters, XI-17 (Paris, 1988)*.
2. L. T. Sin Fai Lam, *J. Phys. B: At. Mol. Phys.* **13**, L427 (1980).
3. J. P. Desclaux, *Comput. Phys. Commun.* **9**, 31 (1975).
4. J. E. Sienkiewicz and W. E. Baylis, *J. Phys. B: At. Mol.* **20**, 5145 (1987).
5. J. E. Sienkiewicz and W. E. Baylis, *J. Phys. B: At. Mol. Opt. Phys.* **22**, 3733 (1989) and references therein.
6. J. E. Sienkiewicz and W. E. Baylis, *Phys. Rev.* **A40**, 3662 (1989).
7. K. Hasenburger, *J. Phys. B: At. Mol. Phys.* **19**, L499 (1986).

XII. EXOTIC ATOMS AND SPECIAL TOPICS

RADIATION OF ATOMIC ELECTRONS IN THE PROCESSES
OF NUCLEAR TRANSFORMATIONS

A.V. Solov'yov

A.F. Ioffe Physical-Technical Institute of the USSR
Academy of Sciences, Leningrad, 194021, USSR

It is shown that the atomic electron shell strongly influences the radiation spectra arising due to various transformations of the nucleus. The following processes have been considered as examples of nuclear transformation: nuclear decays (α -, β -, δ -decays and others), spontaneous fission, nuclear reaction with two or more particles in the final state, scattering of neutral particles (neutron, neutrino) on a nucleus.

All these processes proceed at the distances small as compared with the atomic extent. The characteristic time of the processes is considerably less than the periods of electron motion around the nucleus. It permits to treat a nuclear transformation as a rapid perturbation acting on the atomic electrons. This perturbation generates the atomic electron radiation (AER). Of course, this radiation appears together with that of escaping nuclear particles themselves. However, in many occurrences the AER dominates or gives a large contribution to the total radiation spectrum in the region of characteristic atomic frequencies.

The processes suggested can be simply explained qualitatively. During the nuclear reaction or decay an alternating dipole moment of nuclear particle system is created. This dipole moment interacts with the atomic shells, polarizing them. The alteration of the induced dipole moment of the atom is a source of AER. That is a basic physical idea of all processes proposed in this work, but in any particular case there are some peculiarities in the radiation spectrum. Note that analogous effects were investigated in the process of scattering various particles on the atoms (see review [1]).

For example, during α -decay of the nucleus the emitted AER is due to polarizing the atomic shells by escaping slow particles, that is α -particle and a nucleus remainder. This process gives continuous spectrum radiation into a broad range of atomic frequencies. Its intensity is comparable with the radiation intensity of nuclear

particles themselves during the α -decay.

The AER dominates substantially in the total radiation spectrum near the resonance frequencies which correspond to the transitions between two discrete atomic levels.

The AER forms in the nuclear β -decay process in another manner because of a large velocity of β -electron. Firstly, AER arises as a consequence of rapid alteration of the nucleus charge in the β -decay process. Due to a monopole character of such perturbation a dipole photon is possible to emit in this process if the angular momentum of the atomic state is changed by unity. Secondly, the atomic polarization is induced by the β -electron moving through the atom. It is to be noted that for a fast electron, this effect is not strong. But it is shown that an account for AER is very important near the resonance atomic frequencies and also in the tip region.

In the present work the frequency dependence of photon radiation probability was investigated for all cases mentioned above. The AER effects were taken into account.

1. M.Ya. Amusia, Phys. Rev., v. 162, 248-335 (1988).

EVIDENCE OF FAST EXCITED POSITRONIUM FORMATION FROM
N=2 FINESTRUCTURE TRANSITION

R. Ley, K.D. Niebling and G. Werth
Institut für Physik, Universität Mainz
D-6500 Mainz, Fed.Rep.Germany

Finestructure transitions in the first excited state of Positronium have been measured using "backscatter-Ps" production on a Mo-surface. A beam of about 10^8 slow e^+ /s produced from the bremsstrahlung of a 180 MeV pulsed electron accelerator was guided into a waveguide and the L_{α} -radiation from decaying $n=2$ Ps was observed (Fig. 1). The e^+ kinetic energy was 60 eV where the maximum yield of $n=2$ Ps has been measured (Fig. 2). We observed a change in the L_{α} intensity when the Ps-atoms were irradiated with microwaves at the $2^3S_1-2^3P_{1,2}$ transitions at 8.6 and 13.0 GHz, respectively (Fig. 3). Due to the presence of the magnetic guiding field at the transition region the resonances are shifted from the calculated [1] and previously measured [2] values by a motional Stark shift. Using the calculation of Lewis and Hughes [3] the shift can be attributed to a mean transverse kinetic energy of $n=2$ Ps of several eV.

The work is supported by the Deutsche Forschungsgemeinschaft.

References

- [1] T. Fulton and P.C. Martin, Phys.Rev. 95, 811 (1954)
- [2] S. Hatamian, R.C. Conti, and A. Rich, Phys.Rev.Lett. 58, 1833 (1987)
- [3] M.L. Lewis and V.W. Hughes, Phys.Rev. A8, 625 (1973)

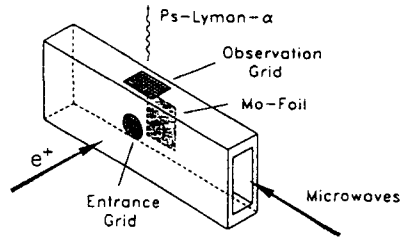


Fig. 1 Production of $n=2$ positronium on a Mo-surface inside a waveguide. A magnetic field ($B=100$ G) is superimposed in the e^+ -beam direction.

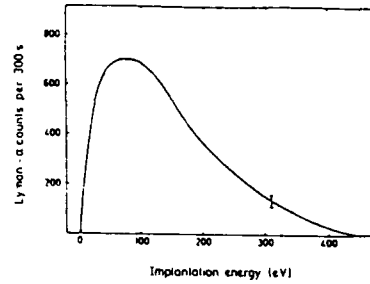


Fig. 2 Observed energy dependence of excited positronium production.

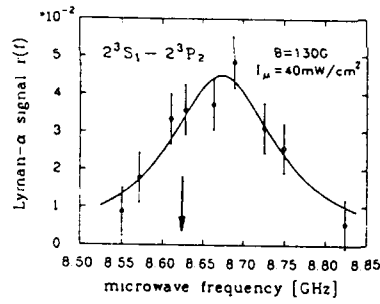
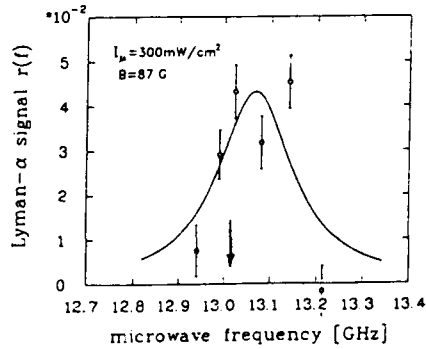
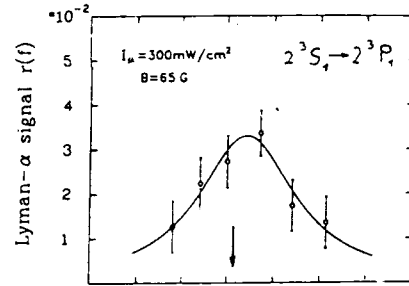


Fig. 3 Observed finestructure transitions in different magnetic fields. The arrows indicate the line position in zero field.



FREE MUONIUM FROM SILICA AEROGELS

V. Ebert, K. Jungmann, V.W. Hughes, S. Kirches, S. Koppe, F. Maas, H.-J. Munding, G. zu Putlitz, J. Rosenkranz, W. Schäfer, W. Schwarz, Z. Zhang
 Physikalisches Institut, Universität Heidelberg, Philosophenweg 12, D-6900 Heidelberg
 Yale University, New Haven, Ct 06520, USA

Muonium is a bound state of a muon (μ^+) and an electron (e^-). The atom is a purely leptonic hydrogenlike system. It is an ideal object for investigating bound state Quantum Electrodynamics (QED) and fundamental properties of the muon and the muon-electron interaction.

The observation of muonium atoms emerging into vacuum with thermal velocities from targets of SiO_2 powders after stopping positive muons (μ^+) from a subsurface beam has launched a number of interesting experiments. Searches for a spontaneous conversion of muonium into antimuonium have reached a sensitivity of below $5 \cdot 10^{-7}$ for the conversion probability [2] and significant improvements of this limit are possible [3]. The optical excitation of the 1S-2S transition by two photon laser spectroscopy allows a precise determination of the 1S Lambshift [4]. Alternatively the experiment may be interpreted as a measurement of mass of the positive muon. With the observation of polarized thermal muonium in vacuum measurements of the muonium ground state hyperfine structure splitting became possible in vacuum [5] and have yielded $\Delta\nu_{\text{HFS}} = 4463.29(3)$ MHz with 16(2) % signal height. Ultimately we expect higher precision from experiments using free muonium than from measurements in gas atmospheres.

Despite the success of the experiments using thermal muonium in vacuum, the details of the formation process in the powder are not very well known yet. In the course of a series of measurements addressing this problem, silica aerogels have been found to release muonium atoms into vacuum.

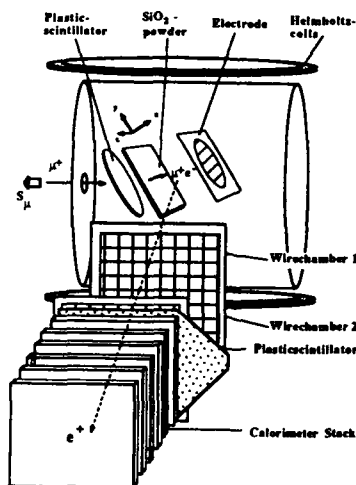


Figure 1: Schematic view of the apparatus used in the measurements.

Muonium is formed inside of SiO_2 aerogel samples of 170 mg/cm^3 density with 60 (8) % efficiency. This fraction is the same as for SiO_2 powders. A fraction of 1.0 (3) % of the atoms leaves the solid material through a flat untreated surface with thermal velocities into the vacuum. Similar results had been obtained for SiO_2 powders which were slightly compressed under a pressure of about 0.1 N/cm^2 .

The aerogel material consists of large highly branched chains of spheroidal SiO_2 particles which have diameters of approximately 8 nm [6]. The material has a specific surface area of $800 \text{ m}^2/\text{g}$. The structure leaves large open cells of typically 15 nm in size, which allow the muonium atoms to escape into vacuum. By shaping the aerogel surface in form of adjacent

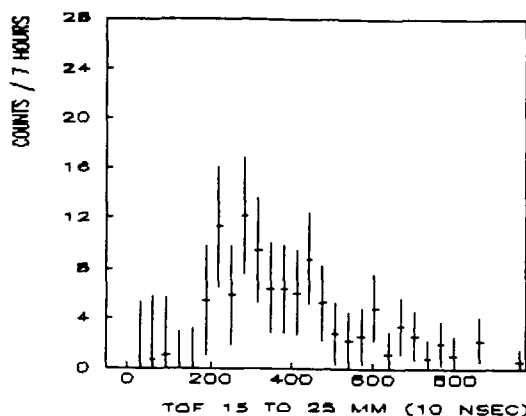


Figure 2. Time of flight spectrum taken at 20 mm distance from the aerogel surface. The distribution is not affected by applied external electric fields and corresponds to a Maxwellian distribution of velocities for muonium at a temperature of 295 K.

pyramids of 1.5 mm high and 2 mm base width the effective outer aerogel surface can be increased. Any clogging of the surface cells can be removed carefully by mechanical or chemical treatment. With such surfaces on 160 mg/cm^3 density aerogels we obtain 2.5 (3) % thermal muonium yield for incoming μ^+ beams of 26.7 MeV/c momentum and 10 % momentum bite.

We expect a much higher muonium yield from aerogels of 30 mg/cm^3 or even lower density and with a specific surface area of $1600 \text{ m}^2/\text{g}$ which are available now. The solid silica aerogel for muonium production are considered an alternative to the fragile SiO_2 powder targets in future precision experiments.

The experiments have been performed at the Paul Scherrer Institute (Villigen, CH) and the Rutherford Appleton Laboratory (Chilton, UK). The aerogel

samples tested have been provided by M. Bourdinaud (Saclay), J. Fricke (Würzburg) and J. van Lierop (Eindhoven). This work has been supported by the Bundesministerium für Forschung und Technologie of the Federal Republic of Germany.

- [1] G.A. Beer et al., Phys. Rev. Lett. **57**, 671 (1986) and K.A. Woodle et al., Z. Phys. D9, **59** (1988)
- [2] H.J. Munding et al., in "Proceedings of the Rare Decay Symposium 1988 in Vancouver", eds. D. Bryman, S. Ny, T. Numao, J.-M. Poutisson, World Scientific Singapore, p. 434 (1989) and T.M. Huber, *ibid.*, p. 439 (1989)
- [3] K. Jungmann, W. Bertl et al., PSI Proposal R 89-06.1 (1990)
- [4] S. Chu et al., Phys. Rev. Lett. **60**, 101 (1988) and K. Jungmann et al., RAL proposal 709 (1987)
- [5] F. Maas et al. "Muonium Hyperfine Structure Transitions in Vacuum", Verhandl. DPG (VI) **25**, A28.2 (1990)
- [6] C.A.M. Mulder and S.G. van Lierop, in "Aerogels", Proceedings of the First Int. Symp. Würzburg, ed. J. Fricke, p. 68 (1985)

ANGULAR DISTRIBUTION MEASUREMENT OF BEAM-FOIL MUONIUM

H.E. Ahn¹, F. Chmely¹, V.W. Hughes¹, S.H. Kettell¹, Y. Kuang¹,
 B.E. Matthias¹, H.-J. Mundinger², B. Nil¹, G. zu Putlitz², H.R. Schaefer¹,
 K.A. Woodle¹

Yale University¹, Universitat Heidelberg²

The angular distributions of low momentum muons (μ^+) and muonium ($M \equiv \mu^+e^-$) produced by the beam-foil method [1] have been measured. A 7.5 MeV/c subsurface μ^+ beam [2] was delivered to our apparatus (Fig. 1) from the stopped muon channel [3] at the Los Alamos Meson Physics Facility (LAMPF). The μ^+ formed M by electron capture in the thin Al target foil (0.21 mg/cm²). A low pressure multiwire proportional chamber [4] (MWPC) upstream of the target foil was used both as a moderator and as a muon counter. To observe muonium in its ground $n=1$ state, muons were swept away by a bending magnet which was placed downstream of the target foil. This magnet was turned off while measuring the μ^+ distribution. Beyond the magnetic field particles were collimated and then stopped by a microchannel plate detector (MCP) located at various angles (0°, 10°, 20°, 30°, and 45°) to the incident muon beam axis. Two pairs of scintillators mounted above (S_c) and below (S_b) the MCP were used to detect the decay positrons to verify from the lifetime spectrum that the particles detected by the MCP are muons.

The intensities of μ^+ and M emerging from the Al foil at different angles were obtained from both a time-of-flight spectrum (between MWPC and MPC) and a lifetime spectrum (between MPC and S_c or S_b). An initial analysis (Fig. 2) shows that the angular distribution of M(1S) is considerably wider than that of positive muons as expected from Monte Carlo simulations [5]. This observation may be quite important for a possible future measurement of the Lamb shift. We expect that the angular distribution of the M(2S) atoms [6] will be similar to that observed for M(1S) and hence broader than that of the μ^+ . Hence for a muonium Lamb shift measurement, it may be preferable from the viewpoint of signal to noise to utilize the M(2S) beam formed at 30° to the incident μ^+ rather than that at 0° as has been done thus far [7] despite the loss of intensity of the M(2S) beam.

This work was supported by DOE, NSF, and BMFT.

REFERENCES

- [1] P.R. Bolton et al., Phys. Rev. Lett. 47, 1441 (1981).
- [2] A. Badertscher, et al., Nucl. Instr. and Meth. A238, 200 (1985).
- [3] P.A. Thompson et al., Nucl. Instr. and Meth. 161, 391 (1979).
- [4] S.H. Kettell, Measurement of the $2^2S_{1/2}-2^2P_{3/2}$ Fine Structure Interval in Muonium. Ph.D. thesis, Yale University, 1990. (Unpublished)
- [5] Y. Kuang, et al., Phys. Rev. A35, 3172 (1987).
- [6] G. Gabrielse, Phys. Rev. A23, 775 (1981).
- [7] K.A. Woodle, et al., Phys. Rev. A41, 93 (1990).

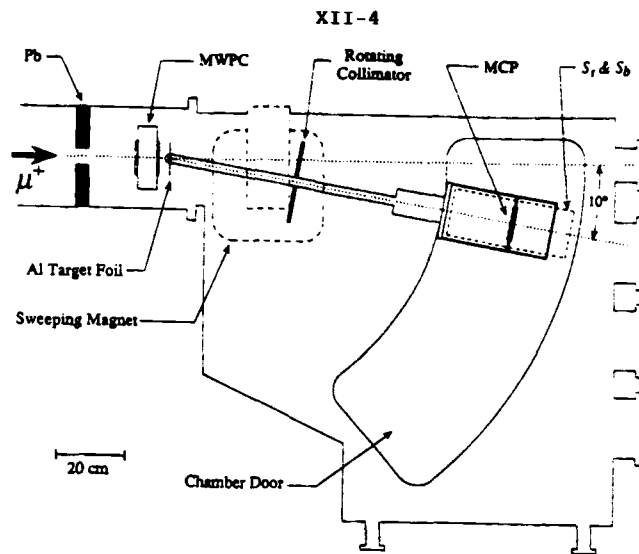


Fig. 1. Schematic diagram of the experimental apparatus. The setup is shown for the case of the angular distribution measurement at 10° from the beam axis.

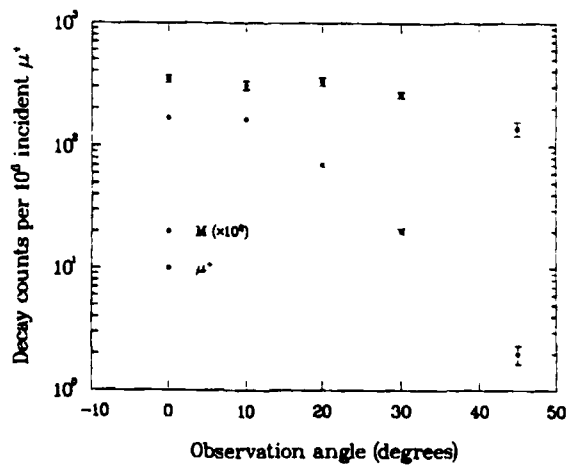


Fig. 2. Total counts of decay positrons per incident μ^+ for different angles.

ATOMIC PHYSICS SEARCHES FOR BOUND STATE BETA DECAY

D. E. Murnick and Namic Kwon
Department of Physics, Rutgers University
Newark, New Jersey 07102

In addition to the well-known mode of β -decay in which the electron is emitted into the continuum, it is, in principle, possible for the decay electron to be created in a bound state of the daughter atom. This mode is normally very improbable since the most favorable final states, the innermost electron states, are usually already filled. The bound state beta decay (BSBD) process has a considerable effect, however, in astrophysics since it becomes a favored decay channel for certain ionized species which exist in stellar plasmas at temperatures between a few keV and several hundred keV.

Despite its importance, this fundamental radioactive decay mode has never been observed in the laboratory. Advances in atomic physics which now allow laser spectroscopy of extremely dilute species and/or long trapping times for selected ions may allow laboratory studies of this process.

The case of tritium is particularly favorable for BSBD to occur in normal matter since the electron can be created in the K-shell or the 1s state of the daughter ^3He atom. The energetics of the process is simple. Starting with a neutral atom of ^3H , a 1s bound-state β -decay results in a neutral atom of ^3He and thus only a monoenergetic neutrino with energy $E_\nu = Q$, the $^3\text{H} - ^3\text{He}$ mass difference, is emitted. Calculations¹ indicate a branching ratio of 0.69% for the process, approximately 80% of which goes into electron creation in the $1\ ^1\text{S}_0$ ground state of the daughter ^3He . The largest source of background in observing bound state β -decay and a major reason that it has not yet been observed is that the usual β -decay which results in $^3\text{He}^+$ is so much more intense.

In an atomic resonance fluorescence experiment, however, the ions themselves offer no interference because they are non resonant. An experiment, recently begun at Rutgers aims to detect the presence of ^3He neutral atoms from the bound state beta decay of tritium by resonance fluorescence at 1.08μ , the $n=2\ ^3\text{S}_1 - ^3\text{P}_1$ resonance transition using a stabilized solid state LNA laser.² A diode pumped laser tunable around 1.08μ has been built and used to pump ^3He metastables in a weak rf discharge. The photogalvanic effect is used for detection, and will allow locking to a particular resonance in the hyperfine structure if required.

A modest 1mC tritium source should yield several thousand decays per second to the 3S_1 , 3He level, assuming that only 1/10 of the BSBD decays are through this level. A carefully designed resonance fluorescence cell using signal enhancement techniques will be used to detect these atoms establishing the existence of BSBD. Subsequent laser scanning with the LNA laser will establish the recoil atom velocity distribution.

Besides its interest as a new fundamental physical phenomenon, BSBD also has intrinsic measurement science significance as it involves a two body final state weak interaction- an antineutrino plus a neutral atom. This opens the possibility for enhanced precision Q value measurements and ultimately a measurement of neutrino mass.³ High resolution measurement (\approx MHz) of line width will provide an independent direct measurement of Q and very high resolution (\approx kHz) may provide information on the neutrino mass.

Another experiment to search for BSBD is planned at the new accelerator SIS-ESR under construction at GSI Darmstadt West Germany.⁴ ^{163}Dy is , as a neutral atom, a stable isotope with a natural abundance of 25%. Highly ionized, however, ^{163}Dy can decay by BSBD to ^{163}Ho . Fully ionized (66+) or hydrogen like (65+) Dysprosium can be stored in the ESR storage ring and the number of Ho atoms produced after BSBD detected. The calculated BSBD lifetime of .16 years should yield detectable signals after a storage time of order 1000 sec.

1. J.N. Bahcall, *Phys. Rev.* **124** (1961) 495
2. L.D. Scheerer, M. Leduc, D. Viven, A. M. Lejus and J. They, *IEEE J. of Quantum Electronics* **22**(1986)713
3. S.G.Cohen, D.E.Murnick, and R.S.Raghavan, *Hyperfine interactions* **33** (1987)1
- 4 . F. Bosch, B. Franzke, W. Henning, P. Kienle, O. Klepper, W. Koenig, R. Mahn, E. Roeckl and K. Summerer, GSI report 87-7 (1987)

Work supported by the National Science Foundation under Grant No. PHY 90-10982

PHYSICS WITH LASER POLARIZED NUCLEI*

T.E. Chupp
Lyman Laboratory of Physics, Harvard University
Cambridge, MA 02138

Polarized nuclei provide a unique tool for several types of nuclear physics investigation including the measurement of nuclear moments, study of weak interaction effects and the spin dependent structure of nuclei and nucleons. Recent advances of optical pumping techniques, driven in part by new laser technologies, have made possible the polarization of large quantities of ^3He and other noble gas nuclei by way of spin exchange with laser optically pumped Rb vapor. Polarized ^3He has been applied in two unique ways for the polarization of neutrons over a broad range of energies and for studies of the structure of the neutron which dominates the spin dependence in electron scattering experiments. Polarized neutrons are used in studies of the structure of the weak interaction involving the strongly interacting nucleons.

Experimental study of Parity Violation in resonance absorption of polarized neutrons has been pursued at the pulsed neutron source at LAMPF. The weak interaction as well as time reversal violation are under study in a series of polarized neutron β -decay experiments at NIST and Grenoble.

The fact that the proton spins are almost completely paired leaves the unpaired neutron highly polarized in a polarized ^3He nucleus. Thus electron scattering from polarized ^3He with quasi-elastic kinematics, where most of the momentum transfer is to the individual nucleons, probes the electric charge distribution of the neutron (the electric form factor). Experiments at the 900 MeV MIT-Bates LINAC are

underway and the results of a first run are being analyzed. In deep inelastic scattering, the distribution of spin among the partons (quarks) in the neutron can be measured. This topic has experienced renewed interest with the results of a recent experiment at CERN that suggests that the valence partons carry very little of the proton's spin. An experiment at SLAC with 23 GeV electrons and a polarized ^3He target has been approved and should run in 1992.

In these experiments, the mixture of atomic and laser physics with accelerator physics is essential to probe new features of sub-atomic physics.

*Supported by the National Science Foundation

¹ Phys. Rev. 115, 850 (1959)

AUTHOR INDEX

Authors	Poster(s)	Authors	Poster(s)
Aashamar, K.	VII-16,39	Becker, T.	VIII-1
Abdel-Raouf, M.A.	IX-2; XI-2	Becker, U.	V-12
Abdullah, K.	I-11	Bederson, B.	XI-24
Ablyazov, A.F.	VII-47	Beigman, I.L.	VII-5
Abshagen, M.	IX-4	Beijerinck, H.C.W.	IV-6; X-1
Abu-Jafar, M.	VII-41	Belkacem, A.	VIII-23
Abutaleb, M.	VIII-19	Bell, A.S.	IV-13
Adachi, H.	IX-1	Bengtsson, J.	VIII-12
Aggarwal, K.M.	XI-14,15	Bennett, C.L.	I-19
Ahn, H.E.	I-9; XII-4	Bergeman, T.	IV-7,8; VIII-25
Ali, R.	XI-25	Berger, J.	V-14
Allegrini, M.	V-22	Bergquist, J.C.	IV-14
Amusia, M. Ya.	V-5; VII-29,34	Bergstrom, P.M.	V-17,19
Andreev, V.A.	I-20	Berrington, K.A.	XI-14,15
Ansbacher, W.	VIII-11	Berry, H.G.	VIII-8,26; X-7
Arimondo, E.	IV-21; V-22	Beyer, H.J.	XI-22,23
Armstrong, P.S.	V-15	Bezuglov, N.N.	V-2
Avdonina, N. B.	V-5	Bhalla, C.P.	XI-25
Azuma, Y.	X-7	Biagini, M.	X-13
Baba, D.T.	VII-48	Biémont, E.	VII-19,20
Badertscher, A.	I-9	Bigelow, N.P.	IV-18,19
Bagnato, V.S.	II-2	Björk, G.	IV-2
Baird, P.E.G.	VIII-13	Bloomfield, L.A.	IV-12
Balazs, N.D.	IV-8	Blumenfeld, L.	VIII-23
Balykin, V.	II-13,16	Blundell, S.A.	I-30
Baruch, M.C.	V-15	Bobashev, S.V.	X-17
Barwood, G.P.	IV-13	Bock, M.	II-13; V-14
Bauer, H.	IX-3	Börner, H.	I-15
Baylis, W. E.	I-4; IX-7; XI-26	Bogdanova, I.P.	IX-6; XI-10
Beau, M.	IX-3	Bollinger, J.J.	IV-16
Bechler, A.	V-10	Bolzinger, T.	VIII-14
Beck, D.R.	VII-32	Boom, W.	X-1
Becker, K.	VI-2	Boos, N.	II-16

Authors	Poster(s)	Authors	Poster(s)
Borisov, E.N.	V-2	Chmely, F.C.	I-9; XII-4
Boshier, M.G.	I-26	Cho, D.	I-25
Bradley, C.C.	II-17	Chung, K.T.	VII-21,22
Brieger, M.	VIII-4	Chupp, T.E.	I-16,17; IV-17; XII-6
Brown, R.E.	I-2	Church, D.A.	X-7
Budker, D.	I-10,12	Chutjian, A.	XI-18
Bukhari, M.A.H.	XI-23	Clark, M.W.	II-1; X-15
Bureyeva, L.	VII-7	Claytor, N.	VIII-23
Burgess, A.	XI-12	Clementi, E.	VII-26
Burke, P.G.	XI-14	Cocke, C.L.	II-1; XI-25
Burnett, K.	II-6	Commins, E.D.	I-10,11,12
Buurman, E.P.	VIII-5	Conti, R.S.	I-22
Cai, Z.	VII-32	Corr, J.J.	XI-11
Cameron, R.	I-32	Costescu, A.	V-19
Camp, J.	I-2	Couty, M.	IX-7
Camparo, J.C.	III-3,5	Cowan, T.E.	I-19
Cantatore, G.	I-32	Dai, C.J.	V-20
Carlberg, C.	I-11	Darling, T.	I-2
Carlsson, J.	VIII-12	Davidson, M.	VIII-5
Carpenter, K.	VII-48	de Graaff, R.J.	VIII-19
Chambaud, G.	IX-7	Dehmelt, H.G.	II-8,11
Chan, F.T.	I-28	Deilamian, K.	I-14
Chang, E.S.	VII-13,14	Dembczynski, J.	VIII-16
Chen, Ce	III-2; V-3,4	Demidov, V.I.	VI-1
Chen, C.-T.	VII-18	DeMille, D.	I-10,12
Chen, J.	II-17	de Oliveira, P.C.	IV-1
Chen, L.	VIII-14	Deslattes, R.D.	I-15
Chen, M.H.	I-19; XI-17	Dewey, M.S.	I-15
Chen, X.	VII-45	DeWitt, D.	II-1
Chen, Z.	VII-36	Dietrich, D.D.	I-19
Cheng, K.-T.	I-19	di Lorenzo-Filho, O.	IV-1
Cheret, M.	VIII-14	Ding, D.	VII-8; VIII-6
Chidichimo, M.C.	XI-12	Dinneen, T.P.	VIII-26

Authors	Poster(s)	Authors	Poster(s)
Aashamar, K.	VII-16,39	Becker, T.	VIII-1
Abdel-Raouf, M.A.	IX-2; XI-2	Becker, U.	V-12
Abdullah, K.	I-11	Bederson, B.	XI-24
Ablyazov, A.F.	VII-47	Beigman, I.L.	VII-5
Abshagen, M.	IX-4	Beijerinck, H.C.W.	IV-6; X-1
Abu-Jafar, M.	VII-41	Belkacem, A.	VIII-23
Abutaleb, M.	VIII-19	Bell, A.S.	IV-13
Adachi, H.	IX-1	Bengtsson, J.	VIII-12
Aggarwal, K.M.	XI-14,15	Bennett, C.L.	I-19
Ahn, H.E.	I-9; XII-4	Bergeman, T.	IV-7,8; VIII-25
Ali, R.	XI-25	Berger, J.	V-14
Allegrini, M.	V-22	Bergquist, J.C.	IV-14
Amusia, M. Ya.	V-5; VII-29,34	Bergstrom, P.M.	V-17,19
Andreev, V.A.	I-20	Berrington, K.A.	XI-14,15
Ansbacher, W.	VIII-11	Berry, H.G.	VIII-8,26; X-7
Arimondo, E.	IV-21; V-22	Beyer, H.J.	XI-22,23
Armstrong, P.S.	V-15	Bezuglov, N.N.	V-2
Avdonina, N. B.	V-5	Bhalla, C.P.	XI-25
Azuma, Y.	X-7	Biagini, M.	X-13
Baba, D.T.	VII-48	Biémont, E.	VII-19,20
Badertscher, A.	I-9	Bigelow, N.P.	IV-18,19
Bagnato, V.S.	II-2	Björk, G.	IV-2
Baird, P.E.G.	VIII-13	Bloomfield, L.A.	IV-12
Balazs, N.D.	IV-8	Blumenfeld, L.	VIII-23
Balykin, V.	II-13,16	Blundell, S.A.	I-30
Baruch, M.C.	V-15	Bobashev, S.V.	X-17
Barwood, G.P.	IV-13	Bock, M.	II-13; V-14
Bauer, H.	IX-3	Börner, H.	I-15
Baylis, W. E.	I-4; IX-7; XI-26	Bogdanova, I.P.	IX-6; XI-10
Beau, M.	IX-3	Bollinger, J.J.	IV-16
Bechler, A.	V-10	Bolzinger, T.	VIII-14
Beck, D.R.	VII-32	Boom, W.	X-1
Becker, K.	VI-2	Boos, N.	II-16

Authors	Poster(s)	Authors	Poster(s)
Dönszelmann, A.	VIII-5	Fuhr, J.R.	VII-2
Drake, G.W.F.	I-31,33	Fuso, F.	V-22
Drukarev, E.G.	XI-1	Gabbanini, C.	II-9,X-13
Dunford, R.W.	VIII-8; X-7	Gallagher, T.F.	III-4; V-20,21; X-18
Dyer, P.	I-2	Galvan, D.H.	VII-41
Dygdala, R.	V-22	Galvez, E.J.	VIII-18
Dzuba, V.A.	VII-25	Gao, Feng	V-18
Ebert, V.	XII-3	Gengsun, Yu	VII-3
Eckhause, M.	I-9	Gerz, Ch.	II-4
Eichler, J.	X-5	Ghaffari, B.	I-22
Eissner, W.B.	XI-15	Giammanco, F.	V-22
Ellert, C.	II-13,16	Gibson, N.D.	V-15
Elliott, D.S.	III-2; V-3,4	Gidley, D.	II-15
Erickson, G.	VII-33	Gien, T.T.	XI-8,9
Ertmer, W.	IV-9,10; VIII-16	Gill, P.	IV-13
Evans, R.M.	VIII-4	Gillaspy, J.D.	I-14
Eyler, E.E.	V-16; VIII-25	Goldberg, I.B.	V-11
Fabrikant, I.I.	V-8	Goldman, S.P.	VII-35,36
Falecki, W.	IV-3,4	Goldman, T.	I-2
Farnham, D.L.	II-7	Gould, H.	I-11; VIII-23
Feinberg, B.	VIII-23	Gozzini, S.	II-9,X-13
Ferguson, S.M.	X-15	Grant, I.P.	VII-37,38; XI-19,20
Fink, M.	IX-5	Gray, L.G.	X-12
Fischer, C.F.	VII-1	Greene, G.L.	I-15
Fischer, J.	IX-3	Gribakin, G.F.	V-7; VII-25; XI-13
Flambaum, V.V.	VII-25	Grieser, M.	II-13
Foot, C.J.	VIII-13	Grieser, R.	II-13,16
Forest, J.L.	X-15	Gross, M.	VIII-14
Fortner, R.	II-1	Gul'tsev, B. V.	V-7; XI-13
Fortson, E.N.	I-34	Guss, P.	I-9
Frueholz, R.P.	III-5	Habs, D.	II-13,16; V-14
Fry, E.S.	V-18	Hagena, D.	II-4
Fu, Panming	V-21	Halama, H.	I-32

Authors	Poster(s)	Authors	Poster(s)
Han, G.	VII-10	Inaba, T.	XI-5
Hannaford, P.	X-4; VIII-13	Indelicato, P.	I-23
Hansen, J.E.	V-13; VII-31	Ishihara, T.	X-10
Hansen, S.B.	X-12	Itano, W.M.	IV-14,16
Hare, J.	VIII-14	Ivanov, V.K.	V-7; XI-13
Hartley, A.C.	I-5,21	Jäger, H.	VIII-17
Hartmann, W.	IV-3,4	Jaeschke, E.	II-13
Havey, M.	X-6	Jarmie, N.	I-2
Heckel, B.R.	I-34	Jensen, R.V.	III-1
Heckmann, P.H.	VIII-7,11	Jiang, T.Y.	XI-24
Heinzen, D.J.	IV-16	Jin, M.	VII-8; VIII-6
Hemmers, O.	V-12	Jönsson, P.	VIII-12
Hennig, G.	IV-9	Johnson, W.R.	I-30
Hettema, J.M.	V-21	Jungmann, K.	XII-3
Hinds, E.A.	I-25,26,27	Kachru, R.	X-18
Hoare, R.J.	I-16,17	Kagawa, T.	VII-40
Hochadel, B.	V-14	Kane, J.R.	I-9
Hogervorst, W.	VIII-19	Kano, S.S.	XI-5
Holt, R.A.	VIII-20	Karashima, S.	X-3
Holtkamp, D.B.	I-2	Kazantsev, S.A.	X-2
Holzscheiter, M.H.	I-2	Kelleher, D.E.	I-14
Hoog, I.	II-16	Kelly, H.P.	VII-17,46
Hoogerland, M.D.	IV-6	Kenefick, R.A.	I-2
Hose, G.	X-16	Kessler, E.G.	I-15
Hou, Q.	XI-16	Kettell, S.H.	I-9; XII-4
Houssin, M.	IV-20	Kharchenko, V.A.	X-17
Huang, G.	II-10	Kheifets, A.S.	VII-29
Huang, K.-N.	VII-18	Kilgus, G.	V-14
Huber, G.	II-13,16	Kim, Y.-K.	I-24
Hubrich, M.	II-3	Kim, Y.S.	V-11
Hughes, R.J.	I-2,8	King, N.S.P.	I-2
Hughes, V.W.	I-9; XII-3,4	Kingston, A.E.	XI-14
Hulet, R.G.	II-17	Kirches, S.	XII-3

Authors	Poster(s)	Authors	Poster(s)
Kiyokawa, S.	VII-40	Lee, Hai-Woong	I-1
Klein, H.A.	IV-13	Lerner, P.B.	I-20; IV-22
Klein, R.	II-13,16	Levick, A.P.	IV-13
Kleinpoppen, H.	XI-22,23	Levine, M.	II-1
Klemz, G.	VII-9	Levy, L.	VIII-23
Klimeck, G.	III-2	Ley, R.	XII-2
Knab, H.	II-3	Li, G.P.	XI-5
Knapp, D.A.	I-19	Li, J.M.	XI-16
Knize, R.J.	II-5	Li, S.	VII-10
Knöll, K.H.	II-3	Li, ShiFang	V-18
Koppe, S.	XII-3	Li, XingFu	V-18
Kostroun, V.E.	VIII-23	Li, Y.F.	VIII-4
Kowalski, J.	IX-4	Lichten, W.	VIII-24
Koyama, N.	X-10	Lieber, M.	I-28
Kronfeldt, H.-D.	VII-9	Lifrieri, K.	X-15
Kuang, Y.	I-9; XII-4	Lin, Fucheng	VIII-2
Kuchiev, M. Yu.	I-3; V-1,7; VII-47; XI-13	Lindgren, I.	VII-43,44
Kühl, T.	II-13,16	Lindroth, E.	I-5; VII-43
Kutzner, M.	VII-46	Liu, C.J.	VIII-8; X-7
Kwela, J.	I-33	Liu, Hang	VII-8; VIII-6
Kwon, N.	XII-5	Liu, J.W.	VII-27
Lambropoulos, L.C.	III-3	Liu, Xuewen	VII-3,4
Lamoreaux, S.K.	I-34	Liu, Z.W.	VII-17
Landtman, M.	VII-31	Livingston, A.E.	VIII-18
Langer, B.	V-12	Lowe, R.M.	X-4
Lapidus, L.	II-15	Lozano, J.A.	X-14
Larson, D.J.	V-15	Lu, K.T.	IV-24; VII-48
Larsson, J.	VIII-12	Lucchesini, A.	X-13
Lawall, J.R.	VIII-15	Luke, T.M.	VII-28,39
Lazarus, D.	I-32	Lupton, J.H.	I-18
Lee, C.Y.	V-21	Lutrus, C.K.	X-11
Lee, D.H.	X-9	Maas, F.	XII-3
		MacAdam, K.B.	X-12

Authors	Poster(s)	Authors	Poster(s)
Machida, S.	IV-2	Möller, G.	VIII-7,11
Macpherson, M.J.D.	I-6	Mohanty, A. K.	VII-26
Madej, A.A.	IV-20	Mohr, P.J.	I-23,24
Maeda, M.	X-10	Moi, L.	II-9; X-13
Majumder, P.K.	I-34	Moore, F.L.	II-7,15,16
Man, K.-F.	XI-18	Moores, D.L.	XI-17
Manning, L.W.	VII-42	Mowat, R.	VIII-23
Mansour, N.B.	VIII-26; X-7	Msezane, A.Z.	V-9
Marrs, R.	II-1	Müller, A.	V-14
Marrs, R.E.	I-19	Müller, J.H.	IV-9
Martin, W.C.	VII-2	Mukoyama, T.	IX-1
Martus, K.E.	VI-2	Mundinger, H.-J.	I-9; XII-3,4
Mårtensson-Pendrill , A.-M.	I-5; VII-15,44	Murnick, D.E.	XII-5
Matsuzawa, M.	X-10	Musgrove, A.	VII-2
Matthias, B.E.	I-9; XII-4	Music, M.	II-13; V-14
Mattison, E.M.	III-6	Musso, M.	VIII-17,21
Mauri, F.	IV-21	Nagourney, W.	II-11
Mawhorter, R.J.	XI-18	Nahar, S.N.	XI-6
McClelland, J.J.	II-14	Nakamatsu, H.	IX-1
McColm, D.	VII-33	Napolitano, R.	II-2
McConkey, J.W.	XI-11	Narumi, H.	XI-21
McCormack, E.	V-16	Nellessen, J.	IV-9
McKibben, J.L.	I-13	Neumann, R.	II-13,16
McLean, R.J.	X-4	Neureither, G.	V-14
Mei, G.	II-10	Nezrick, F.	I-32
Melissinos, A.C.	I-32	Ni, B.	I-9; XII-4
Menzel, A.	V-12	Nico, J.	II-15
Merz, P.	II-16	Niebling, K.D.	XII-2
Meyberg, M.	IX-4	Nienhuis, G.	II-9
Meyer, M.	V-13	Nieto, M.M.	I-2
Miesner, H.	II-13	Norrington, P.H.	XI-15
Misawa, S.	VIII-23	Nussenzweig, A.	VIII-25
		Nyandeh, F.	V-9

Authors	Poster(s)	Authors	Poster(s)
Oakley, D.	I-2	Prior, M.	VIII-23
Öster, P.	VII-43,44	Prodell, A.	I-32
Oh, S.D.	VII-30	Prosihin, V.P.	V-2
Olsgaard, D.	X-6	Putlitz, G. zu	I-9; IX-4; XII-3,4
Onaga, T.	XI-21	Qian, X.-Z.	VII-11
Orth, H.	I-9	Quinet, P.	VII-20
Osterheld, A.L.	I-19	Quiney, H.M.	VII-37
Oteiza, E.R.	I-16,17	Quintana, E.J.	X-14
Paffuti, G.	II-9	Radojevic, W.	VII-46
Pan, S.	VII-8	Raizen, M.G.	IV-14
Papaioannou, D.G.	III-4	Rao, G.N.	VIII-10
Pardo, R.C.	VIII-26	Raphaelian, M.L.A.	VIII-8
Parpia, F.A.	VII-38; XI-19,20	Ratliff, L.P.	V-15
Pathak, A.	XI-14	Raven, E.V.	V-13
Pelletier, R.	VII-24	Rebane, T.K.	X-2
Pelletier-Allard, N.	VII-24	Rebane, V.N.	X-2
Pendrill, L.	VII-15	Redd, E.	X-8
Perger, W.F.	VII-32	Reed, K.	II-1
Persson, H.	VII-43	Reed, K.J.	XI-17
Petrashen, A.G.	X-2	Reyher, H.J.	IX-3
Petrich, W.	II-13,16	Rich, A.	I-22
Pietsch, W.	VIII-21	Richard, P.	X-9; XI-25
Pillet, P.	X-18	Richardson, J.M.	I-17
Pinnington, E.H.	VIII-11	Rinkleff, R.-H.	VIII-1
Pipkin, F.M.	I-7; VIII-15	Rios Leite, J. R.	IV-1
Pisk, K.	V-17	Ristinen, R.	I-2
Plano, L.	X-15	Ritchie, N.W.M.	II-17
Poitzsch, M.E.	I-7	Rizzo, C.	I-32
Polezhaeva, N.T.	X-2	Rogers, J.	I-32
Pollack, E.	VIII-25; X-14	Rosenkranz, J.	IX-3; XII-3
Pratt, R.H.	V-10,11,17,19; VII-30; XI-16	Rosner, A.D.	VIII-20
Prentiss, M.	IV-18,19	Ross, A.W.	IX-5
		Ross, S.B.	I-11

Authors	Poster(s)	Authors	Poster(s)
Roussel, F.	VIII-14	Schwalm, D.	II-13,16; V-14
Rowley, W.R.C.	IV-13	Schwarz, W.	XII-3
Rudakova, T.V.	VI-1	Schweppe, J.	VIII-23
Ryan, R.	IV-7	Schwinberg, P.B.	II-7,8
Sagle, J.	VIII-9	Scofield, J.H.	I-19
Sakai, Y.	XI-5	Semertzidis, Y.	I-32
Salk, S.-H.	X-11	Sengstock, K.	IV-9
Salomon, C.	II-2	Senhorst, H.A.J.	IV-6
Salomonson, S.	VII-15,43,44	Serpa, F.G.	VIII-18
Sandars, P.G.H.	I-21	Sesko, D.	IV-23
Sanders, F.C.	VII-41,42	Shabaev, V.M.	VII-12
Sanders, J.M.	X-9	Shen, Y.T.	VII-31
Sanders, J.P.H.	X-1	Shertzer, J.	VII-23,24
Sandoghdar, V.	I-27	Shiner, D.	VIII-24
Sangster, K.	I-25	Shinpaugh, J.L.	X-9
Sankey, J.D.	IV-20	Sienkiewicz, J.E.	XI-26
Saperstein, J.	I-30	Sigray, P.	II-13
Schaefer, H.R.	I-9; XII-4	Simonov, V.Y.	VI-1
Schäfer, W.	XII-3	Singh, R.	VIII-10
Scheerer, L. D.	IV-5	Skalsey, M.	I-29
Scheinerman, S.A.	V-1	Slaby, J.	IX-4
Scheinefein, M.R.	II-14	Smith, A.M.	II-6
Schinn, G.W.	V-20	Smith, S.J.	XI-18
Schirmacher, A.	VIII-3	Smith, W.W.	X-18
Schmieder, R.	II-1	Solov'yov, A.V.	I-3; XII-1
Schneider, D.	II-1	Sonntag, B.	V-13
Schoenfeld, W.G.	VII-14	Spangenberger, U.	IV-9
Scholl, T.J.	VIII-20	Spiess, G.	VIII-14
Scholz, T.J.	V-21	Sporn, H.	IV-8
Schramm, U.	V-14	Srivastava, R.	XI-3
Schröder, S.	II-13,16	Stacey, D.N.	I-6; VIII-13
Schuch, R.	II-1; V-14	Stachowska, E.	VIII-16
Schuessler, H.A.	VIII-4	Steck, M.	II-13

Authors	Poster(s)	Authors	Poster(s)
Steiger, T.D.	I-22	TSR Group	II-16
Stockli, M.P.	XI-25	Tully, J.A.	XI-12
Story, J.G.	II-17	Ubachs, W.	VIII-19
Strobel, R.	IV-4	Vahala, L.	IV-11
Sturesson, L.	VIII-12	van der Burgt, P.	XI-11
Sturuss, W.G.	V-15	Vandiver, R.	IV-5
Sugar, J.	VII-2; VIII-7	Van Dyck, Jr., R.S.	II-7,8
Sukenik, C.I.	I-26	Van House, J.	I-29
Suric, T.	V-17	van Leeuwen, K.A.H.	IV-6
Sushkov, O.P.	VII-25	van Wijngaarden, A.	I-33
Suzuki, H.	XI-5	van Wijngaarden, W.A.	VIII-9
Suzuki, T.	XI-5	Venema, B.J.	I-34
Svanberg, S.	VIII-12	Venter, K.	IX-3
Swan, J.B.	VIII-13	Verhaar, B.J.	X-1
Sweeney, C.	II-12	Veseth, L.	V-6
Takayanagi, T.	XI-5	Vessot, R.F.C.	III-6
Takuma, H.	XI-5	Vladimirov, V.A.	IX-6
Talman, J.D.	VII-16,28,39	Vondrasek, R.C.	VIII-8
Tanis, J.A.	X-15	Vuskovic, L.	XI-24
Tate, D.A.	III-4	Wagner, M.	V-14
Tauheed, A.	VIII-11	Wagshul, M.E.	I-17; IV-17
Taylor, A.W.	VIII-20	Wakiya, K.	XI-5
Thompson, C.D.	VIII-13	Walker, T.	IV-23
Tiwary, S.N.	XI-4	Wallis, H.	IV-10
Tollett, J.J.	II-17	Walsworth, R.L.	III-6
Tombesi, P.	IV-22	Wang, Z.-W.	VII-4,11
Toshima, N.	X-5	Wanner, B.	II-13,16
Tosto, S.	VII-6	Warston, H.	VII-15
Träbert, E.	VIII-7,11	Watanabe, S.	XI-7
Träger, F.	IX-4	Wehlitz, R.	V-12
Tran, N.H.	X-18	Weihe, F.	II-12
Tsemekhman, K.L.	VII-34		
Tsemekhman, V.L.	VII-34		

Authors	Poster(s)	Authors	Poster(s)
Weiman, C.	IV-23	Zabransky, B.J.	VIII-8
Weimer, C.S.	IV-15	Zavattini, E.	I-32
Werner, J.	IV-9	Zetie, K.P.	I-6
Werth, G.	II-3,4; XII-2	Zhang, Y.	IX-5
Wiese, W.L.	VII-2	Zhang, Z.	XII-3
Wijesundera, W.P.	XI-19; XI-20	Zhao, P.	VIII-15
Wijnands, M.N.J.H.	IV-6	Zheng, S.H.	VI-2
Williams, I.D.	XI-18	Zhou, Z.-X.	VIII-24
Williams, J.F.	VIII-22	Zhu, Xiwen	II-10
Wilsdorf, D.	II-4	Zilio, S.C.	II-2
Windholz, L.	VIII-17,21	Zitzewitz, P.W.	II-15
Wineland, D.J.	IV-14,15,16	Zolotorev, M.	I-10
Winn, D.	VII-46	Zorn, J.	II-12
Winter, H.	VIII-3	Zouros, T.J.M.	X-9
Witteborn, F.C.	I-2	Zuo, M.	XI-24
Wolf, A.	II-13,16; V-14		
Woodgate, G.K.	VIII-13		
Woodle, K.A.	I-9; XII-4		
Woodman, G.H.	VIII-13		
Xie, Chen	III-2		
Yakhoutov, V.L.	I-3		
Yakovleva, V.I.	IX-6		
Yamamoto, Y.	IV-2		
Yan, Z.C.	XI-9		
Yang, D.	II-10		
Yang, H.	VII-10		
Yang, X.L.	I-28		
Yeh, J.R.	II-5		
Yin, Y.-Y.	V-3,4		
Ynnerman, A.	VII-15,44		
Young, L.	VIII-26		
Yu, N.	II-11		
Yurgenson, S.V.	XI-10		

Supplement
POST-DEADLINE POSTERS

TABLE OF CONTENTS TO SUPPLEMENT

Post-Deadline Posters, Session A Tuesday, 31 July 1990

- PD-1 *Interaction of "beaded" atoms with laser radiation*
J. Robert, Ch. Miniatura, F. Perales, Y. Yaun, S. Le Boiteux, G. Vassilev, J. Reihardt and J. Baudon
- PD-2 *Squeezing a squeezed electromagnetic field*
G. A. Barbosa and C. H. Monken
- PD-3 *Velocity selective magnetic resonance laser cooling*
S.-Q. Shang, B. Sheehy, P. van der Straten and H. Metcalf
- PD-4 *Atomic beam deflection with cooling below the Doppler limit*
S.-Q. Shang, B. Sheehy, P. van der Straten and H. Metcalf
- PD-5 *Theory of laser cooling below the Doppler limit in a magnetic field*
S.-Q. Shang, P. van der Straten and G. Nienhuis
- PD-6 *Magnetic-field-induced laser cooling below the Doppler limit*
B. Sheehy, S.-Q. Shang, P. van der Straten and H. Metcalf
- PD-7 *Systematics of antiproton mass spectroscopy*
R. L. Tjoelker, X. Fei, W. Jhe, L. A. Orozco, D. Phillips, G. Gabrielse, J. Haas, H. Kalinowski, T. A. Trainor and W. Kells
- PD-8 *Investigation of long-range states through ultracold collisions*
P. Lett, P. Jessen, C. Westbrook, S. Rolston, W. Phillips and P. Julienne

INTERACTION OF "BEADED" ATOMS WITH LASER RADIATION

J. Robert, Ch. Miniatura, F. Perales*, Y. Yuan, S. Le Boiteux,
 G. Vassilev, J. Reinhardt and J. Baudon
 Laboratoire de Physique des Lasers**, Université Paris-Nord
 Avenue J.B. Clément, 93430-Villetaneuse, France

(*) Present address: Department of Physics, NYU, 10003, New-York, USA

(**) Laboratoire associé au CNRS, URA 282

In a previous paper [1] it has been shown that by use of a longitudinal Stern-Gerlach experiment, "beaded" atoms can be prepared, i.e. atoms described by a wavefunction $|\varphi(\vec{r})\rangle \cdot \Phi(\vec{R})$; $|\varphi(\vec{r})\rangle$ is the internal state (\vec{r} is the electronic coordinate); $\Phi(\vec{R})$, which describes the external (CM) motion, consists of $2j+1$ wave packets (j is the atomic angular momentum), aligned along the atomic velocity. The spatial separation between two successive packets is given by :

$$a = (g \mu_B / 2E_0) \int_0^L B(Z) dZ$$

g is the Landé factor, μ_B is the Bohr magneton, $B(Z)$ the magnetic field profile ($B \neq 0$ within the interval $[0, L]$, $\vec{\nabla} B$ parallel to the direction Z of the atomic velocity), E_0 is the kinetic energy. The distance a can be easily varied over a wide range, from typical atomic wavelengths up to typical optical wavelengths.

When $|\varphi\rangle$ is a radiative state and when a is comparable to the related optical wavelength, the spontaneous emission of these atoms exhibits special properties insofar as the level width, the Lamb-shift and the radiation diagram become a -dependent. Correlatively the behaviour of these atoms in a laser field is also modified by the multiple localisation of $\Phi(\vec{R})$. For sake of simplicity let us consider the case $j = \frac{1}{2}$, with two non-overlapping wave packets, and two internal states $|g\rangle$, $|e\rangle$, connected to each other by a dipolar transition. The standard semi-classical treatment of the atomic evolution, within the frame of the rotating wave approximation, is easily extended to beaded atoms. If all relaxation effects are ignored, it leads to the modified Rabi frequency :

$$\Omega^2 = \delta\omega^2 + \Omega_0^2 \cos^2 \frac{\beta}{2}$$

$\delta\omega$ is the detuning (with respect to the Doppler shifted atomic frequency), $\Omega_0 = p \mathcal{E}_0 / \hbar$ (p dipole momentum, \mathcal{E}_0 laser field amplitude), $\beta = ka \cos \theta$, where k is the optical wavenumber and θ the angle between Z and the laser beam axis. The treatment is readily extended to cases including relaxation effects, $\delta\omega$ being replaced by $\delta\omega + i(\gamma_e - \gamma_g)$, where $\gamma_{e,g}$ are the level widths. It should be pointed out that now the level widths are a -dependent

[1] : $\gamma(a) = \frac{1}{2} \gamma(0) (1 + \sin ka / ka)$.

If one assumes that initially all atoms are in state $|g\rangle$ and that the laser field is switched on at time 0, then one gets the following expression for the upper level population :

$$|C_e(t)|^2 = \Omega_0^2 \cos^2 \beta/2 [\delta\omega^2 + \Omega_0^2 \cos^2 \beta/2]^{-1} \sin^2 [(\delta\omega^2 + \Omega_0^2 \cos^2 \beta/2)^{1/2} t]$$

At resonance :

$$|C_e|^2 = \sin^2 \left(\frac{\Omega_0}{2} \cdot \cos \frac{\beta}{2} \cdot t \right)$$

When the atom passes through a laser beam of rectangular profile such that, for $\theta = \pi/2$, $a = 0$, a π -pulse is achieved, then for $a = \lambda$, one gets the final upper state population as a function of θ as shown in fig.1. It is seen that at particular values of θ , a full transparency of the atoms with respect to the light is obtained.

REFERENCE

- [1] Ch. Miniatura, F. Perales, G. Vassilev, J. Reinhardt, J. Robert and J. Baudon, submitted to J. de Phys.(Paris) (1990)

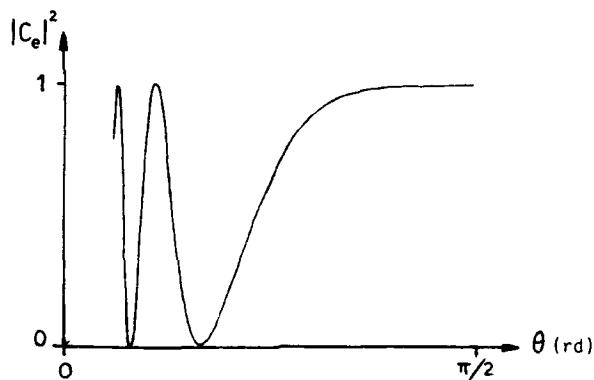


Fig.1

SQUEEZING A SQUEEZED ELECTROMAGNETIC FIELD

Geraldo Alexandre Barbosa and Carlos Henrique Monken

*Department of Physics - ICEx - Universidade Federal de Minas
Gerais - CP 702 - CEP 30161 - Belo Horizonte MG
Fax 5531.4481372. Telex 312308UFMGBR - BRAZIL*

ABSTRACT

A device is proposed to manipulate the photon statistics of a luminescence beam from the down-conversion luminescence produced in a non-linear crystal by laser pumping.

This device, consisting of a Multiple-Quantum-Well (MQW) semiconductor made as a Fabry-Perot cavity for a given frequency ω_s , is supposed being pumped by the two conjugated beams of frequency ω_a and ω_b from the down-conversion luminescence produced in a non-linear crystal. These frequencies are chosen such that ω_a is in the band gap of the MQW and ω_b coincides with the first excitonic level. We have shown that the transmitted ω_a beam, modulated by conjugated fluctuations of number of photons in the ω_b beam, may have its sub-Poissonian character enhanced.

This proposal aims to stimulate a discussion on the theoretical and practical aspects of the device. It is an extension of the ideas presented in *J. Phys. Soc. Japan* 58(1989)2330 and in the 1987 Annual Meeting of the Condensed Matter of the Brazilian Society of Physics.

VELOCITY SELECTIVE MAGNETIC RESONANCE LASER (NG*

S-Q. Shang, B. Sheehy, P. van der Straten, and H. Metcalf
 Physics Dept., S.U.N.Y. Stony Brook, NY 11794, USA

Our magnetically induced laser cooling below the Doppler temperature T_D^1 has been extended to stronger field ($B \sim 1$ Gauss) where the Zeeman frequency ω_Z is much larger than the optical pumping rate γ_p . Thus Zeeman coherences between the ground state sublevels are not readily damped by optical pumping. The motion of the atoms in a standing wave results in intensity modulation of the intensity that induces a magnetic resonance at a particular velocity $v_r = \omega_Z/2k$ where $\omega_Z = g_F \mu_B B/\hbar$ is the the ground state Zeeman splitting¹. As a consequence of this velocity-selective resonance, the atoms are cooled to non-zero velocity $\pm v_r$ with a velocity spread below the one-dimensional (1-D) Doppler limit $v_D = (7k_B T_D/10M)^{1/2} = 10$ cm/s for Rb. In a 1-D atomic beam collimation experiment, we observe the cooling of the atoms to $\pm v_r$ instead of $v = 0$ by the vanishing of the central peak of the spatial distribution and the appearance of two symmetrically placed side peaks (see top part of Fig. 1). We also observed the collimation at low velocities with blue detuning predicted by our model as shown in the bottom part of Fig. 1.

We have extended the model described in an accompanying abstract to the strong field domain where ω_Z and $k v$ are both larger than γ_p . Both the analytic and numerical results show strong, narrow resonances where the force vanishes for atoms moving at v_r . It is instructive to examine the result of an analytic solution found by transforming the optical Bloch Eq's. to a frame rotating at frequency $2k v$. This rotating frame approximation requires $|\omega_Z - 2k v| \ll \omega_Z$ and the light shifts $\omega_j \ll \omega_Z$. The optical force exerted on the atoms is obtained from $F = -\text{Tr}(\rho \nabla H)$ averaged over a wavelength. We find

$$F = \frac{\beta(v-v_r)}{[1+((v-v_r)/v_c)^2]} \quad (1)$$

with the damping constant β and the capture range v_c given by

$$\beta = \hbar k^2 \frac{24\delta\gamma}{(25\gamma^2 + 30\delta^2)} \quad (2a) \quad \text{and} \quad v_c = (\bar{\gamma}_p/k) \sqrt{\frac{25\gamma^2 + 30\delta^2}{25\gamma^2}} \quad (2b)$$

This is a cooling force when the detuning $\delta < 0$. We note that β is independent of s , and both β and v_c are of the same order of magnitude as those calculated for other sub-Doppler cooling schemes. We emphasize that the atoms will not be cooled to $v = 0$ as in the other cooling schemes, but to $v_r \neq 0$.

We have also used numerical methods to calculate the force and diffusion and then calculate the expected velocity distribution by integrating the Fokker-Planck equation for a finite interaction time. We obtain good agreement between the data and our calculations with no adjustable parameters (dashed line in Fig. 1). To our knowledge this represents the first detailed comparison between experiment and the widely studied one-dimensional models of optical molasses that produce sub-Doppler temperatures.

The cooling to non-zero velocity can also be understood as the resonances derived from the exchange of n virtual bosons of energy $2\hbar k v$ between two magnetic

sublevels of the the ground state. It is similar to Doppleron resonances arising from the optical coherences between the ground state and excited state at high intensity. We emphasize that the resonances reported here are a low intensity effect since only the Zeeman coherences between the ground state are involved. They also produce a sign reversal of the damping for small velocity so that atoms are cooled for blue detuning. The width of the velocity peaks is much less than the Doppler limit.

*Supported by NSF and ONR

1. W. Bell and A. Bloom, Phys. Rev. Lett. 6, 280 (1961).
2. B. Sheehy et al., Phys. Rev. Lett. 64, 858 (1990).
3. S-Q. Shang et al., Accepted by Phys. Rev. Letters.

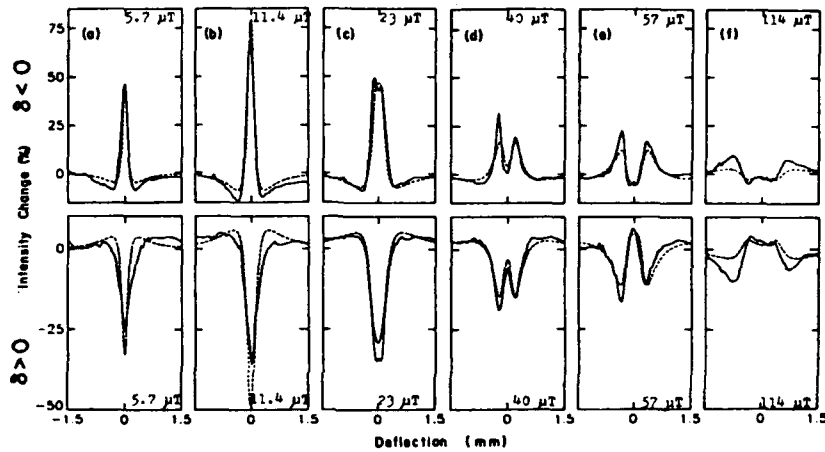
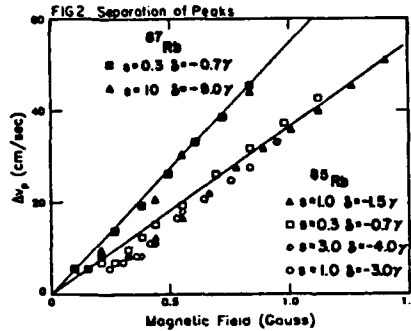


Fig 1: Change in the transverse spatial distribution of the beam as a function of the applied magnetic field. The saturation parameter is 0.25 and the laser detuning is $\delta = -2\gamma/3$. The dashed line represents the expected spatial distribution given the velocity distribution obtained by numerically integrating the Pokker-Planck equation.



ATOMIC BEAM DEFLECTION WITH COOLING BELOW THE DOPPLER LIMIT*

S-Q. Shang, B. Sheehy, P. van der Straten, and H. Metcalf
 Physics Dept., S.U.N.Y. Stony Brook, NY 11794, USA

We have investigated a new one dimensional sub-Doppler cooling process in a polarization gradient and a uniform magnetic field. For an optical molasses made from counterpropagating beams of opposite circular polarizations crossing an atomic beam at right angle, with an applied magnetic field along the direction of the light beams, we have found that the atomic beam is deflected and cooled to the transverse velocity given by $v_r' = 2v_r = \omega_z/k$, where ω_z is the Zeeman frequency. Reversing the magnetic field deflects the atomic beam to the opposite direction (Fig. 1). Note that in this case, v_r' does not depend on detuning or intensity. For orthogonal linear polarizations we apply the field perpendicular to the laser beams and find that the atomic beam is deflected along the direction of the traveling wave whose polarization is parallel to the applied magnetic field. If the magnetic field is along the other laser beam polarization, the deflection is reversed. In this case, the deflection satisfies the condition $v_r = \omega_z/2k$, which is half of the first case (Fig. 2). We wish to emphasize that the atoms are not simply deflected, but in all cases are cooled to this velocity with a width well below the Doppler limit.

In order to demonstrate this phenomenon, we make a velocity selected ^{85}Rb beam using two diode lasers. The first one crosses the beam perpendicularly, and is tuned to optically pump all the atoms into the $F = 2$ hyperfine level of the ground state. The second crosses the atomic beam at an angle $\sim 16^\circ$, and is tuned to excite a particular velocity class chosen by the Doppler shift from the $F = 2$ to $F' = 3$, thus populating the $F = 3$ ground state. The optical molasses (formed by light from a third diode laser) is tuned for $F = 3$ to $F' = 4$ transition. Therefore those atoms participating in the cooling and deflecting process are longitudinally velocity selected. The longitudinal velocity resolution is determined from the angle and the power broadened width of the transition to be about 50 m/s. Our data show a sub-Doppler spread of the transverse velocities for the deflected atoms.

These observations have shown the existence of the velocity-selective ground state resonances¹ even in the presence of a polarization gradient. The resonance is induced by a coherent Raman process when the Doppler shift of the Raman transition $2\hbar kv$ caused by an atom moving in oppositely directed light beams equals the ground state separation (in this case caused by Zeeman splitting). When the narrow Raman resonance condition is met, the atomic ground state coherences are strongly enhanced; near the resonance population differences are created. The resonance width is determined by the rate of optical pumping, which destroys the coherence. The result is a very strong damping of the velocity that cools the atoms to the resonance velocity. This Raman resonance shows that sub-Doppler cooling can work at low intensity because a significant population in the excited state is not necessary.

For our 3 Gauss field we have been able to deflect a transversely cold atomic beam to velocities as large as 1.5 m/s. If the deflection is applied to a beam that has been longitudinally decelerated to 30m/s, this corresponds to a deflection angle of 5° and thus provides a way of extracting a well

defined cold atoms. One could imagine building an atomic storage ring based on this deflecting and cooling technique that could provide a beam which is ideal for precision spectroscopy, the study of cold collisions, and collective effects of cold atoms.

We have previously observed similar ground state resonance in magnetic induced laser cooling.¹ We have developed a theoretical model based on the velocity-selective Raman resonance in a Λ scheme that unifies the well known sub-Doppler cooling processes in the same frame. We emphasize here that the requirement of polarization gradient for sub-Doppler cooling arises because the two ground states coupled by the Raman transition are the magnetic sublevels. In principle this sub-Doppler cooling process could be extended to an atom with two non-degenerate ground states if two lasers were used. In this case neither polarization nor intensity gradient are needed. We will present some examples to show how to obtain sub-Doppler cooling for a more complicated atomic system.

*Supported by NSF and ONR

1. S-Q. Shang *et al.*, Accepted by Phys. Rev. Lett.

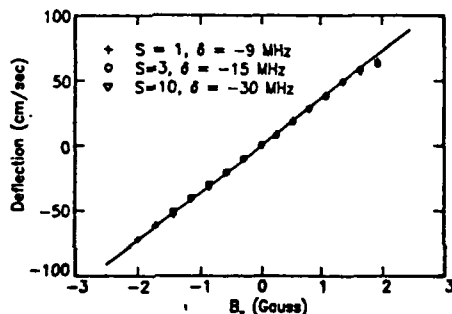


Fig. 1 Deflection of the atomic beam for σ^+, σ^- scheme

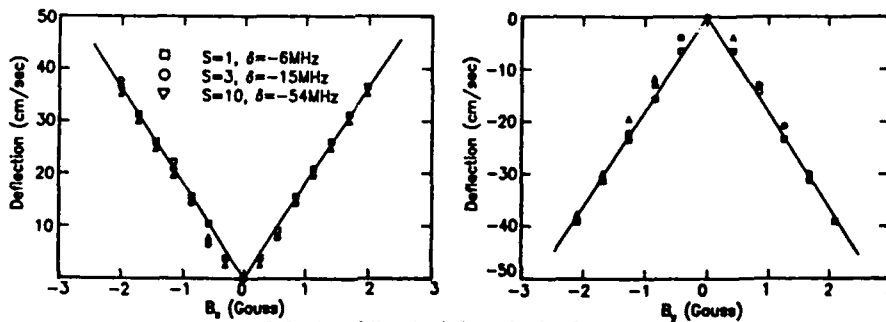


Fig. 2 Deflection of the atomic beam for I.I.I.n. scheme

THEORY OF LASER COOLING BELOW THE DOPPLER LIMIT IN A MAGNETIC FIELD*

S-Q. Shang, P. van der Straten,
Physics Dept., S.U.N.Y. Stony Brook, NY 11794, USA

and G. Nienhuis,
Fysisch Laboratorium, P.B. 80 000, 3508 TA Utrecht, The Netherlands

Recently new experiments in laser cooling have shown temperatures below the Doppler limit $T_D = \hbar\gamma/2k_B$. Theoretical models developed by Dalibard and Cohen-Tannoudji¹ and by the Stanford group² have given an explanation for the observed low temperatures in certain models. However, the results published have not been extended to other experimental situations and a more general theory of sub-Doppler laser cooling is preferable.

We have developed a theoretical description for sub-Doppler laser cooling with or without polarization gradients and with an external field, in particular a magnetic field. In the low velocity regime ($kv \ll \Gamma$) we can adiabatically eliminate the optical coherence from the Optical Bloch Equations (OBE), since the rate of change of the field the atom feels is slow compared to the decay of the optical coherence. The optical force on the atoms can then be expressed in terms of the polarizability of the atoms in the light field. The force has contributions deriving from the gradient of the phase, the amplitude or the polarization of the light field. Each gradient can contribute to the force by the Hermitian or anti-Hermitian part of the polarizability. In this way we can distinguish between the radiation pressure force, the dipole force, the polarization scattering force and polarization redistribution force. The momentum diffusion coefficient contains two parts: the momentum fluctuations due to the spontaneous emission and due to the force fluctuations.

The case of low-intensity is of special interest for sub-Doppler laser cooling, since it has been observed, that sub-Doppler laser cooling works well at low excitation rates¹. In that case we can eliminate the excited state from the OBE and obtain simple relations for the evolution of the atomic state, the force on the atoms, and the diffusion. The evolution equation can be solved for the steady state by expanding the density matrix elements in a spatial Fourier series, obtain recurrence relations between the coefficients, truncating the Fourier series after a number of terms and numerically solving the resulting linear relations. In this way we avoid integrating the OBE directly, which can be a tedious task². For the diffusion coefficient we apply the quantum regression theorem to the multi-level system to obtain the numerical solution.

Our method provides the same results which were previously obtained by Dalibard and Cohen-Tannoudji¹ for specific atomic transitions in the case of polarization gradients, where only two states contribute to the polarizability. However, our method is valid for arbitrary transitions, including hyperfine structure and the Zeeman precession. We have specifically applied our method to Magnetic-Induced Laser Cooling (MILC), where recently new experimental data has been obtained^{3,4}. At low magnetic field, cooling to zero velocity was observed with a width of a few times the recoil limit³. These results were corroborated by our theoretical model described above, which show sub-Doppler

temperatures for low magnetic field and the same trend for the increase of the temperature with the increase of the magnetic field.

At higher magnetic field⁴ sub-Doppler cooling was observed to non-zero velocity $\pm v_r$, with $v_r = \omega_z / 2k$ and ω_z is the Larmor frequency. In this case we can find an approximate analytical solution of the OBE for a $J_g = 1/2$ to $J_e = 3/2$ transition if the optical pumping rate is much smaller than the Larmor frequency by transforming the OBE to a frame rotating with a frequency $2kv$ around the magnetic field axis. The damping coefficient and capture velocity obtained in this way is proportional to the corresponding expression for the polarization gradient models, however, in this case the model shows cooling to a non-zero velocity $\pm v_r$. This is reminiscent of the Doppleron resonances predicted for high-intensity Doppler cooling, but in this case coherence is established between the ground state sublevels. Therefore it can be observed at the low intensities used in the experiments.

With the numerical procedure described above, we have solved the OBE for the case of $J_g = 3$ to $J_e = 4$ transition in rubidium in the case of high magnetic field and observed the ground state resonance in the force curve for this transition (see Fig. 1). To directly compare our model with the experimental results we have also calculated the diffusion for an atom at rest, and used this to numerically integrate the Fokker-Planck equation for a finite interaction time to describe the cooling of the atoms by the light field. The good agreement obtained⁴ (see also a related experimental abstract of our group) indicates that the physics involved in sub-Doppler laser cooling is well described here.

*Supported by NSF and ONR

1. J. Dalibard and C. Cohen-Tannoudji, J. Opt. Am. B6, 2023 (1989).
2. P. Ungar et al., J. Opt. Am. B6, 2058 (1989).
3. B. Sheehy et al., Phys. Rev. Lett. 64, 858 (1990).
4. S-Q. Shang et al., Accepted by Phys. Rev. Lett.

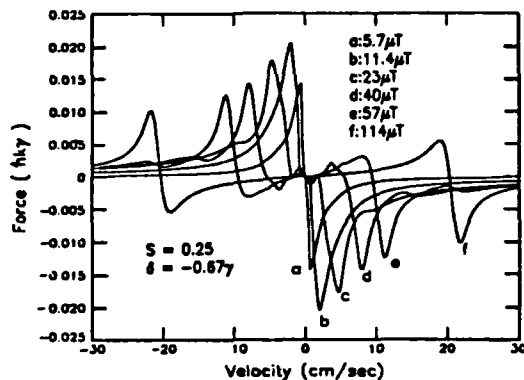


Fig. 1 The force in MILC averaged over a wavelength for $F=3$ to $F=4$ transition of ^{85}Rb .

MAGNETIC-FIELD-INDUCED LASER COOLING BELOW THE DOPPLER LIMIT*

B. Sheehy, S-Q. Shang, P. van der Straten, and H. Metcalf
 Physics Dept., S.U.N.Y. Stony Brook, NY 11794, USA

We report experiments and calculations of sub-Doppler laser cooling in a one-dimensional optical molasses and a uniform magnetic field without polarization gradients. Magnetic field induced laser cooling depends upon the non-adiabatic response of moving atoms to the combination of a circularly polarized laser standing wave and a magnetic field perpendicular to the laser beams. The original idea of damping atomic motion by optical molasses arises from different Doppler shifts of the counterpropagating laser beams seen by the moving atom. In that case, a calculation of the cooling and heating for two level atoms yields the Doppler limit $T_D = \hbar\gamma/2k_B$ ($\sim 140 \mu\text{K}$ for Rb) where $\gamma = 1/\tau$ ($= 2\pi \times 6 \text{ MHz}$ for Rb) is the natural width of the excited atomic state. For two level atoms, the optimum damping of the velocity occurs in a time $\tau_c = 2M/\hbar k^2$ ($\sim 42 \mu\text{sec}$ for Rb) where $k = 2\pi/\lambda$ is the optical wave vector. Still another important parameter is the capture velocity $v_c = \gamma/k$ ($\sim 4.5 \text{ m/s}$ for Rb) that determines the range of velocities where Doppler molasses is most effective.

The experimental discovery of temperatures below T_D led to new theories of optical molasses that attributed these lower temperatures to optical pumping among ground state sublevels in the presence of optical polarization gradients. We report here the discovery of a new cooling process that uses an applied magnetic field instead of motion in a polarization gradient to redistribute atoms among differently light-shifted atomic ground state sublevels¹. We have used this method for optical collimation of a Rb atomic beam to well below the transverse rms velocity width $v_D = (7\hbar\gamma/20M)^{1/2} \approx 10 \text{ cm/s}$ corresponding to the Doppler limit expected for two level atoms in this experimental configuration.

Collimation of atomic beams by optical molasses is limited by the interaction time and the velocity capture range. In Doppler molasses, Rb atoms with thermal velocity ($v \sim 350 \text{ m/s}$) would spend only about $60 \mu\text{s} = 1.4\tau_c$ in a 20 mm long molasses region and could be captured by it if their divergence angles were less than $v_c/350 \text{ m/s} \sim 13 \text{ mrad}$. Because the damping time τ_c' in this new process can be much smaller than τ_c , the velocity distribution of cooled atoms can be much narrower for two reasons: 1) the atoms spend several times τ_c' in the same size interaction region and 2) the temperature limit is much smaller than T_D .

We use a thermal beam of natural Rb produced by an oven at $T \sim 150 \text{ }^\circ\text{C}$ with a horizontal slit aperture 0.1 mm high by 2 mm wide, and a vertical beam defining slit 0.1 mm wide by 2 mm high about 35 cm away. The emerging atoms are optically collimated by a pair of counterpropagating laser beams transverse to their motion. The atomic beam profile is measured with a scanning hot tungsten wire, 25 μm in diameter, 1.3 m away from the region of interaction with the laser beam. The laser light is tuned near the $5S_{1/2}(F_g=3) \rightarrow 5P_{3/2}(F_e=4)$ cycling transition of ^{85}Rb at $\lambda = 780 \text{ nm}$. The laser and atomic beams cross perpendicularly, so the Doppler shifts are small. Atoms can only decay back to the $F_g=3$ ground state, so repumping them out of the $F_g=2$ ground state is not needed. The laser frequency is calibrated with a saturated absorption signal from an auxiliary Rb cell at room temperature. We observed widths of the velocity distribution as low as 2 cm/sec, well below the Doppler limit $v_D = 10 \text{ cm/sec}$ for Rb in a one-dimensional molasses and limited only by experimental geometry. The rms velocity width of the typical data shown in

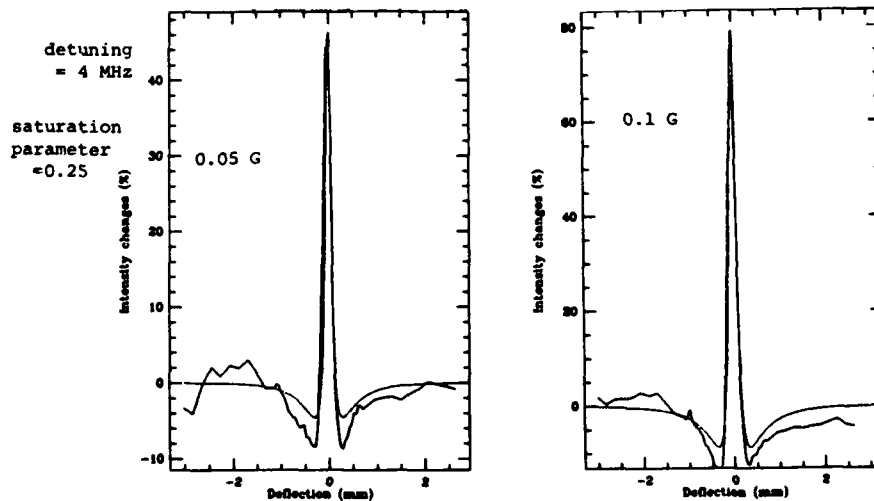
Figure 1 can be estimated to be less than 2 cm/s from the 1.3 m distance between the hot wire and the interaction region, and the thermal velocity ~ 350 m/s.

The main physical idea of this new cooling scheme is based on the different light shifts (ac Stark shift) of the atomic state's magnetic sublevels. Because the light is tuned below resonance, the light shifts are negative for ground state sublevels. Furthermore, atoms are optically pumped to the lowest sublevel (highest M_J) by the circular polarization, and in this process, atoms absorb light with lower frequency than they fluoresce, thus losing internal energy. To sustain the cooling process, atoms must be redistributed among the sublevels when the light shifts are smaller or reversed, and this is done by a weak transverse magnetic field. Thus atoms travelling across the standing wave are optically pumped to the lowest energy sublevel near an antinode, and redistributed among the higher sublevels near a node by Larmor precession. Travel across the next antinode repeats the process and extracts energy from the atoms, thereby damping their motion.

We have developed several different models to describe our experiments. The simplest one is for a $J = 1/2 \rightarrow 3/2$ transition that uses adiabatic elimination of the excited states to reduce the problem to that of the two ground state sublevels. Approximate solution of the Optical Bloch equations yields an expression for the force, and the quantum regression method yields an approximate expression for the momentum diffusion. This model has been extended to the 7 ground sublevels of the $F=3$ ground state of ^{85}Rb , and we have found numerical solutions. We have used these to numerically calculate the expected velocity distribution by integrating the Fokker-Planck Eq. for a finite time. We obtain good agreement between our calculations and data with no adjustable parameters as shown by the smooth lines in Fig. 1.

*Supported by NSF and ONR

1. B. Sheehy et al., Phys. Rev. Lett. **64**, 858 (1990).



SYSTEMATICS OF ANTIPROTON MASS SPECTROSCOPY

R.L. Tjoelker, X. Fei, W. Jhe, L.A. Orozco, D. Phillips, G. Gabrielse
Department of Physics, Harvard University, Cambridge, MA 02138, USA

J. Haas, H. Kalinowsky
Institut für Physik, Universität Mainz, 6500 Mainz, West Germany

T.A. Trainor
*Department of Physics, University of Washington, Seattle, WA 98195,
USA*

W. Kells
Institute for Fusion Studies, Pasadena, CA 91107, USA

Mass spectroscopy is reaching unprecedented accuracies using Penning traps. Such traps consist of a static, uniform magnetic field with an electric quadrupole added for particle confinement. They provide an ideal environment for comparisons of different ions. The measurement of the eigenfrequencies of the particles oscillating in such an environment is a mass measurement.¹ However, several systematic checks are needed to understand the interaction of the electric and magnetic field with the trapped particle(s).

We have successfully measured the inertial mass of the antiproton with an accuracy one thousand times better than with previous techniques. Measurements were performed using an open cylindrical trap geometry with a large effective trap dimension of 0.69 centimeters.²

The axial and cyclotron motions of the freely oscillating particles are *simultaneously observed*. Their dependence on energy, number, and trap

¹L.S. Brown and G. Gabrielse, *Rev. Mod. Phys.*, **58**, 233 (1986)

²G. Gabrielse, L. Haarsma and S.L. Rolston, *Intl. J. of Mass Spec. and Ion Proc.*, **88**, 319 (1989); *ibid.* **93**, 121 (1989).

imperfections is studied. Direct detection of the cyclotron motion using a split ring electrode provides unique means to investigate various possible systematic sources of error. We measure the modified cyclotron eigenfrequency of the confined particles as a function of the applied trapping potential. By extrapolating to zero voltage for both antiprotons and protons, we compare the obtained value to the free space cyclotron frequency determined using an invariance theorem.³ These cyclotron frequency versus voltage measurements also provide a valuable probe for the eigenfrequency dependence on the polarity of charge for equal mass particles, possible space charge and cloud size effects.

This work is supported by AFOSR, the atomic physics program of the NSF, and the BMFT of the Fed. Rep. of Germany.

³L.S. Brown and G. Gabrielse, Phys. Rev. A **25**, 2123 (1982)

INVESTIGATION OF LONG RANGE MOLECULAR STATES THROUGH
ULTRACOLD COLLISIONS

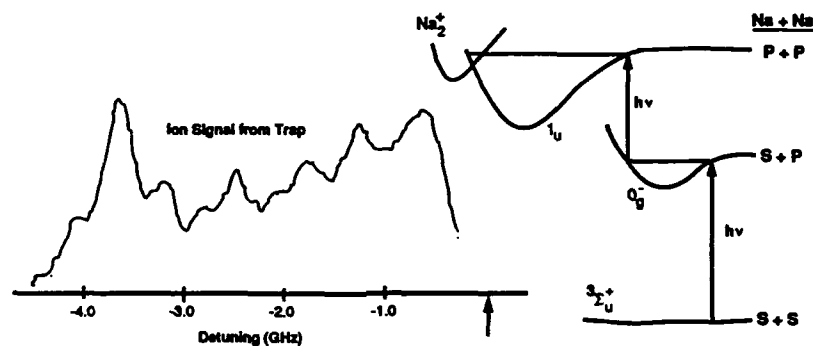
P. Lett, P. Jessen†, C. Westbrook, S. Rolston, W. Phillips and
P. Julienne, National Institute of Standards and Technology,
Gaithersburg, MD 20899 USA,
P. Gould, Univ. of Connecticut, Storrs, CT 06268 USA

We have studied associative ionization (AI) at ultracold temperatures in a two-focus laser trap [1]. In the course of these studies we have investigated the dependence of the AI rate on the trap laser frequency, which shows interesting resonance structure and offers the possibility of investigating "pure long range" molecular states of the Na₂ molecule [2]. In addition, we have begun two-color experiments to help elucidate this resonance structure.

The trap consists of two tightly focussed laser beams counterpropagating in a region of optical molasses [1]. The two trapping lasers are alternated in time to avoid standing wave heating effects and, in addition, alternated with cooling periods during which neither trap beam is on. In the trap the sodium atoms reach densities $\sim 10^{10}$ cm⁻³ and are laser cooled to ~ 1 mK. These atoms undergo ionizing collisions (AI):



In the figure the ionization rate versus trap laser frequency is shown. It is believed that this resonant structure, although complicated by changing trap parameters, (in particular, the temperature and density of the atoms may be changing, due to changing heating rates and the changing depth of the trap) may be a signature of intermediate bound state resonances (vibrational states) on the O_g⁻ long range molecular potential and rotational state structure in the 1_u molecular state leading to AI.



The proposed intermediate 0_g^- state is one of the "pure long range" molecular states that were predicted over a decade ago [2] but have yet to be unambiguously observed. The purely long-range nature of this state (inner turning point near $55 a_0$) has made its creation somewhat problematic by conventional techniques. The extremely slow passage through the appropriate range of large internuclear separations available with ultracold collision techniques may now open up these states to investigation.

This explanation of the structure in the AI signal requires further verification. Two color experiments, performed with the addition of another laser frequency during the trap periods, have been initiated. With the information gained from these experiments and additional theoretical efforts [3], it is hoped that this structure may be identified with particular rotational/ vibrational resonances of the proposed intermediate states.

Work supported by NIST and the U.S. Office of Naval Research.

†Permanent address: Institute of Physics, U. of Aarhus, Århus, Denmark

[1] P. Gould, P. Lett, P. Julienne, W. Phillips, H. Thorsheim and J. Weiner, *Phys. Rev. Lett.* **60**, 788 (1988).

[2] W. Stwalley, Y.-H. Uang and G. Pichler, *Phys. Rev. Lett.* **41**, 1164 (1978).

[3] P. Julienne and R. Heather, private communication. (See also the invited talk by P. Julienne at this conference.)